NORTHWESTERN UNIVERSITY

Using Visible Light to Synthesize Ladder Polymers and Modulate Dynamic Covalent Chemistry

A DISSERTATION

SUBMITTED TO THE GRADUATE SCHOOL
IN PARTIAL FULFILLMENT OF THE REQUIREMENTS

for the degree

DOCTOR OF PHILOSOPHY

Field of Chemistry

By

Emily Robin McClure

EVANSTON, ILLINOIS

September 2023

Abstract

Photochemistry allows chemists to harness the energy in specific wavelengths of light and use it to achieve new chemical transformations. These chemical transformations are often impossible or energetically demanding under traditional thermal conditions. My dissertation focuses broadly on different strategies to apply visible-light photochemistry and photocatalysis to the development of unique materials. Specifically, I synthesized new photoresponsive molecules that can manipulate and control the exchange of dynamic covalent bonds. Through a joint synthetic and computational approach, we explained how adjacent azobenzene photoswitches control boronic acid-ester exchange. Moreover, I have explored photoredox catalysis as an opportunity to access synthetically challenging polymer structures. I adapted a small-molecule photoredox Diels–Alder reaction to the synthesis of non-conjugated ladder polymers that have potential applications in gas and fluid membrane separation. I was able to identify multiple pathways of initiation for the polymerization and broaden the scope of the reaction to include myriad of photocatalysts, monomer structures, solvents, and oxidants. This approach allows us to access a unique fully saturated ladder polymer backbone. Throughout my thesis, I show opportunities to couple light with well-known chemistries to access new materials and address gaps in the application of photochemistry to materials synthesis.

Acknowledgements

I would like to acknowledge that all of my research at Northwestern was completed on occupied homelands of the Council of Three Fires; the Ojibwe, Potawatomi, and Odawa as well as the Menominee, Miami, and Ho-Chunk nations. I would like to acknowledge this history and I hope that those who do research in the future can keep it in mind and find more ways to actively incorporate Indigenous history and knowledge into their scholarship.

First, I would like to acknowledge my advisor, Professor Julia Kalow. Thank you for your compassion, your willingness to try new ideas, and your belief in both the merit of my scientific ideas and me as a scientist. Thank you also for the marvelous book recommendations. I am extremely grateful for your mentorship and guidance, and I can only hope to embody your leadership and thorough approach to thinking about science in my future research endeavors. Your constant feedback and support made me a better scientist, colleague, and instructor.

Julia has also hired a fantastic set of people for the lab who remind me constantly of the joys of doing science. I would like to thank everyone in the lab for their friendship, support, and engagement. I would especially like to thank Dr. Pradipta Das for your friendship and collaboration, and Haley McAllister, Ian Pierce, Dr. Young Ju Yoon, and Alexis Martell. Each of your gestures of friendship came at crucial times for me and will not be forgotten. Thank you also to Dr. Jacob Ishibashi for helping me brainstorm, Dr. Eliot Woods, Dr. Joe Accardo, Dr. Bassil El-Zaatari, Dr, Viraj Kirinda, Dr. Xiaodi Wang, Dr. David Barsoum, Dr. Boyeong Kang, Dr. Alexandra Berl, Dr. Vivian Zhang, Dr. Steven Chapman, Christina Hemmingsen, Dr. Eric Abenojar, Daniel Hart, Jonathan Sklar, Emmanual Garcia Villatoro, Ethan Fuller, Cooper Hanley, and Nina Georgieva. I would also like to thank my dear friend Dr. Christopher Eckdahl for reminding me that molecules are not an apt judge of character.

I would like to thank my committee for their feedback and support during an unprecedented time to take a qualifying exam and subsequently conduct research. Thank you to Dr. Regan Thomson, Dr. Christian Malapit, Dr. Emily Weiss, and Dr. Karl Scheidt.

A huge thank you to all my collaborators over the years, but most especially Dr. Martin Mosquera. Thank you for your patience, mentorship, and friendship. Thank you also to all the staff at the Integrated Molecular Structure Education and Research Center (IMSERC) at Northwestern without whom much of my research would not be possible. Special thanks to Dr. Ralph Tobias, Dr. Yongbo Zhang, Dr. Yuyang Wu, and Saman Shafaie. Thank you also to Feda Jerad and Linda Hickey for your support of Kalow lab operations. Thank you, Feda, for your kindness and enthusiasm.

So much of my PhD happened outside of the lab, and I would like to thank all of those who brought education and knowledge into my life outside of research. Thank you to all board members of Northwestern University Building on Diversity, past and present, but especially thank you to Joshua Zhu, Dr. Qining Wang, Alexis Martell, Jeremy Fisher, Clover Moisanu, Dr. Aidan Caravana, Dr. Dawn Duan, Dr. Ollie Hayes, Dr. Andrea D'Aquino, Dr. Ariana Grey Bé, Dr. Zach Urbach, Cat Ly, Ezra Marker, Dr. Waleed Helweh, and Dr. Nic Watkins. I am inspired by your commitment to providing a welcoming space for students at Northwestern and the opportunity for graduate students to reflect and grow. Thank you also to my fellow activists in Northwestern University Graduate Workers, including Stella Fors and Emma-Rose Newmeyer. I would also like to thank those who have made work with the Northwestern Prison Education Program possible, especially Dr. Emily Ma and Sanjana Subramaniam. An especially big thank you to my tutee through NPEP, Patty Ouska. You have taught me the power of perseverance and what all of us are able to overcome. Thank you for your correspondence and your continued commitment to education in the two years we've known each other.

Thank you to the teaching faculty in the chemistry department at Northwestern, but I owe an especially big thank-you to Dr. Stephanie Knezz. Your commitment to teaching and social change is inspiring, and I am emboldened knowing there are educators and thinkers like you in the world. Thank you for always supporting me in whatever pursuits I took on. Thank you also to the Center for Teaching and Learning (SEARLE Center) at Northwestern.

I am immensely grateful for the opportunities I found at the Center for Civic Engagement at Northwestern, especially with Dr. Ruth Curry and Katrina Weimholdt at NU Votes. Thank you for reminding me of the bigger picture.

Thank you to mentors Dr. Erick Leggans, Dr. Steve Sieck, Dr. Silvia Grama, and Dr. Benjamin Partridge! I would not have gotten to where I am today without your mentorship on my path to Northwestern.

Thank you to Elysse Longetti for your unwavering support and belief that I would find a job! You were right!

I have mentioned many people already that I hold near and dear to my heart, but I would like to take a moment to acknowledge and thank all of my friends in the Northwestern Chemistry Department. Thank you to the soon-to-be Dr. Emilie Lozier without whom graduate school, unionizing, cat sitting, and writing this thesis would have been much harder! Thank you to Dr. Jana Butman for your incredible humor and rollerskating adventures. Thank you to Katie Landy, Dr. Jennifer Rote, Dr. Dan Laorenza, and Dr. Megan Wasson. Thank you to Clover Moisanu for taking the department in promising directions after I leave. I'm so proud of you! Thank you to Dr. Joanna Korpanty for helping me see the best version of myself and for being my friend since day one. You are an inspiring scientist and friend. I'm so grateful you are in my life, and not just because you live in Boston now! Come back! Dr. Aleia Bellcross has been one of my closest friends at Northwestern. Thank you for your support and hype without fail, and for finding moments of friendship and closeness even on walks to Tomate. I am so excited about what our friendship holds for us, as I know you are a once-in-a-lifetime kind of friend.

A big thank you to my best meet-cute friend, Genevieve Schroeder. I know whatever you reach for, you will always land in the stars. Thank you for sharing so much with me in our views of the world, but also always expanding my perspective (and not just about space or eye makeup).

A big thank you to my full-moon intention-setting friends Izzy Zelichenko and Adrienne Seitz. Here's to the amazing dance parties and memories we've made together, and I am holding my breath until we can travel together again! Thank you for reminding me that friendship is about love and intention, not proximity.

As many of my colleagues can confirm, I am extremely grateful for my time at Grinnell College and the friendships my time there has provided me with as I've graduated and entered the next stages of my life. Thank you to Karnika Arora, Charlie Rosenblum, Alex Chang, Patrick McHale, Samanike Hengst, Josie Sloyan, Amal Dadi, Christine Rains, Justin Leuba, and Clara Trippe. Every single one of you means so much to me, and I

feel so lucky for all the unique ways you all bring joy to my life. I look forward to many more years of friendship whether we are in the same city or far away.

I want to extend a special thanks to my friends from Grinnell who are sharing the experience of completing a PhD. Your commiseration and understanding have been crucial to my success, and I know that I thrive when my friends thrive. Thank you to Dr. Philip Gemmel for your mentorship and support, Dr. Valerie McGraw, and Dr. Melissa Hardy. Thank you to my kyooties Dr. Austin Wadle, Emma Friedlander, and Katherine Parrish. I could write paragraphs about what the three of you (plus Churl and Niks) have brought into my life and what you mean to me, but I'll reserve my affections for our next meeting in person. Dr. Wadle, I am so lucky to have been through the thick and thin of graduate school with you and I am so proud of you. I am eternally grateful for the support and friendship of both Sarah McHale and Jillian Rix Mulligan. You are both so inspiring and I feel the warmth of your glow. Sarah, your friendship came into my life right when I needed it, and your loyalty and insight are unparalleled. Jill, I am so lucky you are my friend, and that we can share so much together even when we are far away. I so look forward to when it will be time for both of you to defend your theses as well.

Thank you to friends in Colorado Abby Levitt, Katya Shipyatsky and Ben Pettis. Thank you to Emma Milek for being my longest friend. I am so grateful that we always find time for each other, and I look forward to so many more years of celebrations and catch-ups. Thank you to Hannah Bendiksen for beagle betrothments and helping me learn what it means to lose. It's because of you that I can now espouse the principles of Big Friendship!

Thank you to the friends I've found in Chicago including Erika Greenfelder, Charlotte Boucher, Ingrid Hofeldt, Laura Nevill, Geneva Garcia, and Grace Bell. Thank you also for the people you introduced me to and the communities you invited me into. I feel so lucky to have the network that I do thanks to you. Thank you to my Dungeons and Dragons group Eva Martuzzi, Tim Boex, Trenty Henry, and Bianca Bárcenas. Thank you to Ryan Keaveny for your countless hours of Mario Kart, TV show binging, long talks, and all-around life experiences. There are so few people with whom I could do road trips, quarantine, camping, and rooftop bars without us tiring of each other, and I'm grateful that we still find something new to talk about. You are such a

thoughtful and caring person, and I don't know what my life would have been like in Chicago without you. Luckily, I will not have to find out!

Thank you to my rock climbing (and rock climbing adjacent) buddies Kaushik Rao, Dr. Felix Owusu, Tothyanna White, and Jacob Getzoff. Thank you especially to my fellow coordinator and move-maker Michael Owusu for your friendship and impeccable taste in books and gifs. I owe an especially big thank you to Anita DeWitt, not just because you still remember my order from Dari Barn, but because you have been with me practically every step of the way on my journey as a scientist. You are one of my closest friends and I am always learning from you while also laughing and having the best time, no matter what we do. I'm looking forward to many more years of friendship; thank you for always reminding me of the things we can rejoice in life.

Thank you to my neighbor and absolutely incredible friend (NAIF) Emma Tilden. I can only hope that I have brought a fraction of the joy and enrichment to your life that you have brought to mine. Thank you for always understanding me and being game for most anything. If you ever decide to ditch tech and want to open a multifunctional bookstore/bar/craft café, please let me know. Until then, I am excited for more trivia nights, cook-n-hangs, bach/nails nights, or really any night that we get to spend together.

I attribute the capacity I have for love and friendship in large part to learning how to love big from my family. Thank you to my grandparents Jim Magee, Kathy Hall, and especially my grandmother Jayne McClure. You bought me a microscope when I was a kid and you were one of the first people to help me see myself as a scientist. It is remarkable that you have been gone for so long and yet I still feel your presence in my life so deeply and profoundly. I miss you and I hope you are proud of the woman I am today. Thank you to my grandfathers Bill McClure and Mike Mansfield. Thank you to my Mor Mor Judy for your steadfast email correspondence and your love and support. I also hope to make you proud, and I am so grateful for your support in all my endeavors over the years. You mean so very much to me.

Thank you Mim Neal, Harlan Neal, Marion Weedemann, and Bruce Neal. Your familial support in Chicago made living here so much fun and was such a comfort. Much love and gratitude for Laura and John Maxa. Thank you to my family in Durham including my phenomenal aunt Robin Magee as well as Dr. Henri Gavin and Stephen Magee. Thank you to all the Mansfield-Nevin family for your undying support and fully

embracing me as a member of the family. I am so fortunate! Thank you to Dr. Michael McClure for being the coolest uncle alive and providing much-needed insight into academia.

Thank you to my cat, Scooter, for being a simultaneous joy and menace in my life. You have the biggest capacity for love I have ever seen but please for the love of God stop trying to eat plastic. You can't read but please know how much I love you; everyone else does. Thanks for being my buddy for the last thirteen years.

Lastly, thank you to my parents and my sister. Thank you for reminding me that no matter what I did, I could just be your daughter and you would still celebrate me. I will also credit all of you with my verbose tendencies. Thanks, Ken, for being the best chosen dad I could ask for, but as a gift for my PhD, I might suggest a moratorium on adopting more chihuahuas. Thank you to Kelly for being an amazing mother to me and my sister, and for being an inspiration in all the projects you take on and the ways you built community and find time for artistic expression. You inspire me! Thank you to my sister Iris for being the best sibling I could ever ask for. I love you to the moon and back. Thank you to my mom, Caitlin, and my dad, Lance, for teaching me more about the world than I may ever understand. Dad, congratulations on your retirement after almost three decades of teaching. Thank you for your dedication to art and education. I'm so excited that we can embark on new life journeys together. Mom, I could spend hours listing all the things that I am grateful for, and it wouldn't be enough. I can't wait to watch you win *Jeopardy!*. The best parts of me come from those closest to me, and I hope this PhD brings a well-earned sense of pride to my entire family. I love you.

Table of Contents

List of Abbreviations

ACN	acetonitrile
AIF	aggregation induced fluorescence
AgNO$_3$	silver nitrate
Ar	generic aromatic group
bp	boiling point
BHT	butylated hydroxytoluene
cm^{-1}	wavenumber
conv	conversion
COD	cyclooctadiene
CO$_2$	carbon dioxide
CPCM	conductor-like polarizable continuum model
DA	Diels–Alder
Da	Dalton
DCC	dynamic covalent chemistry
DCM	dichloromethane
DCTB	*trans*-2-[3-(4-*tert*-butylphenyl)-2-methyl-2-propenylidene]malononitrile
DI	deionized
DFT	density functional theory
DIF	dissociation induced fluorescence
DMEM	Dulbecco's Modified Eagle Medium
DMF	*N*,*N*-dimethylformamide
DMSO	dimethylsulfoxide
dn/dc	refractive index increment, used to determine molecular weight
DSC	differential scanning calorimetry

Đ	polydispersity index
E_a	activation energy
ECM	extracellular matrix
EG	ethylene glycol
Et	ethyl
Et_2O	diethyl ether
EtOAc	ethyl acetate
ET	energy transfer
equiv	equivalents
FTIR	Fourier transform infrared radiation
G'	elastic modulus (Pa)
G"	storage modulus (Pa)
GCMS	gas chromatography mass spectrometry
GPC	gel permeation chromatography
GSD	global spectral deconvolution
HAT	hydrogen atom transfer
HCl	hydrochloric acid
HEPES	4-(2-hydroxyethyl)-1-piperazineethanesulfonic acid
Hex	hexanes
HRMS	high resolution mass spectrometry
H_2O	water
Hz	Hertz
IRC	intrinsic reaction coordinate
IR	infrared
K_{eq}	equilibrium constant
k_{ex}	rate constant of exchange

LCMS	liquid chromatography mass spectrometry
LED	light emitting diode
LFER	linear free energy relationships
MALDI	matrix-assisted laser desorption ionization mass spectrometry
MALS	multiangle light scattering
Me	methyl
MeOH	methanol
Mg	magnesium
Mg_2SO_4	magnesium sulfate
ML	metal-ligand
mol	mole
M_n	number average molecular weight
M_w	weight average molecular weight
MWCO	molecular weight cutoff
M	molar
m	milli
NaCl	sodium chloride
$NaHCO_3$	sodium bicarbonate
Na_2SO_4	sodium sulfate
NaOH	sodium hydroxide
Ni	nickel
nm	nanometer
NMR	nuclear magnetic resonance
N_2	nitrogen
O_2	oxygen
Pd	palladium

PDMS	poly(dimethylsiloxane)
PCET	proton coupled electron transfer
PEG	poly(ethylene glycol)
PET	photoinduced electron transfer
ppm	parts per million
PVC	poly(vinylchloride)
PBS	phosphate buffered saline
RBF	round bottom flask
RI	refractive index
RP	reverse phase
rt	room temperature
R	generic alkyl group
SEC	size exclusion chromatography
TBAF	tetra-n-butylammonium fluoride
TBS	*tert*-butyl-dimethylsilyl
TEA	triethylamine
TGA	thermogravimetric analysis
THF	tetrahydrofuran
TLC	thin layer chromatography
TMS	trimethylsilyl
TS	transition state
UV-Vis	ultraviolet-visible
VT-NMR	variable-temperature NMR
V	voltage
2D	two dimensional
Δ	delta, or difference

μ   micro

List of Figures

List of Schemes

List of Tables

Chapter 1: Introduction

As chemists and materials scientists aim to develop materials with increasing precision and control, light presents an ideal stimulus for new chemical transformations. Photochemical transformations were first discussed as an alternative energy source by Ciamician in 1912,[1] but photochemical transformations did not appear in industrial processes until the 1940s.[2] Even then, most developments encompassed ultraviolet (UV)-mediated processes, such as curing ink, resins, and films. Despite the slow implementation of these photochemical transformations, there are several aspects of photochemistry that make it an attractive alternative to thermal transformations. Light consists of photons at various energies, and these photons can excite molecules with appropriate electronic structures. Every molecule contains an energy gap (of various degrees of magnitude depending on the structure) between the ground and excited state, and certain wavelengths of light correspond to the energy required for that gap. Photoexcitation induces electrons in a molecule to populate an excited state, which enables further chemical transformations, such as isomerization, bond breaking, and photoinduced electron transfer (PET). The energy barrier to access these excited states prohibits their population through thermal pathways. For example, one mole of photons at 365 nm, just outside of the range of visible wavelengths, has 130 times more energy than the thermal energy available to activate a reaction at ambient conditions.[3] Moreover, the excitation of a molecule inverts conventional rules for molecule reactivity. Photochemical excitation of a molecule leads to changes in the molecular orbital symmetry[4] and enables thermally disallowed reactions such as [2+2] cycloadditions. As a result, photochemistry enables processes that cannot occur under thermal conditions.[5]

Light-induced reactions provide an additional benefit in the ability to control reactions over time and space, using an external stimulus. Some reactions are photoinitiated, meaning light initiates a process that then propagates thermally, while others are photocontrolled, meaning the reaction progress continuously depends on irradiation with light. Photocontrolled reactions are a powerful tool in chemical synthesis because a flip of a switch can reversibly activate and deactivate a chemical transformation. Beyond temporal control of a reaction, light presents the additional advantage of spatial control. Polymer chemists especially benefit from the ability to the selectively implement photochemical transformations over a space, as this has led to the

development of photomasking for lithography,[6] 3D printing,[7] and fabrication of new materials.[8] However, the penetration depth of light limits the efficacy of photochemical transformations to non-opaque or very thin materials, especially photochemical reactions catalyzed by shorter wavelengths of light, such as UV light. The added environmental toxicity of UV light creates an additional incentive to develop visible light-mediated photochemical transformations. Visible light provides greater penetration depth, requires less energy, and is more biologically benign. In my graduate research, I studied visible light-induced transformations in two specific ways: modifying photoresponsive molecules to control dynamic covalent chemistry (DCC) and developing a new photoredox-catalyzed ladder polymerization.

Part I: Modifying photoswitch architectures to control dynamic covalent chemistry equilibria

Photoresponsive molecules harness the benefits of light as an external stimulus for a variety of applications in small-molecule systems—such as molecular sensing[9], light harvesting,[10] and drug delivery[11]—and the design
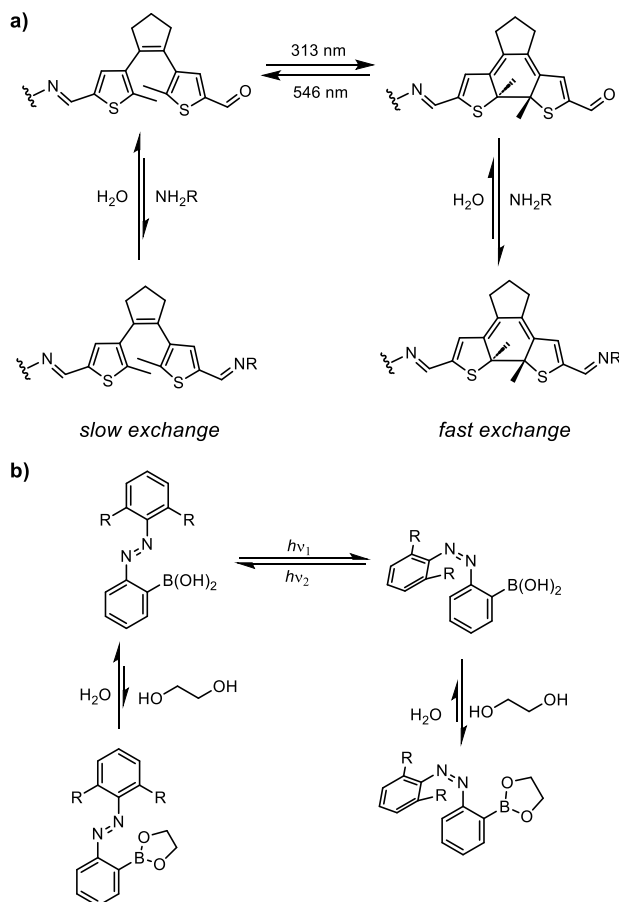
and synthesis of polymeric materials.[12,13] Photoswitches are a class of photoresponsive molecules that undergo a conformational change, such as E to Z isomerization or electrocyclization, upon irradiation with light.[14] These changes result in differences in size, dipole, conjugation, and charge. These changes are often reversible under heating or irradiation with a different wavelength of light. Scientists can modify a wide range of photoswitch properties such as thermal half-life, wavelengths of isomerization, rate of isomerization, and quantum yield through structural diversification.

Figure 1. a) Using diarylethenes to control imine exchange. **b)** Using azobenzenes to control boronic ester exchange.

Dynamic covalent chemistry (DCC) is defined as any reaction with reversible exchange of covalent bonds between molecules.[15] The reversible nature of these reactions has led to their applications in various systems including self-healing materials, templated 2D and 3D organic materials, and materials with potential for closed-loop recycling.[16] Coupling these reactions to a photoresponsive moiety enables an additional non-invasive, rapid tool to control these exchange reactions. Specifically, the ability to tune the kinetics or thermodynamics of dynamic covalent bonds through the structural changes in a photoswitch offers opportunities to control the properties of dynamic materials externally and reversibly with light. Previous attempts to couple dynamic covalent reactions with photoswitches include modifying diarylethenes to control the exchange of reversible Diels–Alder reactions[17] and imine formation (**Figure 1a**).[13,18]

To design dynamic and adaptable materials that reversibly respond to light, the Kalow lab has developed a photoswitchable dynamic bond based on boronic ester exchange. The design included a photoswitchable azobenzene with a boronic acid at the *ortho* position (**Figure 1b**). This molecule was installed into hydrogel networks with a diol partner and resulted in reversible stiffening and softening of the hydrogel upon irradiation with UV (365 nm) or green (530 nm) and blue (450 nm) light, respectively. I sought to red-shift the isomerization of the photoswitch for increased compatibility in biological applications. Additionally, I hypothesized that creating an azobenzene analogue with different substituents to red-shift absorption might also affect the relative binding of the boronic acid. In chapter 2, I report my findings of how a subtle small-molecule synthetic modification drastically changes the properties of a photoswitchable dynamic covalent bond.

This change also allowed us to elucidate the origins of photoswitchable binding through computational and experimental studies.

Part II: Photoredox catalysis for the synthesis of ladder polymers

Photoredox catalysis aims to mimic the action of photosystems I and II by introducing a catalyst that can absorb light and subsequently electron transfer with additional substrates. Similarly, organic and organometallic molecules and complexes absorb light to reach an excited state then undergo electron transfer to a substrate through one of two pathways.[19] In a reductive quenching pathway, the excited photocatalyst oxidizes a substrate, providing a radical cation substrate and a radical anion photocatalyst, which is oxidized by an external oxidant to close the cycle. Conversely, in an oxidative quenching pathway, the excited photocatalyst reduces a substrate, which yields a radical anion substrate and the radical cation photocatalyst, which must be reduced by an external reductant. Whether a photoredox catalyst undergoes oxidative or reductive quenching depends on the oxidation and reduction potentials of the substrates relative to the catalyst excited state.[20] In both cases, the radical ion of the substrate goes on to do productive chemistry.
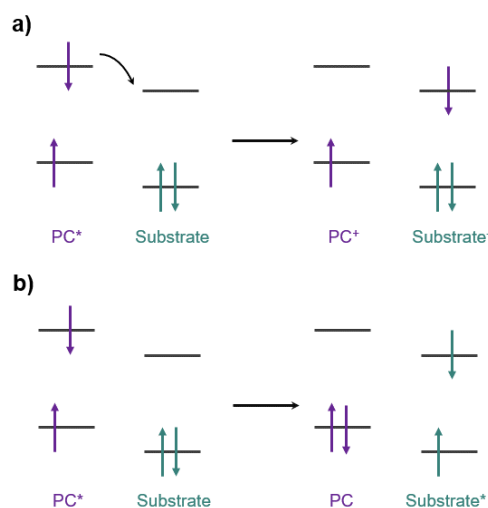
Figure 2. a) Photoinduced electron transfer **b)** Photoinduced energy transfer.

Photoredox catalysis via single electron transfer requires that the substrate has a favorable potential relative to that of the excited photocatalyst (Figure **2a**).[21] If the excited photocatalyst does not have favorable oxidation/reduction potential compared to that of the substrate and a transformation is still observed, this

provides significant evidence for an energy transfer mechanism. In an energy transfer mechanism, the excited photocatalyst induces excitation of an electron in a substrate, typically to the triplet state, while the photocatalyst relaxes (Figure **2b**).[22] A photocatalyzed transformation can also proceed through hydrogen atom transfer (HAT) or proton coupled electron transfer (PCET). In a HAT process, the photocatalyst extracts a proton from a hydrogen donor substrate, generally through a photoxidation process.[23] Recently, this transformation was applied to the post-polymerization functionalization of poly(ethylene)glycol (PEG).[24] Unlike PCET, the movement of the electron and proton in HAT generally occurs at the substrate of interest. In other words, the electron and hydrogen pair transfer between the same donor and acceptor compound. Conversely, PCET refers to reactions in which the proton and electron are transferred between different centers, generally a conjugate base that compliments and propels the reaction.[25] Recently, polymer chemists have applied PCET to the degradation of polymers with ether linkages in the polymer backbone.[26]

Photoredox polymerization strategies largely comprise analogues of known thermal polymerizations, such as the controlled radical polymerization of acrylates,[27] as well as the cationic[28] and radical[29,30] polymerization of vinyl ethers, and radical ring-opening polymerization.[31] Beyond previously reported thermally-initiated radical polymerizations, photoredox catalysis has also been applied to the activation of Si-H bonds for network formation,[32] and to access a radical cation for a metal-free ring-opening metathesis polymerization (ROMP).[33,34] Photoredox catalysis has been applied to the post-polymerization modification of commodity polymers[35,36] for further functionalization and degradation of thermosets.[37] While photoredox catalysis has been applied to the synthesis or modification of many previously characterized polymers, I recognized an opportunity to apply photoredox catalysis to the synthesis of novel polymer architectures that are challenging to access via traditional thermal methods.

Ladder polymers are a class of polymers that have historically presented significant synthetic and characterization obstacles to polymer chemists. Ladder polymers are characterized by an uninterrupted sequence of rings, in which each ring shares at least two atoms with the adjacent repeat unit. The added bond leads to reduced degrees of rotation and a more rigid material.[38] One way chemists and materials scientists evaluate the rigidity of a polymer is through its persistence length. Persistence length is defined as the distance

required for a polymer strand to bend 90º, which is often measured using small-angle neutron scattering (SANS), atomic force microscopy (AFM) or fluorescence microscopy, while SANS remains the dominant technique for synthetic polymers.[39] Double-stranded DNA is an example of a natural ladder polymer with increased rigidity relative to its linear counterpart, single-stranded DNA. Single-stranded DNA, like many typical single-strand monomers, has a short persistence length of 1.5 – 10 nm. Double-stranded DNA has a persistence length of 50 nm.[40]

Chemists have discussed and sought to synthesize ladder polymers for almost a century. Staudinger proposed a synthesis of a ladder polymer structure in 1926 through the repeated [2+2] cycloaddition of cyclopentadiene catalyzed by tin butyl chloride.[41] This proposal was especially remarkable because the first report of a Diels–Alder cycloaddition with cyclopentadiene had not yet been reported. Interest in ladder
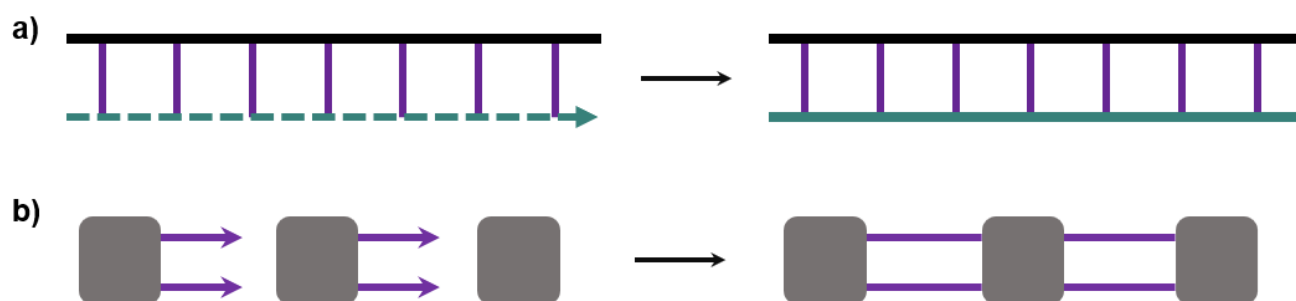
polymers increased in the 1960s and 1970s as chemists anticipated that the additional linkage along the polymer backbone would lead to more rigid and durable materials.[42] For decades, chemists sought to synthesize ladder

Scheme 1. a) Synthesis of ladder polymers through a zipping mechanism. A preliminary polymerization reaction forms the first junction of the ladder polymer connection and a second transformation forms the second connection. **b)** Formation of ladder polymers through a reaction that forms both connections in one reaction (either a multi-step or concerted mechanism).

polymers, but were unable to isolate and fully characterize a soluble material and confirm the ladder structure until the late 1980s.[43] Many of these reaction conditions included heating the reaction to above 200 ºC, which led to carbonization of the material.

Generally, there are two synthetic strategies to synthesize ladder polymers. The first strategy arises from polymerizing a monomer with a single connection across atoms (**Scheme 1a**). This monomer should contain a pendant group that can undergo a second reaction in post-polymerization modification to form the second junction. An example of this includes an organometallic cross coupling to from aromatic carbon-carbon bonds, followed by ring-closing metathesis to from the second bond. This approach requires judicious approach of the second reaction such that few defects are formed and the polymer does not form a highly crosslinked network.[44] This "zipping" of a linear prepolymer as an approach is useful in the synthesis of conjugated ladder polymers; however, to synthesize polymers with microporous properties, chemists must rely on an approach that takes a rigid monomer and forms both bonds in one transformation (**Scheme 1b**). A key strategy enabling the synthesis of ladder polymers is the use of pericylic reactions to form both ladder junctions (**Figure 3**). While some pericyclic reactions proceed through a step-wise mechanism,[45] the majority of pericyclic reactions allow concerted formation of both bonds, leading to the formation of fewer defects along the ladder polymer chain and decreasing the propensity to form cross-linked networks. In 1989, the first fully characterized ladder polymer was reported via a Diels–Alder reaction in which the diene was generated *in situ*.[46] While Diels–Alder
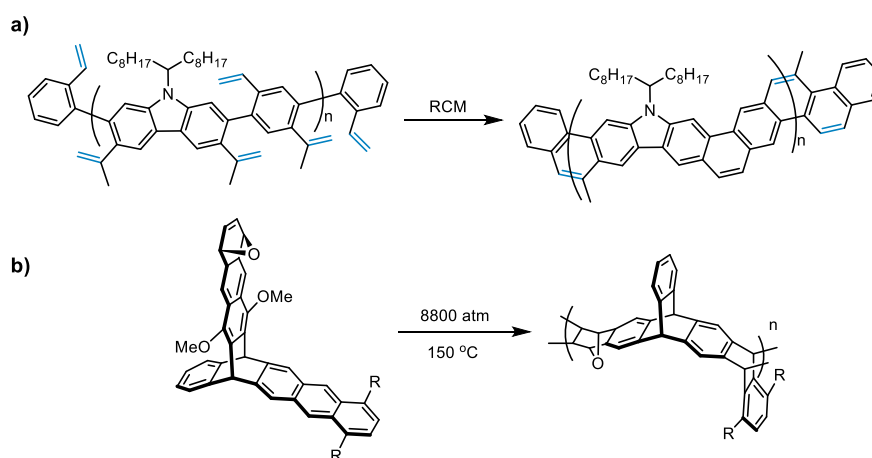
Figure 3. **a)** Synthesis of conjugated ladder polymers through a "zipping" approach. **b)** Synthesis of nonconjugated ladder polymers through Diels–Alder pericyclic reaction.

reactions have been the primary way to synthesize ladder polymers,[47] other pericyclic reactions have included nickel-catalyzed [2+2+2] cycloaddition with isocyantes to form six-membered rings alternating with seven- or

eight-membered rings along the polymer backbone; however, the larger rings decrease the rigidity of the ladder polymer.[48,49]

For ladder polymers without a fully conjugated backbone, their bulk and rigidity frustrate packing of the polymer strands and result in the formation of micropores.[50] Therefore, non-conjugated ladder polymers make up part of a larger class of polymers of intrinsic microporosity (PIMs).[51] Ladder polymers have also been used in the field of polymer physics to study the orientation of more flexible polymer strands through polarized excitation spectra.[52] While some polymers made through Diels–Alder polymerization exhibit microporosity, this is only after they are subjected to post-polymerization functionalization.[53] The majority of ladder PIMs are synthesized via nucleophilic aromatic substitution[54] or Tröger's base catalyzed condensation.[55] More recently, Xia and coworkers developed the catalytic (oxa)norboronene-arene annulation (CANAL), which takes advantage of a reported side reaction in the Catellani reaction,[56] to synthesize porous ladder polymers from aryl halides and norbornenes.[57] Many of these reactions require high temperatures, hyperbaric reaction conditions, or the use of expensive transition-metal catalysts. Regardless of the synthetic route, all the previously reported syntheses of ladder polymers involve a step-growth polymerization, which limits the potential to access more complex architectures like block copolymers. Moreover, step-growth polymerization requires extremely high conversion to reach appreciable molecular weights, and generally leads to less control of the molecular weight of the polymer.

As ladder polymers continue to present an attractive synthetic options for membranes for gas a fluid separation,[51] there is a need to develop ladder polymerization reactions with more benign conditions that enable increased control over molecular weight and sequence. I anticipated that photoredox catalysis would enable chain-growth ladder polymerization through an electronically mismatched, radical-cation Diels–Alder polymerization. In chapter 3, I will discuss how I was inspired by a small-molecule report from the Yoon research group[58] and designed a monomer that would support polymerization to yield a unique ladder polymer architecture.

Chapter 2: Using visible light to tune boronic acid–ester equilibria

Abstract

We report a series of azobenzene boronic acids that reversibly control the extent of diol binding via photochemical isomerization. When the boronic acid is ortho to the azo group, the thermodynamically-favored E isomer binds weakly with diols to form boronic esters. Isomerization of the E azobenzene to its Z isomer enhances diol binding, and the magnitude of this enhancement is affected by the azobenzene structure. 2,6-Dimethoxy azobenzene boronic acids show over 20-fold enhancement in binding upon E–Z isomerization, which can be triggered with red light. Competition experiments and computational studies suggest that the changes in binding affinity originate from stabilization of the E boronic acids and destabilization of the E boronic esters. We demonstrate a correlation between diol binding and photostationary state: different wavelengths of irradiation yield different quantities of bound diol. Higher binding constants for the Z isomer relative to the E isomer was observed with all diols investigated, including cyclic diols, nitrocatechol, biologically relevant compounds, and polyols. This photoswitch was employed to "catch and release" a fluorescently tagged diol in buffered water. By tethering this photoswitch to a poly(ethylene glycol) star polymer, we can tune the stiffness of covalent adaptable hydrogels using different wavelengths of visible light. This work establishes photoswitchable equilibria as a tool for the reversible ligation of molecular and macromolecular species.

Introduction

Dynamic covalent chemistry (DCC) enables thermodynamically-driven reorganization of molecular and macromolecular systems.[15] In the last 20 years, dynamic covalent chemistry has expanded both in utility and scope, with the most popular reactions including transesterification, transimination, Diels-Alder cycloaddition, conjugate addition–elimination, disulfide exchange, metathesis, and boronic ester exchange.[59,60] The reversibility of these reactions enables applications in combinatorial library development, molecular recognition,

self-healing polymers, 2- and 3-D covalent organic frameworks, and matrices for 3D cell-culture.[59,61–65] With insight into the reaction mechanism, DCC equilibria can be adjusted by structural modification of exchange partners, providing materials with a wide range of properties. In stimuli-responsive materials, these equilibria are influenced by stimuli such as light, temperature, pH, and concentration.[66] Light represents an ideal stimulus because it can be applied at readily tuned wavelengths and fluxes with spatiotemporal precision. In applications where sample penetration depth and biocompatibility are of concern, irradiation in the red and near-infrared range is advantageous.[67]

To influence DCC with light, a photoresponsive substrate must be coupled to the exchange reaction.[68–70] Photoswitches are a class of compounds that undergo bidirectional switching in response to light, resulting in a physical change in shape, charge, conjugation, dipole, or pK_a.[71–77,77–79] When a photoswitch is coupled to DCC, the state of the switch may influence the dynamic reaction.[80] In 2006, Branda and coworkers realized the first
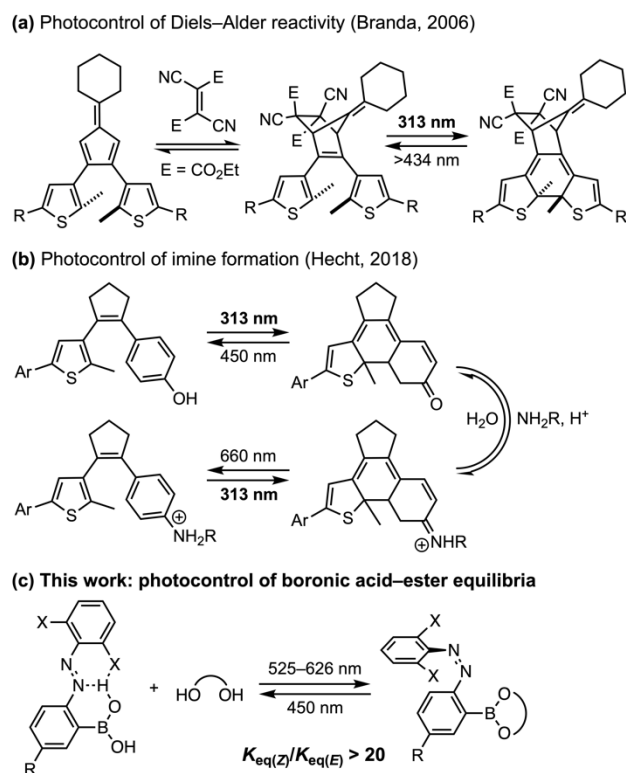
Figure 4. (a) A diarylethene photoswitch gates a reversible Diels–Alder cycloaddition. **(b)** Light regulates the condensation/hydrolysis of amines and hydrazides with a photoswitchable carbonyl. **(c)** In this work, the isomerization of an azobenzene by visible light tunes the equilibrium of a boronic acid–ester dynamic bond.

example of photoswitchable DCC, demonstrating that the Diels-Alder cycloaddition between a diarylethene

photoswitch and a dienophile could be turned on or off (gated) depending upon the isomerization of the photoswitch (Figure 4a).[81] In the open isomer, the diarylethene can undergo a [4+2] cycloaddition with a dienophile. The product could be photoswitched via a 6p electrocyclization to yield a closed "locked" isomer, which is unable to participate in the Diels-Alder equilibrium. This work was further developed by Hecht, who applied this reactivity in photoactivatable maleimide prodrugs and self-healing polymer networks.[12,18,82,83] In these reports, the DCC is either on or off.

We envisioned an alternative approach that modulates the overall equilibrium of a dynamic covalent bond using different wavelengths of light (Figure 4b). In this case, the equilibrium can operate in both states of the photoswitch, but to different extents. This system will enable bidirectional tuning of the reversible bond between small molecules and polymers to our photoswitch. In a complementary study, Hecht and coworkers investigated the effect of photoswitches on the rate of formation of imine dynamic covalent bonds, but did not study the photoswitches' influence on the bond equilibrium.[13] We identified boronic esters as an ideal dynamic covalent bond for this purpose because the exchange occurs at room temperature with many different diol structures and is compatible with aqueous environments (Figure 4c). These attributes have found utility in molecular sensors, stress-relaxing hydrogels, and recyclable thermosets.[84–91] Previous work has shown that the boronic acid–ester equilibrium is highly sensitive to the boronic acid structure.[92–96] We anticipated that photoswitch isomerization could provide the reversible structural change capable of influencing this equilibrium. Towards this goal, we synthesized *ortho*-substituted azobenzene boronic acids (Figure 5a).[97,98] As azobenzenes undergo substantial changes in structure upon $E \rightarrow Z$ isomerization, we hypothesized that the boronic acid–ester equilibrium could be affected by the photoswitch state. Accordingly, we discovered that
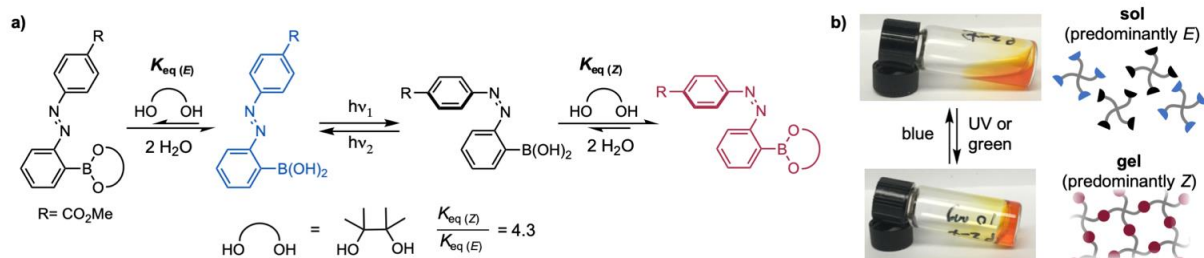
Figure 5. (a) The equilibrium between *ortho*-substituted azobenzene boronic acids and diols is influenced by the isomerization of the photoswitch, with the Z isomer displaying a higher binding affinity with diols than the E isomer. When the diol is pinacol, the Z binding constant is 4 times greater than the E binding constant. **(b)** UV or green and blue light mediate reversible sol-gel transitions of poly(ethylene glycol) hydrogels crosslinked with azobenzene boronic esters (10 w/v%, 0.1 M PBS, pH 7.5).

these compounds have isomerism-dependent equilibria with diols, wherein the Z isomer has a higher binding affinity than the E isomer ($K_{eq(Z)} > K_{eq(E)}$, Figure 2a).[99] When incorporated into poly(ethylene glycol) networks, this preferential binding translated to reversible sol-gel transitions upon $E \rightarrow Z$ photoisomerization (Figure 5b). Interestingly, this dramatic physical change arose from a relatively modest difference in binding affinity to diols (~4:1 for pinacol). We thus sought structural modifications of the azobenzene boronic acid that could increase the difference in binding affinity between the E and Z isomers, allowing us to expand the tunability of this photocontrolled dynamic covalent bond and its potential applications.

In this chapter, we demonstrate that simple modifications of the azobenzene boronic acid allow us to tune the relative binding affinity of Z vs. E azobenzene boronic acids to diols, $K_{rel} = K_{eq(Z)}/K_{eq(E)}$, from 2.4 to over 20. Experimental results and computed structures suggest that the differences in K_{rel} between a series of azobenzene boronic acids are due to both the stabilization of the E boronic acids and the destabilization of the E boronic esters, which can be tuned by azobenzene substitution. Our optimized azobenzene boronic acid can be photoswitched with red light and the Z isomer has a long thermal half-life. Using the azobenzene boronic acid with the largest K_{rel}, the equilibrium between boronic acid and boronic ester can be tuned with different wavelengths of light. We demonstrate that this azobenzene boronic acid can "catch and release" a fluorescently tagged polyol in aqueous buffer. Lastly, we reversibly tune the stiffness of a covalent adaptable hydrogel with several wavelengths of visible light, including red light.

<u>Results and Discussion</u>

Ortho substitution increases the difference in binding affinity between E and Z isomers

The equilibrium between boronic acids and diols strongly depends on the concentration of water and diol. Therefore, we designed ^{1}H and ^{19}F NMR equilibrium competition binding experiments to compare the relative binding affinity between E and Z isomers in the same NMR tube, ensuring that the concentration of water and diol are the same for both isomers (**Figure 6a**; see Supporting Information (SI), section IV for details and derivation). Our investigations commenced with compound **1**, a para-tolyl azobenzene boronic acid (**Figure 6b**). The para-methyl substituent was used in place of the phenyl analog, which exhibits overlapping ^{1}H NMR signals for the E and Z isomers. When a mixture of (E)-**1** and (Z)-**1** was treated with excess ethylene glycol
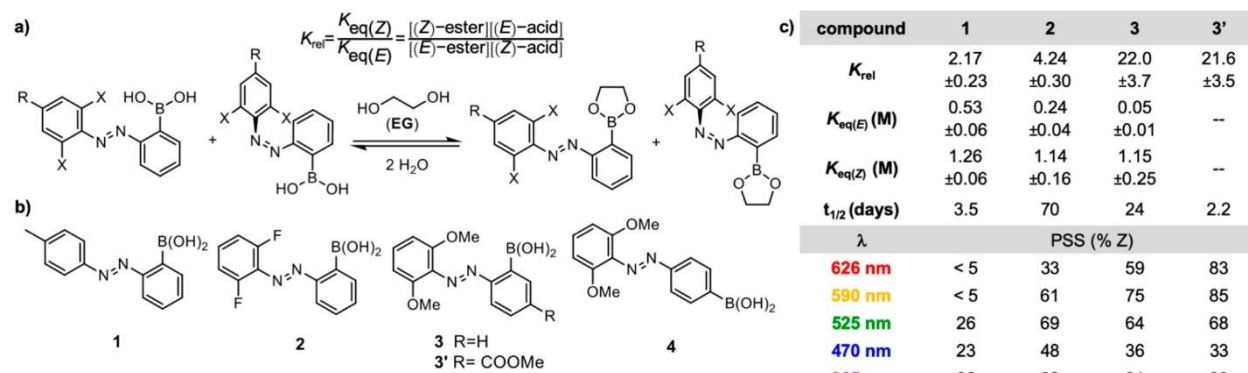
Figure 6. **(a)** Equilibrium competition binding experiment to compare the relative equilibrium binding constants of E and Z azobenzene boronic acids with diol. **(b)** The photoswitches subjected to the equilibrium competition binding experiment in (a). **(c)** Relative and absolute equilibrium constants for azobenzene boronic acids (10 μM) binding EG in DMSO-d_6 at 25 °C, thermal half-lives (days), and photostationary states at different wavelengths of LED irradiation (%Z). For determination of photostationary states, see **Figure 15** through **Figure 19**.

(EG) and D_2O in DMSO-d_6 and allowed to equilibrate for 24 hours, we observed that (Z)-**1** binds EG approximately 2.4 times better than (E)-**1** (Krel = 2.4) (Figure 6).

For our design of photoswitchable equilibria, the ideal photoswitch should feature visible-light bidirectional photoswitching, high photostationary states, and a long thermal half-life for the Z isomer. Unfortunately, in addition to a modest difference between E and Z binding affinities, compound **1** only reached an appreciable photostationary state (PSS, 48% Z) with ultraviolet (UV) irradiation at 365 nm (**Figure 6c**). By measuring the
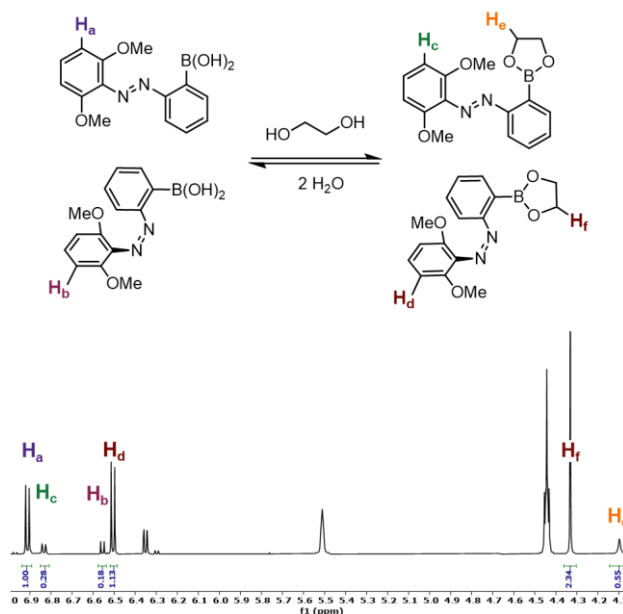
Figure 7. ^{1}H NMR of **3** (10 mM, 1:1 E:Z) and EG subjected to equilibrium competition binding conditions in DMSO-d_6 at 25 °C

rate of thermal relaxation of (Z)-1 to (E)-1 at different temperatures and fitting to an Arrhenius plot (**Figure 23**), we could extrapolate the room-temperature (25 °C) half-life to be 3.5 days. Previous work has established that electronic and steric modifications of the azobenzene can alter key photochemical properties, which has been summarized well by Bandara and Burdette.[72] We anticipated that these modifications could simultaneously alter the equilibrium of the dynamic covalent bond. First, we sought to optimize the photochemical properties to achieve bidirectional visible-light photoswitching. Secondly, we aimed to increase the thermal stability of the Z isomers.

A common strategy to enable azobenzene isomerization with visible light is substituting the aryl rings with resonance electron-donating and -withdrawing groups, creating "push-pull" azobenzenes. These substitution patterns red-shift the $\pi \rightarrow \pi^*$ of the E isomer through a charge-transfer mechanism. Unfortunately, the Z isomers tend to undergo rapid thermal isomerization (< seconds), due to a low activation barrier in the ground state,[100] which would occur much faster than the dynamic covalent reaction. Hecht, Woolley, and others have installed halides or methyl ethers at the *ortho* positions, which separates the $n \rightarrow \pi^*$ absorption bands of the E and Z isomers and enables visible-light $E \rightarrow Z$ photoisomerization with enhanced Z thermal stability.[101–107] Inspired by this work, we synthesized *ortho*-difluoro-substituted azobenzene **2** and dimethoxy analog **3** to access visible-light photoswitching (**Figure 6b**). **2** exhibited a higher PSS (67% Z) with green light (525 nm) irradiation and a dramatically enhanced thermal half-life relative to **1** ($\tau_{1/2}$ = 70 days, Figure S5). The relative binding affinity, as determined by the equilibrium competition binding experiment with EG, increased by a factor of 1.8 relative to **1**, to K_{rel} = 4.2 (**Figure 6c, Figure 31**). When the fluorine atoms were replaced with methyl ethers in compound **3**, photoswitching with red LEDs at 626 nm yielded PSS up to 54%, albeit with a modest decrease in thermal half-life ($\tau_{1/2}$ = 24 days, **Figure 25**). The competition experiment for compound **3** also revealed a dramatic increase in relative binding, where the Z isomer binds EG with over an order of magnitude higher affinity than the E isomer (K_{rel} = 21.5, **Figure 32**). Figure 7 shows the ^{1}H NMR spectrum for the competition experiment of compound **3** with EG, in which (Z)-**3** is predominantly bound, while (E)-**3** is mainly unbound.

As a control, we synthesized an azobenzene derivative with the boronic acid at the 4' (para) position (compound **4**). This compound exhibited little difference in binding affinities between the E and Z isomers

(K_{rel}= 1.1, **Figure 34**). Thus, the proximity of the boronic acid to the phenylazo group is essential for the isomerism-dependent changes in binding affinity.

Ortho substitution influences the esterification equilibrium of the E isomers
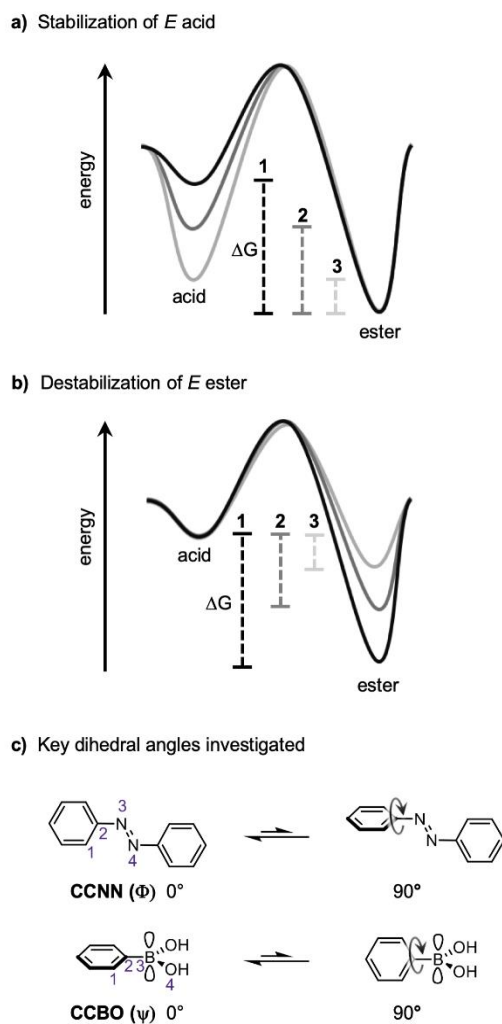
Figure 8. **(a,b)** Energy diagrams portraying two potential origins of the observed trend in Keq, (E)-1 > (E)-2 > (E)-3. **(c)** Key bond rotations that can influence the energy of azobenzene boronic acids and esters.

We next set out to understand the origin of the dramatic increase in K_{rel} for compound **3** compared to compounds **1** and **2**. As K_{rel} is defined as the ratio of $K_{eq(Z)}$ to $K_{eq(E)}$, this trend could originate in an *increase* in $K_{eq(Z)}$, a *decrease* in $K_{eq(E)}$, or a combination of both effects. To distinguish between these possibilities, and validate our equilibrium competition binding assay, we measured individual K_{eq} values for **1–3** by ¹H NMR in DMSO-d_6 (**Figure 6c**; **Table 1**-**Table 2**). The *E* isomers for **1–3** displayed significantly different binding affinities for EG, following the K_{eq} trend (E)-**3** << (E)-**2** < (E)-**1**, consistent with the overall changes in K_{rel}. In contrast, the *Z* isomers of **1–3** revealed similar binding affinities to EG. Therefore, we concluded that the changes in $K_{eq(E)}$,

and not $K_{eq(Z)}$, lead to the observed differences in K_{rel} between compounds **1–3**. Importantly, the K_{rel} values obtained from individual measurements of $K_{eq(E)}$ and $K_{eq(Z)}$ were in good agreement with those determined from equilibrium competition binding experiments.

Calculated structures and control experiments suggest a combination of reactant stabilization and product destabilization disfavors E esterification

Why do E isomers of azobenzene boronic acids consistently display lower binding affinities for diols than their corresponding Z isomers? Why does (E)-**3** bind EG significantly worse than (E)-**2** and (E)-**1**? Structural changes that result in the stabilization of the (E)-acid, destabilization of destabilization of the (E)-ester, or a combination will correspond to less negative ΔG and decreased diol binding affinity (**Figure 8.** (a,b) Energy diagrams portraying two potential origins of the observed trend in Keq, (E)-1 > (E)-2 > (E)-3. (c) Key bond rotations that can influence the energy of azobenzene boronic acids and esters. **a-b**). We hypothesized that there are two main structural parameters influencing the degree of conjugation through the system and therefore the energy of the azobenzene boronic acid and ester. The first is the planarity of the azobenzene, which is described by the dihedral angle between the aryl rings and diazo (CCNN, Φ) (**Figure 8c**). For unsubstituted azobenzene, the energy is lowest when this angle is 0° and highest at 90° (**Figure 55**). The second parameter is the coplanarity of the azobenzene and the boronic acid or ester, which can be described by the CCBO dihedral angle ψ . This parameter correlates with the degree of conjugation between the boronic acid or ester with the adjacent aryl group (**Figure 8c**). Previous reports suggest that arylboronic acids and esters are

a) Calculated structures of unbound azobenzene boronic acids (E)-1 through (E)-3

b) X-ray crystal structures of compound (E)-1 though (E)-3

c) Calculated structures of bound azobenzene boronic esters (E)-1 through (E)-3

d) Control compounds 5–7

	1	2	3
ΔG_{exp} (kcal/mol)	−3.5	−4.1	−1.6
ΔG_{comp} (kcal/mol)	0.36	0.75	1.70

decreasing conjugation, increasing energy

5 K_{rel} = 2.1

6 R = Et **6'** R = OEt K_{rel} = 1.3 K_{rel} = 10.3

7 K_{rel} = 1.8
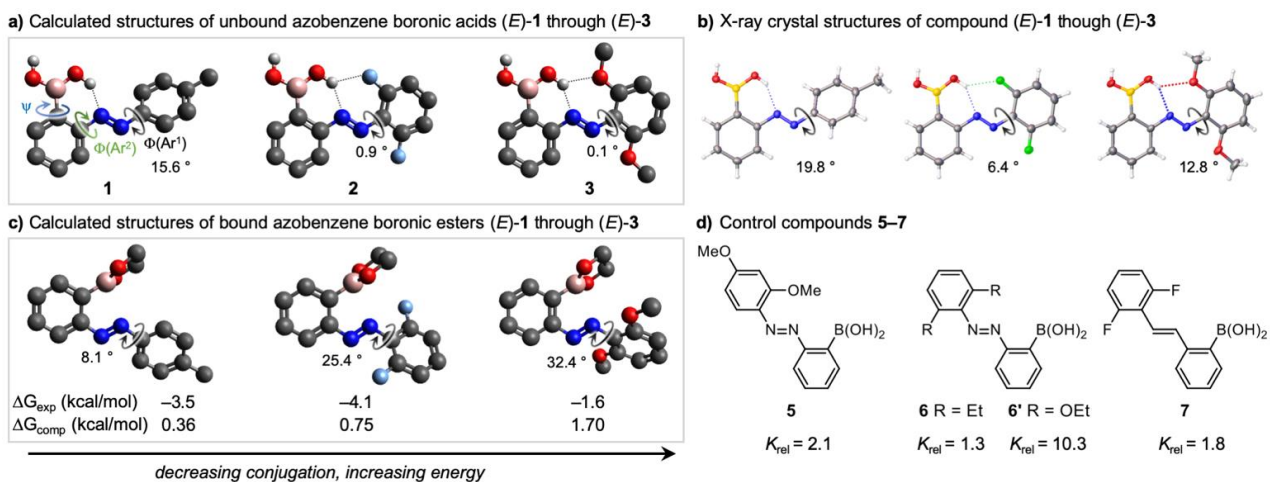
stabilized when the non-bonding oxygen lone pairs and vacant p orbital are in conjugation with the π-system of the aryl group, with a CCBO dihedral angle of 0°. We performed geometry scans of phenylboronic acid and the corresponding ester, confirming an energetic maximum at 90° and a minimum at 0°, when conjugation is enhanced. (**Figure 55**).

To understand which scenario might be responsible for the decrease in $K_{eq}(E)$ from **1>2>>3**, we calculated the optimized structures of (*E*)-**1**, **2**, and **3** in their bound and unbound forms with the B3LYP/6-31+G** level of theory and performed frequency calculations to determine the lowest-energy rotamers. We modeled the boronic acids and esters in their trigonal planar form based on ^{11}B NMR studies (**Figure 33**). We first examined the geometry-optimized structures of (*E*)-**1** through (*E*)-**3** in their unbound forms (**Figure 9a**). Each azobenzene is nearly planar, and the two CCNN dihedrals angles Φ (Ar[1]) and Φ (Ar[2]) are between 11° and 17° for (*E*)-**1** and between 0° and 2° for (*E*)-**2** and (*E*)-**3**. The CCBO dihedral angles ψ are close to 0° for **1–3**, and an intramolecular hydrogen bond is present between the boronic acid proton and the proximal azobenzene nitrogen.

The boronic acid protons in the calculated structures of (*E*)-**2** and (*E*)-**3** also engage in H-bonding with one of the *ortho*-heteroatom substituents (fluorine or methoxy, respectively). This additional H-bonding interaction was confirmed in the single-crystal X-ray structures of (*E*)-**2** and (*E*)-**3** (**Figure 9b**). We hypothesize that the additional hydrogen bonds stabilize the boronic acid and lead to a less negative Δ*G* for esterification. While the O-H···F-C interaction in **2** is expected to be much weaker than with the methoxy group in **3**, the H– F distance of 2.27 Å is consistent with previously reported H-bonding interactions involving a C–F acceptor.[108,109] In both **2** and **3**, these additional hydrogen bonds assist in keeping the azobenzene nearly planar, whereas (*E*)-**1**, which lacks H-bond acceptors at the *ortho* positions, is slightly more twisted. Again, these features were corroborated by the single-crystal X-ray structure of (*E*)-**1**, in which Φ (Ar[1]) is 19.8°.

Binding of EG to the (*E*)-azobenzene boronic acids is accompanied by varying degrees of twisting of the aryl rings and deviation of the CCNN dihedral angles from 0°. In the calculated structures, *ortho*-unsubstituted (*E*)-**1** remains slightly twisted after binding EG (11.6°), while (*E*)-**2** and (*E*)-**3** display more significant twisting,

exemplified by Φ (Ar^1) angles of 24.6° and 40.4°, respectively (Figure 6c, see Figure S31 for full list of angles). This twisting likely arises from repulsive steric interactions between the halide or methoxy *ortho* substituents and the boronic ester. For all compounds, we observe that the boronic ester is nearly perpendicular to the aryl ring (75° $\leq \psi \leq$ 84°), which avoids Van der Waals repulsion between the ester oxygen and distal nitrogen. We hypothesize that the large conformational changes engendered by diol binding reduce the degree of conjugation in the azobenzene and raise the energy of the boronic ester relative to the boronic acid. Since these conformational changes become more significant across the series **1 < 2 < 3**, ΔG becomes correspondingly less negative across this series, and the esterification becomes less favorable for **3** compared to **1** and **2**. Alternative rotamers for the esters of (*E*)-**1** through (*E*)-**3** (**Figure 57**) are less than 3 kcal/mol higher in energy but follow similar trends to those shown here, with the smallest conformational changes upon binding occurring for (*E*)-**1** and the largest changes occurring for (*E*)-**3**.

The optimized structures for the *Z* isomers place the boronic acids away from the *ortho* substituents. Each boronic acid still displays an intramolecular hydrogen bond with the proximal nitrogen; however, there are no additional H-bonds with the *ortho*-fluoro or methoxy substituents in (*Z*)-**2** and **3.** The absence of steric interactions between the boronic esters and *ortho* substituents in the *Z* isomers allows diol binding to occur with minimal structural rearrangement for compounds (*Z*)-**1** through (*Z*)-**3**, as exemplified by small changes in Φ(Ar^1), Φ(Ar^2), and ψ upon diol binding (Figure 10 for **3**; see **Figure 58** for compounds **1-2**). These small changes are consistent with the similar diol binding affinities exhibited by the *Z* isomers of **1–3** in equilibrium competition binding experiments. Additionally, the boronic esters maintain conjugation with the aryl ring (0.6° $\leq \psi \leq$ 20°) after binding EG. This favorable conformation, combined with the absence of repulsive interactions with the *ortho* groups, likely underlies the improved binding of *Z* azobenzene boronic acids compared to their *E* isomers.

$\Phi°$ (Ar^1)   62.7 °   68.3 °
$\Phi°$ (Ar^2)   44.4 °   55.2 °
ψ 10.5 °   0.6 °
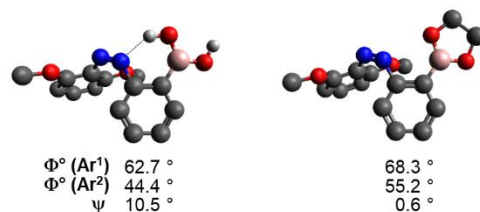
Figure 10 Calculated structure of (*Z*)-3 before and after binding EG.

Based on the calculated structures, we designed control compounds to experimentally demonstrate that the high K_{rel} for **3** arises from a combination of (i) H-bonding to the azo group, which stabilizes the (*E*)-boronic acid; (ii) additional H-bonding to one of the *ortho*-methoxy groups, providing further stabilization; and (iii) steric destabilization of the (*E*)-boronic ester. First, we synthesized compound **5**, in which one of the methoxy substituents was moved from the *ortho* position to the *para* position. When **5** was subjected to the competition experiment, K_{rel} was determined to be 2.4, almost an order of magnitude lower than that of **3** (see **Figure 38** for ^{1}H NMR). The calculated structures of **5** show that the boronic acid and ester both adopt planar conformations. (**Figure 59**-**Figure 60**). This control experiment suggests that stabilization of the boronic acid by double H-bonding only partially disfavors esterification; steric interactions that destabilize the ester are also required to achieve high K_{rel}.

Next, we synthesized di-*ortho*-ethyl azobenzene **6**, which is sterically comparable to compound **3,** but lacks the ability to participate in additional hydrogen bonding with the *ortho* positions. When subjected to the competition experiment, K_{rel} was determined to be only 1.3 (**Figure 39**). Calculated structure of **6** show significant twisting in both the boronic acid (Φ (Ar^1) = 43°, Figure S35) and boronic ester (Φ (Ar^1) = 42°). This control experiment demonstrates that steric interactions alone cannot explain the K_{rel} trend for **1–3**; H-bonding to stabilize the boronic acid and planarize the (*E*)-azobenzene are essential.

Lastly, we synthesized stilbene **7**, which is sterically comparable to **2** and capable of $E \rightarrow Z$ isomerization but is unable to engage in intramolecular hydrogen bonding (**Figure 62**). For compound **7**, K_{rel} was determined to be only 1.8 (**Figure 40**). This modest K_{rel} value likely arises from steric effects alone. Stilbene **7** also allowed us to experimentally probe the relative effect of intramolecular H-bonding on the thermodynamics of boronic

acid esterification for E vs. Z isomers. We performed an equilibrium competition binding experiment between **2** and **7** and observed that the stilbenes have higher binding affinities for diols compared to their azobenzene analogs. Specifically, E stilbene bound EG 6-fold more than the E azobenzene, whereas the Z stilbene bound EG 2.6-fold more than the Z azobenzene. While the O–H⋯N H-bond is present in both E and Z azobenzene isomers, its stabilizing influence is more significant in the E isomer; furthermore, the E isomer presents multiple H-bond acceptors.

In summary, calculated structures, supported by experimental results with control compounds **5–7**, lead us to the following conclusions:

1) Stabilization of boronic acids by adjacent H-bond acceptors can disfavor esterification. This effect is further exacerbated by the presence of multiple H-bond acceptors, as in the case of **3** and, to a lesser extent, **2**, in which both the proximal azo N and the *ortho* groups of the distal arene act as H-bond acceptors.

2) In E azobenzenes, the degree of twisting away from the planar conformation imposed by steric interactions offers an additional synthetic handle to tune the stability of dynamic covalent bonds. Previous approaches have considered the effect of photoswitch conjugation on its propensity to form a dynamic bond;[1] our work suggests a complementary design principle, in which the structure of the dynamic bond can also affect the stabilization of the photoswitch by conjugation.

3) The twisted structure of Z azobenzenes requires fewer conformational changes to accommodate boronic acid esterification, and also precludes additional H-bonding interactions. Thus, esterification is more favorable for the Z isomer than for the E isomer.

While previous studies have probed the structural features that affect the thermodynamics of the boronic acid–ester dynamic bond in detail, they have generally focused on parameters such as the electronics of the boronic acid, the presence of proximal basic amines, or the diol structure.[91,93,94,96,110] The insights gained from our studies provide a framework for future designs of boronic acids where proximal functional groups can enhance or disrupt the stability of the dynamic bond.

Diol binding can be tuned through irradiation with different wavelengths of light

We selected **3** as the optimal photoswitch to tune diol binding because of its large K_{rel} and favorable

photochemical properties. We envisioned that the ratio of the *E* and *Z* isomers should dictate the overall

boronic acid–ester equilibrium, wherein the amount of bound diol should increase as the ratio of (*Z*)-**3** to (*E*)-

3 increases. As the PSS (%*Z*) is wavelength dependent, the ratio of *Z* to *E* can be tuned by irradiation with

different wavelengths of light. We prepared a solution of (*E*)-**3** and EG (1:1) in DMSO-d_6, in which the
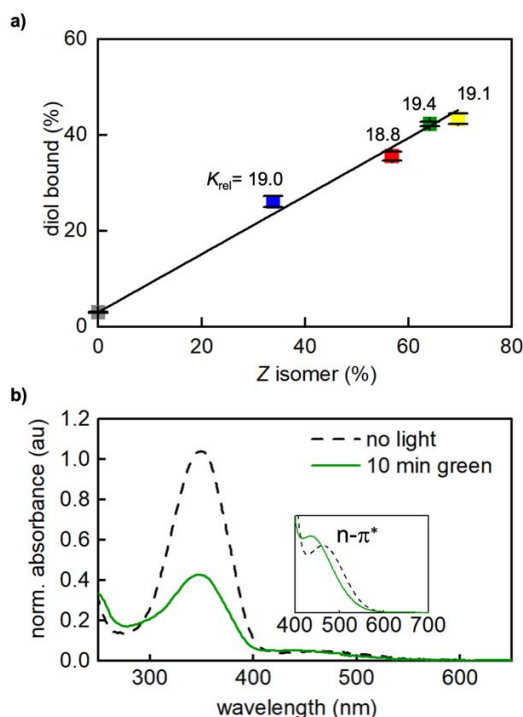
Figure 11. **(a)** Percent diol binding as a function of PSS, which is achieved thermally (gray) or with blue, red, green, or yellow light. Error bars represent integration er-ror, and the line is the least squares fit. The Krel value calcu-lated for each E/Z mixture is indicated. **(b)** UV-Vis profile of 3 in acetonitrile (21 uM) before (black) and after (green) irradiation with green LEDs for 10 minutes.

azobenzene bound 30% of the available EG prior to irradiation (**Figure 11a**, see **Figure 43** for ¹H NMR

spectrum). Irradiating the sample with blue, red, or green irradiation yielded different photostationary states,

and higher photostationary states correlated linearly with increased diol binding. Up to 70% of the diol could

be bound with green light. The high barrier for *Z*→*E* thermal isomerization ensures that the resulting

equilibrium is maintained for the duration of the experiment (24 hours), such that continuous irradiation is not

required. By irradiating with a wavelength of light corresponding to a lower PSS, the equilibrium can be shifted

to favor boronic acid and enables release of diol into solution. Figure 11b shows the UV-Vis absorbance

spectrum of 3 before and after irradiation with green light. The ability to achieve high PSS for both E→Z and

Z→E isomerization arises from the separation of the n-π* transitions of the E and Z isomers (Figure 11b, inset).

Photoswitching modulates boronic ester equilibria with different diols

Next, we investigated the generality of photoswitchable binding to boronic acid **3** with different diols. Using **3**, we observed K_{rel} values between 6 and 20 for a variety of diols, including a 1,3-diol (**8**), simple cyclic diols (**9-10**), nitro-catechol (**11**), and a variety of complex and biologically relevant diols, including glucose (**14**), adenosine (**15**), and the chemotherapeutic drug capecitabine (**16**) (**Figure 12**). Phenylboronic acid-containing polycarbonates have previously been used for the pH-dependent release of diols including capecitabine.[111] We

8 (14.4) **9** (17.2[a]) **10** (14.7) **11** (9.75)

12 (11.5) **13** (16.7[a]) **14** (6.30)

15 (7.27) **16** (8.89)
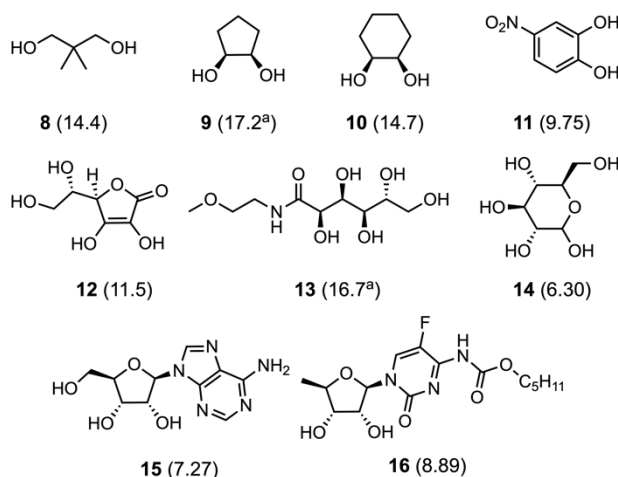
Figure 12 K_{rel} (reported in parentheses) between (Z)-3 and (E)-3 with various diols (20 mM in DMSO-d$_6$). Standard deviations were between 0.1 and 2.4 and are reported in **Figure 45** through **Figure 53**. [a]Excess D$_2$O was added due to high binding affinity.

envision **3** could provide a complementary light-driven strategy. Diols of interest could first be bound in the Z state, where release could be controlled by isomerization to the E isomer.

We qualitatively observed that some diols bound 3 poorly in the standard NMR assay conditions (<1% D2O in DMSO-d6); when exogenous water was added to the 4-nitrocatechol (9) equilibrium competition binding experiment, we exclusively observed only boronic acid for both isomers. In contrast, some cyclic diols and polyols (such as cis-1,2-cylcopentanediol (9) and gluconolactone derivative (13)) have higher binding constants, and additional exogenous water (6% in DMSO-d6) was needed in the competition experiment to observe any unbound acid, consistent with previous studies using simple arylboronic acids.[93] These results demonstrate that while the relative binding affinities between Z and E are similar across a range of diols, the

absolute equilibrium constants are highly dependent on diol structure. For applications of 3 in an aqueous environment, cyclic diols such as 9 or polyols such as 13 will be optimal.

Azobenzene boronic acids reversibly bind diols in fully aqueous environments

To overcome the low aqueous solubility of small molecule **3**, we designed and synthesized a carboxylate analog of **3**, SI-**11**, and coupled it to amine-terminated 4-arm poly(ethylene glycol) (PEG, M_w 5 kg/mol) (polymer **P1**, **Figure 13a**; see SI for details). While installing the electron-withdrawing ester shortens the thermal half-life of the *Z* azobenzene to 2.2 days by creating push-pull character (**Figure 26**), it increases the PSS (%*Z*).
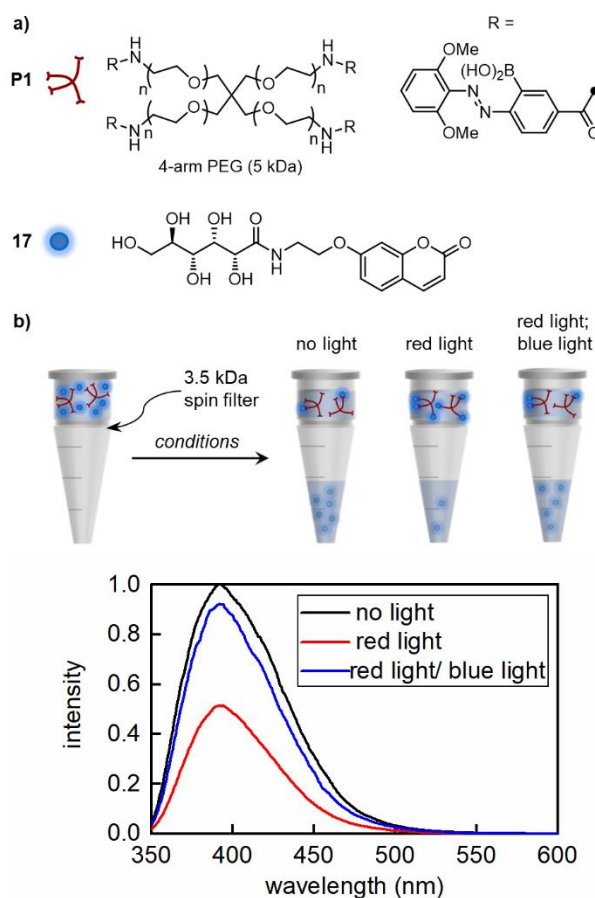
Figure 13. **(a)** Structures of P1 and gluconolactone-tagged coumarin 17. **(b)** Illustration of experimental setup and fluorescence spectra of eluents after irradiating and spin filtering each solution.

The methyl ester of compound SI-**10**, reaches 76% *Z* after red light irradiation, and returns to 29% *Z* after blue light irradiation (**Figure 6c**).

We also synthesized a coumarin-tagged gluconolactone derivative (compound **17**) to provide a fluorescent output for reversible binding. The gluconolactone tag was chosen based on the performance of **13** in the

presence of excess water, suggesting esterification would be favorable in an aqueous environment. The ratio of bound **17** should be increased after irradiation to predominantly Z isomer with red light and decreased after irradiation to predominantly E isomer with blue light. We mixed the boronic acid polymer **P1** and compound **17** in a 1:4 molar ratio (1:1 boronic acid:**17**) in a phosphate buffered saline (PBS) solution at pH 7.5. To analyze the amount of unbound **17**, we filtered the mixture with a 3.0 kDa molecular weight cut-off (MWCO) centrifugal filter such that only free fluorophore (MW 383 g/mol) can pass through the membrane. We next performed UV-vis and fluorescence spectroscopy of the resulting dialysate. Without any irradiation, we observed strong fluorescence in the dialysate indicating that unbound **17** had passed through the filter (**Figure 13b**). When the solution was irradiated with red light for 60 minutes before spin filtering, we observed decreased emission, indicating more fluorophore was bound to **P1** and unable to pass through the filter. In an analogous experiment, we first irradiated the mixture with red light for 60 minutes, then with blue light for 10 minutes, before centrifugal filtration. In this case, the fluorescence of the dialysate increased to nearly the same level as the no-irradiation control, demonstrating that the fluorophore bound to red-irradiated **P1** was released by blue light.

Reversible changes in binding affinity lead to reversible stiffening of hydrogels

Lastly, we sought to translate the reversible changes in binding affinity to control crosslink density in a hydrogel network. Previously, we demonstrated that reversible changes in binding affinity could lead to sol-gel transitions in a boronic ester crosslinked poly(ethylene glycol) hydrogel, with stiffening occurring with UV or green light and softening occurring with blue light. Based on the photochemical properties of compound **3**, we reasoned that its incorporation as a crosslink into hydrogels would enable stiffening with red light. We prepared diol-terminated polymer **P2** by ring-opening glucono-δ-lactone with amine- terminated 4-arm poly(ethylene glycol) (M_w= 5 kDa), according to a previous literature procedure.[112] When **P1** and **P2** were mixed in a 1:1 ratio in 0.1 M phosphate-buffered saline at pH 7.5 (10 w/v%), a sol was observed, according to the flow-inversion method. Irradiation with red LEDs (626 nm) for 3 hours promotes the $E{\rightarrow}Z$ isomerization of the terminal azobenzene boronic acids and leads to the gelation of the mixture. Irradiating this gel for 5 minutes with blue LEDs promotes $Z{\rightarrow}E$ isomerization and returns the mixture to the sol state (**Figure 14**a). By alternating

irradiation with red and blue light, we could continue to cycle the gel between sol and gel states. Addition of excess free diol **13** leads to the dissolution of the network, presumably by outcompeting **P2** and disrupting the boronic ester crosslinks.

Toward our lab's effort to design photoreversible matrices for 3D cell culture, we prepared a hydrogel with **P1** and **P2** (10 w/v%) in Dulbecco's Modified Eagle Medium (DMEM), a common growth medium for a variety of cell types. While the glucose, amino acids, or vitamins in DMEM could interfere with the boronic ester dynamic bond, we were gratified to observe that gelation can still occur in this medium. Bulk mechanical characterization of this hydrogel was performed by oscillatory photorheology at constant strain in the linear viscoelastic region. We first investigated the frequency-dependent properties of this hydrogel from 100 to 0.1 rad/s, which yields information on the dynamics of the crosslinks. The storage modulus (G') represents the material's ability to store energy elastically like a solid, while the loss modulus (G") represents the material's able to dissipate energy into the surrounding environment like a liquid. In materials that behave as elastic solids, such as permanently crosslinked hydrogels, G' and G" are frequency independent. Viscoelastic materials display both solid- and liquid-like behaviors, which depend upon the frequency of the deformation. At high frequencies (> 1 rad/s), where deformation is faster than the dynamic bond exchange, the **P1/P2** gel has solid-like behavior, wherein G' > G". The crossover point (where G' = G") occurs at 0.5 rad/s, and below this frequency the gel flows like a liquid due to the reversible hydrolysis of boronic ester crosslinks (**Figure 14**b). Interestingly, this hydrogel does not undergo sol-gel transitions by the flow inversion method, which are observed when PBS is the solvent. We hypothesize that the additives in DMEM reduce the rate of exchange of the dynamic crosslinks, shifting the crossover point to lower frequencies. The relationship between molecular kinetics and the crossover frequency is the subject of ongoing studies in our laboratory.

The hydrogel in DMEM also demonstrates photodependent changes in stiffness (**Figure 14c**). The gel was stiffened for three hours with red light, yielding a G' of 60 Pa. Irradiation for 10 minutes with blue light led to a softer gel, decreasing G' by 33%. The gel could be stiffened again with yellow light irradiation, increasing G' to 54 Pa after 3 hours. We propose that the photo-dependent changes in stiffness arise from changes in the hydrogel crosslink density. We hypothesize that the softness of these gels, compared to those previously reported in the literature,[84,99,112,113] is due to the unusually low binding of the E azobenzene. While these hydrogels may be practical as tools for studying soft tissue mechanics, we envision that increasing the binding constant of the Z isomer while maintaining high K_{rel} will enable larger ranges of photocontrolled stiffness.
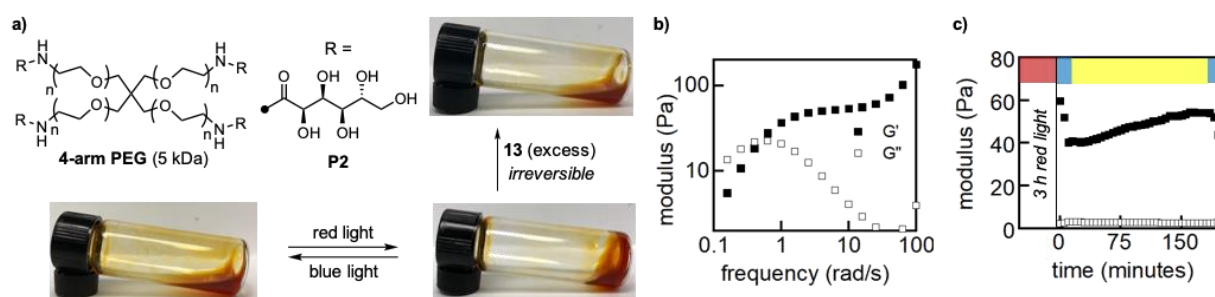
Figure 14. **(a)** Structure of P2 and reversible gelation of P1 and P2 with red and blue light (10 w/v%, PBS pH 7.5). **(b)** Frequency sweep of P1 and P2 in DMEM (10 w/v%, 10% strain) after stiffening with red light for 3 hours. **(c)** Reversible mechanical response of P1 and P2 in DMEM (10 w/v%, 10% strain, 25 rad/s) to different wavelengths of visible light.

Conclusion

We have shown how multiple wavelengths of light can be used to tune the equilibrium of a dynamic covalent bond by harnessing the photostationary state of a photoswitch. While previous reports of photocontrolled dynamic covalent chemistry turn equilibria on or off, our approach offers the ability to modulate the boronic acid/ester equilibrium depending upon the isomerism of an azobenzene photoswitch. The binding equilibrium becomes more favorable as the percentage of Z isomer is increased. Moreover, we show that the range of equilibrium binding constants achieved by a single photoswitch is highly dependent upon ortho,ortho-substitution of the distal ring. In addition to increasing the difference in E and Z binding constants, these ortho substituents impart improved photochemical properties including longer thermal half-lives, increased photostationary states, and visible light photoswitching, making them promising for biomedical applications. The optimized azobenzene identified in these studies can reversibly bind a range of biologically relevant diols. We further demonstrated the application of photoswitchable equilibria to a dynamic covalent

hydrogel that can be stiffened with red light. Tuning equilibria with photoswitches represents a powerful approach to noninvasively control the interaction between molecular and macromolecular species. While this work applies this concept to boronic acid–ester exchange, the underlying principles may be used to impart photocontrol on other dynamic reactions, such as imine exchange or thia-Michael addition.

Supporting Information

General information

General procedures. Unless otherwise noted, reactions were performed under N_2 atmosphere in oven-dried (150 ºC) glassware. Reaction progress was monitored by thin layer chromatography (Merck silica gel 60 F_{254} plates), visualizing with fluorescence quenching, $KMnO_4$, or ninhydrin stains. Automated column chromatography was performed using SiliCycle SiliaFlash F60 (40-63 μm, 60 Å) in SNAP cartridges on a Biotage Isolera One. Organic solvents were removed *in vacuo* using a rotary evaporator (Büchi Rotovapor R-100, ~20–300 torr) and residual solvent was removed under high vacuum (<200 mtorr). Water-soluble polymers were purified by dialysis using SnakeSkin Dialysis Tubing (3.5 kDa cutoff, 16 mm diameter) purchased from Fisher Scientific.

Materials. Commercial reagents were purchased from Sigma-Aldrich, Acros, Alfa Aesar, TCI, or Oakwood and used as received. 4-Arm PEG-NH_2 HCl salt (M_w 5 kDa) was purchased from JenKem and was melted under high vacuum (<100 mtorr) prior to functionalization.

Instrumentation. Proton nuclear magnetic resonance (^1H NMR) spectra and carbon nuclear magnetic resonance (^{13}C NMR) spectra were recorded on Bruker AVANCE-500 spectrometers at 500 MHz and 125 MHz, and referenced to the solvent residual peaks. ^{19}F NMR spectra were recorded on Bruker AVANCE-500 spectrometers at 470 MHz. Boron nuclear magnetic resonance (^{11}B NMR) spectra were recorded on Bruker AVANCE-400 spectrometers at 128 MHz in Wilmad Precision NMR tubes (CFQ, 500 MHz, OD: 5 mm, wall thickness: 0.38 mm). NMR data are represented as follows: chemical shift ($\square$ ppm), multiplicity (s = singlet, d = doublet, t = triplet, q = quartet, m = multiplet), coupling constant in Hertz (Hz) and integration. UV-Vis spectra were collected on a Cary 5000 UV-vis-NIR spectrophotometer with an Hg lamp; cuvettes were 10-mm path length quartz cells (Starna 23-Q-10). Blue LED strip lights (wavelength = 470 nm, power = 6.6 W) green

LED strip lights (wavelength = 525 nm, low power = 5.7 W, high power = 16 W), yellow LED strip lights (wavelength= 590 nm), red LED strip lights (wavelength = 626 nm, power = 6.6W), were purchased from superbrightleds.com. Size exclusion chromatography (SEC) measurements were performed in BHT stabilized, HPLC-grade tetrahydrofuran using an Agilent 1260 Infinity II system with variable-wavelength diode array (254, 450, and 530 nm) and refractive index detectors, guard column (Agilent PLgel; 5μm; 50 x 7.5 mm), and three analytical columns (Agilent PLgel; 5μm; 300 x 7.5 mm; 10^5, 10^4, and 10^3 Å pore sizes). The instrument was calibrated with narrow-dispersity polystyrene standards between 640 Da and 2300 kDa (Polymer Standards Service GmbH). All runs were performed at 1.0 mL/min flow rate and 40 °C. Molecular weight values are calculated based on the refractive index signal.

Synthesis

Nitroso compounds were prepared by the oxidation of the aniline precursor using the Oxone method developed by Rück-Braun.[1]

1-bromo-2-nitrosobenzene (SI-1)
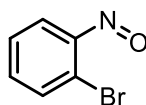
2-bromoaniline (1.00g, 1 equiv, 5.81 mmol) was added to a 100 mL round bottom flask (RBF) equipped with a stir bar and dissolved in 17 mL of DCM. Oxone (7.15g, 2 equiv, 11.6 mmol) was dissolved into 20 mL of deionized water and added to the reaction, which was left to stir vigorously for 3 hours at ambient temperature. The reaction was diluted with DCM and washed with 1M NaOH (2x) and 1M HCl. The organic layer was collected, dried with sodium sulfate and concentrated. The crude solid was carried on to the following reaction.

(*E*)-1-(2-bromophenyl)-2-(p-tolyl)diazene (SI-2)
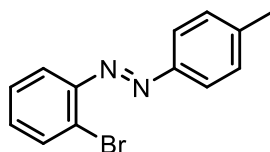
SI-**1** (400 mg, 1 equiv, 2.15 mmol) and p-toluidine (242 mg, 1.05 equiv, 2.26 mmol) were added to a 100 mL round-bottom flask (RBF) equipped with a stir bar. DCM (28 mL) and acetic acid (7 mL) were added and the

reaction was stirred at ambient temperature for 4 hours. The reaction mixture was concentrated and dissolved into EtOAc and washed with 1M NaOH to remove acetic acid. The organic fraction was collected, dried with sodium sulfate, and concentrated *in vacuo*. The crude residue was purified by column chromatography (5% EtOAc in hexane) to yield (*E*)-1-(2-bromophenyl)-2-(p-tolyl)diazene (367 mg, 1.33 mmol, 62%) as a red solid. **¹H NMR** (500 MHz, CDCl₃-*d*) δ 7.90 (d, *J* = 8.5 Hz, 2H), 7.75 (dd, *J* = 8.0, 1.4 Hz, 1H), 7.67 (dd, *J* = 8.0, 1.7 Hz, 1H), 7.42 – 7.36 (m, 1H), 7.36 – 7.28 (m, 3H), 2.45 (s, 3H).**¹³C NMR** (125 MHz, CDCl₃-*d*) δ 150.84, 149.75, 142.29, 133.69, 131.57, 129.84, 127.96, 125.46, 123.44, 117.81, 21.60. **HRMS**: m/z expected for C₁₃H₁₂BrN₂ [M+H]⁺ 275.01, measured 275.02.

(*E*)-(2-(p-tolyldiazenyl)phenyl)boronic acid (1)
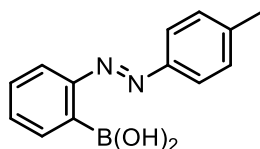
Bis(pinacolato)diboron (299 mg, 1.1 equiv, 1.18 mmol), potassium acetate (316 mg, 3 equiv, 3.22 mmol), and Pd(dppf)Cl₂*dcm (88 mg, 0.1 equiv, 0.107 mmol) were added to a 25-mL Schlenk flask equipped with a stir bar. The reaction was backfilled with nitrogen (3x) and then SI-**2** (295 mg, 1 equiv, 1.07 mmol) was added in 10 mL of dry toluene. The reaction was stirred for 12 hours at 80 °C and then filtered through a Celite plug, concentrated, and re-dissolved into EtOAc. The organic layer was washed with aq. NH₄Cl followed by DI water. The organic layer was collected, dried over sodium sulfate, concentrated and then dissolved in 10 mL of THF and 2 mL of DI water. Sodium periodate (459 mg, 2 equiv, 2.14 mmol) and 1 mL of 1M HCl were added and the reaction was left to stir overnight. The THF was removed *in vacuo* and the crude was re-dissolved in EtOAc. The boronic acid was extracted into water with 1M NaOH. The organic layer was discarded and the aqueous layer was neutralized with 1M HCl leading to boronic acid precipitation. It was further re-extracted with EtOAc and concentrated to give a brown-yellow oil. 25 mL of hexane was added to the oil which was sonicated for 30 minutes leading to the precipitation of a yellow solid. This was collected on a filter to yield (*E*)-(2-(p-tolyldiazenyl)phenyl)boronic acid (70 mg, 0.29 mmol, 27%) as a yellow solid.

¹H NMR (500 MHz, DMSO-d_6) δ 7.86 (d, J = 8.0 Hz, 1H), 7.79 (d, J = 8.3 Hz, 2H), 7.57 – 7.46 (m, 3H), 7.42 (d, J = 8.1 Hz, 2H), 2.42 (s, 3H). **¹³C NMR** (125 MHz, DMSO-d_6) δ 155.21, 149.47, 142.29, 133.15, 130.99, 130.42, 129.62, 122.94, 122.74, 21.53. **HRMS** m/z expected for $C_{13}H_{14}BN_2O_2$ [M+H]⁺ 241.11, measured 241.11.

1,3-difluoro-2-nitrosobenzene (SI-3)
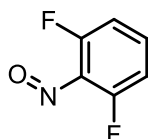
2,6-difluoroaniline (560 mg, 500 µL, 1 equiv, 4.34 mmol) was added to a 100 mL RBF equipped with a stir bar and dissolved in 14 mL of DCM. Oxone (5.33 g, 2 equiv, 8.67 mmol) was dissolved into 16 mL of DI water, and added to the reaction. The reaction was stirred vigorously for 24 hours at ambient temperature. The reaction was diluted with DCM and washed with 1M NaOH (2x) and 1M HCl. The organic layer was collected, dried with sodium sulfate and concentrated. The crude was carried on to the following reaction.

(*E*)-(2-((2,6-difluorophenyl)diazenyl)phenyl)boronic acid (2)
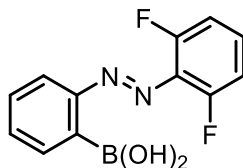
SI-**3** (350 mg, 1 equiv, 2.45 mmol) and 2-(4,4,5,5-tetramethyl-1,3,2-dioxaborolan-2-yl)aniline (536 mg, 1 equiv, 2.45 mmol) were added to a 25 mL RBF equipped with a stir bar. Acetic acid (10 mL) was added and the reaction was stirred at ambient temperature for 24 hours. The reaction was then diluted with DCM and washed with sodium bicarbonate (2x) to remove AcOH. The organic layers were dried with sodium sulfate and concentrated and carried through to the deprotection step without any further purification. The crude residue was dissolved into 60 mL of THF into a 250 mL RBF, to which sodium periodate (1.57 g, 3 equiv, 7.34 mmol) and 2 mL of 1M HCl were added. The reaction was stirred overnight. The solvent was then removed, and the product was dissolved into EtOAc and washed with water. The organic layer was collected and dried over

sodium sulfate. It was then passed through a small silica plug, first with 40:60 EtOAc in hexane to remove the byproduct and then with 5% MeOH in DCM. The MeOH-DCM fractions were collected and concentrated *in vacuo*. The crude boronic acid was further purified with 1M NaOH basic extraction against EtOAc (1x). The basic aqueous layer was then neutralized with 1M HCl and the boronic acid was re-extracted with EtOAc. Finally, the organic layers were collected and concentrated and washed with cold ACN to yield (*E*)-(2-((2,6-difluorophenyl)diazenyl)phenyl)boronic acid (75 mg, 0.29 mmol, 12%) as an orange solid.

¹H NMR (500 MHz, DMSO-d_6) δ 8.01 (s, 2H), 7.84 – 7.78 (m, 1H), 7.78 – 7.72 (m, 1H), 7.65 – 7.57 (m, 3H), 7.42 – 7.32 (m, 2H).**¹³C NMR** (125 MHz, DMSO-d_6) δ 156.69, 156.24, 154.65, 134.58, 132.80, 130.44, 119.28, 113.72, 113.56. **¹⁹F NMR** (470 MHz, DMSO-d_6) δ -121.16. **HRMS:** m/z expected for $C_{12}H_{10}BF_2N_2O_2$ [M+H]⁺ 263.07, measured 263.08.

(*E*)-1-(2-bromophenyl)-2-(2,6-dimethoxyphenyl)diazene (SI-4)
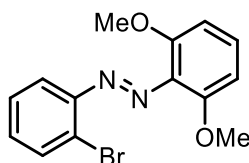
SI-**1** (885 mg, 1 equiv, 4.67 mmol) was added to a flask charged with a stir bar and dissolved in 36 mL of DCM. 2,6-dimethoxyaniline (729 mg, 1 equiv, 4.76 mmol) and acetic acid (5.7 mL, 21 equiv, 100 mmol) were added to the flask which was allowed to stir open to air overnight at ambient temperature. The reaction mixture was then concentrated *in vacuo*, re-dissolved in EtOAc (40 mL) and washed with 40 mL 1 M HCl (3x). The organic layers were collected, dried over sodium sulfate and concentrated *in vacuo*. The resulting crude was purified *via* flash column chromatography (20% EtOAc in hexane) to yield (*E*)-1-(2-bromophenyl)-2-(2,6-dimethoxyphenyl)diazene (835 mg, 55%) as a red powder.

¹H NMR (500 MHz, CDCl₃-*d*) δ 7.73 (dd, J = 7.9, 1.3 Hz, 1H), 7.61 (dd, J = 7.9, 1.4 Hz, 1H)*, 7.57 (dd, J = 7.9, 1.7 Hz, 1H), 7.41 – 7.34 (m, 1H), 7.32 – 7.27 (m, 2H), 7.08 (t, J = 8.4 Hz, 1H)*, 7.00 (td, J = 7.6, 1.7 Hz, 1H)*, 6.95 (td, J = 7.6, 1.4 Hz, 1H)*, 6.70 (d, J = 8.4 Hz, 2H), 6.43 (d, J = 8.4 Hz, 2H)*, 6.39 (dd, J = 7.8, 1.7 Hz, 1H)*, 3.89 (s, 6H), 3.71 (s, 6H)*. **¹³C NMR** (126 MHz, CDCl₃-*d*) δ 153.26, 152.44*, 151.43, 149.04*, 133.45,

133.27, 132.99*, 131.32, 130.70, 128.73*, 128.57*, 127.99, 126.59*, 124.37, 118.13, 116.83*, 105.29, 103.99*, 56.70, 55.71*.

*indicate observed *Z* isomer peaks

HRMS: m/z expected for $C_{14}H_{14}BrN_2O_2$ [M+H]$^+$ 321.02, measured 321.02.

(*E*)-(2-((2,6-dimethoxyphenyl)diazenyl)phenyl)boronic acid (3)
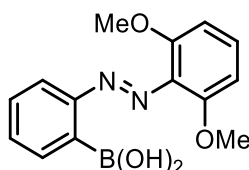
SI-**4** (2.50 g, 1 equiv, 7.78 mmol), bis(pinacolato)diboron (2.17 g, 1.1 equiv, 8.56 mmol), potassium acetate (2.29 g, 3 equiv, 23.4 mmol), and Pd(dppf)Cl$_2$*dcm (636 mg, 0.1 equiv, 0.778 mmol) were added to a flask equipped with stir bar and degassed and back-filled with nitrogen (3x). Toluene (85 mL) was added *via* cannula and the reaction was stirred under nitrogen at 80°C overnight. The solution was filtered through a celite plug, using EtOAc to elute additional product. The product was concentrated *in vacuo*, and diluted with 150 mL of THF and 39 mL of DI water. Sodium periodate (3.33 g, 2 equiv, 15.6 mmol) was added and allowed to stir for 30 minutes before adding 1 M HCl (7.7 mL). The reaction was stirred overnight at ambient temperature. The organic solvent was removed *in vacuo* and the product was washed with EtOAc. The resulting organic layer was extracted with 1 M NaOH. The aqueous layer was neutralized with 1 M HCl and extracted with EtOAc. The resulting organic layer was dried over sodium sulfate and concentrated to yield a crude product that was washed with DCM on a fritted funnel to yield (*E*)-(2-((2,6-dimethoxyphenyl)diazenyl)phenyl)boronic acid (672 mg, 30%) as a free-flowing dark orange powder.

¹H NMR (500 MHz, DMSO-*d₆*) δ 8.52 (s, 2H), 8.00 (dd, J = 7.4, 1.7 Hz, 1H), 7.73 (dd, J = 8.1, 1.2 Hz, 1H), 7.67 (d, J = 6.3 Hz, 1H)*, 7.61 – 7.45 (m, 3H), 7.14 (d, J = 7.4 Hz, 1H)*, 7.12 – 7.03 (m, 1H)*, 6.90 (d, J = 8.5 Hz, 2H), 6.55 (d, J = 8.4 Hz, 2H)*, 6.29 (d, J = 7.8 Hz, 1H)*, 3.90 (s, 6H), 3.60 (s, 6H)*. **¹³C NMR** (126 MHz, DMSO-*d₆*) δ 159.64*, 157.71, 154.61, 148.09*, 136.51, 135.02*, 133.64, 132.62*, 131.74, 131.14, 130.52, 129.62*, 128.84*, 127.67*, 114.11, 113.68*, 105.79, 104.78*, 56.62, 56.07*. *indicate observed *Z* isomer peaks

HRMS: m/z expected for $C_{14}H_{16}BN_2O_4$ [M+H]$^+$ 287.11, measured 287.12

1-bromo-4-nitrosobenzene (SI-5)
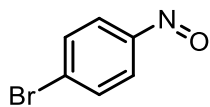
4-bromoaniline (500 mg, 1 equiv, 2.91 mmol) was added to a 100 mL RBF equipped with a stir bar and dissolved in 7 mL of DCM. Oxone (3.57 g, 2 equiv, 5.81 mmol) was dissolved into 28 mL of deionized water and added to the reaction, which was left to stir vigorously for 3 hours at ambient temperature. The reaction was diluted with DCM and washed with 1M NaOH (2x) and 1M HCl. The organic layer was collected, dried with sodium sulfate, and concentrated. The crude was carried on to the following reaction.

(*E*)-1-(4-bromophenyl)-2-(2,6-dimethoxyphenyl)diazene (SI-6)
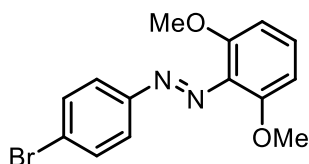
SI-**5** (910 mg, 1.1 equiv, 4.89 mmol) was added to a flask equipped with a stir bar and dissolved in 40 mL of DCM. 2,6-dimethoxy aniline (681 mg, 1.0 equiv, 4.45 mmol) and acetic acid (5.34 mL, 21 equiv, 93.4 mmol) were added and the reaction was left to stir at ambient temperature overnight. The reaction mixture was then concentrated *in vacuo* and diluted with 100 mL EtOAc and washed with 1 M HCl. The aqueous layer was washed with 75 mL EtOAc (3x) and the combined organic layers were dried over sodium sulfate and concentrated *in vacuo*. The resulting crude red oil was purified by column chromatography (30% EtOAc in hexane) to yield (*E*)-1-(4-bromophenyl)-2-(2,6-dimethoxyphenyl)diazene (719.4 mg, 51%) as a red powder.

^{1}H NMR (500 MHz, CDCl$_3$-*d*) δ 7.76 (d, J = 8.6 Hz, 2H), 7.62 (d, J = 8.7 Hz, 2H), 7.32 (d, J = 8.6 Hz, 2H)*, 7.29 – 7.23 (m, 1H), 7.08 (t, J = 8.4 Hz, 1H)*, 6.78 (d, J = 8.6 Hz, 2H)*, 6.68 (d, J = 8.4 Hz, 2H), 6.42 (d, J = 8.4 Hz, 2H)*, 3.83 (s, 6H), 3.68 (s, 6H)*. **^{13}C NMR** (126 MHz, CDCl$_3$-*d*) δ 152.52, 152.19, 148.26*, 133.47, 132.19, 131.11*, 130.00, 128.52*, 125.18, 124.13, 120.44*, 105.12, 104.08*, 56.48, 55.66*.

*denotes observed *Z* isomer peaks

LRMS: m/z expected for C$_{14}$H$_{14}$BrN$_2$O$_2$ [M+H]$^+$ 321.02, measured 321.0

(*E*)-(4-((2,6-dimethoxyphenyl)diazenyl)phenyl)boronic acid (4)
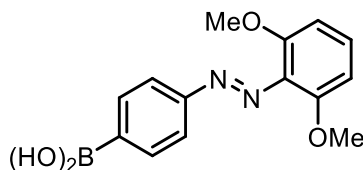
SI-**6** (670 mg, 1 equiv, 2.09 mmol), bis(pinacolato)diboron (583 mg, 1.1 equiv, 2.29 mmol), potassium acetate (614 mg, 3 equiv, 6.26 mmol), and Pd(dppf)Cl2*dcm (170 mg, 0.1 equiv, 0.209 mmol) were added to a flask charged with stir bar and degassed and back-filled with nitrogen (3x). Toluene (20 mL) was added *via* cannula and the reaction was stirred under nitrogen at 80 °C overnight. It was then filtered through celite, using EtOAc to elute additional product. The filtrate was then concentrated and re-dissolved in THF (27 mL) followed by addition of sodium periodate (892 mg, 2 equiv, 4.17 mmol) in 7 mL of DI water. After 30 minutes of stirring, 1.3 mL of 1 M HCl was added to the reaction mixture and stirred overnight at ambient temperature. The organic layer was removed *in vacuo* and the resulting aqueous solution was extracted with EtOAc. The crude was then purified *via* flash column chromatography (10% MeOH in DCM), followed by a base extraction and a plug column first with 50% EtOAc in Hexanes then 10% MeOH in DCM to yield (E)-(4-((2,6-dimethoxyphenyl)diazenyl)phenyl)boronic acid (39 mg, 7%) as a dark red powder.

¹H NMR (500 MHz, DMSO-d_6) δ 8.28 (s, 2H), 7.97 (d, J = 8.3 Hz, 1H), 7.71 (d, J = 8.3 Hz, 1H), 7.64 (d, J = 8.3 Hz, 2H)*, 7.31 (t, J = 8.4 Hz, 1H), 7.07 (t, J = 8.4 Hz, 1H)*, 6.81 (d, J = 8.5 Hz, 2H), 6.74 (d, J = 8.3 Hz, 2H)*, 6.54 (d, J = 8.4 Hz, 2H)*, 3.74 (s, 6H), 3.62 (s, 6H)*. **¹³C NMR** (126 MHz, DMSO-d_6) δ 156.57*, 153.67, 151.53, 147.77*, 137.16*, 135.10, 134.08*, 133.19*, 132.20*, 129.66, 128.42*, 121.08, 116.63, 105.27, 104.42*, 56.22, 55.67, 54.96*.

*denotes observed *Z* isomer peaks

LRMS: m/z expected for $C_{14}H_{16}BN_2O_4$ [M+H]⁺ 287.11, measured 287.12

(*E*)-1-(2-bromophenyl)-2-(2,4-dimethoxyphenyl)diazene (SI-7)
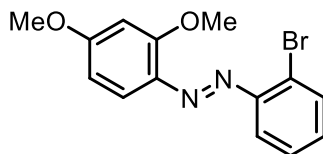
To a flask equipped with a stir bar, SI-**1** (500 mg, 1.2 equiv, 2.69 mmol) in 20 mL of DCM was added followed by 2,4 dimethoxy aniline (343 mg, 1 equiv, 2.24 mmol) and acetic acid (2.69 mL, 21 equiv, 47 mmol). The reaction was left to stir overnight at ambient temperature. The reaction mixture was washed with 75 mL of sodium bicarbonate (3x), followed by 75 mL of 1 M HCl (2x). The combined organic layers were dried over sodium sulfate and concentrated *in vacuo*. The resulting product was purified *via* column chromatography (25% EtOAc in hexane) to yield (*E*)-1-(2-bromophenyl)-2-(2,4-dimethoxyphenyl)diazene (624 mg, 87%) as a red powder.

¹H NMR (500 MHz, CDCl$_3$-*d*) δ 7.85 (d, J = 8.9 Hz, 1H), 7.75 – 7.68 (m, 1H), 7.63 (dd, J = 8.0, 1.7 Hz, 1H), 7.35 (ddd, J = 8.1, 7.3, 1.4 Hz, 1H), 7.28 – 7.20 (m, 2H), 7.04 (td, J = 7.6, 1.4 Hz, 1H)*, 7.00 – 6.93 (m, 1H)*, 6.67 (d, J = 8.6 Hz, 1H)*, 6.59 – 6.42 (m, 1H), 6.38 – 6.33 (m, 1H)*, 6.31 (dd, J = 8.7, 2.4 Hz, 1H)*, 4.02 (s, 3H), 3.89 (s, 3H), 3.75 (s, 3H)*, 3.71 (s, 3H)*. **¹³C NMR** (126 MHz, CDCl$_3$-*d*) δ 164.34, 160.94*, 159.26, 151.76*, 150.43, 137.08*, 136.77, 133.47*, 133.07, 130.88, 128.02, 127.89*, 127.38*, 124.75, 121.49*, 118.89, 118.33, 117.60*, 105.95, 104.21*, 98.99, 56.41, 55.72, 55.56*, 55.50*. *denotes observed *Z* isomer peaks

**HRMS:** m/z expected for C$_{14}$H$_{14}$BrN$_2$O$_2$ [M+H]$^+$ 321.02, measured 321.02

(*E*)-(2-((2,4-dimethoxyphenyl)diazenyl)phenyl)boronic acid (5)
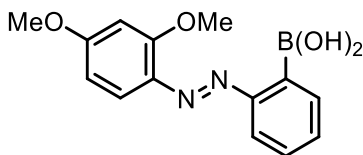

SI-**7** (600 mg, 1 equiv, 1.87 mmol), bis(pinacolato)diboron (522 mg, 1.1 equiv, 2.05 mmol), potassium acetate (550 mg, 3 equiv, 5.60 mmol), and Pd(dppf)Cl2*dcm (137 mg, 0.1 equiv, 0.187 mmol) were added to a flask

charged with stir bar and degassed and back-filled with nitrogen (3x). Toluene (20 mL) was added *via* cannula and the reaction was stirred under nitrogen at 80 ºC overnight. The reaction mixture was then filtered through celite, using EtOAc to elute additional product. The filtrate was concentrated and re-dissolved in THF (36 mL). To it sodium periodate (799 mg, 2 equiv, 3.74 mmol) in 9 mL of DI water was added and after 30 minutes of stirring, 0.9 mL of 1 M HCl was added to the reaction mixture which was then left to stir overnight at room temperature. The organic layer was removed *in vacuo* and the resulting aqueous solution was extracted with EtOAc and dried over sodium sulfate. The organic layer was concentrated and purified *via* column chromatography (10% MeOH in DCM). The resulting product was concentrated and re-dissolved in EtOAc, extracted with 1 M NaOH. The basic layer was neutralized with 1 M HCl and extracted with EtOAc, dried over sodium sulfate, and concentrated to yield (E)-(2-((2,4-dimethoxyphenyl)diazenyl)phenyl)boronic acid (181 mg, 34%) as a red powder.

^{1}H NMR (500 MHz, DMSO-d_6) δ 8.27 (s, 2H), 8.08 (s, 2H)*, 7.79 (dd, J = 7.3, 1.6 Hz, 0H), 7.71 (dd, J = 8.1, 1.2 Hz, 0H), 7.67 (d, J = 8.9 Hz, 1H), 7.63 (d, J = 9.0 Hz, 1H)*, 7.55 (m, 1H)*, 7.52 (td, J = 7.7, 1.6 Hz, 1H), 7.46 (td, J = 7.2, 1.2 Hz, 1H), 6.79 (d, J = 2.6 Hz, 1H), 6.73 (dd, J = 8.9, 2.5 Hz, 1H), 6.63 (dd, J = 8.9, 2.5 Hz, 1H)*, 3.96 (s, 3H), 3.89 (s, 3H), 3.72 (s, 3H)*, 3.69 (s, 3H)*. **^{13}C NMR** (126 MHz, DMSO-d_6) δ 164.13, 159.26*, 157.22, 156.67, 153.03*, 135.88, 135.07, 133.60*, 130.73, 130.29, 129.76, 124.02, 122.69, 117.80*, 116.32, 106.89, 106.77*, 99.84, 99.63*, 56.48, 56.30 *denotes observed *Z* isomer peaks.

HRMS: m/z expected for $C_{14}H_{16}BN_2O_4$ [M+H]$^+$ 287.11, measured 287.12

methyl 3-bromo-4-nitrosobenzoate (SI-8)
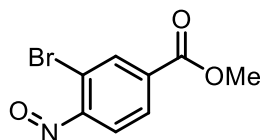
Methyl 4-amino-3-bromobenzoate (230 mg, 1 equiv, 1.00 mmol) was dissolved into 6 mL of DCM into a 50 mL RBF equipped with a stir bar. Oxone (1.84 g, 3 equiv, 3.00 mmol) was dissolved into 24 mL of water and was added into the RBF. The reaction was left to stir for 36 hours at ambient temperature. The reaction was

diluted with DCM and washed with 1M NaOH (2x) and 1M HCl. The organic layer was collected, dried with sodium sulfate and concentrated. The crude was purified by flash chromatography (10% EtOAc in hexane) to yield the product as a yellow solid methyl 3-bromo-4-nitrosobenzoate (87 mg, 0.36 mmol, 36 %), which was carried on to the following reaction

^{1}H NMR (500 MHz, CDCl$_3$) δ 8.66 (d, J = 1.6 Hz, 1H), 7.92 (dd, J = 8.3, 1.7 Hz, 1H), 6.18 (d, J = 8.3 Hz, 1H), 3.98 (s, 3H).

methyl (*E*)-3-bromo-4-((2,6-dimethoxyphenyl)diazenyl)benzoate (SI-9)
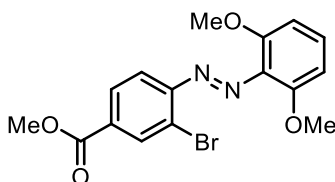
In a 250-mL RBF equipped with a stir bar, SI-**8** (560 mg, 1 equiv, 2.29 mmol) and 2,6-dimethoxyaniline (352 mg, 1 equiv, 2.29 mmol) were dissolved into DCM. To it 10 mL of AcOH was added and the reaction was capped and let stir for 24 hours at ambient temperature. Initially the reaction solution was a dark green color, which quickly became darker and the green color faded away. After 24 hours, the reaction was a deep red/black solution. The reaction was then diluted with DCM and washed with 1M NaOH and then with 1M HCl. The organic layer was collected, dried over sodium sulfate, and concentrated. The crude was purified with flash chromatography (20% EtOAc in hexane) to yield methyl (*E*)-3-bromo-4-((2,6-dimethoxyphenyl)diazenyl)benzoate (301 mg, 35%) as red solid.

^{1}H NMR (500 MHz, CDCl$_3$-*d*) δ 8.38 (s, 1H), 8.27 (s, 1H)*, 8.01 (d, J = 8.0 Hz, 1H), 7.80 (d, J = 8.3 Hz, 1H)*, 7.62 (d, J = 8.2 Hz, 1H)*, 7.54 (d, J = 8.3 Hz, 1H), 7.31 (t, J = 8.4 Hz, 1H), 7.08 (s, 1H)*, 6.68 (d, J = 8.4 Hz, 2H), 6.41 (d, J = 8.3 Hz, 2H)*, 3.93 (s, 3H), 3.89 (s, 6H) 3.70 (s, 6H)*.**^{13}C NMR** (125 MHz, CDCl$_3$-*d*) δ 165.54, 154.20, 153.72, 134.78, 133.00, 132.16, 131.84, 129.35, 123.58, 117.99, 105.12, 56.66, 52.52. *denotes observed *Z* isomer peaks

HRMS: m/z expected for $C_{16}H_{16}BrN_2O_4$ [M+H]$^+$ 379.02, measured 379.03

(*E*)-(2-((2,6-dimethoxyphenyl)diazenyl)-5-(methoxycarbonyl)phenyl)boronic acid (3')
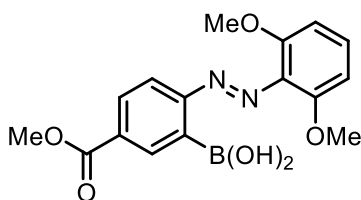
Bis(pinacolato)diboron (222 mg, 1.1 equiv, 873 μmol), potassium acetate (234 mg, 3 equiv, 2.38 mmol) and Pd(dppf)Cl$_2$*dcm (64.8 mg, 0.1 equiv, 79.4 μmol) were added to a 50 mL Schlenk flask equipped with a stir rod. The reaction was backfilled (3x) with nitrogen and then SI-**9** (301 mg, 1 equiv, 794 μmol) was added in 35 mL of dry toluene. The reaction was stirred for 18 hours at 80 °C. Upon completion, the reaction was cooled to room temperature and filtered through a celite plug. The filtrate was then concentrated and re-dissolved in EtOAc. The organic layer was washed with saturated NH$_4$Cl followed by DI water. Combined organic layers were collected, dried over sodium sulfate, concentrated and then re-dissolved in 10 mL of THF into a 25 mL RBF equipped with a stir bar. 2 mL of DI water and sodium periodate (340 mg, 1.59 mmol) were added to it and stirred overnight. Upon completion, the organic solvent was removed *in vacuo*. The crude was dissolved in EtOAc and washed with saturated NH$_4$Cl. The organic layer was collected, dried over sodium sulfate and concentrated to yield (*E*)-(2-((2,6-dimethoxyphenyl)diazenyl)-5-(methoxycarbonyl)phenyl)boronic acid (154 mg, 448 μmol, 56%) as a red solid.

¹H NMR (500 MHz, DMSO-d_6) δ 8.67 (s, 2H), 8.60 (s, 1H), 8.14 (d, *J* = 8.5 Hz, 1H), 7.81 (d, *J* = 8.6 Hz, 1H), 7.55 (t, *J* = 8.5 Hz, 1H), 6.93 (d, *J* = 8.5 Hz, 2H), 3.93 (s, 6H), 3.91 (s, 3H). **¹³C NMR** (125 MHz, DMSO-d_6) δ 166.38, 160.05, 155.04, 137.73, 134.91, 132.54, 131.04, 130.55, 114.60, 105.82, 56.72, 52.78. **HRMS:** m/z expected for $C_{16}H_{17}BN_2O_6$ [M+H]$^+$ 345.12 , measured 345.12.

(*E*)-3-borono-4-((2,6-dimethoxyphenyl)diazenyl)benzoic acid (SI-10)
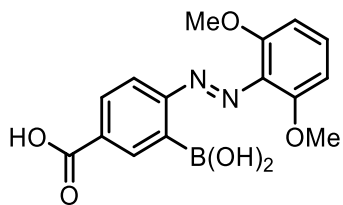
To a 100 mL RBF equipped with a stir bar, compound **3'** (200 mg, 1 equiv, 581 µmol) in methanol (21 mL) was added followed by LiOH (41.8 mg, 3 equiv, 1.74 mmol) in 8 mL of water. It was then stirred for 48 hours at ambient temperature, then diluted with EtOAc and DI water (1:1). The product remained in the aqueous layer, so the organic layer was discarded. The aqueous layer was then neutralized with 1M HCl and extracted back into EtOAc. The organic layer was collected, dried over sodium sulfate and concentrated. The product was washed extensively with acetonitrile to yield (*E*)-3-borono-4-((2,6-dimethoxyphenyl)diazenyl)benzoic acid (153 mg, 80%) as an orange solid.

¹H NMR (500 MHz, DMSO-d_6) δ 8.67 (s, 2H), 8.58 (s, 1H), 8.11 (dd, *J* = 8.5, 2.1 Hz, 1H), 7.78 (d, *J* = 8.4 Hz, 1H), 7.54 (t, *J* = 8.5 Hz, 1H), 6.92 (d, *J* = 8.5 Hz, 2H), 3.92 (s, 6H).**¹³C NMR** (125 MHz, DMSO-d_6) δ 167.47, 159.89, 155.00, 137.93, 134.84, 132.72, 132.22, 130.43, 114.38, 105.77, 56.69. **LRMS:** m/z expected for $C_{15}H_{16}BN_2O_6$ [M+H]$^+$ 331.1 , measured 331.1

7-(2-aminoethoxy)-2H-chromen-2-one hydrochloride (SI-11)
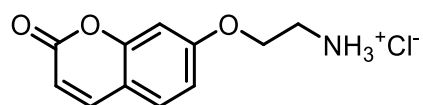
7-Hydroxy-2H-chromen-2-one (635 mg, 1 equiv, 3.92 mmol) and potassium carbonate (388 mg, 1 equiv, 3.92 mmol) were dissolved in acetonitrile (10 mL) into a 25 mL 3-neck RBF equipped with a stir bar and condenser. To it, tert-butyl (2-bromoethyl)carbamate (878 mg, 1 equiv, 3.92 mmol) in 10 mL of dry acetonitrile was added and stirred at refluxing conditions for 20 hours, leading to the formation of bright yellow solid precipitates. Upon completion, the reaction was concentrated and dissolved into EtOAc and washed with saturated NaHCO$_3$. The organic layer was dried and concentrated to about 20 mL, to which 25 drops of concentrated HCl was added. This led to the precipitation of a white solid over two hours which was collected by filtration and characterized as the HCl salt. The salt was then free based by dissolving 50 mg into 10 mL of MeOH

followed by addition of 10 eq of solid NaHCO₃ and letting stir for 3 hours. After the solvent was removed and the crude was dissolved in DCM and washed with water. The organic layer was dried over sodium sulfate and concentrated. The amine was unstable at room temperature, so was immediately carried on to the next reaction without further purification.

Data for compound SI-12 : **¹H NMR** (500 MHz, DMSO-d_6) δ 8.11 (s, 3H), 8.03 (d, J = 9.5 Hz, 1H), 7.69 (d, J = 8.6 Hz, 1H), 7.06 (d, J = 2.4 Hz, 1H), 7.01 (dd, J = 8.6, 2.4 Hz, 1H), 6.34 (d, J = 9.5 Hz, 1H), 4.29 (t, J = 5.1 Hz, 2H), 3.25 (p, J = 5.4 Hz, 2H). **¹³C NMR** (125 MHz, DMSO-d_6) δ 161.33, 160.65, 155.73, 144.74, 130.10, 113.40, 113.31, 113.21, 101.97, 65.53, 38.62. **HRMS:** m/z expected for $C_{11}H_{12}NO_3$ [M+H]⁺ 206.07 , measured 206.08.

2,3,4,5,6-pentahydroxy-N-(2-((2-oxo-2H-chromen-7-yl)oxy)ethyl)hexanamide (17)
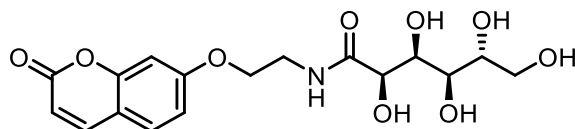
7-(2-Aminoethoxy)-2H-chromen-2-one (30.0 mg, 1 equiv, 146 μmol, free base of **SI-11**) was dissolved into acetonitrile (10 mL) in a 20 mL scintillation vial equipped with a stir bar, and 3,4,5-trihydroxy-6-(hydroxymethyl)tetrahydro-2H-pyran-2-one (24.7 mg, 0.95 equiv, 139 μmol) was added. The reaction was heated to 70 °C overnight. The reaction was then filtered over Celite and the filtrate was concentrated and washed with MeOH to yield 2,3,4,5,6-pentahydroxy-N-(2-((2-oxo-2H-chromen-7-yl)oxy)ethyl)hexanamide (25 mg, 65 μmol, 45%) as a white solid.

¹H NMR (500 MHz, DMSO-d_6) δ 8.06 (d, J = 9.5 Hz, 1H), 7.70 (d, J = 8.6 Hz, 1H), 7.09 (s, 1H), 7.03 (dd, J = 8.6, 2.4 Hz, 1H), 6.36 (d, J = 9.5 Hz, 1H), 4.19 (t, J = 6.1 Hz, 2H), 4.10 (d, J = 3.8 Hz, 1H), 3.99 (s, 1H), 3.66 – 3.49 (m, 6H). **¹³C NMR** (125 MHz, DMSO-d_6) δ 173.39, 161.96, 160.80, 155.82, 144.81, 130.01, 113.22, 113.01, 112.93, 101.71, 73.81, 72.57, 71.80, 70.43, 67.21, 63.63, 37.81. **LRMS:** m/z expected for $C_{17}H_{20}NO_9$ [M-H]⁻ 382.12 , measured 382.0.

(*E*)-1-(2-bromophenyl)-2-(2,6-diethylphenyl)diazene (SI-12)
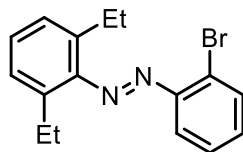
To a 250 mL flask equipped with a stir bar, SI-**1** (872 mg, 1 equiv, 4.69 mmol) and 2,6-diethylaniline (735 mg, 811 μL, 1.05 equiv, 4.92 mmol) were dissolved into 60 mL of DCM, to which 15 mL of AcOH was added to. The reaction was left to run for 7 days at ambient temperature, which was then diluted with DCM and washed with 1M NaOH (2x). The organic fraction was collected, dried with sodium sulfate, and concentrated. The crude was dissolved into hexane and passed through a silica plug with hexane. The eluent was collected, concentrated, and then passed through an alumina plug with hexane. The hexane was concentrated to approximately 10 mL and cooled to –20 °C, which led to the crystallization of an impurity. The product was collected as a dark red oil, (*E*)-1-(2-bromophenyl)-2-(2,6-diethylphenyl)diazene (187 mg, 0.53 mmol, 11%, >90% ^{1}H NMR purity), and carried on to the next reaction without further purification. **^{1}H NMR** (500 MHz, CDCl$_3$-*d*) δ 7.70 (dd, J = 7.9, 1.3 Hz, 1H), 7.53 (dd, J = 8.0, 1.7 Hz, 1H), 7.34 (ddd, J = 8.0, 7.2, 1.4 Hz, 1H), 7.26 (ddd, J = 7.8, 7.2, 1.7 Hz, 1H), 7.20 – 7.16 (m, 1H), 7.11 (d, J = 7.6 Hz, 2H).

(*E*)-1-(2,6-diethylphenyl)-2-(2-(4,4,5,5-tetramethyl-1,3,2-dioxaborolan-2-yl)phenyl)diazene (6)
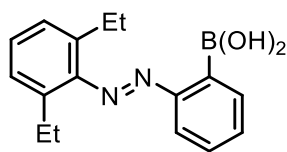
Bis(pinacolato)diboron (165 mg, 1.1 equiv, 648 μmol), potassium acetate (174 mg, 3 equiv, 1.77 mmol) and Pd(dppf)Cl$_2$*dcm (48.1 mg, 0.1 equiv, 58.9 μmol) were added to a 25 mL Schlenk flask equipped with a stir rod. The reaction was backfilled (3x) with nitrogen and then SI-**12** (187 mg, 1 equiv, 589 μmol) was added in 8 mL of dry toluene. The reaction was stirred for 18 hours at 80 °C. Upon completion, the reaction was cooled to room temperature and filtered through a celite plug. The solvent was removed, the crude was diluted in DCM and washed with water. The organic layer was dried with sodium sulfate, and concentrated. The crude

was dissolved into 9 mL of THF into a 100 mL RBF equipped with a stir bar, to which 2.25 mL of water and sodium periodate (379 mg, 3 equiv, 1.77 μmol) were added to. 0.5 mL of 1M HCl was added and the reaction was left to react overnight at ambient temperature. After the reaction was diluted with EtOAc and washed with water. The organic layer was collected, dried with sodium sulfate, and concentrated. The crude was purified by flash chromatography (20% EtOAc in hexane) to yield , (*E*)-(2-((2,6-diethylphenyl)diazenyl)phenyl)boronic acid (99 mg, 350 μmol, 59%) as a red oil.

¹H NMR (500 MHz, DMSO-*d₆*) δ 7.94 – 7.87 (m, 1H), 7.69 – 7.57 (m, 3H), 7.33 (dd, *J* = 8.4, 6.6 Hz, 1H), 7.30 – 7.23 (m, 2H), 2.69 (q, *J* = 7.5 Hz, 4H), 1.14 (t, *J* = 7.5 Hz, 6H). **¹³C NMR** (125 MHz, DMSO-*d₆*) δ 155.14, 150.96, 136.36, 133.08, 131.20, 129.57, 128.70, 127.71, 122.24, 24.72, 16.23. **LRMS:** m/z expected for $C_{16}H_{19}BN_2O_2$ [M+H]⁺ 283.15 , measured 283.1

(*E*)-2-(2-bromostyryl)-1,3-difluorobenzene (SI-13)
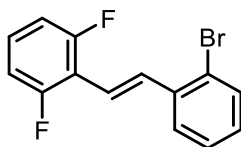
A 25 mL Schlenk flask equipped with a stir rod was charged with dimethyl (2,6-difluorobenzyl)phosphonate (150 mg, 1.00 equiv, 635 μmol), to which 33 mg of NaH powder (57% NaH) was added to slowly on ice, leading to a cloudy yellow reaction. After 30 minutes, 2-bromobenzaldehyde (118 mg, 74.1 μL, 1.00 equiv, 635 μmol) was added to the reaction, which was allowed to warm to room temperature. After 15 hours the reaction appeared as a clear yellow solution. The THF was removed *in vacuo* and the solution was diluted with EtOAc and washed with DI water 2x. The organic layer was collected and dried with sodium sulfate and concentrated to yield a light yellow oil, ((*E*)-2-(2-bromostyryl)-1,3-difluorobenzene (114 mg, 386 μmol, 61%) and carried through to the next reaction.

Crude **¹H NMR** (500 MHz, CDCl₃-*d*) δ 7.80 (d, J = 16.6 Hz, 1H), 7.69 (dd, J = 7.9, 1.7 Hz, 1H), 7.60 (dd, J = 8.0, 1.3 Hz, 1H), 7.34 (tdd, J = 7.9, 1.3, 0.7 Hz, 1H), 7.22 – 7.12 (m, 2H), 7.06 (d, J = 16.6 Hz, 1H), 6.98 – 6.90 (m, 2H).

(*E*)-(2-(2,6-difluorostyryl)phenyl)boronic acid (7)
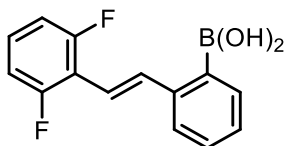
(SI-**14**) (136 mg, 1 equiv, 461 μmol) was dissolved into 3 mL of dry THF and transferred into a 25 mL Schlenk flask equipped with a stir rod. The solution was cooled to -78 ºC for 15 minutes and n-butyllithium (44.3 mg, 278 μL, 1.5 equiv, 691 μmol) was added dropwise. This was allowed to stir for 30 minutes, to which triisopropyl borate (130 mg, 0.16 mL, 1.5 equiv, 691 μmol) was added. The reaction was allowed to warm to room temperature and run for 12 hours. The reaction was quenched with 1M HCl and allowed to run for an hour. The organic solvent was removed and the product was diluted in EtOAc and washed with 1M HCl and DI water (2x). The organic layer was dried with sodium sulfate and concentrated. The product was dissolved in DCM in a RBF layered with hexane and purified by slow evaporation of the DCM *in vacuo* to yield the product as a white powder: (*E*)-(2-(2,6-difluorostyryl)phenyl)boronic acid (33 mg, 0.13 mmol, 28%).

¹H NMR (500 MHz, DMSO-*d₆*) δ 7.87 (dd, *J* = 16.8, 2.4 Hz, 1H), 7.74 (d, *J* = 7.9 Hz, 1H), 7.51 (dd, *J* = 7.4, 1.5 Hz, 1H), 7.42 – 7.31 (m, 2H), 7.31 – 7.25 (m, 1H), 7.19 – 7.11 (m, 2H), 6.99 (d, *J* = 16.8 Hz, 1H). **¹³C NMR** (125 MHz, DMSO-*d₆*) δ 161.54, 159.62, 140.52, 137.39, 133.87, 129.55, 129.36, 127.69, 124.74, 114.92, 112.61. **¹⁹F NMR** (470 MHz, DMSO-*d₆*) δ -113.27 **LRMS:** m/z expected for $C_{14}H_{11}BF_2O_2$ [M+FA]⁻ 305.06, measured 305.1

(*E*)-1-(2-bromophenyl)-2-(2,6-diethoxyphenyl)diazene (SI-14)
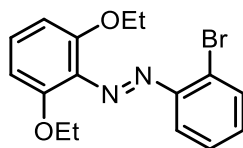
2,6-Diethoxyaniline[2] (540 mg, 1 equiv, 2.98 mmol) and 1-bromo-2-nitrosobenzene (554 mg, 1 equiv, 2.98 mmol) were added to a 100-mL RBF equipped with a stir bar, and dissolved in 40 mL of DCM. 10 mL of AcOH was added and the reaction was left to run overnight at ambient temperature. In the morning, the reaction was washed with potassium carbonate (2x). The organic layer was collected, dried with sodium sulfate, and purified with flash chromatography (5% EtOAc in hexane) to yield (*E*)-1-(2-bromophenyl)-2-(2,6-diethoxyphenyl)diazene (320 mg, 0.77 mmol, 26 %, 84% purity). This material was carried on to the following reaction.

¹H NMR (500 MHz, CDCl$_3$-*d*) δ 7.68 – 7.65 (m, 1H), 7.53 (dd, *J* = 7.9, 1.7 Hz, 1H), 7.31 (ddd, *J* = 8.0, 7.3, 1.4 Hz, 1H), 7.21 (ddd, *J* = 7.9, 7.2, 1.7 Hz, 1H), 7.18 – 7.13 (m, 1H), 6.60 (d, *J* = 8.4 Hz, 2H), 4.04 (q, *J* = 6.9 Hz, 5H), 1.35 (t, *J* = 7.0 Hz, 7H).

(*E*)-(2-((2,6-diethoxyphenyl)diazenyl)phenyl)boronic acid (6')
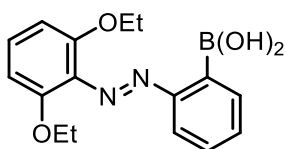
SI-14 (320 mg, 1 equiv, 916 μmol), bis(pinacolato)diboron (256 mg, 1.1 equiv, 1.01 mmol), potassium acetate (270 mg, 3 equiv, 2.75 mmol), and Pd(dppf)Cl2*dcm (74.8 mg, 0.1 equiv, 0.091 mmol) were added to a 100-mL Schlenk flask equipped with stir bar, and degassed and back-filled with nitrogen (3x). Toluene (18 mL) was added via cannula and the reaction was stirred under nitrogen at 80 °C overnight. The solution was filtered through a plug, using acetone/DCM (5:95). The product was concentrated in vacuo, and diluted with 9 mL of THF and 2.5 mL of DI water. Sodium periodate (387 mg, 3 equiv, 1.81 mmol) was added to the reaction followed by 0.5 mL of 1M HCl, and the reaction was left to stir overnight at ambient temperature. The reaction

was diluted in EtOAc and washed with water (1x) and brine (1x) The organic layer was collected dried with sodium sulfate, and purified by column chromatography (10% Acetone in DCM) to yield the product (*E*)-(2-((2,6-diethoxyphenyl)diazenyl)phenyl)boronic acid (88 mg, 0.28 mmol, 31 %) as a red solid.

^{1}H NMR (600 MHz, DMSO-*d$_6$*) δ 8.49 (s, 2H), 8.05 (dd, *J* = 7.3, 1.7 Hz, 1H), 7.83 (dd, *J* = 7.5, 1.5 Hz, 1H)*, 7.81 (s, 2H)*,7.78 (dd, *J* = 8.1, 1.2 Hz, 1H), 7.65 (td, *J* = 7.7, 1.7 Hz, 1H), 7.60 (td, *J* = 7.2, 1.3 Hz, 1H), 7.46 (t, *J* = 8.5 Hz, 1H), 7.27 (td, *J* = 7.4, 1.1 Hz, 1H)*, 7.17 (td, *J* = 7.7, 1.5 Hz, 1H)*, 7.12 (t, *J* = 8.4 Hz, 1H)*, 6.93 (d, *J* = 8.5 Hz, 2H), 6.60 (d, *J* = 8.4 Hz, 2H)*, 6.45 (d, *J* = 7.9 Hz, 1H)*, 4.24 (q, *J* = 7.0 Hz, 4H), 3.96 (d, *J* = 39.0 Hz, 4H)*, 1.40 (t, *J* = 7.0 Hz, 7H), 1.26 (t, *J* = 7.0 Hz, 6H)*.*denotes observed Z isomer peaks

^{13}C NMR (151 MHz, DMSO-*d$_6$*) δ 157.06, 152.82, 135.95, 132.36, 131.27, 131.23, 130.74, 113.75, 106.19, 64.65, 14.43.

LRMS: m/z expected for C16H19BN2O4 [M+H]$^{+}$ 315.14 , measured 315.1

P1
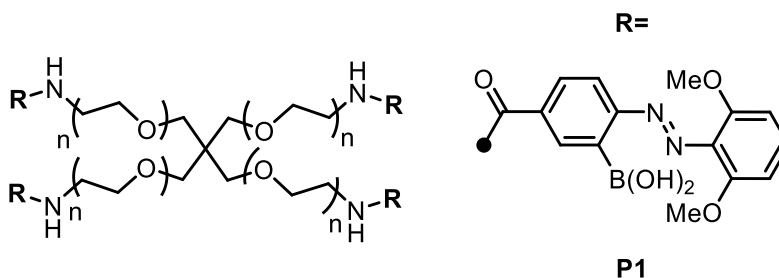
125 mg of 4-arm PEG amine hydrochloride salt (MW = 5000) was added to a Schlenk flask (25 mL) and melted under high vaccum (2x) to remove excess water. 2-methoxyethan-1-aminium (0.125 g, 1 equiv, 23.6 µmol), HOBt (36.1 mg, 10 equiv, 236 µmol), and (E)-3-borono-4-((2,6-dimethoxyphenyl)diazenyl)benzoic acid (77.9 mg, 10 equiv, 236 µmol) were then added as solids along with a stir bar, the vessel was sealed and backfilled with nitrogen (3x). 2 mL of DCM and 2 mL of DMF were then added to solubilize the reagents leading to a clear red solution. TEA (23.9 mg, 33 µL, 10 equiv, 236 µmol) was then added to the solution, which was stirred at room temperature for 24 hours. Upon completion, the reaction was diluted with DCM and filtered through a glass-fritted filter. The filtrate was concentrated *in vacuo* and then diluted with EtOAc and water (1:1). The EtOAc layer was separated and further washed with DI water (3x). Combined aqueous layers were concentrated

in vacuo to ~30 mL and dialyzed for 3 days against DI water (MWCO = 3.5 kDa) while the water being changed daily. The sample was then lyophilized for 48 hours to yield 88 mg of the polymer product.

NOTE: Addition of NaCl was useful for clearing the emulsion at the organic/water interface.

P2

R=

P2
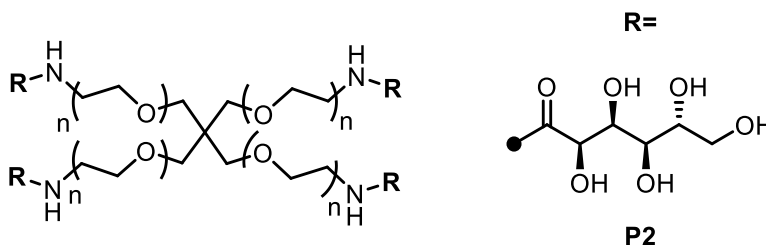
P2 was prepared following a literature procedure.[3]

Photochemical characterization

Determination of photostationary state (PSS): Stock solutions of pure (*E*)-**1** through (*E*)-**3'** (which had not been exposed to light) were prepared at concentrations of 750, 1246, 599 and 421 µM in DMSO. Concentration versus LC area (monitored at 300 nm) calibration curves were prepared by serial dilution of these mixtures. To generate the calibration curves for the *Z* isomers, these samples were then irradiated with either 365 nm light (for compound **1**) or 525 nm light (**2-3'**) to generate a mixture of *E* and *Z* isomers. These mixtures were subject to LC separation, and the LC area at 300 nm was recorded for both the *E* and *Z* isomer. The concentration of the *E* isomers could be calculated using the generated calibration curve, which allows for the *Z* concentration to be determined (as the total concentration is known).

Once the calibration curves were prepared, pure solutions of (*E*)-**1** through (*E*)-**3'** were irradiated with UV (365 nm), blue (470 nm), green (525 nm), yellow (590 nm), or red (626 nm) LEDs for various time intervals. The percent *Z* isomer was determined by LC and plotted as a function of irradiation time. The photostationary state was determined once the ratio of *Z:E* stopped changing.
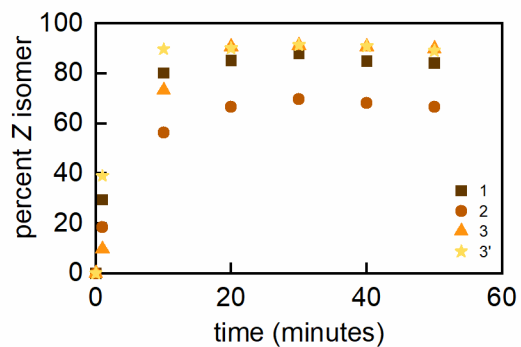
Figure 15. Percent Z isomer of compounds 1-3 and 3' as a function of irradiation time with 365 nm (UV) irradiation.
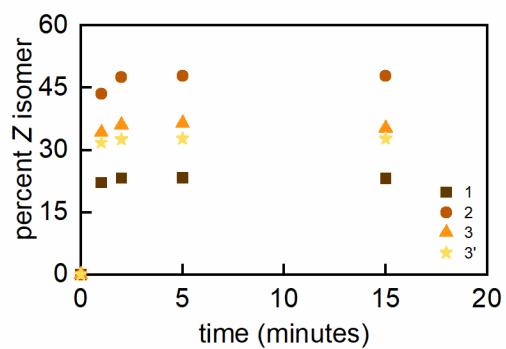
Figure 16. Percent Z isomer of compounds 1-3 and 3' as a function of irradiation time with 470 nm (blue) irradiation.
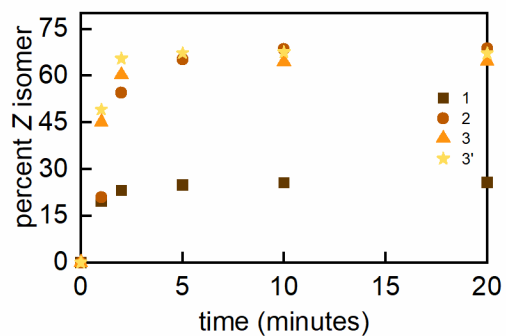
Figure 17. Percent Z isomer of compounds 1-3 and 3' as a function of irradiation time with 525 nm (green) irradiation.
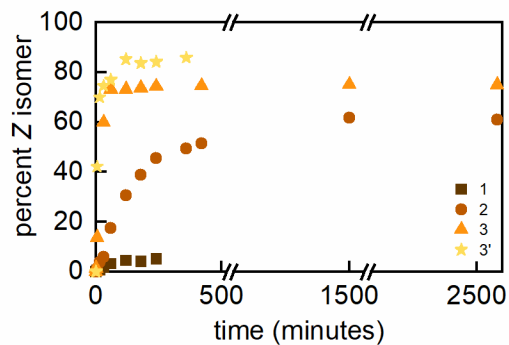
Figure 18. Percent Z isomer of compounds 1-3 and 3' as a function of irradiation time with 590 nm (yellow) irradiation.
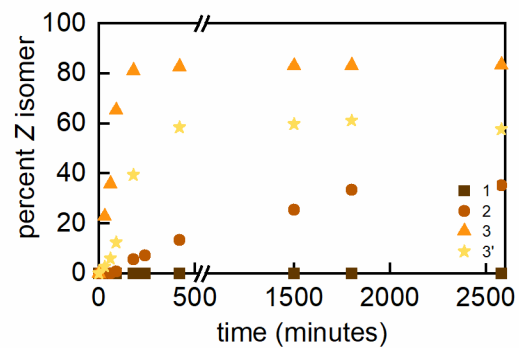
Figure 19. Percent Z isomer of compounds 1-3 and 3' as a function of irradiation time with 626 nm (red) irradiation.

UV-vis Spectra
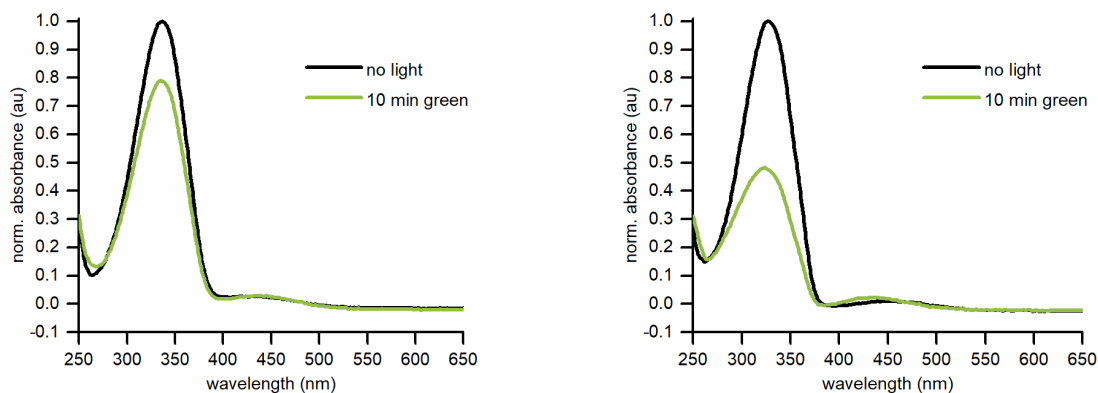
Figure 20 Left: Normalized UV-Vis absorbance spectra of (E)-1 (33 µM in acetonitrile) before (black) and after (green) ten minutes of irradiation. Right: Normalized UV-Vis of (E)-2 (15 µM in acetonitrile) before (black) and after (green) ten minutes of irradiation.
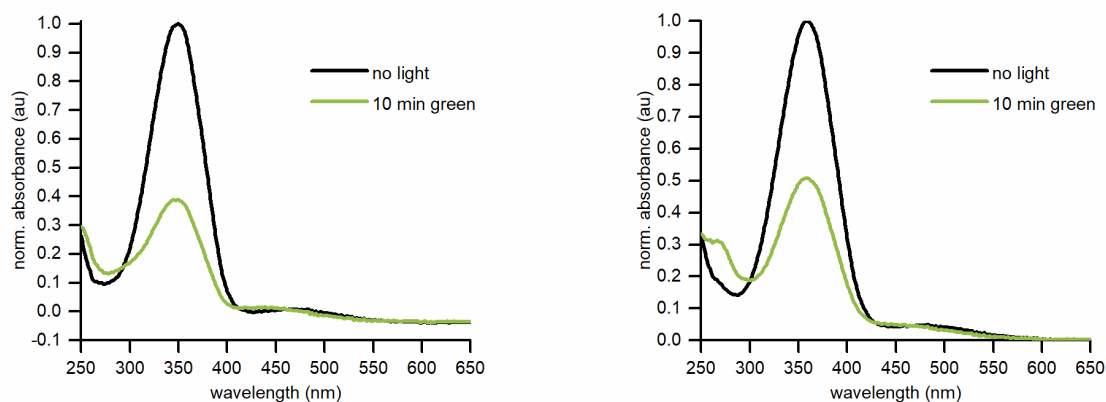
Figure 21. Left: Normalized UV-Vis absorbance spectra of (E)-3 (21 µM in acetonitrile) before (black) and after (green) ten minutes of irradiation. Right: Normalized UV-Vis absorbance spectra of (E)-3'(12 µM in acetonitrile) before (black) and after (green) ten minutes of irradiation.
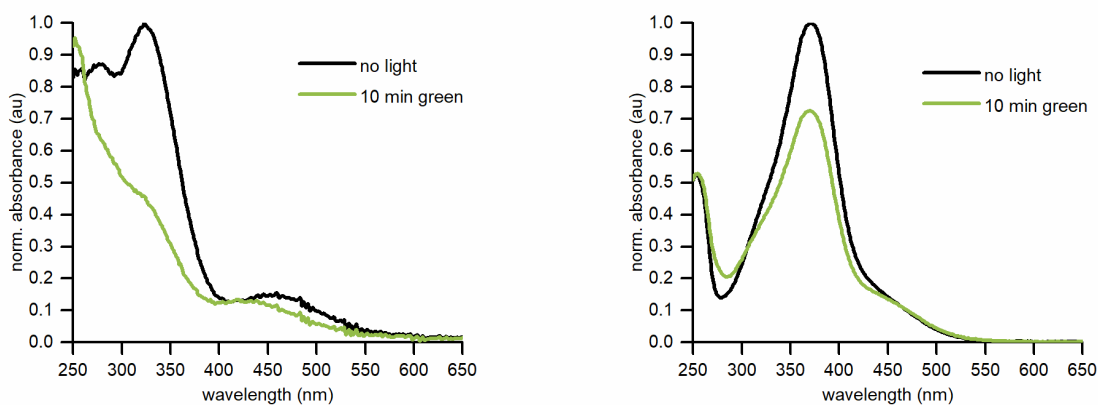
Figure 22. Left: Normalized UV-Vis absorbance spectra of (E)-4 (14 µM in acetonitrile) before (black) and after (green) ten minutes of irradiation. Right: Normalized UV-Vis absorbance spectra of (E)-5 (35 µM in acetonitrile) before (black) and after (green) ten minutes of irradiation.

Determination of thermal half-lives: Each azobenzene (at a concentration of between 1-4 mg/mL) was irradiated with green or red LEDs for at least 30 minutes to produce Z isomer and placed into the NMR, which was set at the appropriate temperature. ^{1}H or ^{19}F NMR spectra were recorded every five minutes at variable temperatures between 30 and 80 °C to monitor the thermal conversion of azobenzene from the Z to E isomer. Rate constants for the first order thermal isomerization were determined from exponential fits and Arrhenius plots were constructed for the rate of isomerization versus temperature. Thermal half-lives at room temperatures (25 °C) were determined by extrapolation of these graphs, where $\tau_{1/2} = \ln(2)/k$.
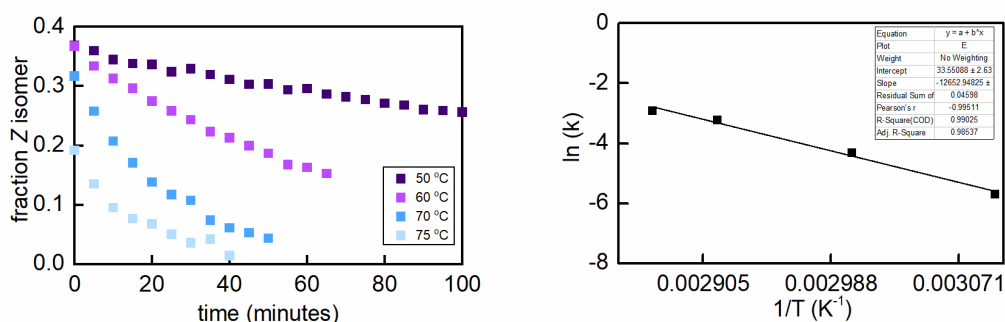
Figure 23. Left: Thermal isomerization of (Z)-1 to (E)-1 as determined by 1H NMR at 50 °C, 60 °C, 70 °C, and 75 °C. Right: Arrhenius plot of thermal isomerization of (Z)-1 to (E)-1. The half-life was determined to 3.5 days at 25 °C.
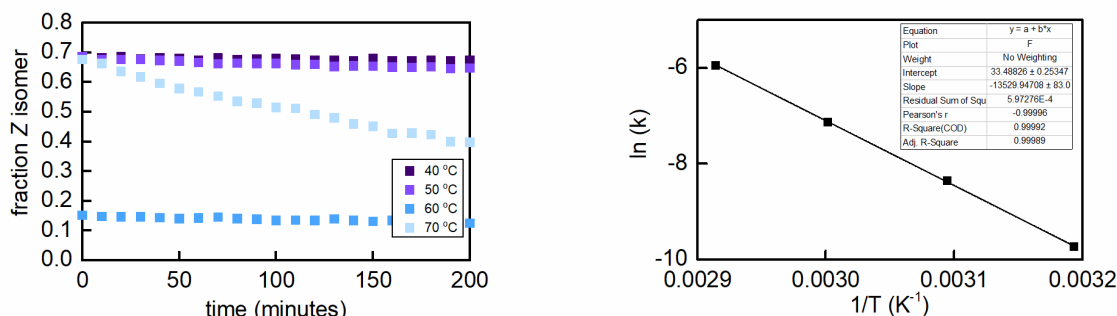
Figure 24. Left: Thermal isomerization of (Z)-2 to (E)-2 as determined by ^{1}H NMR at 40 °C, 50 °C, 60 °C, and 70 °C. Right: Arrhenius plot of thermal isomerization of (Z)-2 to (E)-2. The half-life was determined to 70 days at 25 °C.
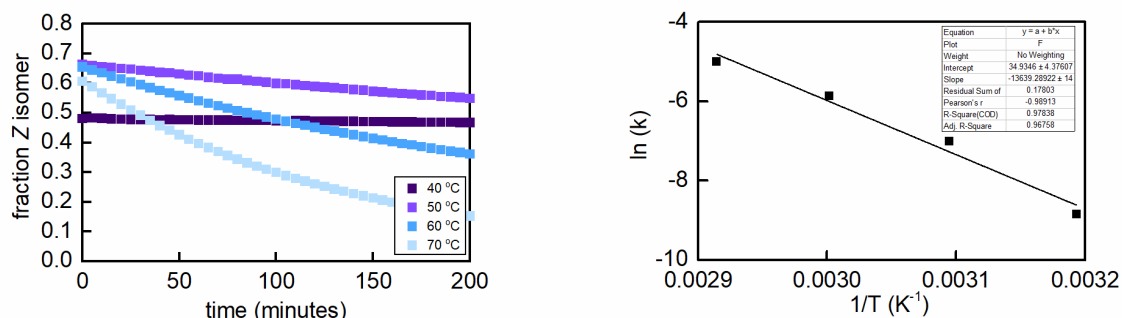
Figure 25. Left: Thermal isomerization of (Z)-3 to (E)-3 as determined by ^{1}H NMR at 40 °C, 50 °C, 60 °C, and 70 °C. Right: Arrhenius plot of thermal isomerization of (Z)-3 to (E)-3. The half-life was determined to 24 days at 25 °C.
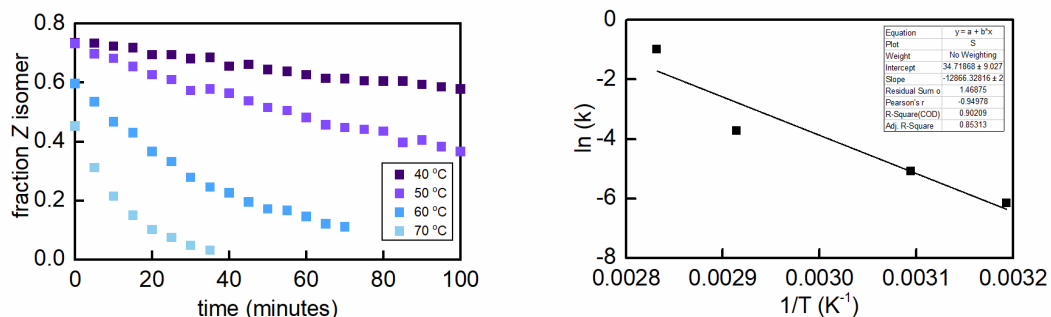
Figure 26. Left: Thermal isomerization of (Z)-3' to (E)-3' determined by ^{1}H NMR at 40 °C, 50 °C, 60 °C, and 70 °C. Right: Arrhenius plot of thermal isomerization of (Z)-1 to (E)-1. The half-life was determined to 2.2 days at 25 °C.

Competition experiments

General procedure for competition experiment: 10 µmol of the given azobenzene boronic acid was dissolved into 500 µL of DMSO-d_6 and irradiated with green or red LEDs for 30 minutes to produce a mixture of the E and Z isomers. Diol (2 equivalents) was added to the solution; if necessary, cyclooctadiene (as an internal standard) was added, as noted in the specific experiments. Cyclopentane diol **9** and guconolactone derivative **13** were treated with excess D_2O (30 µL) to ensure that boronic acid was present. The solution was monitored at 25 °C until equilibrium was reached (see S22 and S23 for further information), and then ^{1}H and/or ^{19}F (if applicable) NMR spectra were recorded using a Bruker AVANCE-500 spectrometers at 500 MHz using a 30° pulse, or a Bruker Neo 600 MHz system with a QCI-F cryoprobe at 600 MHz at 25 °C. Relaxation times for a variety of signals were measured to determine the appropriate delay time, which ranged from 0.7 to 2.7 seconds. Unless noted otherwise, each experiment was subject to 16 scans, and a delay time of 10 seconds. NMR spectra were processed in MestReNova (version 14.1.1) with Whittaker smoother baseline processing,[4] and peaks that could not be fully resolved at baseline were integrated using the global spectral deconvolution (GSD) peak picking integration method. The method of obtaining K_{rel} and integration method is reported under the specific experiments. The amount of bound and unbound boronic acid for both the E and Z isomer were determined by integration and the relative K_{eq} (K_{rel}) was determined from below formula. Protons that could be accurately assigned have been included.

$K_{eq}(E)$ is expressed by equation 1 and $K_{eq}(Z)$ is expressed by equation 2. Because both equilibria are present in the same NMR tube, the concentration of water and diol are the same, and the K_{rel} can be simplified as in equation 3.

$$K_{eq}(E) = \frac{[(E)\text{-ester}][H_2O]^2}{[(E)\text{-acid}][diol]} \quad (1)$$

$$K_{eq}(Z) = \frac{[(Z)\text{-ester}][H_2O]^2}{[(Z)\text{-acid}][diol]} \quad (2)$$

$$K_{rel} = \frac{K_{eq}(Z)}{K_{eq}(E)} = \frac{[(Z)\text{-ester}][H_2O]^2}{[(Z)\text{-acid}][diol]} * \frac{[(E)\text{-acid}][diol]}{[(E)\text{-ester}][H_2O]^2} = \frac{[Z\text{-ester}][E\text{-acid}]}{[Z\text{-acid}][E\text{-ester}]} \quad (3)$$

Determination of T1 relaxation times

Peak	T1	Standard deviation
A	1.92	0.003
B	1.79	0.003
C	0.71	0.008
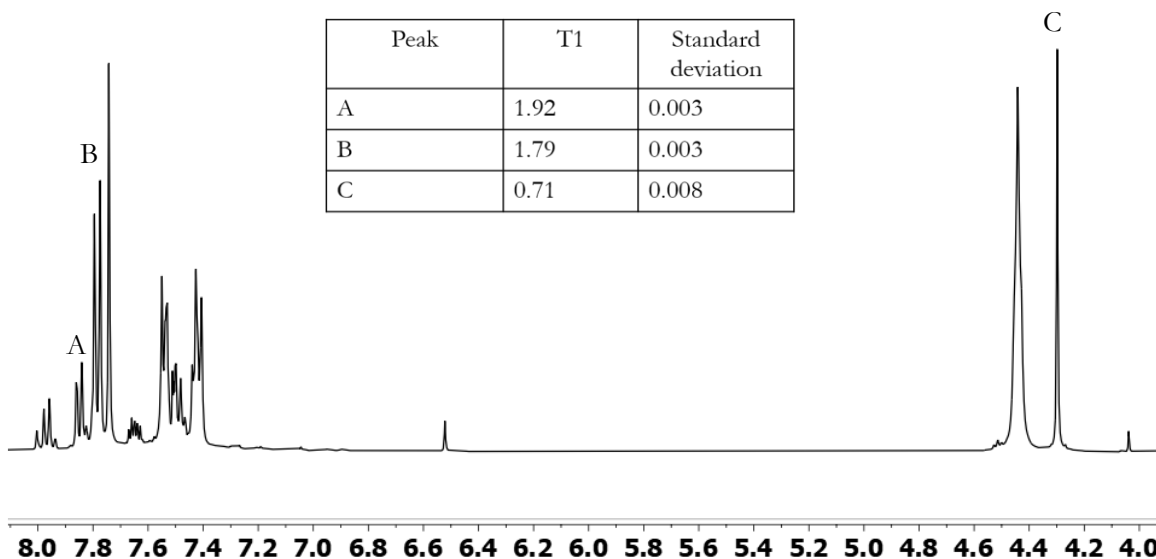
Figure 27. ^{1}H NMR and T1 (in seconds) of compound (E)-1 with EG in DMSO-d$_6$ at 25 °C.

Peak	T1	Standard deviation
A	1.89	0.007
B	1.77	0.002
C	2.68	0.003
D	0.94	0.001
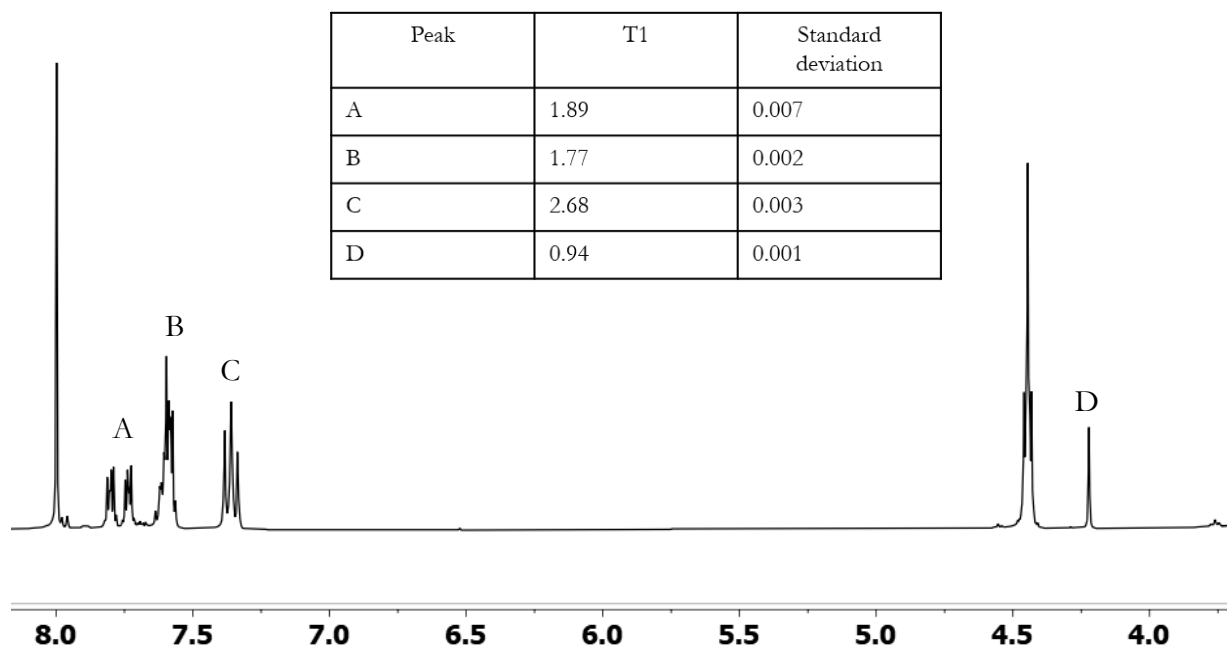
Figure 28. ^{1}H NMR and T1 (in seconds) of compound (E)-2 with EG in DMSO-d$_6$ at 25 °C.

Peak	T1	Standard deviation
A	2.17	0.003
B	1.58	0.004
C	1.912	0.006
D	1.063	0.007
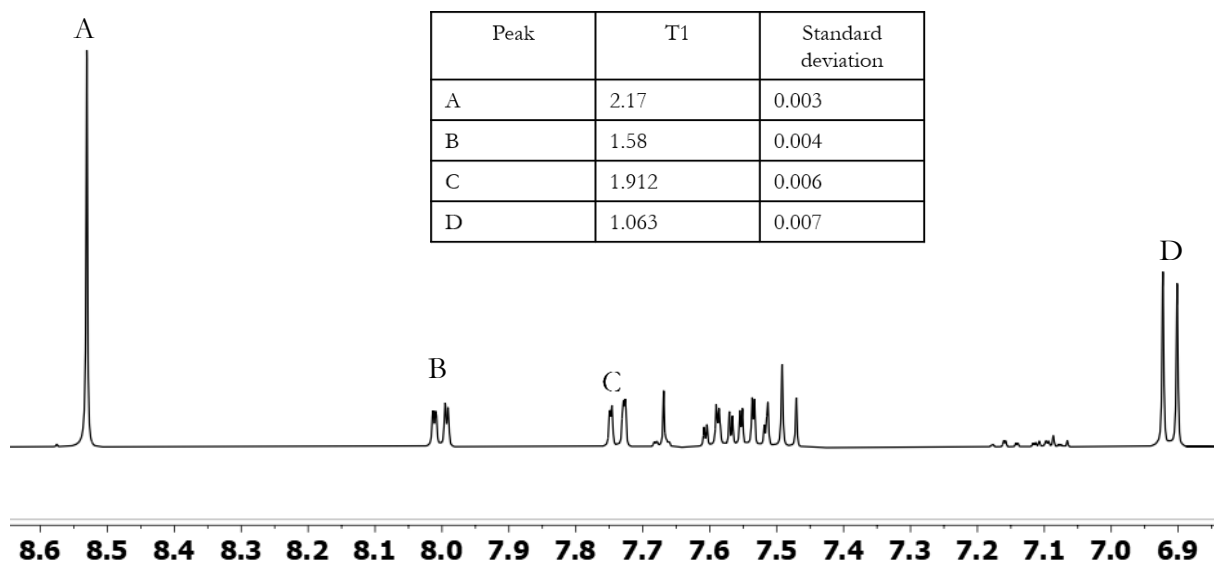
Figure 29. ^{1}H NMR and T1 (in seconds) of compound (E)-3 with EG in DMSO-d$_6$ at 25 °C.
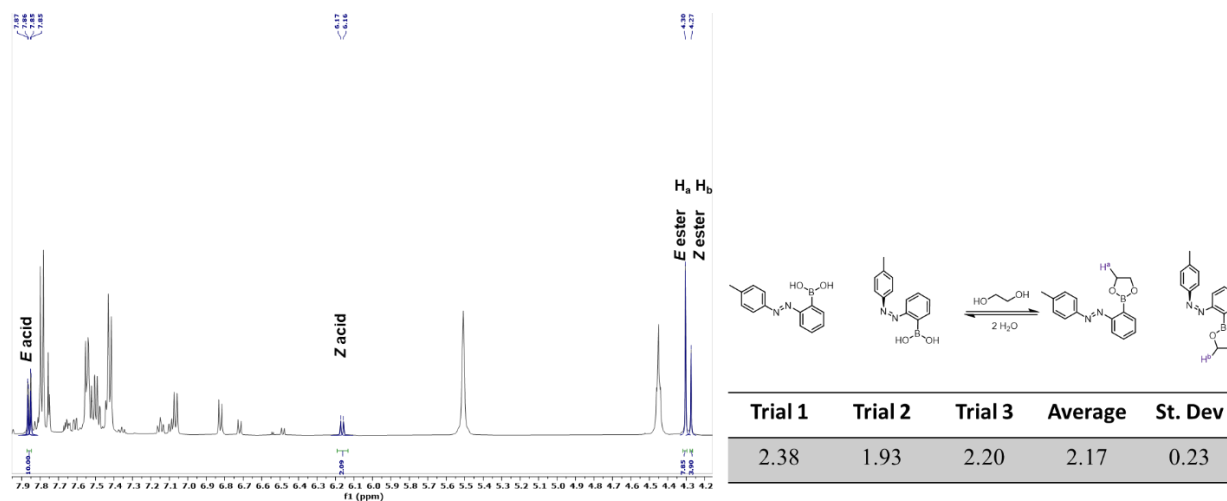
Figure 30. Competition experiments to determine K_{rel} of compound 3 with EG in DMSO-d$_6$ at 25 °C. No additional D$_2$O was added to the experiment and protons were integrated using GSD.
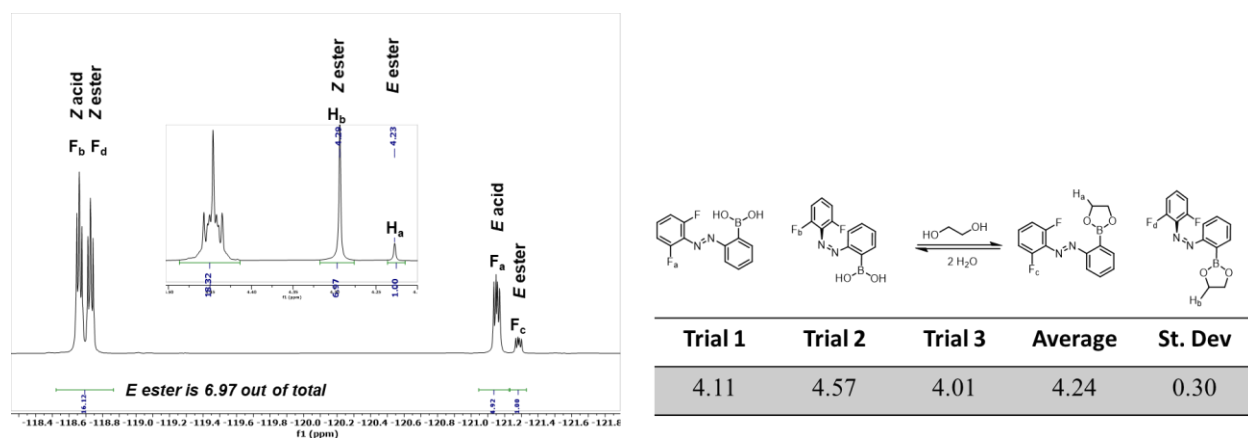
Figure 31. Competition experiments to determine K_{rel} of compound 2 with EG in DMSO-d$_6$ at 25 °C.

No additional D$_2$O was added to the experiment. Protons were integrated using GSD and fluorine signals were integrated with the area under the curve. As the *Z* acid and ester are not baseline resolved by ^{19}F NMR, ^{1}H NMR was employed to determine the ratio of bound *Z* to bound *E*. Using this, the amount of *Z* ester in the ^{19}F NMR can be deduced.
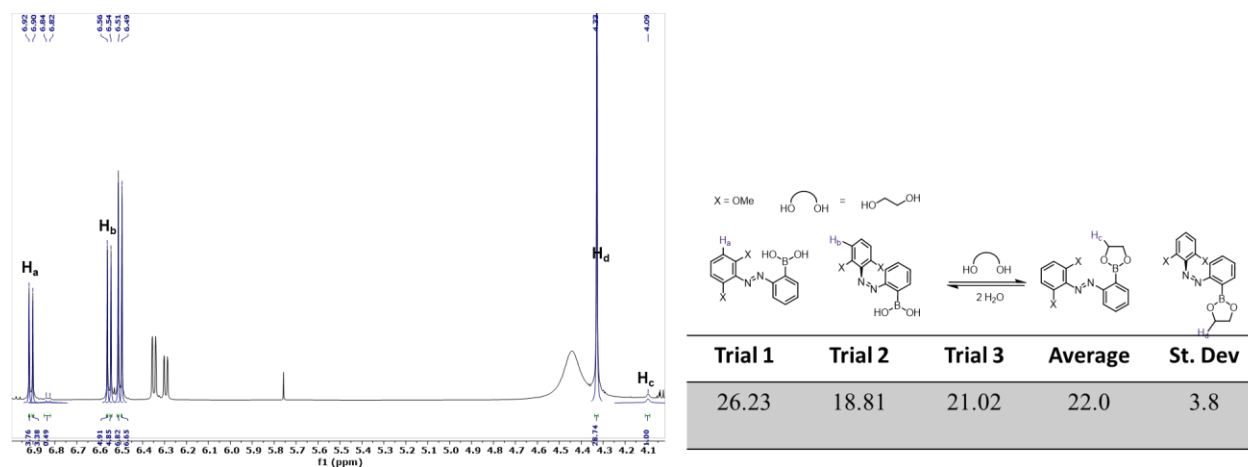
Figure 32. Competition experiments to determine K_{rel} of compound 3 with EG in DMSO-d_6 at 25 °C. X = OMe. Aromatic doublets, H_a and H_b, and aliphatic singlets H_d and H_c were integrated with GSD.

Trial 1	Trial 2	Trial 3	Average	St. Dev
26.23	18.81	21.02	22.0	3.8
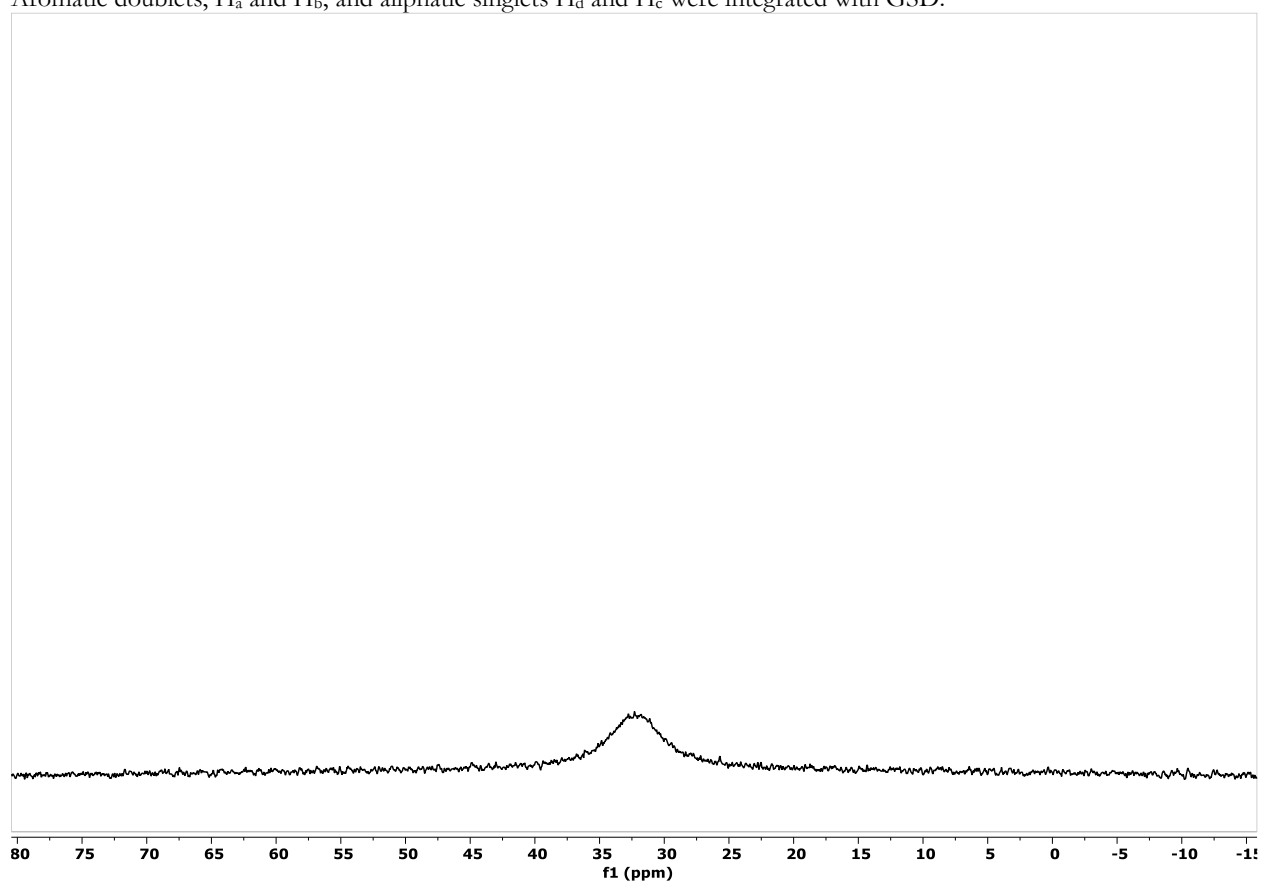
Figure 33. ^{11}B NMR spectrum of competition experiment between (E)-3 and (Z)-3 with EG in DMSO-d_6 at 25 °C.
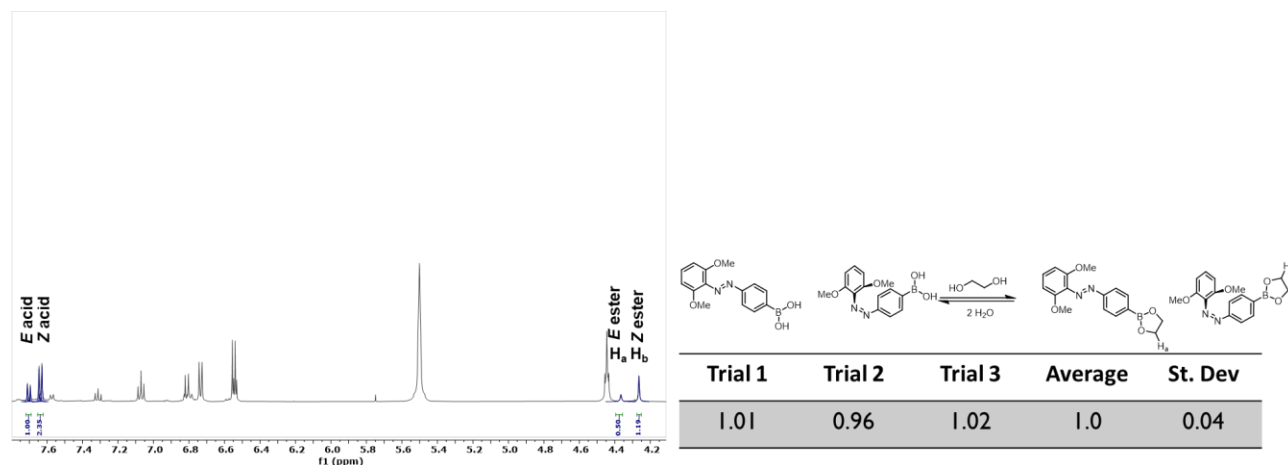
Figure 34. Competition experiment between (*E*)-**4** and (*Z*)-**4** with EG in DMSO-d_6 at 25 °C. 2 μL of D_2O was added to the experiment and protons were integrated using GSD.
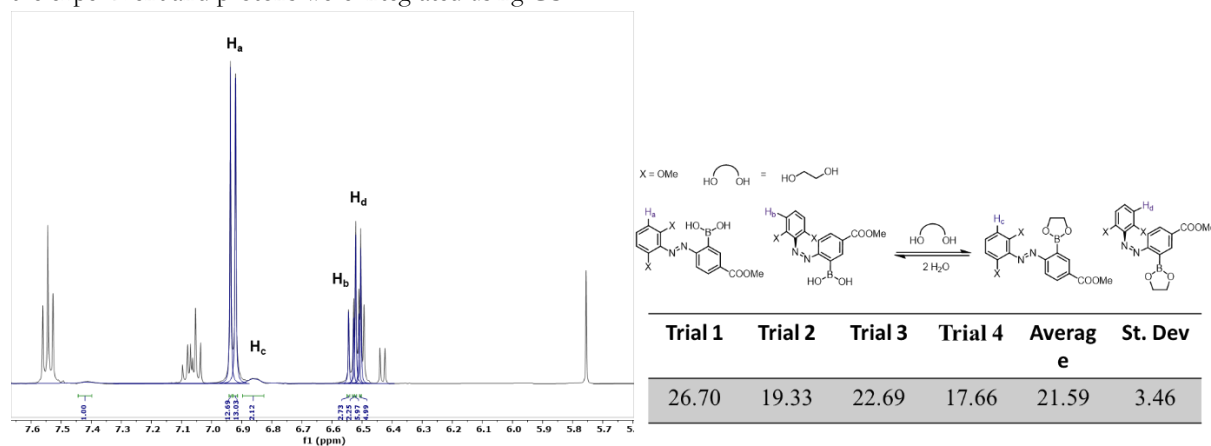
Figure 35. Competition experiment between (E)-3' and (Z)-3' with EG in DMSO-d_6 at 25 °C.

No additional D_2O was added to the experiment and protons were integrated using GSD, except for the broad peak corresponding to the E-ester, likely indicating fast exchange with diol. This peak was integrated with the sum function, and an additional trial was performed.
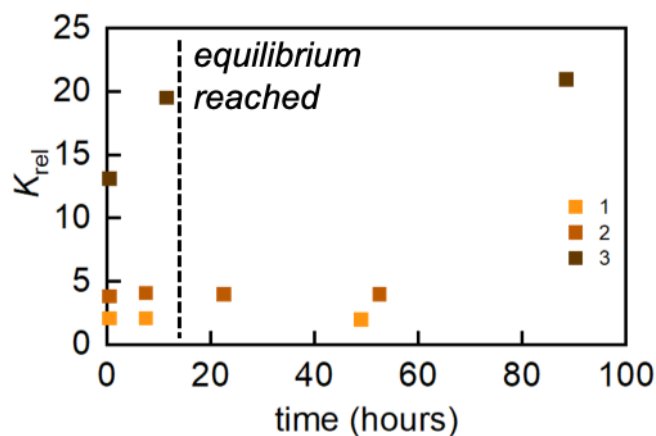
Figure 36. K_{rel} vs time for competition experiment for 1-3 with EG in DMSO-d_6 at 25 °C.
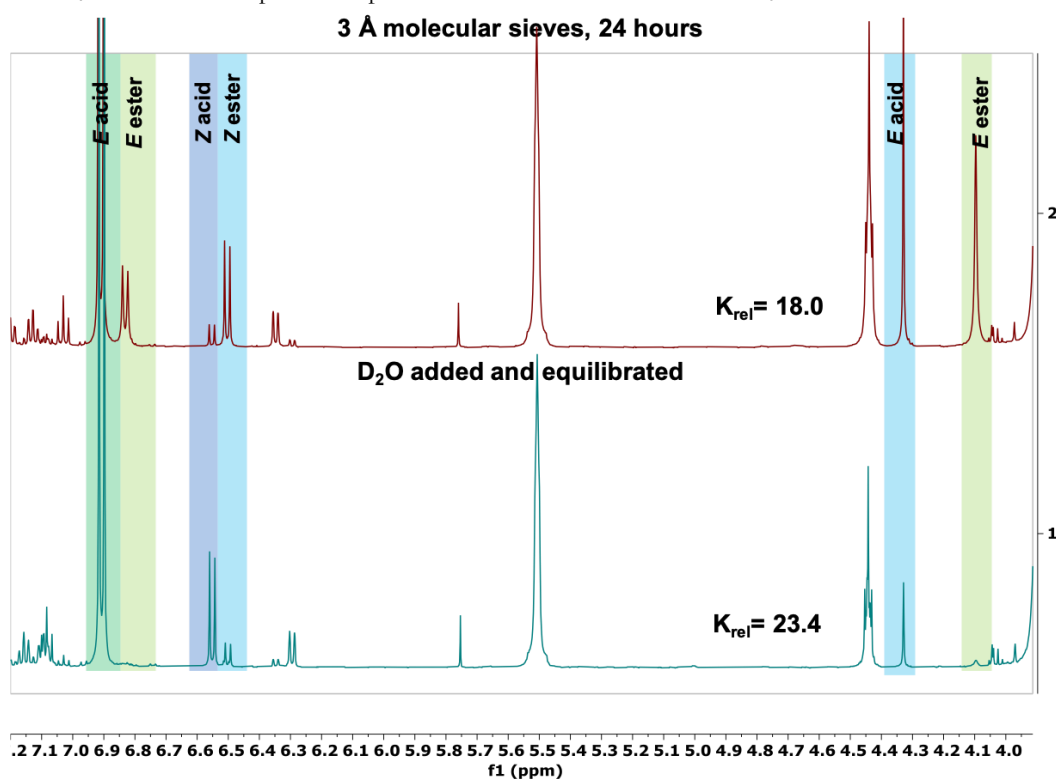
Figure 37. (top) ^{1}H NMR spectrum of the competition experiment of **3** in DMSO-d_6 at 25 °C after drying with sieves overnight. (bottom) ^{1}H NMR spectrum of the same mixture after addition of 1 μL of D_2O to perturb the equilibrium. After perturbation of the stationary state and allowing the system to equilibrate for 24 hours at 25 °C, K_{rel} returns to the average value.

Determination of equilibrium constants

To determine the absolute K_{eq} of **1-3**, we first prepared triplicate samples of pure E **1-3** at 20 mM in 480 μL DMSO-d_6, to which EG was added (2 equivalents in 20 μL of DMSO-d_6). These reactions were set to equilibrate for 48 hours at 25 °C (based on previous experiments) and then the concentration of E acid, E ester, diol, and H_2O were quantified by ^{1}H NMR at 25 °C. K_{eq} was calculated using equation 1. The average values and standard

deviation for this method are reported below in Table 1. Next, we irradiated these samples with either 365 nm (for compound **1**) or 525 nm light (for **2** and **3**). We again determined K_{eq} for the E isomer and the Z isomer using equation 2, which are plotted in Table S2.

	average K_{eq} (M)
(*E*)-**1**	0.528 ± 0.059
(*E*)-**2**	0.235 ± 0.038
(*E*)-**3**	0.052 ± 0.009

Table 1. Equilibrium constants (K_{eq}) of (E)-1 through (E)-3 determined in DMSO-d_6 at 25 °C using samples that had not been irradiated.

	average K_{eq} (M)
(*E*)-**1**	0.542 ± 0.047
(*E*)-**2**	0.284 ± 0.045
(*E*)-**3**	0.057 ± 0.012
(*Z*)-**1**	1.262 ± 0.064
(*Z*)-**2**	1.139 ± 0.157
(Z)-**3**	1.153 ± 0.254

Table 2. Equilibrium constants (K_{eq}) of (E)-1 through (E)-3 and (Z)-1 through (Z)-3 determined in DMSO-d_6 at 25 °C using samples that had been irradiated.

	Trial 1	Trial 2	Trial 3	Average	St. Dev
	2.13	2.07	2.10	2.10	0.03
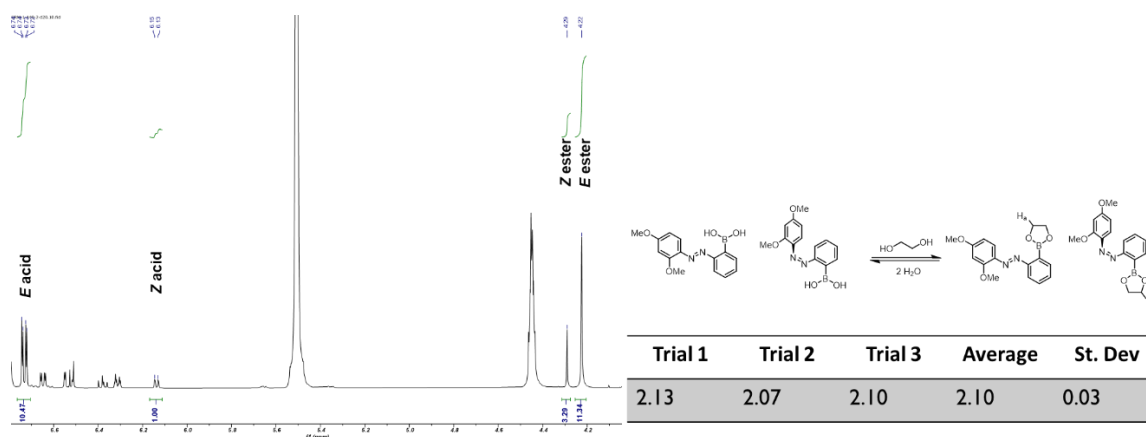
Figure 38. Competition experiment between (E)-5 and (Z)-5 with EG in DMSO-d_6 at 25 °C.
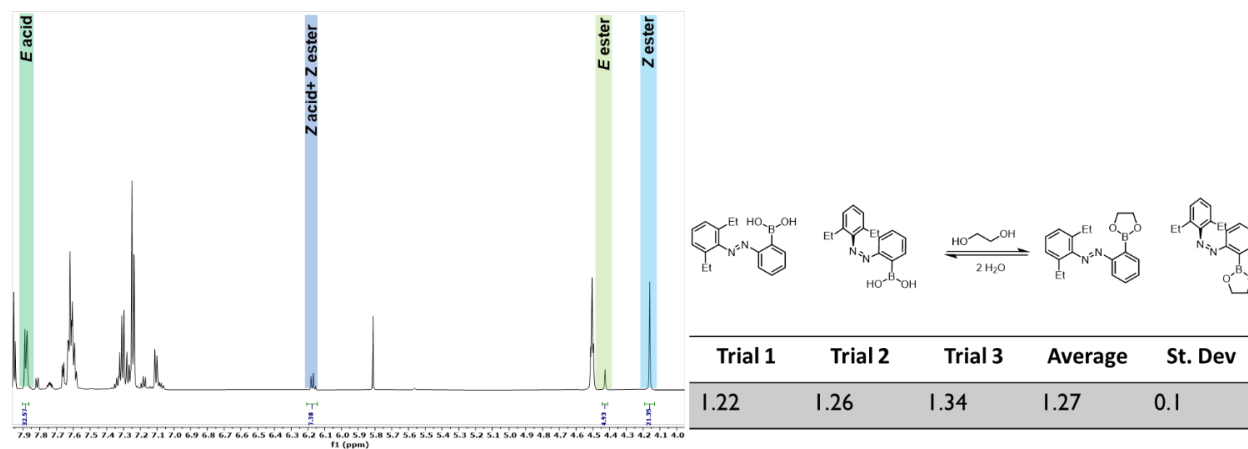
Figure 39. Competition experiment between (E)-6 and (Z)-6 with EG in DMSO-d$_6$ at 25 °C with a delay time of 1s. The amount of Z acid could be determined by subtracting the amount of Z ester from the overlapped peaks. We performed an additional experiment with a 10s delay time, which yielded a similar K$_{rel}$ value of 1.36.
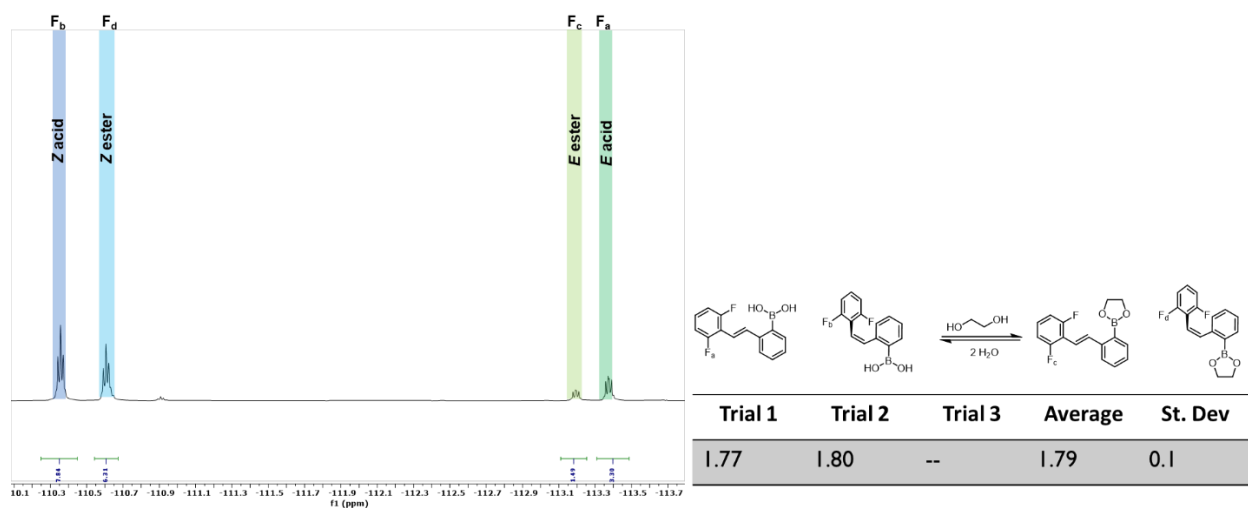
Figure 40. Competition experiment between (E)-7 and (Z)-7 with EG in DMSO-d$_6$ at 25 °C. The integrations were performed with the area (sum) under the curves. The Z isomer was accessed by irradiation of the solution with 305 nm light for 20 minutes.
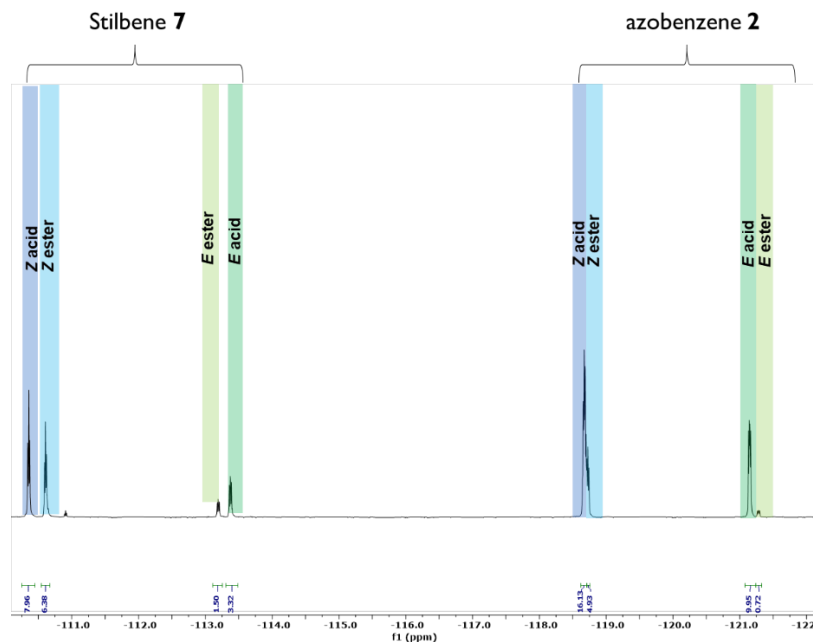
Figure 41. Competition experiment between 2 and 7 with EG in DMSO-d$_6$ at 25 °C.
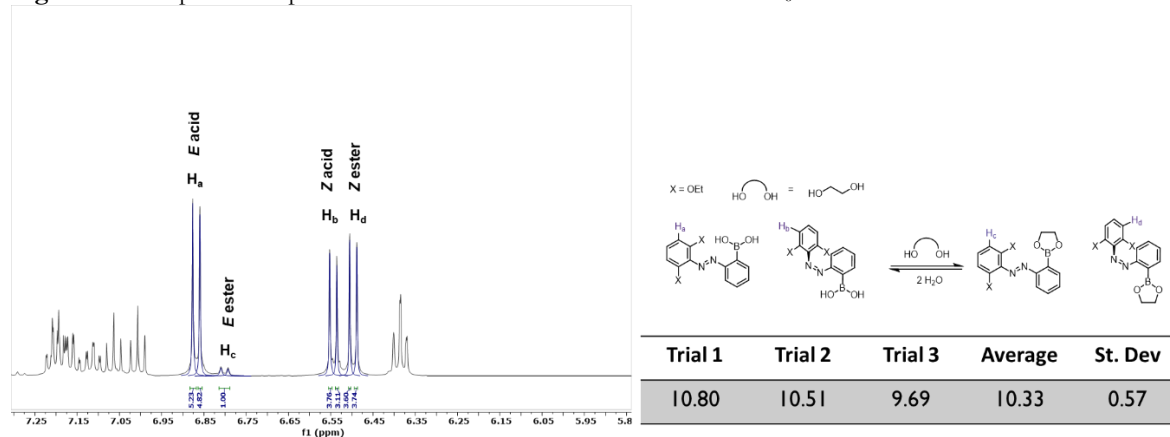
Figure 42. Competition experiment between (E)-6' and (Z)-6' with EG in DMSO-d$_6$ at 25 °C. Protons were integrated using GSD highlighted in blue.

Wavelength-dependent diol binding with compound 3 and ethylene glycol

50 μmol of compound **3** was dissolved into 5 mL of DMSO-d_6 and evenly divided into 10 samples. Two samples were left in the dark while two were irradiated with blue (470 nm), green (525 nm), red (626 nm), or yellow (590 nm) LEDs for 8 hours at 25 °C. Then, 1 equivalent of ethylene glycol (EG) in 10 μL of DMSO-d_6 was added to each sample and the reaction was equilibrated at 25 °C. After reaching equilibrium, ¹H NMR spectra were recorded to determine how much EG was bound, relative to the total amount of EG in solution. The % Z

isomer and % diol bound are an average of the two experiments, as well as the K_{rel} values reported in Figure 8a.

irradiation color	% Z isomer	% diol bound
None (Δ)	0	2.98
blue	33.8	26.1
green	64.1	42.3
yellow	69.5	43.4
red	56.7	35.6
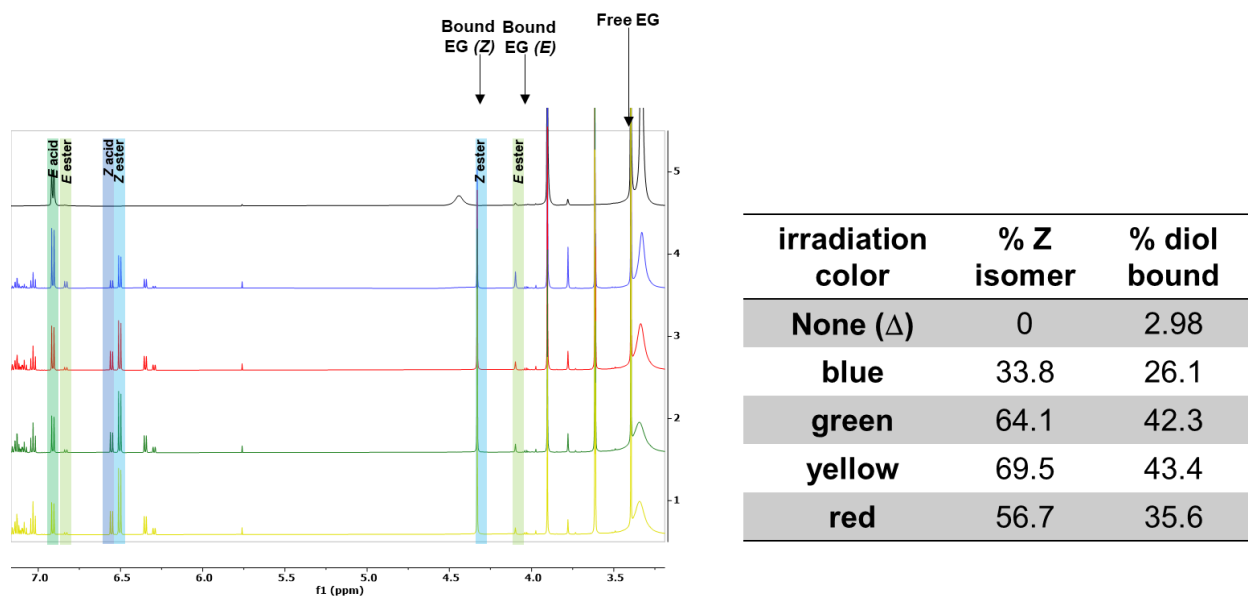
Figure 43. (left) ^{1}H NMR spectra highlighting bound and unbound (E)- and (Z)-3 with EG after irradiation with no light (black trace), blue light (blue trace), red light (red trace), green light (green trace), and yellow light (yellow trace). (right) Table of % Z isomer achieved with different wavelengths of irradiation and the % diol bound.

Irradiation time-dependent diol binding with compound 3 and ethylene glycol

40 μmol of compound **3** was dissolved into 2000 μL of DMSO-d$_6$, along with 1 μL of cyclooctadiene as an internal standard, and divided into four vials. One vial was left in the dark, while the other vials were irradiated with either 0.5, 2, or 10 minutes of green light. After the designated irradiation time, 1 equivalent of EG was added to each vial. After equilibrating for 12 hours, a ^{1}H NMR spectrum was recorded of each sample and the ratio of bound: total ethylene glycol was recorded.
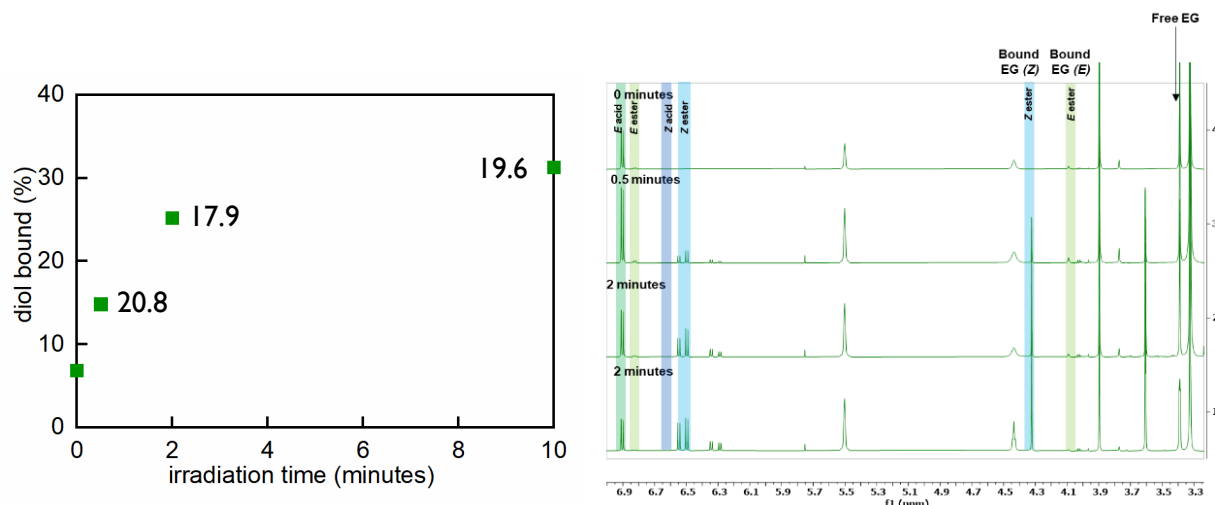
Figure 44. (left): % Diol bound vs. irradiation time with green light (minutes). The numbers represent the K_{rel} value measured for each system after equilibration. Right: [1]H Spectra highlighting bound and unbound (E)- and (Z)-3 with EG after irradiation with different intervals of green light.

Binding experiments with compound 3 and various diols

30 % mol of (E)-**3** was dissolved into 1500 uL of DMSO-d_6 and divided evenly among three vials. Each vial was irradiated for 30 minutes with green LEDs at 25°C to generate a mixture of the E and Z isomer, to which 2 equivalents of the relevant diol was added. The reaction was left to equilibrate for 24–48 hours; upon confirming the reaction was at equilibrium, spectra were recorded in triplicate. The specific details for equilibration time, including K_{rel} values for additional timepoints, are listed under the individual experiments.

Trial 1	Trial 2	Trial 3	Average	St. Dev
14.34	15.73	13.14	14.4	1.30
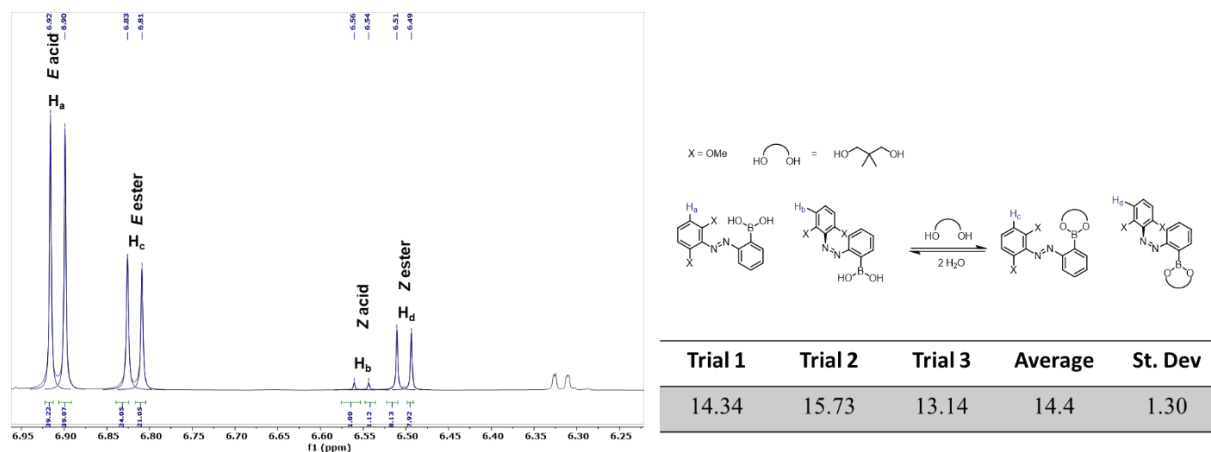
Figure 45. Competition experiment between (E)-3 and (Z)-3 with neopentyl glycol (8) in DMSO-d$_6$ at 25 °C. Protons were integrated using GSD highlighted in blue. K_{rel} was recorded after 48 hours, and, and additional scans at 24 hours (K_{rel}=14.0) and 96 hours (K_{rel}= 14.9) confirmed the system was at equilibrium.
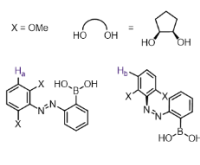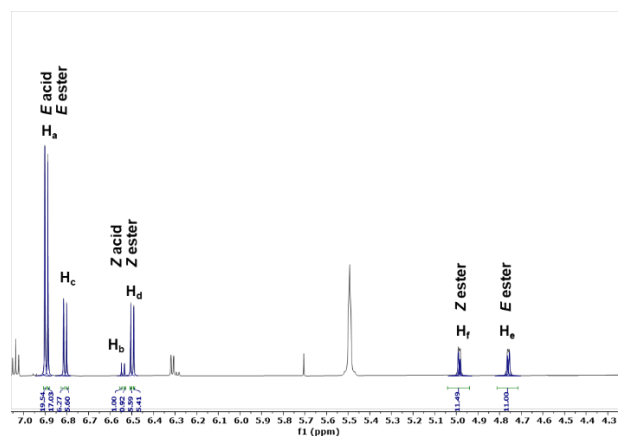
Figure 46. Competition experiment between (E)-3 and (Z)-3 with cis-1,2-cyclopentanediol (9) in DMSO-d_6 at 25 °C. Protons were integrated using GSD highlighted in blue. K_{rel} was recorded after 48 hours, and additional scans at 24 hours (K_{rel}=15.1) and 96 hours (K_{rel}= 15.3) confirmed the system was at equilibrium.
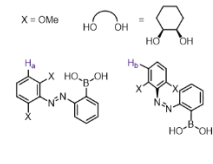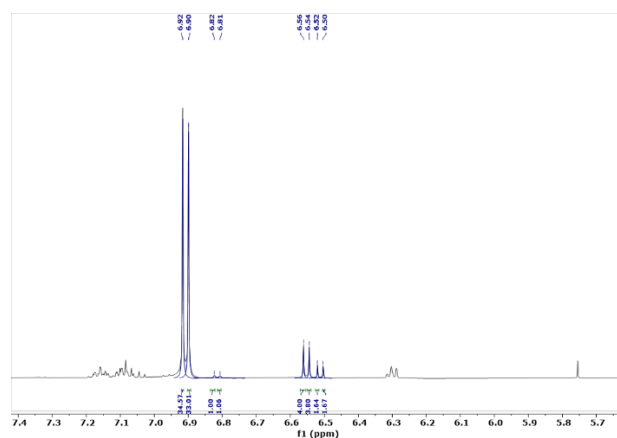
Figure 47. Competition experiment between (E)-3 and (Z)-3 with cis-1,2-cyclohexanediol (10) in DMSO-d_6 at 25 °C. Protons were integrated using GSD highlighted in blue. K_{rel} was recorded after 48 hours, and again at 72 hours (K_{rel}= 13.9), confirming the system was at equilibrium.
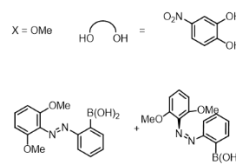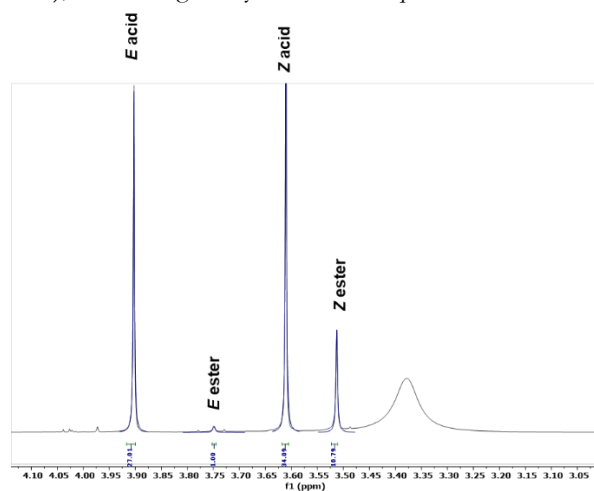
Figure 48. Competition experiment between (E)-3 and (Z)-3 with 4-nitrocatechol (11) in DMSO-d_6 at 25 °C. Protons were integrated using GSD highlighted in blue. As the ester was prone to hydrolysis, the nitrocatechol was dried in a vacuum oven prior to the experiment. K_{rel} was recorded after 24 hours, and again at 48 hours (K_{rel}= 9.13), confirming the system was at equilibrium.
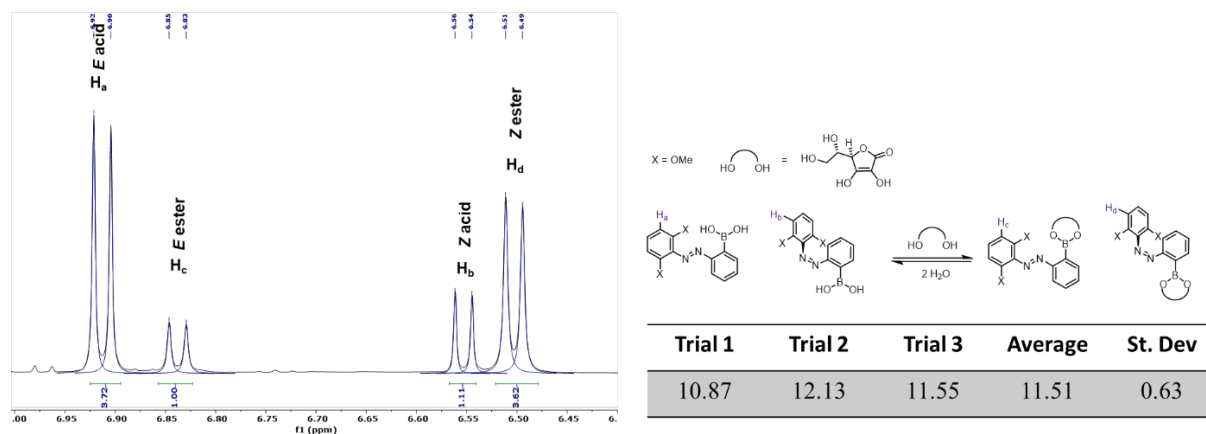
Figure 49. Competition experiment between (E)-3 and (Z)-3 with L-ascorbic acid (12) in DMSO-d_6 at 25 °C. Protons were integrated using GSD highlighted in blue. K_{rel} was recorded after 24 hours, and another scan at 20 hours (K_{rel}= 10.9) confirmed the system was at equilibrium. We observed small new peaks around 6.7 that increased over the course of multiple days, which we hypothesize is the reduction of the azobenzene by ascorbic acid, a known reductant.
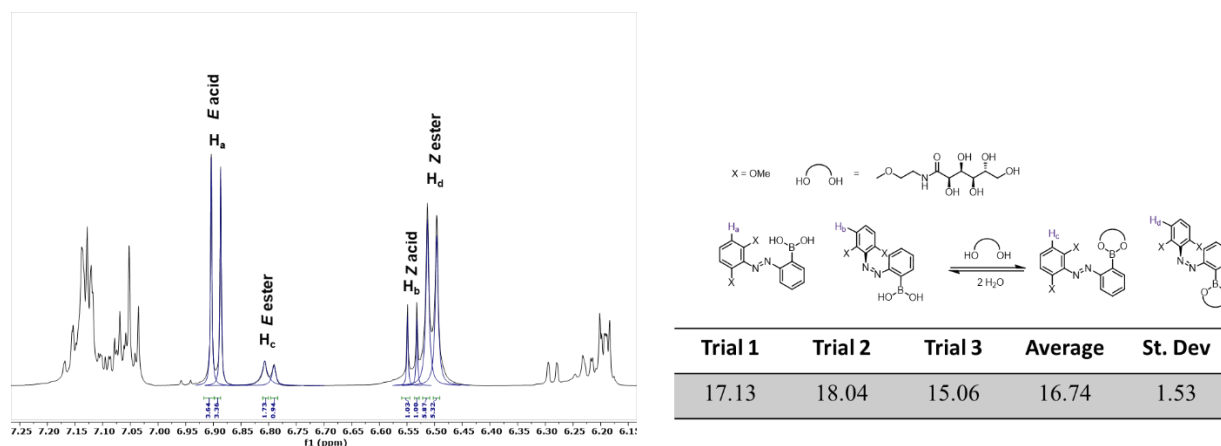
Figure 50. Competition experiment between (E)-3 and (Z)-3 with gluconolactone derivative (13) in DMSO-d_6 at 25 °C. Protons were integrated using GSD highlighted in blue. K_{rel} was recorded after 48 hours, and another scan at 24 hours (K_{rel}= 14.7) and 96 hours (K_{rel}= 19.3) confirmed the system was at equilibrium.
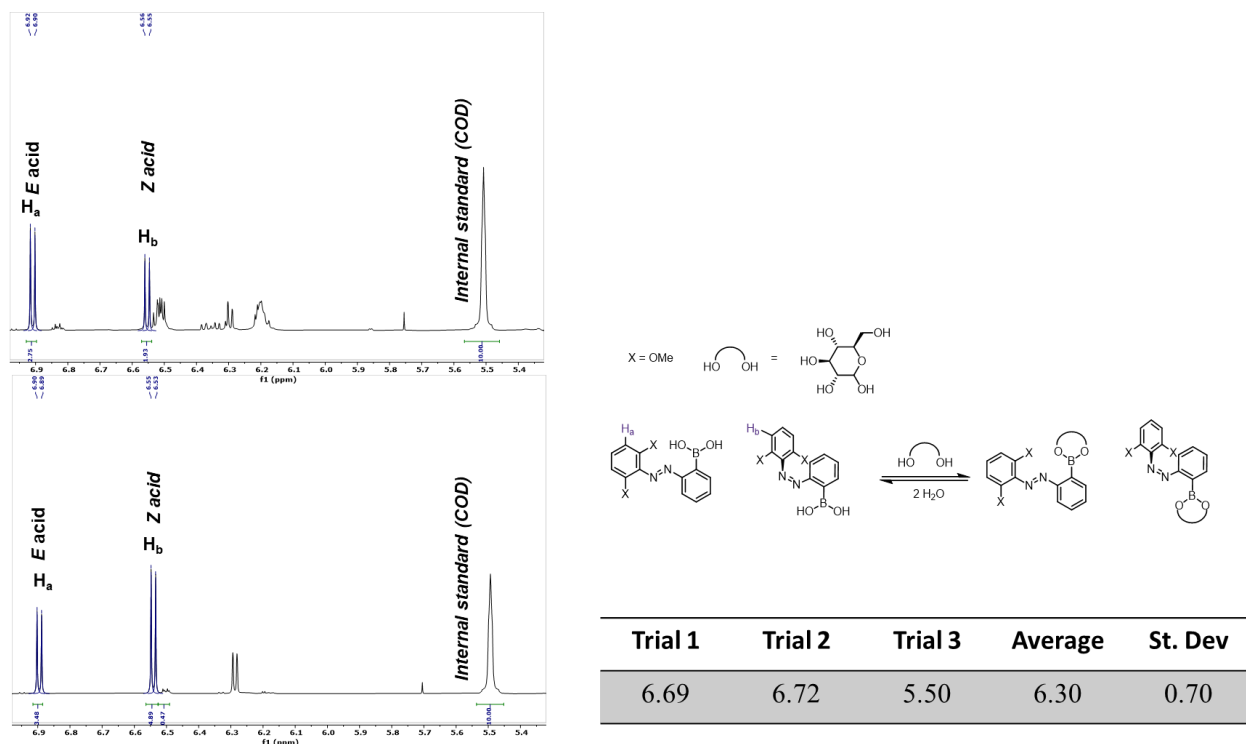
Figure 51. Competition experiment between (E)-3 and (Z)-3 with glucose (14) in DMSO-d$_6$ at 25 °C. Protons were integrated using GSD highlighted in blue. K$_{rel}$ was determined after 72 hours. An identical experiment that was allowed to equilibrate for 24 hours yielded similar results, with K$_{rel}$= 7.05, indicating the systems are at equilibrium.

NOTE: Competition experiments with glucose were complicated to analyze due to multiple binding modes of glucose which was evident by ^{1}H NMR. To account for these, we let the experiments equilibrate and determined the amount of unbound boronic acid relative to a cyclooctadiene internal standard. Afterwards, excess D$_2$O was added to the experiment to hydrolyze all the boronic ester. We then compared the integration of the boronic acids to the internal standard to determine how much boronic acid was consumed prior to hydrolysis. The ^{1}H NMR shows the peaks that were used in the integration as the unbound E or Z azobenzene boronic acid and the COD internal standard.
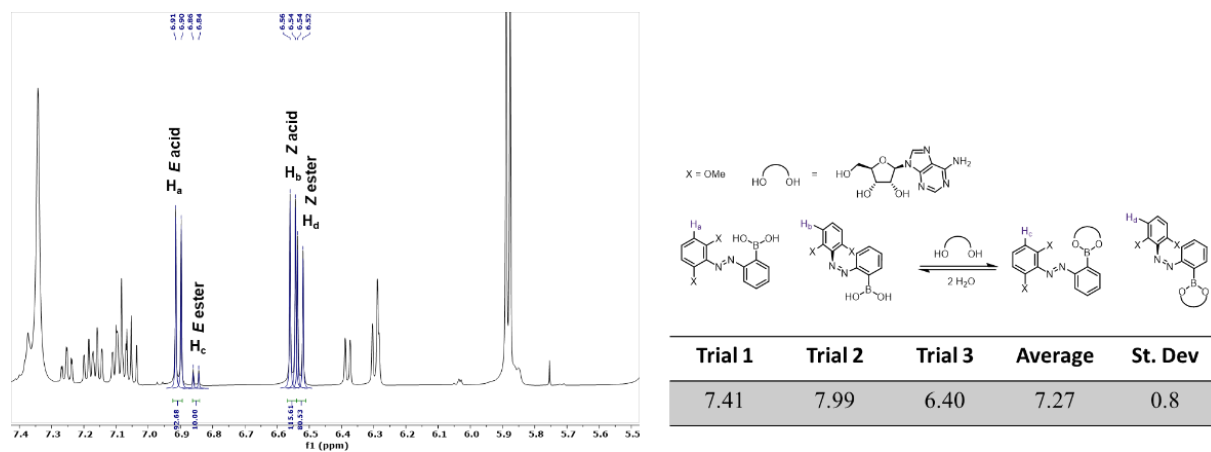
Figure 52. Competition experiment between (E)-3 and (Z)-3 with adenosine (15) in DMSO-d$_6$ at 25 °C. Protons were integrated using GSD highlighted in blue. K$_{rel}$ was determined after 48 hours, and another scan at 72 hours (K$_{rel}$= 7.9) and 96 hours (K$_{rel}$= 7.2) confirmed the system was at equilibrium.
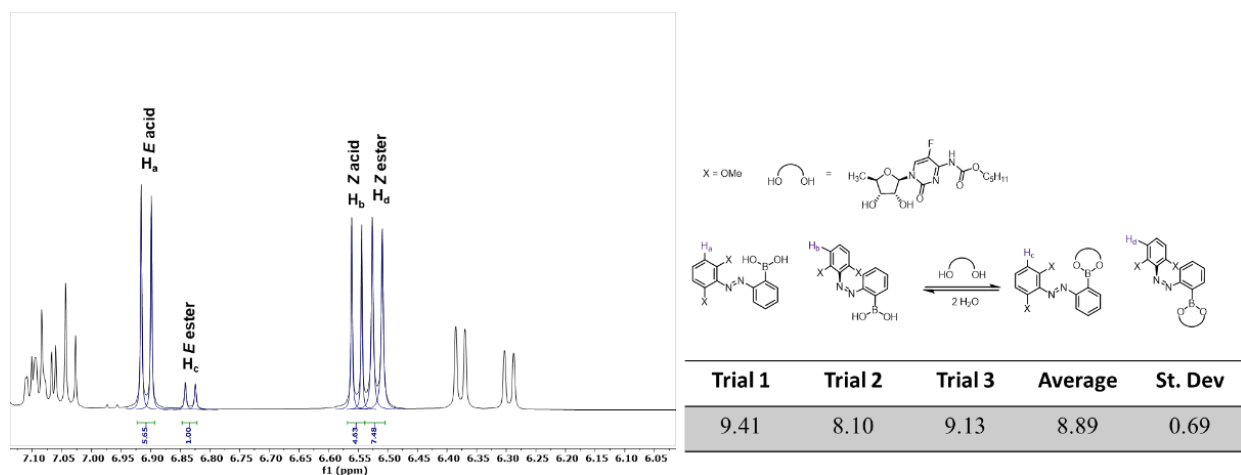
Figure 53. Competition experiment between (*E*)-**3** and (*Z*)-**3** with capecitabine (**16**) in DMSO-*d$_6$* at 25 °C. Protons were integrated using GSD highlighted in blue. *K*$_{rel}$ was determined after 24 hours, and another scan at 72 hours (*K*$_{rel}$= 7.98) confirmed the system was at equilibrium.
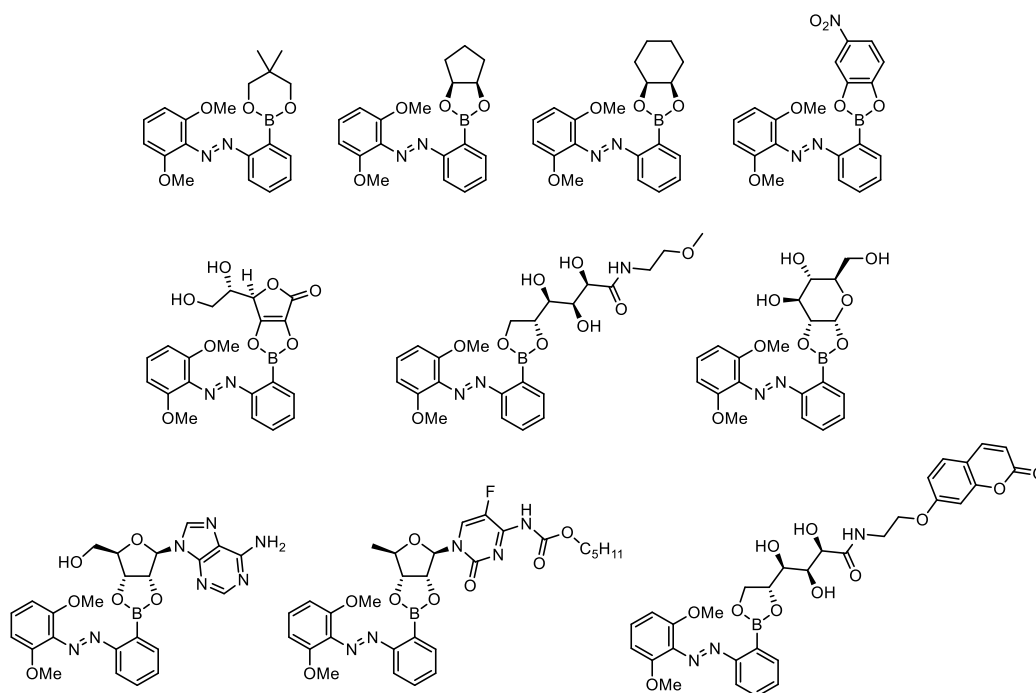
Figure 54. Proposed structures for the esters of the condensation of compound 3 with 8–17. Glucose and ascorbic acid binding structures are predicted based on literature precedence.[5,6]

Computational calculation details

Calculations were performed on the Northwestern University's 'Quest' computational cluster. Preliminary optimizations were performed using the restricted Hartree-Fock theory with the def2-SVP basis set, the input files were generated by Avogadro, and were then further optimized using B3LYP hybrid functional and the 6-31+G** basis set as implemented in Orca.[7] Frequency scans, which were employed to compute the relative energy of the rotamers, were performed with a 6-31+G** basis set and B3LYP method. Geometry scans were performed with a 6-31+G** basis set and B3LYP method from 0–180° in 9.5° intervals.
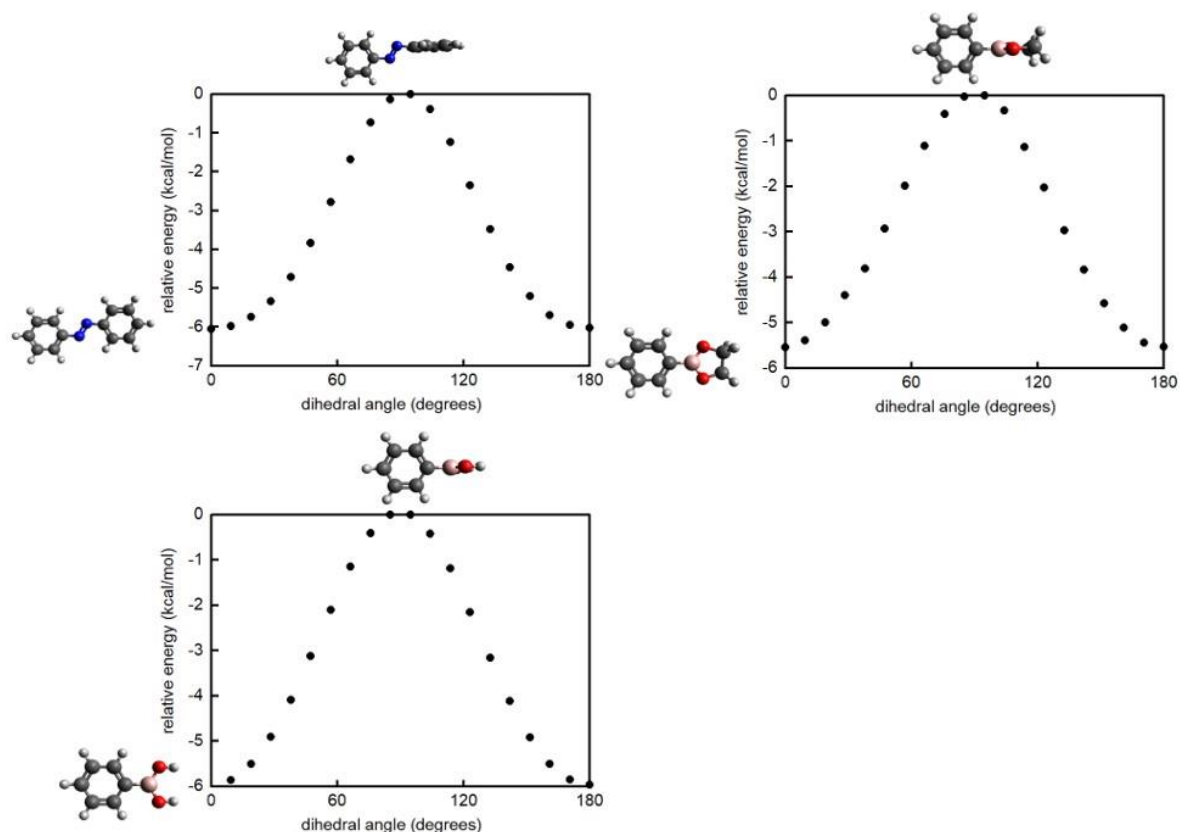
Figure 55. (top left) Geometry scan of azobenzene dihedral angle Φ from 0 to 180° in 9.5° intervals. (top right) Geometry scans of phenyl boronic acid ethylene glycol ester. Dihedral angle Φ (bottom right) from 0 to 180° in 9.5° intervals. (bottom left) Geometry scan of phenyl boronic acid from dihedral angle Φ (bottom right) from 0 to 180° in 9.5° intervals. The optimized structures are depicted for the compounds at 0° and 85°.
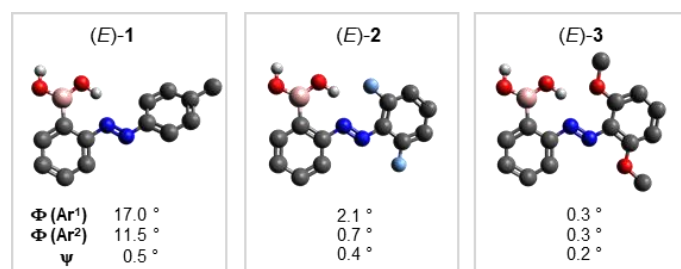
Figure 56. Geometry-optimized structures of unbound (E)-1 through (E)-3.
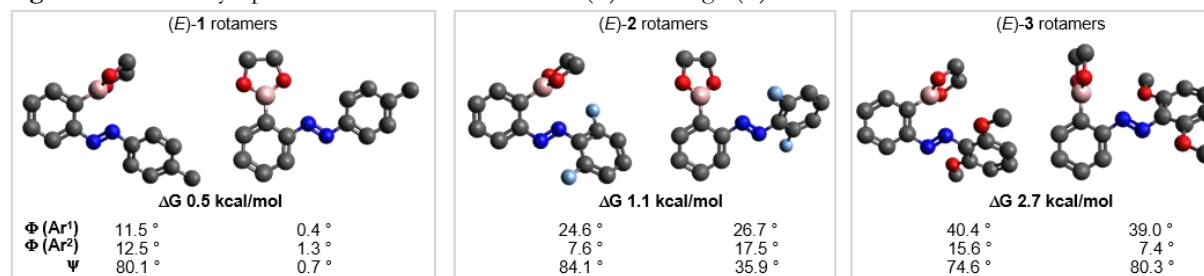
Figure 57. Geometry-optimized rotamers of (E)-1 through (E)-3 bound with EG. The most stable rotamers (rotamer 1) are the left structures in each box, and the differences in energy between the rotamers are reported below (ΔG). The less stable isomers ("rotamer 2", shown on the right side of each box) follow a similar trend to Figure 6, with the smaller conformation changes upon binding occurring for compound 1 and the largest changes for compound 3.
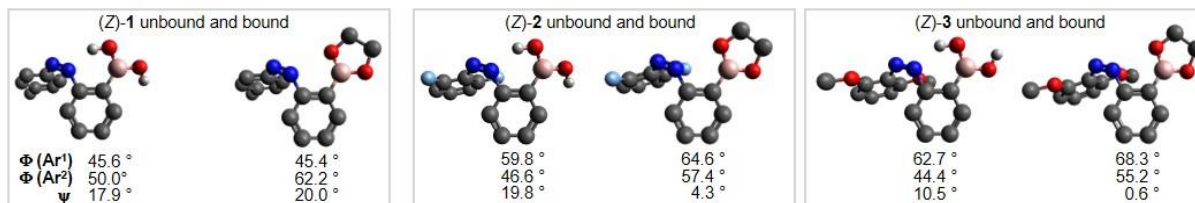
Figure 58. Geometry-optimized rotamers and relative energies of (Z)-1 through (Z)-3.
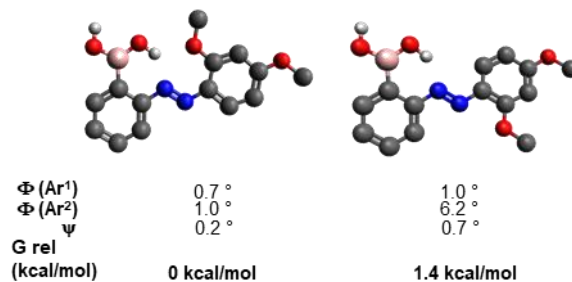
Figure 59. Geometry-optimized rotamers and relative energies of unbound (E)-5.
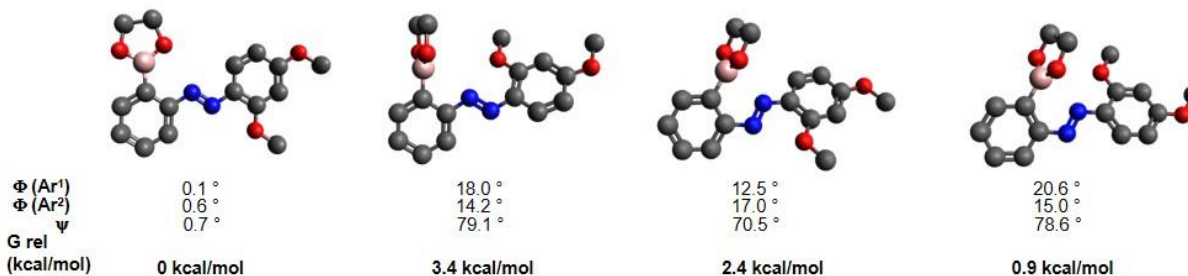
Figure 60. Geometry-optimized rotamers and relative energies of bound (*E*)-**5.**
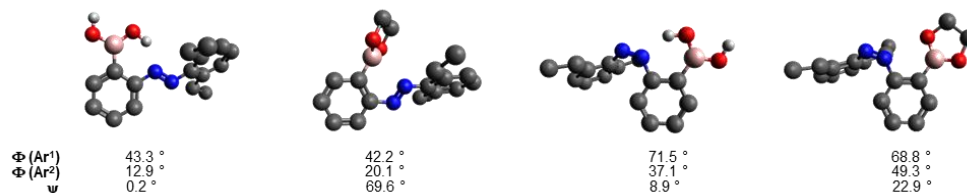
Figure 61. Geometry optimized structures of (E)-6 and (Z)-6.
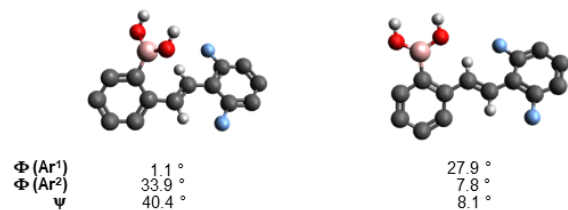
Figure 62. Geometry optimized rotamers of (E)-7 showing the absence of any intramolecular hydrogen bond.

Φ (Ar¹)	24.0 °
Φ (Ar²)	16.6 °
ψ	5.2 °

Φ (Ar¹)	36.2 °
Φ (Ar²)	19.0 °
ψ	72.8 °
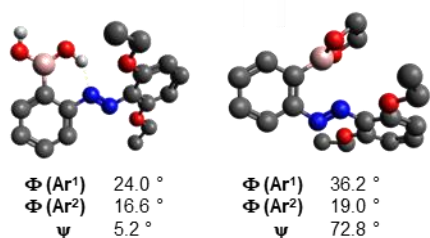
Figure 63. Geometry optimized structures of unbound and bound (E)-6'.

Computing ΔG^o of esterification for E isomers

To calculate the ΔG^o of esterification for compounds (*E*)-**1** through (*E*)-**3**, geometry optimization and frequency calculations for the boronic acids and esters, as well as ethylene glycol and water, were computed with the DMSO COSMO solvent model in Orca. $\Delta G°$ was calculated using the following equation:

$$\Delta G = (G_{\text{boronic ester}} + 2G_{\text{H2O}}) - (G_{\text{boronic acid}} + G_{\text{diol}}) \quad (4)$$

	energy in hartree						
	boronic acid	ethylene glycol	boronic ester	water		ΔG (hartree)	ΔG kcal/mol
(E)-1	-787.5007865	-230.1054329	-864.7994395	-76.4062		-0.005571	-3.4958025
(E)-2	-946.6590306	-230.1054329	-1023.958601	-76.4062		-0.006488	-4.07123883
(E)-3	-977.108483	-230.1054329	-1054.404117	-76.4062		-0.0025518	-1.60124195
(E)-6'	-1055.639417	-230.1054329	-1132.935536	-76.4062		-0.0030369	-1.90567357

Table 3. Calculated energies of (*E*)-**1** through (*E*)-**3** in their boronic acid and ester form, as well as the calculated energies of ethylene glycol and water. $\Delta G°$ were calculated using equation 4.

XYZ coordinates of ground state optimized geometries

(*E*)-**1** unbound

```
O  -6.0010460000  1.4416190000  4.4030960000

O  -4.2112380000  0.4830540000  3.1996130000

N  -7.3996820000  5.0027090000  3.6878310000

N  -6.8035700000  3.9096640000  3.4986180000

C  -11.6261420000  5.2849730000  7.5674580000

C  -8.8694630000  6.2413310000  5.0961940000

C  -9.8867480000  6.3383150000  6.0457850000

C  -10.5160090000  5.1907000000  6.5479580000

C  -10.0943130000  3.9357640000  6.0650170000

C  -9.0741280000  3.8238670000  5.1282730000

C  -8.4405940000  4.9850910000  4.6433430000
```

```
C  -5.6343830000  4.9873180000  1.5984840000
C  -4.6375580000  4.9378780000  0.6300550000
C  -3.7944410000  3.8209930000  0.5464040000
C  -3.9602700000  2.7575610000  1.4343570000
C  -4.9586240000  2.7694920000  2.4261290000
C  -5.7921520000  3.9144740000  2.4951060000
B  -5.0832560000  1.5262140000  3.3972150000
H  -6.5478110000  2.2548360000  4.3987000000
H  -4.3579020000 -0.2298930000  3.8350510000
H  -12.5527890000 4.8388650000  7.1867570000
H  -11.3649780000 4.7475340000  8.4871040000
H  -11.8376730000 6.3240200000  7.8337940000
H  -8.7813160000  2.8493280000  4.7535390000
H  -8.3854590000  7.1287250000  4.6995760000
H  -6.2997490000  5.8400430000  1.6753810000
H  -10.2000800000 7.3181560000  6.3967090000
H  -10.5839200000 3.0348040000  6.4273730000
H  -4.5177810000  5.7656790000 -0.0645800000
H  -3.3085480000  1.8912870000  1.3675320000
H  -3.0168070000  3.7812870000 -0.2122120000
```

(*E*)-1 bound rotamer 1

```
O  -0.3029680000  3.9273400000  1.3293140000
O   0.1651730000  3.5614400000 -0.8922940000
N  -2.5671660000  5.2277670000 -0.2136110000
N  -3.5928760000  4.5324730000  0.0027560000
C  -2.9874660000 10.9589840000 -0.1017030000
C   1.3426170000  4.1801630000 -0.3433630000
C   0.9180960000  4.6401040000  1.0718410000
C  -1.7618570000  8.8008030000 -0.6158130000
C  -1.6784040000  7.4100360000 -0.6293770000
C  -2.9061260000  9.4502770000 -0.1237590000
C  -3.9669560000  8.6574710000  0.3504190000
C  -3.8996860000  7.2667270000  0.3355900000
C  -2.7480190000  6.6317710000 -0.1596760000
```

C   -3.3595110000   3.1348850000   -0.0191960000

C   -2.0638170000   2.5678900000   -0.0058540000

C   -1.9757900000   1.1712020000   -0.0695970000

C   -3.1192610000   0.3623470000   -0.1267360000

C   -4.3898330000   0.9444520000   -0.1176750000

C   -4.5089680000   2.3329900000   -0.0598040000

B   -0.7615750000   3.4374360000   0.1224190000

H   -0.7977320000   6.9050080000   -1.0153700000

H   -4.7203740000   6.6622780000   0.7057750000

H   -2.1955200000 11.3906790000   0.5224850000

H   -2.8693450000 11.3776070000   -1.1084340000

H   -3.9482680000 11.3023630000   0.2930180000

H   -0.9293240000   9.3915890000   -0.9913520000

H   -4.8588960000   9.1429350000   0.7403990000

H   -3.0143460000 -0.7187750000   -0.1716010000

H   -5.2795470000   0.3223430000   -0.1570970000

H   -0.9965610000   0.6977000000   -0.0682570000

H   -5.4801840000   2.8191680000   -0.0568320000

H   1.6502170000   5.0089880000   -0.9890640000

H   2.1488590000   3.4369760000   -0.3182300000

H   0.7140730000   5.7170280000   1.1150220000

H   1.6507140000   4.3878140000   1.8445850000

(*E*)-1 bound rotamer 2

O   -2.5123990000   2.2349240000   -0.2084720000

O   -1.7095570000   4.3807760000   -0.2713990000

N   2.2860140000   5.1061920000   -0.0847050000

N   1.1835980000   4.4989050000   -0.1017240000

C   2.1951010000 10.8529810000   -0.1528350000

C   -3.6786650000   3.0737000000   -0.1777960000

C   -3.1342780000   4.4961450000   -0.4430180000

C   3.3923890000   7.2274890000   -0.0759530000

C   3.3931170000   8.6211160000   -0.0903430000

C   2.1887440000   9.3419300000   -0.1331300000

C   0.9817520000   8.6188260000   -0.1605510000

C 0.9652340000 7.2269740000 -0.1461260000

C 2.1806700000 6.5202630000 -0.1030060000

C 1.2612590000 3.0817310000 -0.0826140000

C 2.4827350000 2.3851760000 -0.0205880000

C 2.4937520000 0.9948260000 0.0018380000

C 1.2868870000 0.2829630000 -0.0356460000

C 0.0776880000 0.9750390000 -0.0959080000

C 0.0288240000 2.3842590000 -0.1224850000

B -1.3899640000 3.0449200000 -0.1999480000

H 2.7219810000 11.2602500000 0.7187870000

H 2.7058980000 11.2363460000 -1.0450440000

H 1.1789660000 11.2573600000 -0.1499090000

H -4.1509000000 2.9817740000 0.8077750000

H -4.3859610000 2.7343560000 -0.9404860000

H -3.5193510000 5.2411860000 0.2594980000

H -3.3350800000 4.8376700000 -1.4653320000

H -0.8560800000 0.4215980000 -0.1235590000

H 3.4400040000 0.4615900000 0.0506350000

H 1.2924520000 -0.8039540000 -0.0164650000

H 3.4050810000 2.9543750000 0.0107430000

H 0.0345000000 6.6689900000 -0.1681470000

H 0.0399290000 9.1626620000 -0.1941770000

H 4.3392800000 9.1577510000 -0.0676670000

H 4.3211700000 6.6649900000 -0.0427130000

(*E*)-2 unbound

F 1.3736400000 8.5415580000 0.3027720000

F -3.3702760000 8.8567290000 0.1149910000

O -4.7387200000 6.2742120000 -0.2651310000

O -5.4734140000 4.0512600000 -0.4908650000

N -0.9023440000 7.1840140000 0.1199340000

N -1.9716090000 6.5249990000 -0.0054020000

C 0.2383740000 9.2663450000 0.2964590000

C 0.3448640000 10.6467490000 0.3858590000

C -0.8243780000 11.4100430000 0.3809680000

C -2.0742920000 10.7918910000 0.2882040000

C -2.1412230000 9.4090530000 0.1988040000

C -0.9949180000 8.5808100000 0.1981660000

C -1.8024110000 5.1138460000 -0.0774820000

C -0.5348030000 4.5042520000 0.0011860000

C -0.4274580000 3.1211270000 -0.0778780000

C -1.5786410000 2.3358910000 -0.2354960000

C -2.8314100000 2.9449560000 -0.3120060000

C -2.9819440000 4.3423930000 -0.2351470000

B -4.4431290000 4.9478250000 -0.3305560000

H -0.7633870000 12.4917460000 0.4509880000

H -3.9324590000 6.8117990000 -0.1510820000

H -6.3270720000 4.5013210000 -0.5413260000

H -2.9976320000 11.3609850000 0.2842150000

H 1.3278780000 11.0988820000 0.4574320000

H -1.4946360000 1.2538770000 -0.2986570000

H -3.7213500000 2.3354710000 -0.4342410000

H 0.3437100000 5.1273360000 0.1223900000

H 0.5504710000 2.6506980000 -0.0169690000

(*E*)-2 bound rotamer 1

F -1.5375010000 6.1672990000 -0.9959340000

F 2.5814160000 5.6473970000 1.3159090000

O 2.8536640000 2.2782150000 0.9738530000

O 2.5395460000 2.7333520000 -1.2584030000

N 0.4631370000 4.3948600000 0.2283150000

N -0.6748990000 3.8661240000 0.1178100000

C 3.8677650000 3.1995780000 -0.9606360000

C 4.1280570000 2.7516160000 0.5014530000

C 1.6308480000 6.4288880000 0.7559110000

C 1.8205520000 7.8029070000 0.7704940000

C 0.8477870000 8.6169220000 0.1850770000

C -0.2870740000 8.0525550000 -0.4023400000

C -0.4495900000 6.6726690000 -0.3850990000

C 0.4960850000 5.8027210000 0.2029910000

C -0.8755760000 -0.3220150000 0.0656650000

C 0.3852210000 0.2896520000 0.0130130000

C 0.5300050000 1.6825100000 0.0144200000

C -0.6562420000 2.4512430000 0.0859410000

C -1.9221760000 1.8481360000 0.1303280000

C -2.0333620000 0.4583170000 0.1224230000

B 1.9651980000 2.3196890000 -0.0752720000

H 3.8918500000 4.2896990000 -1.0703110000

H 4.5673740000 2.7560460000 -1.6759520000

H 4.4622020000 3.5732930000 1.1414180000

H 4.8508260000 1.9299880000 0.5685410000

H 1.2716620000 -0.3386660000 -0.0337190000

H -3.0121010000 -0.0117810000 0.1606740000

H -0.9494710000 -1.4067420000 0.0583000000

H -2.7977800000 2.4887500000 0.1754380000

H 0.9764350000 9.6951390000 0.1820800000

H -1.0486760000 8.6613530000 -0.8779400000

H 2.7131180000 8.2111960000 1.2316820000

(*E*)-2 bound rotamer 2

F 0.1406860000 6.5857480000 1.4009430000

F 4.0166070000 6.5267000000 -1.3457530000

O -2.5553140000 2.3458680000 0.1612250000

O -1.6587660000 4.0514420000 -1.0840490000

N 2.1519540000 5.0505640000 -0.1028120000

N 1.0720880000 4.4236760000 0.0603130000

C -3.6848960000 3.0725420000 -0.3599650000

C -3.0671780000 4.3361820000 -1.0053780000

C 3.0758570000 7.1975320000 -0.6485380000

C 3.1482650000 8.5828670000 -0.6114730000

C 2.1779720000 9.2830860000 0.1097160000

C 1.1598940000 8.5984570000 0.7784090000

C 1.1112360000 7.2114990000 0.7065780000

C 2.0599390000 6.4539720000 -0.0146300000

```
C 1.1979940000 3.0083810000 0.0361790000
C 2.4309800000 2.3535000000 0.2050900000
C 2.4784610000 0.9630190000 0.2389730000
C 1.2981390000 0.2178100000 0.1167990000
C 0.0755710000 0.8730750000 -0.0436620000
C -0.0055660000 2.2771140000 -0.0945110000
B -1.4072900000 2.9337020000 -0.3292130000
H -4.3718700000 3.3007340000 0.4600010000
H -4.2016030000 2.4375170000 -1.0894170000
H -3.2061490000 5.2318510000 -0.3892540000
H -3.4487270000 4.5346900000 -2.0109560000
H -0.8375360000 0.2905410000 -0.1284580000
H 3.4311140000 0.4576300000 0.3749810000
H 1.3319510000 -0.8680000000 0.1562880000
H 3.3301230000 2.9488430000 0.3208470000
H 0.4058770000 9.1196150000 1.3587510000
H 2.2176990000 10.3673810000 0.1556100000
H 3.9509490000 9.0874640000 -1.1379040000
```

(*E*)-3 unbound

```
O 0.7843370000 -0.7060310000 7.4753550000
O 1.2757030000 -0.5036100000 5.1758660000
O -2.7922900000 -0.2821800000 0.1865920000
O 1.4481050000 -0.2727760000 2.3057910000
N -0.9065950000 -0.4772510000 3.5383660000
N -1.4630670000 -0.4106150000 2.4060810000
C 2.8757410000 -0.2144850000 2.2666820000
C -3.6110840000 -0.2255180000 -0.9767480000
C -1.2089920000 -0.6867090000 5.9234990000
C -1.8025020000 -0.6135180000 4.6383300000
C -3.1997580000 -0.6749080000 4.4771290000
C -4.0192160000 -0.8096860000 5.5924480000
C -3.4562660000 -0.8830300000 6.8750300000
C -2.0711520000 -0.8213570000 7.0284670000
C 1.3552200000 -0.0846830000 -0.0991620000
```

C 0.5750980000 -0.0258910000 -1.2525660000

C -0.8164130000 -0.0888820000 -1.1972560000

C -1.4465970000 -0.2146790000 0.0465480000

C -0.6841680000 -0.2804200000 1.2564280000

C 0.7397870000 -0.2108830000 1.1544340000

B 0.3527310000 -0.6265680000 6.1698530000

H 1.0646600000 0.0724040000 -2.2177110000

H 3.2874940000 -1.0535400000 1.6933630000

H 3.2185960000 0.7350270000 1.8385670000

H 3.1888880000 -0.2867070000 3.3081040000

H -3.4802030000 0.7226190000 -1.5138530000

H -3.4043660000 -1.0642700000 -1.6533360000

H -4.6373940000 -0.2968890000 -0.6135270000

H 1.7476100000 -0.6592170000 7.5316930000

H 0.8234980000 -0.4566290000 4.3020940000

H -3.6136520000 -0.6153220000 3.4767250000

H -5.0984100000 -0.8584270000 5.4671260000

H -4.0973000000 -0.9882750000 7.7464210000

H -1.6346640000 -0.8787110000 8.0212660000

H 2.4335240000 -0.0316640000 -0.1800980000

H -1.3934130000 -0.0396760000 -2.1116290000

(*E*)-3 bound rotamer 1

O -4.7042730000 6.4312870000 0.7476270000

O -0.5689780000 6.7021490000 -1.5002980000

O -1.1243980000 4.0190110000 1.8908390000

O 0.3453870000 3.5258740000 0.1912320000

N -2.4555830000 5.1938560000 -0.4668000000

N -3.4759530000 4.4887110000 -0.6783730000

C 1.1193570000 4.2117810000 1.1899560000

C 0.0716430000 4.7565530000 2.1884550000

C 0.5176920000 7.4287610000 -2.0606190000

C -5.7306280000 7.0113170000 1.5441450000

C -1.6314430000 8.7838540000 -0.8221370000

C -1.5853410000 7.3871460000 -0.9123690000

```
C -2.7262190000 9.3872460000 -0.2013310000
C -3.7705590000 8.6311590000 0.3287280000
C -3.7429120000 7.2309410000 0.2250910000
C -2.6438210000 6.5892180000 -0.4062240000
C -3.2156260000 3.0945770000 -0.6252070000
C -2.0402960000 2.5529870000 -0.0554780000
C -1.8834090000 1.1616230000 -0.1116420000
C -2.8593840000 0.3335180000 -0.6825590000
C -4.0258000000 0.8904280000 -1.2157570000
C -4.2057790000 2.2734300000 -1.1819210000
B -0.9570910000 3.4511900000 0.6406240000
H -0.8361590000 9.3958460000 -1.2287050000
H -2.7658120000 10.4709810000 -0.1287740000
H -4.6008050000 9.1298420000 0.8129870000
H -2.7101210000 -0.7431830000 -0.7031760000
H -4.7880070000 0.2522180000 -1.6543660000
H -0.9863850000 0.7096280000 0.3052680000
H -5.0964220000 2.7408430000 -1.5916220000
H 1.7047470000 5.0036710000 0.7125320000
H 1.8067870000 3.4939910000 1.6544850000
H -0.1253610000 5.8253510000 2.0370040000
H 0.3454370000 4.5906140000 3.2351720000
H 1.0418040000 8.0216080000 -1.2995070000
H 1.1946460000 6.6744850000 -2.4648040000
H 0.1813180000 8.0893030000 -2.8701150000
H -6.3685240000 7.6784420000 0.9506190000
H -6.3254100000 6.1719910000 1.9072030000
H -5.3140000000 7.5615940000 2.3975490000
```

(*E*)-3 bound rotamer 2

```
O 3.3450510000 4.6932760000 -0.3472940000
O 2.1595190000 5.0002000000 -2.2890320000
O -2.5904870000 8.8715540000 -0.6259900000
O 1.8544050000 8.3363410000 0.8704960000
N -0.7045710000 7.2589630000 0.2314730000
```

```
N 0.1955020000 6.4236750000 -0.0430970000
C 4.3208120000 5.0685830000 -1.3386890000
C 3.4830310000 5.4897160000 -2.5697540000
C -3.7109100000 9.6745010000 -0.9760700000
C 3.0386790000 8.8707380000 1.4500060000
C 0.8895790000 9.1877930000 0.4370230000
C 1.0705040000 10.5785330000 0.3781870000
C 0.0218280000 11.3975190000 -0.0379090000
C -1.2226940000 10.8683340000 -0.3820660000
C -1.4194210000 9.4835980000 -0.3074560000
C -0.3654160000 8.6184270000 0.0881400000
C -0.1548780000 5.0634940000 0.1880800000
C 0.8125840000 4.1350740000 -0.2453510000
C 0.5655900000 2.7705910000 -0.0248530000
C -0.6106190000 2.3450560000 0.5983810000
C -1.5620480000 3.2854430000 1.0196000000
C -1.3378180000 4.6447600000 0.8211160000
B 2.1130360000 4.6460770000 -0.9609130000
H 4.9622370000 4.2028230000 -1.5420250000
H 4.9395980000 5.8801800000 -0.9437650000
H 3.8391690000 5.0458730000 -3.5037650000
H 3.4328230000 6.5781110000 -2.6884960000
H -2.0530270000 5.3915410000 1.1480920000
H -3.5248020000 10.2420820000 -1.8969520000
H -4.5316180000 8.9751210000 -1.1426660000
H -3.9778540000 10.3662570000 -0.1664700000
H 2.8098670000 9.5317280000 2.2959730000
H 3.6037910000 8.0065990000 1.8028300000
H 3.6358500000 9.4186420000 0.7094930000
H 0.1776590000 12.4715280000 -0.0955560000
H -2.0184250000 11.5282310000 -0.7031730000
H 2.0204100000 11.0219370000 0.6492480000
H -2.4733960000 2.9524610000 1.5097440000
H 1.2971510000 2.0313070000 -0.3418550000
```

H -0.7847030000 1.2846910000 0.7630540000

(*Z*)-1 unbound

O -8.2581260000 1.3404190000 1.3224050000

O -6.7910390000 2.3456200000 -0.1614520000

N -3.6652450000 0.7699940000 -1.2647260000

N -4.9143330000 0.7018580000 -1.2918190000

C 0.1439220000 -2.8485870000 1.0894230000

C -0.6672250000 -1.3318510000 -0.7725670000

C -0.8897670000 -1.9311470000 0.4791840000

C -2.0858790000 -1.6312870000 1.1496080000

C -3.0499540000 -0.7961620000 0.5848260000

C -1.6003540000 -0.4607430000 -1.3288620000

C -5.3888530000 -1.7093450000 -1.5029440000

C -6.2451170000 -2.7881100000 -1.2930070000

C -7.3983660000 -2.6233730000 -0.5194050000

C -7.6971120000 -1.3669510000 0.0125220000

C -6.8766860000 -0.2431390000 -0.1982060000

C -5.6923640000 -0.4567930000 -0.9461650000

C -2.8183530000 -0.2200020000 -0.6736460000

B -7.3090890000 1.1940250000 0.3391330000

H -6.1063250000 2.1657370000 -0.8329360000

H -8.5692720000 0.5152950000 1.7072560000

H 0.3359260000 -3.7140290000 0.4439960000

H 1.1008500000 -2.3313580000 1.2284790000

H -0.1794040000 -3.2223460000 2.0647110000

H -6.0139190000 -3.7534850000 -1.7343560000

H -8.0694530000 -3.4609550000 -0.3508760000

H -8.6211750000 -1.2585910000 0.5773570000

H -4.4955710000 -1.8295880000 -2.1068600000

H -3.9632310000 -0.5786950000 1.1281860000

H -2.2681300000 -2.0580420000 2.1327150000

H -1.4066480000 0.0362020000 -2.2749320000

H 0.2601820000 -1.5298430000 -1.3053920000

(*Z*)-1 bound

O -8.4177770000 1.3218840000 0.7807870000

O -6.2683320000 2.0340970000 0.4042060000

N -3.7833710000 0.6527090000 -1.6952210000

N -5.0241640000 0.5404330000 -1.7613570000

C -6.9127260000 3.1363350000 1.0684970000

C -8.3669280000 2.6544340000 1.3234950000

C -0.0617650000 -2.4827280000 1.3946290000

C -0.7900100000 -1.2922020000 -0.7228110000

C -1.0692230000 -1.6863110000 0.5973640000

C -2.2971060000 -1.2988450000 1.1540350000

C -3.2364250000 -0.5742460000 0.4183120000

C -1.7018220000 -0.5362510000 -1.4552480000

C -5.5170920000 -1.8534300000 -1.7928850000

C -6.3570240000 -2.9213570000 -1.4774610000

C -7.4459350000 -2.7316220000 -0.6204960000

C -7.6898020000 -1.4619200000 -0.0931300000

C -6.8683190000 -0.3600360000 -0.3978210000

C -5.7617030000 -0.5828170000 -1.2490820000

C -2.9498330000 -0.2070970000 -0.9041750000

B -7.1821300000 1.0206040000 0.2502040000

H -6.8637470000 4.0150300000 0.4174450000

H -6.3698690000 3.3533580000 1.9939310000

H -9.1116900000 3.2703900000 0.8097460000

H -8.6192580000 2.6116650000 2.3880490000

H 0.1702390000 -3.4350990000 0.9031400000

H 0.8831060000 -1.9361760000 1.5010310000

H -0.4340640000 -2.7064820000 2.3983200000

H -6.1609950000 -3.9010200000 -1.9051840000

H -8.1023840000 -3.5615890000 -0.3749070000

H -8.5396230000 -1.3079300000 0.5667760000

H -4.6801750000 -1.9933790000 -2.4702970000

H -4.1730910000 -0.2770340000 0.8753210000

H -2.5247270000 -1.5685300000 2.1825050000

H -1.4679970000 -0.1976120000 -2.4603250000

H 0.1628110000 -1.5624190000 -1.1727540000

(*Z*)-2 unbound

F -3.9705770000 -0.2881050000 1.4562180000

F -1.5800800000 -0.1908280000 -2.6142720000

O -8.3268870000 1.2663470000 1.3230200000

O -6.8782220000 2.3569770000 -0.1160860000

N -3.6562640000 0.8240810000 -1.1472660000

N -4.9022810000 0.7629300000 -1.1955260000

C -0.7484380000 -1.4965430000 -0.8288690000

C -0.8934970000 -1.9519080000 0.4855420000

C -1.9847560000 -1.5497320000 1.2599960000

C -2.9285500000 -0.7009350000 0.6972000000

C -1.7055920000 -0.6336520000 -1.3426080000

C -5.3280070000 -1.6448690000 -1.5096940000

C -6.1682960000 -2.7457590000 -1.3491620000

C -7.3477800000 -2.6177820000 -0.6110340000

C -7.6914120000 -1.3786300000 -0.0632980000

C -6.8887470000 -0.2360760000 -0.2223200000

C -5.6778450000 -0.4125850000 -0.9366210000

C -2.8369830000 -0.2281050000 -0.6201870000

B -7.3630820000 1.1769080000 0.3493430000

H -0.1500410000 -2.6199460000 0.9088710000

H -6.1650500000 2.2224710000 -0.7651580000

H -8.6039690000 0.4242330000 1.6968150000

H -5.9063700000 -3.6955900000 -1.8062870000

H -8.0073130000 -3.4714830000 -0.4821100000

H -8.6349060000 -1.3014410000 0.4730840000

H -4.4264630000 -1.7313720000 -2.1063100000

H -2.1135060000 -1.8766660000 2.2858530000

H 0.0887240000 -1.7930790000 -1.4513130000

(*Z*)-2 bound

```
F -4.0766560000 0.1518420000 1.3942640000
F -1.4001260000 -0.2622920000 -2.4735280000
O -8.4440440000 1.1214270000 0.8466760000
O -6.5322570000 2.2655640000 0.2965570000
N -3.5396800000 0.9768760000 -1.2846350000
N -4.7637790000 0.8867610000 -1.4913920000
C -7.2957530000 3.1749710000 1.1101650000
C -8.6546640000 2.4621440000 1.3282220000
C -0.7419340000 -1.3820080000 -0.4984810000
C -0.9952860000 -1.6871670000 0.8427840000
C -2.1256020000 -1.1742310000 1.4834740000
C -2.9945540000 -0.3634140000 0.7634680000
C -1.6303970000 -0.5551590000 -1.1706810000
C -5.1351240000 -1.4995790000 -1.8625570000
C -5.9398260000 -2.6338010000 -1.7466640000
C -7.1187170000 -2.5813190000 -0.9980200000
C -7.4953290000 -1.3832750000 -0.3863390000
C -6.7202040000 -0.2146460000 -0.4985800000
C -5.5150650000 -0.3053650000 -1.2317880000
C -2.7915570000 -0.0368790000 -0.5834710000
B -7.2182260000 1.0823090000 0.2133980000
H -0.3085420000 -2.3257220000 1.3895160000
H -7.3918050000 4.1282630000 0.5824530000
H -6.7528110000 3.3422070000 2.0467580000
H -9.4653140000 2.9171690000 0.7484320000
H -8.9526700000 2.4204980000 2.3799940000
H -5.6459030000 -3.5535900000 -2.2448920000
H -7.7468290000 -3.4628040000 -0.9036560000
H -8.4164980000 -1.3394400000 0.1874900000
H -4.2340620000 -1.5262300000 -2.4670840000
H -2.3436060000 -1.3888400000 2.5239490000
H 0.1247590000 -1.7692180000 -1.0229340000
```

(*Z*)-3 unbound

O -6.8887400000 2.2203960000 -0.4012660000

O -8.6084770000 0.9824400000 0.6313070000

O -4.0110670000 -0.0988600000 1.4034910000

O -1.4955610000 -0.1316830000 -2.5452520000

N -3.5546510000 0.8324230000 -1.1582870000

N -4.7905240000 0.7130500000 -1.3012110000

C -4.2214470000 -0.4062130000 2.7786450000

C -0.3084330000 -0.3822190000 -3.2914490000

C -0.5874900000 -1.3488470000 -0.6276540000

C -0.7809380000 -1.7380940000 0.6997720000

C -1.9152240000 -1.3515260000 1.4141580000

C -2.8898840000 -0.5615200000 0.7875660000

C -1.5558330000 -0.5518210000 -1.2504970000

C -5.0631490000 -1.7293040000 -1.5889260000

C -5.8592400000 -2.8673870000 -1.4623930000

C -7.1075930000 -2.7843800000 -0.8363670000

C -7.5715030000 -1.5496650000 -0.3755650000

C -6.8120990000 -0.3752880000 -0.5172740000

C -5.5260360000 -0.4999150000 -1.0952730000

C -2.7233620000 -0.1700000000 -0.5586520000

B -7.4319360000 1.0116210000 -0.0808170000

H -8.9303710000 1.8746200000 0.8164630000

H -6.0576730000 2.1019100000 -0.9051170000

H -5.1613400000 0.0778350000 3.0462080000

H -4.3114240000 -1.4882600000 2.9335900000

H -3.4122100000 -0.0074510000 3.4024150000

H -0.1477270000 -1.4580290000 -3.4358050000

H -0.4647650000 0.0936700000 -4.2603290000

H 0.5689250000 0.0599460000 -2.8039180000

H -0.0310910000 -2.3549070000 1.1872790000

H -5.5059830000 -3.8164760000 -1.8564340000

H -7.7241240000 -3.6729950000 -0.7301600000

H -8.5515100000 -1.4793790000 0.0867340000

H -4.1038460000 -1.7869210000 -2.0903760000

H -2.0343400000 -1.6607400000 2.4450080000

H 0.2999050000 -1.6672110000 -1.1608420000

(*Z*)-3 bound

O -8.4641650000 1.1119220000 0.8742860000

O -6.6140190000 2.3279190000 0.2747760000

O -3.9713780000 0.2036220000 1.4618630000

O -1.5669090000 -0.2730560000 -2.5280890000

N -3.4828950000 0.9744570000 -1.1607000000

N -4.7090680000 0.9149450000 -1.3675920000

C -4.1748060000 -0.0263670000 2.8501190000

C -0.4254780000 -0.6696610000 -3.2797960000

C -7.4237460000 3.2287300000 1.0486520000

C -8.7441430000 2.4572080000 1.2989830000

C -0.7285020000 -1.4672750000 -0.5643860000

C -0.9240340000 -1.7685420000 0.7853800000

C -2.0002380000 -1.2394690000 1.4977320000

C -2.9074940000 -0.3877730000 0.8486860000

C -1.6324080000 -0.6127810000 -1.2075610000

C -5.0985900000 -1.4615020000 -1.8025760000

C -5.9162820000 -2.5895570000 -1.7284880000

C -7.1136670000 -2.5408710000 -1.0084820000

C -7.4954540000 -1.3493580000 -0.3880880000

C -6.7061150000 -0.1856230000 -0.4598280000

C -5.4792000000 -0.2748350000 -1.1579250000

C -2.7356060000 -0.0773190000 -0.5148260000

B -7.2395140000 1.1085520000 0.2292990000

H -5.0575880000 0.5557170000 3.1188170000

H -4.3630700000 -1.0877060000 3.0561450000

H -3.3174640000 0.3182200000 3.4421910000

H -0.3651660000 -1.7619570000 -3.3703030000

H -0.5580290000 -0.2314210000 -4.2699560000

H 0.4995050000 -0.2863690000 -2.8315050000

H -0.2255950000 -2.4302050000 1.2902340000

H −7.5693800000 4.1530740000 0.4817470000

H −6.8922470000 3.4676970000 1.9769010000

H −9.5766900000 2.8467060000 0.7023000000

H −9.0420030000 2.4458960000 2.3519900000

H −5.6181150000 −3.5034890000 −2.2355690000

H −7.7522990000 −3.4179130000 −0.9465060000

H −8.4344340000 −1.3052150000 0.1561590000

H −4.1803680000 −1.4845010000 −2.3800630000

H −2.1275230000 −1.4897210000 2.5435930000

H 0.1100070000 −1.8966780000 −1.0989840000

(*E*)-5 unbound

O 1.2718100000 0.0362650000 −2.3682450000

O 0.8265380000 −1.0191130000 7.4987750000

O 1.3060960000 −0.7810440000 5.2017320000

O 1.4968560000 −0.4325140000 2.3435570000

N −0.8971430000 −0.5109600000 3.6017720000

N −1.4524690000 −0.3792500000 2.4748160000

C 2.9242120000 −0.4562840000 2.2735700000

C 0.5549360000 0.1665420000 −3.5938670000

C −1.1772260000 −0.7592420000 5.9841650000

C −1.7837180000 −0.5932060000 4.7135470000

C −3.1829110000 −0.5129400000 4.5822050000

C −3.9915560000 −0.5986530000 5.7105450000

C −3.4152590000 −0.7640890000 6.9781240000

C −2.0280650000 −0.8422520000 7.1028650000

C 1.3581310000 −0.1926610000 −0.0497730000

C 0.5716970000 −0.0627350000 −1.2065610000

C −0.8275940000 −0.0423450000 −1.1168850000

C −1.4063680000 −0.1536220000 0.1430830000

C −0.6586600000 −0.2863960000 1.3259550000

C 0.7705250000 −0.3050990000 1.2099240000

B 0.3870830000 −0.8537930000 6.2039820000

H 3.3119990000 0.4794440000 1.8535470000

H 3.2556230000 −0.5665720000 3.3059740000

```
H 3.2735140000 -1.3069850000 1.6761800000
H -2.4867210000 -0.1400830000 0.2517610000
H 0.8554590000 -0.6631210000 4.3351210000
H 1.7905650000 -1.0675900000 7.5395660000
H -0.0905920000 -0.7027660000 -3.7702120000
H -0.0478390000 1.0828250000 -3.6053910000
H 1.3142400000 0.2206680000 -4.3748570000
H -3.6122350000 -0.3833420000 3.5953360000
H -5.0722000000 -0.5356330000 5.6064700000
H -4.0470180000 -0.8305810000 7.8600120000
H -1.5805670000 -0.9703340000 8.0839870000
H 2.4336190000 -0.2027910000 -0.1752060000
H -1.4545550000 0.0579230000 -1.9936970000
```

(*E*)-5 bound (most stable rotamer)

```
O 0.1221370000 12.6606530000 -0.3143930000
O 3.3403580000 3.6250170000 -0.6607050000
O 2.8760620000 5.8696090000 -0.6435740000
O -2.9606840000 8.9356780000 0.1746330000
N -0.9392610000 7.1909520000 -0.0811040000
N 0.0602980000 6.4300390000 -0.2107870000
C -0.9131130000 13.6287830000 -0.1968780000
C 4.6181250000 4.2753620000 -0.7434720000
C 4.2742840000 5.7651890000 -0.9679390000
C -4.0789480000 9.8013050000 0.3155530000
C 0.6541660000 9.0832170000 -0.3218040000
C 0.8874570000 10.4454950000 -0.3757540000
C -0.1936820000 11.3366470000 -0.2455180000
C -1.4961310000 10.8559230000 -0.0594850000
C -1.7255990000 9.4700680000 -0.0039630000
C -0.6437830000 8.5634330000 -0.1377660000
C -0.2265840000 5.0422100000 -0.1580210000
C 0.8742330000 4.1626580000 -0.3103900000
C 0.6145560000 2.7770860000 -0.2572660000
C -0.6727940000 2.2770300000 -0.0642530000
```

```
C -1.7463490000 3.1663750000 0.0833380000

C -1.5272550000 4.5386730000 0.0377410000

B 2.3607650000 4.5973950000 -0.5376170000

H -1.6560080000 13.5191170000 -0.9976730000

H -1.4114330000 13.5652080000 0.7791380000

H -0.4234060000 14.5993460000 -0.2887630000

H 1.4671220000 8.3714070000 -0.4219530000

H 5.1937360000 3.8370460000 -1.5645620000

H 5.1597290000 4.1071140000 0.1955910000

H 4.4140840000 6.0742700000 -2.0105940000

H 4.8431450000 6.4397260000 -0.3214360000

H -2.3436060000 5.2429870000 0.1513690000

H -4.2258560000 10.4190570000 -0.5804470000

H -4.9418010000 9.1466850000 0.4466160000

H -3.9779190000 10.4488990000 1.1962850000

H -2.3228030000 11.5439550000 0.0409490000

H 1.8846870000 10.8486530000 -0.5190740000

H -2.7531260000 2.7848260000 0.2357550000

H 1.4458710000 2.0877920000 -0.3708530000

H -0.8417710000 1.2037340000 -0.0281710000
```

(*E*)-6 unbound

```
O 0.7036140000 0.9542870000 5.1037820000

O 0.6855200000 0.7880970000 7.4578200000

N -1.1582950000 -0.6022750000 3.8276320000

N -1.8614050000 -0.8426970000 2.8122880000

C 2.1385310000 -2.0454340000 1.2950460000

C -4.7908910000 0.6197880000 0.0635200000

C -1.0304120000 -0.6131590000 6.2436180000

C -1.6642230000 -1.0915580000 5.0701850000

C -2.7210350000 -2.0167310000 5.1344080000

C -3.1705780000 -2.4666210000 6.3717850000

C -2.5694090000 -1.9993500000 7.5483000000

C -1.5154670000 -1.0876000000 7.4765240000

C 0.3589840000 -0.1528810000 -0.1183180000
```

```
C -0.5790150000 0.4118970000 -0.9801820000
C -1.9138840000 0.5335870000 -0.5873500000
C -3.7693520000 0.2325410000 1.1386130000
C -2.3257740000 0.1061550000 0.6764580000
C -1.3456680000 -0.4189920000 1.5643350000
C 0.0114730000 -0.5814800000 1.1714230000
C 1.0585690000 -1.2541160000 2.0505840000
B 0.1684900000 0.4211200000 6.2390230000
H 0.2333840000 0.5851490000 4.3268060000
H 2.7997870000 -1.4002570000 0.7072980000
H 2.7685650000 -2.5827830000 2.0121020000
H 1.6957120000 -2.7826920000 0.6156240000
H -5.7970710000 0.6285540000 0.4957740000
H -4.6039060000 1.6195970000 -0.3442190000
H -4.7936740000 -0.0906860000 -0.7712830000
H 1.4107440000 1.4193950000 7.3610720000
H -3.1674850000 -2.3720090000 4.2126060000
H -3.9854240000 -3.1842860000 6.4227990000
H -2.9189170000 -2.3521770000 8.5147200000
H -1.0481420000 -0.7295390000 8.3885980000
H 1.3820660000 -0.2700730000 -0.4590370000
H -0.2726150000 0.7441900000 -1.9682900000
H -2.6348950000 0.9593300000 -1.2762780000
H -3.8158830000 0.9656680000 1.9553010000
H -4.0636890000 -0.7174440000 1.6001800000
H 1.5501320000 -0.5004190000 2.6792480000
H 0.5590190000 -1.9273980000 2.7533720000
O -2.9585220000 -2.7882630000 3.6474900000
O -4.9277770000 -1.6020410000 3.7156810000
N -1.3215780000 0.2255070000 3.8378330000
N -2.0840550000 -0.0699540000 2.8824740000
C -5.1833630000 -2.7390380000 2.8686470000
C -3.7888190000 -3.3571760000 2.6199510000
C 1.8257480000 -1.9263370000 1.6875190000
```

```
C -4.8337560000 1.2573240000 -0.1048880000
C -3.0407290000 -0.7990160000 5.3101350000
C -1.9181380000 0.0375430000 5.1138800000
C -1.3310090000 0.7402720000 6.1738110000
C -1.8871600000 0.6601750000 7.4512110000
C -3.0196910000 -0.1317330000 7.6634080000
C -3.5833130000 -0.8516670000 6.6014770000
C 0.1232800000 -0.3569430000 -0.1212200000
C -0.7414900000 0.1594890000 -1.0862510000
C -2.0210060000 0.5885740000 -0.7297100000
C -3.8295870000 0.9975700000 1.0247480000
C -2.4532350000 0.5109950000 0.5973360000
C -1.5478000000 0.0130340000 1.5726710000
C -0.2464060000 -0.4419370000 1.2285500000
```

(*E*)-6 bound

```
C 0.7027610000 -1.0464170000 2.2539310000
B -3.6229760000 -1.6880800000 4.1561710000
H -5.6736590000 -2.4028090000 1.9503290000
H -5.8569030000 -3.4238040000 3.3984840000
H -3.3807490000 -3.0775530000 1.6411330000
H -3.7775890000 -4.4474570000 2.7121610000
H -3.7065860000 1.9198850000 1.6100450000
H -4.2510730000 0.2770070000 1.7347340000
H 1.1425490000 -0.2398360000 2.8516270000
H 0.1171040000 -1.6367360000 2.9674830000
H -0.4188470000 0.2193470000 -2.1226310000
H 1.4336180000 -2.7339660000 1.0585020000
H 2.5459760000 -1.3543450000 1.0923670000
H 2.3808310000 -2.3848630000 2.5126840000
H -4.5180090000 2.0734380000 -0.7645180000
H -4.9885450000 0.3654030000 -0.7241300000
H -5.8026490000 1.5391980000 0.3199060000
H -0.4578530000 1.3541280000 5.9727730000
H -1.4422660000 1.2120600000 8.2742700000
```

H -3.4592730000 -0.1986550000 8.6550610000

H -4.4545790000 -1.4747760000 6.7888400000

H 1.1026640000 -0.7060310000 -0.4283210000

H -2.6833000000 0.9825040000 -1.4929200000

(*Z*)-6 unbound

O -7.1655830000 2.0332840000 -0.8147220000

O -9.0235890000 0.7851470000 -0.0691680000

N -3.7162850000 0.7164310000 -1.0558730000

N -4.9331400000 0.5430000000 -1.2835240000

C -3.8880050000 -0.2368890000 3.2518570000

C -0.3566830000 -0.4613160000 -3.4776000000

C -4.0703130000 -0.0901730000 1.7361100000

C -1.6598070000 -0.1620110000 -2.7288960000

C -0.7848400000 -1.5113590000 -0.7309890000

C -0.8904450000 -1.9218570000 0.5998940000

C -1.9459950000 -1.4693310000 1.3920240000

C -2.9396720000 -0.6281800000 0.8725520000

C -1.7384600000 -0.6574220000 -1.2946990000

C -5.0997530000 -1.9463840000 -1.4779890000

C -5.8955750000 -3.0893210000 -1.4157140000

C -7.2315730000 -2.9944870000 -1.0118860000

C -7.7784980000 -1.7455280000 -0.7095300000

C -7.0191980000 -0.5655290000 -0.7988420000

C -5.6505420000 -0.6953410000 -1.1501490000

C -2.8336920000 -0.2681880000 -0.4903620000

B -7.7367410000 0.8254970000 -0.5492700000

H -1.8391490000 0.9214840000 -2.7198050000

H -2.5008470000 -0.5806210000 -3.3014570000

H -4.2111850000 0.9722460000 1.5002960000

H -5.0095940000 -0.5801380000 1.4481930000

H -9.3949960000 1.6720040000 0.0274830000

H -6.2556400000 1.9034170000 -1.1549830000

H -4.7232930000 0.2432970000 3.7717900000

H -3.8702470000 -1.2861720000 3.5660490000

H -2.9621440000 0.2364390000 3.5970570000

H -0.1879370000 -1.5373100000 -3.5978860000

H -0.3935090000 -0.0216790000 -4.4792070000

H 0.5114770000 -0.0383080000 -2.9603250000

H -0.1368130000 -2.5788310000 1.0260250000

H -5.4698180000 -4.0532070000 -1.6807560000

H -7.8464710000 -3.8883530000 -0.9509000000

H -8.8209470000 -1.6682760000 -0.4165440000

H -4.0677210000 -2.0267300000 -1.7945480000

H -1.9922930000 -1.7703180000 2.4332750000

H 0.0554780000 -1.8506280000 -1.3279010000

(*Z*)-6 bound

O -6.9406260000 1.6781840000 -0.3268860000

O -8.9405560000 0.6249520000 -0.7185880000

N -3.6169030000 0.4983340000 -1.4902400000

N -4.8113970000 0.2862780000 -1.7777750000

C -3.0299750000 -0.5241920000 0.7039920000

C -9.2864890000 1.9277920000 -0.2115100000

C -7.9461910000 2.6996220000 -0.1860660000

C -4.1042020000 0.3914830000 2.8723000000

C 0.0076290000 -0.8761750000 -3.3254470000

C -4.2521210000 0.0821500000 1.3753610000

C -1.3827760000 -0.5414140000 -2.7752730000

C -0.7030070000 -1.5595480000 -0.5248060000

C -0.9372950000 -1.7721190000 0.8362140000

C -2.0775860000 -1.2447960000 1.4400360000

C -1.6101270000 -0.8325400000 -1.3008920000

C -4.9579820000 -2.1821650000 -1.8179620000

C -5.7292260000 -3.3398430000 -1.7103840000

C -7.0530270000 -3.2634100000 -1.2683240000

C -7.6030510000 -2.0182640000 -0.9549980000

C -6.8586580000 -0.8296600000 -1.0676700000

C -5.5093890000 -0.9349880000 -1.4853840000

C -2.7945410000 -0.3649230000 -0.6810160000

B −7.5644910000 0.5174240000 −0.7137510000

(*E*)-7 rotamer 1

F 1.2135790000 8.9596490000 1.3139750000

F −3.1737780000 9.0386390000 −0.5003450000

O 2.1629150000 4.6731470000 −0.2864440000

O 0.8931760000 6.0202980000 −1.8460440000

C 0.1016440000 9.6327210000 0.9057360000

C 0.1184450000 11.0156850000 1.0078990000

C −1.0081170000 11.7289920000 0.5906610000

C −2.1158700000 11.0462520000 0.0818550000

C −2.0741910000 9.6615400000 0.0015530000

C −0.9777610000 8.8746530000 0.4058930000

C −0.8758930000 7.4165260000 0.3539340000

C −1.7843430000 6.5268960000 −0.1023630000

C −1.5957440000 5.0659400000 −0.0982510000

C −2.7375240000 4.2827150000 0.1645520000

C −2.6564040000 2.8981260000 0.3021670000

C −1.4179790000 2.2634620000 0.1773280000

C −0.2844130000 3.0251590000 −0.1171660000

C −0.3431990000 4.4214370000 −0.2920630000

B 0.9699210000 5.1064290000 −0.8230410000

H 0.0586750000 7.0337570000 0.7519680000

H −2.7552730000 6.8719840000 −0.4415060000

H 2.9646590000 5.0320900000 −0.6851460000

H 1.7262020000 6.4095810000 −2.1366440000

(*E*)-7 rotamer 2

F 1.1937670000 8.6768220000 1.3792800000

F −2.9235480000 9.1330900000 −0.9412290000

O −4.7289050000 6.0621960000 0.2770270000

O −5.4702870000 3.7948730000 −0.0749730000

C 0.2109490000 9.4430170000 0.8312750000

C 0.3535030000 10.8201810000 0.9130370000

C −0.6411730000 11.6279040000 0.3565710000

C −1.7463200000 11.0422500000 −0.2661710000

C -1.8355900000 9.6581430000 -0.3180860000

C -0.8755880000 8.7800770000 0.2229180000

C -0.9028350000 7.3169310000 0.1872520000

C -1.9087000000 6.5154590000 -0.2349760000

C -1.8279800000 5.0428700000 -0.2702630000

C -0.5713720000 4.4223210000 -0.4330120000

C -0.4387460000 3.0370070000 -0.4742550000

C -1.5726810000 2.2262350000 -0.3698720000

C -2.8249560000 2.8232190000 -0.2298490000

C -2.9921590000 4.2230190000 -0.1767660000

B -4.4651260000 4.7366240000 0.0160080000

H 0.0008830000 6.8598670000 0.5776390000

H -2.8459160000 6.9525960000 -0.5476420000

H -0.5558320000 12.7090600000 0.4072800000

H -5.6579840000 6.3049980000 0.3665040000

H -6.3665910000 4.1112800000 0.0842070000

H -2.5354760000 11.6370450000 -0.7134360000

H 1.2269050000 11.2361260000 1.4034010000

H -1.4826900000 1.1436470000 -0.4079570000

H -3.7072570000 2.1948630000 -0.1572470000

H 0.3121580000 5.0402680000 -0.5605510000

H 0.5448560000 2.5926040000 -0.6045510000

(*E*)-6' unbound

O 0.2384150000 1.0655330000 7.3455050000
O 0.8706890000 0.8951660000 5.0738150000
O -2.7688300000 -0.0525340000 0.1703140000
O 1.4713360000 -0.5071880000 2.2504660000
N -0.8959310000 -0.3940240000 3.4853600000
N -1.4193410000 -0.5518450000 2.3448420000
C 3.3918450000 -1.1926800000 3.5117360000
C -5.0507350000 0.0094780000 -0.5373420000
C 2.8997950000 -0.7318900000 2.1521750000
C -3.6078920000 0.1254140000 -0.9933080000
C -1.2972360000 -0.2976690000 5.8631860000
C -1.7118820000 -0.7681140000 4.5900120000
C -2.8519800000 -1.5809020000 4.4513950000
C -3.6040520000 -1.9191970000 5.5741980000
C -3.2258290000 -1.4518810000 6.8411200000
C -2.0872460000 -0.6532970000 6.9732190000
C 1.3878500000 -0.0153800000 -0.1158830000
C 0.6083340000 0.2133020000 -1.2502640000
C -0.7863680000 0.2052990000 -1.2005380000
C -1.4224030000 -0.0357840000 0.0226920000

```
C -0.6590310000 -0.2563370000 1.2131940000
C 0.7700850000 -0.2455400000 1.1218520000
B -0.0074700000 0.5913940000 6.0760880000
H 3.1886320000 -0.4400660000 4.2791060000
H 2.9108640000 -2.1318920000 3.8033730000
H 4.4731660000 -1.3589530000 3.4616560000
H -5.2479160000 -0.9777920000 -0.1067520000
H -5.2885730000 0.7741430000 0.2094490000
H -5.7133990000 0.1485730000 -1.3978320000
H 1.1023580000 0.4037470000 -2.1990730000
H 3.0881640000 -1.4915910000 1.3851820000
H 3.3861230000 0.2029750000 1.8505600000
H -3.4095300000 1.1115990000 -1.4302660000
H -3.3630370000 -0.6441880000 -1.7346260000
H 1.0558380000 1.5831750000 7.3920210000
H 0.5657940000 0.4742890000 4.2338850000
H -3.1282860000 -1.9445290000 3.4680510000
H -4.4815720000 -2.5512530000 5.4655480000
H -3.8111470000 -1.7168350000 7.7172780000
H -1.7974190000 -0.2993550000 7.9582200000
H 2.4670390000 -0.0081960000 -0.2022770000
H -1.3584940000 0.3893040000 -2.1003070000
```

(*E*)-6' bound

```
O -4.7479490000 6.4886710000 0.6762110000
O -0.5805010000 6.7417680000 -1.5467580000
O -1.1763180000 4.1192030000 1.8641580000
O 0.3156860000 3.5811680000 0.1978070000
N -2.4894060000 5.2400920000 -0.5451570000
N -3.5175720000 4.5229410000 -0.6946920000
C 1.0869740000 4.2800290000 1.2067060000
C 0.0281790000 4.8679360000 2.1600920000
C 1.5299120000 6.4543310000 -2.6293350000
C 0.5767780000 7.4651410000 -2.0185550000
C -6.6583170000 5.9477140000 2.0065980000
C -5.7629400000 7.0733680000 1.5224100000
C -1.5906910000 8.8144560000 -0.7805740000
C -1.5775850000 7.4221290000 -0.9281340000
C -2.6774390000 9.4184680000 -0.1447740000
C -3.7493930000 8.6721040000 0.3456740000
C -3.7587090000 7.2767660000 0.1906100000
C -2.6628430000 6.6299640000 -0.4541480000
C -3.2465410000 3.1309150000 -0.6372310000
C -2.0668440000 2.6037680000 -0.0581140000
C -1.8989070000 1.2107950000 -0.0935560000
C -2.8678230000 0.3669890000 -0.6556820000
C -4.0382590000 0.9094290000 -1.1983680000
C -4.2308510000 2.2921220000 -1.1823010000
B -0.9907490000 3.5136130000 0.6346170000
H -6.0889630000 5.2153920000 2.5885690000
H -7.4454070000 6.3616870000 2.6462020000
H -7.1334310000 5.4357320000 1.1637540000
H 2.4215560000 6.9727540000 -2.9969780000
H 1.8404910000 5.7120140000 -1.8877060000
H 1.0620190000 5.9349110000 -3.4721530000
H -0.7774670000 9.4232080000 -1.1540800000
H -2.6898450000 10.4990270000 -0.0291830000
H -4.5691480000 9.1762160000 0.8412130000
H -2.7120150000 -0.7087140000 -0.6586670000
H -4.7956770000 0.2602390000 -1.6285680000
H -1.0038010000 0.7690910000 0.3384880000
H -5.1295580000 2.7376670000 -1.5997260000
H 1.6978090000 5.0467860000 0.7246770000
```

```
H 1.7395740000 3.5552590000 1.7042160000
H -0.1643680000 5.9279700000 1.9622290000
H 0.2811250000 4.7366110000 3.2149140000
H 1.0420350000 7.9904420000 -1.1757870000
H 0.2600370000 8.2070160000 -2.7616390000
H -6.3352560000 7.8080180000 0.9436830000
H -5.2799730000 7.5861450000 2.3630570000
```

(*E*)-1 unbound (solvated)

```
O -5.4686010000 -7.2978080000 0.6810500000

O -4.6028600000 -5.1026980000 0.5005230000

N -1.9551650000 -4.9382930000 -0.0757470000

N -0.8794920000 -4.2816740000 -0.0426720000

C -2.8913800000 -8.5127500000 0.0793190000

C -1.6796650000 -9.1464430000 -0.2061240000

C -0.5346070000 -8.3781270000 -0.4612750000

C -0.6050340000 -6.9880310000 -0.4219970000

C -3.0036900000 -7.1098850000 0.1234940000

C -1.8262460000 -6.3558180000 -0.1224200000

C -1.0096220000 1.4587430000 0.0270050000

C 0.1525190000 -0.7720960000 0.3307300000

C 0.1630700000 -2.1644590000 0.2961850000

C -1.0008100000 -2.8751860000 -0.0510270000

C -1.0078440000 -0.0502100000 -0.0022260000

C -2.1652800000 -2.1652090000 -0.4015060000

C -2.1582800000 -0.7729050000 -0.3746720000

B -4.4073200000 -6.4567230000 0.4478070000

H -6.2872480000 -6.8166390000 0.8725620000

H -3.7455040000 -4.6624040000 0.2960380000

H 0.4079430000 -8.8643490000 -0.6979000000

H 0.2712150000 -6.3844360000 -0.6300890000

H -1.6263550000 -10.2314990000 -0.2383320000

H -3.7741820000 -9.1155400000 0.2710990000

H -0.7751410000 1.8298500000 1.0320450000

H -0.2492120000 1.8650600000 -0.6504870000

H -1.9816180000 1.8635640000 -0.2678620000

H -3.0570730000 -2.6959480000 -0.7162670000

H -3.0583480000 -0.2320060000 -0.6562100000
```

H 1.0558110000 -0.2371110000 0.6133530000

H 1.0617210000 -2.7207120000 0.5475420000

(*E*)-2 unbound (solvated)

F 1.3640350000 8.5348720000 0.3531770000

F -3.3765760000 8.8564410000 0.0571710000

O -4.6983040000 6.2920400000 -0.2520490000

O -5.4897430000 4.0760970000 -0.4530100000

N -0.9099290000 7.1886630000 0.1184520000

N -1.9741320000 6.5216290000 -0.0100030000

C 0.2276170000 9.2697350000 0.3216420000

C 0.3378710000 10.6475990000 0.4128800000

C -0.8319800000 11.4113650000 0.3809300000

C -2.0824820000 10.7956800000 0.2600820000

C -2.1468940000 9.4149630000 0.1709710000

C -1.0027820000 8.5833200000 0.1965640000

C -1.8016120000 5.1097550000 -0.0837360000

C -0.5344260000 4.4988660000 -0.0162850000

C -0.4266540000 3.1142850000 -0.0964780000

C -1.5787630000 2.3277490000 -0.2439210000

C -2.8326260000 2.9385510000 -0.3090180000

C -2.9833230000 4.3365630000 -0.2314660000

B -4.4389150000 4.9515270000 -0.3135560000

H -0.7711720000 12.4927680000 0.4516060000

H -3.8559210000 6.7862090000 -0.1501180000

H -6.3450060000 4.5290310000 -0.4963980000

H -3.0017580000 11.3711210000 0.2341690000

H 1.3176550000 11.1029640000 0.5069100000

H -1.4952330000 1.2460370000 -0.3082350000

H -3.7187800000 2.3216860000 -0.4235860000

H 0.3493350000 5.1158420000 0.0976940000

H 0.5519290000 2.6447050000 -0.0442800000

(*E*)-3 unbound (solvated)

O 0.7788000000 -0.7208900000 7.4937600000

O 1.2645100000 -0.5147700000 5.1896100000

```
O -2.7907400000 -0.2845400000 0.1972300000
O 1.4680600000 -0.2672700000 2.3005700000
N -0.8935100000 -0.4775200000 3.5505900000
N -1.4434300000 -0.4083400000 2.4115100000
C 2.9043600000 -0.1996700000 2.2340300000
C -3.6171300000 -0.2289200000 -0.9761100000
C -1.2164300000 -0.6908100000 5.9361700000
C -1.7993500000 -0.6121800000 4.6445800000
C -3.1969000000 -0.6677600000 4.4775300000
C -4.0264600000 -0.8016800000 5.5872600000
C -3.4738400000 -0.8805000000 6.8745600000
C -2.0883400000 -0.8246800000 7.0351000000
C 1.3594300000 -0.0852400000 -0.1030700000
C 0.5699200000 -0.0299900000 -1.2521300000
C -0.8224500000 -0.0937200000 -1.1931400000
C -1.4464300000 -0.2170600000 0.0525000000
C -0.6746100000 -0.2800700000 1.2620000000
C 0.7528800000 -0.2092600000 1.1534600000
B 0.3424400000 -0.6371900000 6.1895800000
H 1.0549000000 0.0659900000 -2.2196800000
H 3.3048900000 -1.0379700000 1.6554600000
H 3.2272100000 0.7502200000 1.7964400000
H 3.2400300000 -0.2664900000 3.2679600000
H -3.4800300000 0.7188900000 -1.5077500000
H -3.4029700000 -1.0681800000 -1.6461100000
H -4.6415800000 -0.3009300000 -0.6100600000
H 1.7442000000 -0.6778000000 7.5614200000
H 0.8063200000 -0.4642600000 4.3152000000
H -3.6131900000 -0.6050100000 3.4785000000
H -5.1045300000 -0.8452700000 5.4528700000
H -4.1208700000 -0.9847600000 7.7412600000
H -1.6656200000 -0.8869100000 8.0337800000
H 2.4367700000 -0.0313000000 -0.1932600000
H -1.4028300000 -0.0471600000 -2.1052500000
```

(*E*)-1 bound (solvated)

O -0.2095240000 3.8445010000 1.2984030000

O 0.0740350000 3.6518580000 -0.9766060000

N -2.5734540000 5.2356540000 -0.1271880000

N -3.6109160000 4.5310280000 -0.0081980000

C -2.9942960000 10.9673870000 -0.1159400000

C 1.3088900000 4.2257760000 -0.4756520000

C 1.0043760000 4.5766050000 0.9958520000

C -1.7063110000 8.8054230000 -0.4139830000

C -1.6249760000 7.4141230000 -0.4052010000

C -2.9136560000 9.4597750000 -0.1123240000

C -4.0388040000 8.6706010000 0.1974810000

C -3.9728540000 7.2794840000 0.2038600000

C -2.7579660000 6.6386000000 -0.1033530000

C -3.3702390000 3.1333490000 -0.0114370000

C -2.0710600000 2.5714680000 0.0151520000

C -1.9759920000 1.1728560000 -0.0100380000

C -3.1171680000 0.3566830000 -0.0519880000

C -4.3906080000 0.9338650000 -0.0673640000

C -4.5163200000 2.3243360000 -0.0446560000

B -0.7664620000 3.4458530000 0.0987950000

H -0.6912270000 6.9136470000 -0.6435160000

H -4.8477500000 6.6877770000 0.4499810000

H -2.3078110000 11.3988270000 0.6224410000

H -2.7094630000 11.3733750000 -1.0941140000

H -4.0052000000 11.3138020000 0.1160180000

H -0.8231940000 9.3910400000 -0.6571990000

H -4.9792990000 9.1588990000 0.4409880000

H -3.0067700000 -0.7245180000 -0.0680830000

H -5.2778170000 0.3079710000 -0.0979330000

H -0.9956920000 0.7017670000 0.0096610000

H -5.4934310000 2.7990790000 -0.0586330000

H 1.5676980000 5.1009900000 -1.0766040000

H 2.0994950000 3.4747420000 -0.5708130000

H 0.8108990000 5.6449750000 1.1385460000

H 1.7922070000 4.2586600000 1.6825740000

(*E*)-2 bound (solvated)

F −1.3682620000 6.1406190000 −1.2207700000

F 2.3950540000 5.6288700000 1.6366120000

O 2.8837660000 2.2747480000 0.9196700000

O 2.4582610000 2.8135000000 −1.2754650000

N 0.4223730000 4.3879230000 0.3089240000

N −0.6990610000 3.8575680000 0.0815570000

C 3.7894190000 3.3196430000 −1.0028020000

C 4.1498060000 2.7325620000 0.3782770000

C 1.5521210000 6.4152850000 0.9235040000

C 1.7740320000 7.7830670000 0.9149540000

C 0.9056940000 8.5922740000 0.1760190000

C −0.1589640000 8.0308160000 −0.5363060000

C −0.3540490000 6.6581710000 −0.4884630000

C 0.4853150000 5.7912010000 0.2453550000

C −0.8589430000 −0.3375750000 0.1442690000

C 0.3957550000 0.2881680000 0.0805650000

C 0.5210100000 1.6840060000 0.0409230000

C −0.6757350000 2.4411000000 0.0843870000

C −1.9351140000 1.8231350000 0.1303170000

C −2.0270640000 0.4308910000 0.1663380000

B 1.9447960000 2.3382060000 −0.0857030000

H 3.7495010000 4.4136910000 −0.9914240000

H 4.4646850000 2.9904180000 −1.7959600000

H 4.5804850000 3.4745840000 1.0546540000

H 4.8221410000 1.8722040000 0.3045450000

H 1.2895140000 −0.3305780000 0.0501400000

H −3.0002780000 −0.0494830000 0.2104620000

H −0.9196240000 −1.4225170000 0.1681560000

H −2.8251510000 2.4454140000 0.1493530000

H 1.0619580000 9.6661700000 0.1501600000

H −0.8328160000 8.6409020000 −1.1286410000

H 2.6076730000 8.1959370000 1.4725130000

(*E*)-3 bound (solvated)

O -4.7840320000 6.4554380000 0.6833010000

O -0.5884040000 6.6750150000 -1.4938500000

O -1.0970010000 4.0631780000 1.8253100000

O 0.3427650000 3.5517550000 0.1058230000

N -2.5143920000 5.1864160000 -0.5235570000

N -3.5421010000 4.4584420000 -0.6215320000

C 1.1413990000 4.2517640000 1.0930690000

C 0.1102420000 4.8197000000 2.0882230000

C 0.5640340000 7.3968870000 -1.9507530000

C -5.8094240000 7.0615490000 1.4861290000

C -1.6022590000 8.7542590000 -0.7589380000

C -1.5933850000 7.3614480000 -0.8941740000

C -2.6930000000 9.3679910000 -0.1396300000

C -3.7722750000 8.6291590000 0.3461840000

C -3.7842350000 7.2337310000 0.2020930000

C -2.6861050000 6.5740400000 -0.4260590000

C -3.2500900000 3.0696560000 -0.5924990000

C -2.0376510000 2.5520420000 -0.0754550000

C -1.8506870000 1.1626240000 -0.1409280000

C -2.8312280000 0.3123900000 -0.6723510000

C -4.0335480000 0.8445920000 -1.1516180000

C -4.2460360000 2.2236570000 -1.1046430000

B -0.9471280000 3.4668490000 0.5867560000

H -0.7826580000 9.3568800000 -1.1288120000

H -2.7026110000 10.4493910000 -0.0328840000

H -4.5951650000 9.1393230000 0.8303970000

H -2.6589820000 -0.7603690000 -0.7009060000

H -4.7999810000 0.1903780000 -1.5575260000

H -0.9304810000 0.7285450000 0.2432940000

H -5.1689080000 2.6610540000 -1.4752130000

H 1.7260720000 5.0294030000 0.5962470000

H 1.8194440000 3.5308280000 1.5610450000

```
H -0.0983470000 5.8800530000 1.9095630000

H 0.4001490000 4.6790080000 3.1321890000

H 1.0548290000 7.9196070000 -1.1228570000

H 1.2358300000 6.6413820000 -2.3593550000

H 0.2932530000 8.1123990000 -2.7347020000

H -6.3984920000 7.7726550000 0.8975410000

H -6.4461530000 6.2377500000 1.8093550000

H -5.3789190000 7.5629690000 2.3594450000
```

Reversible binding of fluorophore

A stock solution (**A**) of **17** was prepared by dissolving 4.0 mg into 5 mL of 0.1 M PBS buffered at pH 7.5 in a 5 mL volumetric flask. Another stock solution (**B**) of **P1** was prepared by dissolving 44 mg into 440 µL of 0.1 M PBS buffered at pH 7.5. 306 uL of stock solution **A** and 10 µL of stock solution **B** (such that ratio of boronic acid to diol was 1:1) were added to a scintillation vial which was diluted to 3 mL with the PBS buffer. Three of these solutions were prepared. Solution 1 was placed in the dark for one hour, solution 2 was irradiated with red LEDs for one hour, and solution 3 was irradiated with red LEDs for one hour, followed by blue LEDs for 10 minutes. After, 3 mL of each sample was loaded into a 15 mL Amicon ultra-15 centrifugal filter (MWCO= 3 kDa) and spin filtered for 20 minutes at 5000 RPM. The eluents were characterized by UV-Vis (Figure S24) and fluorescence (Figure 8b).
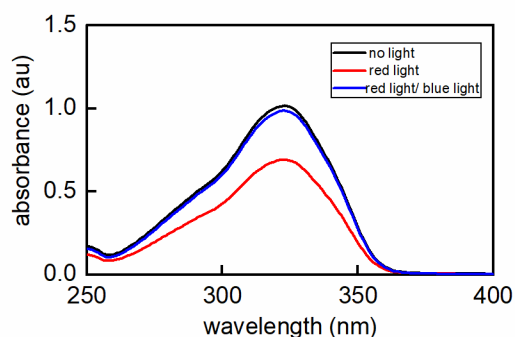

Figure 64. Results of reversible binding of fluorescence diol. Fluorescence spectrum of solution 1 eluents (no irradiation, black trace), solution 2 (60 min red light, red trace) and solution 3 (60 min red light, 10 min blue light, blue trace) in 0.1 M PBS pH 7.5.
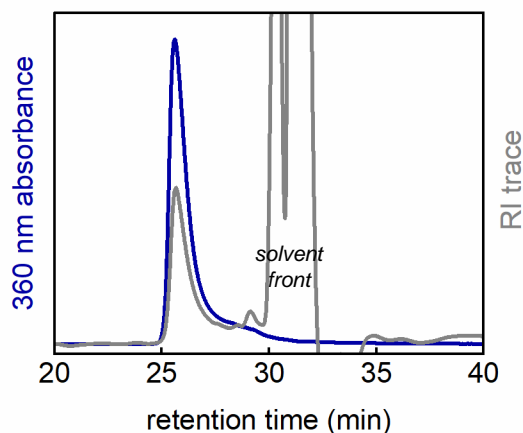
Figure 65. Normalized GPC traces of P1 (1 mg/mL) in THF measured by 365 nm absorbance and RI trace.

Hydrogel fabrication and rheological characterization

Gels were prepared by mixing 200 μL of **P1** (10 w/v%) with **P2** (10 w/v%) in either DMEM or 0.1 M PBS pH 7.5. Hydrogels prepared in PBS were too sticky and difficult to transfer from vials to the rheometer, as such were only characterized by the flow inversion method. Hydrogels in DMEM could easy be removed from the vial, and as such were characterized by photorheology. Mechanical characterization of the prepared hydrogels was performed using an Anton Paar MCR 302 Rheometer with a 25 mm, 5° cone-plate attachment. 10% strain was established to be within the linear viscoelastic regime for all time points tested (Figure S52). Unless noted otherwise, oscillatory strain amplitude sweeps were conducted using a frequency of 25 rad/s and oscillatory frequencies were conducted using 10% strain. Gelation profiles were conducted with 10% strain and a frequency of 25 rad/s. Frequency sweeps were performed at 10% strain, with a frequency range of 100 to 0.1 rad/s. Data were collected at 25 °C.
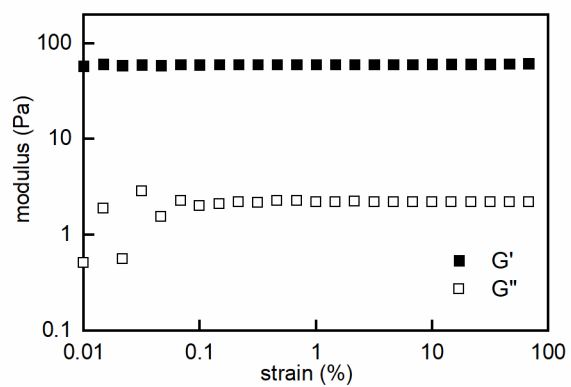
Figure 66. Amplitude sweep (25 rad/s) of hydrogel (1:1 P1/P2, 10 w/v% in DMEM) after three hours of irradiation with red light.

X-ray crystallographic data

<p align="center">(E)-1</p>

Single crystals of (E)-1 were grown by cooling a concentrated solution in acetonitrile.

Table 4. Crystal data and structure refinement for (E)-1.

(E)-(2-(p-tolyldiazenyl)phenyl)boronic acid

Table 1 Crystal data and structure refinement for (E)-1.

Identification code   CCDC# 2022207

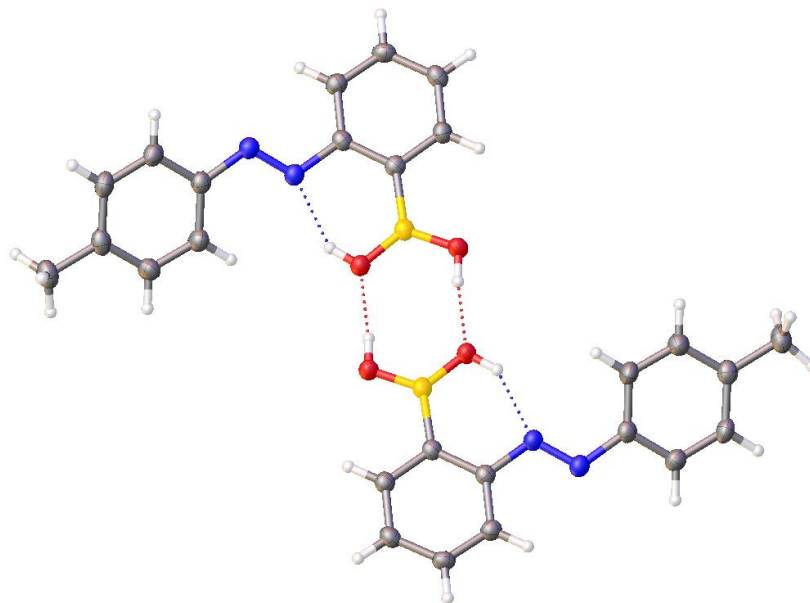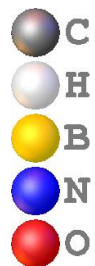|	
Empirical formula	$C_{26}H_{26}B_2N_4O_4$
Formula weight	480.13
Temperature/K	102(3)
Crystal system	monoclinic
Space group	$P2_1/c$
a/Å	10.7395(3)
b/Å	11.9528(2)
c/Å	19.6161(5)
α/°	90
β/°	101.882(2)
γ/°	90
Volume/Å³	2464.11(10)
Z	4
ϱ_{calc}g/cm³	1.294
μ/mm⁻¹	0.705
F(000)	1008.0
Crystal size/mm³	0.14 × 0.07 × 0.02
Radiation	CuKα (λ = 1.54184)
2Θ range for data collection/°	8.414 to 157.658
Index ranges	-12 ≤ h ≤ 13, -14 ≤ k ≤ 14, -22 ≤ l ≤ 24
Reflections collected	20929
Independent reflections	5174 [R_{int} = 0.0384, R_{sigma} = 0.0331]
Data/restraints/parameters	5174/0/331
Goodness-of-fit on F^2	1.062
Final R indexes [I>=2σ (I)]	R_1 = 0.0462, wR_2 = 0.1175
Final R indexes [all data]	R_1 = 0.0569, wR_2 = 0.1235
Largest diff. peak/hole / e Å⁻³	0.27/-0.21

Table 5. Fractional Atomic Coordinates (×10⁴) and Equivalent Isotropic Displacement Parameters (Å²×10³) for cx1429xprep. U_eq is defined as 1/3 of of the trace of the orthogonalised U_{IJ} tensor.

Table 2 Fractional Atomic Coordinates (×10⁴) and Equivalent Isotropic Displacement Parameters (Å²×10³) for cx1429xprep. U_eq is defined as 1/3 of of the trace of the orthogonalised U_{IJ} tensor.

Atom	x	y	z	U(eq)
O001	6233.4(10)	4991.6(8)	4579.8(5)	28.3(2)
O002	5912.1(10)	3015.5(9)	5262.4(5)	29.3(2)
O003	4132.4(10)	2798.6(8)	4338.4(5)	28.8(2)
O004	4512.1(10)	4715.0(9)	3634.7(5)	30.0(2)
N005	2625.4(11)	1032.7(10)	4453.0(6)	25.3(3)
N006	7854.3(12)	6650.2(10)	4400.2(6)	25.7(3)
N007	1584.0(12)	521.7(10)	4294.8(7)	28.1(3)
N008	8955.2(12)	7059.1(10)	4518.0(7)	28.3(3)
C009	5975.9(14)	6311.8(11)	3513.0(7)	24.7(3)
C00A	4505.4(14)	1360.7(11)	5345.2(7)	24.1(3)
C00B	7077.3(14)	6954.3(11)	3744.0(7)	24.5(3)
C00C	3416.9(14)	705.6(11)	5102.6(7)	24.0(3)
C00D	5300.8(14)	1040.9(12)	5972.6(8)	26.3(3)
C00E	9707.3(14)	6795.7(12)	5183.7(8)	27.5(3)
C00F	826.3(14)	801.2(12)	3634.6(8)	27.2(3)
C00G	5216.7(14)	6593.9(12)	2867.7(7)	26.8(3)
C00H	5524.6(15)	7478.3(12)	2474.8(8)	29.2(3)
C00I	7379.7(15)	7862.9(12)	3356.9(8)	27.3(3)
C00J	3947.1(15)	-514.9(12)	6090.3(8)	29.0(3)
C00K	5033.2(15)	114.7(12)	6343.9(8)	28.7(3)
C00L	11000.3(15)	7031.5(13)	5274.0(8)	31.2(3)
C00M	6602.5(15)	8117.4(12)	2724.1(8)	29.5(3)
C00N	3137.4(14)	-230.5(12)	5474.7(8)	27.7(3)
C00O	11345.4(15)	6384.8(12)	6465.1(8)	32.1(3)

C00P	-833.8(15)	1220.4(13)	2357.0(8)	31.3(3)
C00Q	-1267.5(15)	714.9(14)	2903.1(9)	33.2(3)
C00R	9226.5(15)	6368.3(13)	5740.2(8)	32.2(3)
C00S	1279.8(15)	1308.6(13)	3092.7(8)	32.0(3)
C00T	10044.8(16)	6173.3(13)	6371.5(9)	34.3(3)
C00U	11806.0(15)	6816.6(13)	5906.6(8)	32.3(3)
C00V	-447.6(15)	496.4(13)	3532.8(8)	31.9(3)
C00W	453.6(16)	1506.5(14)	2465.2(8)	35.0(4)
C00X	-1702.2(17)	1441.7(16)	1662.1(9)	39.7(4)
C00Y	12223.5(17)	6162.7(15)	7156.1(9)	40.6(4)
B1	5558.1(16)	5298.2(13)	3937.8(8)	25.1(3)
B2	4865.6(16)	2440.3(13)	4956.7(8)	24.6(3)

Table 6 Anisotropic Displacement Parameters ($Å^2×10^3$) for cx1429xprep. The Anisotropic displacement factor exponent takes the form: $-2\pi^2[h^2a^{*2}U_{11}+2hka^*b^*U_{12}+…]$.

Anisotropic Displacement Parameters ($Å^2×10^3$) for cx1429xprep. The Anisotropic displacement factor exponent takes the form: $-2\pi^2[h^2a^{*2}U_{11}+2hka^*b^*U_{12}+…]$.

Atom	U_{11}	U_{22}	U_{33}	U_{23}	U_{13}	U_{12}
O001	29.1(6)	25.3(5)	28.2(5)	2.2(4)	0.7(4)	-4.4(4)
O002	31.1(6)	26.4(5)	27.8(5)	4.1(4)	0.1(4)	-5.4(4)
O003	31.3(6)	24.9(5)	27.2(5)	2.3(4)	-0.7(4)	-6.6(4)
O004	36.0(6)	26.2(5)	25.4(5)	2.2(4)	0.4(4)	-6.0(4)
N005	26.0(6)	23.0(6)	26.3(6)	-2.4(4)	3.8(5)	-2.3(5)
N006	26.4(6)	23.0(6)	26.8(6)	-1.6(5)	3.5(5)	-0.6(5)
N007	28.0(6)	26.8(6)	28.7(6)	-1.9(5)	3.7(5)	-3.3(5)
N008	28.4(7)	27.0(6)	28.6(6)	-1.3(5)	4.0(5)	-2.1(5)
C009	27.5(7)	20.9(6)	26.0(7)	-3.0(5)	6.3(6)	1.7(5)
C00A	27.0(7)	21.6(6)	23.5(7)	-3.0(5)	5.2(5)	0.5(5)
C00B	26.9(7)	23.5(6)	22.9(7)	-2.1(5)	4.8(5)	2.4(5)

C00C	26.0(7)	22.9(6)	23.4(7)	-2.5(5)	5.7(6)	0.9(5)
C00D	28.0(7)	25.0(7)	25.6(7)	-2.6(5)	4.9(6)	-0.8(5)
C00E	28.8(8)	24.3(7)	28.2(7)	-2.6(5)	2.8(6)	-0.7(6)
C00F	29.1(8)	24.6(7)	26.6(7)	-4.6(5)	2.6(6)	-2.8(6)
C00G	28.1(7)	25.9(7)	25.4(7)	-3.8(5)	3.2(6)	-0.8(6)
C00H	33.8(8)	28.8(7)	23.6(7)	-0.8(6)	2.7(6)	3.8(6)
C00I	29.1(7)	24.0(7)	29.3(7)	-2.1(5)	7.2(6)	-0.8(6)
C00J	36.7(8)	24.1(7)	27.4(7)	2.7(5)	9.3(6)	-1.6(6)
C00K	34.3(8)	29.0(7)	22.1(7)	0.6(5)	3.7(6)	2.1(6)
C00L	30.2(8)	31.5(8)	31.2(8)	-5.5(6)	5.1(6)	-5.8(6)
C00M	35.8(8)	24.7(7)	29.4(8)	3.2(6)	9.9(6)	0.6(6)
C00N	30.5(8)	24.9(7)	28.2(7)	-2.5(6)	7.1(6)	-3.5(6)
C00O	33.5(8)	25.5(7)	33.2(8)	-4.8(6)	-2.6(6)	2.4(6)
C00P	31.3(8)	30.7(8)	30.6(8)	-5.5(6)	3.0(6)	-0.2(6)
C00Q	24.4(7)	36.4(8)	36.9(8)	-3.8(6)	2.0(6)	-6.1(6)
C00R	27.3(8)	33.7(8)	33.9(8)	2.7(6)	2.7(6)	-1.9(6)
C00S	25.6(8)	38.1(8)	31.2(8)	-2.3(6)	3.1(6)	-7.5(6)
C00T	36.4(9)	34.1(8)	30.8(8)	4.9(6)	3.1(7)	-0.7(7)
C00U	26.0(8)	32.4(8)	36.2(8)	-7.6(6)	1.3(6)	-2.5(6)
C00V	31.0(8)	31.5(8)	32.7(8)	-0.5(6)	5.7(6)	-6.7(6)
C00W	33.7(8)	41.7(9)	28.6(8)	1.1(6)	4.0(6)	-5.5(7)
C00X	35.7(9)	46.6(10)	33.1(9)	-2.5(7)	-1.6(7)	-1.3(7)
C00Y	38.8(9)	40.3(9)	37.0(9)	-1.4(7)	-5.3(7)	4.0(7)
B1	26.8(8)	22.7(7)	25.3(8)	-3.4(6)	4.5(6)	0.9(6)
B2	25.9(8)	23.7(7)	23.9(8)	-3.5(6)	4.6(6)	-0.6(6)

Table 7. Bond Lengths for cx1429xprep.

Bond Lengths for cx1429xprep.

Atom	Atom	Length/Å	Atom	Atom	Length/Å
O001	B1	1.3675(19)	C00E	C00L	1.392(2)
O002	B2	1.3483(19)	C00E	C00R	1.397(2)
O003	B2	1.3716(19)	C00F	C00S	1.396(2)
O004	B1	1.3514(19)	C00F	C00V	1.390(2)
N005	N007	1.2559(17)	C00G	C00H	1.388(2)
N005	C00C	1.4329(19)	C00H	C00M	1.389(2)
N006	N008	1.2561(17)	C00I	C00M	1.380(2)
N006	C00B	1.4294(19)	C00J	C00K	1.391(2)
N007	C00F	1.420(2)	C00J	C00N	1.378(2)
N008	C00E	1.422(2)	C00L	C00U	1.383(2)
C009	C00B	1.405(2)	C00O	C00T	1.394(2)
C009	C00G	1.399(2)	C00O	C00U	1.391(2)
C009	B1	1.587(2)	C00O	C00Y	1.507(2)
C00A	C00C	1.406(2)	C00P	C00Q	1.391(2)
C00A	C00D	1.399(2)	C00P	C00W	1.397(2)
C00A	B2	1.586(2)	C00P	C00X	1.508(2)
C00B	C00I	1.401(2)	C00Q	C00V	1.386(2)
C00C	C00N	1.402(2)	C00R	C00T	1.383(2)
C00D	C00K	1.387(2)	C00S	C00W	1.382(2)

Table 8. Bond Angles for cx1429xprep.

Bond Angles for cx1429xprep.

Atom	Atom	Atom	Angle/°	Atom	Atom	Atom	Angle/°
N007	N005	C00C	114.96(12)	C00M	C00I	C00B	119.58(14)
N008	N006	C00B	114.81(12)	C00N	C00J	C00K	120.76(13)
N005	N007	C00F	115.14(12)	C00D	C00K	C00J	119.53(14)
N006	N008	C00E	114.71(12)	C00U	C00L	C00E	120.00(15)

C00B C009 B1	123.94(13)	C00I C00M C00H	120.10(14)
C00G C009 C00B	117.09(13)	C00J C00N C00C	119.29(14)
C00G C009 B1	118.97(13)	C00T C00O C00Y	120.74(16)
C00C C00A B2	123.94(13)	C00U C00O C00T	118.21(15)
C00D C00A C00C	117.39(13)	C00U C00O C00Y	121.04(15)
C00D C00A B2	118.66(13)	C00Q C00P C00W	117.85(15)
C009 C00B N006	116.62(12)	C00Q C00P C00X	121.96(15)
C00I C00B N006	121.85(13)	C00W C00P C00X	120.18(15)
C00I C00B C009	121.51(13)	C00V C00Q C00P	121.06(15)
C00A C00C N005	116.66(12)	C00T C00R C00E	119.51(15)
C00N C00C N005	121.97(13)	C00W C00S C00F	119.49(14)
C00N C00C C00A	121.37(13)	C00R C00T C00O	121.48(15)
C00K C00D C00A	121.66(14)	C00L C00U C00O	121.16(15)
C00L C00E N008	115.80(13)	C00Q C00V C00F	120.31(15)
C00L C00E C00R	119.61(14)	C00S C00W C00P	121.82(15)
C00R C00E N008	124.54(14)	O001 B1 C009	122.32(13)
C00S C00F N007	124.92(14)	O004 B1 O001	120.14(13)
C00V C00F N007	115.58(13)	O004 B1 C009	117.53(13)
C00V C00F C00S	119.46(14)	O002 B2 O003	120.55(13)
C00H C00G C009	121.68(14)	O002 B2 C00A	117.68(13)
C00G C00H C00M	120.00(14)	O003 B2 C00A	121.76(13)

Table 9. Hydrogen Atom Coordinates (Å×10^4) and Isotropic Displacement Parameters (Å^2×10^3) for cx1429xprep.

Hydrogen Atom Coordinates (Å×10^4) and Isotropic Displacement Parameters (Å^2×10^3) for cx1429xprep.

Atom	x	y	z	U(eq)
H001	6880	5400	4689	42
H002	5965	3605	5036	44
H003	3539	2341	4205	43

H004	4408	4176	3892	45
H00D	6043	1469	6149	32
H00G	4471	6169	2694	32
H00H	4998	7647	2035	35
H00I	8115	8301	3529	33
H00J	3762	-1148	6345	35
H00K	5588	-88	6768	34
H00L	11329	7340	4901	37
H00M	6805	8731	2458	35
H00N	2397	-664	5304	33
H00Q	-2140	516	2843	40
H00R	8344	6213	5685	39
H00S	2150	1516	3155	38
H00T	9713	5889	6750	41
H00U	12690	6967	5961	39
H00V	-758	137	3896	38
H00W	769	1846	2097	42
H00E	-2543	1122	1660	60
H00F	-1346	1096	1291	60
H00O	-1782	2250	1583	60
H00A	11719	6019	7510	61
H00B	12769	6816	7292	61
H00C	12753	5509	7115	61

(E)-**2**

Single crystals of (E)-**2** were grown by cooling a concentrated solution in DCM.
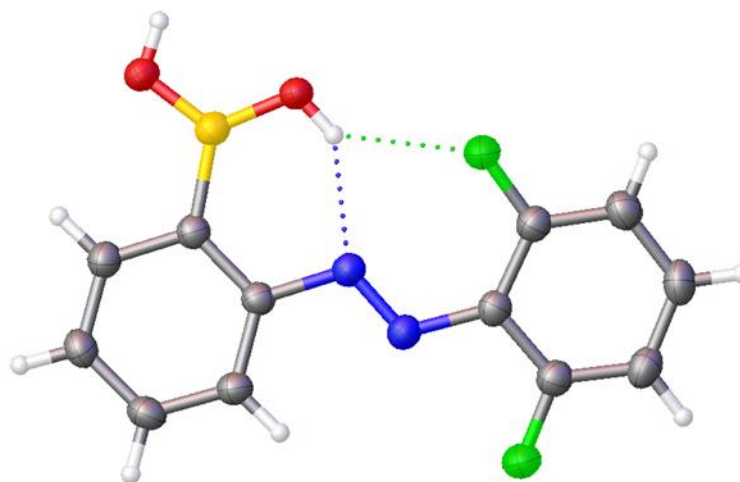
Table 10. Crystal data and structure refinement for (E)-2.

(E)-(2-((2,6-difluorophenyl)diazenyl)phenyl)boronic acid

Table 1 Crystal data and structure refinement for (E)-2.

Identification code	CCDC # 2020825
Empirical formula	$C_{12}H_9BF_2N_2O_2$
Formula weight	262.02
Temperature/K	200.00(10)
Crystal system	triclinic

Space group	P-1
a/Å	3.81460(10)
b/Å	11.3358(2)
c/Å	14.5651(3)
$\alpha/°$	112.536(2)
$\beta/°$	93.972(2)
$\gamma/°$	92.375(2)
Volume/Å^3	578.74(2)
Z	2
ϱ_{calc}g/cm^3	1.504
μ/mm^{-1}	1.063
F(000)	268.0
Crystal size/mm^3	0.342 × 0.096 × 0.031
Radiation	CuKα (λ = 1.54184)
2Θ range for data collection/°	6.598 to 152.982
Index ranges	-4 ≤ h ≤ 4, -14 ≤ k ≤ 14, -18 ≤ l ≤ 18
Reflections collected	17174
Independent reflections	2389 [R_{int} = 0.0454, R_{sigma} = 0.0241]
Data/restraints/parameters	2389/0/174
Goodness-of-fit on F^2	1.088
Final R indexes [I>=2σ (I)]	R_1 = 0.0355, wR_2 = 0.1035
Final R indexes [all data]	R_1 = 0.0382, wR_2 = 0.1066
Largest diff. peak/hole / e Å^{-3}	0.30/-0.20

Table 11 Fractional Atomic Coordinates (×10^4) and Equivalent Isotropic Displacement Parameters (Å^2×10^3) for cx1948. U_{eq} is defined as 1/3 of of the trace of the orthogonalised U_{IJ} tensor.

Table 2 Fractional Atomic Coordinates (×10^4) and Equivalent Isotropic Displacement Parameters (Å^2×10^3) for cx1948. U_{eq} is defined as 1/3 of of the trace of the orthogonalised U_{IJ} tensor.

Atom	*x*	*y*	*z*	U(eq)

F18	6269(2)	2483.5(7)	6190.5(5)	47.1(2)
F19	2662(2)	5826.2(7)	9001.0(5)	47.4(2)
O17	7265(3)	10269.1(8)	8971.4(6)	43.5(2)
O16	5085(3)	8407.9(8)	9152.3(6)	41.5(2)
N8	5851(3)	6172.1(9)	7523.4(7)	31.1(2)
N7	5770(3)	4982.2(9)	7060.4(7)	33.4(2)
C9	7120(3)	6890.3(10)	6978.1(8)	28.9(2)
C14	7543(3)	8225.8(10)	7490.2(8)	29.8(2)
C1	4608(3)	4216.8(10)	7565.9(8)	31.5(3)
C2	4937(3)	2900.1(11)	7083.3(9)	35.3(3)
C6	3203(3)	4583.3(11)	8492.3(9)	34.1(3)
C10	7905(3)	6302.7(11)	5985.1(8)	33.9(3)
C13	8839(3)	8932.8(11)	6962.4(9)	34.3(3)
C12	9618(3)	8357.8(12)	5982.1(9)	37.2(3)
C3	4026(3)	2016.8(11)	7475.5(10)	39.7(3)
C11	9139(3)	7034.2(12)	5490.6(9)	37.3(3)
C5	2297(3)	3726.7(12)	8911.4(9)	38.7(3)
C4	2717(3)	2437.0(12)	8400.1(10)	40.8(3)
B15	6598(4)	8985.7(12)	8594.0(10)	33.4(3)

Table 12 Anisotropic Displacement Parameters ($Å^2×10^3$) for cx1948. The Anisotropic displacement factor exponent takes the form: $-2\pi^2[h^2a*^2U_{11}+2hka*b*U_{12}+\ldots]$.

Anisotropic Displacement Parameters ($Å^2×10^3$) for cx1948. The Anisotropic displacement factor exponent takes the form: $-2\pi^2[h^2a*^2U_{11}+2hka*b*U_{12}+\ldots]$.

Atom	U_{11}	U_{22}	U_{33}	U_{23}	U_{13}	U_{12}
F18	64.6(5)	32.3(4)	41.8(4)	8.9(3)	20.1(4)	3.8(3)
F19	70.8(5)	30.8(4)	40.0(4)	10.0(3)	23.5(4)	3.5(3)
O17	62.8(6)	27.5(4)	36.5(5)	6.6(3)	18.2(4)	-2.8(4)
O16	61.9(6)	26.7(4)	32.4(4)	6.0(3)	17.5(4)	-3.1(4)
N8	34.2(5)	27.1(4)	30.2(5)	8.9(4)	5.6(4)	-0.6(4)

N7	38.6(5)	27.5(5)	32.2(5)	9.5(4)	6.2(4)	-1.0(4)
C9	27.3(5)	29.3(5)	29.0(5)	10.0(4)	4.8(4)	0.6(4)
C14	28.4(5)	29.1(5)	30.8(5)	10.3(4)	4.7(4)	0.2(4)
C1	31.2(6)	29.2(5)	32.8(6)	11.2(4)	2.0(4)	-2.3(4)
C2	35.9(6)	31.8(6)	35.3(6)	10.0(5)	5.4(5)	-1.4(4)
C6	35.8(6)	30.0(5)	33.9(6)	10.0(4)	3.8(5)	-1.3(4)
C10	37.9(6)	30.0(5)	30.7(5)	7.9(4)	7.0(4)	1.5(4)
C13	35.9(6)	29.5(5)	36.7(6)	11.5(5)	7.2(5)	-1.3(4)
C12	38.2(6)	38.7(6)	39.3(6)	19.2(5)	10.3(5)	0.0(5)
C3	39.3(7)	28.7(6)	50.5(7)	15.1(5)	4.9(5)	-1.4(5)
C11	40.9(7)	40.4(6)	29.7(5)	11.4(5)	10.6(5)	3.3(5)
C5	39.4(6)	40.5(6)	37.8(6)	16.7(5)	6.7(5)	-2.3(5)
C4	39.0(6)	38.4(6)	51.1(7)	24.5(6)	5.1(5)	-4.5(5)
B15	36.7(7)	28.3(6)	32.5(6)	8.6(5)	6.2(5)	0.0(5)

Table 4 Bond Lengths for cx1948.

Atom	Atom	Length/Å	Atom	Atom	Length/Å
F18	C2	1.3466(14)	C14	B15	1.5815(16)
F19	C6	1.3497(13)	C1	C2	1.4004(16)
O17	B15	1.3492(15)	C1	C6	1.4034(16)
O16	B15	1.3658(15)	C2	C3	1.3736(17)
N8	N7	1.2536(13)	C6	C5	1.3750(16)
N8	C9	1.4298(13)	C10	C11	1.3786(16)
N7	C1	1.4121(14)	C13	C12	1.3834(16)
C9	C14	1.4043(15)	C12	C11	1.3903(17)
C9	C10	1.4011(15)	C3	C4	1.3823(19)
C14	C13	1.4033(15)	C5	C4	1.3853(18)

Table 5 Bond Angles for cx1948.

Atom	Atom	Atom	Angle/°	Atom	Atom	Atom	Angle/°
N7	N8	C9	113.99(9)	F19	C6	C1	119.43(10)
N8	N7	C1	116.83(9)	F19	C6	C5	117.61(10)
C14	C9	N8	116.45(9)	C5	C6	C1	122.96(11)
C10	C9	N8	122.22(10)	C11	C10	C9	120.18(10)
C10	C9	C14	121.32(10)	C12	C13	C14	122.28(10)
C9	C14	B15	125.30(10)	C13	C12	C11	119.81(10)
C13	C14	C9	116.63(10)	C2	C3	C4	118.86(11)
C13	C14	B15	118.05(10)	C10	C11	C12	119.76(10)
C2	C1	N7	115.73(10)	C6	C5	C4	119.41(11)
C2	C1	C6	114.82(10)	C3	C4	C5	120.19(11)
C6	C1	N7	129.45(10)	O17	B15	O16	119.91(10)
F18	C2	C1	117.87(10)	O17	B15	C14	116.90(10)
F18	C2	C3	118.38(10)	O16	B15	C14	123.17(10)
C3	C2	C1	123.74(11)				

Table 6 Hydrogen Bonds for cx1948.

D	H	A	d(D-H)/Å	d(H-A)/Å	d(D-A)/Å	D-H-A/°
O17	H17	O16[1]	0.84	1.97	2.7982(11)	169.3
O16	H16	F19	0.84	2.27	2.9531(11)	138.9
O16	H16	N8	0.84	2.05	2.7724(12)	144.1

[1]1-X,2-Y,2-Z

Table 7 Torsion Angles for cx1948.

A	B	C	D	Angle/°	A	B	C	D	Angle/°
F18	C2	C3	C4	178.80(11)	C9	C10	C11	C12	0.30(19)
F19	C6	C5	C4	178.18(11)	C14	C9	C10	C11	0.38(18)

N8 N7 C1 C2	-172.67(10)	C14 C13 C12 C11	-0.35(19)
N8 N7 C1 C6	6.46(18)	C1 C2 C3 C4	-0.2(2)
N8 C9 C14 C13	179.08(9)	C1 C6 C5 C4	-1.10(19)
N8 C9 C14 B15	-2.43(17)	C2 C1 C6 F19	-177.65(10)
N8 C9 C10 C11	-179.69(10)	C2 C1 C6 C5	1.62(18)
N7 N8 C9 C14	-174.93(10)	C2 C3 C4 C5	0.8(2)
N7 N8 C9 C10	5.14(16)	C6 C1 C2 F18	-179.98(10)
N7 C1 C2 F18	-0.72(16)	C6 C1 C2 C3	-0.96(18)
N7 C1 C2 C3	178.30(11)	C6 C5 C4 C3	-0.2(2)
N7 C1 C6 F19	3.22(19)	C10 C9 C14 C13	-0.99(16)
N7 C1 C6 C5	-177.52(11)	C10 C9 C14 B15	177.51(11)
C9 N8 N7 C1	178.75(9)	C13 C14 B15 O17	-3.07(17)
C9 C14 C13 C12	0.98(17)	C13 C14 B15 O16	175.15(11)
C9 C14 B15 O17	178.46(11)	C13 C12 C11 C10	-0.31(19)
C9 C14 B15 O16	-3.32(19)	B15 C14 C13 C12	-177.63(11)

Table 8 Hydrogen Atom Coordinates ($Å×10^4$) and Isotropic Displacement Parameters ($Å^2×10^3$) for cx1948.

Atom	x	y	z	U(eq)
H17	6621.28	10582	9551.21	65
H16	4921.82	7610.25	8836.64	62
H10	7585.68	5397.8	5651.68	41
H13	9191.99	9837.77	7289.76	41
H12	10479.26	8865.9	5645.74	45
H3	4291.04	1132.21	7117.49	48
H11	9659.72	6635.36	4816.29	45
H5	1391.12	4016.68	9545.98	46

| H4 | 2103.61 | 1839.6 | 8685.6 | 49 |

(*E*)-**3**

Single crystals of (*E*)-**3** were grown by slow evaporation of a solution of ACN.
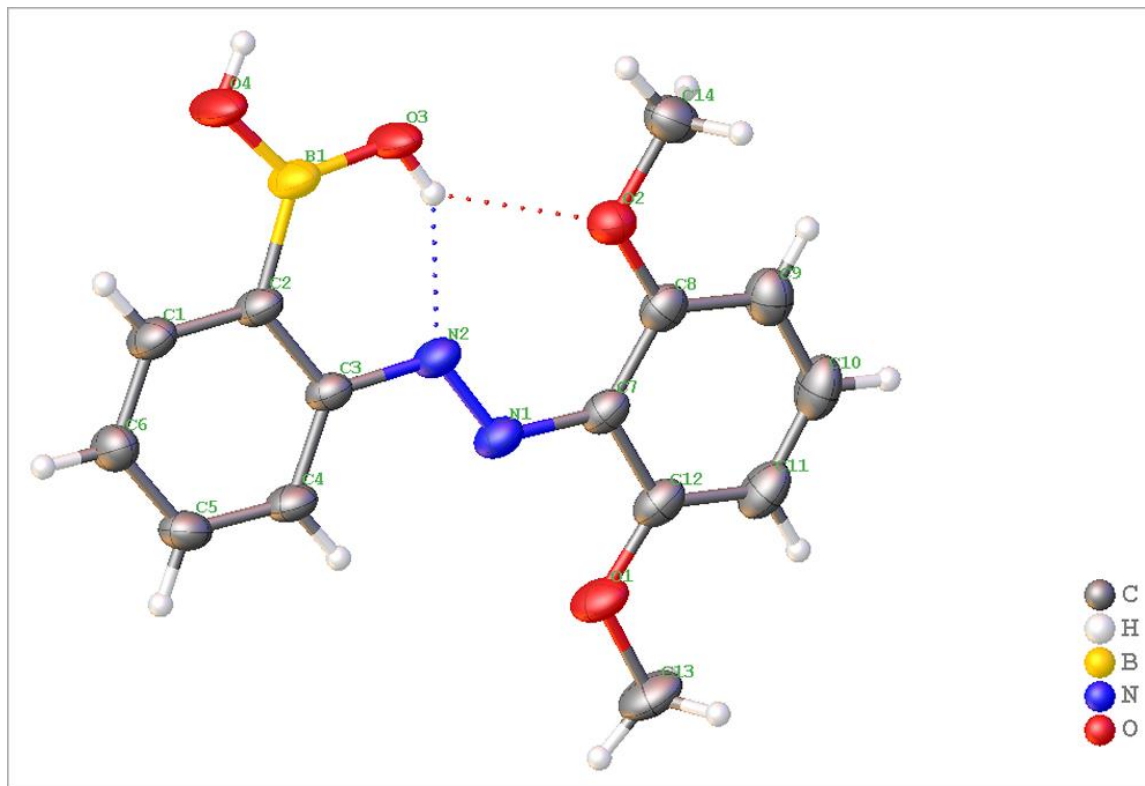
(*E*)-(2-((2,6-dimethoxyphenyl)diazenyl)phenyl)boronic acid

Table 1 Crystal data and structure refinement for (*E*)-3

Identification code	CCDC #2008419
Empirical formula	$C_{14}H_{15}BN_2O_4$
Formula weight	286.09
Temperature/K	200.01(10)
Crystal system	monoclinic
Space group	$P2_1/n$

a/Å	17.8347(3)
b/Å	4.10813(10)
c/Å	19.0734(4)
$\alpha/°$	90
$\beta/°$	101.795(2)
$\gamma/°$	90
Volume/Å^3	1367.95(5)
Z	4
ϱ_{calc}g/cm^3	1.389
μ/mm^{-1}	0.840
F(000)	600.0
Crystal size/mm^3	0.228 × 0.104 × 0.048
Radiation	CuKα (λ = 1.54184)
2Θ range for data collection/°	6.184 to 154.312
Index ranges	-17 ≤ h ≤ 21, -4 ≤ k ≤ 5, -24 ≤ l ≤ 24
Reflections collected	8314
Independent reflections	2755 [R_{int} = 0.0349, R_{sigma} = 0.0361]
Data/restraints/parameters	2755/0/194
Goodness-of-fit on F^2	1.060
Final R indexes [I>=2σ (I)]	R_1 = 0.0419, wR_2 = 0.1185
Final R indexes [all data]	R_1 = 0.0471, wR_2 = 0.1227
Largest diff. peak/hole / e Å^{-3}	0.18/-0.21

Table 2 Fractional Atomic Coordinates (×10^4) and Equivalent Isotropic Displacement Parameters (Å^2×10^3) for cx1670. U_{eq} is defined as 1/3 of of the trace of the 143rthogonalized U_{IJ} tensor.

Atom	x	y	z	U(eq)

Atom				
N2	2422.0(6)	1268(3)	9953.9(6)	32.3(3)
N1	3136.7(6)	1030(3)	10151.5(6)	32.8(3)
O2	2264.0(5)	-2697(3)	11002.0(5)	38.0(3)
O1	4584.0(5)	1789(3)	10622.5(5)	44.1(3)
O3	957.8(5)	19(3)	10055.4(5)	46.5(3)
O4	24.4(5)	1800(4)	9076.7(6)	57.6(4)
C2	1384.9(6)	3012(4)	9010.7(6)	32.6(3)
C3	2181.2(6)	2865(3)	9281.2(6)	29.2(3)
C4	2694.5(7)	4297(4)	8910.7(7)	34.6(3)
C7	3428.6(7)	-420(3)	10818.3(7)	32.2(3)
C5	2429.3(7)	5873(4)	8272.9(7)	37.2(3)
C8	3026.3(7)	-2225(4)	11255.5(7)	34.1(3)
C12	4229.5(7)	42(4)	11063.8(7)	37.0(3)
C9	3408.5(9)	-3453(4)	11909.7(8)	43.3(4)
C6	1645.1(8)	6030(4)	7991.8(7)	38.4(3)
C1	1138.1(7)	4610(4)	8359.0(7)	37.9(3)
C11	4599.7(8)	-1186(4)	11719.8(8)	44.2(4)
B1	768.6(8)	1518(5)	9407.0(8)	39.3(4)
C10	4188.0(9)	-2907(4)	12136.2(8)	48.4(4)
C13	5392.2(7)	2254(5)	10829.7(9)	49.1(4)
C14	1853.1(9)	-4674(4)	11412.8(8)	44.0(4)

Table 3 Anisotropic Displacement Parameters (Å^2×10^3) for cx1670. The Anisotropic displacement factor exponent takes the form: -2π^2[h^{2}a*^{2}U$_{11}$+2hka*b*U$_{12}$+…].

Atom	U_{11}	U_{22}	U_{33}	U_{23}	U_{13}	U_{12}
N2	20.0(5)	45.4(7)	30.6(5)	-1.6(5)	3.3(4)	0.7(4)
N1	20.8(5)	44.3(7)	32.1(5)	-3.5(5)	2.7(4)	0.2(4)

O2	30.1(5)	45.7(6)	38.5(5)	4.6(4)	7.6(4)	-1.6(4)
O1	20.8(4)	66.9(7)	42.6(5)	-2.5(5)	1.5(4)	-3.0(4)
O3	19.0(4)	81.6(8)	39.1(5)	14.6(5)	6.0(4)	-3.3(5)
O4	19.7(5)	106.6(11)	46.1(6)	26.6(6)	5.4(4)	-2.3(5)
C2	20.5(6)	47.6(8)	29.6(6)	-2.2(6)	4.7(4)	0.2(5)
C3	21.4(5)	38.3(7)	28.1(6)	-3.6(5)	5.2(4)	-0.8(5)
C4	21.0(5)	46.1(8)	37.1(7)	-2.3(6)	7.1(5)	-3.7(5)
C7	24.9(6)	40.0(7)	30.5(6)	-6.0(5)	2.8(5)	3.5(5)
C5	30.4(6)	46.1(8)	37.7(7)	0.8(6)	12.9(5)	-5.0(6)
C8	31.3(6)	37.3(7)	33.0(6)	-5.7(5)	4.7(5)	4.5(5)
C12	26.9(6)	44.8(8)	37.4(7)	-8.9(6)	2.2(5)	4.2(5)
C9	48.5(8)	44.6(8)	34.7(7)	0.4(6)	3.9(6)	4.9(6)
C6	34.0(7)	50.0(8)	30.9(6)	4.4(6)	6.0(5)	1.4(6)
C1	24.0(6)	55.5(9)	33.3(6)	2.4(6)	3.9(5)	1.2(6)
C11	32.1(7)	54.6(9)	40.5(7)	-8.3(7)	-5.5(6)	6.9(6)
B1	21.3(6)	61.2(10)	35.3(7)	3.9(7)	5.4(5)	-1.4(7)
C10	48.4(8)	55.2(10)	35.0(7)	-1.3(7)	-7.2(6)	12.1(7)
C13	21.9(6)	66.8(11)	55.6(9)	-12.2(8)	0.6(6)	-2.4(6)
C14	45.2(8)	43.9(8)	46.5(8)	3.6(7)	17.6(6)	-2.4(6)

Table 4 Bond Lengths for cx1670.

Atom	Atom	Length/Å	Atom	Atom	Length/Å
N2	N1	1.2569(14)	C2	B1	1.580(2)
N2	C3	1.4270(17)	C3	C4	1.3957(18)
N1	C7	1.4046(17)	C4	C5	1.3738(19)
O2	C8	1.3605(15)	C7	C8	1.416(2)
O2	C14	1.4303(17)	C7	C12	1.4221(17)

O1	C12	1.3565(19)		C5	C6	1.3932(18)
O1	C13	1.4275(15)		C8	C9	1.3886(19)
O3	B1	1.3608(19)		C12	C11	1.385(2)
O4	B1	1.3528(17)		C9	C10	1.387(2)
C2	C3	1.4096(15)		C6	C1	1.381(2)
C2	C1	1.3950(19)		C11	C10	1.381(2)

Table 5 Bond Angles for cx1670.

Atom	Atom	Atom	Angle/˚	Atom	Atom	Atom	Angle/˚
N1	N2	C3	113.93(10)	O2	C8	C7	117.07(11)
N2	N1	C7	118.03(11)	O2	C8	C9	122.61(13)
C8	O2	C14	118.22(11)	C9	C8	C7	120.31(12)
C12	O1	C13	118.11(11)	O1	C12	C7	115.50(12)
C3	C2	B1	123.76(12)	O1	C12	C11	123.83(12)
C1	C2	C3	117.20(11)	C11	C12	C7	120.66(14)
C1	C2	B1	119.04(11)	C10	C9	C8	119.85(15)
C2	C3	N2	116.38(11)	C1	C6	C5	119.68(12)
C4	C3	N2	122.76(11)	C6	C1	C2	122.04(12)
C4	C3	C2	120.84(12)	C10	C11	C12	119.65(13)
C5	C4	C3	120.28(11)	O3	B1	C2	122.89(11)
N1	C7	C8	128.08(11)	O4	B1	O3	119.96(12)
N1	C7	C12	113.76(12)	O4	B1	C2	117.15(13)
C8	C7	C12	118.16(12)	C11	C10	C9	121.36(13)
C4	C5	C6	119.96(12)				

Table 6 Hydrogen Bonds for cx1670.

D H A	d(D-H)/Å	d(H-A)/Å	d(D-A)/Å	D-H-A/°
O3 H3 N2	0.82	1.99	2.7067(13)	145.7
O3 H3 O2	0.82	2.22	2.8657(14)	136.3
O4 H4 O3[1]	0.82	1.93	2.7483(14)	171.9

[1]-X,-Y,2-Z

Table 7 Hydrogen Atom Coordinates ($Å×10^4$) and Isotropic Displacement Parameters ($Å^2×10^3$) for cx1670.

Atom	x	y	z	U(eq)
H3	1425	-32	10185	70
H4	-248	1078	9338	86
H4A	3218	4185	9096	41
H5	2773	6834	8029	45
H9	3142	-4639	12195	52
H6	1464	7085	7559	46
H1	616	4722	8166	45
H11	5123	-854	11879	53
H10	4439	-3716	12577	58
H13A	5568	3518	10472	74
H13B	5644	176	10877	74
H13C	5508	3380	11280	74
H14A	1331	-4889	11162	66
H14B	1867	-3673	11870	66
H14C	2086	-6788	11482	66

NMR data

SI-**2**

¹H NMR, CDCl₃-*d*

^{13}C NMR, CDCl$_3$-d

1

¹H NMR, DMSO-*d₆*

155.21
149.47
142.29
133.15
130.99
130.42
129.62
122.94
122.74
21.53

f1 (ppm)
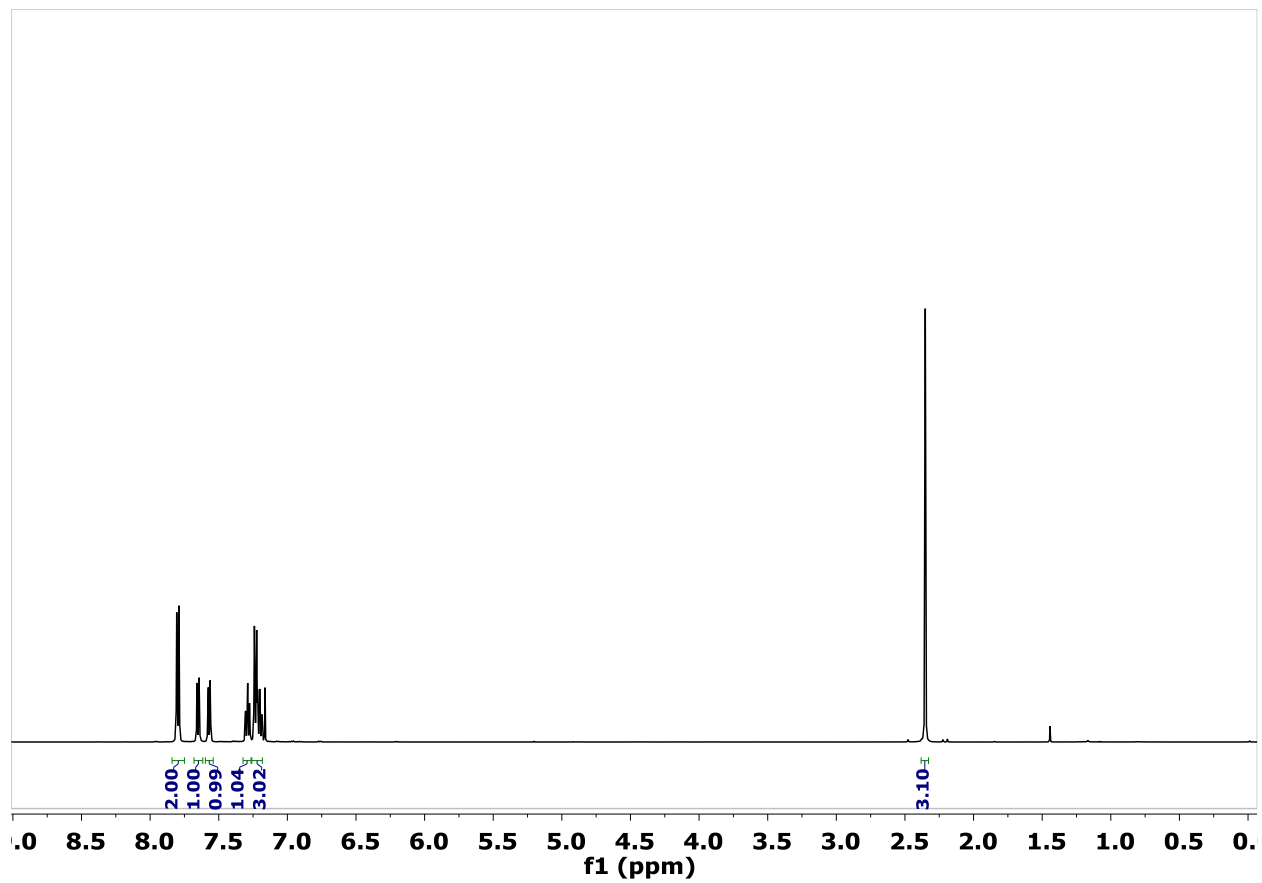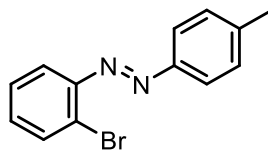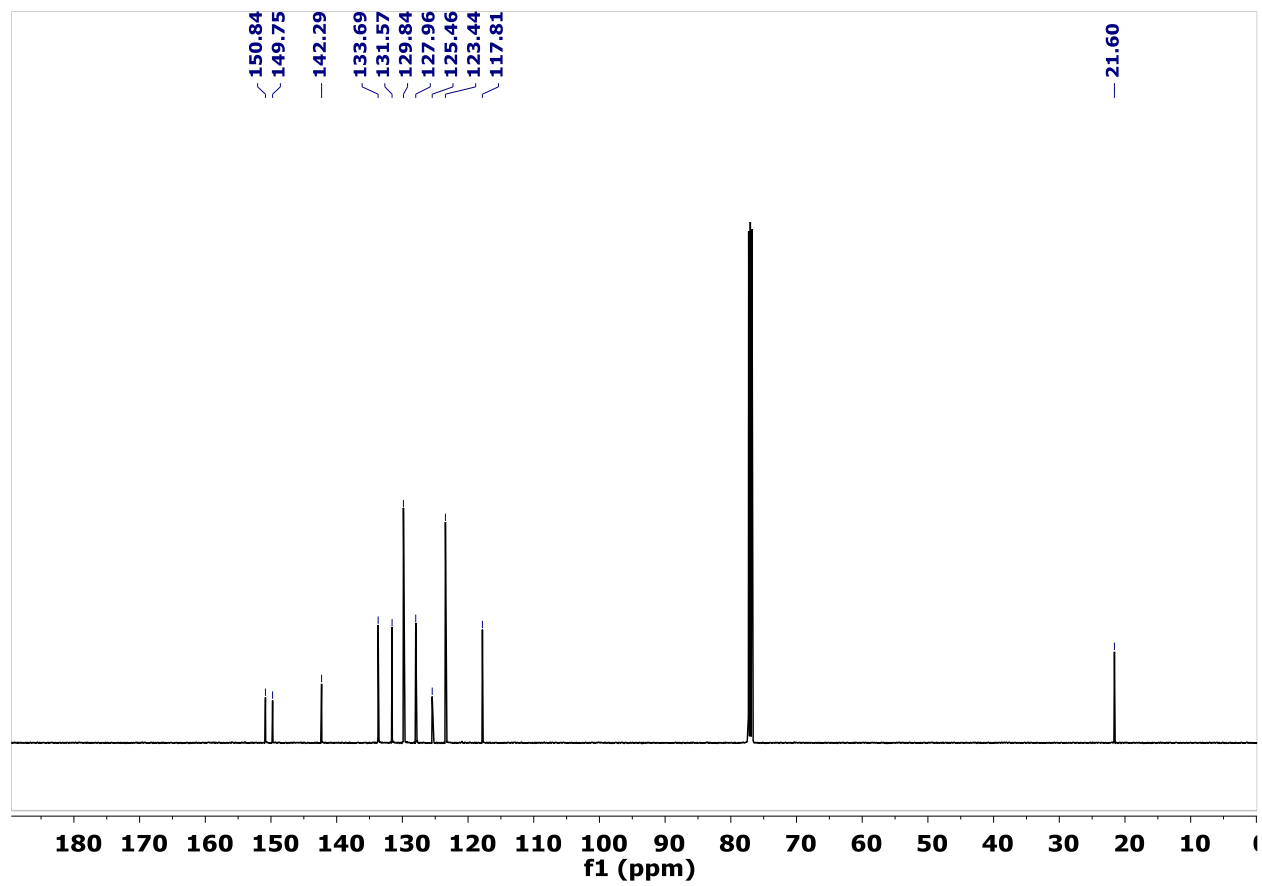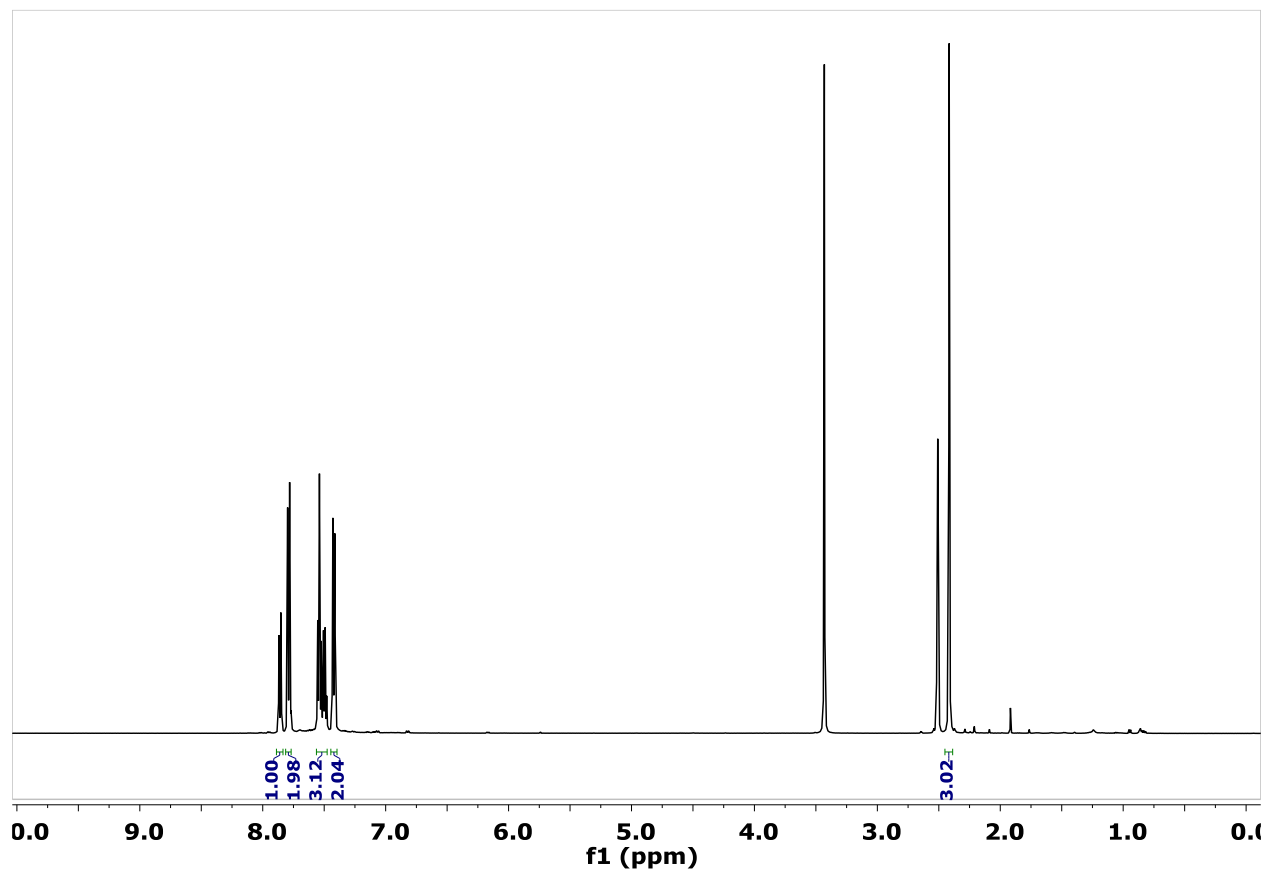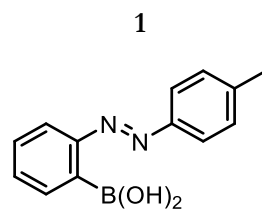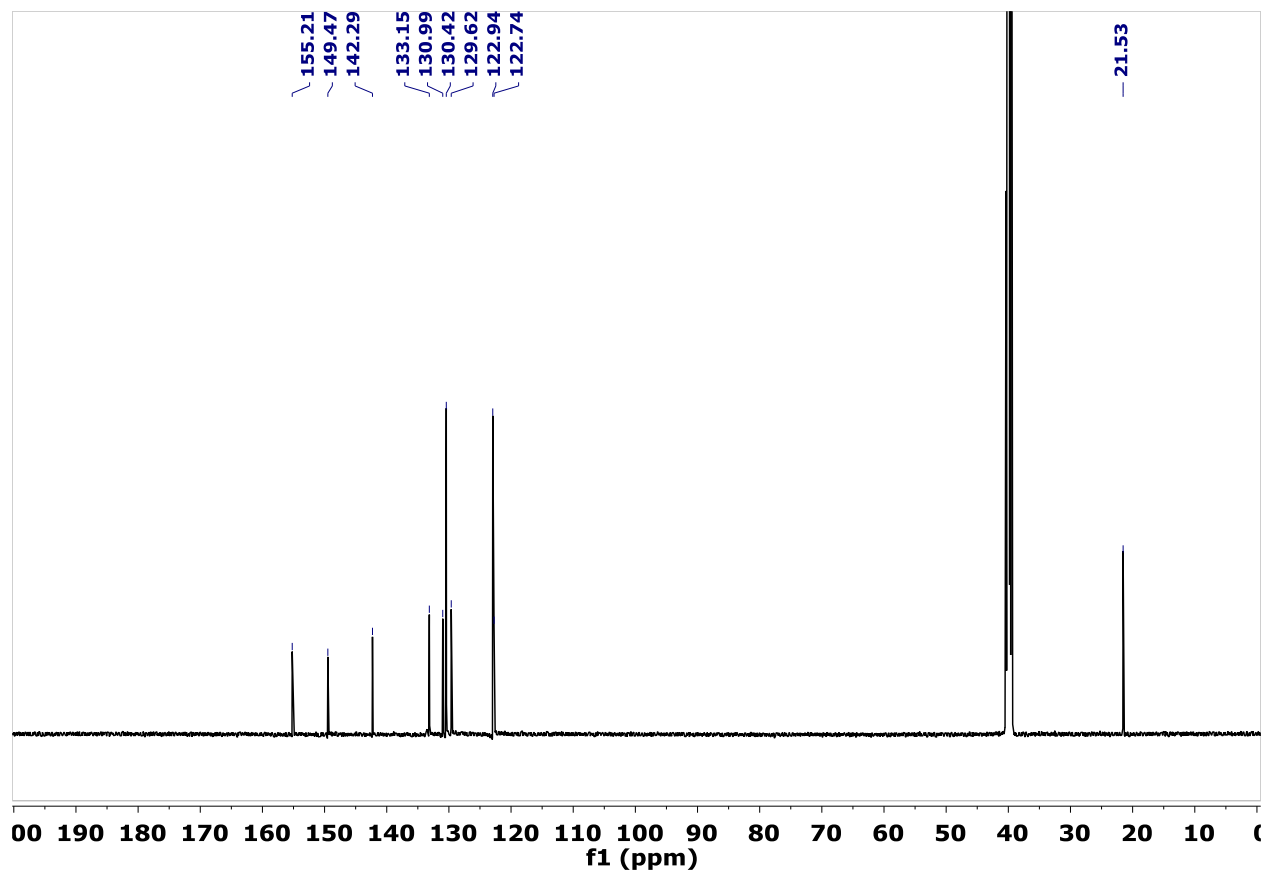
¹³C NMR, DMSO-*d₆*

2
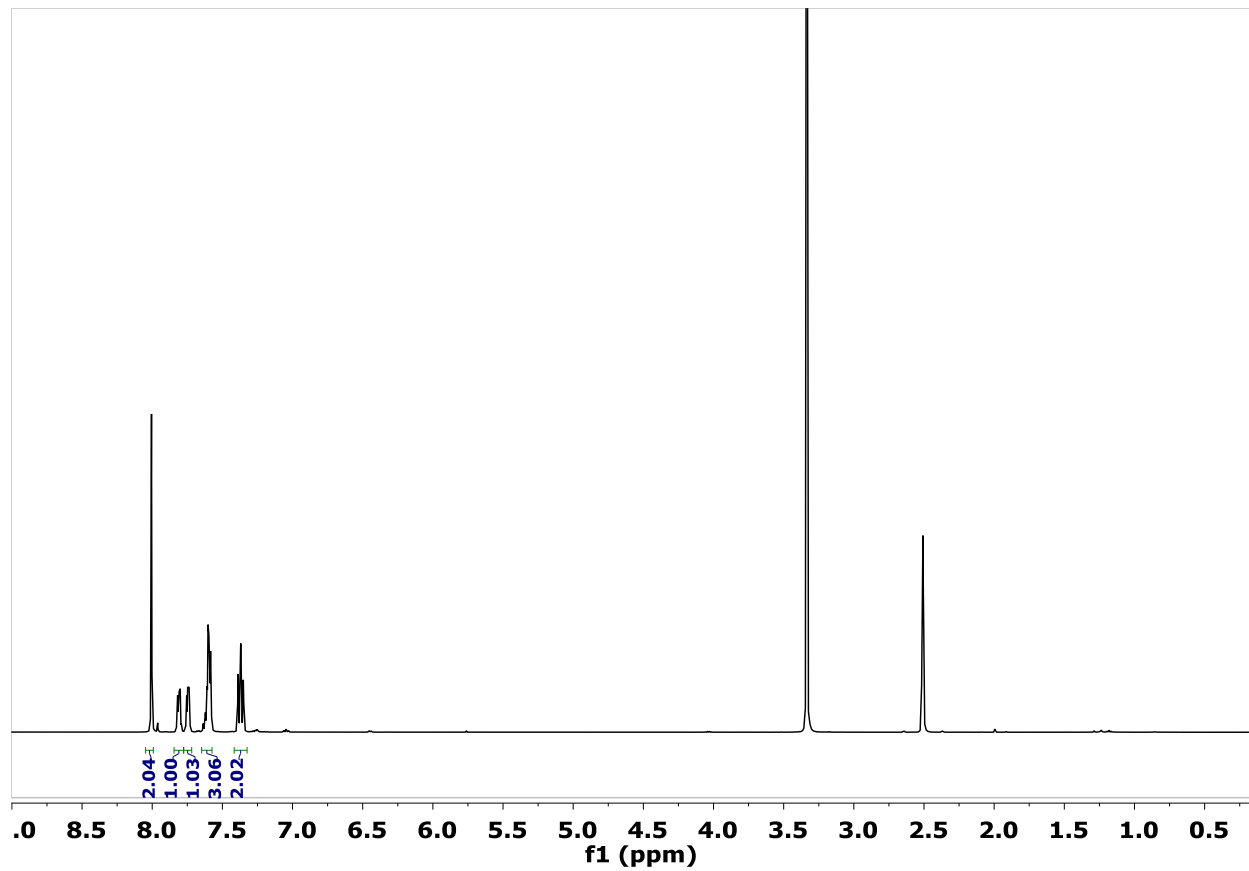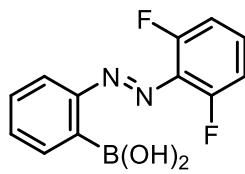
¹H NMR, DMSO-*d₆*
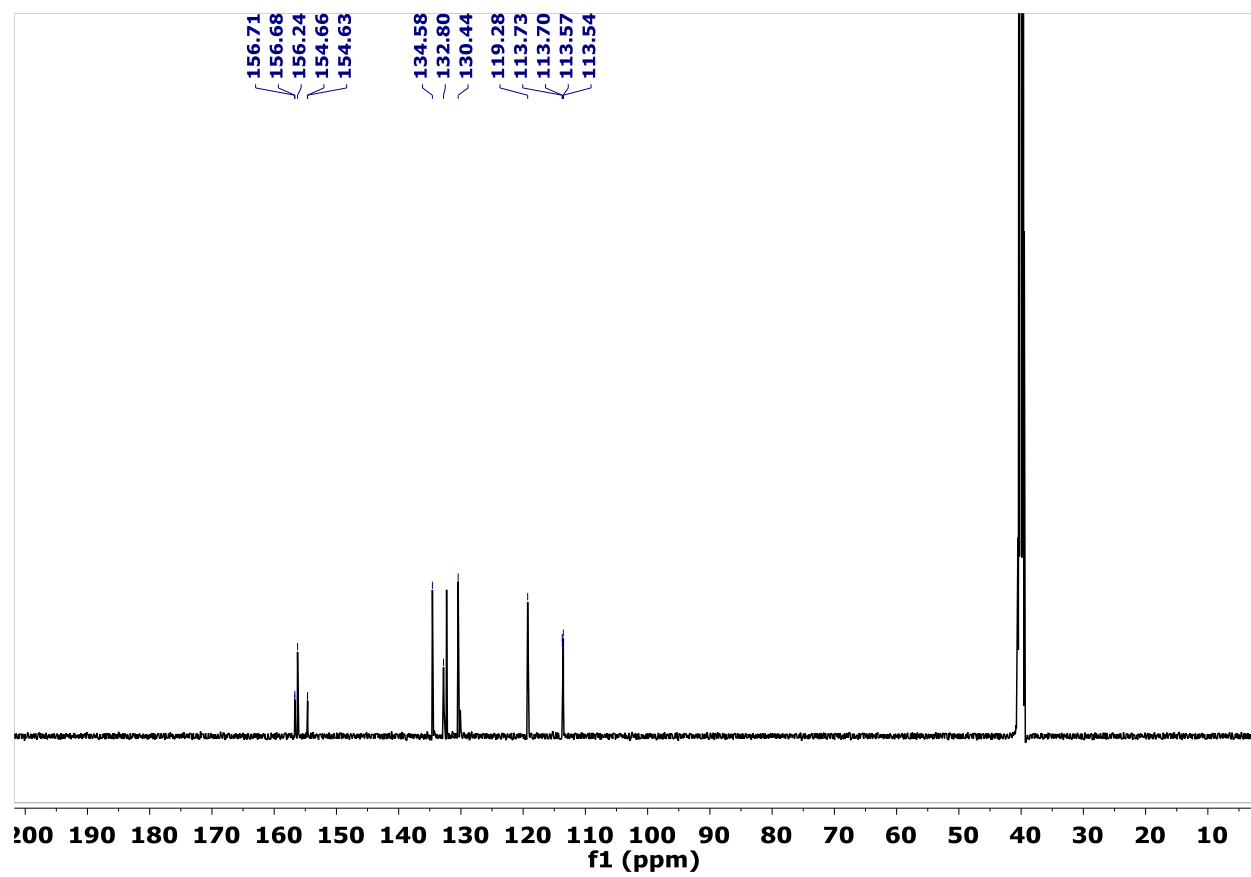
^{13}C NMR, DMSO-d_6

-121.16
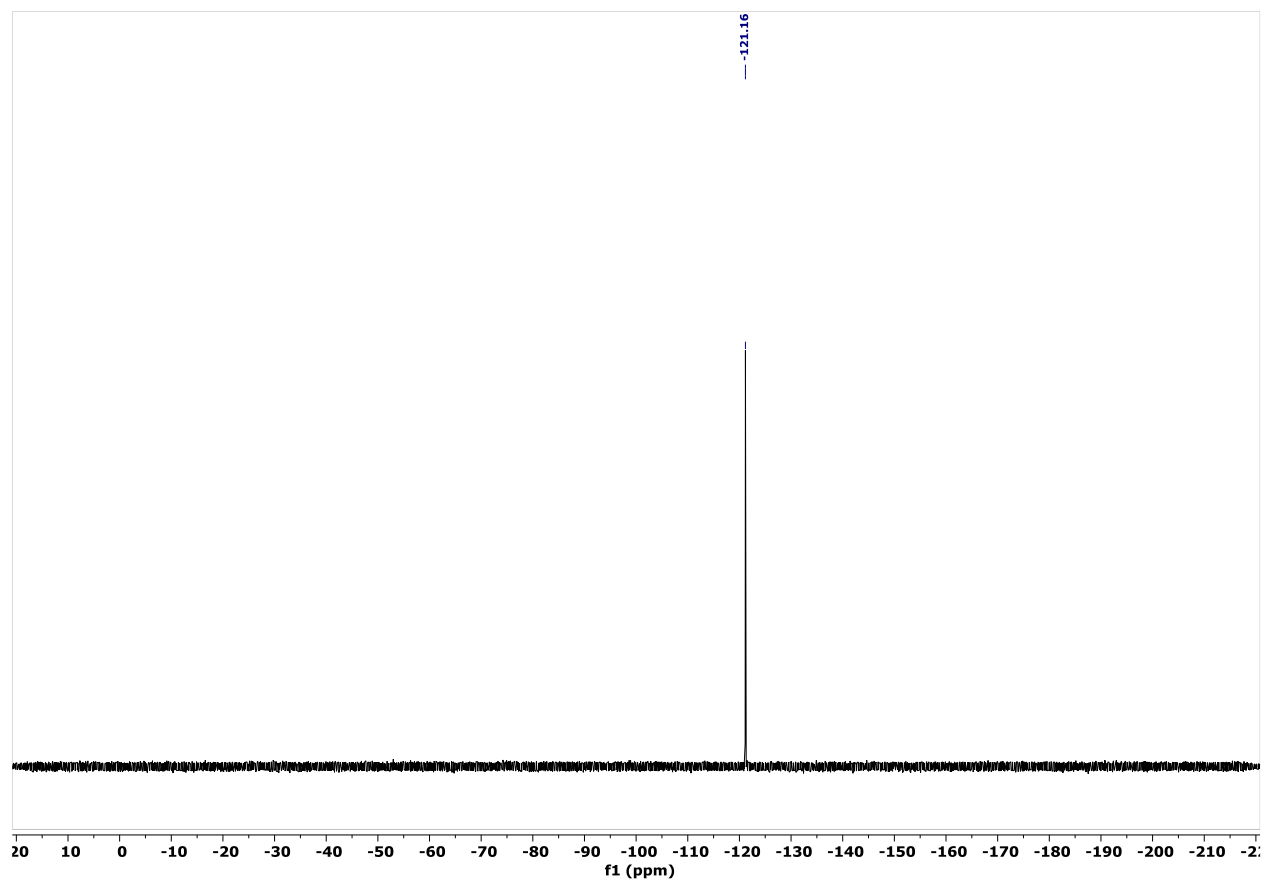
^{19}F NMR (DMSO-d_6).

SI-**4**
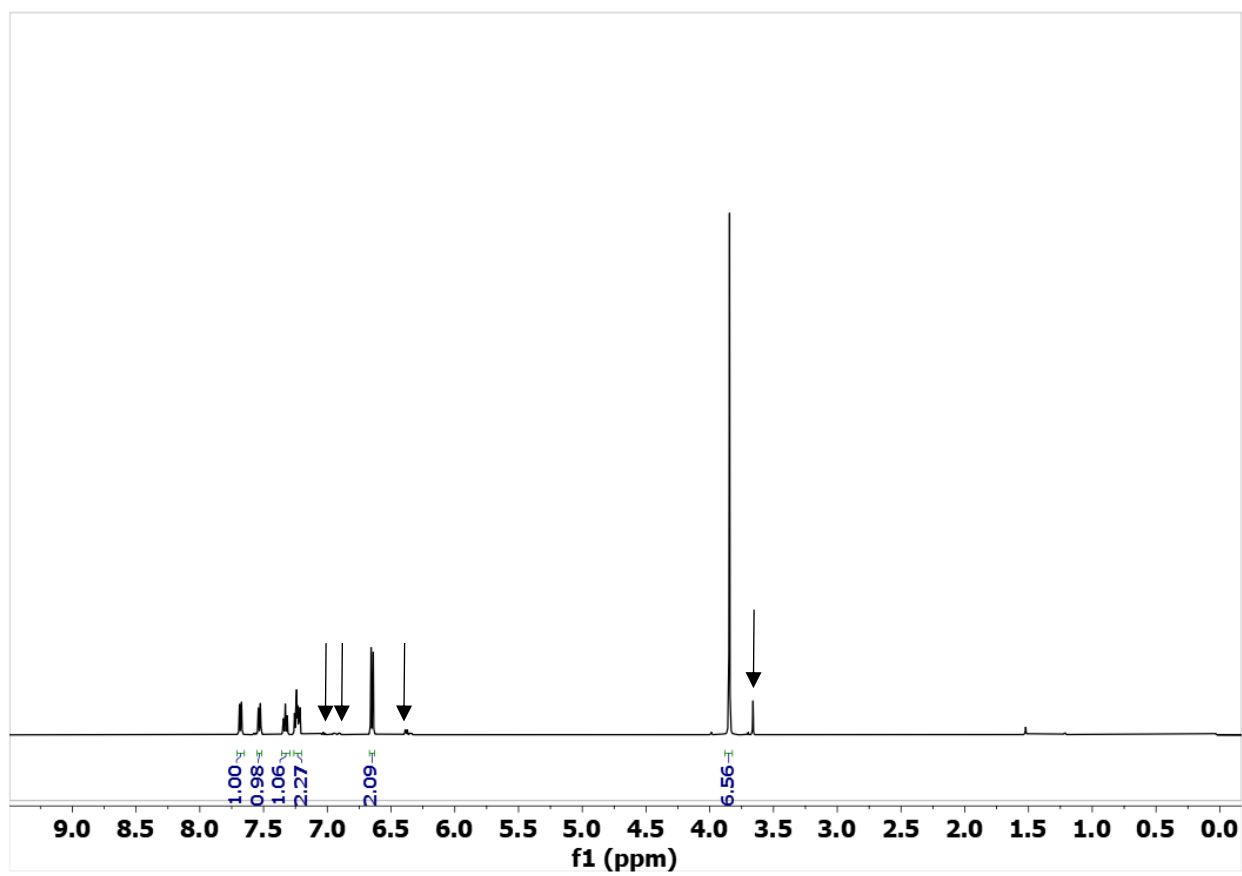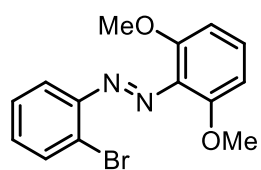
^{1}H NMR, DMSO-*d₆*. 16.3% *Z* isomer (denoted with arrows)

¹³C NMR, DMSO-*d₆*

3

MeO

OMe

N=N

B(OH)₂
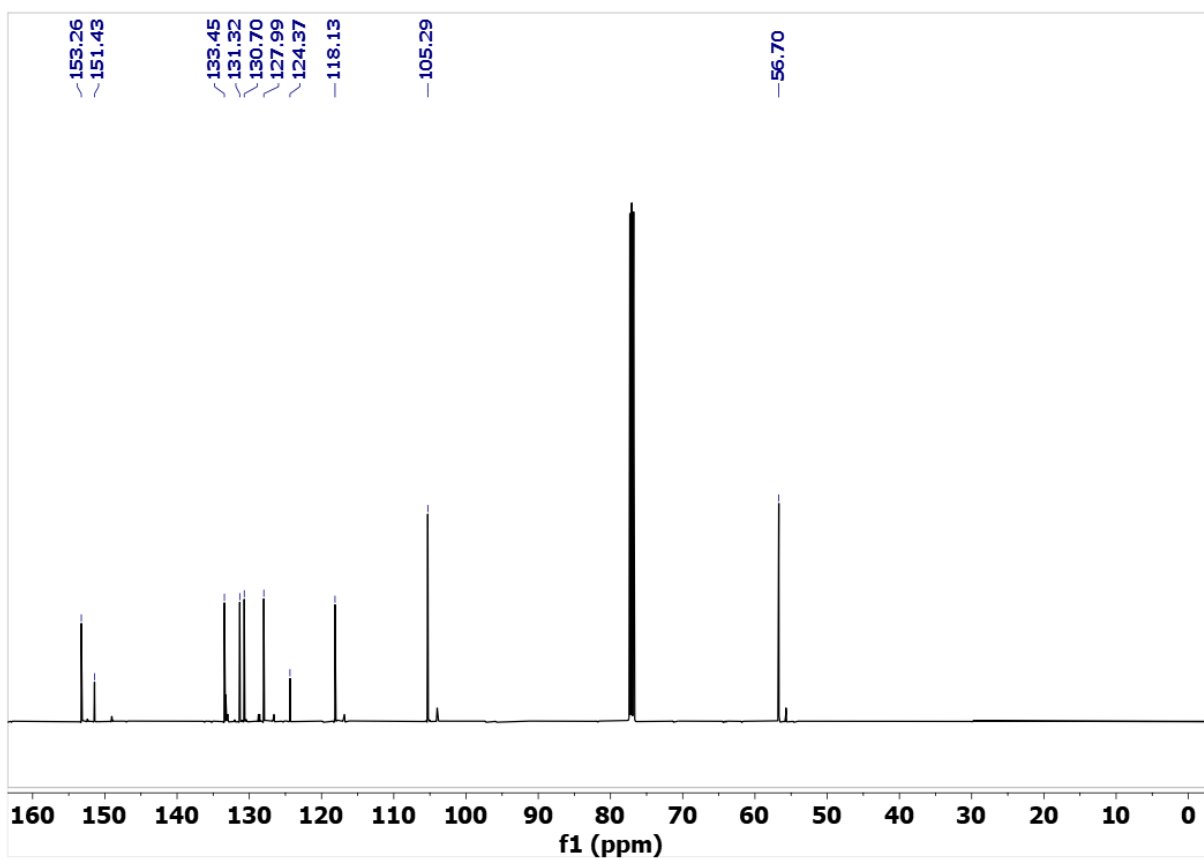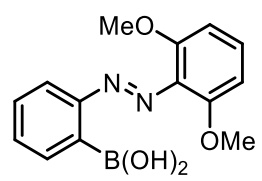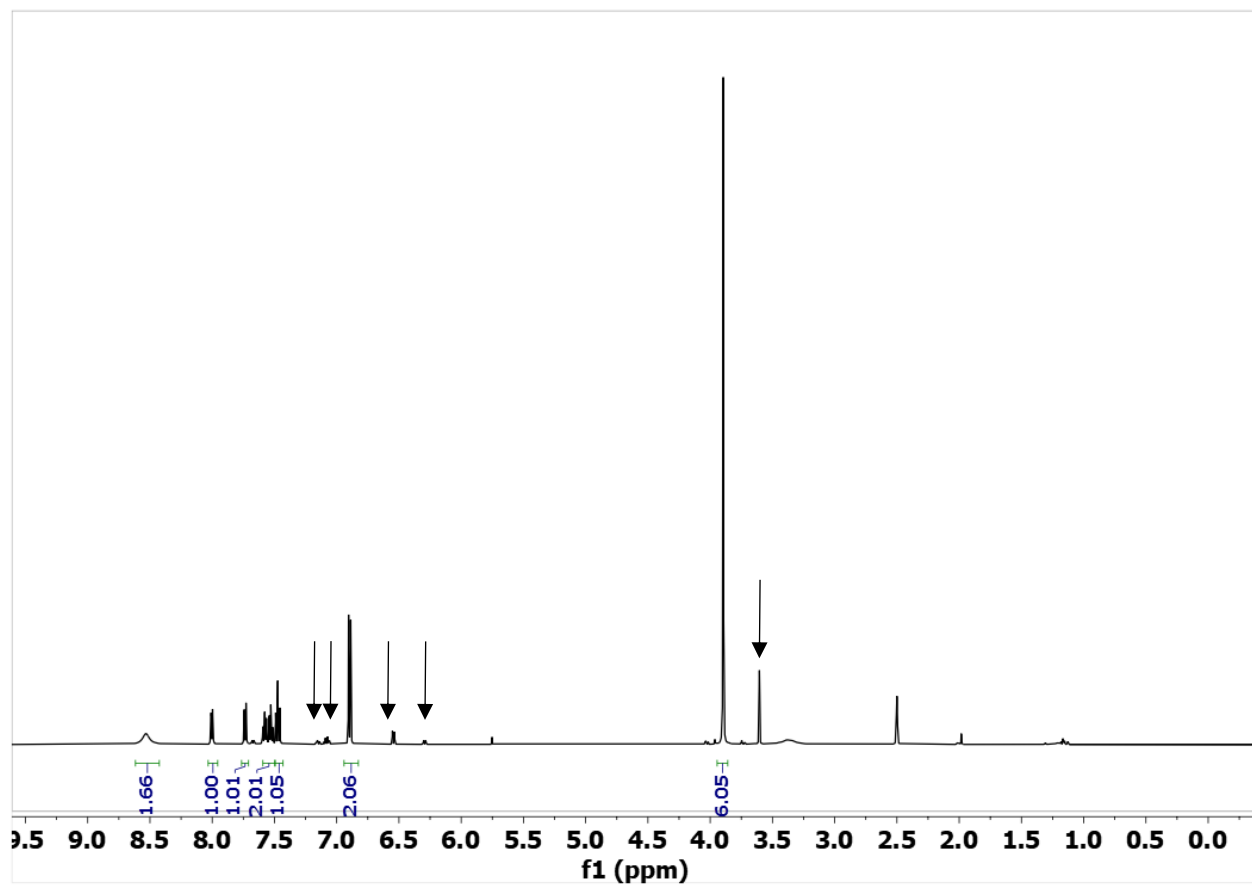
¹H NMR, DMSO-*d₆*. 4.2% *Z* isomer (denoted with arrows)
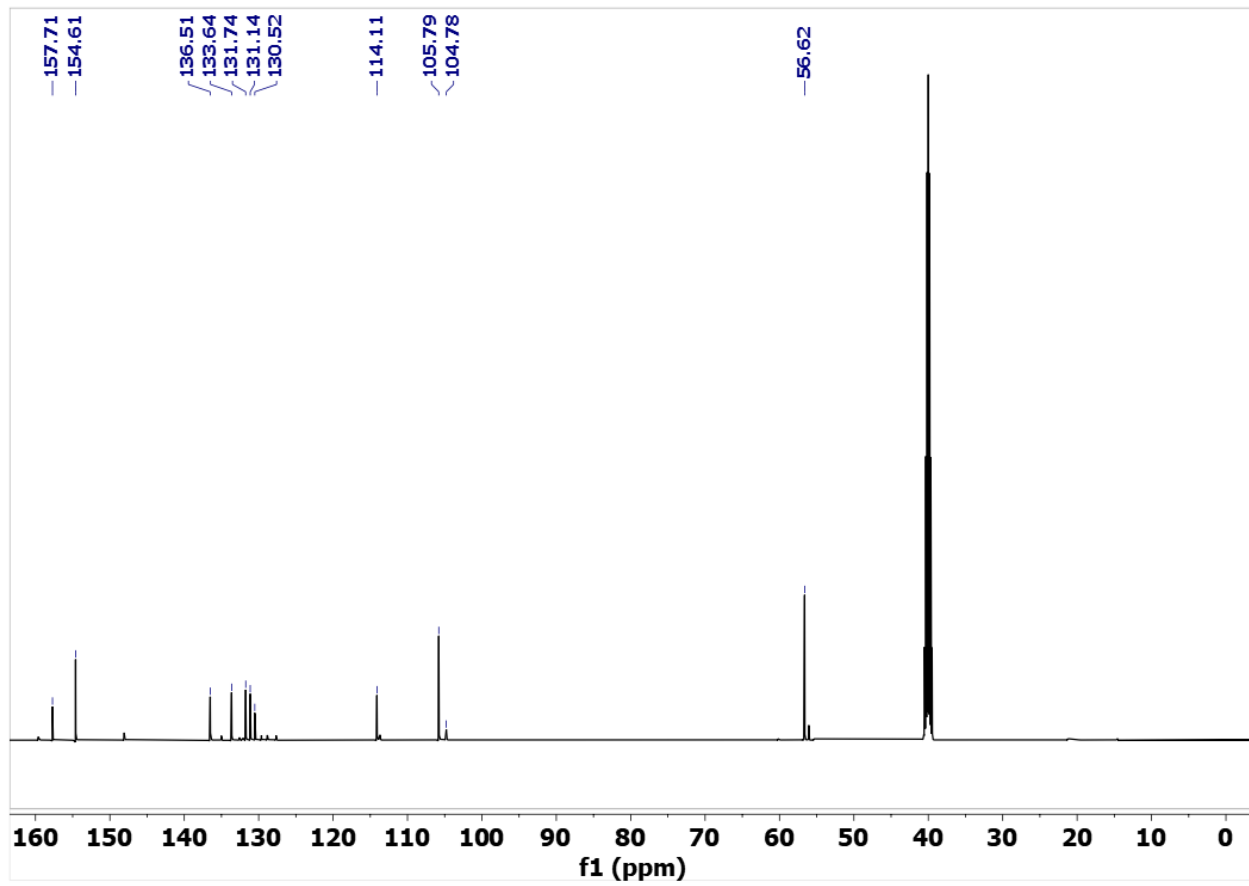
^{13}C NMR, DMSO-d_6

SI-**6**
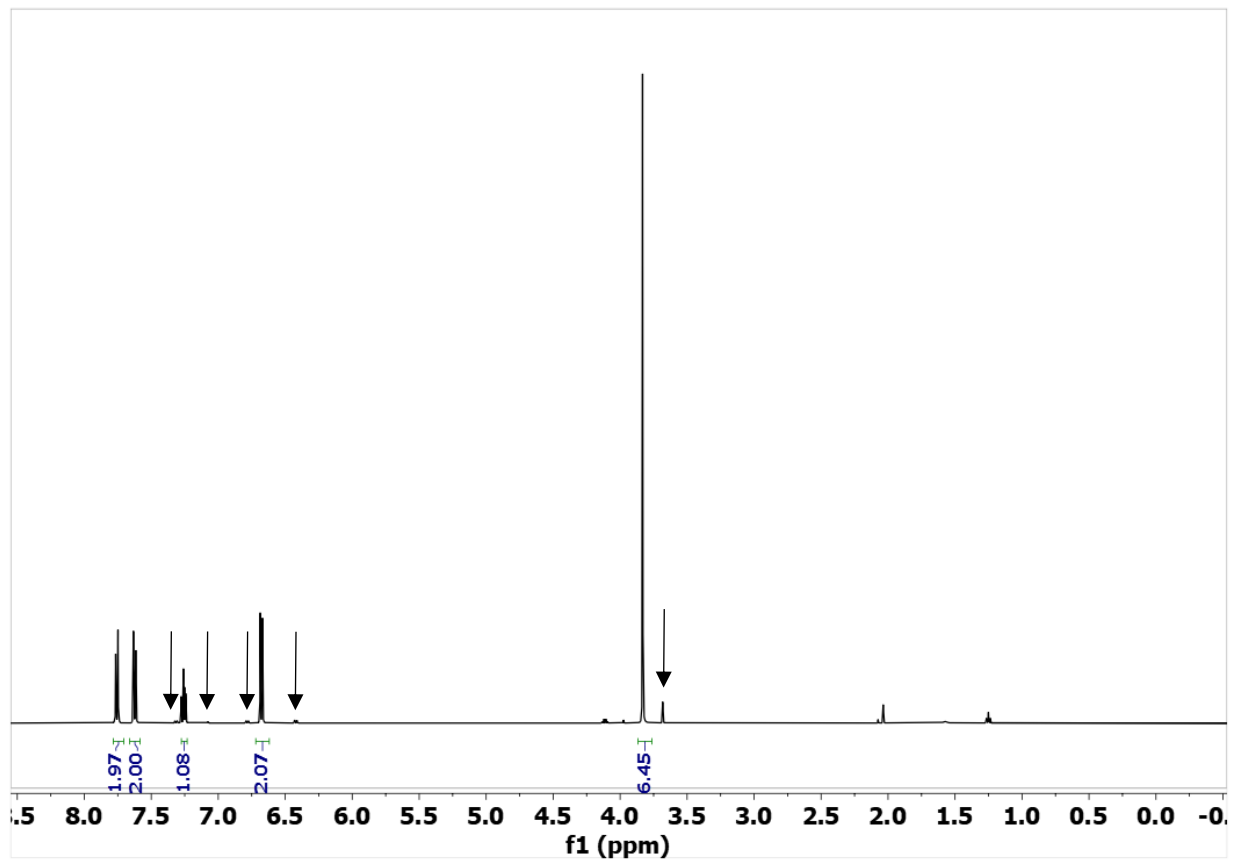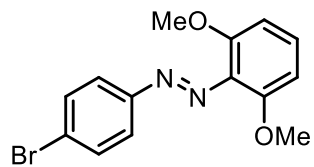
¹H NMR, DMSO-*d₆*. 2.9% *Z* isomer (denoted with arrows)
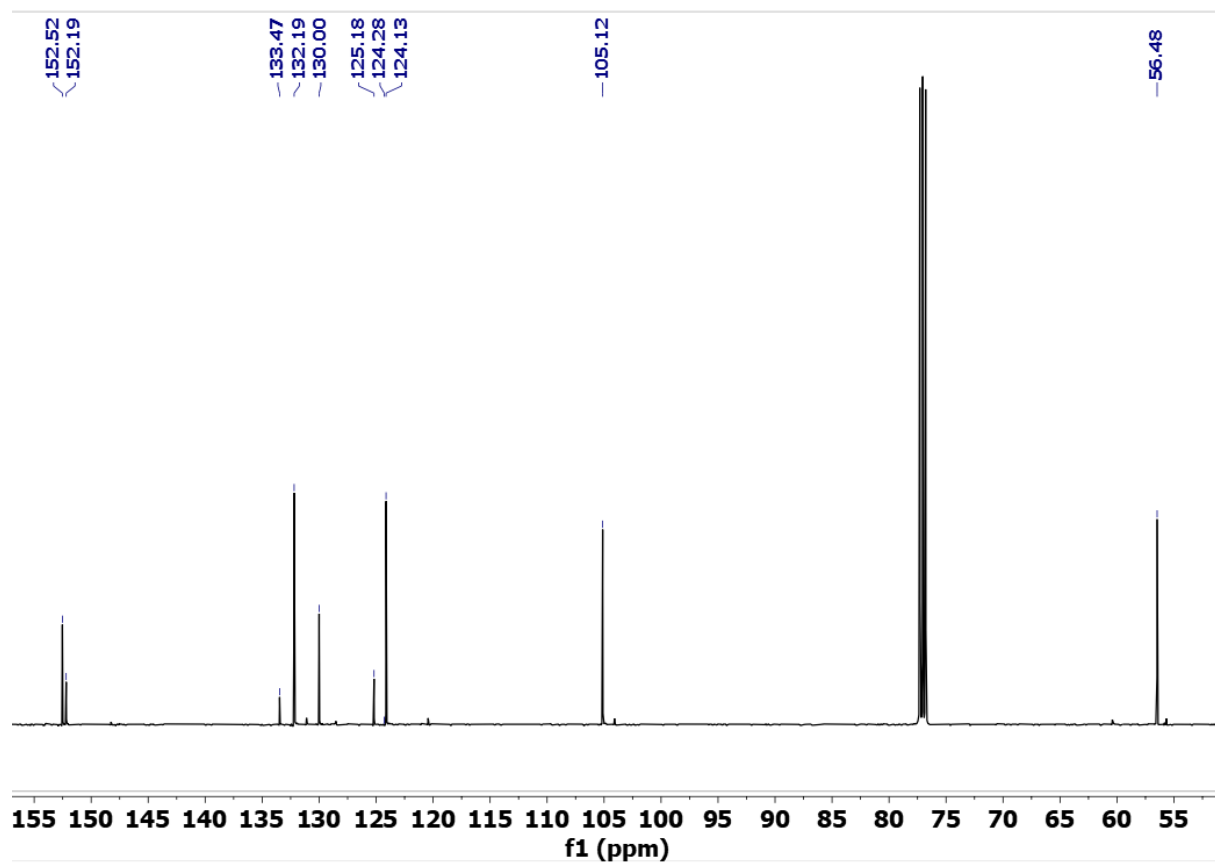
^{13}C NMR, DMSO-d_6

4
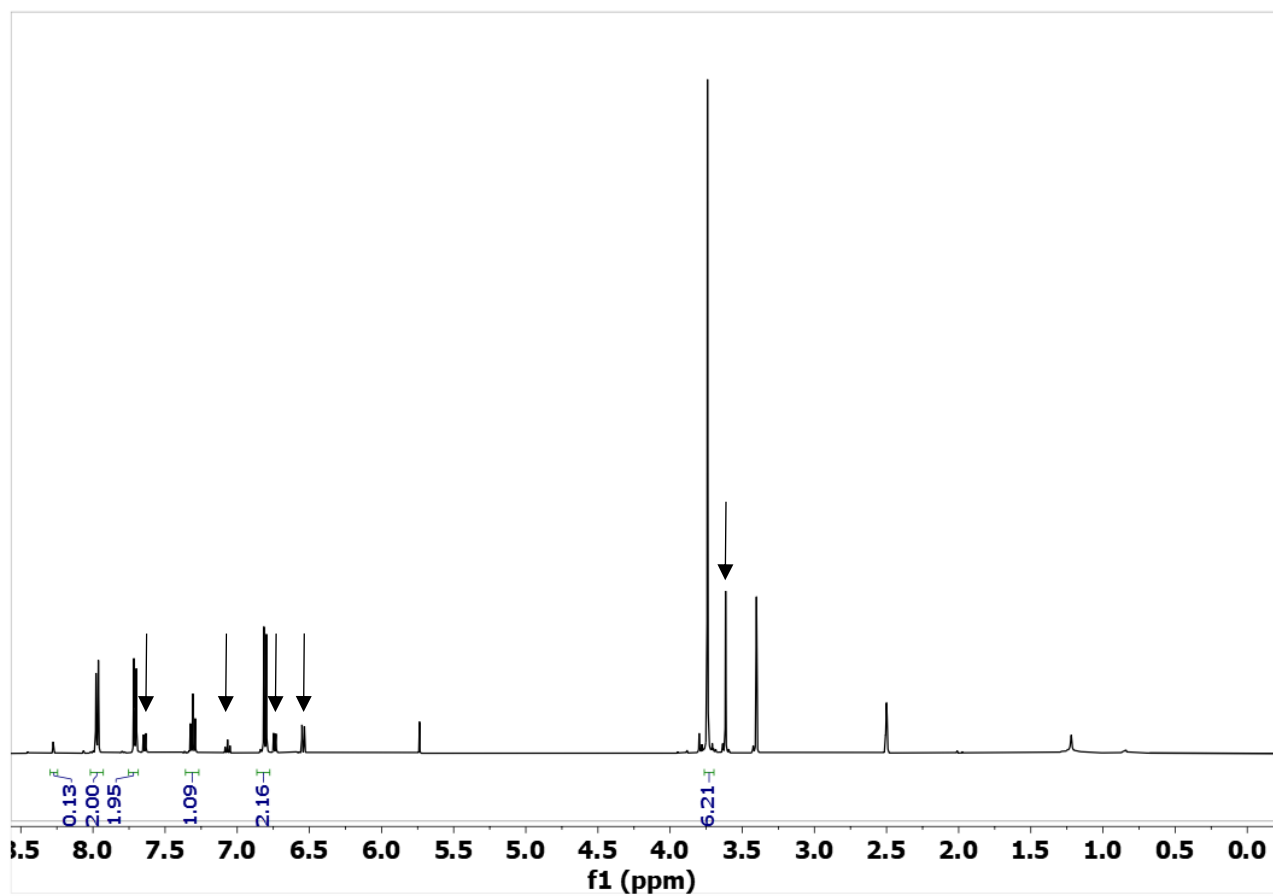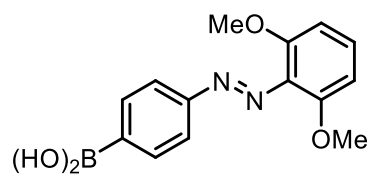
¹H NMR, DMSO-*d₆*. 18.5% *Z* isomer (denoted by arrows)
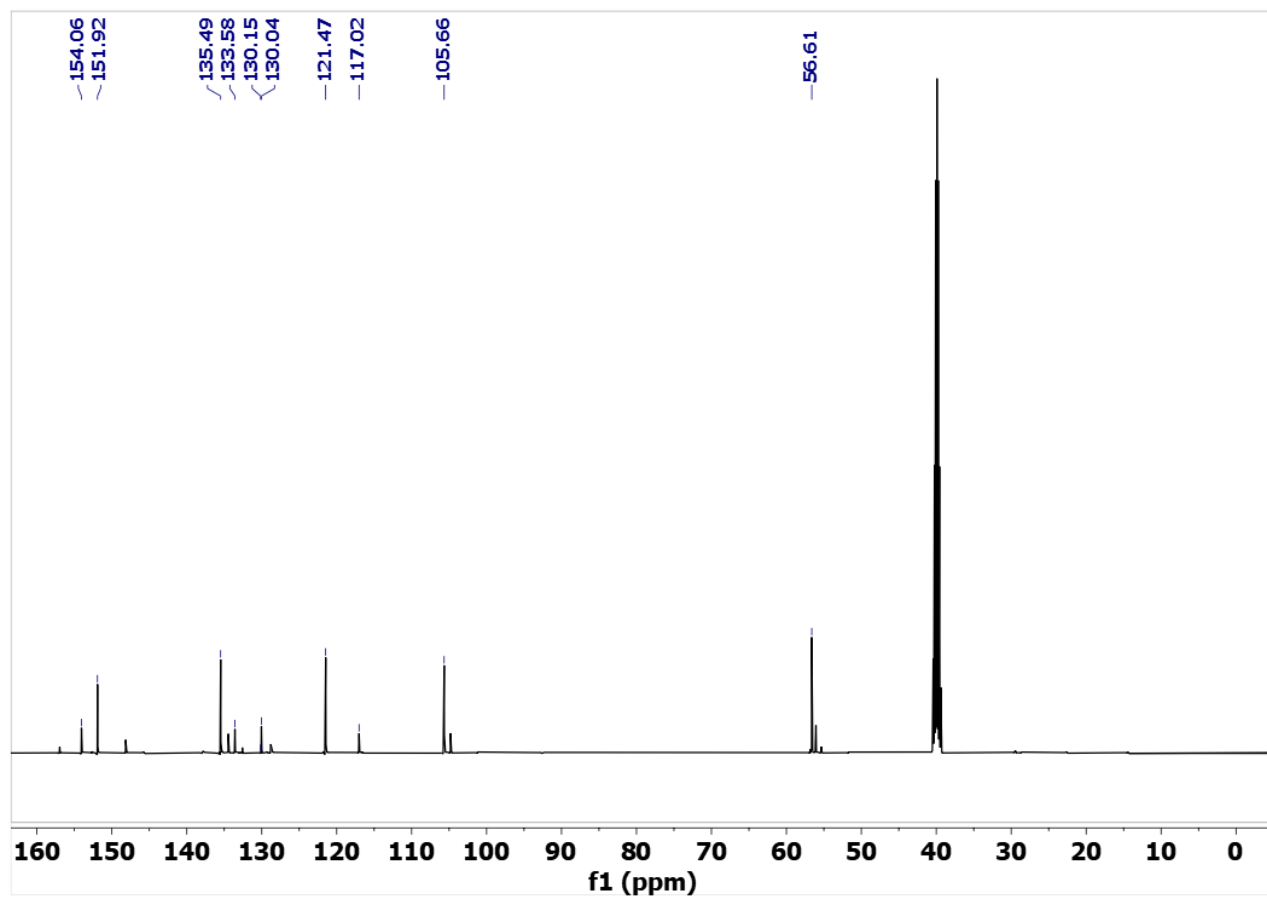
^{13}C NMR, DMSO-d_6

SI-**7**
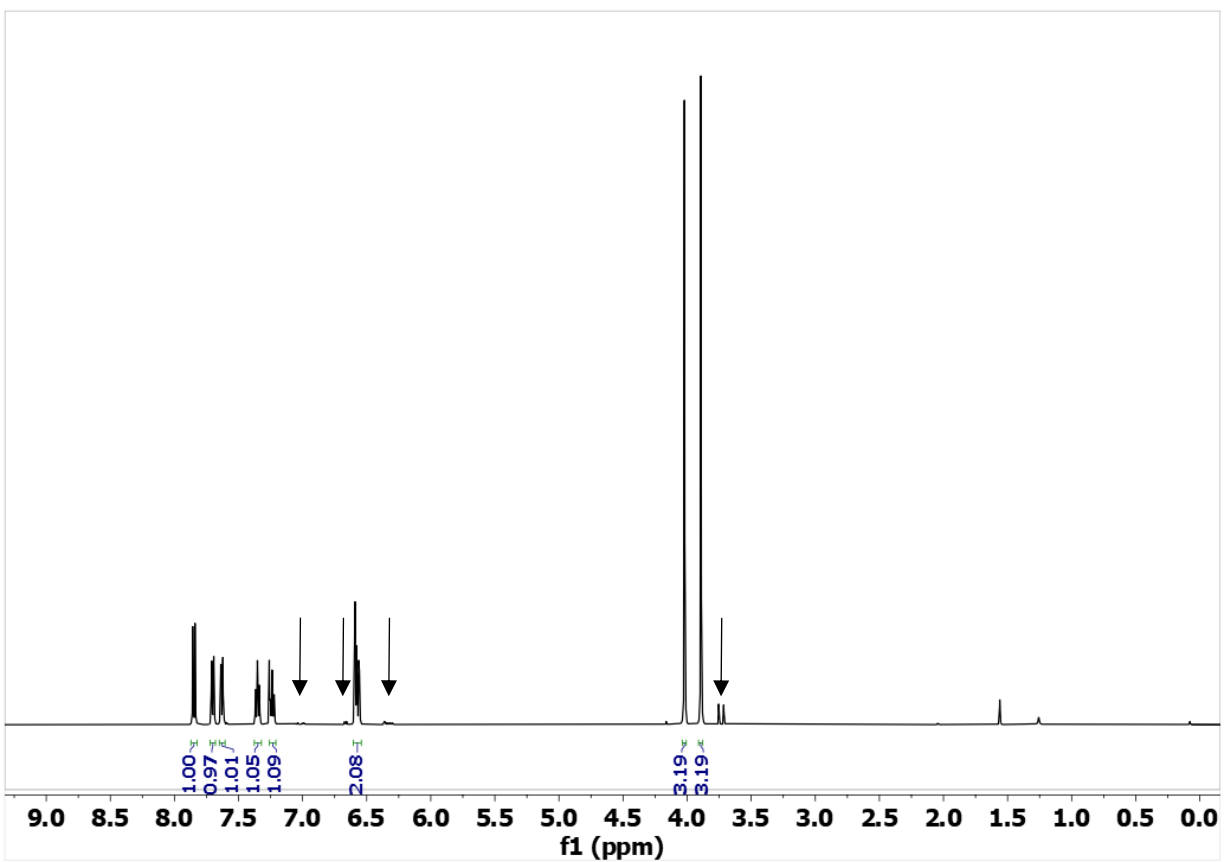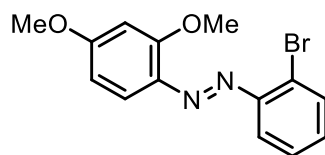
^{1}H NMR, DMSO-d_6. 2.7% Z isomer (denoted with arrows)
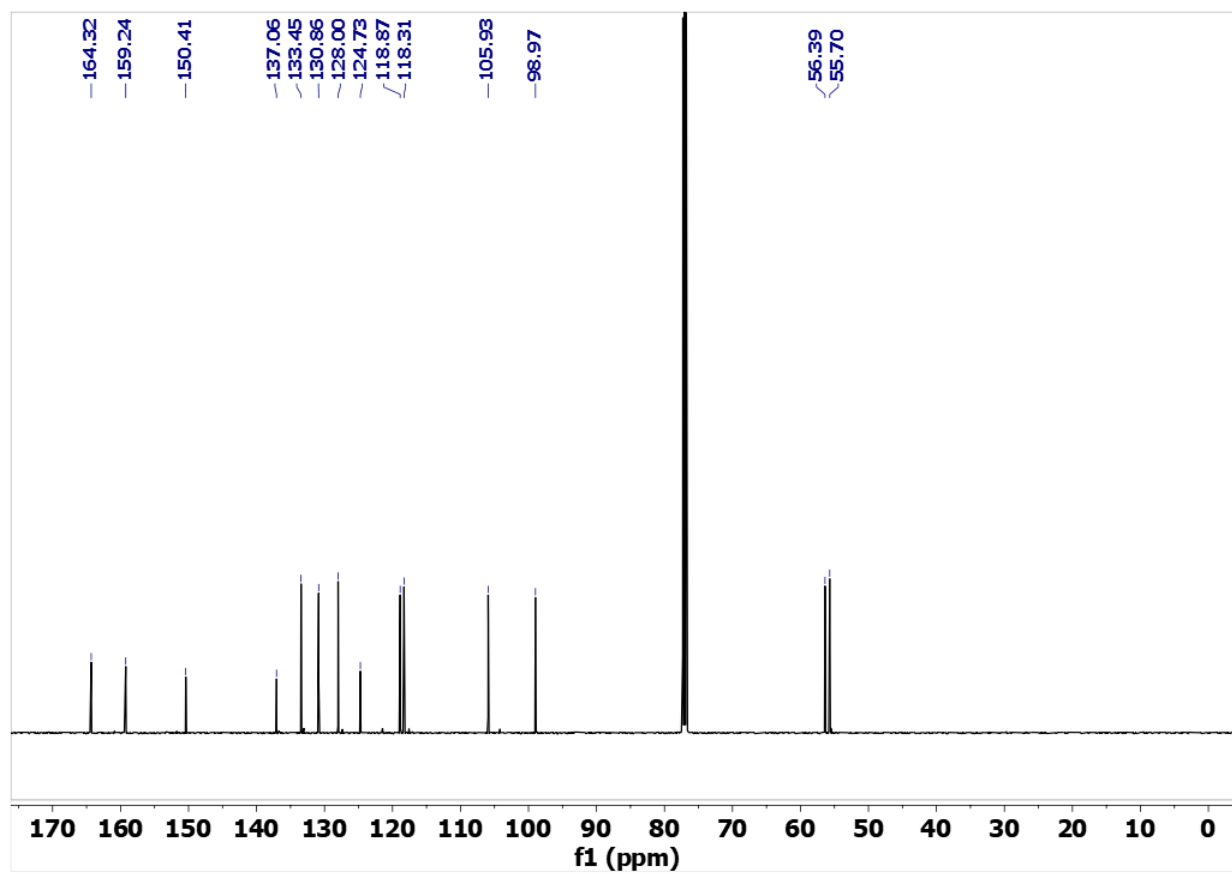
^{13}C NMR, DMSO-d_6

5
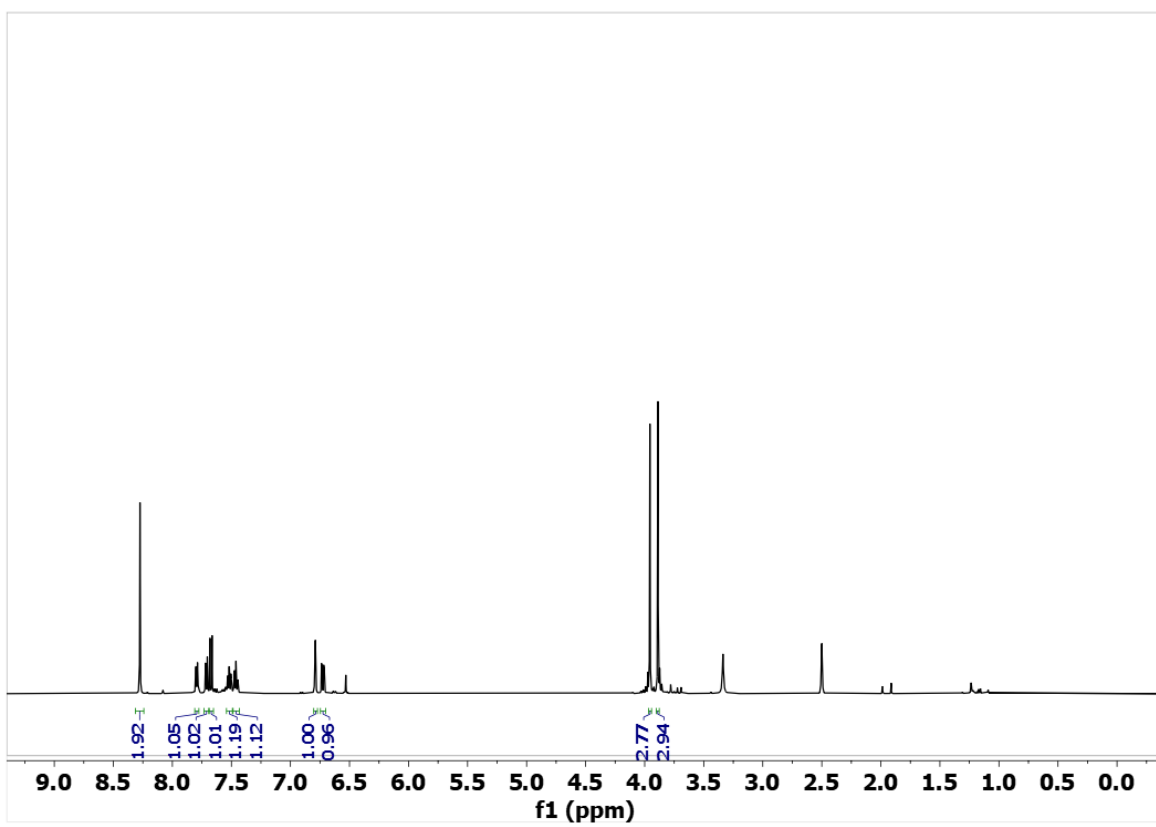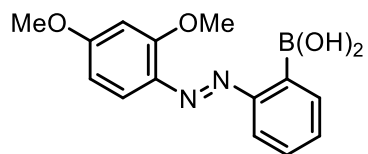
^{1}H NMR, DMSO-d_6. 1.0% Z isomer
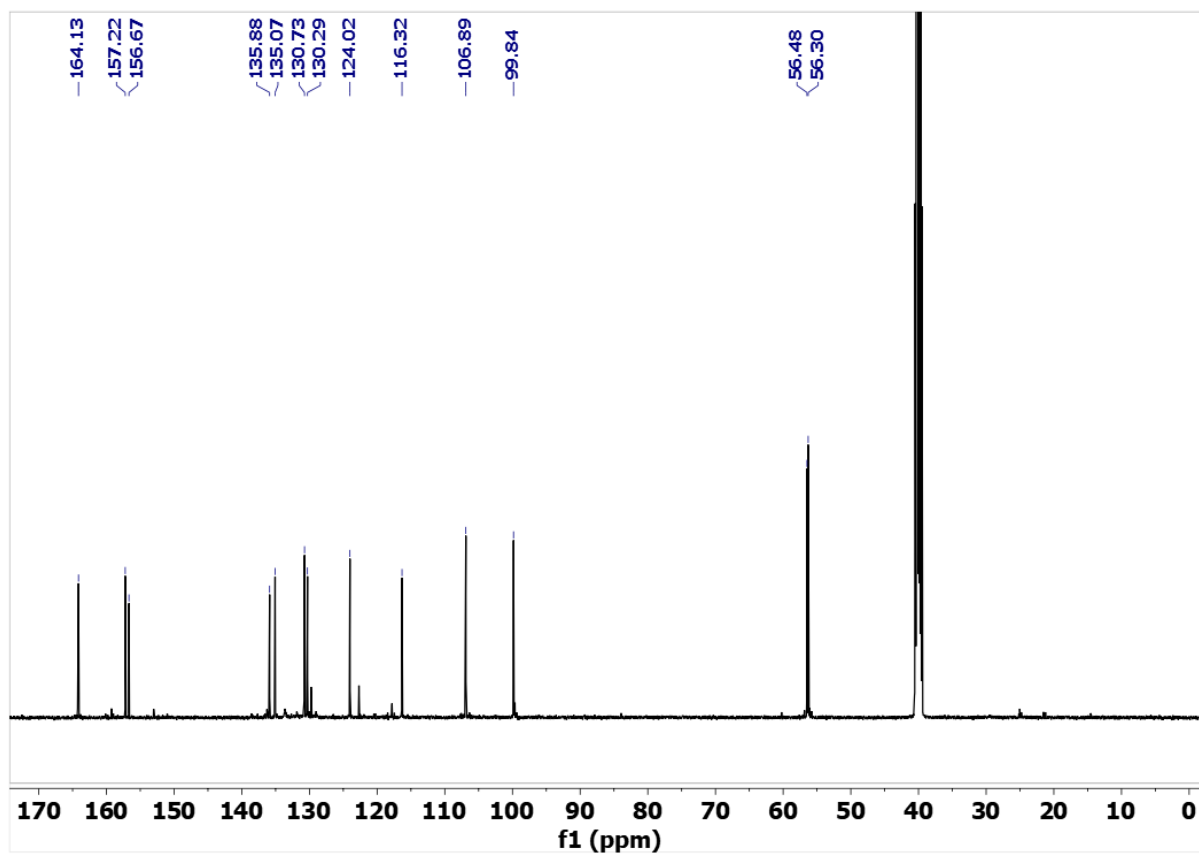
^{13}C NMR, DMSO-d_6

SI-**9**
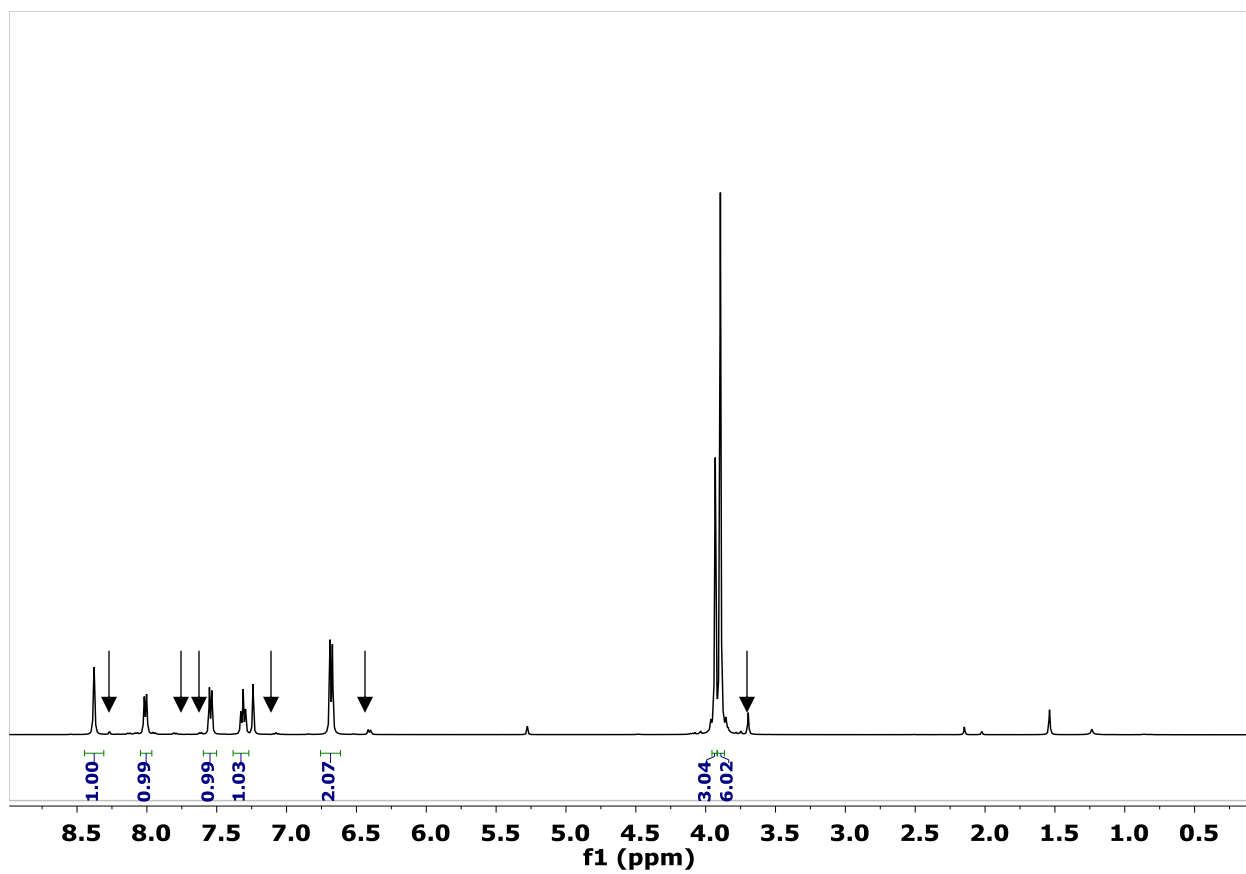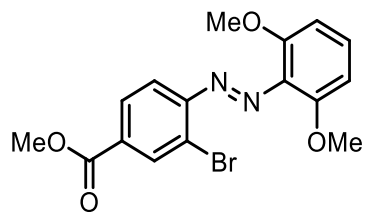
¹H NMR, CDCl$_3$-*d*. 6.7% *Z* isomer (denoted with arrows).
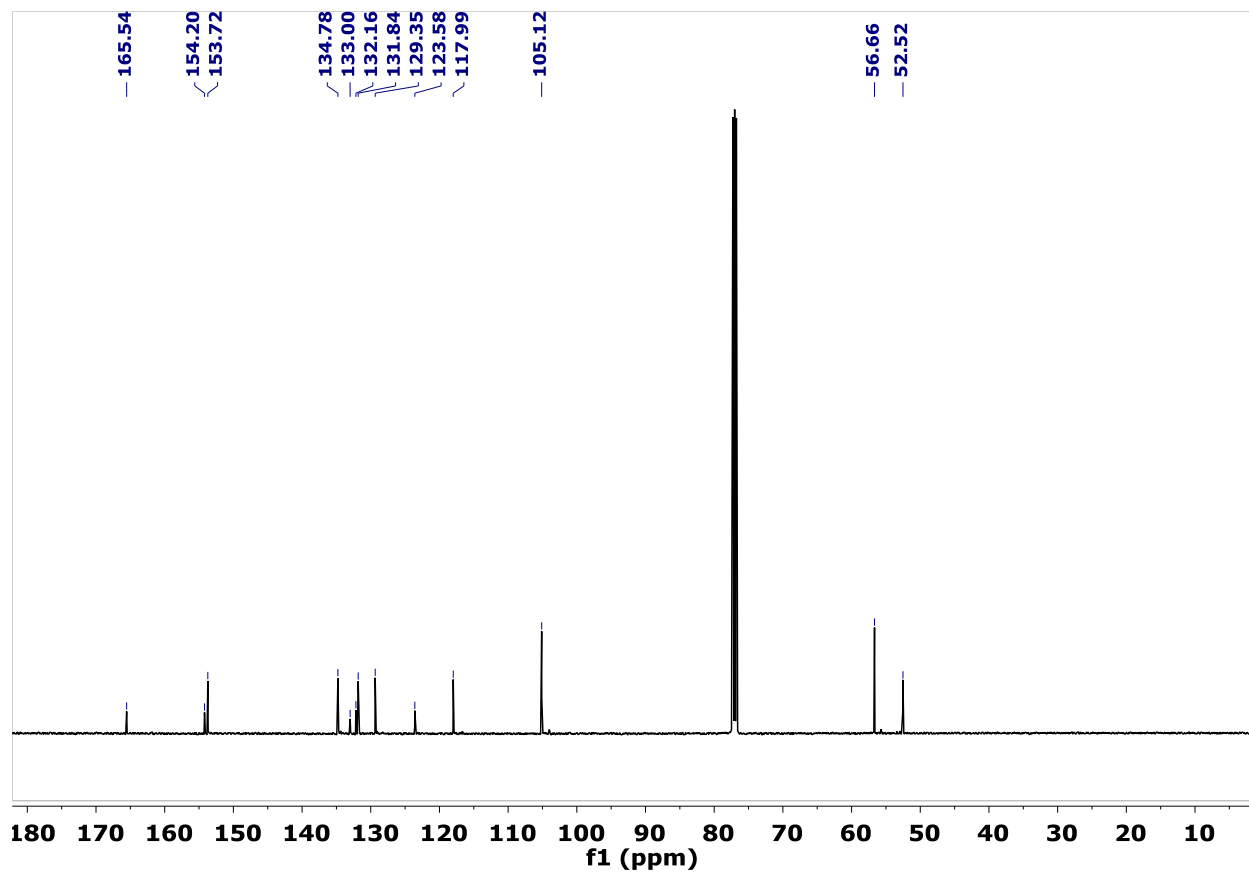
^{13}C NMR, CDCl$_3$-d

3'

¹H NMR, DMSO-*d₆*

166.38
160.05
155.04
137.73
134.91
132.54
131.04
130.55
114.60
105.82
56.72
52.78

f1 (ppm)
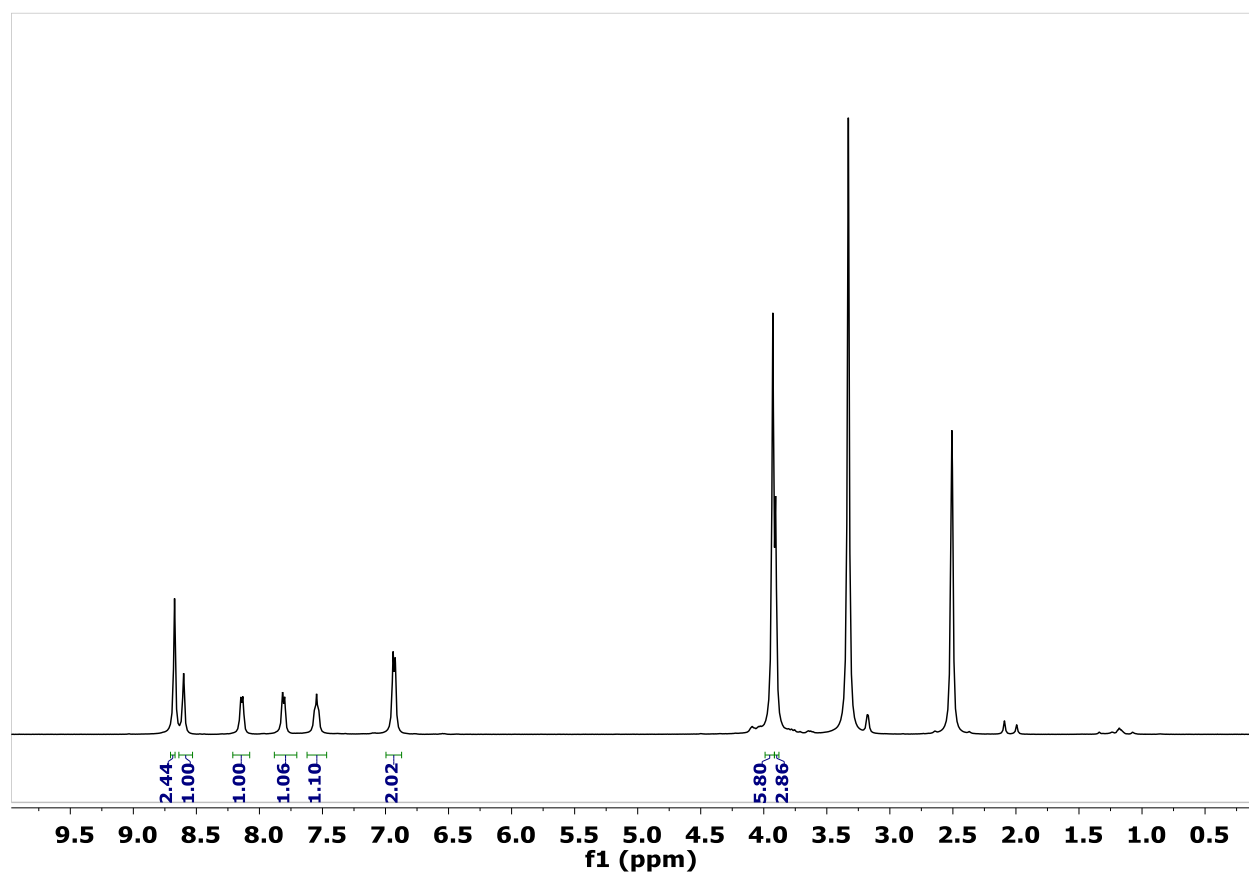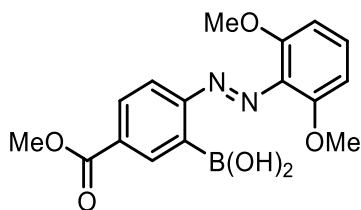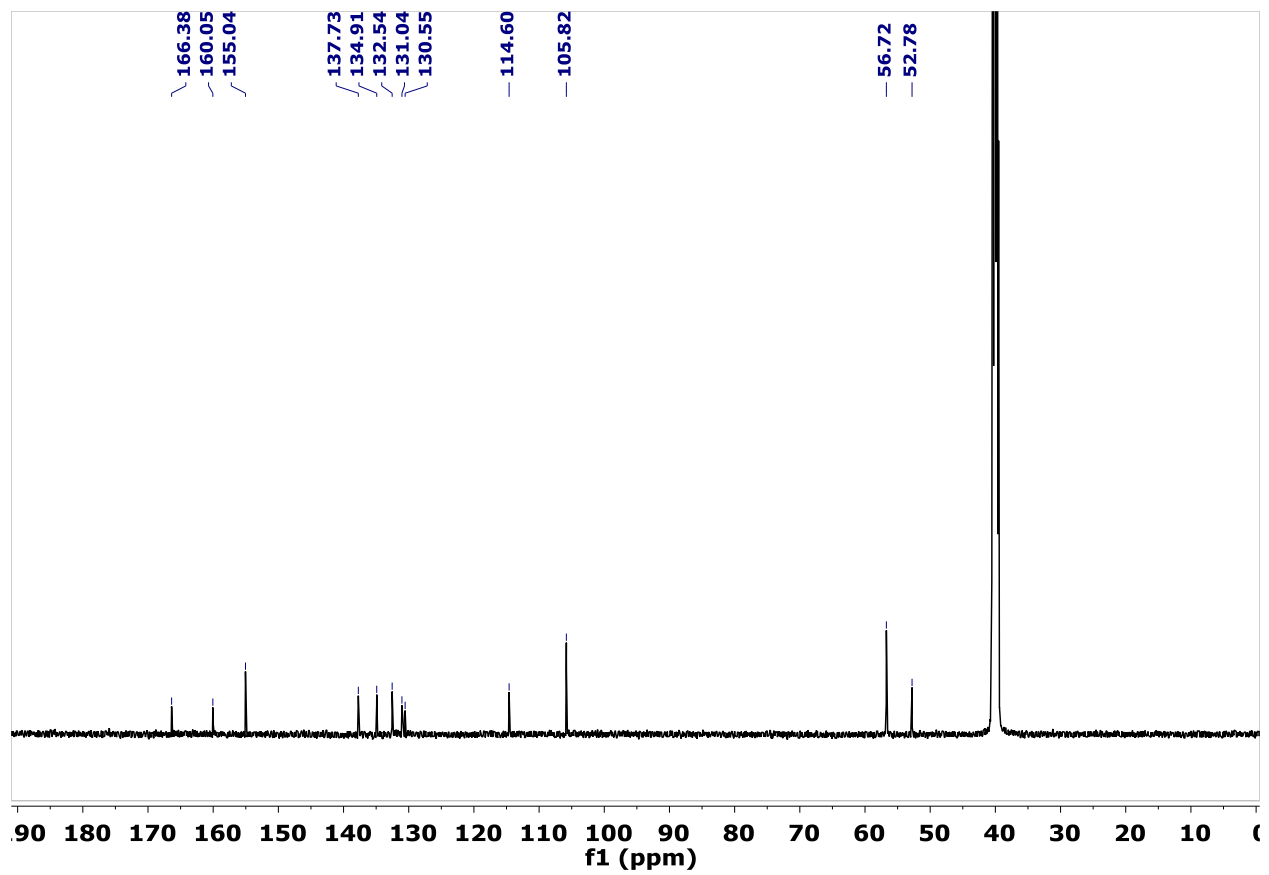
^{13}C NMR, DMSO-d_6

SI-**10**
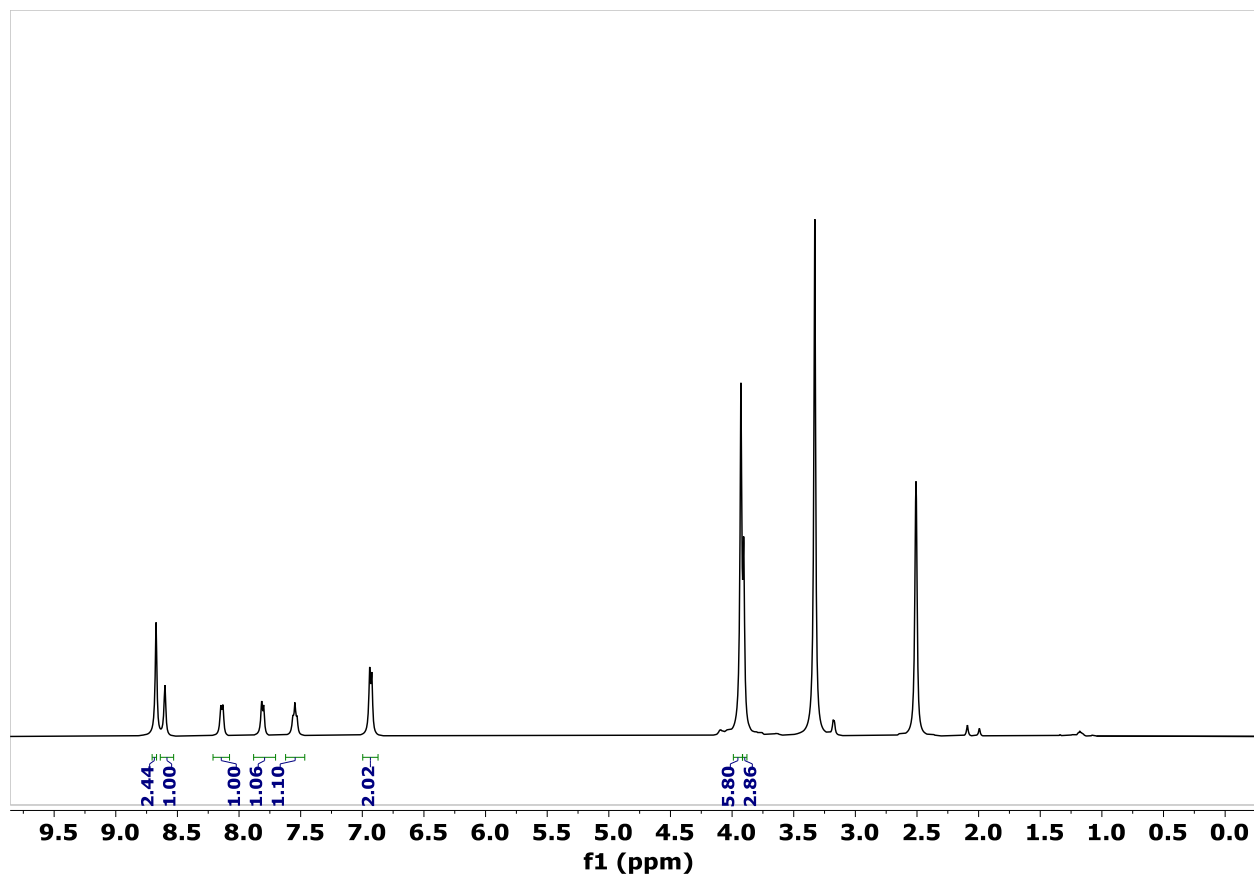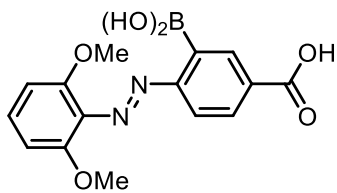
¹H NMR, DMSO-*d₆*
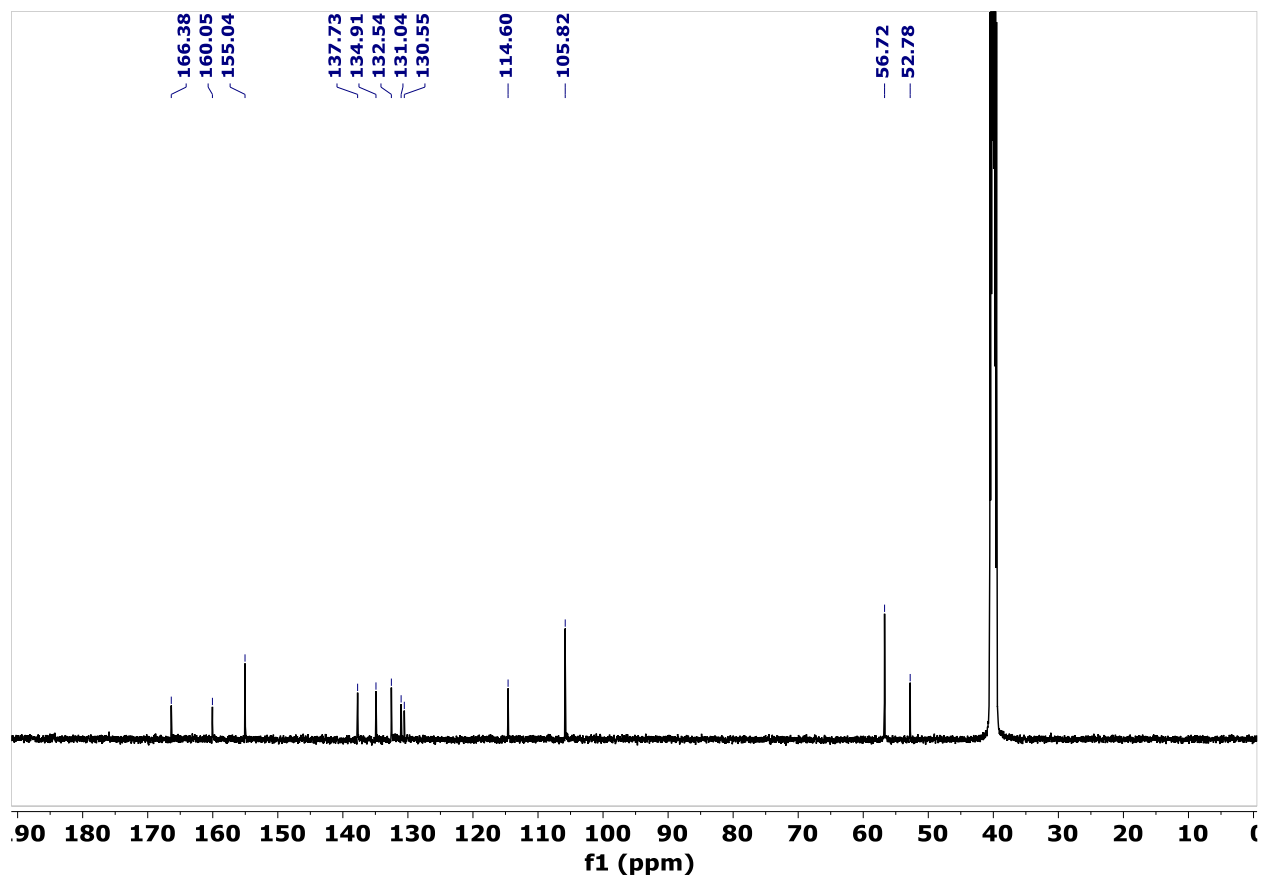
¹³C NMR, DMSO-*d₆*

SI-**11**
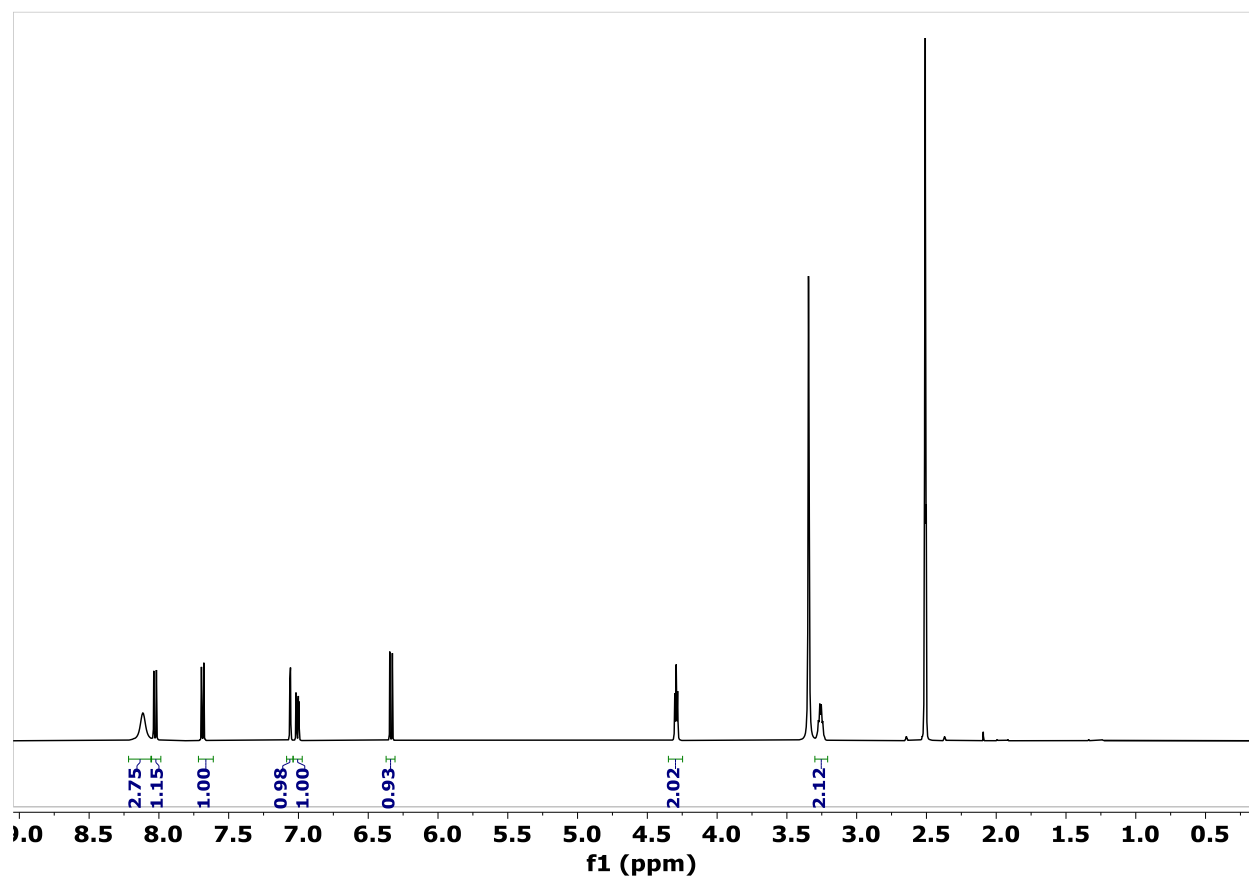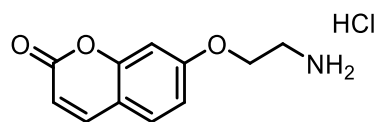
1H NMR, DMSO-*d₆*
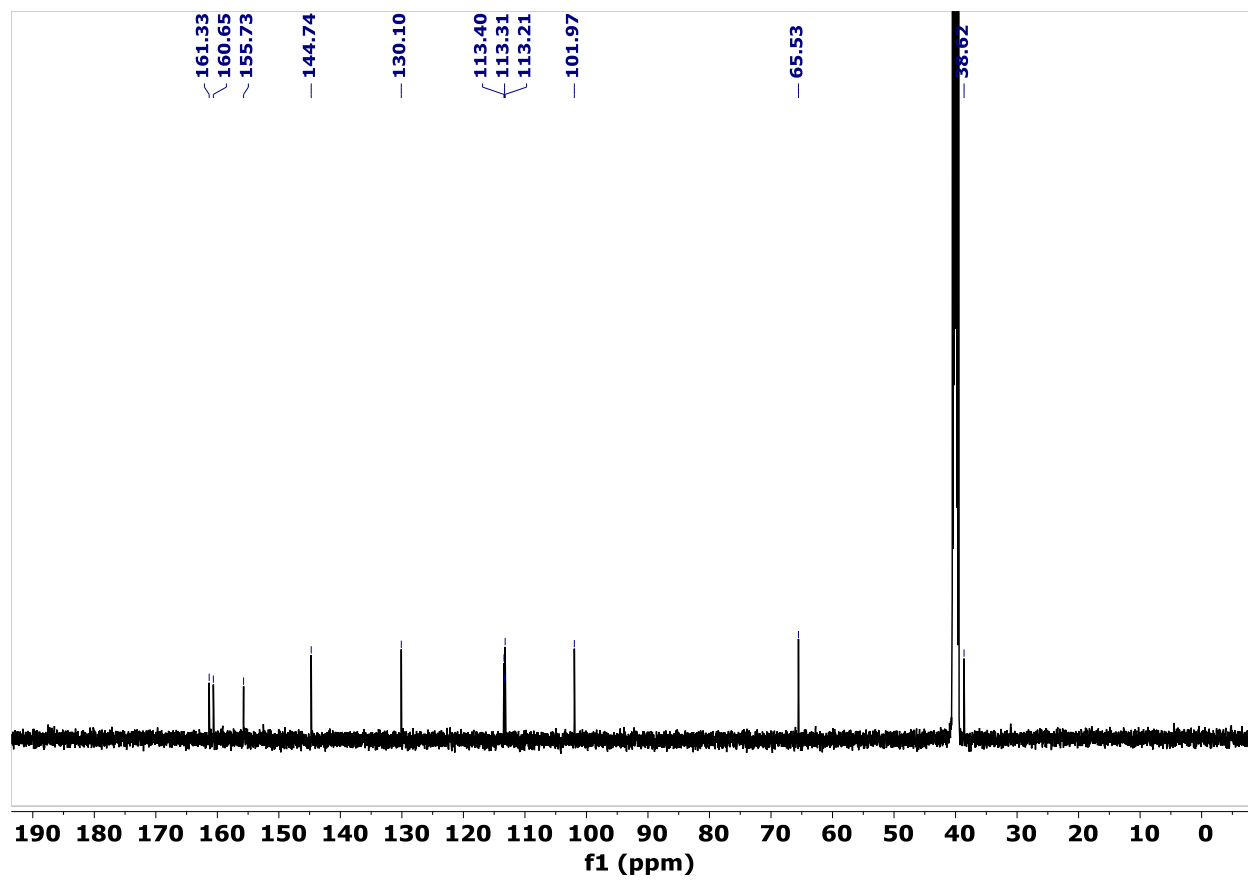
^{13}C NMR, DMSO-d_6

17
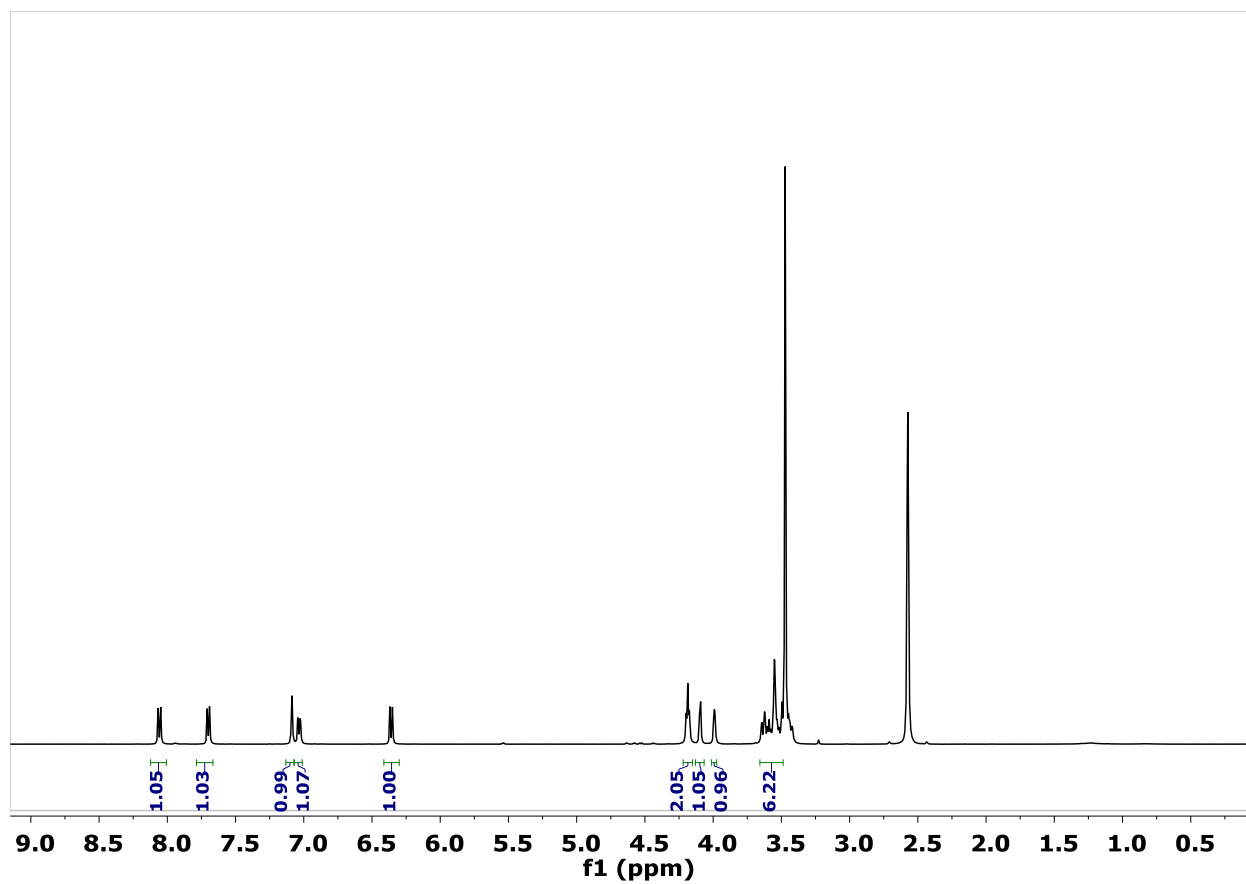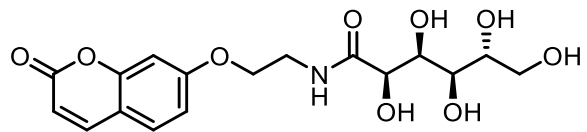
^{1}H NMR, DMSO-d_6
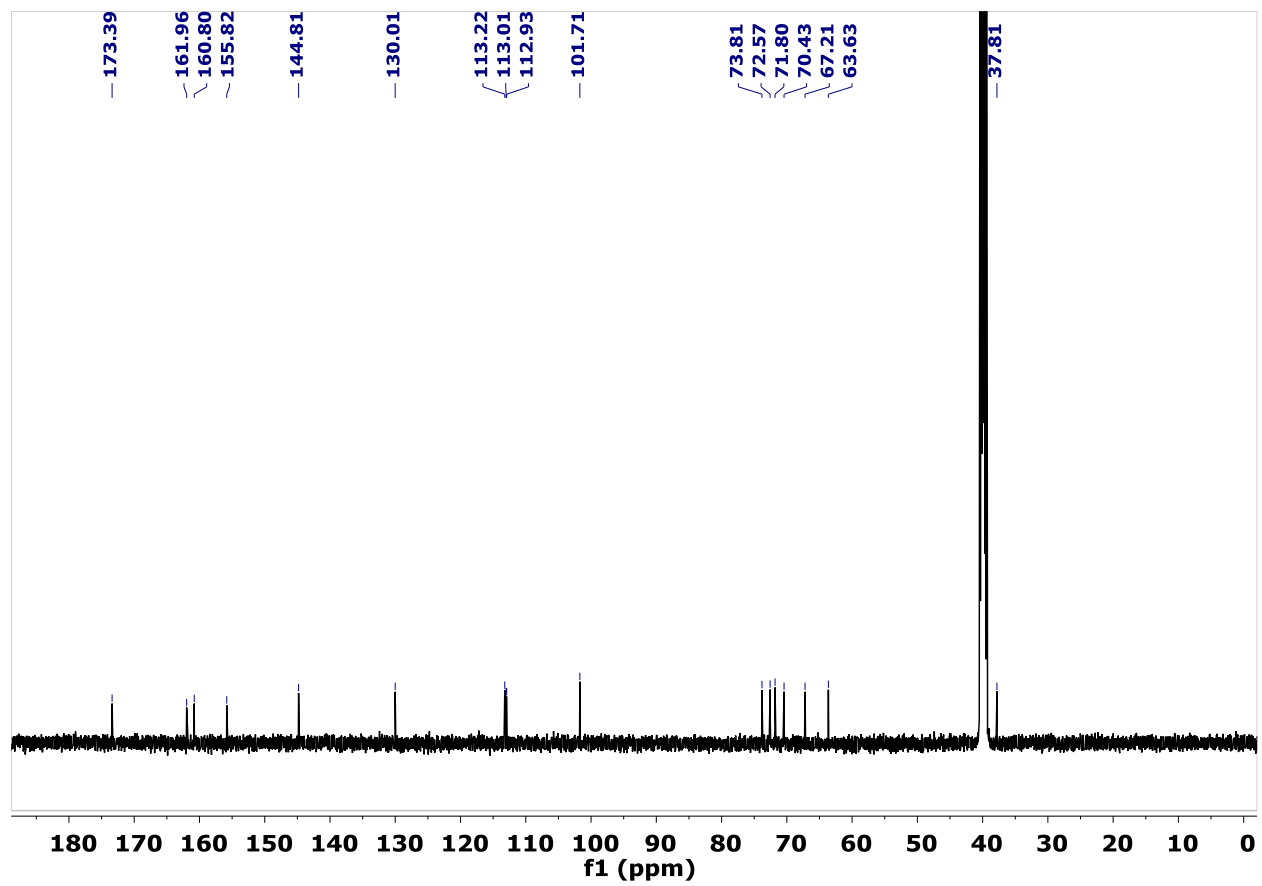
^{13}C NMR, DMSO-d_6

SI-**12**
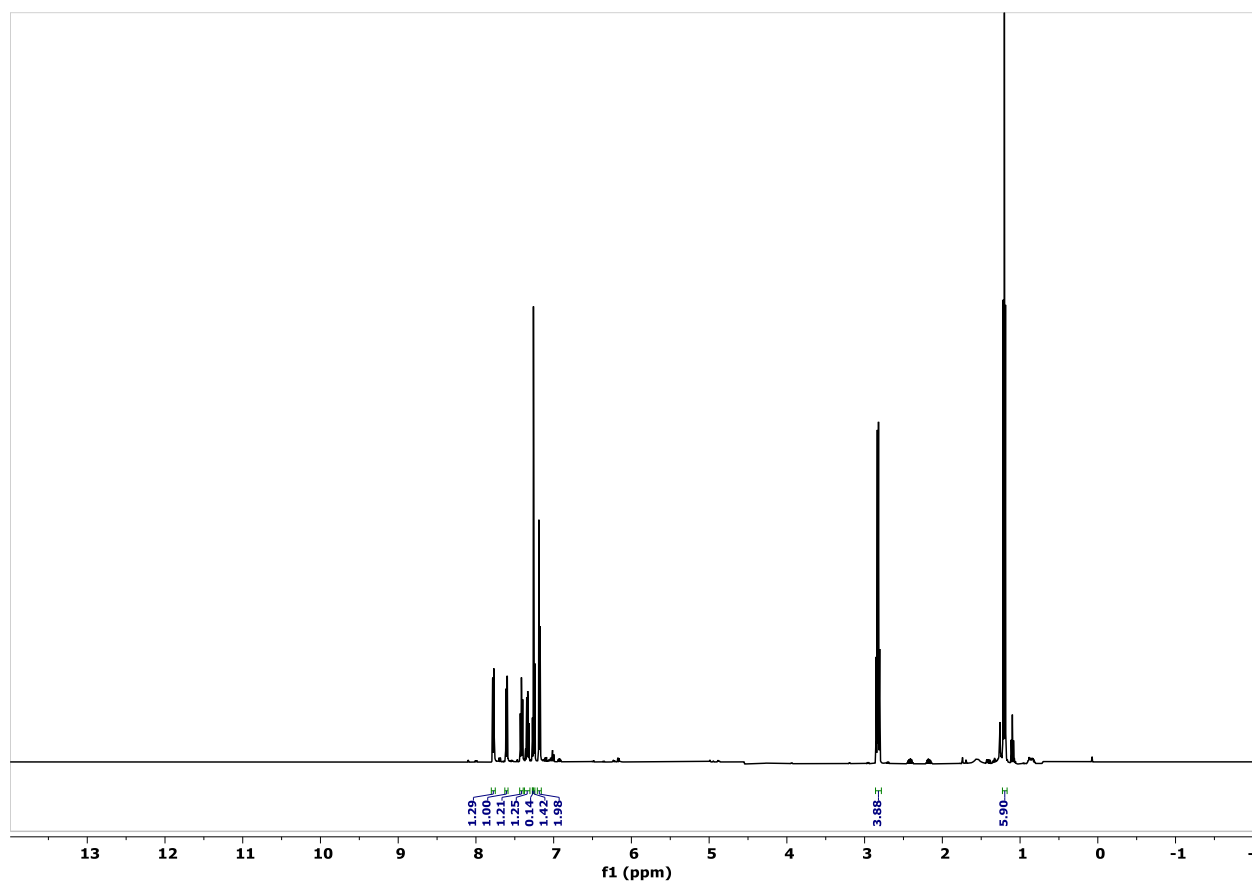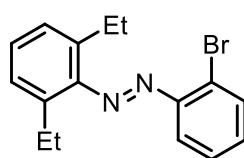
¹H NMR, CDCl₃-*d* (crude)
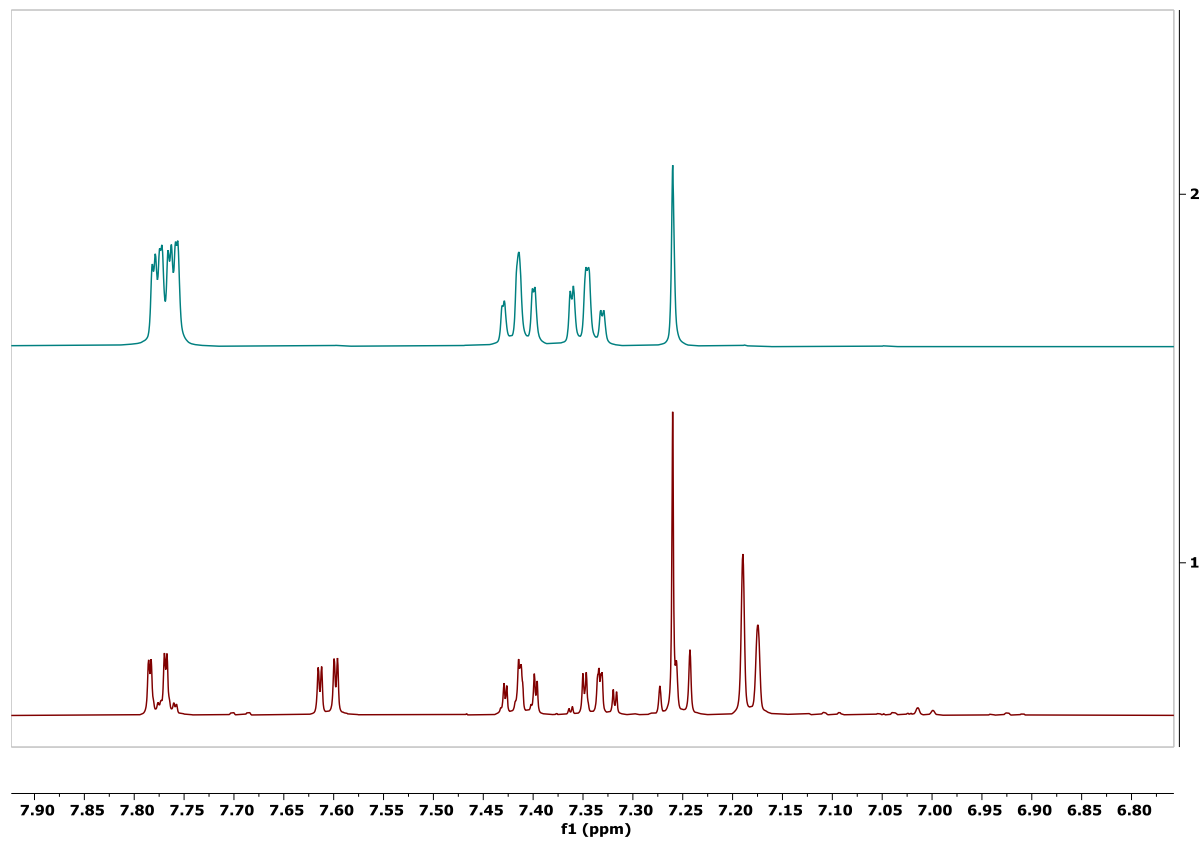
¹H NMR, CDCl₃-*d* (crude) and unknown impurity, which was largely removed through crystallization in cool hexane.

(E)-**6**
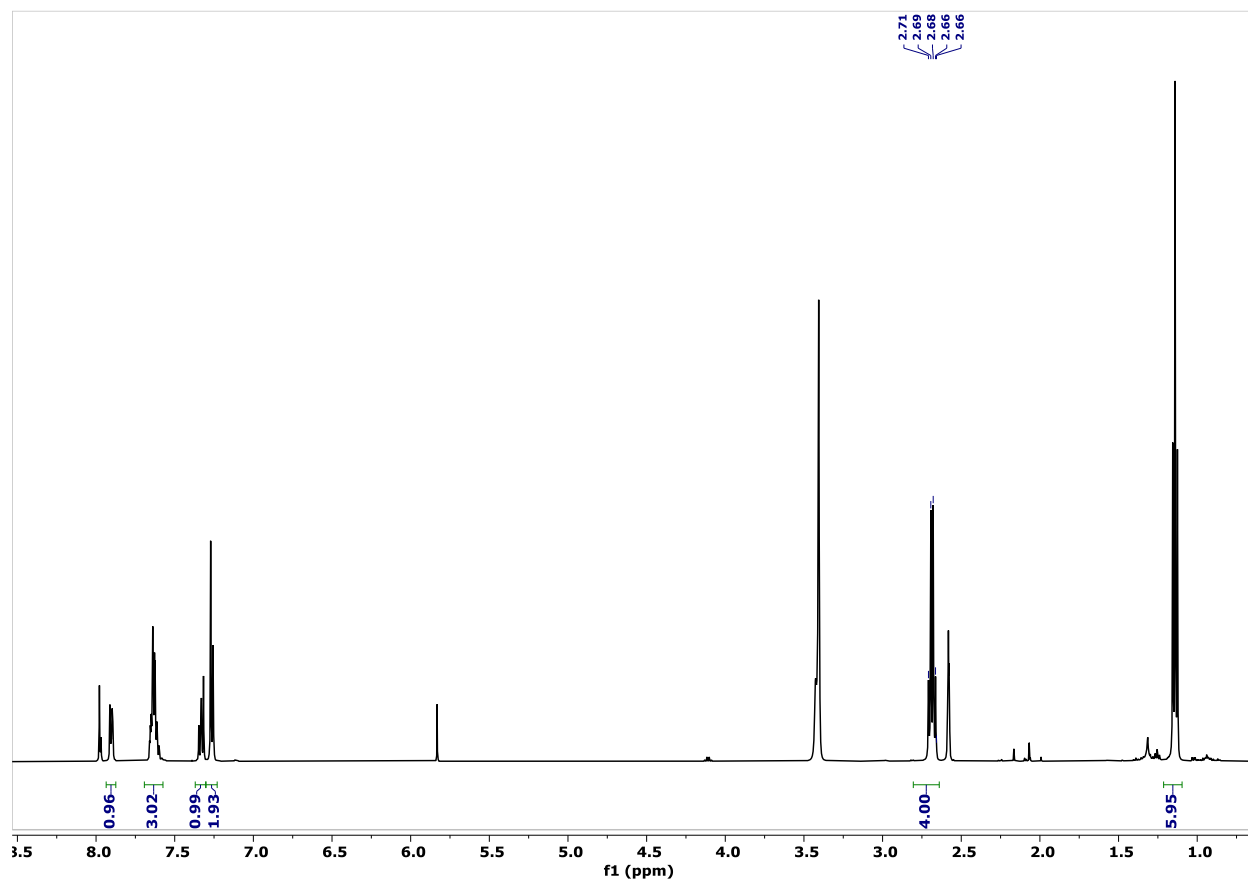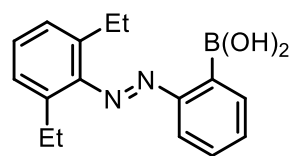
^{1}H NMR, DMSO-d_6
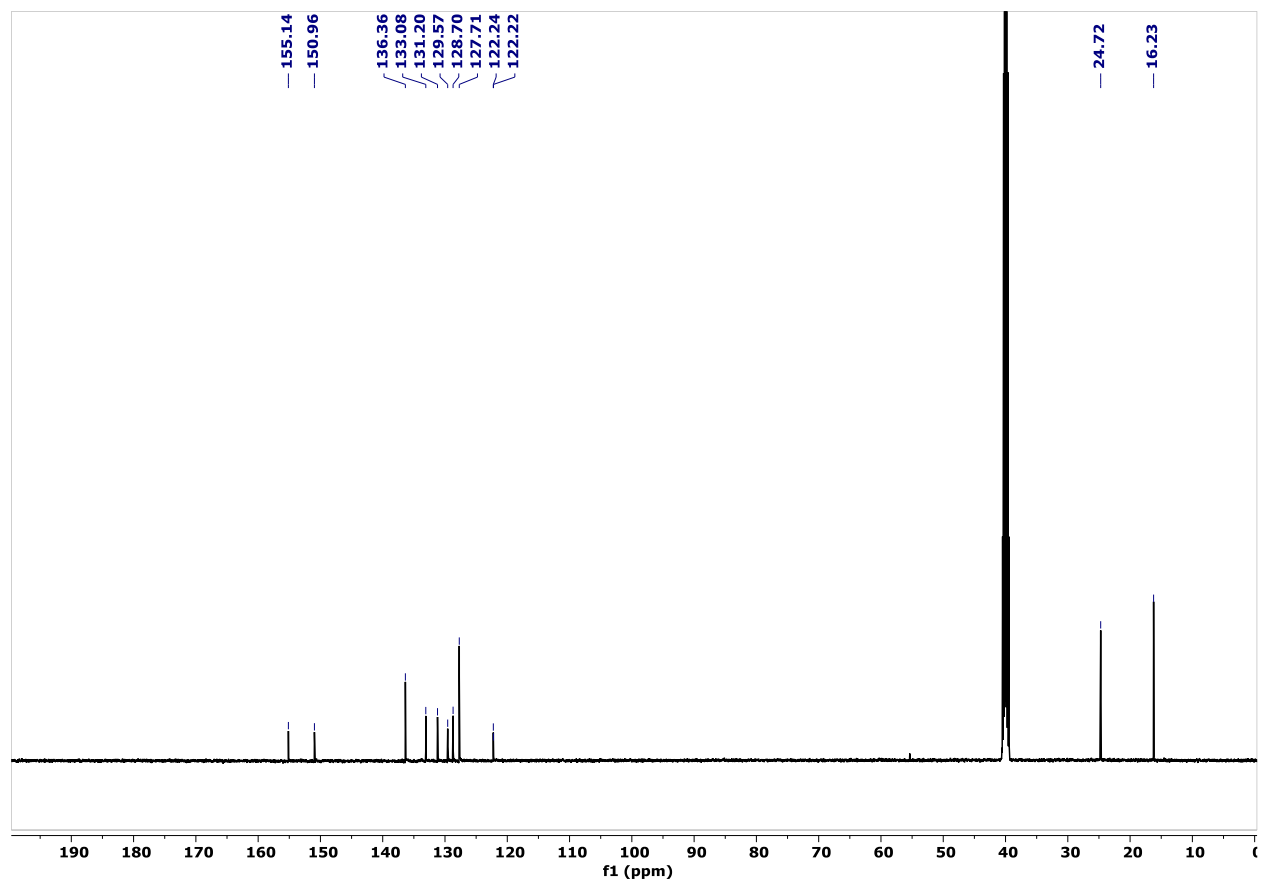
^{13}C NMR, DMSO-d_6

SI-**13**
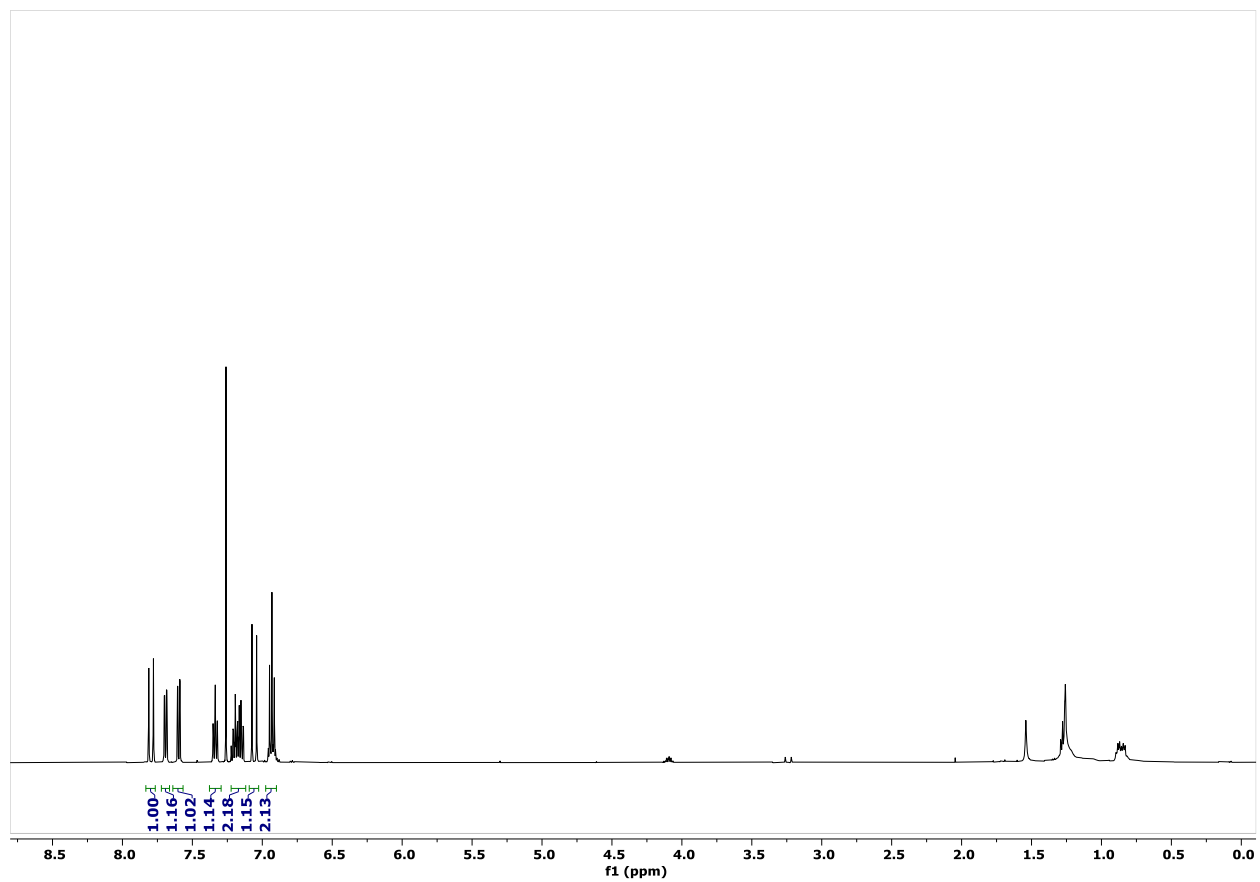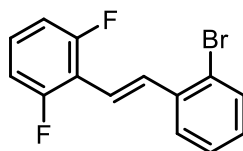
¹H NMR, CDCl₃-*d* (crude)
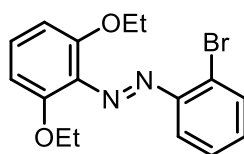
(*E*)-**7**

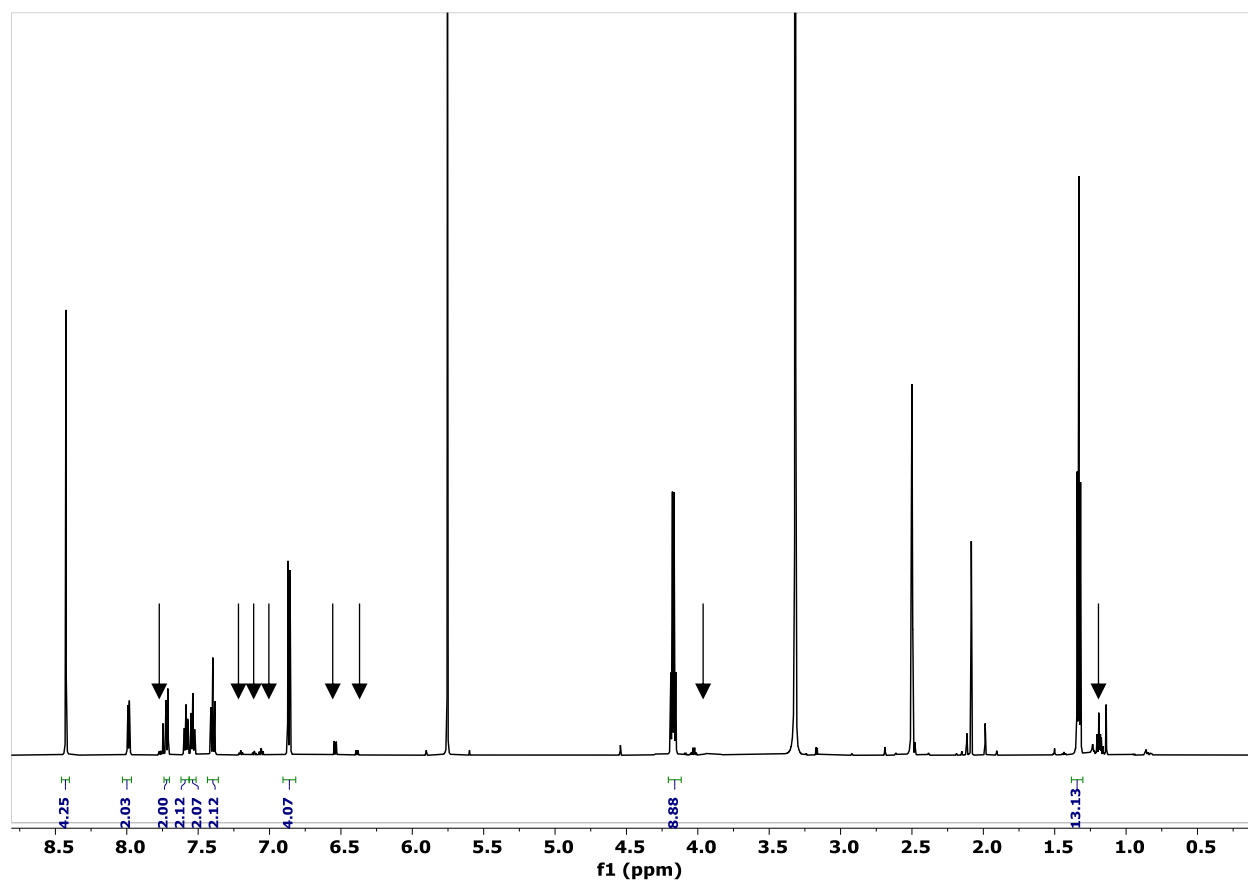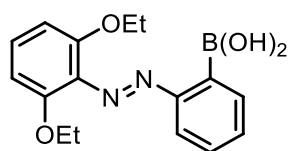¹H NMR, DMSO-*d₆*

^{13}C NMR, DMSO-d_6

-113.27
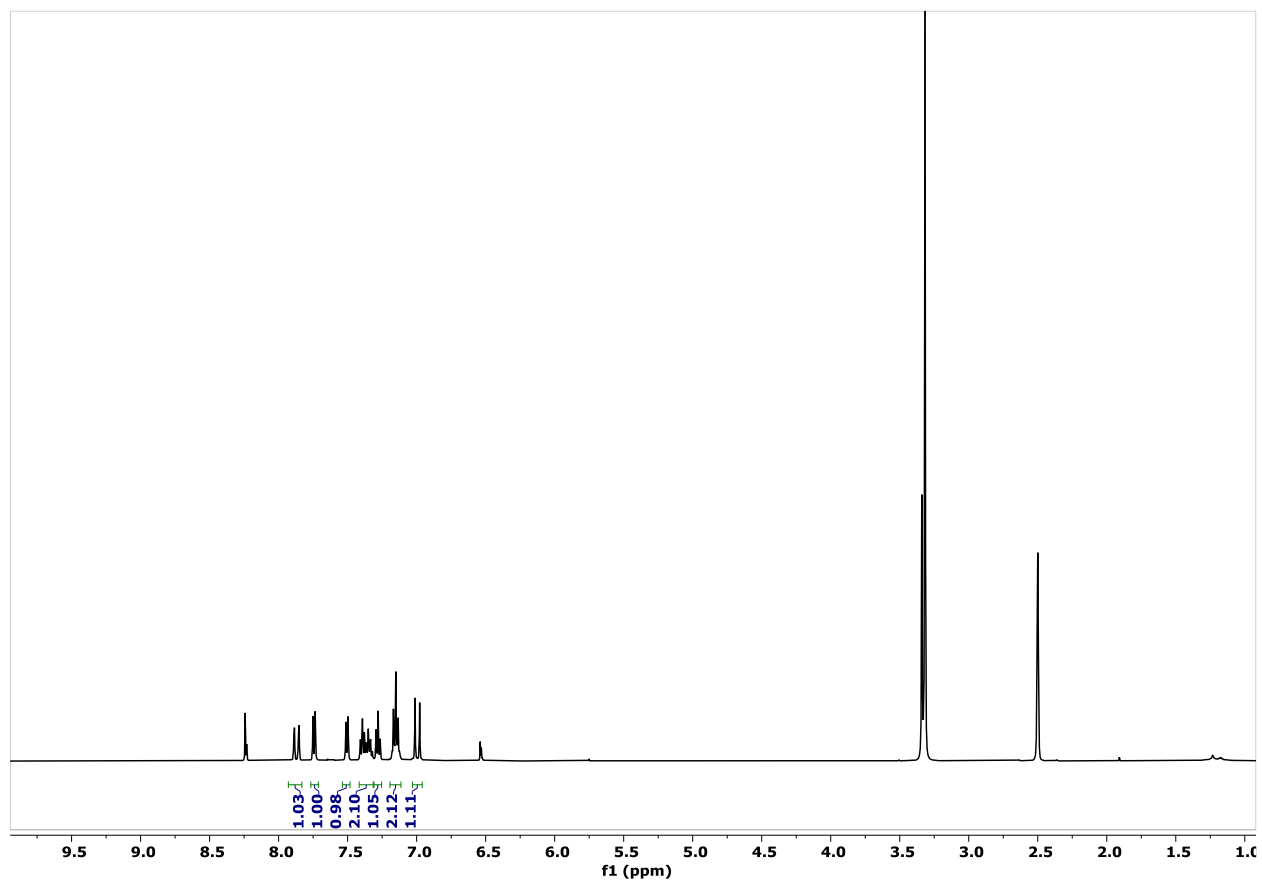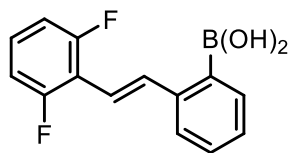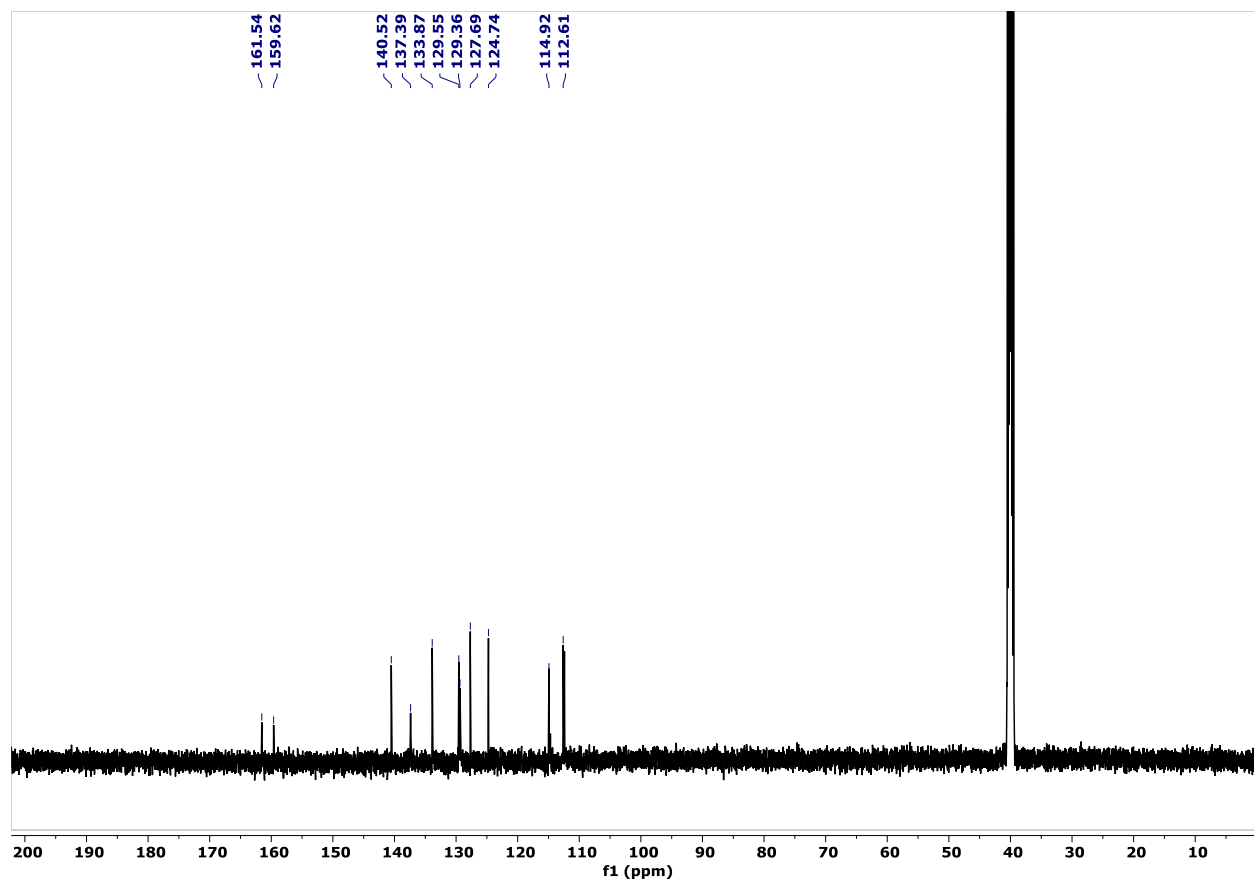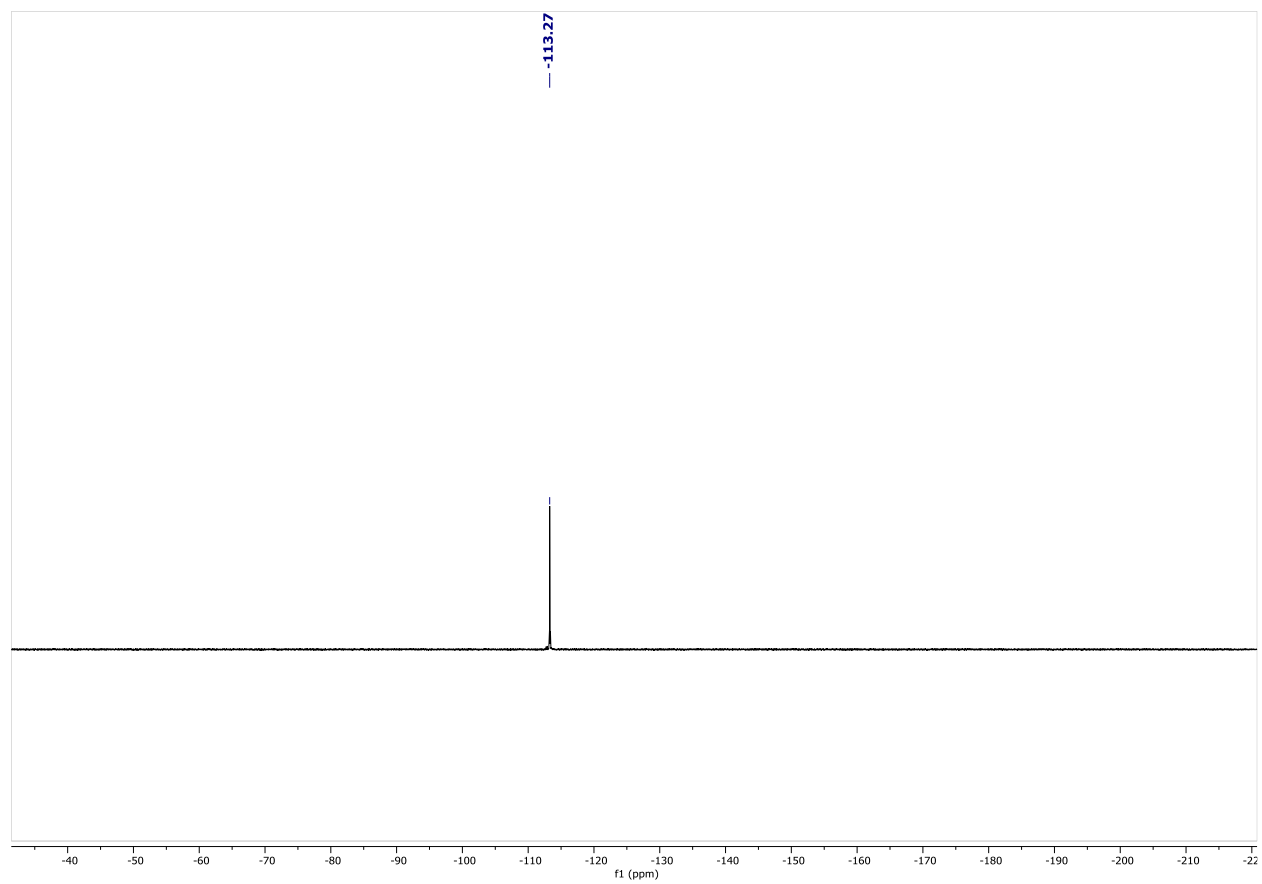
^{19}F NMR (DMSO-d_6).

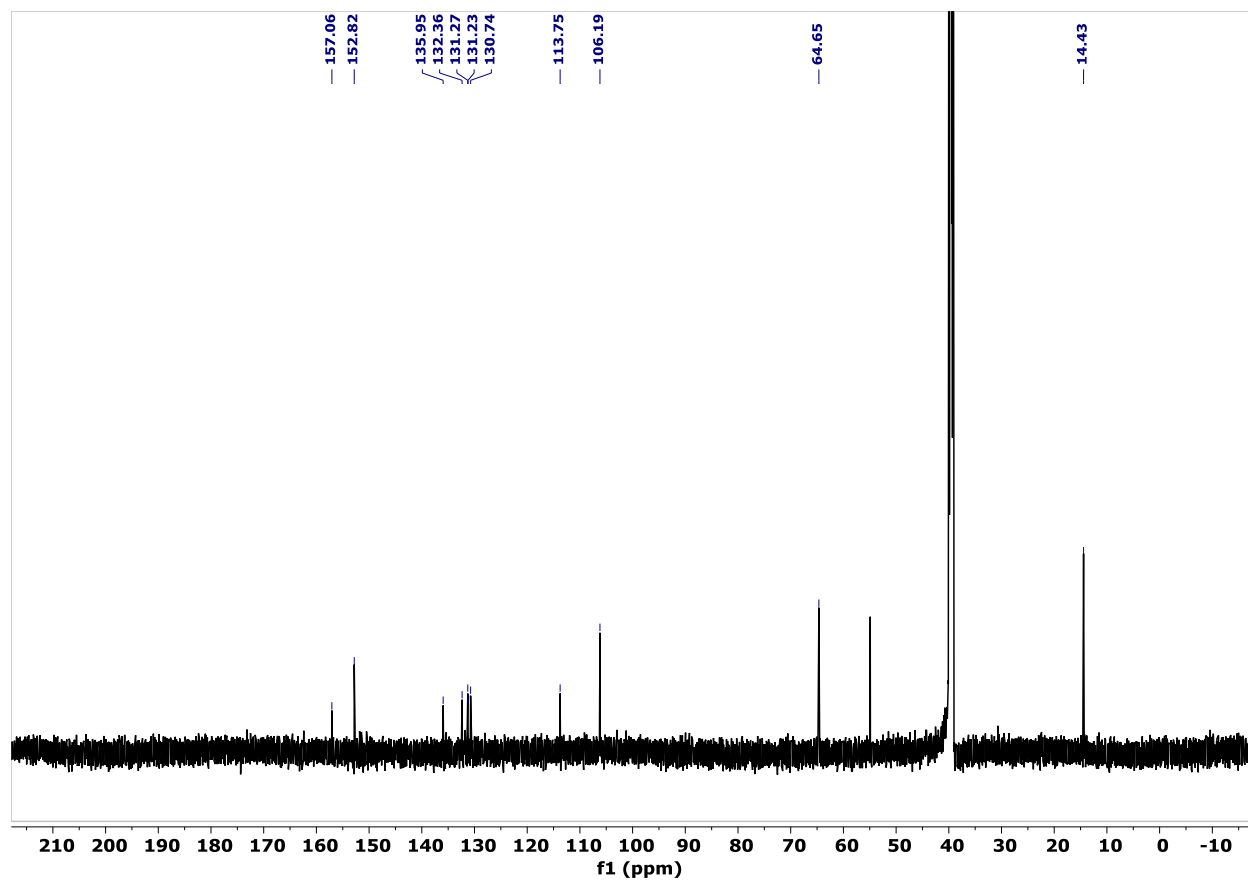**(*E*)-1-(2-bromophenyl)-2-(2,6-diethoxyphenyl)diazene (SI-14)**
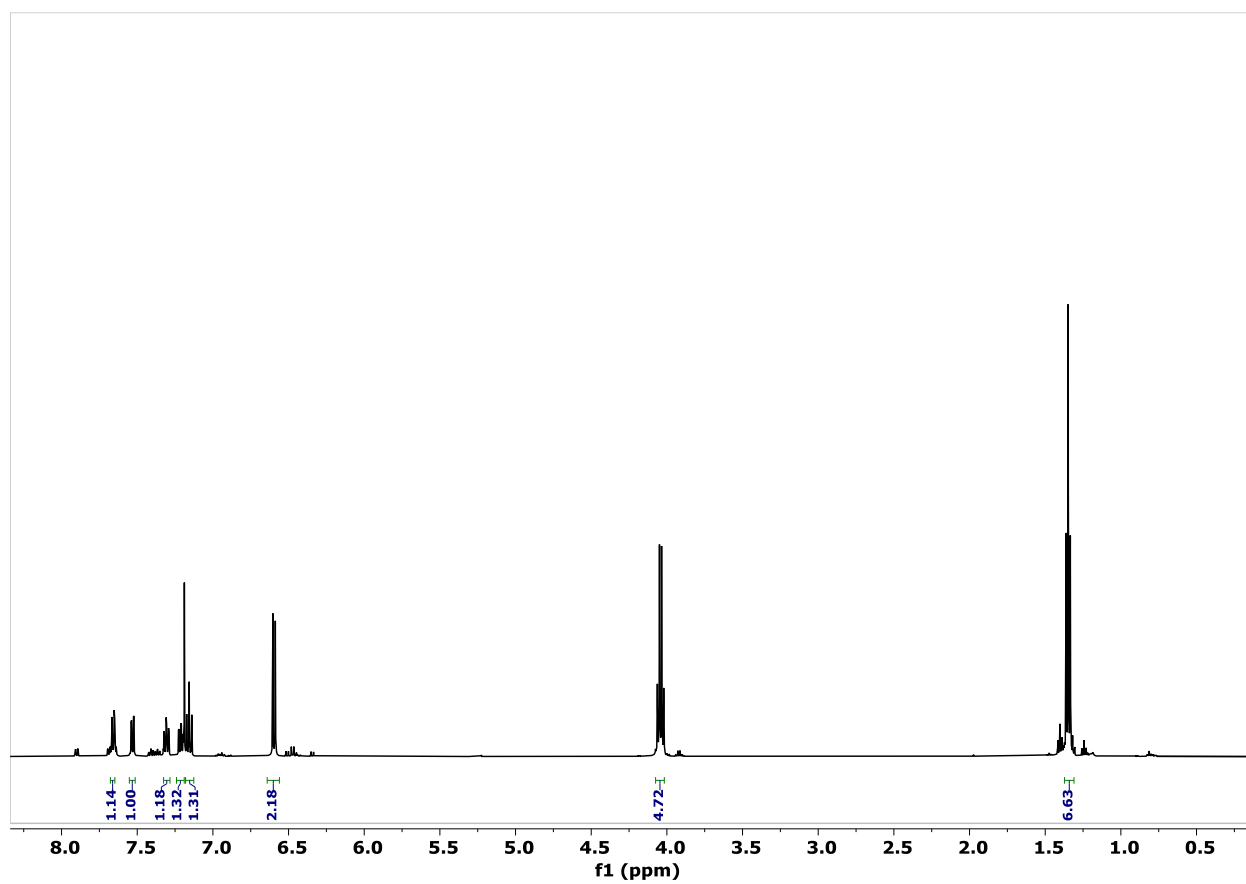
^{1}H NMR, CDCl$_3$-*d*

(*E*)-(2-((2,6-diethoxyphenyl)diazenyl)phenyl)boronic acid (6')

^{1}H NMR, DMSO-*d_6*. 7.5 % *Z* isomer (denoted with arrows)

157.06
152.82
135.95
132.36
131.27
131.23
130.74
113.75
106.19
64.65
14.43

^{13}C NMR, DMSO-d_6

P1
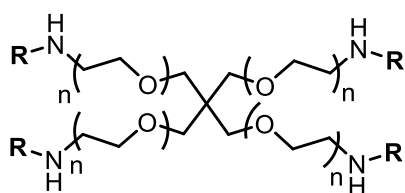
R=
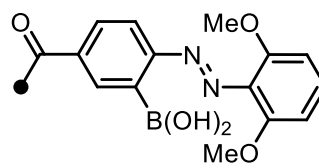
P1
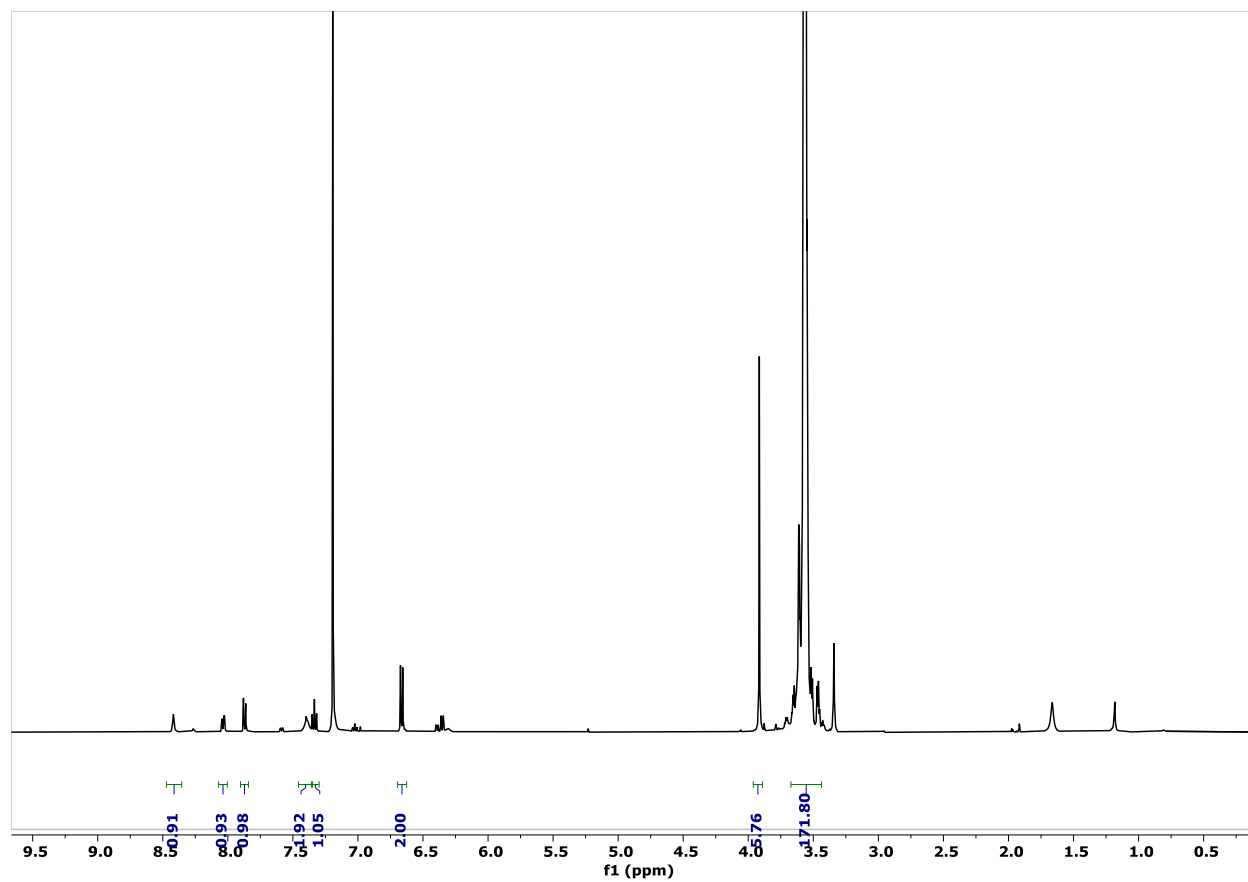
^{1}H NMR, CDCl$_3$-d. Minor peaks represent the Z isomer. The functionality of PEG-NH$_2$ was determined to be ≥80 % by end-group analysis.

Chapter 3: Photoredox Diels—Alder ladder polymerization

Abstract

Ladder polymers are synthetically challenging targets that comprise a sequence of rings in which each repeat unit shares at least two atoms with the adjacent one. Ladder polymers with sp^3-hybridized backbones feature kinked structures with restricted bond rotation. Such ladder polymers are typically synthesized through a mechanism that allows simultaneous formation of both bonds during polymerization, such as the Diels–Alder cycloaddition. Prior Diels–Alder polymerizations yielding ladder polymers required elevated temperature and/or pressure to achieve the desired reactivity, and the resulting products include aromatic linkages within the backbone. Here, we show that photoredox catalysis provides access to unique ladder polymers with sp^3 backbones under mild reaction conditions. We design 2-arylbutadiene monomers that enable propagation of the cyclohexene formed by each successive cycloaddition by stabilizing the required radical cation. The polymerization achieves molecular weights up to 4,400 g/mol with various electron-rich 2-aryl butadiene monomers. The resulting products may also be treated as macromonomers to form ladder bottlebrush polymers through a cationic polymerization. This report represents the first example of applying photoredox catalysis to the synthesis of ladder polymers and yields a novel sp^3-rich ladder polymer structure.

Introduction

Ladder polymers, which have two continuous junctions along the polymer backbone, have long enticed and puzzled chemists with their distinctive structures and challenging synthesis.[38] Because each repeat unit shares two atoms with the adjacent one, forming an uninterrupted sequence of rings,[114] ladder polymers have significantly limited degrees of rotation. These restricted conformations prevent efficient chain packing and can lead to materials that are intrinsically microporous, with applications in gas-phase separation, water purification, and chemical warfare agent detoxification.[50] The Diels–Alder cycloaddition presents an attractive synthetic route to ladder polymers because of the concerted nature of the ring-forming reaction. In 1926, Staudinger posited the first synthesis of a ladder polymer through the repeated cycloaddition of cyclopentadiene, and found that heating dicyclopentadiene at 200 °C for 90 h yielded an insoluble white powder that depolymerized to cyclopentadiene at 500 °C (**Figure 67a**).[41] While Staudinger's proposed polymerization involves a

thermodynamically disfavored [2+2] cycloaddition, a [4+2] cycloaddition, which had not yet been reported by

Diels and Alder,[115] is more likely. Schlüter used the Diels–Alder cycloaddition to prepare the first soluble, fully

characterized ladder polymer using a highly reactive diene that was generated *in situ*.[46,116] Despite the popularity

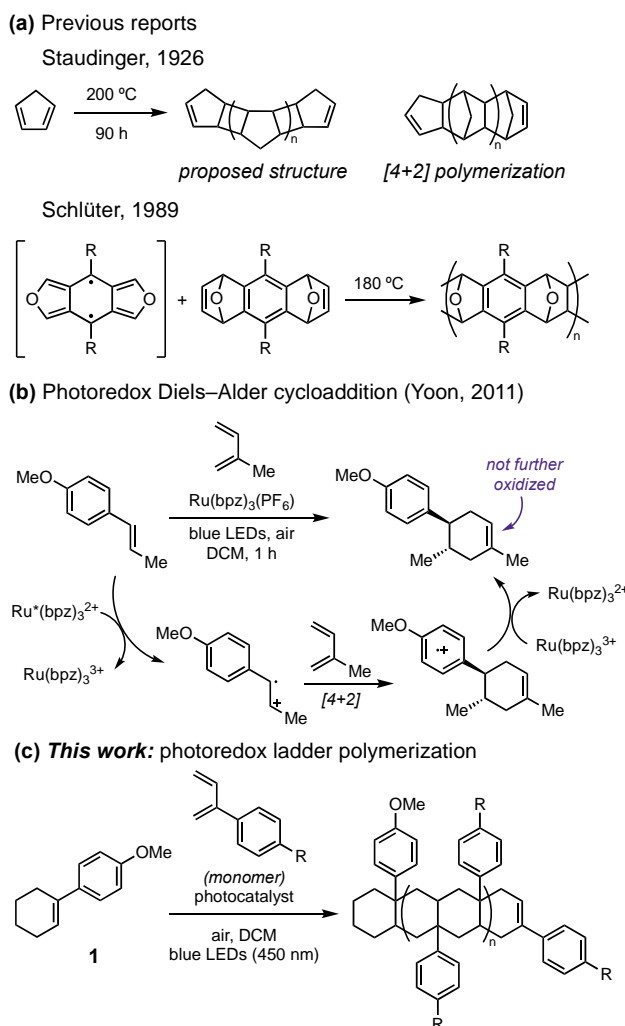of the Diels–Alder reaction for the synthesis of ladder polymers, efficient polymerization often requires high-

(a) Previous reports

Staudinger, 1926

(b) Photoredox Diels–Alder cycloaddition (Yoon, 2011)

(c) *This work:* photoredox ladder polymerization

Figure 67. (a) Previous attempts and successful reports of ladder polymerization based on cycloaddition reactions. **(b)** Radical cation Diels–Alder of trans-anethole and isoprene using photoredox catalysis. **(c)** Our proposed ladder polymerization via photoredox catalysis.

temperature or hyperbaric[52] reaction conditions. Since then, other reactions commonly used to form both

bonds along the polymer backbone include Pd-catalyzed annulation,[57] S$_N$Ar polycondensation,[54] and Tröger's

base formation.[55] Notably, all previous reports involve aromatic monomers, so the resulting ladder polymers

include some sp^2 atoms along the backbone even though they are not fully conjugated.

We envisioned that photoredox catalysis could be used to access ladder polymers with saturated backbones without elevated temperature or pressure. The advent of photoredox catalysis in polymer chemistry has enabled spatiotemporal control and mild reaction conditions.[117] Photoredox catalysis has been applied to many classes of polymerization,[117] including RAFT,[30,118,119] ATRP,[120,121] ROMP,[33,34] ROP,[31] and cationic polymerization of vinyl ethers.[29,122] Surprisingly, photoredox catalysis has not yet been applied to the synthesis of ladder polymers. We were inspired by the photoredox Diels–Alder cycloaddition reported by Yoon and coworkers, in which an electronically mismatched diene and dienophile react through a radical cationic pathway (**Figure 67b**).[58] In this small-molecule example, the dienophile must contain an electron-rich aryl group to allow oxidation by the photoredox catalyst.[123] However, the unactivated alkene in the product derived from isoprene cannot be oxidized, preventing further cycloadditions.

We hypothesized that the diene could be modified to support subsequent oxidation of the cycloadduct, thus enabling multiple sequential Diels–Alder reactions to ultimately form a ladder structure (**Figure 67c**). We envisioned that cyclohexene **1** could serve as a readily oxidized initiator, while 2-arylbutadiene monomers would produce cycloadducts with activated alkenes capable of propagation by the radical cation Diels–Alder mechanism. Unlike the ladder polymers accessed by prior approaches, including Diels–Alder polymerizations, the resulting ladder polymer would possess a fully sp^3-hybridized backbone with the exception of the propagating terminus. The properties of such saturated ladder polymers are entirely unknown. Such a polymerization could also follow a chain-growth mechanism, distinct from other Diels–Alder polymerization, which are step-growth in nature. Herein, we report the first photoredox ladder polymerization, explore the scope of this reaction, and demonstrate the ability to chain-extend the resulting products to achieve higher molecular weight polymers.

<u>Results and Discussion</u>

We first sought to confirm that the expected product of the proposed Diels–Alder cycloaddition, a 1-arylcyclohexene, can serve as a dienophile for subsequent propagation. Using cyclic voltammetry, we studied the oxidation of *p*-methoxyphenyl cyclohexene **1** (**Figure 68a**). Cyclohexene **1** underwent an irreversible oxidation event at +0.85 V *vs.* ferrocene/ferrocenium, suggesting that it has an even lower oxidation potential

than *trans*-anethole, the model substrate in Yoon's original study (+0.9 V).[58] These comparable oxidation potentials suggest that the electronics of **1** would support a radical cation cycloaddition. However, **1** is also a trisubstituted alkene, making it more sterically hindered than *trans*-anethole. To confirm that the radical cation derived from **1** can undergo cycloaddition, we subjected **1** and excess isoprene to various photocatalysts and oxidants (**Figure 68b**). Gratifyingly, **1** underwent successful cycloaddition with several oxidizing photocatalysts, and the structure of adduct **2** was confirmed by both mass spectrometry (MS) and ^{1}H nuclear magnetic resonance spectroscopy (NMR) (see Supplementary Information (SI)). As expected, the unactivated alkene in **2** did not undergo further propagation, but we anticipated that these photoredox conditions could be extended to the proposed ladder polymerization with appropriate monomers. To demonstrate that other aryl groups could support propagation, we synthesized and tested several cyclohexenes with different electron-rich aryl groups, and observed the desired cycloadducts by gas chromatography–mass spectrometry (GCMS, **Table 14**). These results demonstrate that a 1-arylcyclohexene can serve as a dienophile in the radical cation Diels–Alder cycloaddition promoted by photoredox catalysis, supporting the propagation step of the proposed ladder polymerization.
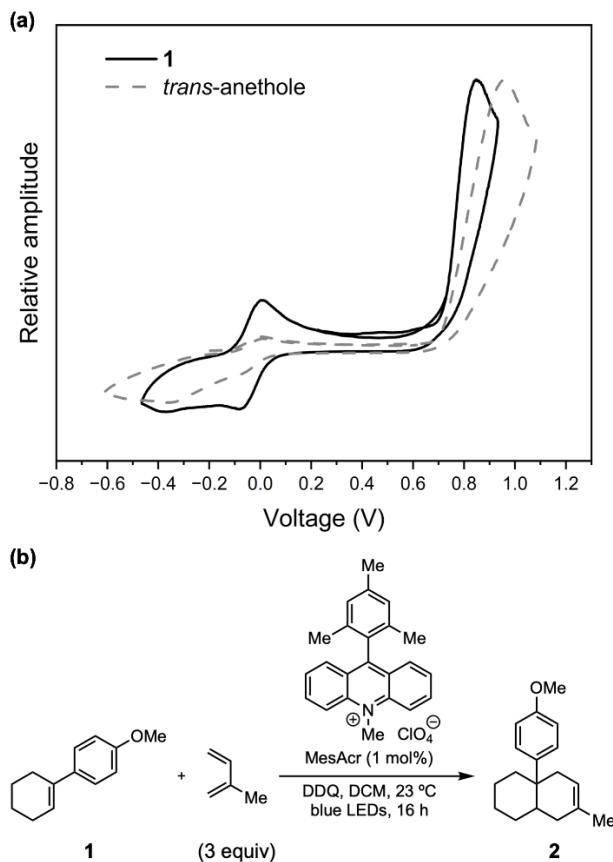
Figure 68. (a) Cyclic voltammetry comparing 1 and trans-anethole. Conditions: 0.1 M TBAPF$_6$ in acetonitrile, Pt working electrode, Pt auxiliary electrode, AgCl reference electrode, and ferrocene as a reference. **(b)** Small-molecule test reaction with isoprene.

Emboldened by these small-molecule results, we sought to apply these conditions to polymerization using 2-aryl-1,3-diene monomers in place of isoprene. We hypothesized that the electronics of the aryl group would influence its ability to support subsequent oxidation of the terminal cyclohexene and thus undergo propagation. Initially, we performed polymerization experiments with cyclohexene **1** as the initiator and 5 equivalents of *p*-methoxyphenyl diene **3a** (**Figure 69a**). These conditions resulted in low-molecular-weight oligomers with M$_n$ 490 g/mol (Đ 1.4) (expected 988 g/mol) as indicated by gel permeation chromatography (GPC). Additionally, during vacuum distillation of **3a** at elevated temperatures, we observed side products arising from a single Diels–Alder cycloaddition, suggesting reactivity outside of the radical cation manifold. Fortunately, replacing the methoxy group with a silyl ether suppressed the thermal reactivity and improved the solubility of the products; furthermore, the silyl ether could be deprotected for post-polymerization modifications. With 5 equivalents TBS-protected diene **3b** relative to **1,** we obtained oligomer with M$_n$ 780

g/mol (expected 1,488 g/mol). Further increasing the amount of monomer relative to initiator to 15:1 increased the molecular weight to 1,300 g/mol (Đ=1.5, expected 4,088 g/mol) with a yield of 71%. The disparity between the theoretical and experimental molecular weights suggests that the polymerization is not well controlled (*vide infra*). The polymerization of diene **3b** proceeded with a variety of photocatalysts, solvents, oxidants, and at a variety of concentrations, but with minimal effect on the molecular weight of the product (see SI for additional conditions).

Using monomer **3b** and initiator **1**, we performed several control experiments to confirm the role of light in the reaction. We do not obtain polymer in the absence of light, photocatalyst, or when diene (SI, **Table 18**). We questioned whether the modest molecular weights arise from a competing retro-Diels–Alder process. However, when we subjected the isolated polymer to the standard reaction conditions (photocatalyst, light, no monomer), we did not observe a decrease in M_n. Under the standard photoredox conditions in the absence of **3b**, **1** undergoes [2+2] dimerization;[124] this side reaction is not observed when the diene is present. Interestingly, we still observed polymer formation with M_n 1,200 g/mol when **1** was not added to the reaction mixture, suggesting that the initiator is not necessary.

These observations prompted us to investigate the products of the reaction in more detail. Since ^{1}H NMR of the polymeric products was complex, preventing detailed structural elucidation, we isolated and characterized oligomeric products formed from **1** and **3b** under the photoredox conditions. After precipitation into methanol, we separated the oligomeric products in the supernatant via preparative thin-layer chromatography and analyzed their structures using 1D and 2D NMR. The products we isolated correspond to well-defined Diels–Alder cycloadducts derived from **1** and **3b** in various ratios up to DP = 4. The double addition of **3b** to **1** was fully characterized and assignments for key protons in the ^{1}H NMR spectrum are in **Figure 68b**. In addition to oligomers containing **1**, we also observe Diels–Alder adducts lacking **1** and containing an additional monosubstituted olefin, which we assign to [4+2] cycloaddition between two dienes. Based on this assignment, we propose that the polymerization may either be initiated by **1** (forming **LP3b**, **Figure 69a**) or by the diene itself (forming **LP3b'**). While **LP3b'** contains two alkenes, the monosubstituted alkene would not be oxidized by the photocatalyst, thus propagation should still occur unidirectionally. These

assignments are consistent with MALDI-TOF analysis of the reaction products (SI, **Figure 105** through **Figure 107**). In the absence of **1**, masses corresponding to multiples of **3b** are observed, while polymerization in the presence of **1** yields the same set of peaks in addition to a set indicating incorporation of initiator. Initiation by the diene partly accounts for the discrepancy between theoretical and experimental molecular weights.

^{1}H NMR analysis of the polymers includes the same characteristic signals observed in the oligomers, including the cyclohexene vinyl proton at 6.1 ppm and the OMe proton of **1** at 3.8 ppm, but the presence of several peaks in each region suggests that these protons exist in a variety of environments. For example, an incoming diene can react with either the top or bottom face of the cyclohexene terminus, resulting in different diastereomers of the product. While the oligomers we isolated were predominantly a single diastereomer, we cannot confirm diastereoselectivity. The ^{1}H NMR spectra of these ladder polymers are notably distinct from those of the linear polymers synthesized from 2-aryldiene monomers using a Mg-initiated polymerization reported by Fiorito et al.[125]
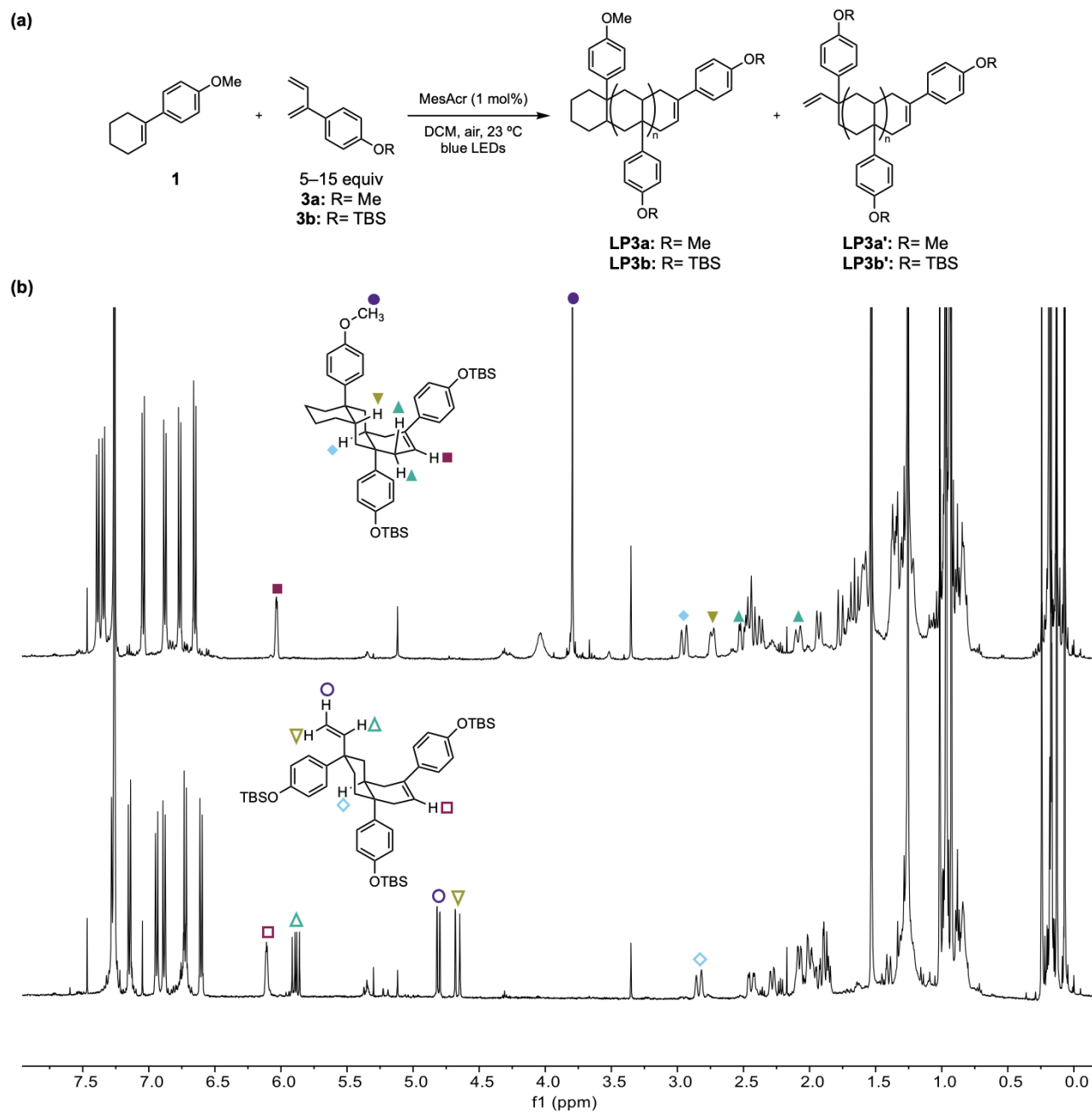
Figure 69. (a) Initiation pathways for the photoredox Diels–Alder polymerization assigned based on MALDI-TOF and NMR analysis (see ESI for details). (b) ^{1}H NMR spectra of the bis-addition product for both initiation pathways; see ESI for isolation procedure and additional spectroscopic data.

We next synthesized a library of 2-aryl diene monomers and subjected them to our optimized conditions. Polymerizations were evaluated based on the yield after precipitation into methanol and molecular weight by gel permeation chromatography (GPC). Because of the rigid structure of ladder polymers, GPC

evaluation of molecular weights using polystyrene standards on GPC are generally accepted as less accurate.[126,127] Therefore, we used GPC coupled with multiangle light scattering (MALS) to determine the absolute molecular weights of the polymers. For most dienes evaluated, GPC indicated formation of oligomeric (~1500 g/mol) species in low to moderate yields (**Figure 70**). **3c**, bearing a *para*-tertbutylphenyl group, provided one of the highest yields and molecular weights, most likely due to the electron-donating and solubilizing nature of this substituent. A *para*-methyl group (**3d**) also provided modest yield of an oligomer. As expected, based on the radical cation mechanism, electron-poor aryl dienes such as **3e** had deleterious effects on the molecular weight and yield. Beyond substitution at the *para* position, *ortho* substituents decreased the yield of oligomer/polymer with variable effects on molecular weight. Compared to *para*-substituted arenes, 2-naphthyl (**3g**) and 2,4-dimethylphenyl (**3h**) dienes provided improved molecular weight, while sterically hindered **3i** prevented efficient polymerization. While *para*-methoxy-substituted **3a** was too reactive, undergoing background thermal reactions, *meta*-substituted **3j** and **3k** provided modest yields and molecular weights. Molecular weights were not significantly influenced by photocatalyst, solvent, and reaction concentration, suggesting the versatility of the polymerization (see SI for additional conditions). Further attempts to increase the molecular weight of the polymers are beyond the scope of this report. Synthesizing ladder polymers of high molecular weights has historically been a challenge due to the limited degrees of rotation of the polymers, which leads to lower solubility.[126] Solubility limitations, as well as unknown termination mechanisms, may account for the lower yields observed for some of the reactions. We also speculate that the rigid, kinked conformation of these materials may render the propagating alkene sterically inaccessible after multiple cycloadditions, limiting the molecular weight of the polymers.
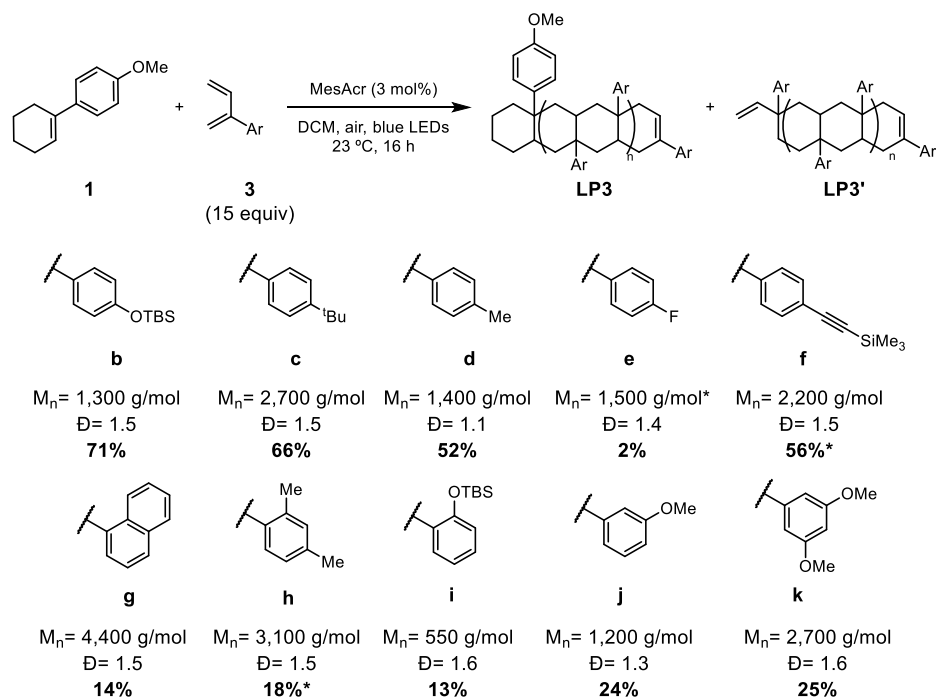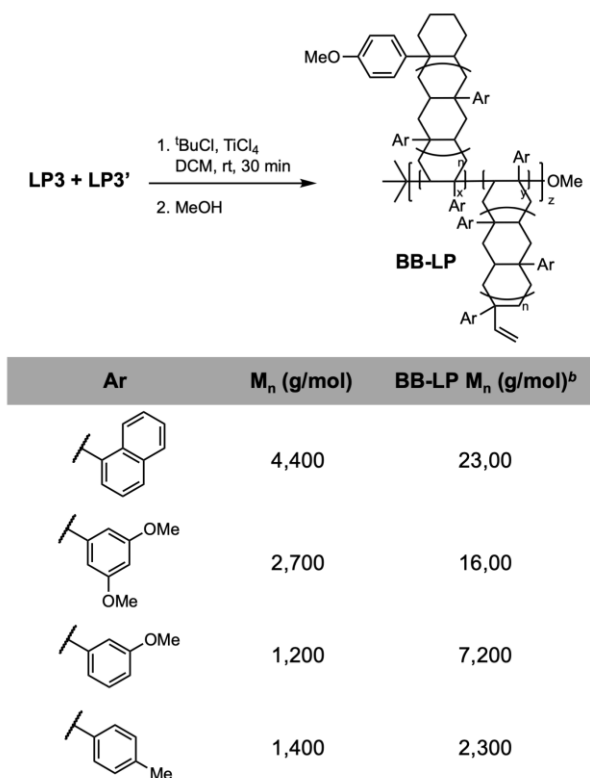
Figure 70. Scope of Diels—Alder polymerization. Polymerizations were conducted with a 1:15 initiator:monomer ratio and precipitated into 7:1 methanol:water. The resulting polymer was analyzed using GPC. *Polymer did not precipitate into methanol; in these cases yield and molecular weight are based on the supernatant.

The surface areas of the ladder polymers obtained through the photoredox polymerization are modest (ESI, **Figure 75** through **Figure 76**). The microporosity of ladder polymers often increases with their molecular weight.[128] Therefore, we sought to increase the molecular weight of these oligomers by using them as macroinitiators for a different polymerization mechanism. Inspired by recent reports by Swager and coworkers,[53,129] we hoped to convert the oligomeric products of the photoredox pathway to bottlebrush ladder polymers. Unlike the ladder polymers synthesized by Swager and coworkers, the cyclic alkene of the Diels–Alder adduct is not amenable to ring-opening metathesis polymerization. Instead, we hypothesized that the cyclohexene at the propagating end of both **LP3** and **LP3'** would be sufficiently electron-rich to engage in Lewis acid-initiated cationic polymerization. A subset of polymers from **Figure 70** was subjected to previously reported cationic polymerization conditions and the polymers were evaluated by GPC-MALS (**Table 13**). Indeed, we observed increases in molecular weight for each polymer sample. For some polymers, we observed significant increases in molecular weight, while polymers with less electron-rich arene end groups led to more marginal increases. This reactivity provides additional support for the presence of the cyclohexene end group.

Future experiments include evaluating the gas-sorption characteristics of these bottlebrush polymers and comparing them to their precursors.

Table 13. Cationic polymerization to synthesize bottlebrush ladder polymers.[a]

Ar	M_n (g/mol)	BB-LP M_n (g/mol)[b]
(naphthalenyl)	4,400	23,00
(3,5-dimethoxyphenyl)	2,700	16,00
(3-methoxyphenyl)	1,200	7,200
(4-methylphenyl)	1,400	2,300

[a]Polymers were precipitated into 7:1 methanol–water. [b] Molecular weights determined by GPC-MALS.

In conclusion, we have developed mild conditions for synthesizing highly saturated ladder polymers through a photoredox Diels–Alder cycloaddition. The polymerization proceeds with a variety of photocatalysts, solvents, and electron-rich aryl diene monomers. Evidence for the cycloadduct structure of the products is obtained from NMR analysis of isolated oligomers. Although a cyclohexene initiator is incorporated into the polymers, we also found evidence for initiation by the monomer itself. Furthermore, we can exploit the resulting alkene end groups to synthesize higher-molecular-weight bottlebrush polymers through a cationic mechanism. While the polymerization is not well controlled, it likely proceeds through a chain-growth mechanism initiated or mediated by light.[130] Future experiments include characterizing the microporosity of these polymers, comparing their microporosity to linear analogues, and investigating the polymerization kinetics.

<u>Supporting Information</u>

General Procedures Unless otherwise noted, reactions were performed under N_2 atmosphere in oven-dried (150 °C) glassware. Reaction progress was monitored by thin layer chromatography (Merck silica gel 60 F_{254} plates) or by either liquid chromatography-mass spectrometry using an Agilent 6120 Quadrupole LC/MS or gas-chromatography mass-spectrometry using an Agilent GCMSD-Headspace. TLC plates were visualized using mainly UV-light (254 nm) fluorescence quenching, potassium permanganate stain, ceric ammonium molybdate followed by heat. Automated column chromatography was performed using SiliCycle SiliaFlash F60 (40-63 μm, 60 Å) in SNAP cartridges on a Biotage Isolera One. Organic solvents were removed *in vacuo* using a rotary evaporator (Büchi Rotovapor R-100, ~20–300 torr) and residual solvent was removed under high vacuum (<200 mtorr).

Materials and Methods Commercial reagents were purchased from Sigma-Aldrich, Acros, Alfa Aesar, TCI, or Oakwood and used as received. All solvents were purified and dried using a solvent-purification system that contained activated alumina. Additionally, THF used for glovebox experiments was degassed before being stored in a nitrogen-filled glove box over activated 3Å sieves.

Instrumentation Proton nuclear magnetic resonance (^{1}H NMR) spectra and carbon nuclear magnetic resonance (^{13}C NMR) spectra were recorded on Bruker AVANCE-500 spectrometers at 500 MHz and 125 MHz, and referenced to the solvent residual peaks. ^{19}F NMR spectra were recorded on Bruker AVANCE-500 spectrometers at 470 MHz. NMR data are represented as follows: chemical shift (δ ppm), multiplicity (s = singlet, d = doublet, t = triplet, q = quartet, m = multiplet), coupling constant in Hertz (Hz) and integration. Blue LED strip lights (wavelength = 470 nm, power = 6.6 W) and green LED strip lights (wavelength = 525 nm, low power = 5.7 W, high power = 16 W) were purchased from superbrightleds.com. Size exclusion chromatography (SEC) measurements were performed in stabilized, HPLC-grade tetrahydrofuran using one of two instruments; the first is a Agilent 1260 Infinity II system with variable-wavelength diode array (254, 400, 480, 530, and 890 nm) and refractive index detectors, guard column (Agilent PLgel; 5μm; 50 x 7.5 mm), and

three analytical columns (Agilent PLgel; 5μm; 300 x 7.5 mm; 105 , 104 , and 103 Å pore sizes). The instrument was calibrated with narrow dispersity polystyrene standards between 640 g/mol and 2300 kg/mol (Polymer Standards Service GmbH). All runs were performed at 1.0 mL/min flow rate and 40 °C. Molecular weight values are calculated based on the refractive index signal. The other GPC instrument used in this report was an Agielnt Infinity II series system running with tetrahydrofuran as the mobile phase and two PolyPore 300 × 7.5 mm columns (Varian p/n 5M-POLY-008-112). The instrument is equipped with 18-angle DAWN HELEOS II multiangle light scattering (MALS) detector, a ViscoStar II viscometer, and a Optilab T-rEX differential refractive index detector (Wyatt). All runs were performed at 1.0 mL/min flow rate and at 27 °C. Matrix-assisted laser desorption/ionization time of flight mass spectrometry (MALDI-TOF-MS) was performed on Bruker rapiflex MALDI-TOF Tissue typer in reflector positive mode. Samples were prepared by preparing solutions of *trans*-2-[3-(4-*tert*-butylphenyl)-2-methyl-2-propenylidene]malononitrile (DCTB, 10 mg/mL) in THF, silver nitrate (5mg/mL) in deionized water, and sample (1 mg/mL) in THF. Approximately 2.5 μL of silver nitrate, polymer solution, and matrix were spotted on the MALDI chip and dried, respectively. The sample:additive:matrix ratios were varied to achieve good signal to noise. The glove box in which specified procedures were carried out was an MBraun Unilab Pro with N_2 atmosphere. N_2 and CO_2 isotherms were obtained at 77 K on a micromeritics Tristar after further activation at 100 °C under vacuum overnight.

Cyclic Voltammetry All cyclic voltammetry experiments were conducted in a nitrogen-filled glovebox using acetonitrile with 0.1 M tetrabutylamonnium hexafluorophosphate electrolyte. Ferrocene was added as an internal standard following every run. Due to irreversibility of most of the measured redox events, potentials are reported as half-peak potentials determined by finding the potential at which the measured current reaches the average of the maximum and pre-onset currents of a peak. These values were referenced to the half-wave potential of ferrocene.

Experimental Procedures
Part A: Synthesis of cyclohexene initiators

(4-bromophenoxy)(*tert*-butyl)dimethylsilane
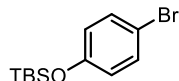
4-bromophenol (5.0g, 29 mmol) was dissolved in 60 mL of dry DCM. Add imidazole (4.7 g, 69 mmol, 2.4 equivalents), and let stir under nitrogen for 10 minutes before adding tert-butylchlorodimethylsilane (5.2 g, 35 mmol, 1.2 equivalents) and let stir overnight at room temperature. The reaction was quenched with saturated ammonium chloride (40 mL) and the organic layer was separated and washed with brine (20 mL) before drying over sodium sulfate. The crude was purified via flash column (10% EtOAc:Hexanes) to afforded the desired (4-bromophenoxy)(tert-butyl)dimethylsilaneas clear liquid (7.195 g, 87%).

¹H NMR: (500 MHz, CDCl₃-*d*₃) δ 7.32 (dd, *J* = 8.8, 2.2 Hz, 2H), 6.71 (dd, *J* = 8.9, 2.2 Hz, 2H), 0.97 (s, 10H), 0.18 (s, 6H).

Scheme 2 Synthesis of cyclohexene initiators[131]
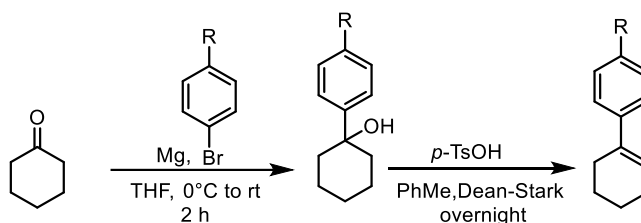
R=OMe To a 100mL three-necked round bottom flask, magnesium (1.07 g, 1.1 equivalents, 44.0 mmol) was added. Dry THF (10 mL) and 0.4 mL of 1-bromo-4-methoxybenzene was added. The solution was heated to reflux with a heat gun under nitrogen. Add the remaining 1-bromo-4-methoxybenzene (7.9 g, 5.3 mL total, 1.1 equivalents 42.0 mmol) in 30 mL of dry THF and reflux. After one hour, cool the flask to 0°C and add cyclohexanone (3.9 g, 4.1 mL, 40 mmol) in 20 mL of dry THF dropwise via addition funnel. Bring solution to reflux for one hour. After reflux, cool solution to 0°C and quench reaction by adding 6 M HCl dropwise (approximately 60 mL). Extract with ethyl acetate (100 mL), wash with brine (40 mL) and dry with sodium sulfate. The organic layer was concentrated *in vacuo* and the crude product (dark amber oil) was immediately carried forward to the subsequent elimination step. The oil was dissolved in 40 mL of dry toluene in a 100mL round-bottom flask. To this flask, *p*-toluenesulfonic acid monohydrate (0.76g, 4.0 mmol, 0.1 eq) was added and the solution was refluxed under a Dean-Stark trap under nitrogen overnight. The reaction was quenched at

room temperature with 1 M NaOH (50 mL) and extracted with diethyl ether. The organic layer was dried over sodium sulfate and concentrated *in vacuo* with additional toluene removed via distillation. The crude oil was purified by column chromatography (100% pentane) to yield 4'-methoxy-2,3,4,5-tetrahydro-1,1'-biphenyl (1.2 g, 16%) as a clear oil. Characterization of this material matched literature reports.[131]

¹H NMR: (500 MHz, CDCl₃-d_3) δ 7.31 dd (J = 8.8, 2.1 Hz, 2H), 6.85 (dd, J = 8.8, 2.0 Hz, 2H), 6.04-6.02 (m, 1H), 3.81 (s, 3 H), 2.40-2.36 (m, 2 H), 2.21-2.17, (m, 2H), 1.79-1.75 (m, 2 H), 1.68-1.63 (m, 2H). **LRMS:** m/z expected for $C_{13}H_{17}O$ [M+H]⁺ 188.1, measured 188.2

R= H To a 100mL three-necked round bottom flask, magnesium (1.07 g, 1.1 equivalents, 44.0 mmol) was added. Dry THF (10 mL) and 0.4 mL of 1-bromo-benzene was added. The solution was heated to reflux with a heat gun under nitrogen. Add the remaining 1-bromo-benzene (6.6 g, 4.4 mL total, 1.1 equivalents 42.0 mmol) in 30 mL of dry THF and reflux. After one hour, cool the flask to 0°C and add cyclohexanone (3.9 g, 4.1 mL, 40 mmol) in 20 mL of dry THF dropwise via addition funnel. Bring solution to reflux for one hour. After reflux, cool solution to 0°C and quench reaction by adding 6 M HCl dropwise (approximately 60 mL). Extract with ethyl acetate (100 mL), wash with brine (40 mL) and dry with sodium sulfate. The organic layer was concentrated *in vacuo* and the crude product (dark amber oil) was immediately carried forward to the subsequent elimination step. The oil was dissolved in 40 mL of dry toluene in a 100mL round-bottom flask. To this flask, *p*-toluenesulfonic acid monohydrate (0.76g, 4.0 mmol, 0.1 eq) was added and the solution was refluxed under a Dean Stark trap under nitrogen overnight. The reaction was quenched at room temperature with 1 M NaOH (50 mL) and extracted with diethyl ether. The organic layer was dried with sodium sulfate and concentrated *in vacuo*. The crude oil was purified by column chromatography (100% pentane) to yield 2,3,4,5-tetrahydro-1,1'-biphenyl (1.2 g, 19%) as a clear oil. Characterization of this material matched literature reports.[131]

¹H NMR: (500 MHz, CDCl₃-d_3) δ 7.41 – 7.36 (m, 2H), 7.33 – 7.28 (m, 2H), 7.24 – 7.18 (m, 1H), 6.12 (tt, J = 3.9, 1.7 Hz, 1H), 2.42 (tdt, J = 6.3, 4.3, 2.4 Hz, 2H), 2.25 – 2.17 (m, 2H), 1.83 – 1.75 (m, 2H), 1.71 – 1.61 (m, 2H).

R= Me To a 100mL three-necked round bottom flask, magnesium (1.07 g, 1.1 equivalents, 44.0 mmol) was added. Dry THF (10 mL) and 0.4 mL of 1-bromo-4-methylbenzene was added. The solution was heated to reflux with a heat gun under nitrogen. Add the remaining 1-bromo-4-methylbenzene (7.2 g, 5.2 mL total, 1.1 equivalents 42.0 mmol) in 30 mL of dry THF and reflux. After one hour, cool the flask to 0°C and add cyclohexanone (3.9 g, 4.1 mL, 40 mmol) in 20 mL of dry THF dropwise via addition funnel. Bring solution to reflux for one hour. After reflux, cool solution to 0°C and quench reaction by adding 6 M HCl dropwise (approximately 60 mL). Extract with ethyl acetate (100 mL), wash with brine (40 mL) and dry with sodium sulfate. The organic layer was concentrated *in vacuo* and the crude product (dark amber oil) was immediately carried forward to the subsequent elimination step. The oil was dissolved in 40 mL of dry toluene in a 100mL round-bottom flask. To this flask, *p*-toluenesulfonic acid monohydrate (0.76g, 4.0 mmol, 0.1 eq) was added and the solution was refluxed under a Dean Stark trap under nitrogen overnight. The reaction was quenched at room temperature with 1 M NaOH (50 mL) and extracted with diethyl ether. The organic layer was dried with sodium sulfate and concentrated *in vacuo*. The crude oil was purified by column chromatography (100% pentane) to yield 4'-methyl-2,3,4,5-tetrahydro-1,1'-biphenyl (4.0 g, 58%) as a clear oil. Characterization of this material matched literature reports.[131]

¹H NMR: (500 MHz, CDCl₃-*d₃*) δ 7.32 – 7.26 (m, 2H), 7.16 – 7.09 (m, 2H), 6.09 (tt, *J* = 3.9, 1.7 Hz, 1H), 2.45 – 2.39 (m, 1H), 2.42 – 2.34 (m, 1H), 2.34 (s, 3H), 2.21 (dtt, *J* = 6.3, 3.8, 2.2 Hz, 2H), 1.83 – 1.75 (m, 2H), 1.71 – 1.63 (m, 2H).

**R= ᵗBu** To a 100mL three-necked round bottom flask, magnesium (1.07 g, 1.1 equivalents, 44.0 mmol) was added. Dry THF (10 mL) and 0.4 mL of 1-bromo-4-(tert-butyl)benzene was added. The solution was heated to reflux with a heat gun under nitrogen. Add the remaining 1-bromo-4-(tert-butyl)benzene (9.0 g, 7.3 mL total, 1.1 equivalents 42.0 mmol) in 30 mL of dry THF and reflux. After one hour, cool the flask to 0°C and add cyclohexanone (3.9 g, 4.1 mL, 40 mmol) in 20 mL of dry THF dropwise via addition funnel. Bring solution to reflux for one hour. After reflux, cool solution to 0°C and quench reaction by adding 6 M HCl dropwise (approximately 60 mL). Extract with ethyl acetate (100 mL), wash with brine (40 mL) and dry with sodium

sulfate. The organic layer was concentrated *in vacuo* and the crude product (dark amber oil) was immediately carried forward to the subsequent elimination step. The oil was dissolved in 40 mL of dry toluene in a 100mL round-bottom flask. To this flask, *p*-toluenesulfonic acid monohydrate (0.76g, 4.0 mmol, 0.1 eq) was added and the solution was refluxed under a Dean Stark trap under nitrogen overnight. The reaction was quenched at room temperature with 1 M NaOH (50 mL) and extracted with diethyl ether. The organic layer was dried with sodium sulfate and concentrated *in vacuo*. The crude oil was purified by column chromatography (100% pentane) to yield 4'-(tert-butyl)-2,3,4,5-tetrahydro-1,1'-biphenyl (6.7 g, 78%) as a clear oil. Characterization of this material matched literature reports.[131]

¹H NMR: (500 MHz, CDCl$_3$-*d$_3$*) δ 7.34 (s, 4H), 6.11 (tt, *J* = 3.9, 1.7 Hz, 1H), 2.41 (dddd, *J* = 6.3, 4.4, 3.1, 1.8 Hz, 2H), 2.21 (ddt, *J* = 7.7, 6.3, 3.2 Hz, 2H), 1.84 – 1.74 (m, 2H), 1.71 – 1.63 (m, 2H), 1.33 (s, 9H).

R= F To a 100mL three-necked round bottom flask under nitrogen, add solution of (4-fluorophenyl)magnesium bromide (0.8 M, 45 mL, 36 mmol). Add cyclohexanone (2.9 mmol, 3.1 mL, 30 mmol) in 15 mL of dry THF dropwise at room temperature. Bring solution to reflux for one hour. After reflux, cool solution to 0°C and quench reaction by adding 6 M HCl dropwise (approximately 50 mL). Extract with ethyl acetate (75 mL), wash with brine (30 mL) and dry with sodium sulfate. The organic layer was concentrated *in vacuo* and the crude product was immediately carried forward to the subsequent elimination step. The crude product was dissolved in 25 mL of dry toluene in a 100mL round-bottom flask. To this flask, *p*-toluenesulfonic acid monohydrate (0.57 g, 3.0 mmol, 0.1 eq) was added and the solution was refluxed under a Dean Stark trap under nitrogen overnight. The reaction was quenched at room temperature with 1 M NaOH (30 mL) and extracted with ethyl acetate. The organic layer was dried with sodium sulfate and concentrated *in vacuo*. The crude oil was purified by column chromatography (100% pentane) to yield 4'-fluoro-2,3,4,5-tetrahydro-1,1'-biphenyl (3.8 g, 72%) as a clear oil. Characterization of this material matched literature reports.[131]

¹H NMR: (500 MHz, CDCl$_3$-*d$_3$*) δ 7.36 – 7.30 (m, 2H), 7.01 – 6.95 (m, 2H), 6.05 (tt, *J* = 3.9, 1.7 Hz, 1H), 2.40 – 2.35 (m, 2H), 2.23 – 2.18 (m, 2H), 1.81 – 1.75 (m, 2H), 1.65 (dtt, *J* = 9.5, 6.5, 3.0 Hz, 2H). **¹⁹F NMR** (470 MHz, CDCl$_3$-*d$_3$*) δ -116.81 (tt, *J* = 9.7, 5.1 Hz)

R= OTBS To a 100mL three-necked round bottom flask, magnesium (1.07 g, 2.2 equivalents, 44.0 mmol) was added. Dry THF (10 mL) and 0.4 mL of (4-bromophenoxy)-(tert-butyl)dimethylsilane

was added. The solution was heated to reflux with a heat gun under nitrogen. Add the remaining (4-bromophenoxy)-(tert-butyl)dimethylsilane

(6.0 g, 1.1 equivalents 21.0 mmol) in 30 mL of dry THF and reflux. After one hour, cool the flask to 0°C and add cyclohexanone (1.96 g, 2.1 mL, 20 mmol) in 20 mL of dry THF dropwise via addition funnel. Bring solution to reflux for two hours. After reflux, cool solution to 0°C and quench reaction by adding saturated ammonium chloride dropwise (approximately 60 mL). Extract with ethyl acetate (100 mL), wash with brine (40 mL) and dry with sodium sulfate. The organic layer was concentrated *in vacuo* and the crude product (dark amber oil) was immediately carried forward to the subsequent elimination step. The oil was dissolved in 40 mL of dry toluene in a 100mL round-bottom flask. To this flask, *p*-toluenesulfonic acid monohydrate (0.76g, 4.0 mmol, 0.1 eq) was added and the solution was refluxed under a Dean Stark trap under nitrogen overnight. The reaction was quenched at room temperature with 1 M NaOH (50 mL) and extracted with diethyl ether. The organic layer was dried with sodium sulfate and concentrated *in vacuo*. The crude oil was purified by column chromatography (100% pentane) to yield 4'-(tert-butyl)-2,3,4,5-tetrahydro-1,1'-biphenyl (6.7 g, 78%) as a clear oil.

¹H NMR: (500 MHz, CDCl$_3$-d_3) δ 7.15 (dd, J = 7.2, 1.5 Hz, 3H), 6.67 (dd, J = 8.7, 2.3 Hz, 2H), 5.94 (tt, J = 3.9, 1.7 Hz, 1H), 2.27 (tdd, J = 6.3, 4.0, 2.1 Hz, 2H), 2.09 (ddt, J = 7.7, 6.2, 3.2 Hz, 2H), 1.71 – 1.62 (m, 2H), 1.58 – 1.50 (m, 2H), 0.88 (s, 10H), 0.78 (t, J = 7.1 Hz, 6H).

Part B: Synthesis of diene monomers

We sought to synthesize aryl dienes through a synthetic route originally reported by Mazet and coworkers (**Scheme S3a**) .[132] However, we found that while we synthesized the diene in moderate yields, we often also obtained the styrene product, most likely due to a hydrate addition that can happen during Grignard addition reactions.[133] This styrene product was incredibly challenging to separate from the diene *via* column chromatography, so we chose to synthesize many dienes through a Grignard addition-elimination pathway (**Scheme S3b**).[134] In this way, any carbonyl reduction product could be more easily separated from the Grignard addition product via column chromatography before proceeding to the elimination step.

**Scheme S3 Synthetic routes for diene monomers**
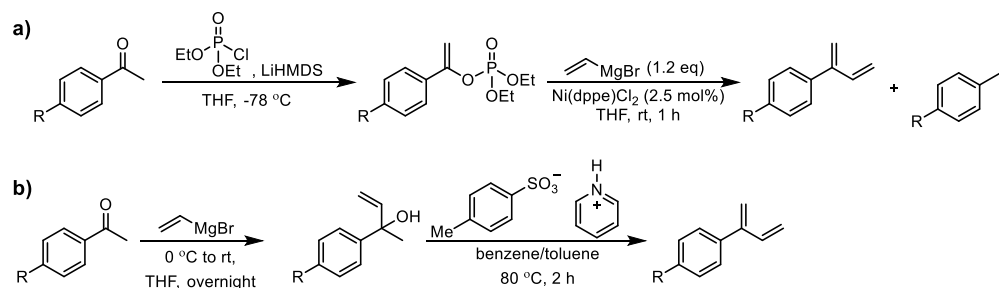
2-(4-(tert-butyl)phenyl)but-3-en-2-ol
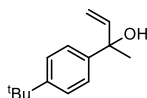
A solution of vinyl magnesium bromide (1.0 M in THF, 41 mL, 41 mmol, 1.8 equiv) was cooled to 0°C and a solution of 1-(4-(tert-butyl)phenyl)ethan-1-one (4.1 g, 4.2 mL, 23 mmol, 1 equiv) in 36 mL of diethyl ether was added dropwise under nitrogen. The reaction was stirred at room temperature overnight and quenched with saturated ammonium chloride (80 mL). The product was extracted with ether (50 mL), and washed with brine. The organic layer was dried with sodium sulfate and concentrated *in vacuo*. The crude oil was purified by column chromatography (10-30% ethyl acetate in hexanes) to yield 2-(4-(tert-butyl)phenyl)but-3-en-2-ol (1.3 g, 27%) as a yellow oil.

¹H NMR: (500 MHz, CDCl₃-d_3) δ 7.44 – 7.33 (m, 4H), 6.18 (dd, J = 17.3, 10.6 Hz, 1H), 5.31 (dd, J = 17.3, 1.1 Hz, 1H), 5.14 (dd, J = 10.6, 1.1 Hz, 1H), 1.86 (s, 1H), 1.66 (s, 3H), 1.32 (s, 10H).

¹³C NMR: (126 MHz, CDCl3) δ 149.95, 145.09, 143.56, 125.25, 125.00, 112.11, 74.67, 34.52, 31.47, 29.49.

1-(4-((tert-butyldimethylsilyl)oxy)phenyl)ethan-1-one
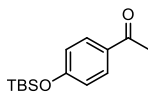
Under nitrogen atmosphere, to a solution of 4-hydroxyacetophenone (5.0 g, 36.7 mmol) and imidazole (5.0 g, 36.7 mmol) in anhydrous dimethyl formamide (50 mL) was added chloro tert-butyldimethylsilane (TBSCl, 6.64 g, 44.1 mmol). The resulting solution was stirred for 24 h at room temperature. The reaction mixture was diluted with hexane/Et2O = 1/1 (200 mL), and organic layer was washed three times with H2O (100 mL) and once with brine (100 mL), dried over Na₂SO₄, filtered, and the filtrate was concentrated to give a colorless liquid, which crystallized on standing to yield 1-(4-((tert-butyldimethylsilyl)oxy)phenyl)ethan-1-one as a colorless solid (9.23g, quantitative).

¹H NMR: (400 MHz, CDCl₃, δ): 7.86 (d, J = 6.9 Hz, Ar H-2, 6, 2H), 6.84 (d, J = 6.9 Hz, Ar H-3, 5, 2H), 2.53 (s, -COCH₃, 3H), 0.97 (s, -SiC(CH₃)₃, 9H), 0.22, (s, -Si(CH₃)₂, 6H)

1-(2-((tert-butyldimethylsilyl)oxy)phenyl)ethan-1-one
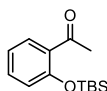
Under nitrogen atmosphere, to a solution of 1-(2-hydroxyphenyl)ethan-1-one (4.1 g, 3.6 mL, 30 mmol) and imidazole (4.9 g, 72 mmol, 2.4 equiv) in anhydrous dichloromethane (60 mL) was added chloro tert-butyldimethylsilane (TBSCl, 5.4 g, 36 mmol). The resulting solution was stirred for 24 h at room temperature. The organic layer was washed three times with H₂O (100 mL) and once with brine (100 mL), dried over Na₂SO₄, filtered, and the filtrate was concentrated to give a colorless liquid, which crystallized on standing to yield 1-(2-((tert-butyldimethylsilyl)oxy)phenyl)ethan-1-one as a colorless solid (2.92 g, 39%).

¹H NMR: 1H NMR (500 MHz, CDCl₃) δ 7.59 (dd, *J* = 7.7, 1.9 Hz, 1H), 7.33 (ddd, *J* = 8.2, 7.3, 1.9 Hz, 1H), 6.98 (td, *J* = 7.5, 1.1 Hz, 1H), 6.86 (dd, *J* = 8.2, 1.0 Hz, 1H), 2.60 (s, 3H), 0.99 (s, 9H), 0.26 (s, 6H).

2-(4-((tert-butyldimethylsilyl)oxy)phenyl)but-3-en-2-ol
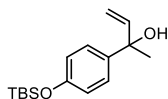
A solution of vinyl magnesium bromide (1.0 M in THF, 36 mL, 36 mmol, 1.8 equiv) was cooled to 0°C and a solution of 1-(4-((tert-butyldimethylsilyl)oxy)phenyl)ethan-1-one (5.0 g, 20 mmol, 1 equiv) in 36 mL of diethyl ether was added dropwise under nitrogen. The reaction was stirred at room temperature overnight and quenched with saturated ammonium chloride (80 mL). The product was extracted with ether (50 mL) and washed with brine. The organic layer was dried with sodium sulfate and concentrated *in vacuo*. The crude oil was purified by column chromatography (10-30% ethyl acetate in hexanes) to yield 2-(4-((tert-butyldimethylsilyl)oxy)phenyl)but-3-en-2-ol (2.1 g, 38%) as a pale yellow oil.

¹H NMR: (500 MHz, CDCl₃) δ 7.34 – 7.29 (m, 2H), 6.83 – 6.77 (m, 2H), 6.15 (dd, *J* = 17.3, 10.6 Hz, 1H), 5.20 (ddd, *J* = 78.7, 17.3, 1.0 Hz, 2H), 1.81 (s, 1H), 1.63 (s, 3H), 0.98 (s, 9H), 0.19 (s, 6H).

2-(3-methoxyphenyl)but-3-en-2-ol
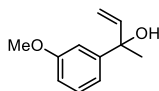
A solution of vinyl magnesium bromide (1.0 M in THF, 39 mL, 39 mmol, 1.7 equiv) was cooled to 0°C and a solution of 1-(3-methoxyphenyl)ethan-1-one (3.5 g, 3.2 mL, 23 mmol, 1 equiv) in 36 mL of tetrahydrofuran was added dropwise under nitrogen. The reaction was stirred at room temperature overnight and quenched with saturated ammonium chloride (80 mL). The product was extracted with ether (50 mL) and washed with brine. The organic layer was dried with sodium sulfate and concentrated *in vacuo*. The crude oil was purified by column chromatography (10-30% ethyl acetate in hexanes) to yield 2-(3-methoxyphenyl)but-3-en-2-ol (1.6 g, 38%) as a yellow oil.

¹H NMR: (500 MHz, CDCl₃) δ 7.30 – 7.22 (m, 2H), 7.09 – 6.99 (m, 1H), 6.80 (ddd, *J* = 8.2, 2.6, 1.0 Hz, 1H), 6.16 (dd, *J* = 17.3, 10.6 Hz, 1H), 5.31 (dd, *J* = 17.3, 1.1 Hz, 1H), 5.15 (dd, *J* = 10.6, 1.1 Hz, 1H), 3.82 (s, 3H), 1.87 (s, 1H), 1.65 (s, 3H).

2-(3,5-dimethoxyphenyl)but-3-en-2-ol
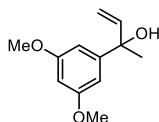
A solution of vinyl magnesium bromide (1.0 M in THF, 17 mL, 15 mmol, 1.8 equiv) was cooled to 0°C and a solution of 1-(3,5-dimethoxyphenyl)ethan-1-one (1.5 g, 8.3 mmol, 1 equiv) in 17 mL of tetrahydrofuran was added dropwise under nitrogen. The reaction was stirred at room temperature overnight and quenched with saturated ammonium chloride (80 mL). The product was extracted with ether (50 mL) and washed with brine. The organic layer was dried with sodium sulfate and concentrated *in vacuo*. The crude oil was purified by column chromatography (10-30% ethyl acetate in hexanes) to yield 2-(3,5-dimethoxyphenyl)but-3-en-2-ol (1.6 g, 92%) as a yellow oil.

¹H NMR: (500 MHz, CDCl₃) δ 6.63 (d, *J* = 2.3 Hz, 2H), 6.36 (t, *J* = 2.3 Hz, 1H), 6.14 (dd, *J* = 17.3, 10.6 Hz, 1H), 5.31 (dd, *J* = 17.2, 1.1 Hz, 1H), 5.14 (dd, *J* = 10.6, 1.1 Hz, 1H), 3.80 (s, 6H), 1.87 (s, 1H), 1.63 (s, 3H).

2-(4-fluorophenyl)but-3-en-2-ol
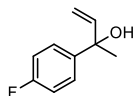
A solution of vinyl magnesium bromide (0.7 M in THF, 59 mL, 42 mmol, 1.8 equiv) was cooled to 0°C and a solution of 1-(4-fluorophenyl)ethan-1-one (3.2 g, 2.8 mL, 23 mmol, 1 equiv) in 36 mL of tetrahydrofuran was added dropwise under nitrogen. The reaction was stirred at room temperature overnight and quenched with saturated ammonium chloride (80 mL). The product was extracted with ether (50 mL) and washed with brine. The organic layer was dried with sodium sulfate and concentrated *in vacuo*. The crude oil was purified by column

chromatography (10-30% ethyl acetate in hexanes) to yield 2-(4-fluorophenyl)but-3-en-2-ol (1.6 g, 43%) as a pale yellow oil.

¹H NMR: (500 MHz, CDCl₃) δ 7.48 – 7.40 (m, 2H), 7.05 – 6.97 (m, 2H), 6.14 (dd, *J* = 17.3, 10.6 Hz, 1H), 5.22 (ddd, *J* = 68.8, 17.4, 0.6 Hz, 2H), 1.89 (s, 1H), 1.64 (s, 3H).

¹⁹F NMR: (470 MHz, CDCl₃-*d₃*) δ -116.24 (tt, *J* = 8.7, 5.5 Hz).

diethyl (1-(naphthalen-1-yl)vinyl) phosphate
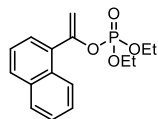
To a stirred solution of 1-(naphthalen-1-yl)ethan-1-one (2.47 g, 14.5 mmol, 1.0 equiv.) in anhydrous THF (45.0 mL, 0.2 M overall concentration) at –78 ºC and under an inert atmosphere of nitrogen, LiHMDS (18.9 mL of 1 M solution in THF/ethylbenzene, 18.9 mmol, 1.3 equiv.) was added dropwise. After 30 min, diethyl chlorophosphate (3.15 mL, 21.8 mmol, 1.5 equiv.) was added dropwise and the reaction mixture was stirred at -78 °C 2 hours. The reaction mixture was warmed up to room temperature for 10 hours, quenched with saturated ammonium chloride solution and then extracted with ethyl acetate (3 x 100 mL). The combined organics were dried over sodium sulfate, filtered, and concentrated under reduced pressure. The crude residue was purified by flash chromatography (20 – 50% ethyl acetate in hexanes) affording pure diethyl (1-(naphthalen-1-yl)vinyl) phosphate (4.18 g, 94%) as an orange oil.

¹H NMR: (500 MHz, CDCl₃) δ 8.24 (dq, *J* = 8.7, 0.9 Hz, 1H), 7.88 – 7.83 (m, 2H), 7.60 (dd, *J* = 7.1, 1.3 Hz, 1H), 7.51 (dddd, *J* = 18.0, 8.1, 6.8, 1.4 Hz, 2H), 7.45 (dd, *J* = 8.3, 7.0 Hz, 1H), 5.49 (t, *J* = 2.1 Hz, 1H), 5.06 (t, *J* = 2.1 Hz, 1H), 4.10 – 3.96 (m, 4H), 1.21 (td, *J* = 7.1, 1.1 Hz, 6H).

³¹P NMR: (202 MHz, CDCl₃) δ -6.78 (p, *J* = 7.9 Hz).

¹³C NMR: (126 MHz, CDCl₃) δ 152.94, 152.87, 133.65, 133.60, 133.56, 130.97, 129.78, 128.39, 127.38, 126.68, 126.16, 125.73, 125.13, 103.20, 103.17, 64.48, 64.43, 16.07, 16.02.
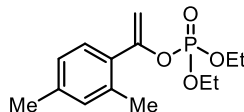
1-(2,4-dimethylphenyl)vinyl diethyl phosphate To a stirred solution 1-(2,4-dimethylphenyl)ethan-1-one (2.15 g, 2.16 mL, 14.5 mmol, 1.0 equiv.) in anhydrous THF (45.0 mL, 0.2 M overall concentration) at –78 ºC and under an inert atmosphere of nitrogen, LiHMDS (18.9 mL of 1 M solution in THF/ethylbenzene, 18.9 mmol, 1.3 equiv.) was added dropwise. After 30 min, diethyl chlorophosphate (3.15 mL, 21.8 mmol, 1.5 equiv.) was added dropwise and the reaction mixture was stirred at -78 °C 2 hours. The reaction mixture was warmed up to room temperature for 10 hours, quenched with saturated ammonium chloride solution and then extracted with ethyl acetate (3 x 100 mL). The combined organics were dried over sodium sulfate, filtered and concentrated under reduced pressure. The crude residue was purified by flash chromatography (30 – 60% ethyl acetate in hexanes) affording pure 1-(2,4-dimethylphenyl)vinyl diethyl phosphate (4.04 g, 98%) as an amber oil.

¹H NMR: (500 MHz, CDCl₃) δ 7.28 – 7.24 (m, 1H), 7.01 – 6.96 (m, 2H), 5.27 (t, J = 2.1 Hz, 1H), 4.80 (t, J = 2.1 Hz, 1H), 4.18 – 4.01 (m, 4H), 2.38 (s, 3H), 2.31 (s, 3H), 1.32 – 1.24 (m, 9H).

³¹P NMR: (202 MHz, CDCl₃) δ -6.79 (p, J = 8.1 Hz).
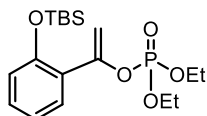
1-(2-((tert-butyldimethylsilyl)oxy)phenyl)vinyl diethyl phosphate To a stirred solution 1-(2-((tert-butyldimethylsilyl)oxy)phenyl)ethan-1-one (2.91 g, 11.6 mmol, 1.0 equiv.) in anhydrous THF (45.0 mL, 0.17 M overall concentration) at –78 ºC and under an inert atmosphere of nitrogen, LiHMDS (15.1 mL of 1 M solution in THF/ethylbenzene, 15.1 mmol, 1.3 equiv.) was added dropwise. After 30 min, diethyl chlorophosphate (3.01 g, 2.53 mL, 17.4 mmol, 1.5 equiv.) was added dropwise and the reaction mixture was stirred at -78 °C 2 hours. The reaction mixture was warmed up to room temperature for 10 hours, quenched with saturated ammonium chloride solution and then extracted with ethyl acetate (3 x 100 mL). The combined organics were dried over

sodium sulfate, filtered and concentrated under reduced pressure. The crude residue was purified by flash chromatography (30 – 60% ethyl acetate in hexanes) affording pure 1-(2,4-dimethylphenyl)vinyl diethyl phosphate (2.6 g, 58%) as an amber oil.

¹H NMR: (500 MHz, CDCl₃) δ 7.47 (dd, *J* = 7.8, 1.8 Hz, 1H), 7.18 (ddd, *J* = 8.1, 7.3, 1.8 Hz, 1H), 6.94 (td, *J* = 7.6, 1.2 Hz, 1H), 6.83 (dd, *J* = 8.2, 1.2 Hz, 1H), 5.35 (dt, *J* = 12.8, 2.1 Hz, 2H), 4.19 – 4.07 (m, 4H), 1.29 (td, *J* = 7.1, 1.1 Hz, 6H), 0.99 (s, 9H), 0.22 (s, 6H).

³¹P NMR: (202 MHz, CDCl₃) δ -6.53 (p, *J* = 8.1 Hz).
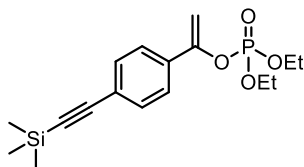
diethyl (1-(4-((trimethylsilyl)ethynyl)phenyl)vinyl) phosphate To a stirred solution 1-(4-((trimethylsilyl)ethynyl)phenyl)ethan-1-one (2.0 g, 9.2 mmol, 1.0 equiv.) in anhydrous THF (34.0 mL, 0.2 M overall concentration) at –78 °C and under an inert atmosphere of nitrogen, LiHMDS (12 mL of 1 M solution in THF/ethylbenzene, 12 mmol, 1.3 equiv.) was added dropwise. After 30 min, diethyl chlorophosphate (2.4 g, 2.0 mL, 14 mmol, 1.5 equiv.) was added dropwise and the reaction mixture was stirred at -78 °C 2 hours. The reaction mixture was warmed up to room temperature for 10 hours, quenched with saturated ammonium chloride solution and then extracted with ethyl acetate (3 x 25 mL). The combined organics were dried over sodium sulfate, filtered and concentrated under reduced pressure. The crude residue was purified by flash chromatography (30 – 60% ethyl acetate in hexanes) affording pure 1-(2,4-dimethylphenyl)vinyl diethyl phosphate (2.53 g, 78%) as an orange oil.

¹H NMR: (500 MHz, CDCl₃) δ 7.54 – 7.42 (m, 4H), 5.33 – 5.24 (m, 2H), 4.20 (dqt, *J* = 8.2, 7.1, 3.5 Hz, 4H), 1.34 (td, *J* = 7.1, 1.1 Hz, 6H), 0.25 (s, 9H).

³¹P NMR: (202 MHz, CDCl₃) δ 31P NMR (162 MHz, CDCl3) δ -6.28 (s).
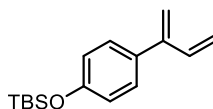
(4-(buta-1,3-dien-2-yl)phenoxy)(tert-butyl)dimethylsilane To a solution of 2 2-(4-((tert-butyldimethylsilyl)oxy)phenyl)but-3-en-2-ol (1.6 g, 5.7 mmol, 1.0 equiv) in 40 mL of benzene, pyridinium p-toluenesulfonate (14 mg, 0.057 mmol, 0.01 equiv), dibutylhydroxytoluene (13 mg, 0.057 mmol, 0.01 equiv), and sodium sulfate (50 mg, 0.35 mmol, 0.061 equiv) were added. The reaction was stirred at reflux for overnight. After, the reaction was quenched with saturated sodium bicarbonate (60 mL), extracted with ethyl acetate (30 mL) and the organic layer was dried with sodium sulfate before being concentrated under reduced pressure. The crude product was redissolved in 60 mL of dichloromethane and imidazole (1.1 g, 16 mmol, 2.8 equiv) and stirred for 5 minutes. After, tert-butylchlorodimethylsilane (1.2 g, 8.0 mmol, 1.4 equiv) was added and the reaction was stirred at room temperature overnight under nitrogen. The resulting product was quenched with saturated ammonium chloride (60 mL) and washed with brine (75 mL) and water (75 mL). The organic layer was dried with sodium sulfate and concentrated *in vacuo*. The crude product was purified by flash column chromatography (100% hexanes) to afford (4-(buta-1,3-dien-2-yl)phenoxy)(tert-butyl)dimethylsilane (1.07g, 72%) as a colorless oil which was stored at -20 °C with 1 mol % BHT. The spectra of the compound match that of previous reports.[132]

¹H NMR: (500 MHz, CDCl₃) δ 7.23 – 7.16 (m, 2H), 6.86 – 6.78 (m, 2H), 6.61 (ddd, *J* = 17.4, 10.6, 0.8 Hz, 1H), 5.26 – 5.15 (m, 4H), 1.00 (s, 9H), 0.22 (s, 6H).
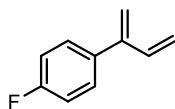
1-(buta-1,3-dien-2-yl)-4-fluorobenzene To a solution of 2-(4-fluorophenyl)but-3-en-2-ol (1.6 g, 9.6 mmol, 1.0 equiv) in 40 mL of benzene, pyridinium p-toluenesulfonate (24 mg, 0.096 mmol, 0.01 equiv), dibutylhydroxytoluene (21 mg, 0.096 mmol, 0.01 equiv), and sodium sulfate (50 mg, 0.32 mmol, 0.042) were added. The reaction was stirred at reflux for overnight. After, the reaction was quenched with saturated sodium bicarbonate (60 mL), extracted with ethyl acetate (30 mL) and the organic layer was dried with sodium sulfate before being concentrated under reduced pressure. The crude product was purified by flash column chromatography (100% hexanes) to afford 1-(buta-1,3-dien-2-yl)-4-fluorobenzene (617 mg, 43%) as a colorless

oil which was stored at -20 °C with 1 mol % BHT. The spectra of the compound match that of previous reports.[132]

¹H NMR: (500 MHz, CDCl₃) δ 7.31 – 7.26 (m, 2H), 7.07 – 7.00 (m, 2H), 6.61 (dd, J = 17.4, 10.7 Hz, 1H), 5.30 – 5.12 (m, 4H).

¹⁹F NMR: (470 MHz, CDCl₃-d_3) δ -115.16 (ddd, J = 14.0, 9.7, 5.3 Hz).
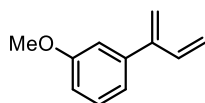
1-(buta-1,3-dien-2-yl)-3-methoxybenzene To a solution of 2-(3-methoxyphenyl)but-3-en-2-ol (1.5 g, 8.4 mmol, 1.0 equiv) in 20 mL of benzene, pyridinium p-toluenesulfonate (21 mg, 0.084 mmol, 0.01 equiv) and sodium sulfate (50 mg, 0.32 mmol, 0.042) was added. The reaction was stirred at reflux for 2 hours. After, the reaction was quenched with saturated sodium bicarbonate (50 mL), extracted with ethyl acetate (20 mL) and the organic layer was dried with sodium sulfate before being concentrated under reduced pressure. The crude product was purified by flash column chromatography (100% hexanes) to afford 1-(buta-1,3-dien-2-yl)-3-methoxybenzene (120 mg, 9%) as a colorless oil. The spectra of the compound match that of previous reports.[132]

¹H NMR (500 MHz, CDCl₃) δ 7.27 (td, J = 7.7, 0.8 Hz, 1H), 6.95 – 6.83 (m, 3H), 6.65 – 6.55 (m, 1H), 5.34 – 5.19 (m, 4H), 3.82 (s, 3H).
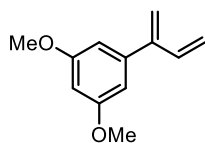
1-(buta-1,3-dien-2-yl)-3,5-dimethoxybenzene To a solution of 2-(3,5-dimethoxyphenyl)but-3-en-2-ol (1.6 g, 7.7 mmol, 1.0 equiv) in 20 mL of benzene, pyridinium p-toluenesulfonate (19 mg, 0.077 mmol, 0.01 equiv) and sodium sulfate (50 mg, 0.35 mmol, 0.046) was added. The reaction was stirred at reflux for 2 hours. After, the reaction was quenched with saturated sodium bicarbonate (50 mL), extracted with ethyl acetate (20 mL) and the organic layer was dried with sodium sulfate before being concentrated under reduced pressure. The crude

product was purified by flash column chromatography (100% hexanes) to afford 1-(buta-1,3-dien-2-yl)-3,5-dimethoxybenzene (323 mg, 22%) as a colorless oil.

¹H NMR (500 MHz, CDCl₃) δ 6.62 – 6.54 (m, 1H), 6.48 (d, *J* = 2.3 Hz, 2H), 6.43 (t, *J* = 2.3 Hz, 1H), 5.31 – 5.18 (m, 4H), 3.80 (s, 6H).
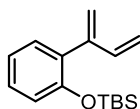
(2-(buta-1,3-dien-2-yl)phenoxy)(tert-butyl)dimethylsilane Under an argon atmosphere, [(dppe)NiCl2] (25.50 mg, 0.07093 mmol, 2.5 mol%) was weighted in a 25 mL Schlenk flask and suspended in 4.0 mL of anhydrous and degassed tetrahydrofuran. The flask was sealed and removed from argon atmosphere. The heterogeneous mixture was cooled to 0°C and 1-(2-((tert-butyldimethylsilyl)oxy)phenyl)vinyl diethyl phosphate (1.4 g, 3.65 mmol, 1.0 equiv.) was added to the mixture using a syringe. Vinylmagnesium bromide(5.5 mL of a 0.7 M solution in THF, 3.83 mmol, 1.05 equiv.) was added dropwise by syringe at 0°C (final volume: 14.56 mL, concentration: 0.25 M). The reaction mixture was stirred for 1 hour at room temperature. The reaction was then quenched by addition of 5.0mL of a saturated solution of ammonium chloride at 0°C and extracted with diethyl ether (3 x 25 mL). The organic layers were dried over sodium sulfate, filtered and the solvent removed under vacuum affording the crude residue that, after purification by silica gel flash chromatography (100% pentane), afforded (2-(buta-1,3-dien-2-yl)phenoxy)(tert-butyl)dimethylsilane (498 mg, 52%) as a colorless oil.

¹H NMR (500 MHz, CDCl₃) δ 7.18 (ddd, *J* = 8.1, 7.3, 1.8 Hz, 1H), 7.11 (dd, *J* = 7.5, 1.8 Hz, 1H), 6.94 (td, *J* = 7.4, 1.2 Hz, 1H), 6.83 (dd, *J* = 8.1, 1.2 Hz, 1H), 6.55 (ddd, *J* = 17.2, 10.3, 0.7 Hz, 1H), 5.39 – 5.11 (m, 3H), 5.12 – 4.83 (m, 3H), 0.94 (s, 11H), 0.14 (s, 7H).

¹³C NMR: (126 MHz, CDCl₃) δ 153.07, 146.43, 138.52, 131.60, 131.22, 128.50, 120.98, 119.42, 118.61, 116.45, 25.94, 25.82, 18.25, 0.15.
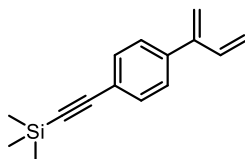
((4-(buta-1,3-dien-2-yl)phenyl)ethynyl)trimethylsilane Under an argon atmosphere, [(dppe)NiCl2] (39.7 mg, 0.00141 mmol, 2.5 mol%) was weighted in a 25 mL Schlenk flask and suspended in 4.0 mL of anhydrous and degassed tetrahydrofuran. The flask was sealed and removed from argon atmosphere. The heterogeneous mixture was cooled to 0°C and diethyl (1-(4-((trimethylsilyl)ethynyl)phenyl)vinyl) phosphate (1.00 g, 2.84 mmol, 1.0 equiv.) was added to the mixture using a syringe. Vinylmagnesium bromide(4.3 mL of a 0.7 M solution in THF, 2.98 mmol, 1.05 equiv.) was added dropwise by syringe at 0°C (final volume: 11.35 mL, concentration: 0.25 M). The reaction mixture was stirred for 1 hour at room temperature. The reaction was then quenched by addition of 5.0mL of a saturated solution of ammonium chloride at 0°C and extracted with diethyl ether (3 x 25 mL). The organic layers were dried over sodium sulfate, filtered and the solvent removed under vacuum affording the crude residue that, after purification by silica gel flash chromatography (pentane buffered with 0.1% triethylamine), afforded ((4-(buta-1,3-dien-2-yl)phenyl)ethynyl)trimethylsilane (465 mg, 72%) as a yellow oil. The spectra matched that of literature reports.[132]

¹H NMR (500 MHz, CDCl₃) δ 7.48 – 7.42 (m, 2H), 7.26 (dt, J = 6.3, 1.8 Hz, 2H), 6.64 – 6.55 (m, 1H), 5.33 – 5.13 (m, 4H), 0.26 (s, 9H).
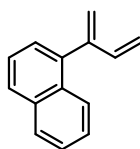
1-(buta-1,3-dien-2-yl)naphthalene To a stirred 1.0 M solution of vinyl magnesium bromide in THF (3.7 g, 28 mmol, 28 mL, 1.2 equiv), a solution of 1-(p-tolyl)ethan-1-one in 36 mL of THF was added dropwise over thirty minutes at 0°C under a nitrogen atmosphere. The reaction mixture was stirred at the same temperature for two hours and then quenched with saturated ammonium chloride (200 mL) and extracted with ethyl acetate (100 mL). The organic layer was dried with sodium sulfate and concentrated under reduced pressure. The crude product was dissolved in 60 mL of toluene with pyridinium p-toluenesulfonate (38 mg, 0.15 mmol, 0.005 equiv) and sodium sulfate (50 mg, 0.35 mmol, 0.012 equiv) and heated to 80°C for three hours. The reaction was quenched with 75 mL of saturated sodium bicarbonate and washed with brine (80 mL). The organic layer was

dried with sodium sulfate and concentrated *in vacuo* before being purified by column chromatography (100%

hexanes) to yield 1-(buta-1,3-dien-2-yl)-4-methylbenzene (72 mg, 2% yield) as a colorless oil.

¹H NMR (500 MHz, CDCl₃) δ 7.99 – 7.83 (m, 3H), 7.55 – 7.46 (m, 3H), 7.38 (dd, *J* = 7.0, 1.3 Hz, 1H), 6.83

(dd, *J* = 17.3, 10.5 Hz, 1H), 5.65 (d, *J* = 2.0 Hz, 1H), 5.32 (t, *J* = 1.7 Hz, 1H), 5.19 (dq, *J* = 10.5, 1.2 Hz, 1H),

4.77 (dd, *J* = 17.3, 1.2 Hz, 1H).

¹³C NMR (126 MHz, CDCl3) δ 147.49, 139.21, 137.83, 133.58, 131.94, 128.16, 127.71, 126.70, 126.39, 125.79,

125.74, 125.40, 119.69, 117.81.
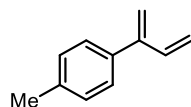
1-(buta-1,3-dien-2-yl)-4-methylbenzene To a stirred 1.0 M solution of vinyl magnesium bromide in THF

(3.7 g, 28 mmol, 28 mL, 1.2 equiv), a solution of 1-(p-tolyl)ethan-1-one in 36 mL of THF was added dropwise

over thirty minutes at 0°C under a nitrogen atmosphere. The reaction mixture was stirred at the same

temperature for two hours and then quenched with saturated ammonium chloride (200 mL) and extracted with

ethyl acetate (100 mL). The organic layer was dried with sodium sulfate and concentrated under reduced

pressure. The crude product was dissolved in 60 mL of toluene with pyridinium p-toluenesulfonate (38 mg,

0.15 mmol, 0.005 equiv) and sodium sulfate (50 mg, 0.35 mmol, 0.012 equiv) and heated to 80°C for three

hours. The reaction was quenched with 75 mL of saturated sodium bicarbonate and washed with brine (80

mL). The organic layer was dried with sodium sulfate and concentrated *in vacuo* before being purified by column

chromatography (100% hexanes) to yield 1-(buta-1,3-dien-2-yl)-4-methylbenzene (72 mg, 2% yield) as a

colorless oil.

¹H NMR (500 MHz, CDCl₃) δ 7.25 – 7.20 (m, 2H), 7.16 (dt, *J* = 7.8, 0.7 Hz, 2H), 6.65 – 6.57 (m, 1H), 5.28 –

5.17 (m, 4H), 2.37 (s, 3H).
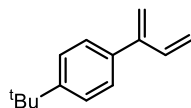
1-(buta-1,3-dien-2-yl)-4-(tert-butyl)benzene To a solution of 2-(4-(tert-butyl)phenyl)but-3-en-2-ol (2.8 g, 14

mmol, 1.0 equiv) in 40 mL of benzene, pyridinium p-toluenesulfonate (34 mg, 0.14 mmol, 0.01 equiv) and

sodium sulfate (50 mg, 0.35 mmol, 0.026 equiv) was added. The reaction was stirred at reflux for 2 hours. After, the reaction was quenched with saturated sodium bicarbonate (80 mL), extracted with ethyl acetate (40 mL) and the organic layer was dried with sodium sulfate before being concentrated under reduced pressure. The crude product was purified by flash column chromatography (100% hexanes) to afford 1-(buta-1,3-dien-2-yl)-4-(tert-butyl)benzene (932 mg, 37%) as a colorless oil.

¹H NMR (500 MHz, CDCl₃) δ 7.39 – 7.35 (m, 2H), 7.29 – 7.25 (m, 2H), 6.66 – 6.56 (m, 1H), 5.30 – 5.17 (m, 4H), 1.34 (s, 9H).
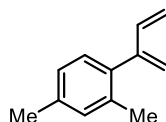
1-(buta-1,3-dien-2-yl)-2,4-dimethylbenzene Under an argon atmosphere, [(dppe)NiCl2] (25.50 mg, 0.07093 mmol, 2.5 mol%) was weighted in a 25 mL Schlenk flask and suspended in 4.0 mL of anhydrous and degassed tetrahydrofuran. The flask was sealed and removed from argon atmosphere. The heterogeneous mixture was cooled to 0°C and 1-(2,4-dimethylphenyl)vinyl diethyl phosphate (1g, 3.65 mmol, 1.0 equiv.) was added to the mixture using a syringe. Vinylmagnesium bromide(5.5 mL of a 0.7 M solution in THF, 3.83 mmol, 1.05 equiv.) was added dropwise by syringe at 0°C (final volume: 14.56 mL, concentration: 0.25 M). The reaction mixture was stirred for 1 hour at room temperature. The reaction was then quenched by addition of 5.0mL of a saturated solution of ammonium chloride at 0°C and extracted with diethyl ether (3 x 25 mL). The organic layers were dried over sodium sulfate, filtered and the solvent removed under vacuum affording the crude residue that, after purification by silica gel flash chromatography (100% pentane), afforded 1-(buta-1,3-dien-2-yl)-2,4-dimethylbenzene (221 mg, 38%) as a colorless oil.

¹H NMR (500 MHz, CDCl₃) δ 7.04 – 6.94 (m, 3H), 6.59 (dd, J = 17.3, 10.4 Hz, 1H), 5.36 (d, J = 2.0 Hz, 1H), 5.11 (dq, J = 10.3, 1.2 Hz, 1H), 5.04 (t, J = 1.8 Hz, 1H), 4.72 (dd, J = 17.2, 1.5 Hz, 1H), 2.33 (s, 3H), 2.17 (s, 3H).

LED emission profiles
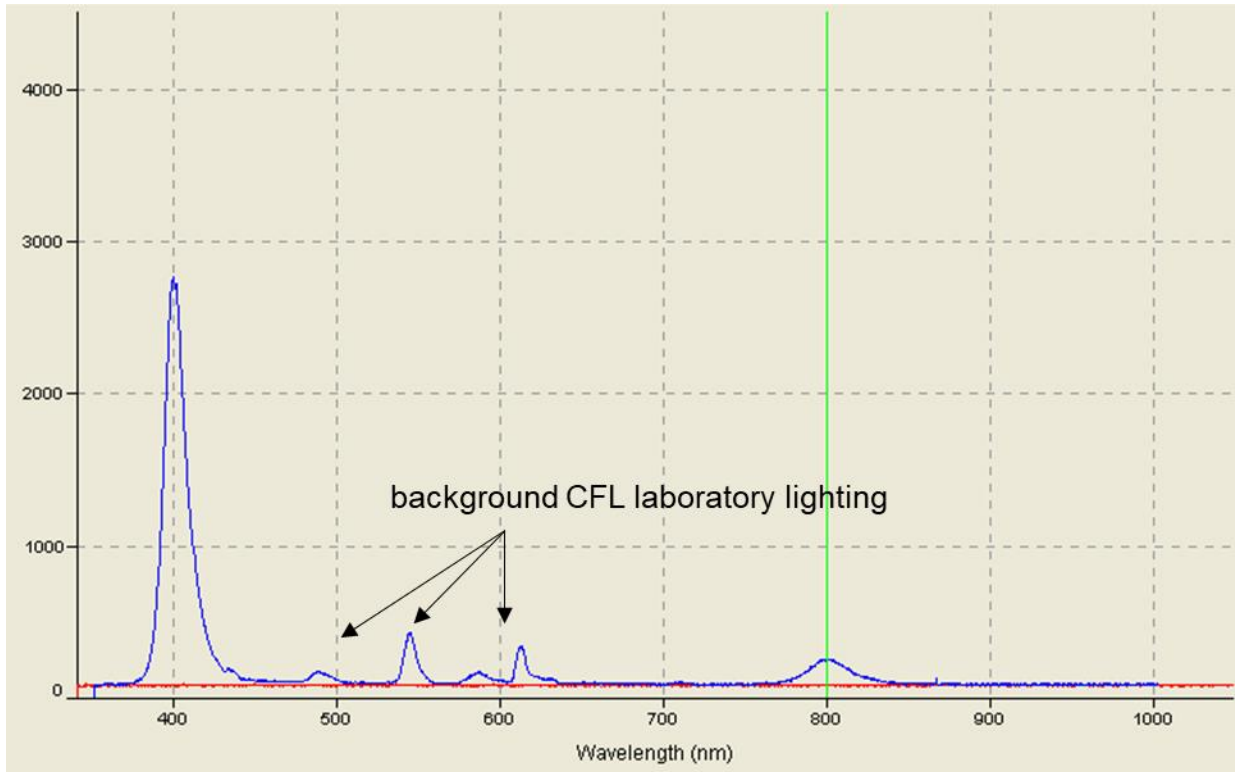
Figure 71. Measured emission spectra of "470 nm" LEDs used.
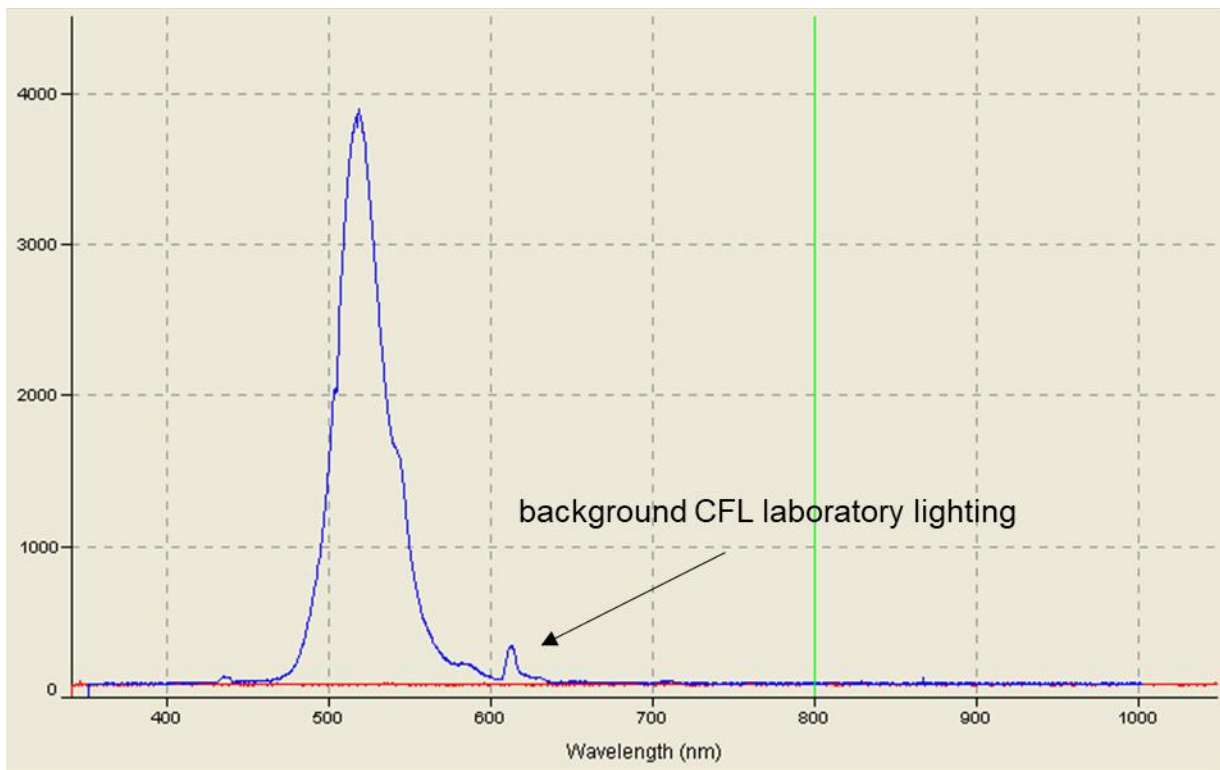
Figure 72. Measured emission spectra of "525 nm" LEDs used.

Procedure for the small-molecule photoredox Diels–Alder

Procedure for identification of small-molecule Diels–Alder product: An oven-dried 1-dram vial was charged with a stir bar and sealed with a septa cap. In three separate, sealed, oven-dried 1-dram vials, solutions of cyclohexene **1** (50 mg/mL), photocatalyst (8μmol/mL), and isoprene (50 mg/mL) were prepared in dichloromethane or acetonitrile. To each 1-dram vial with a stir bar, 0.1 mL of each solution was added under nitrogen. The reactions were then stirred at 450 rpm either under a steady flow of nitrogen or with a 25 G needle to vent the reaction and introduce oxygen. The reaction was irradiated with blue LEDs (470 nm) and cooled with a fan for 16 hours. After which, the reactions were concentrated *in vacuo* and redissolved in solvent for GC-MS (dichloromethane) or LC-MS (10:1 acetonitrile:water with 0.1% formic acid) analysis. To isolate the cycloaddition product **2**, four reaction vials were combined and purified using preparatory thin-layer chromatography in 100% pentane.

2
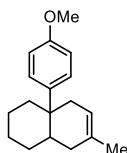
¹H NMR (500 MHz, CDCl₃) δ 7.32 – 7.29 (m, 2H), 6.83 – 6.80 (m, 2H), 5.39 (s, 1H), 3.79 (s, 3H), 2.53 (d, J = 18.7 Hz, 1H), 2.19 (dd, J = 5.6, 2.7 Hz, 1H), 2.15 (d, J = 4.8 Hz, 1H), 1.98 – 1.92 (m, 1H), 1.84 (t, J = 9.3 Hz, 2H), 1.79 – 1.65 (m, 5H), 1.53 – 1.50 (m, 3H), 1.40 – 1.35 (m, 2H).

LRMS m/z expected for $C_{18}H_{25}O$ [M+H]+ 257.18, measured 257.1

Table 14. Cycloaddition products measured using GC-MS (LRMS). Reaction procedure for product identification follows that for product identification of 2.

	*t*Bu	Me	F
[M+H]+	$C_{21}H_{30}$	$C_{18}H_{25}$	$C_{17}H_{22}F$
m/z expected	282.23	240.19	244.16
m/z measured	282.2	240.2	244.2

Procedure for optimization and quantification of small-molecule Diels–Alder reaction: An oven-dried 1-dram vial was charged with a stir bar (and external oxidant if that was a variable for screening) and sealed with a septa cap. In three separate, sealed, oven-dried 1-dram vials, solutions of cyclohexene **1** (50 mg/mL, 0.3mmol/mL), photocatalyst (8μmol/mL), and isoprene (50 mg/mL) were prepared in deuterated dichloromethane (0.12 M concentration total). To each 1-dram vial with a stir bar, 0.1 mL of each solution was added under nitrogen. The reactions were then stirred at 450 rpm either under static nitrogen (if an external oxidant was added) or with a 25 G needle to vent the reaction and introduce oxygen. The reaction was irradiated with blue LEDs (470 nm) and cooled with a fan for 16 hours. The reactions were diluted with an additional 0.2 mL of deuterated DCM. A solution of benzaldehyde as an external standard was prepared (30mg/mL, 0.3mmol/mL) in deuterated dichloromethane and 0.1 mL of this solution was added to each reaction vile. The resulting solutions were analyzed via ^{1}H NMR to measure conversion of starting cyclohexene and product formation.

Table 15. Optimization of small-molecule reaction.
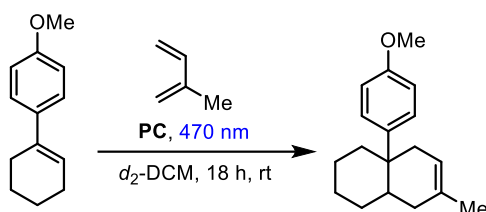
Entry	Catalyst	Oxidant	Solvent	Conversion	Yield
1	MesAcr (1 mol%)	Air	DCM	68%	1%
2	TPT-OMe	Air	DCM	100%	1%
3	TPT	Air	DCM	64%	<1%
4	CzIPn	Air	DCM	90%	<1%
5	MesAcr	DDQ (0.2 eq)	DCM	96%	<1%
6	MesAcr	DDQ (1 eq)	DCM	74%	13%
7	MesAcr	CAN (0.2 eq)	DCM	77%	<1%
8	MesAcr	CAN (1 eq)	DCM	85%	n.d.

n.d.= not detected

Procedure for the optimization of photoredox Diels–Alder polymerization

General procedure for reaction optimization. An oven-dried 1-dram vial was charged with a stir bar (and external oxidant if that was a variable for screening) and sealed with a septa cap. In three separate, sealed, oven-

dried 1-dram vials, solutions of cyclohexene **1** (50 mg/mL, 0.3mmol/mL), photocatalyst (8μmol/mL), and **3b** (1.10 g/mL) were prepared in solvent (0.09 M concentration total). To each 1-dram vial with a stir bar, 0.1 mL of each solution was added under nitrogen. For reactions without initiator, 0.1 mL of solvent was added. The reactions were then stirred at 450 rpm with a 25 G needle to vent the reaction and introduce oxygen. The reaction was irradiated with blue LEDs (470 nm) and cooled with a fan for 16 hours. The reaction solution in each vial was precipitated into a 7:1 methanol:water solution and centrifuged at 10,000 rpm at 0 ˚C for 10 minutes.

Table 16. Optimization of standard reaction conditions.
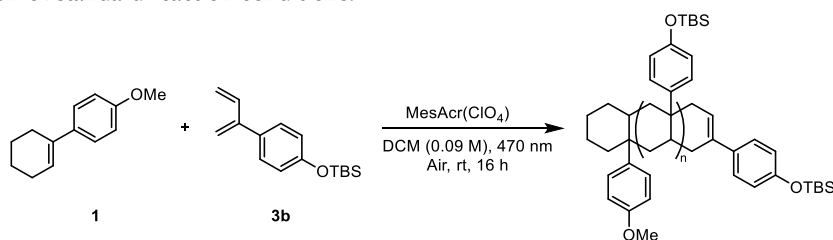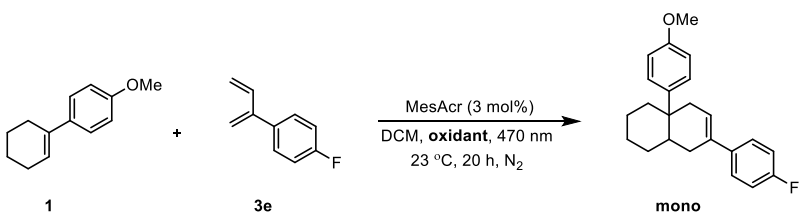
Entry	Deviation from standard conditions	M_n	Đ	Yield
1	None	1500	1.2	16
2	No initiator	1300	1.2	38
3	F-Cyclohexene	1800	1.3	25
4	TPT-OMe	1200	1.2	33
5	TPT	860	1.1	7.2
6	^{t}BuMesAcr	1000	1.3	40
7	(Ir[dF(CF$_3$)ppy]$_2$(dtbpy))PF$_6$	1300	1.4	15
8	No solvent	860	1.03	No precipitate
9	Chloroform	1600	1.2	12
10	DMSO	2700	1.6	11
11	Nitromethane	1100	1.1	59
12	DMF	n.d.	n.d.	n.d.
13	THF	1500	1.4	6
14	4 M	1500	1.3	46
15	2 M	1600	1.3	44
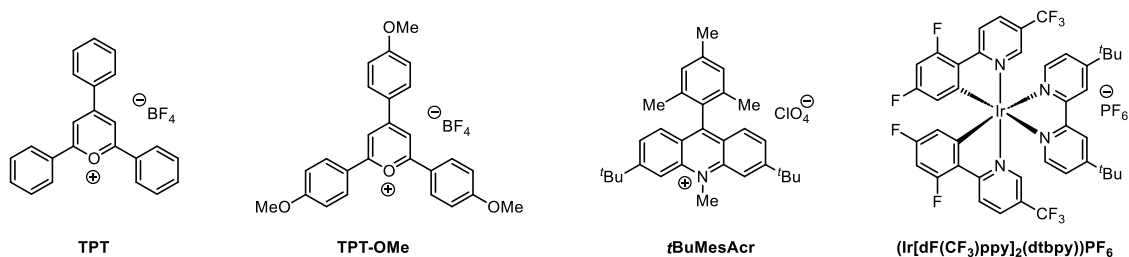
Scheme 4. Photocatalysts used in Table 16.

Procedure for external oxidant screens. In 6 separate 1 dram vials the following solutions were prepared: 15 mg of **1** was dissolved in 0.3 mL of DCM or THF (50 mg/mL), 59.1 mg of diene **3e** was dissolved in 0.3 mL of DCM or THF (197 mg/mL), and 2.0 mg of MesAcr was dissolved in 0.61 mL of DCM or THF (3.2 mg/mL, 3 mol%). Six 1-dram vials were charged with a stir bar and external oxidant (0.2 eq) was added and the vials were sealed with septa and kept under nitrogen. Two vials contained CAN (2.91 mg), two contained DDQ (1.12 mg), and two contained methyl viologen (1.37 mg). To three vials with different oxidants in each, 0.1mL of each solution (photocatalyst, **1**, and **3e**) were added via syringe under nitrogen. The reactions were run at room temperature with irradiation with blue light (470 nm) for 20 hours. Then, the samples were concentrated and prepared for GC-MS analysis by creating 0.5 mg/mL solutions of crude reaction mixture in HPLC DCM with toluene as an external standard. Toluene internal standard was made by dissolving 2.61 mg of toluene in 1.0 mL of HPLC DCM (0.0284 mmol). Samples were redissolved in 1.0 mL of HPLC DCM (0.0284 mmol) from which 0.1 mL of this solution was combined with toluene standard and 0.8 mL of HPLC DCM. Reactions were evaluated based on conversion of **3e** and formation of **1+3e** product according to MS (336.2 m/z). Note: diene **3e** was used due to the ability to detect the **1+3e** product using GC-MS.

Table 17. Optimization of external oxidant.

Oxidant	Solvent	% 3e conversion	% mono
CAN	THF	47	14
DDQ	THF	40	4
Methyl violegen	THF	37	0
Air	THF	62	48
CAN	DCM	55	16
DDQ	DCM	63	2
Methyl violegen	DCM	38	1.1
Air	DCM	82	43

Procedure for elimination experiments. Solutions of photocatalyst, diene **3b**, and **1** were made by dissolving MesAcr (1.5 mg) in 0.5 mL of DCM, 440 mg **3b** 0.4 mL of DCM, and 25 mg of **1** in 0.5 mL of DCM. Reactions were set up where in two 1-dram vials charged with stir bars, 0.1 mL of each solution was added. One of these

vials was the control, while the other was prepared in the dark and the vial was wrapped in electrical tape. In the three remaining vials, only two of the three solutions were added to each vial, and 0.1 mL of DCM was added to replace the omitted solution (0.3 mL total volume). The reactions were vented with 25 G needles, irradiated with blue light (470 nm), and stirred at 450 rpm for 16 hours. Then, the reactions were precipitated into 8 mL of a 7:1 methanol:water mixture and centrifuged at 10,000 rpm at 0 °C for 10 minutes. Molecular weights were determined either from the polymer from precipitate or—if not precipitate was formed—from the isolated products in the supernatant.

Table 18. Elimination experiments. M_n was determined using GPC with MALS detector.
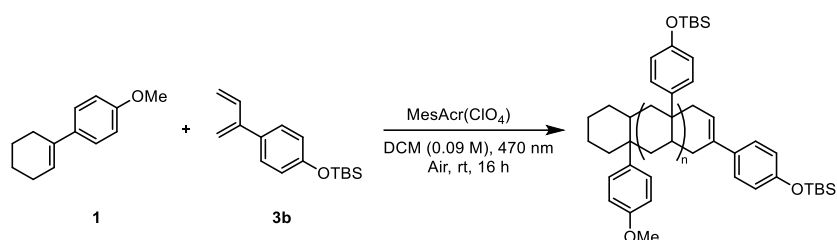
Entry	Eliminated component	M_n (Đ)
1	None	1500 (1.6)
2	MesAcr	n.d.
3	**1**	1200 (1.3)
4	**3e**	n.d.
5	Light (run in dark)	n.d.

Procedure for substrate scope experiments. An oven-dried 1-dram vial was charged with a stir bar (and external oxidant if that was a variable for screening) and sealed with a septa cap. In three separate, sealed, oven-dried 1-dram vials, solutions of cyclohexene **1** (50 mg/mL, 0.3mmol/mL), photocatalyst (8µmol/mL), and diene (4.0 mmol/mL) were prepared in solvent (0.09 M concentration total). To each 1-dram vial with a stir bar, 0.1 mL of each solution was added under nitrogen. The reactions were then stirred at 450 rpm either with a 25 G needle to vent the reaction and introduce oxygen. The reaction was irradiated with blue LEDs (470 nm) and cooled with a fan for 16 hours. The reaction solution in each vial was precipitated into a 7:1 methanol:water solution and centrifuged at 10,000 rpm at 0 °C for 10 minutes.

Procedure for cationic polymer extension experiments. In a 1 dram vial with stir bar, 10 mg of polymer sample was dissolved in 0.15 mL of DCM under nitrogen. Stock solutions of *tert*-butyl chloride were prepared

(115 µL in 0.5 mL, 2.0 mmol/mL) and 0.1 mL of this solution was added to the vial with dissolved polymer under nitrogen. This reaction was stirred as titanium tetrachloride (18 µL, 18 µmol, 1.0 M in DCM) was added and the reaction was stirred for 30 minutes before precipitation into 8mL of a 7:1 methanol:water solution and centrifuged at 10,000 rpm at 0 °C for 10 minutes. The precipitate was isolated and analyzed via GPC using MALS detection.

Procedure for probing polymerization initiation and characterization of oligomers. Supernatant from polymerizations with **1** and **3b** with MesAcr was concentrated in vacuo and redissolved in ~1 mL of DCM to deposit at the baseline of a preparatory TLC plate. The plate was developed in a solution of 2% ether in pentane with 0.1% triethylamine. The top six lines which were isolated and purified using ^{1}H NMR and various 2D NMR experiments including COSY, HSQC, HMBC, TOCSY, and NOSY.

Electrochemical data
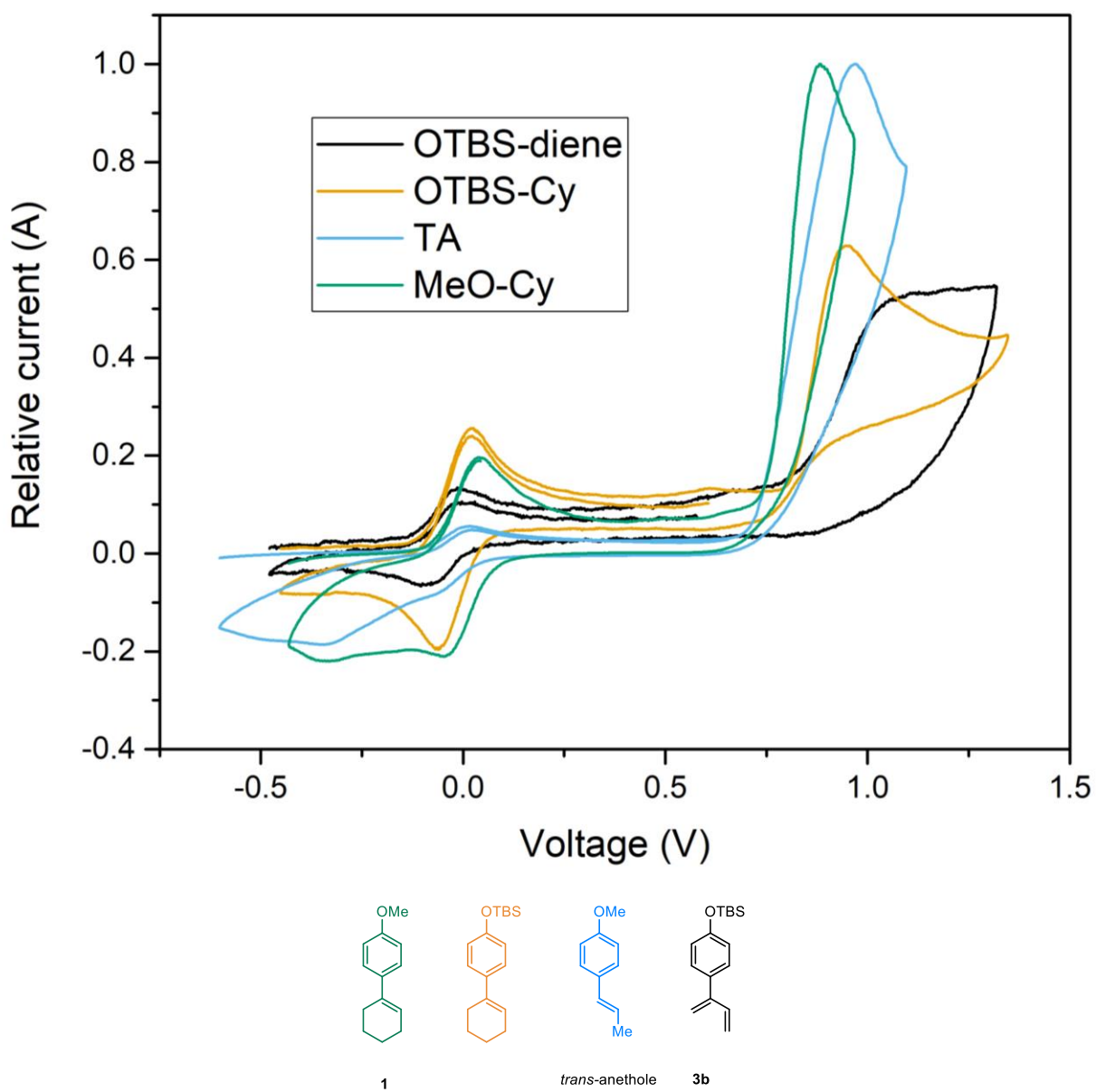
Figure 73. CV comparison of multiple initiators and 3b acetonitrile with TBAPF$_6$ electrolyte.
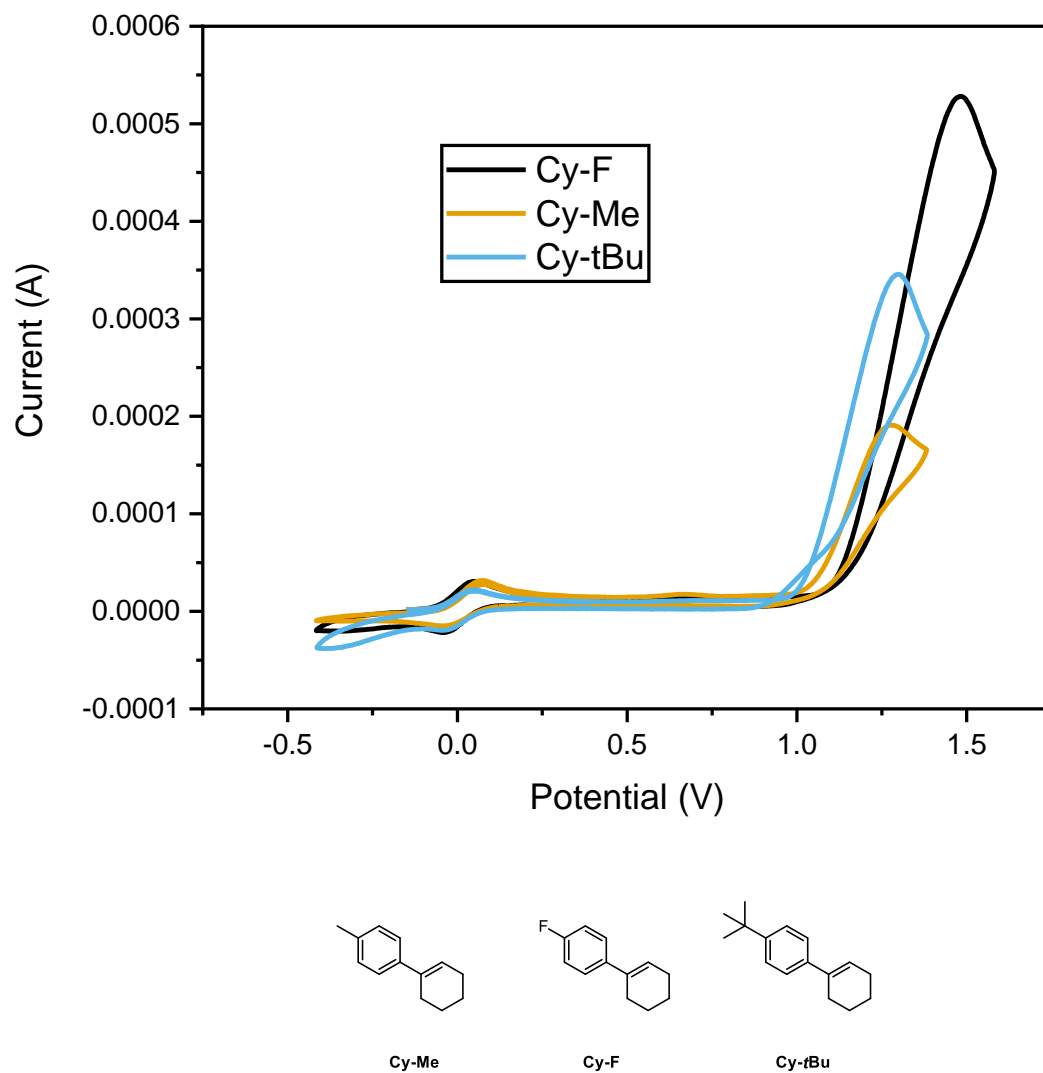
Figure 74. CV of oxidation potential of multiple cyclohexenes in acetonitrile with TBAPF$_6$ electrolyte.

Gas sorption experiments
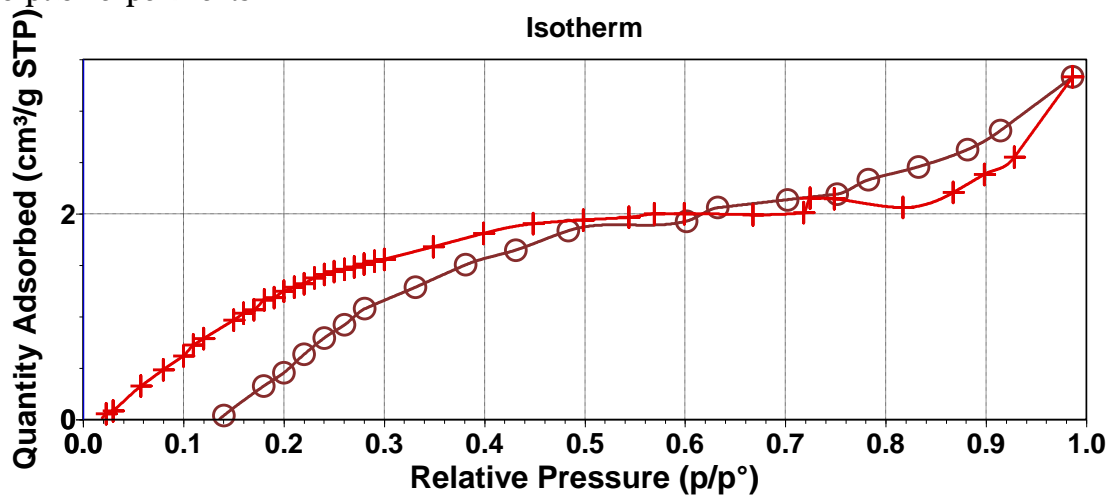
Figure 75. N_2 isotherms of LP-3b (5.7 m²/g).
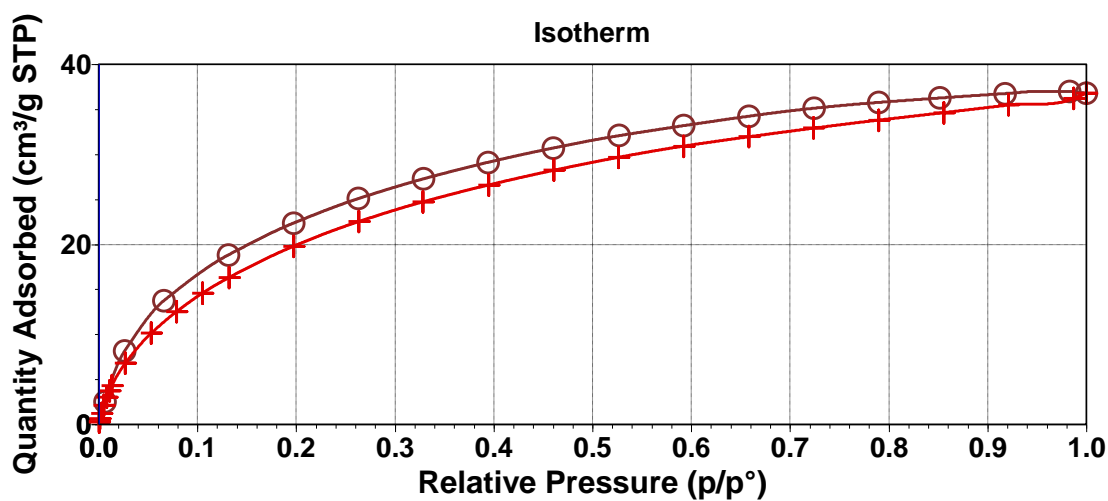
Figure 76. CO_2 isotherms of LP-3b (110 m²/g).

GPC Traces
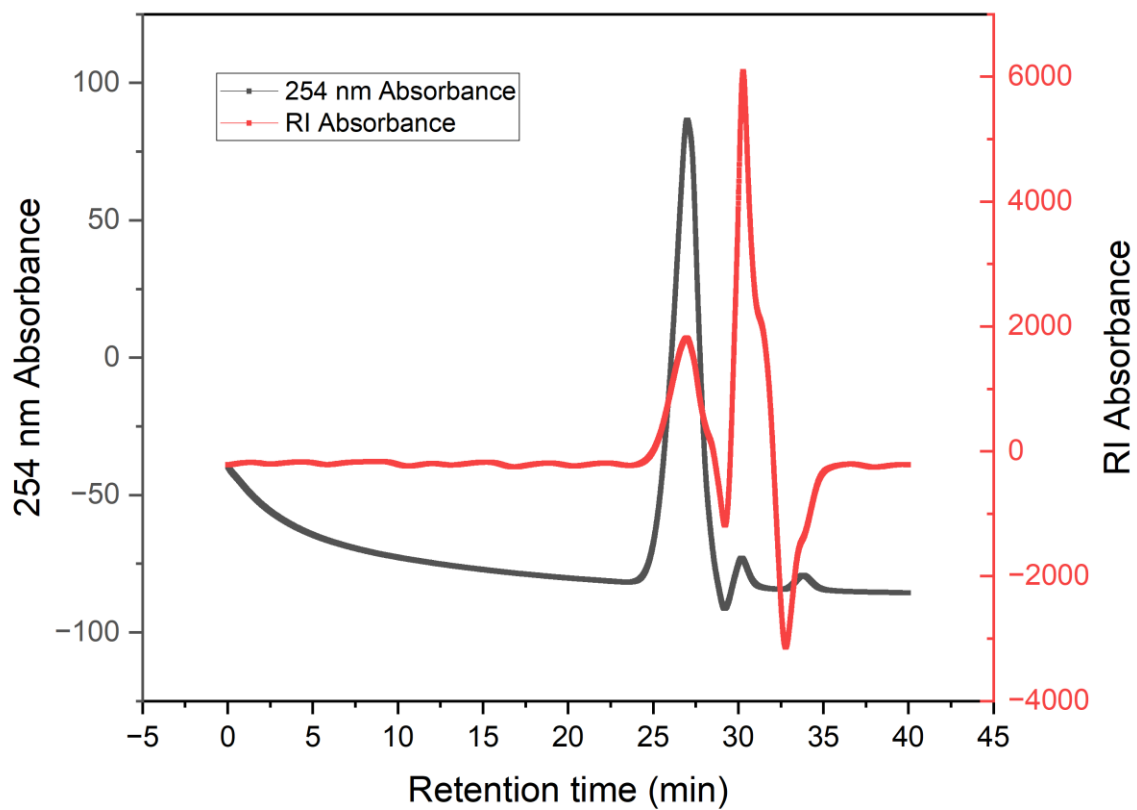
Figure 77. GPC traces of reaction in Table 16, entry 1 using RID detection.
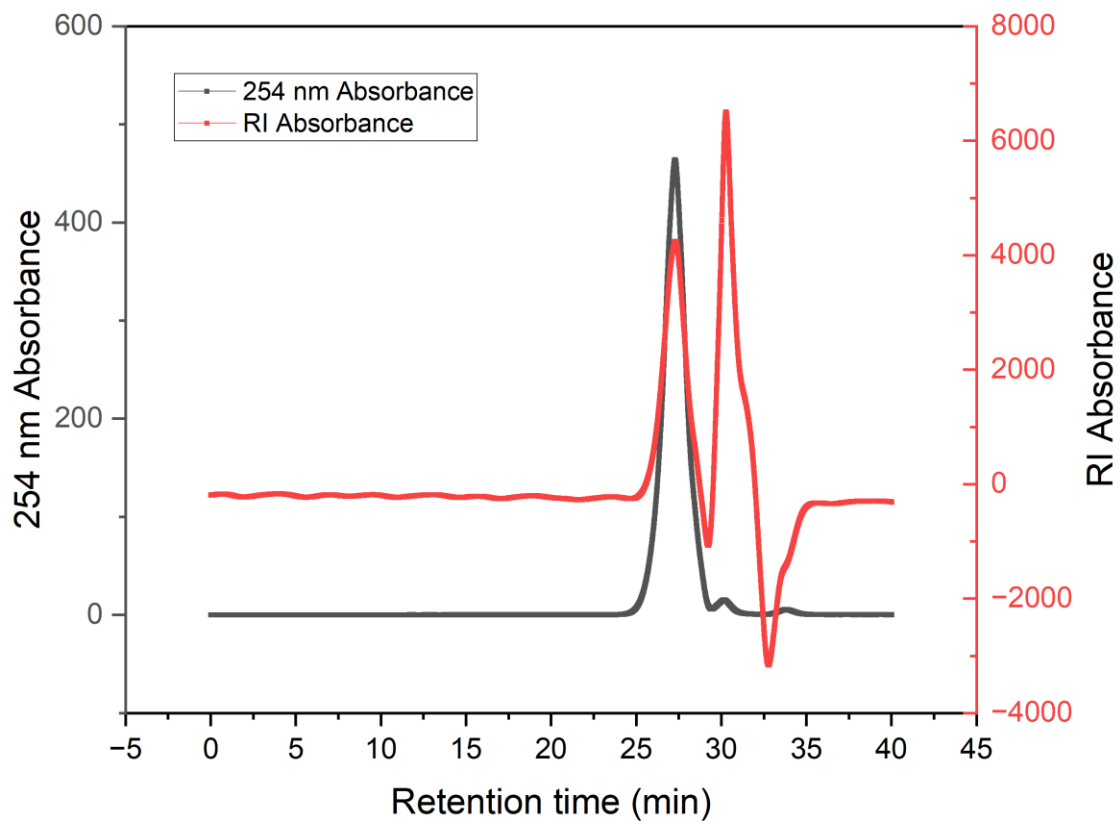
Figure 78. GPC traces of reaction from Table 16, entry 2 using RID detection.
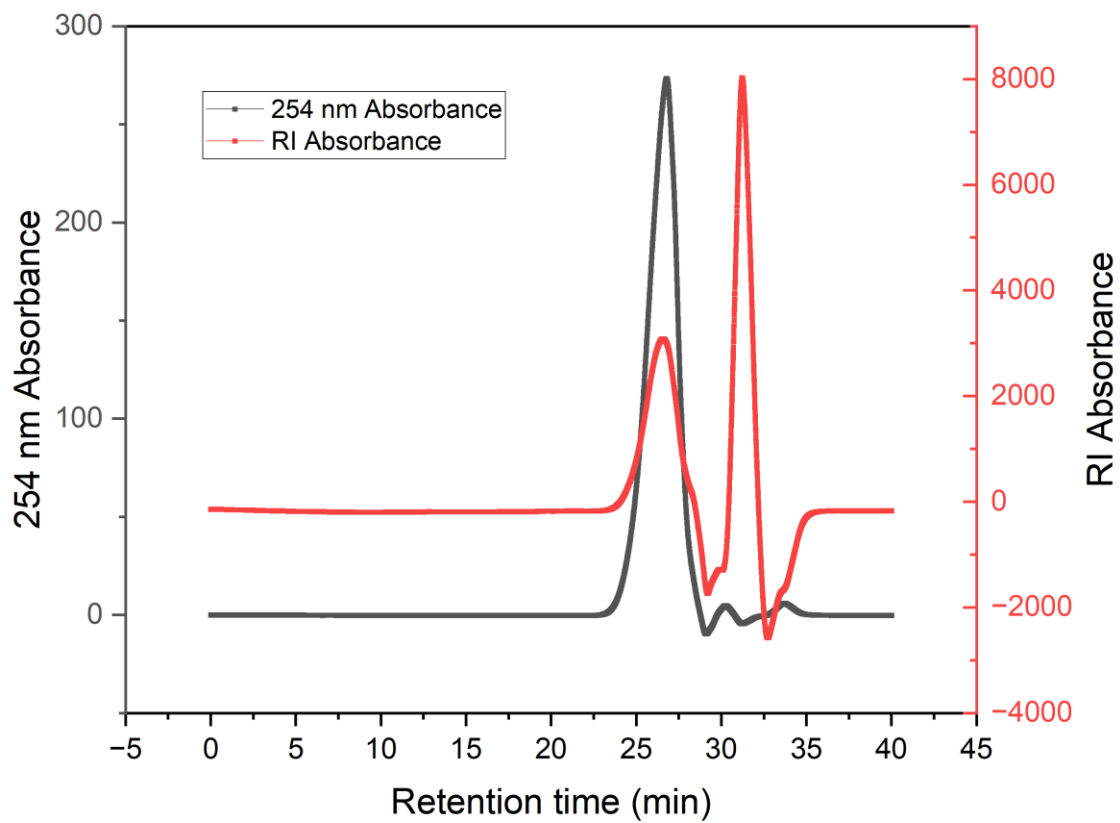
Figure 79. GPC traces of reaction in Table 16, entry 3 using RID detection.
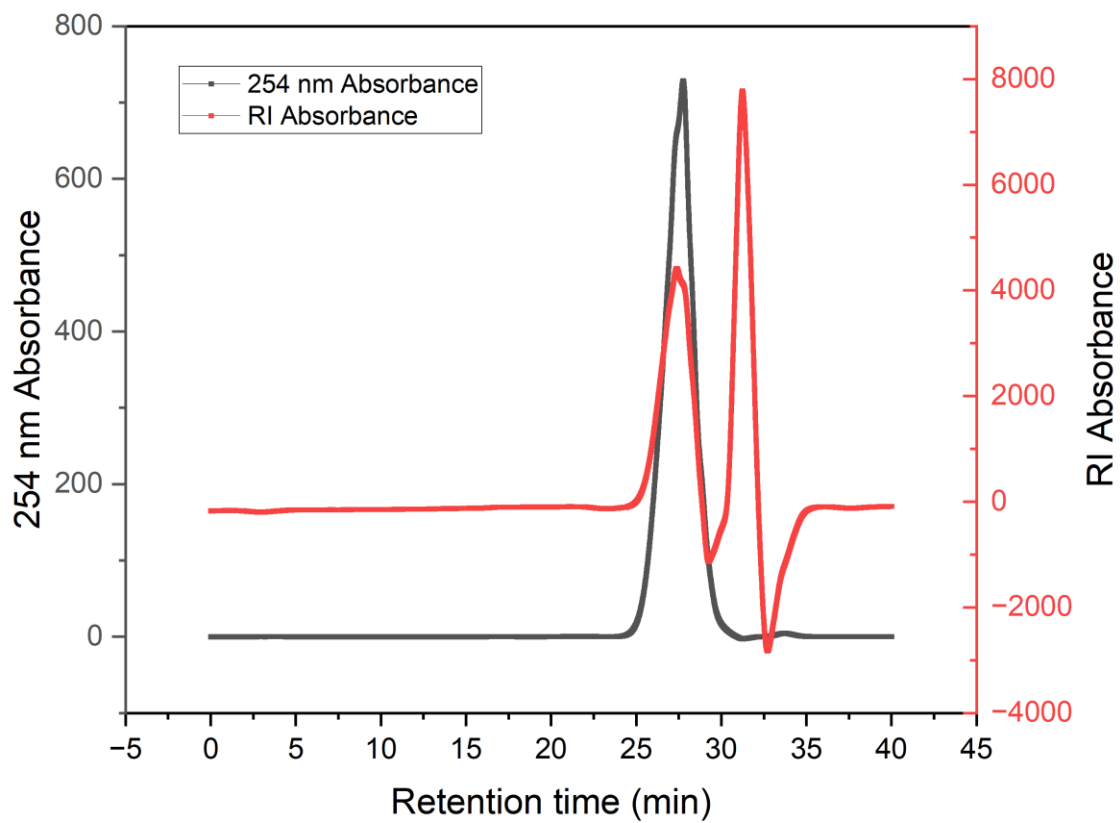
Figure 80. GPC of reaction from Table 16, entry 4 using RID detection.
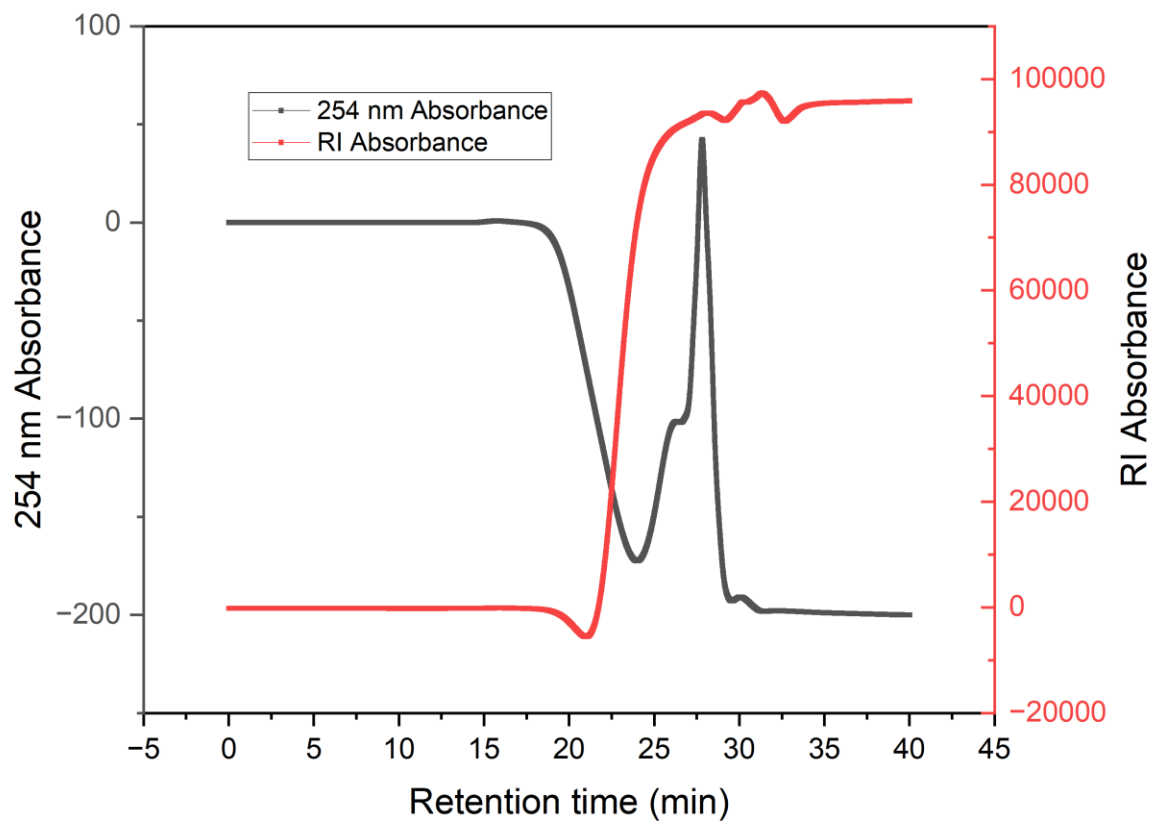
Figure 81. GPC of reaction from Table 16, entry 5 using RID detection.
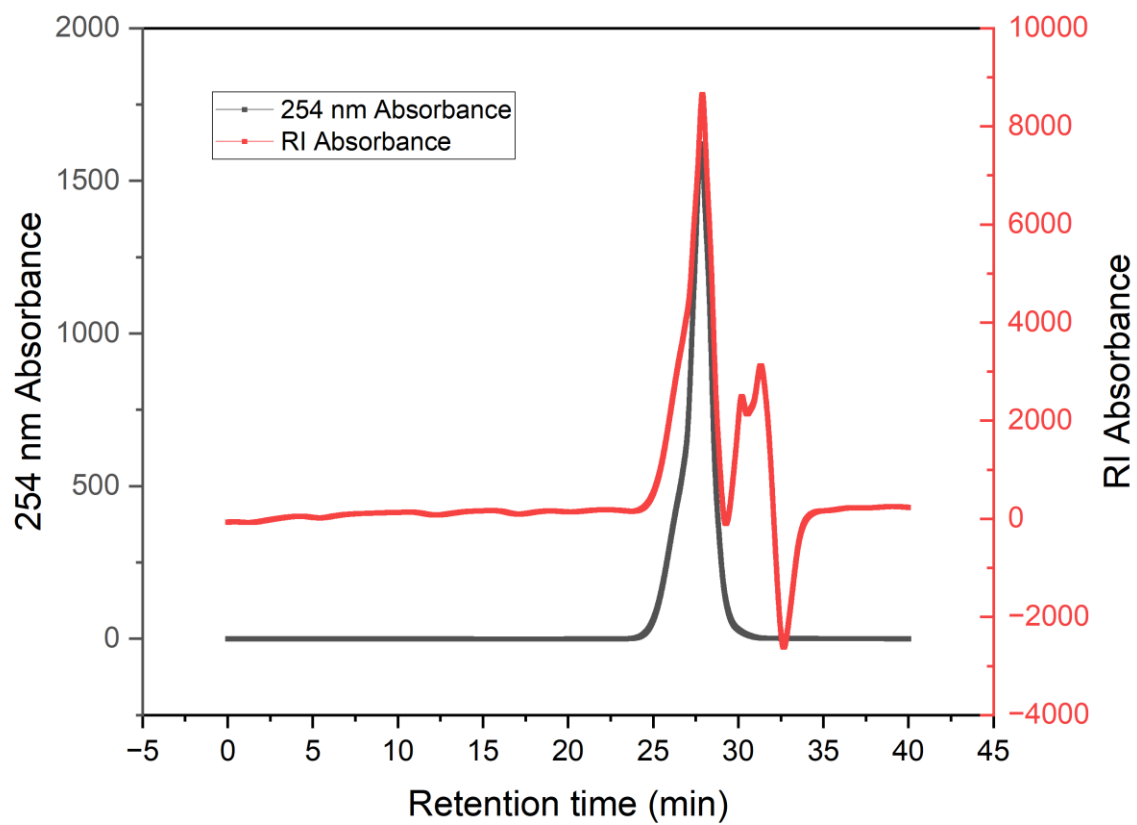
Figure 82. GPC traces of reaction from Table 16, entry 6 using RID detection.
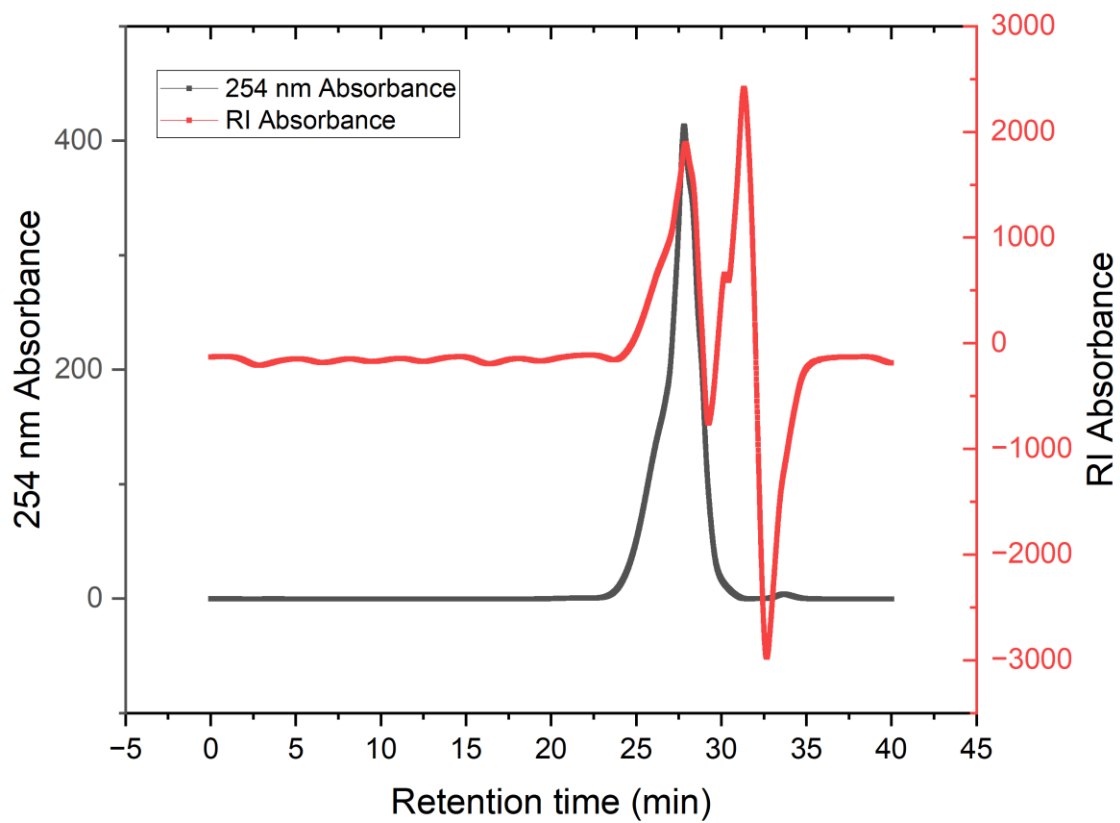
Figure 83. GPC traces of reaction in Table 16, entry 7 using RID detection.
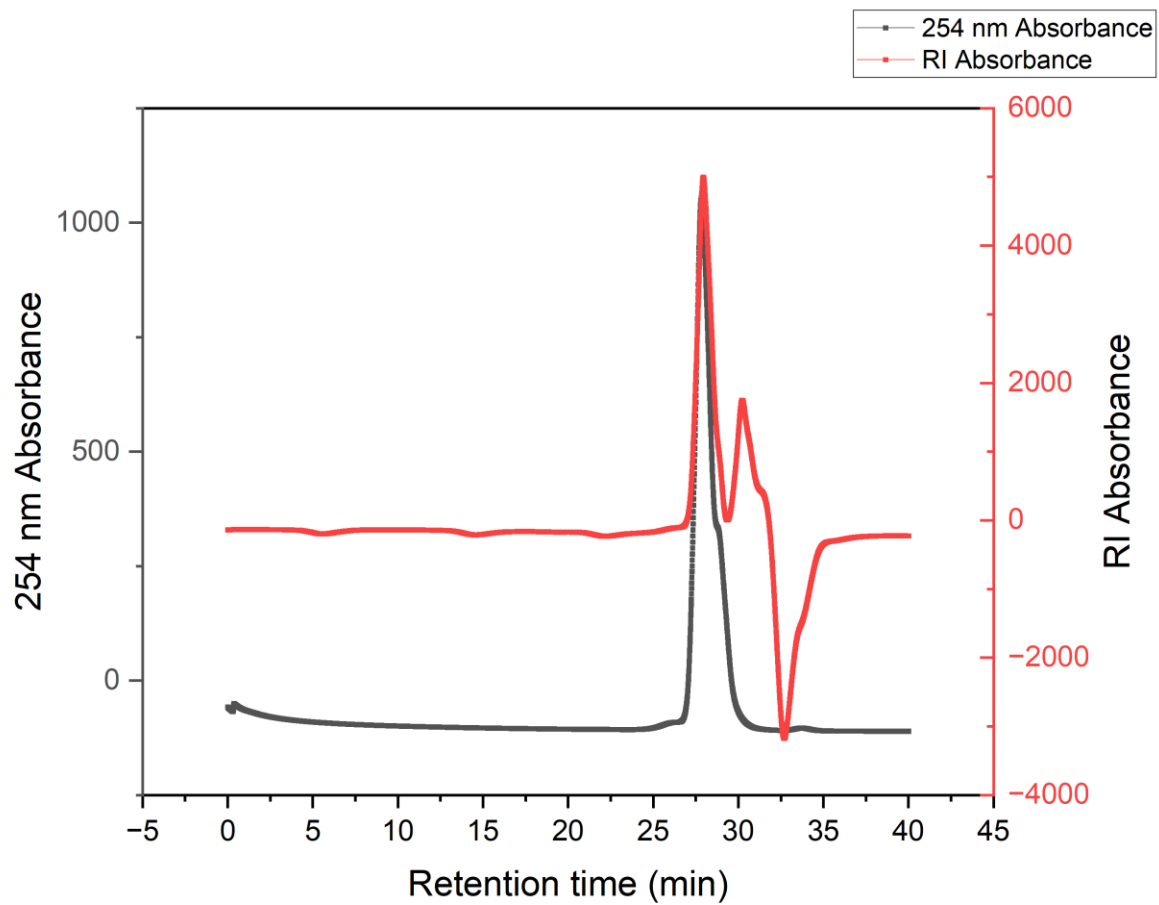
Figure 84. GPC traces of reaction in Table 16, entry 8 using RID detection.
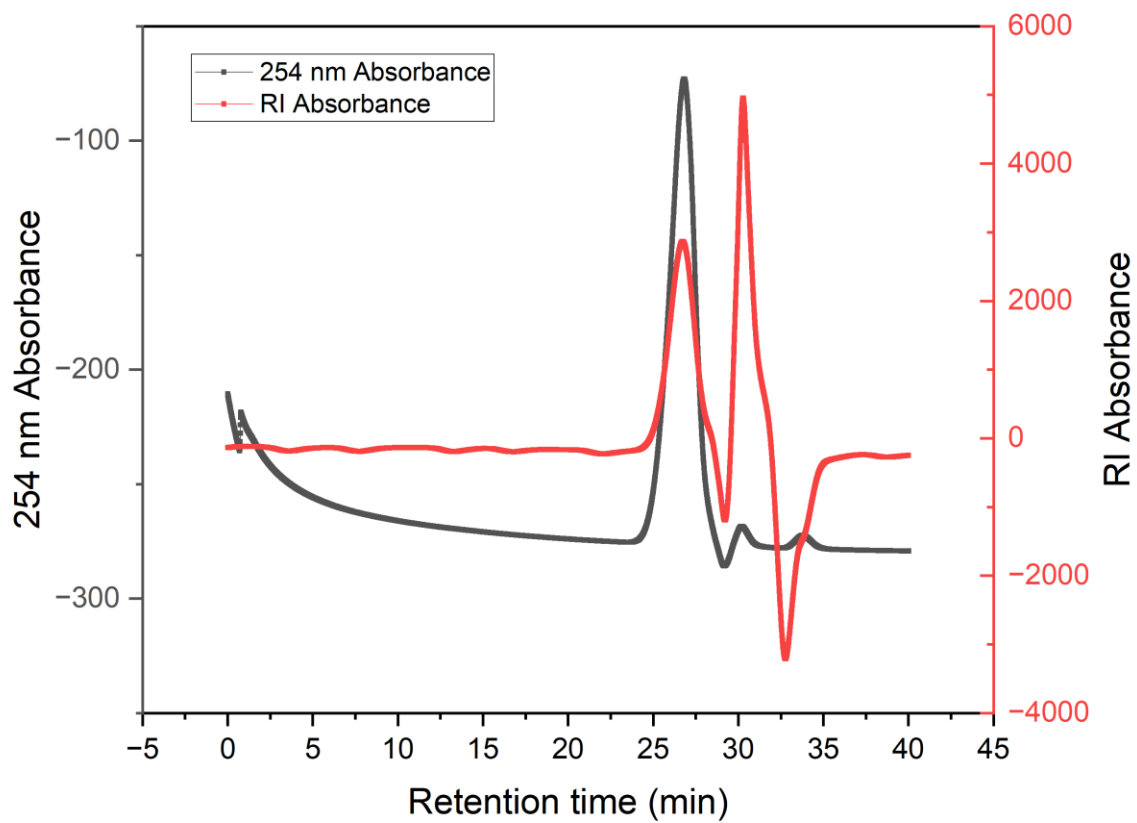
Figure 85. GPC traces of Table 16, entry 9 using RID detection.
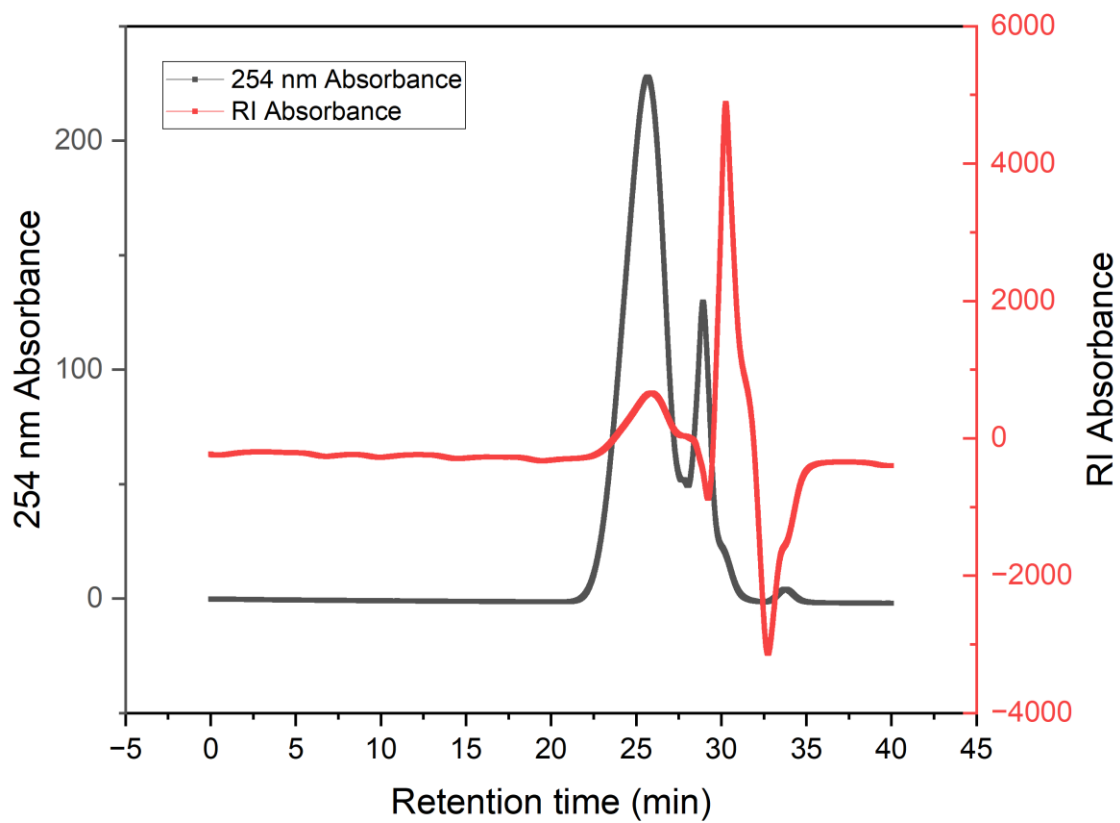
Figure 86. GPC traces of Table 16, entry 10 using RID detection.
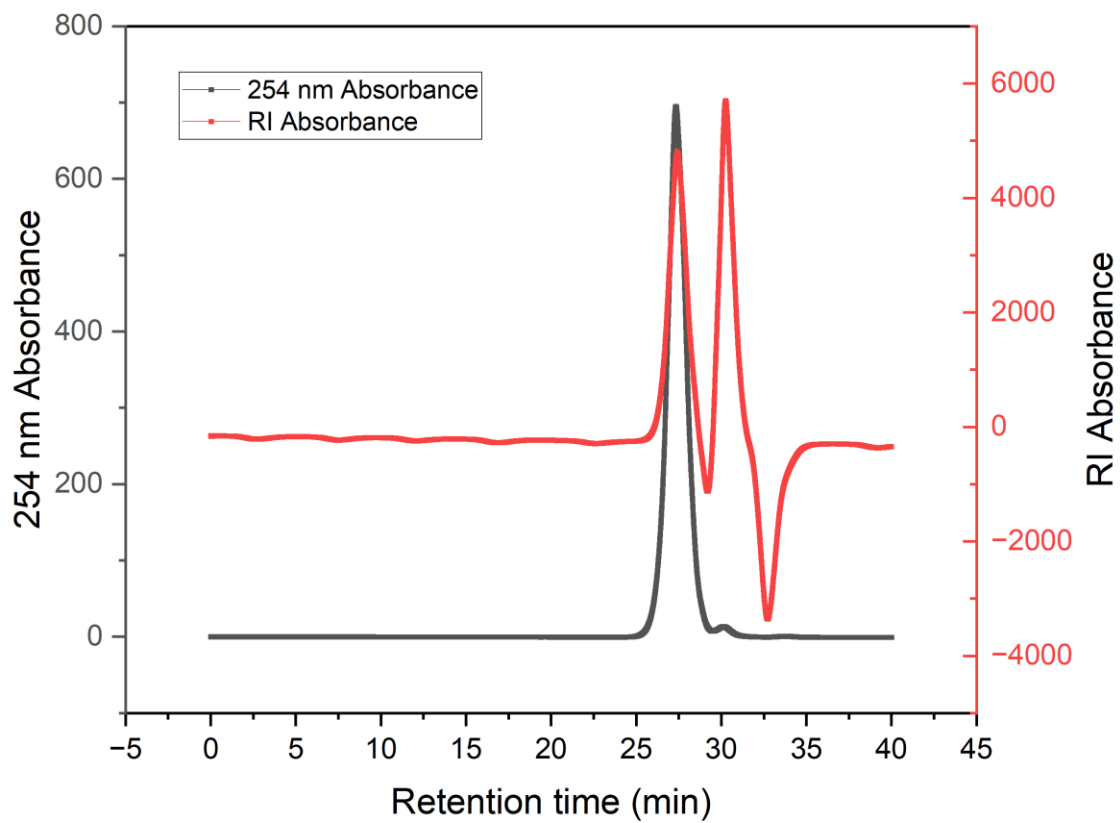
Figure 87. GPC traces of Table 16, entry 11 using RID detection.
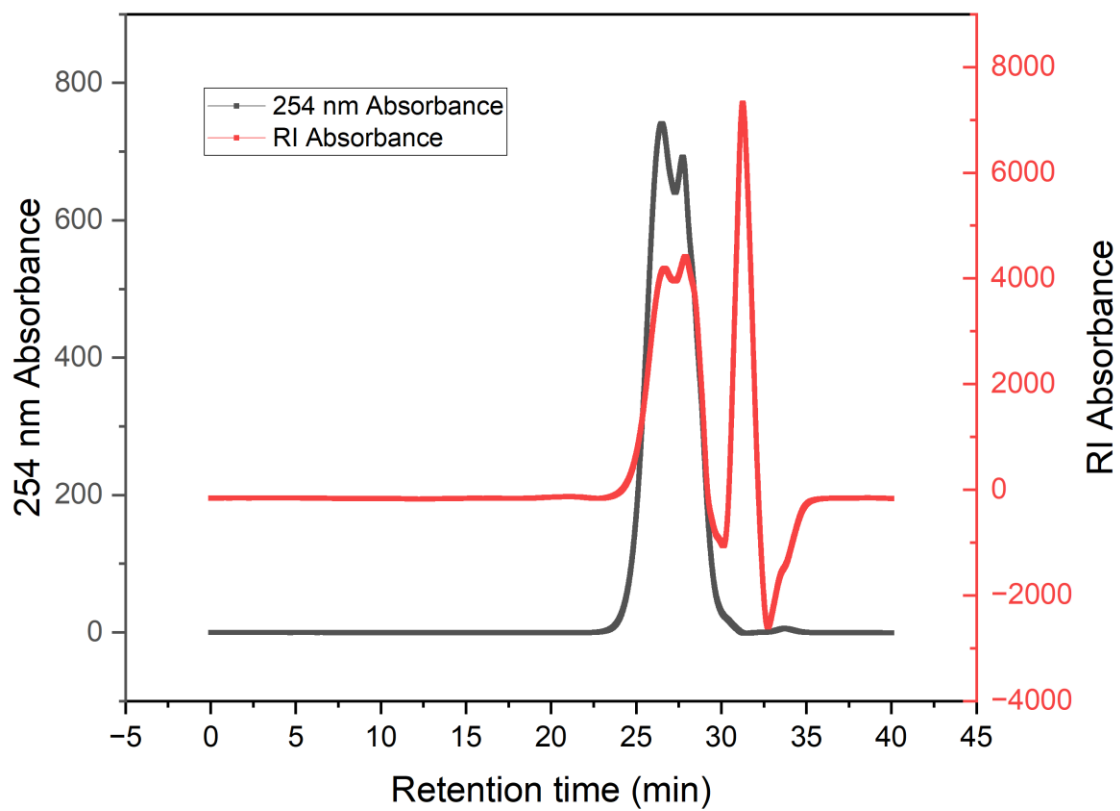
Figure 88. GPC traces of reaction in Table 16, entry 13 using RID detection.
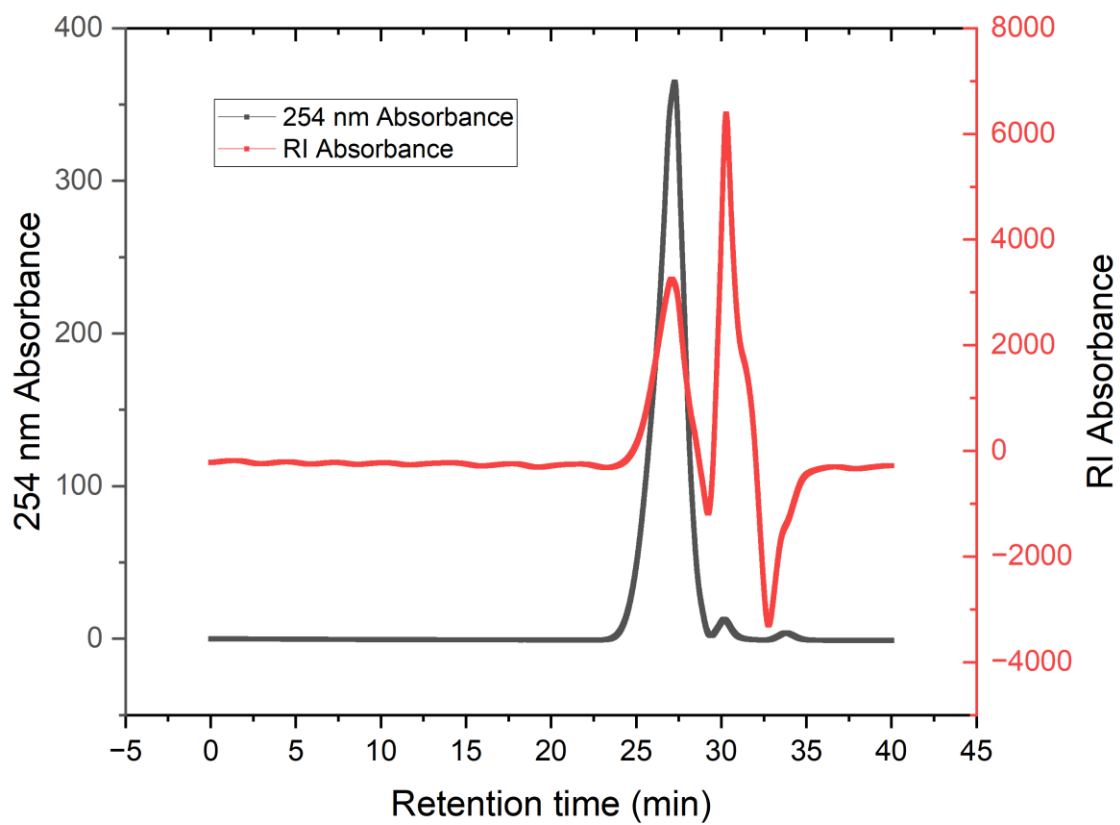
Figure 89. GPC traces of the reaction in Table 16, entry 14 using RID detection.
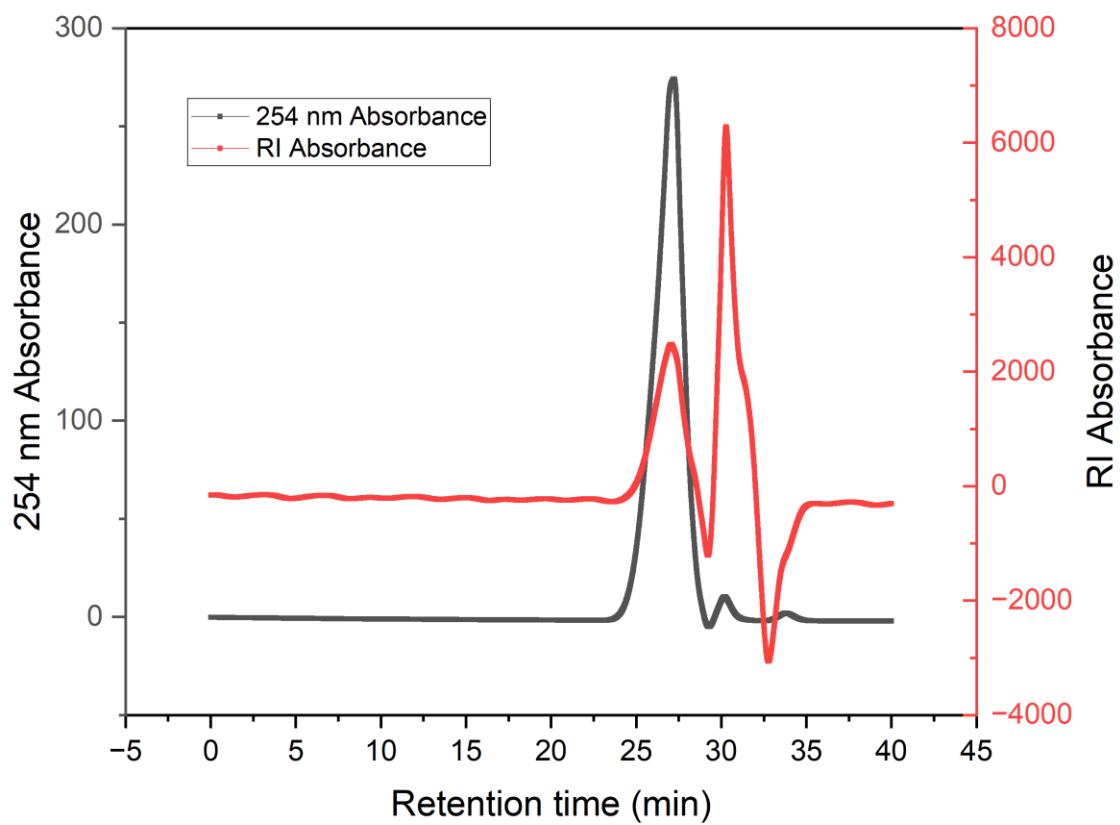
Figure 90. GPC traces of reaction in Table 16, entry 15.

dn/dc: 0.1429 mL/g
Concentration: 1.000 mg/mL
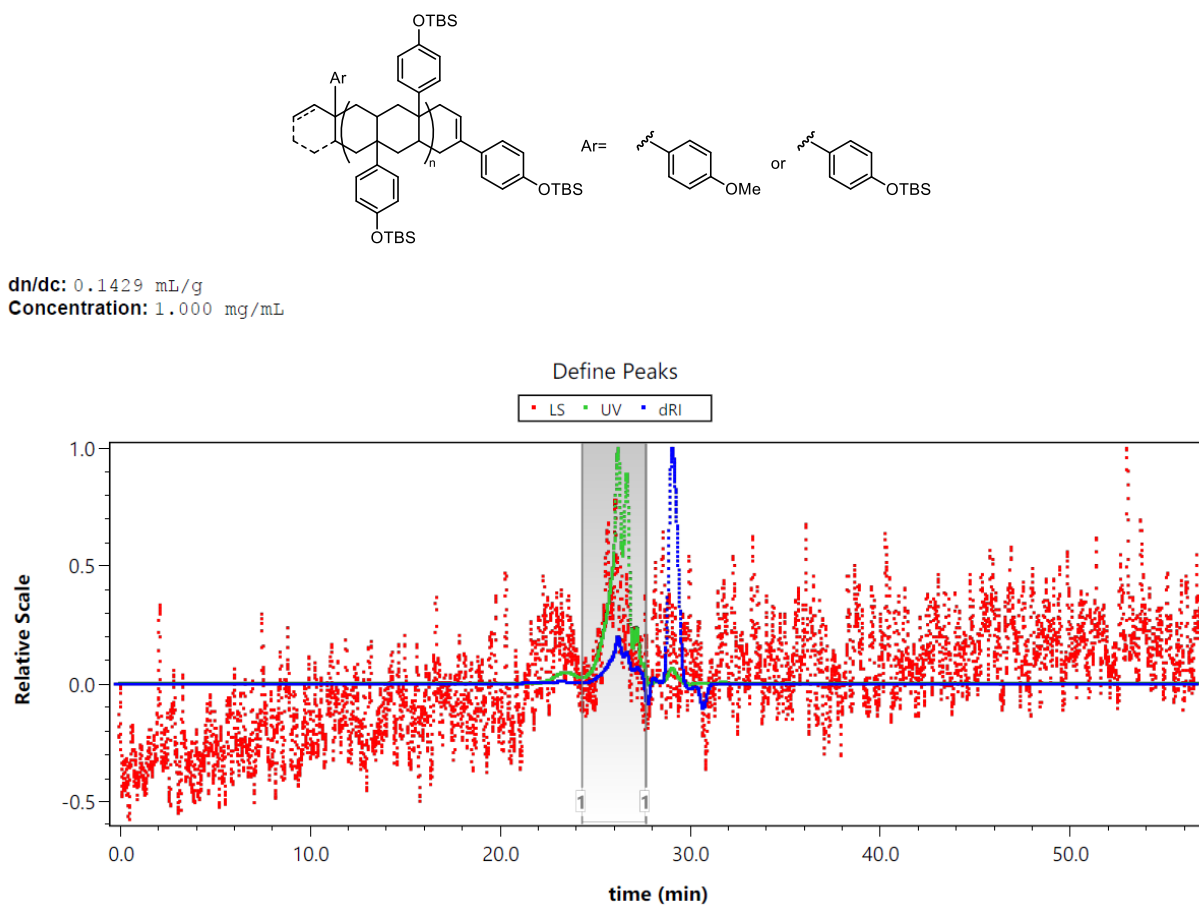
Figure 91. GPC traces of LP-3b measured with a MALS detector.

dn/dc: 0.1450 mL/g
Concentration: 1.000 mg/mL
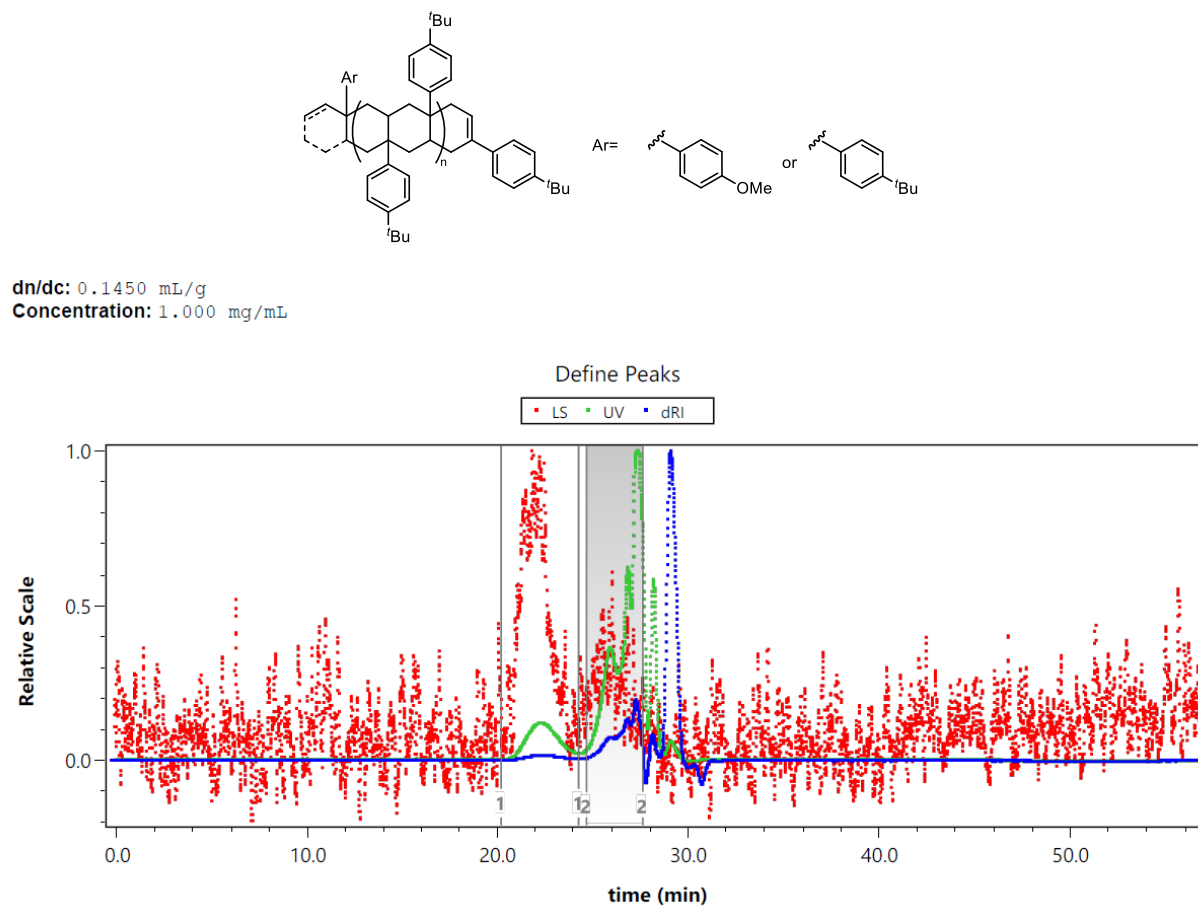
Figure 92. GPC traces of LP-3c measured with a MALS detector.

dn/dc: 0.3967 mL/g
Concentration: 1.000 mg/mL
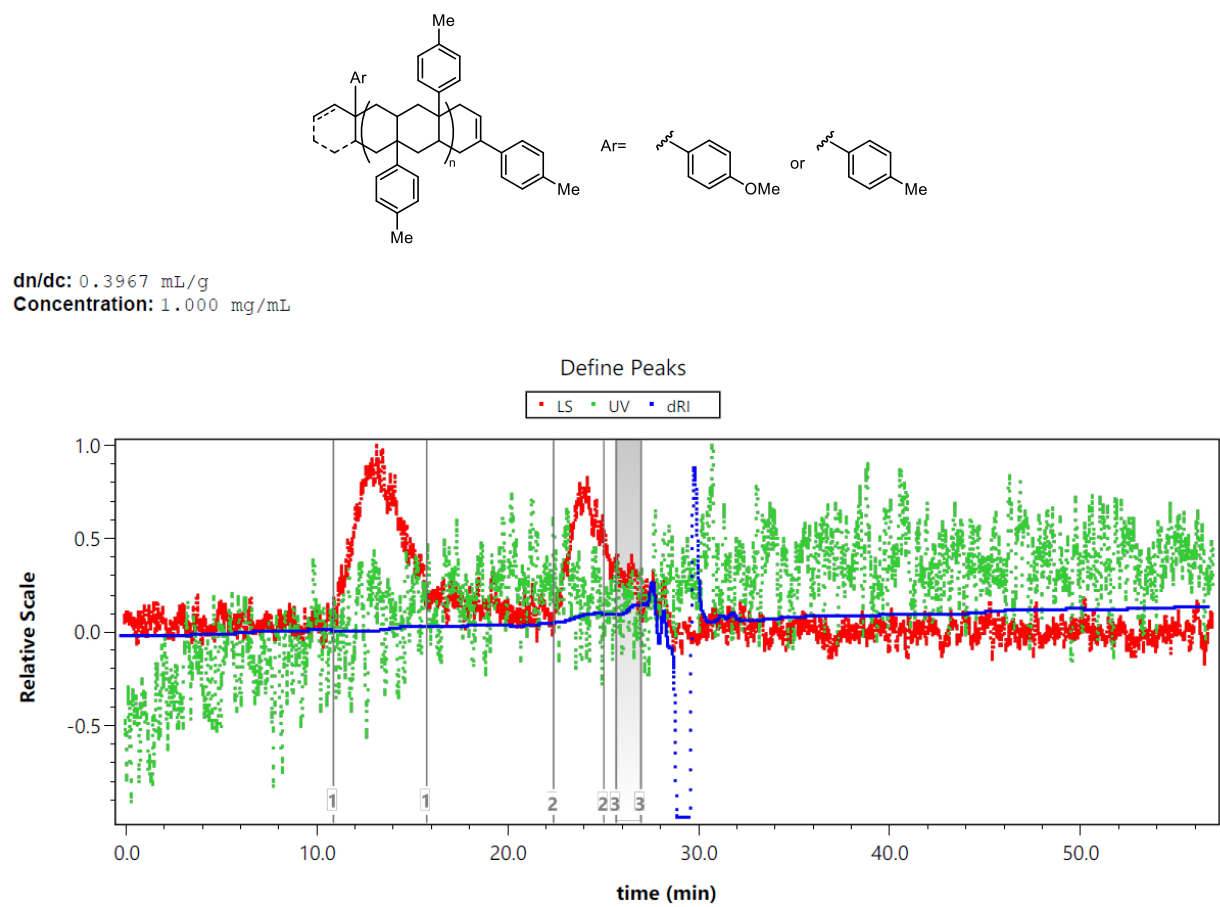
Figure 93. GPC traces of LP-3d using a MALS detector. M_n, M_w, and Đ were determined based on region 2.
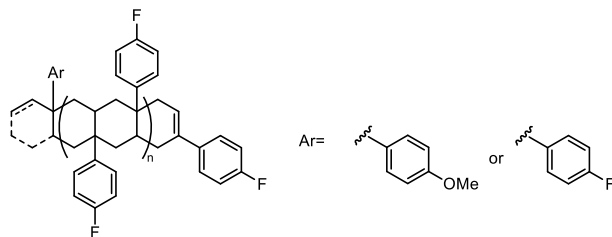
dn/dc: 0.2666 mL/g
Concentration: 1.000 mg/mL
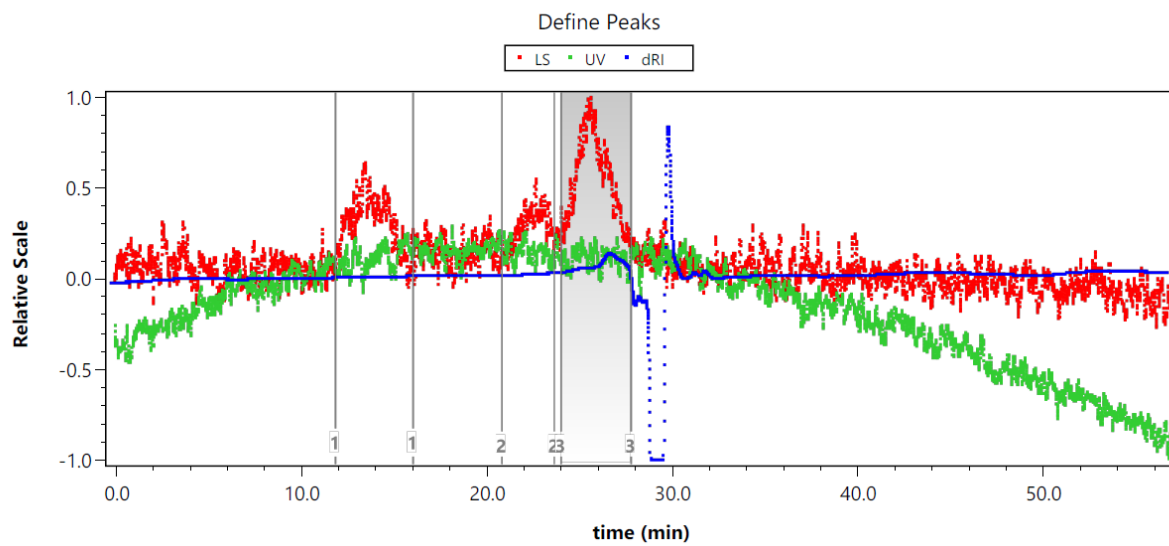
Figure 94. GPC traces of LP-3e using a MALS detector.
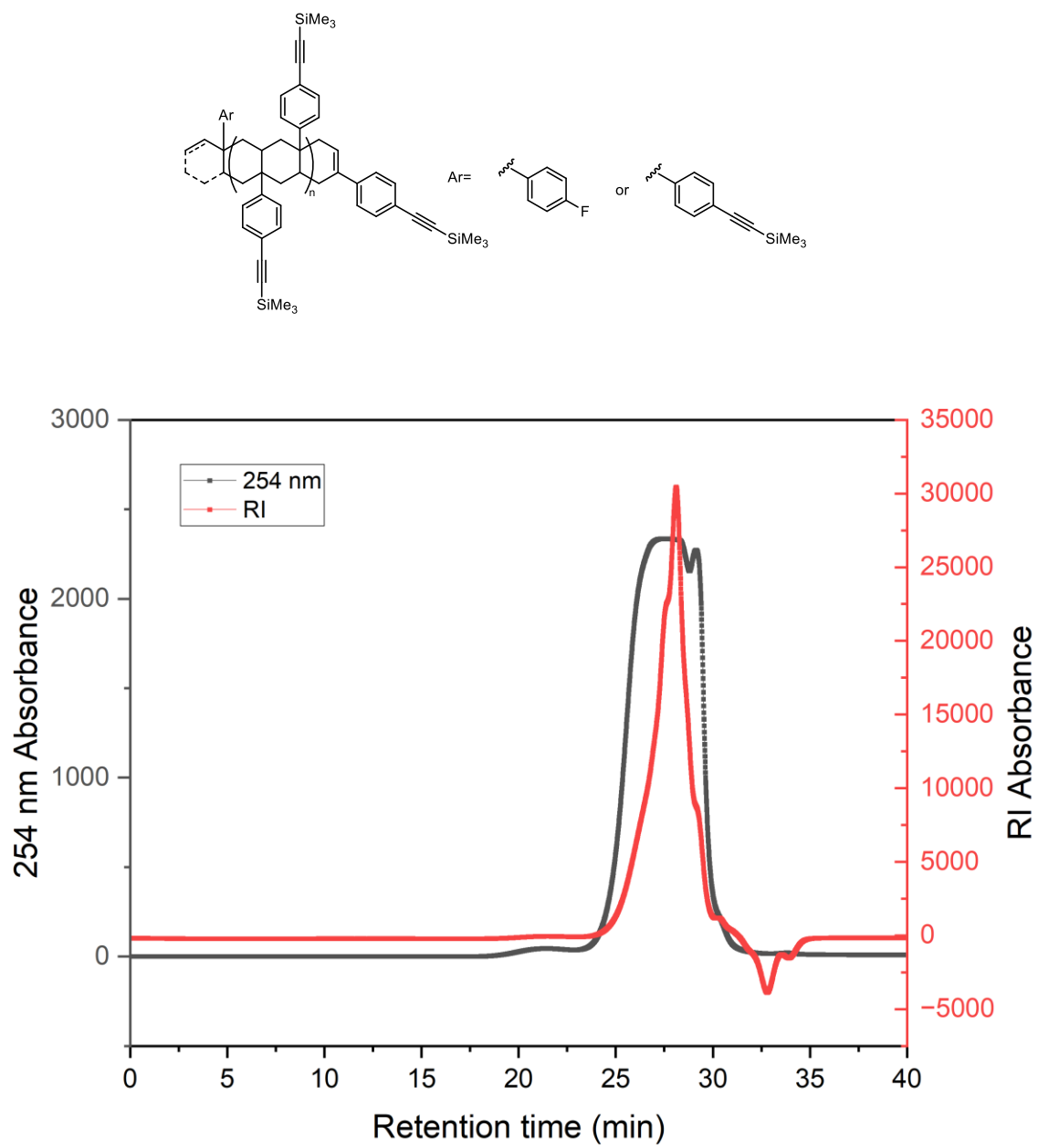
Figure 95. GPC of LP-3f using RI detection.

dn/dc: 0.1013 mL/g
Concentration: 1.000 mg/mL
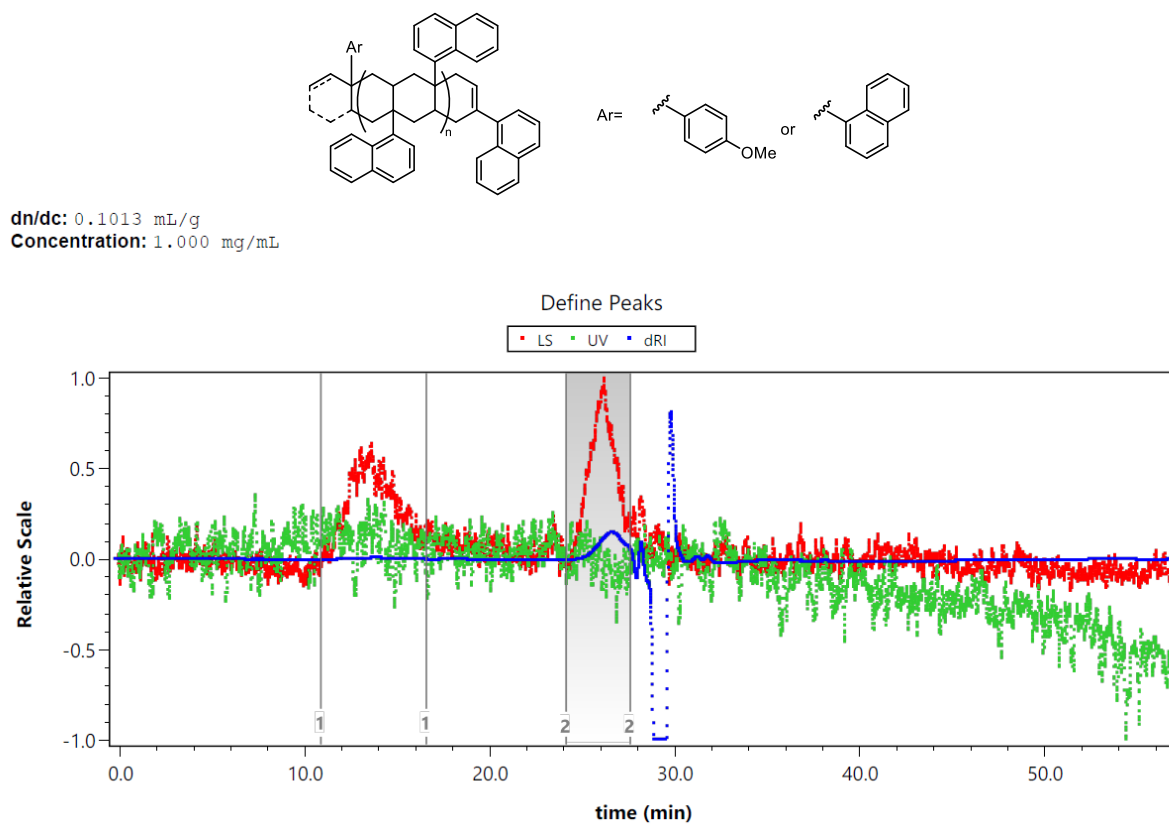
Figure 96. GPC traces of LP-3g using a MALS detector.
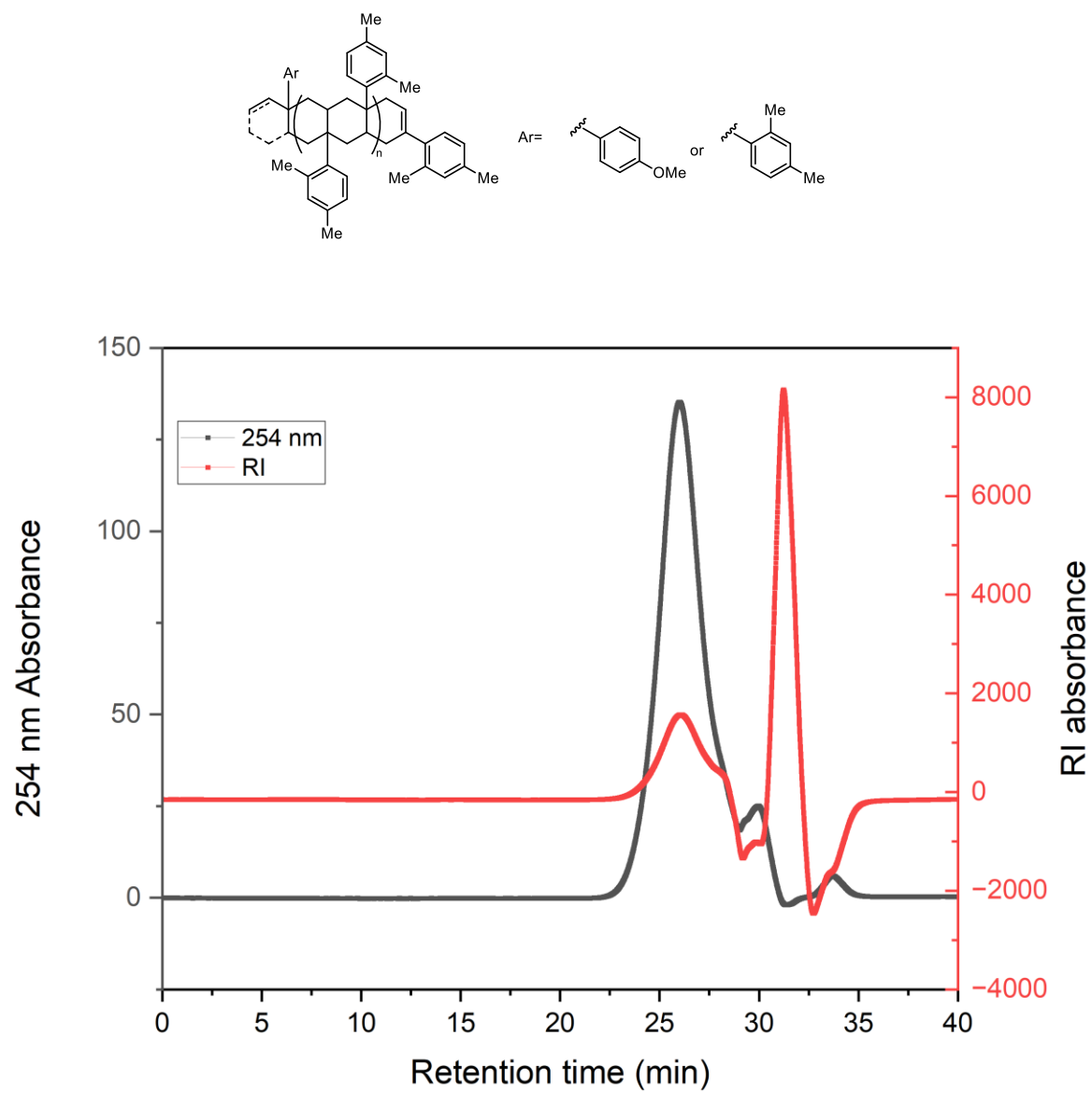
Figure 97. GPC of LP-3h using RID detection.

dn/dc: 0.3462 mL/g
Concentration: 1.000 mg/mL
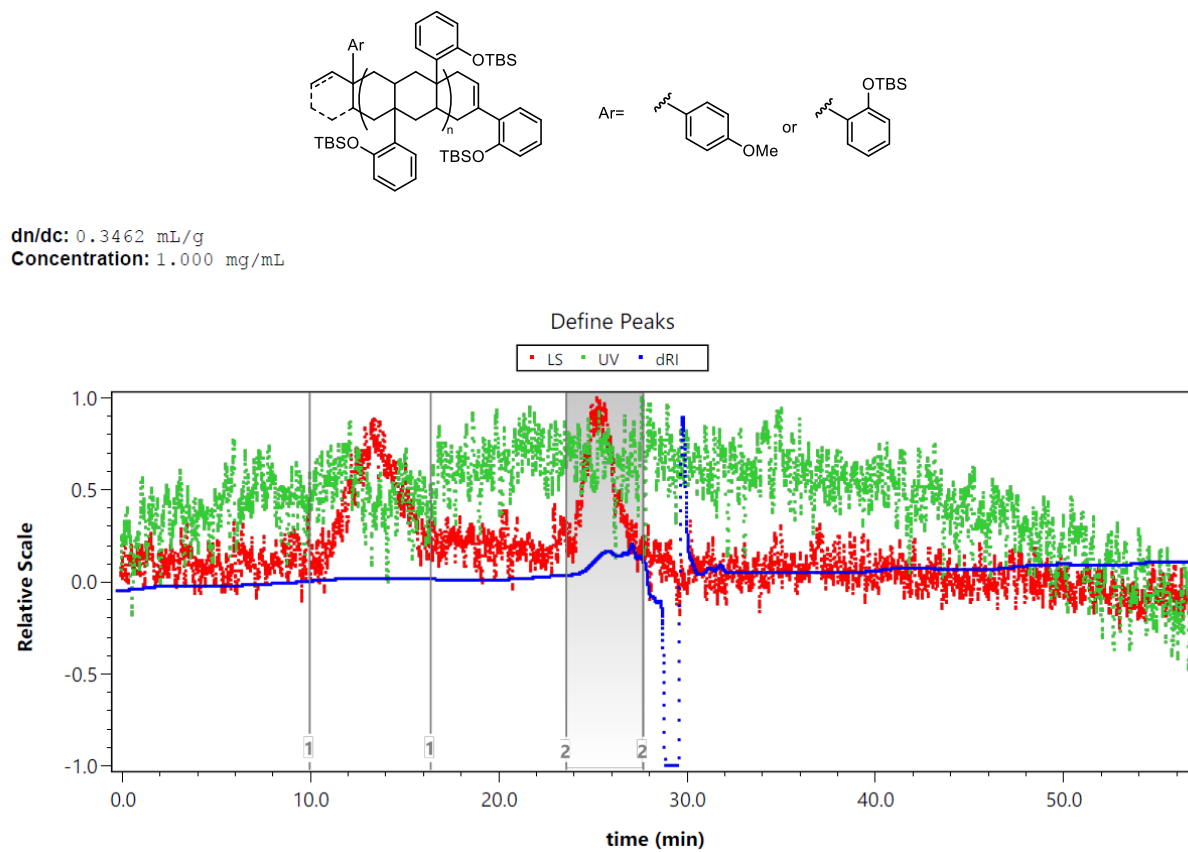
Figure 98. GPC traces of LP-3i using a MALS detector.

dn/dc: 0.3407 mL/g
Concentration: 1.000 mg/mL
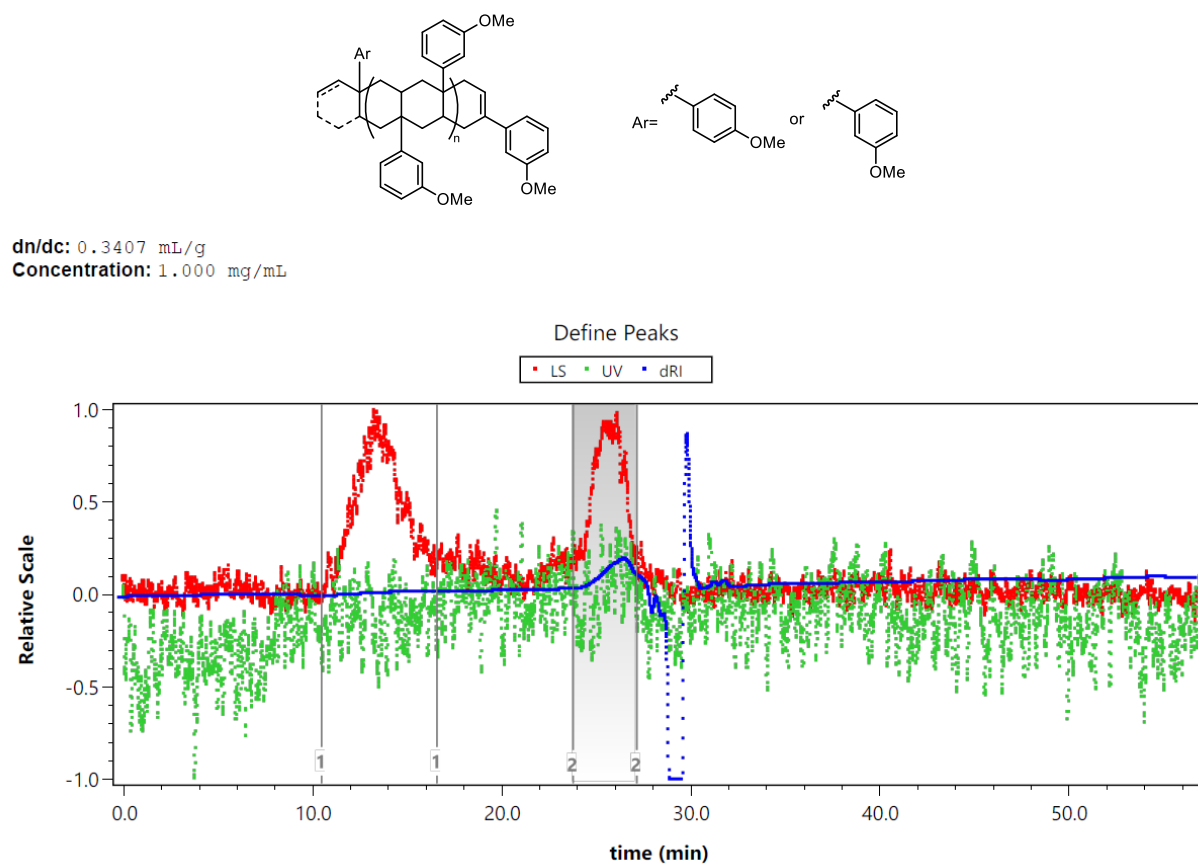
Figure 99. GPC traces of LP-3*J* using a MALS detector.

dn/dc: 0.2230 mL/g
Concentration: 1.000 mg/mL
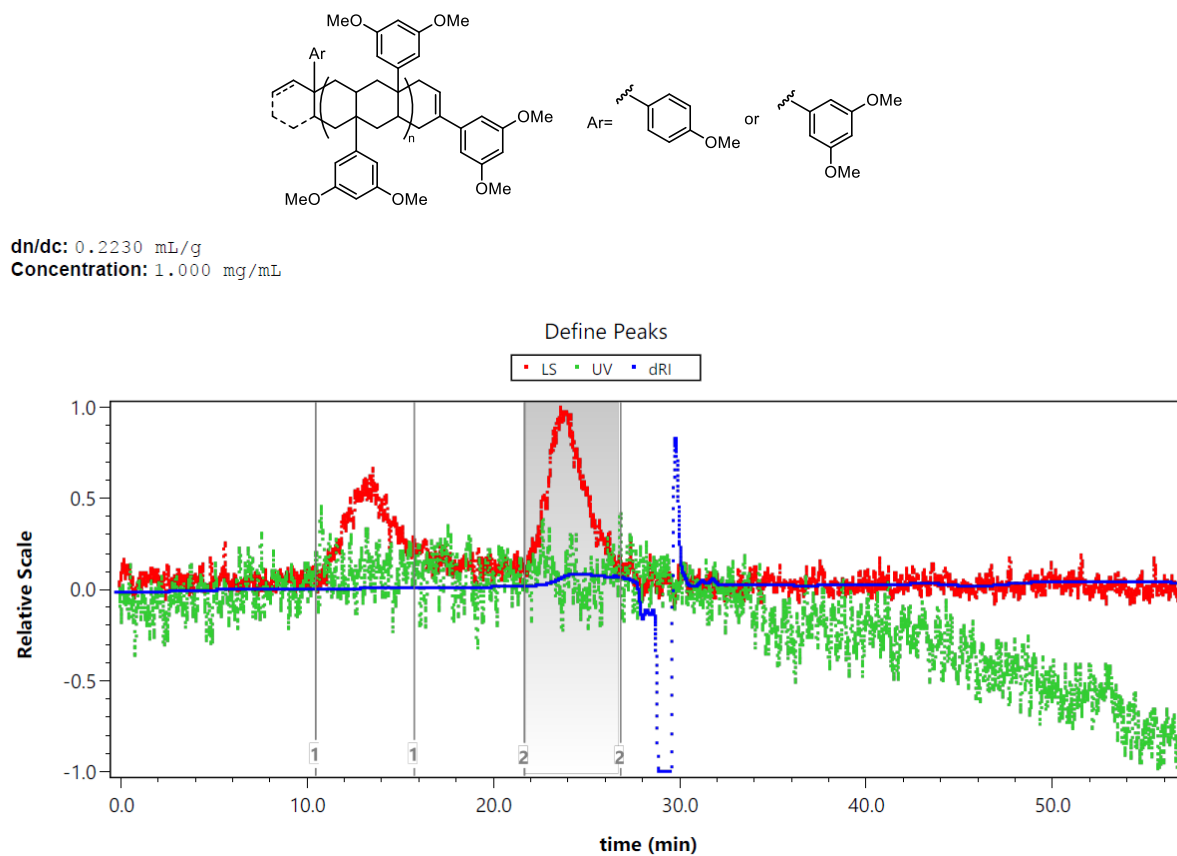
Figure 100. GPC traces of LP-3k using a MALS detector.
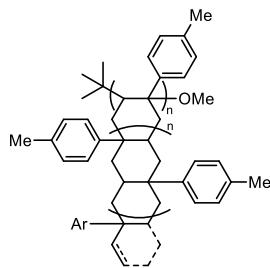
dn/dc: 0.0910 mL/g
Concentration: 1.000 mg/mL
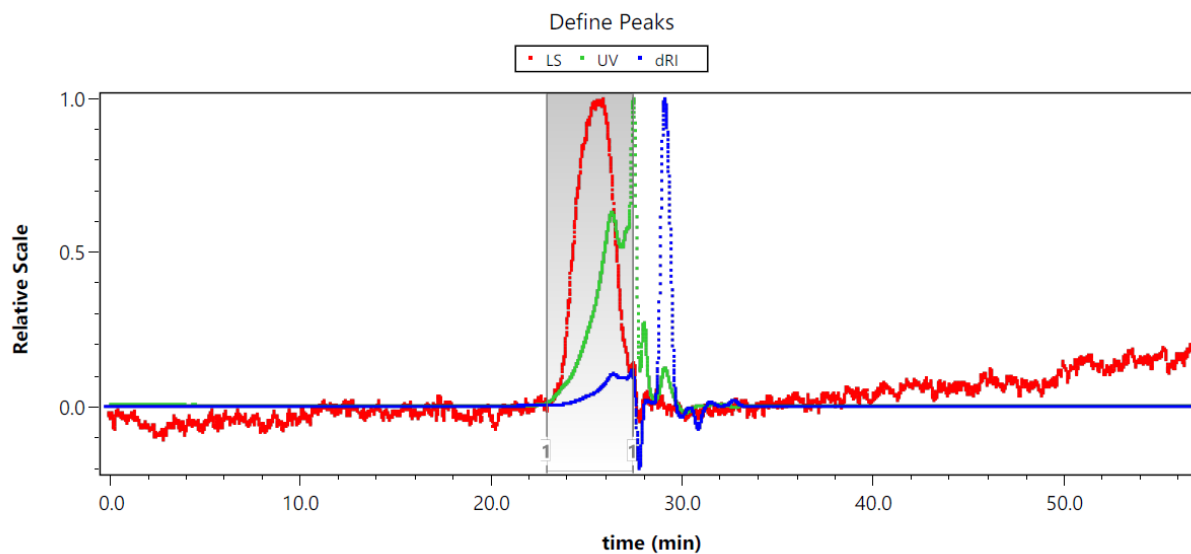
Figure 101. GPC traces of LP-3d-ext using a MALS detector.
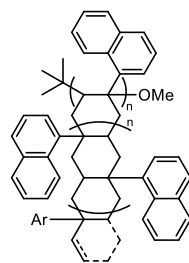
dn/dc: 0.0578 mL/g
Concentration: 1.000 mg/mL
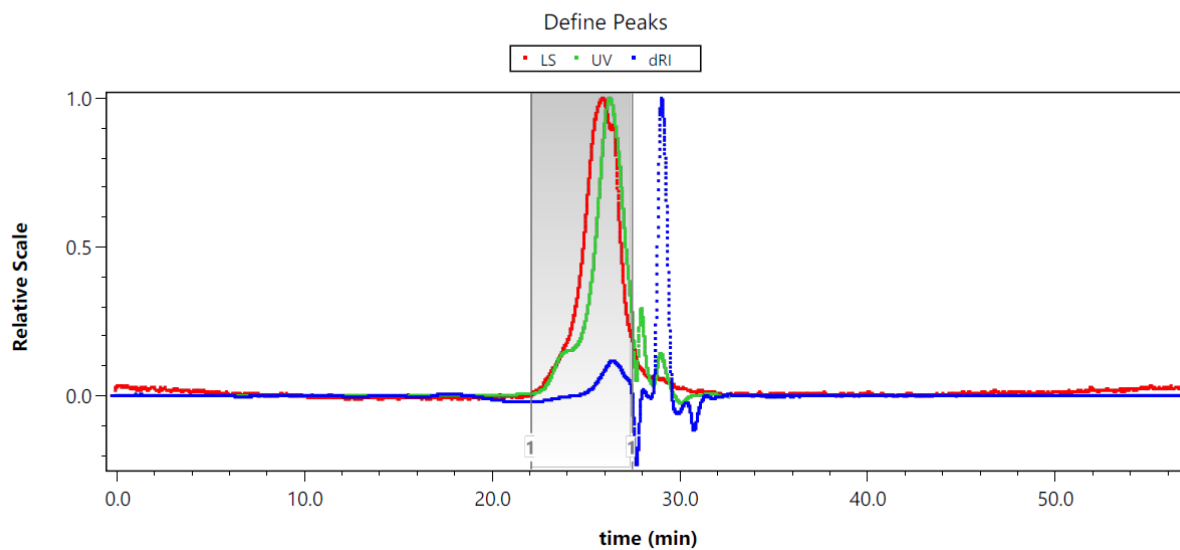
Figure 102. GPC traces of LP-3g-ext using a MALS detector.

dn/dc: 0.1423 mL/g
Concentration: 1.000 mg/mL
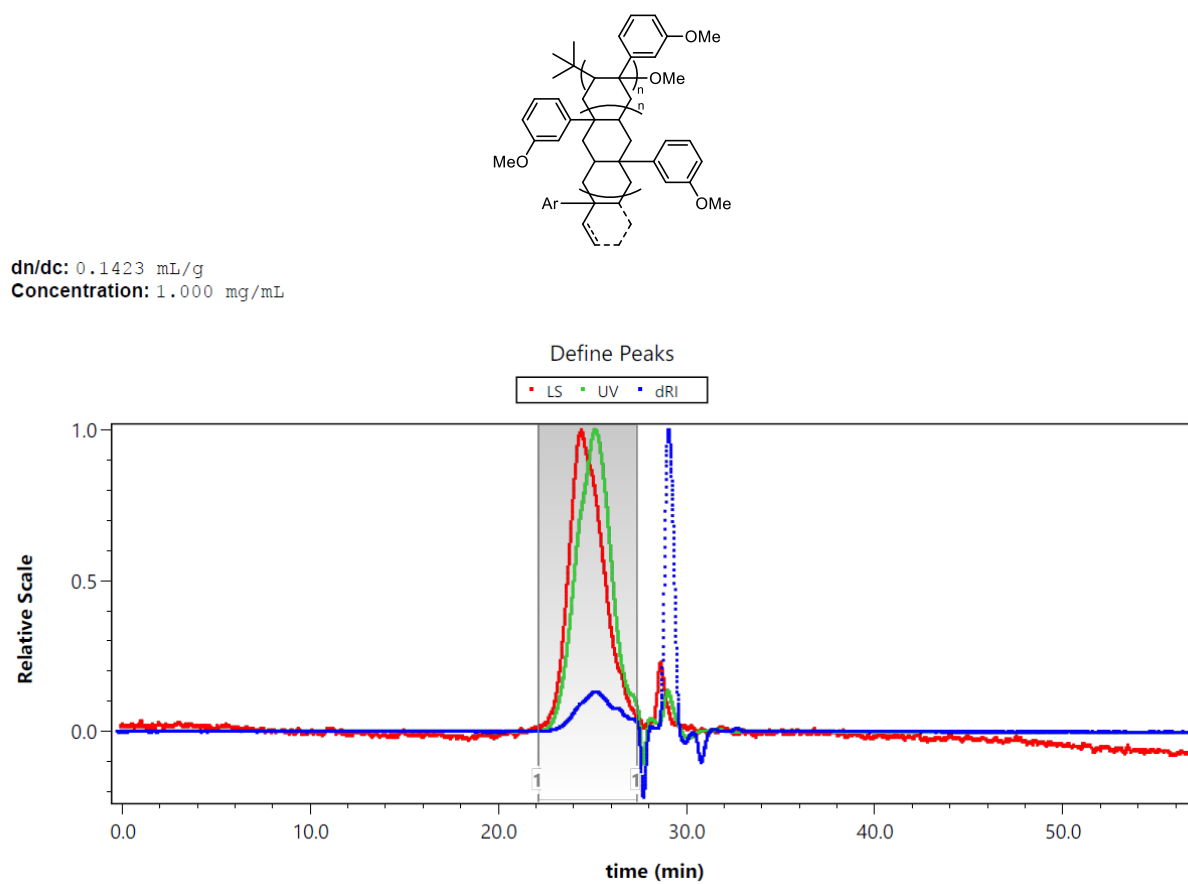
Figure 103. GPC trace of LP-3j-ext using a MALS detector.
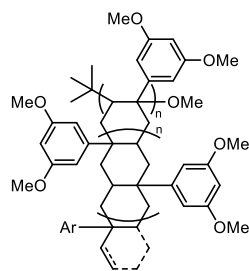
dn/dc: 0.0771 mL/g
Concentration: 1.000 mg/mL
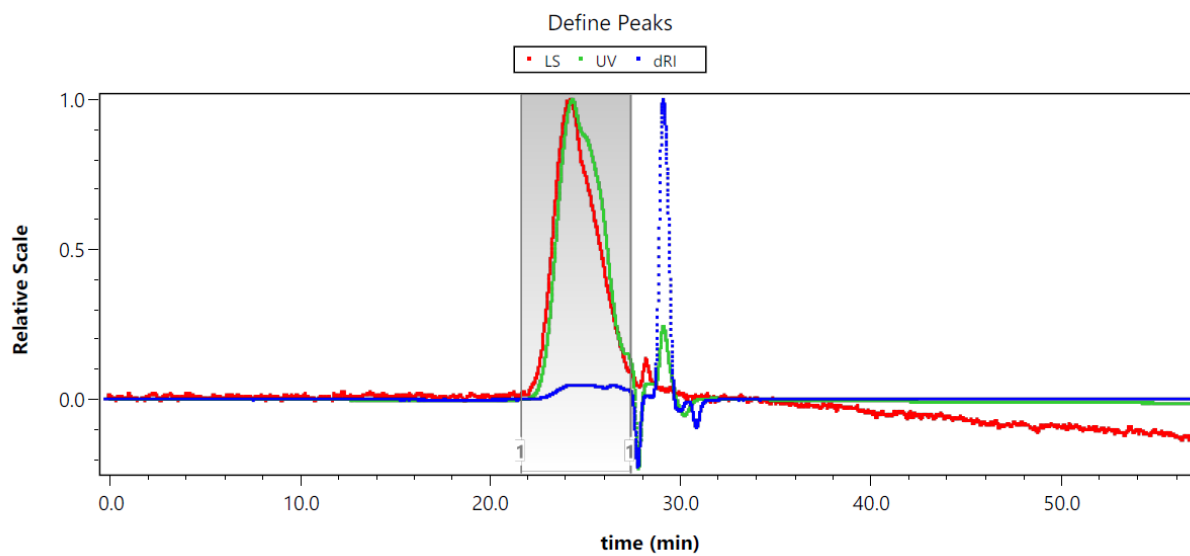
Figure 104. GPC trace of LP-3k-ext using a MALS detector.

NMR Spectra

(4-bromophenoxy)(*tert*-butyl)dimethylsilane
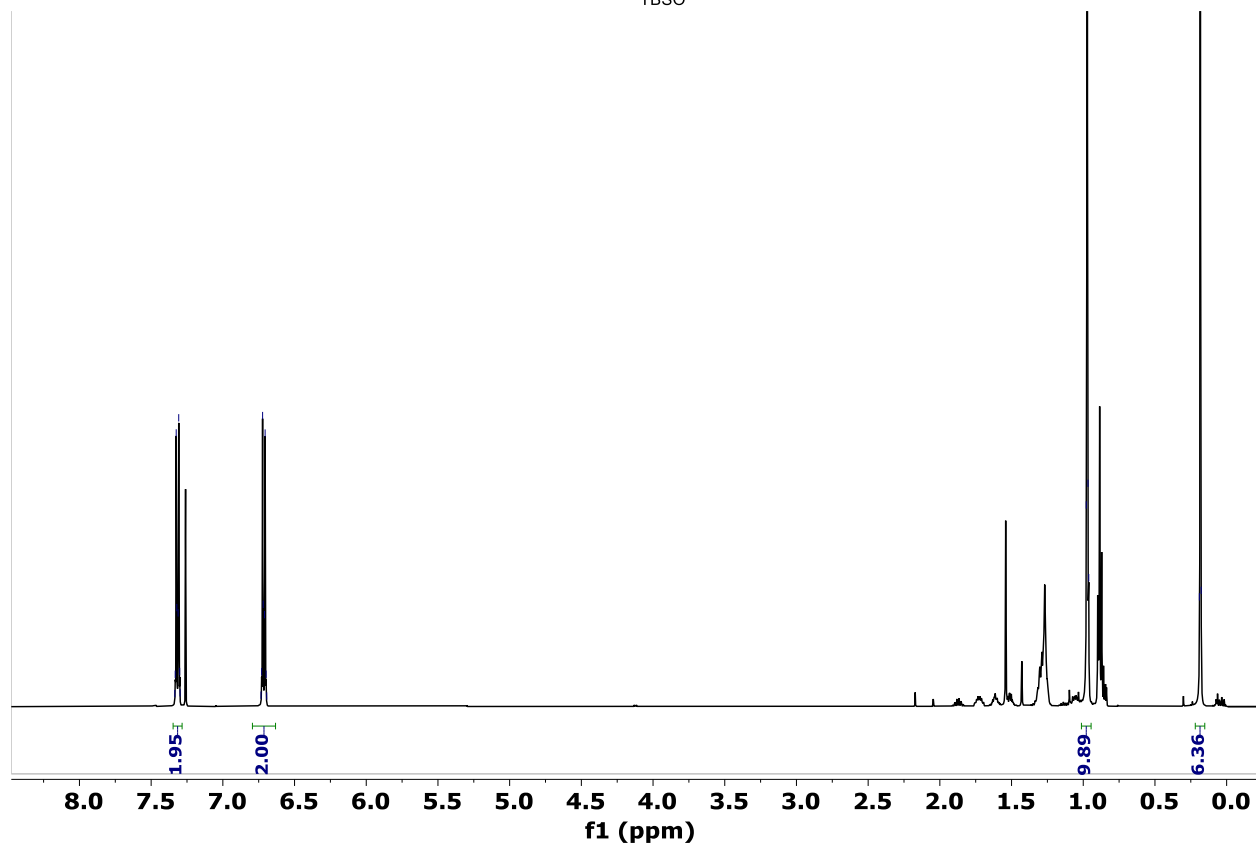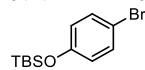
^{1}H NMR, CDCl$_3$-*d*

4'-methoxy-2,3,4,5-tetrahydro-1,1'-biphenyl (1)
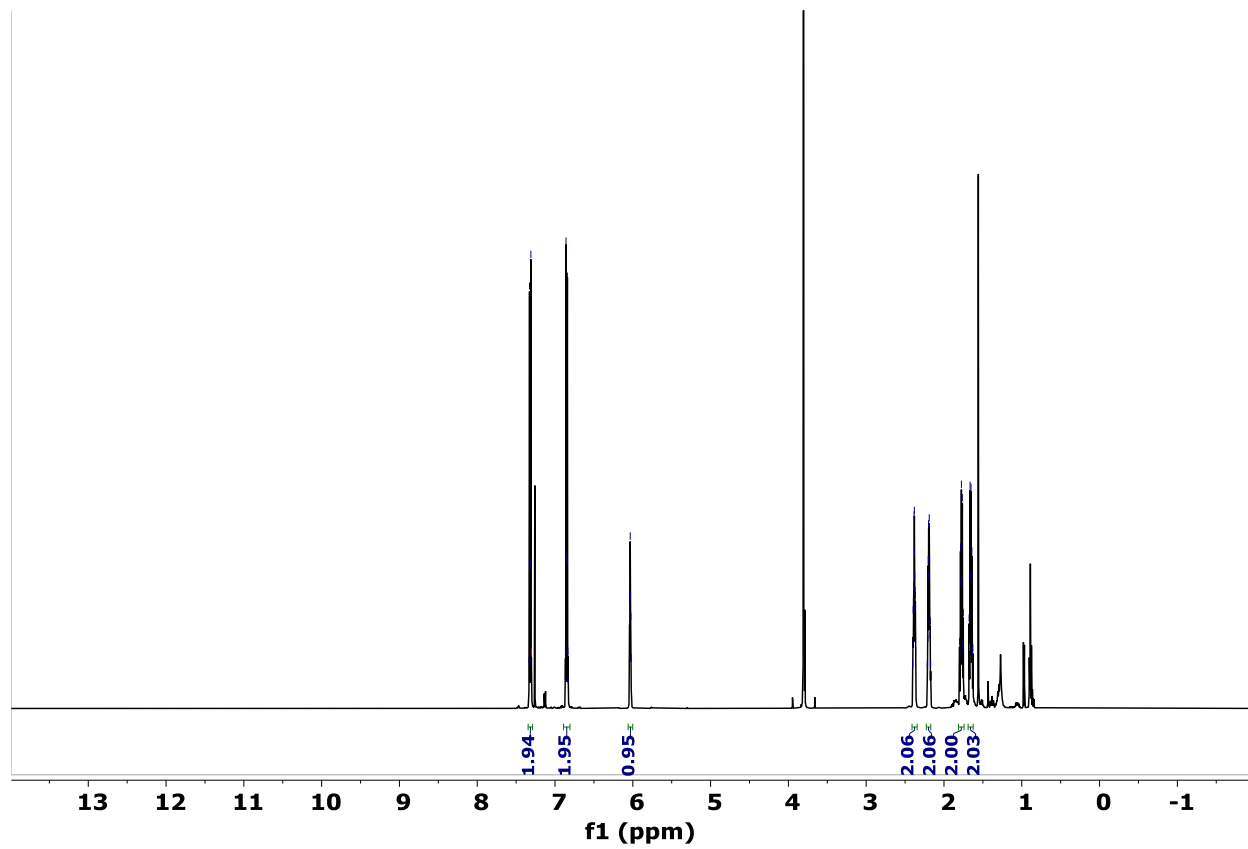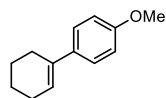
^{1}H NMR, CDCl$_3$-*d*

2,3,4,5-tetrahydro-1,1'-biphenyl
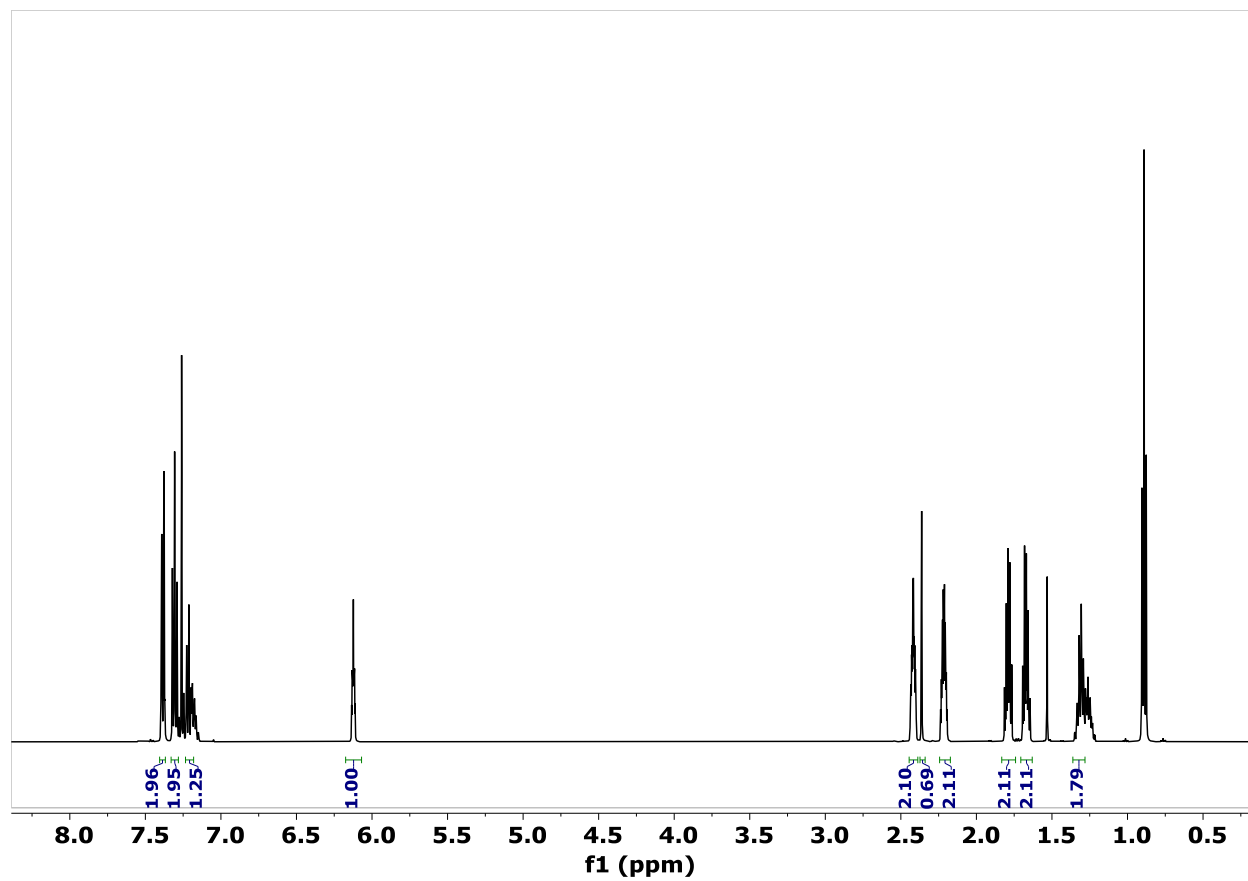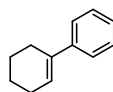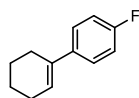

¹H NMR, CDCl₃-*d*

4'-methyl-2,3,4,5-tetrahydro-1,1'-biphenyl
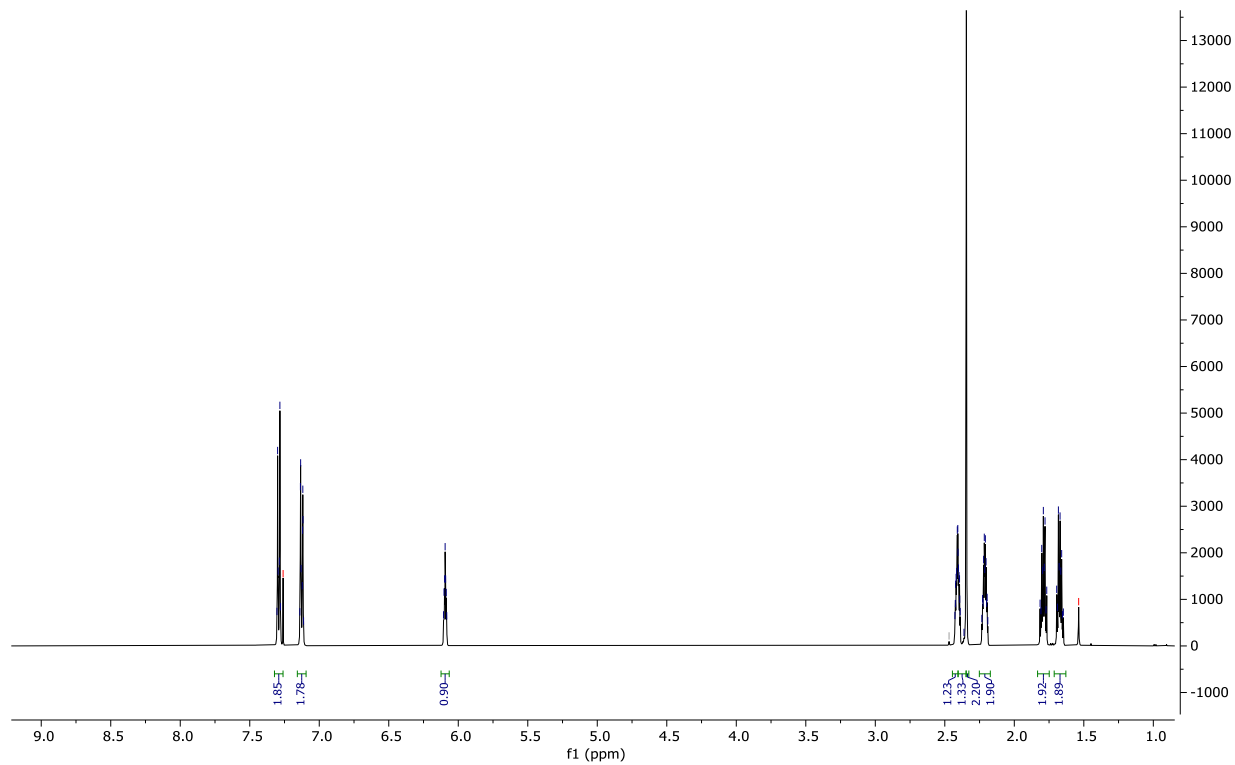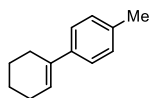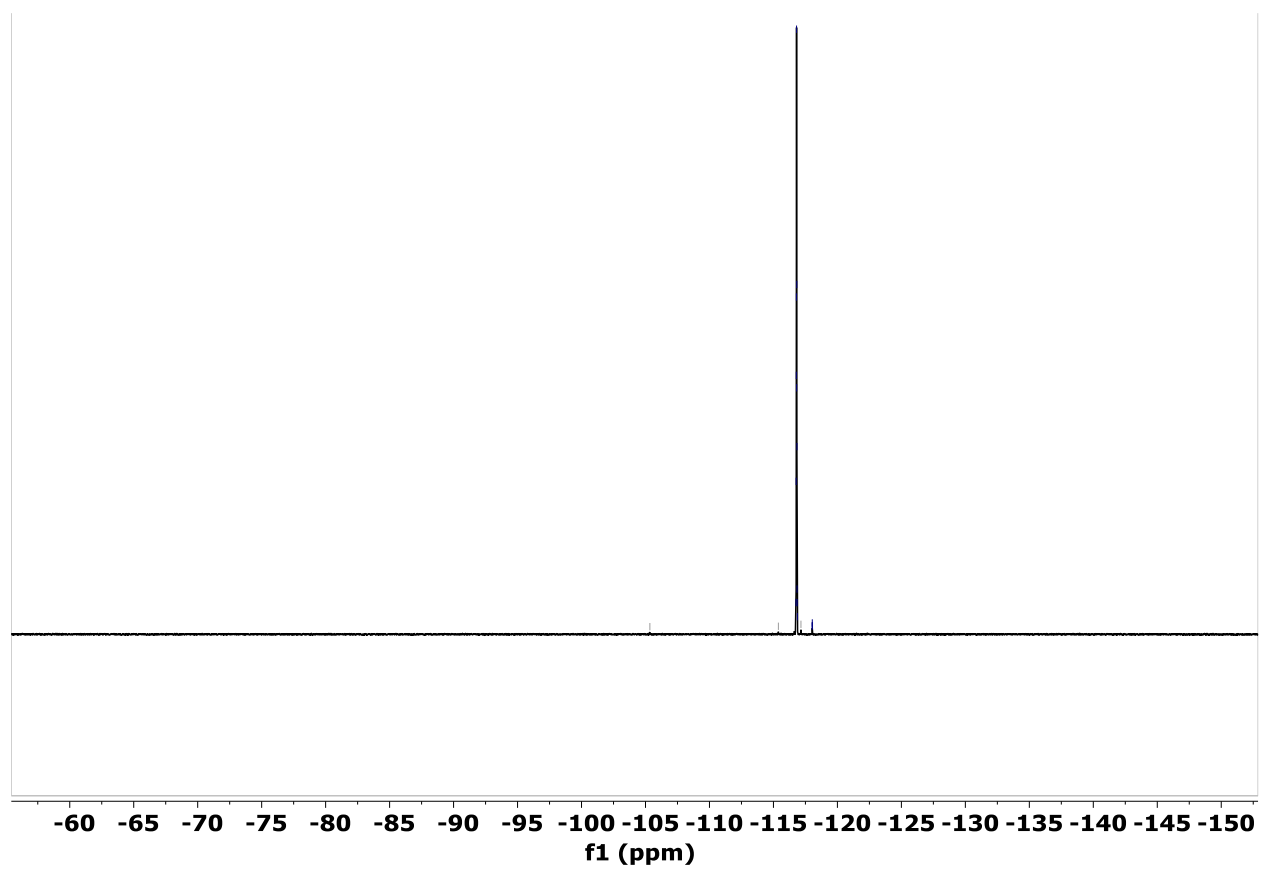

¹H NMR, CDCl₃-*d*

4'-(*tert*-butyl)-2,3,4,5-tetrahydro-1,1'-biphenyl
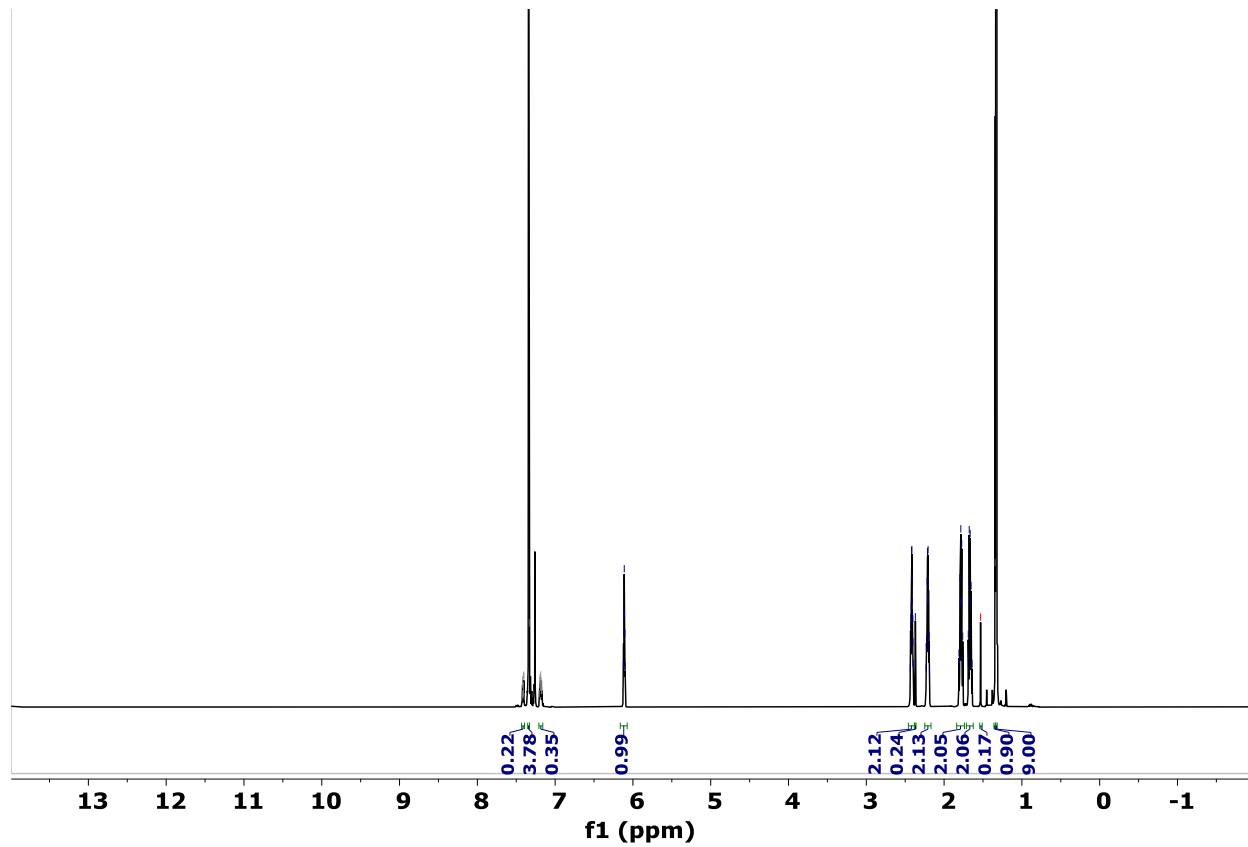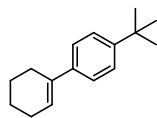
¹H NMR, CDCl₃-*d*

4'-fluoro-2,3,4,5-tetrahydro-1,1'-biphenyl
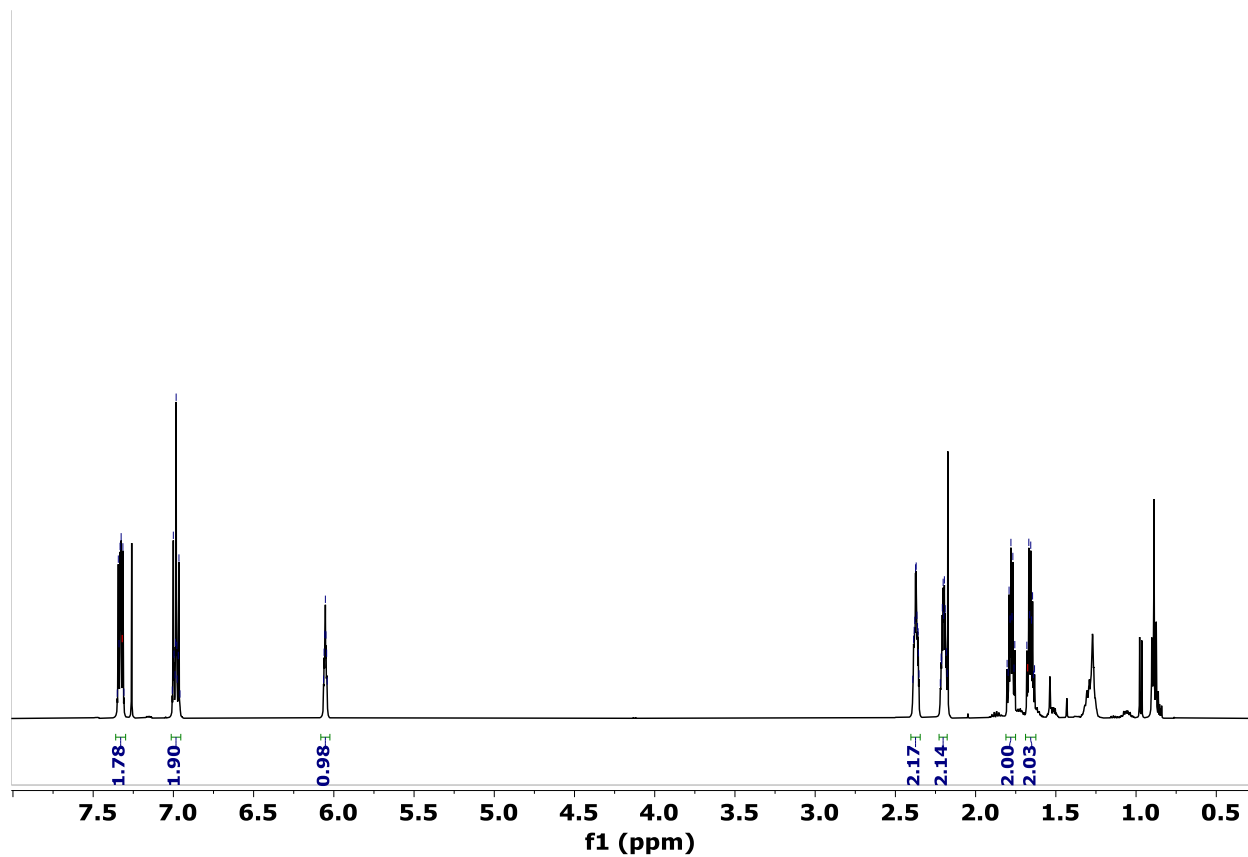
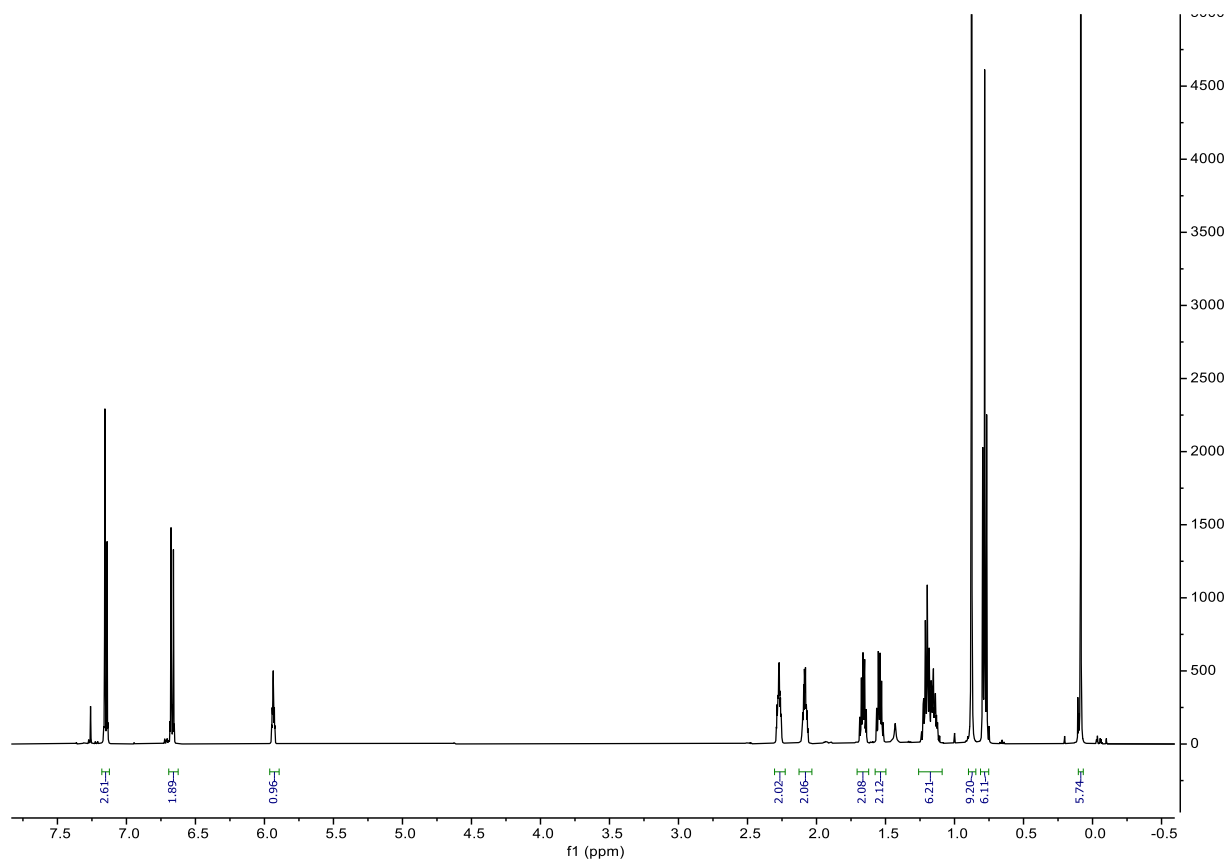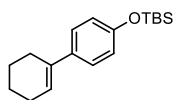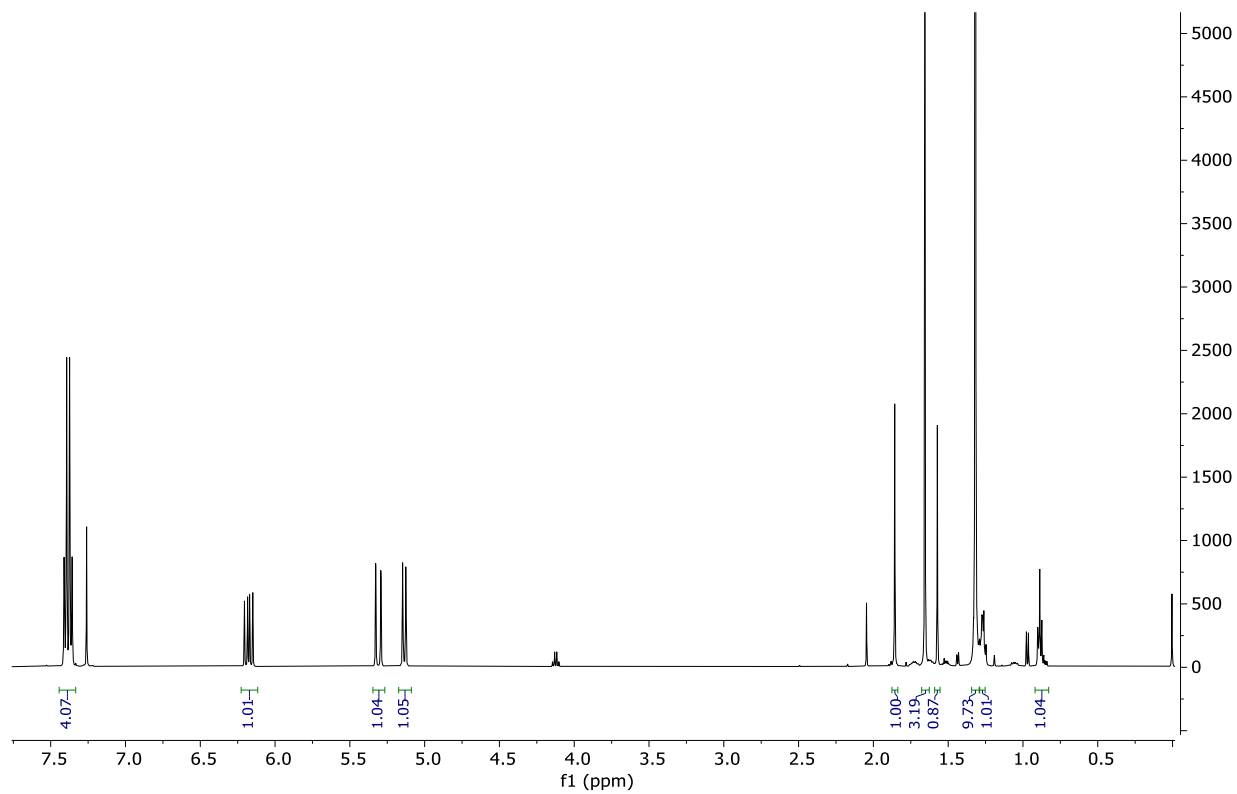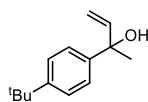1H NMR, CDCl$_3$-*d*

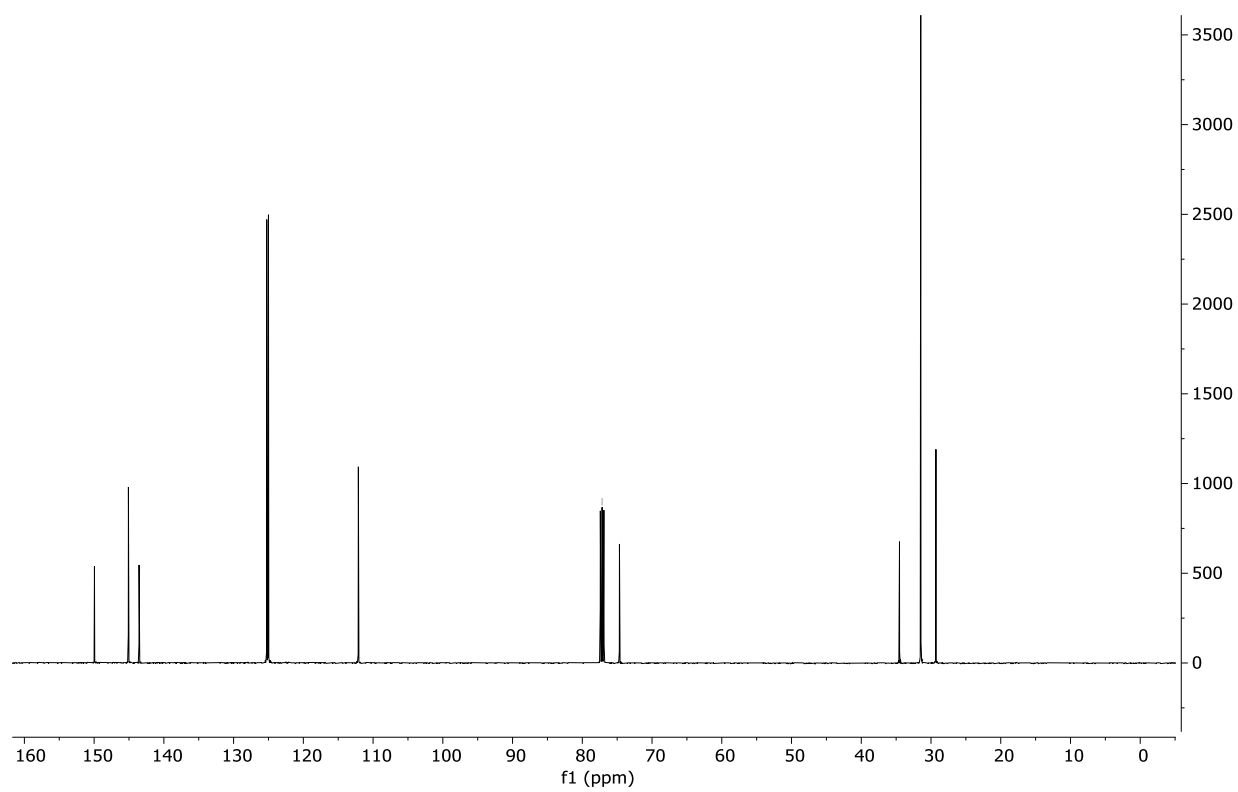^{19}F NMR, CDCl$_3$-*d*

4'-(tert-butyl)-2,3,4,5-tetrahydro-1,1'-biphenyl

^{1}H NMR, CDCl$_3$-*d*

2-(4-(tert-butyl)phenyl)but-3-en-2-ol

¹H NMR, CDCl₃-*d*

^{13}C NMR, CDCl$_3$-*d*

1-(4-((tert-butyldimethylsilyl)oxy)phenyl)ethan-1-one
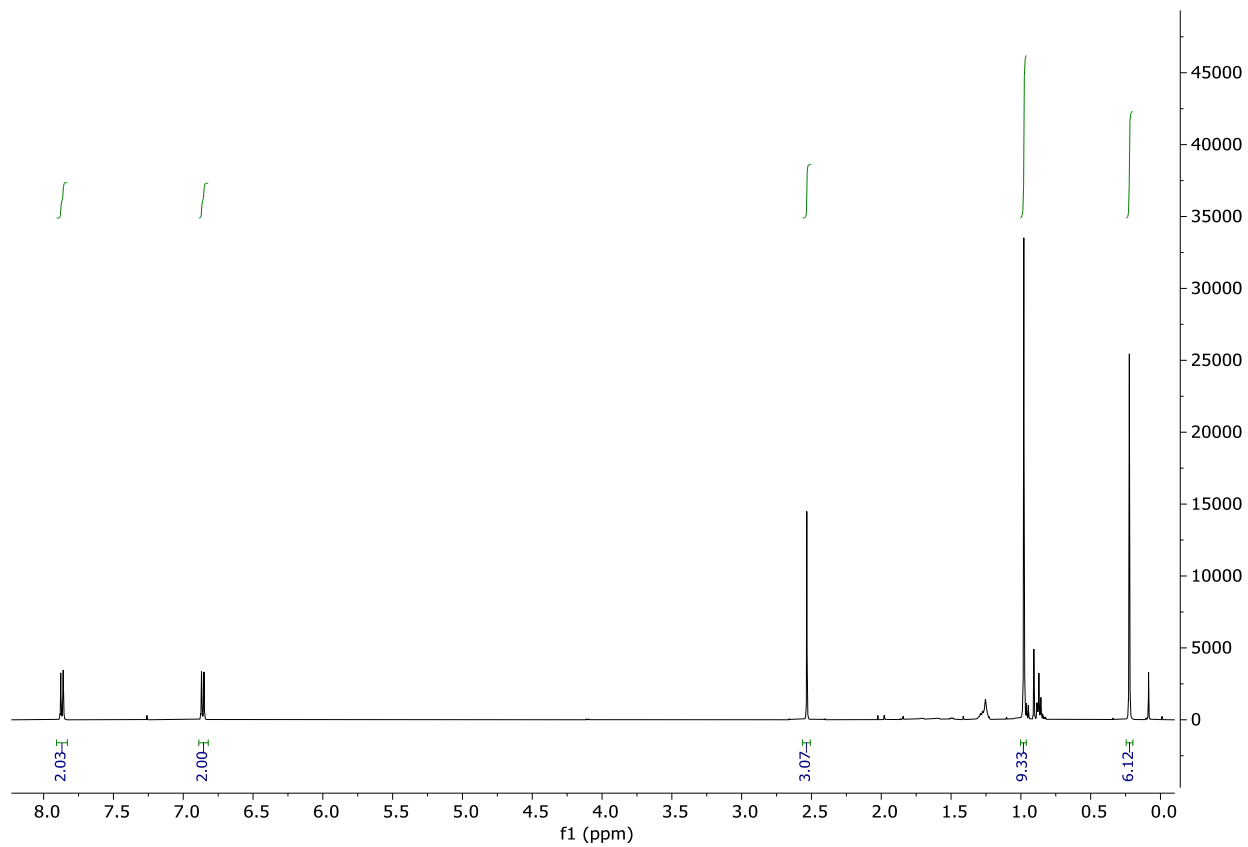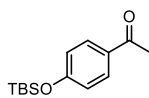
^{1}H NMR, CDCl$_3$-*d*

1-(2-((tert-butyldimethylsilyl)oxy)phenyl)ethan-1-one
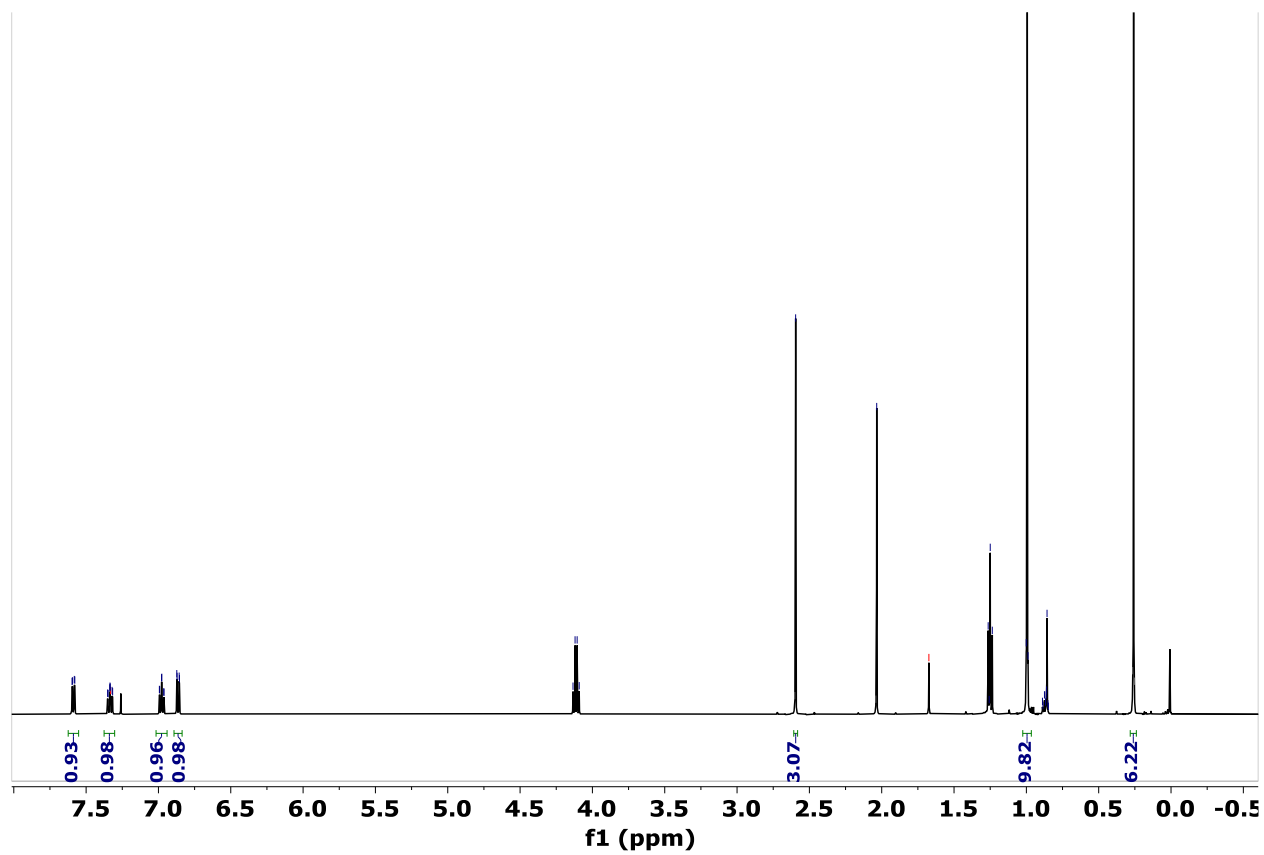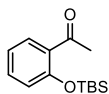
^{1}H NMR, CDCl$_3$-d

2-(4-((tert-butyldimethylsilyl)oxy)phenyl)but-3-en-2-ol
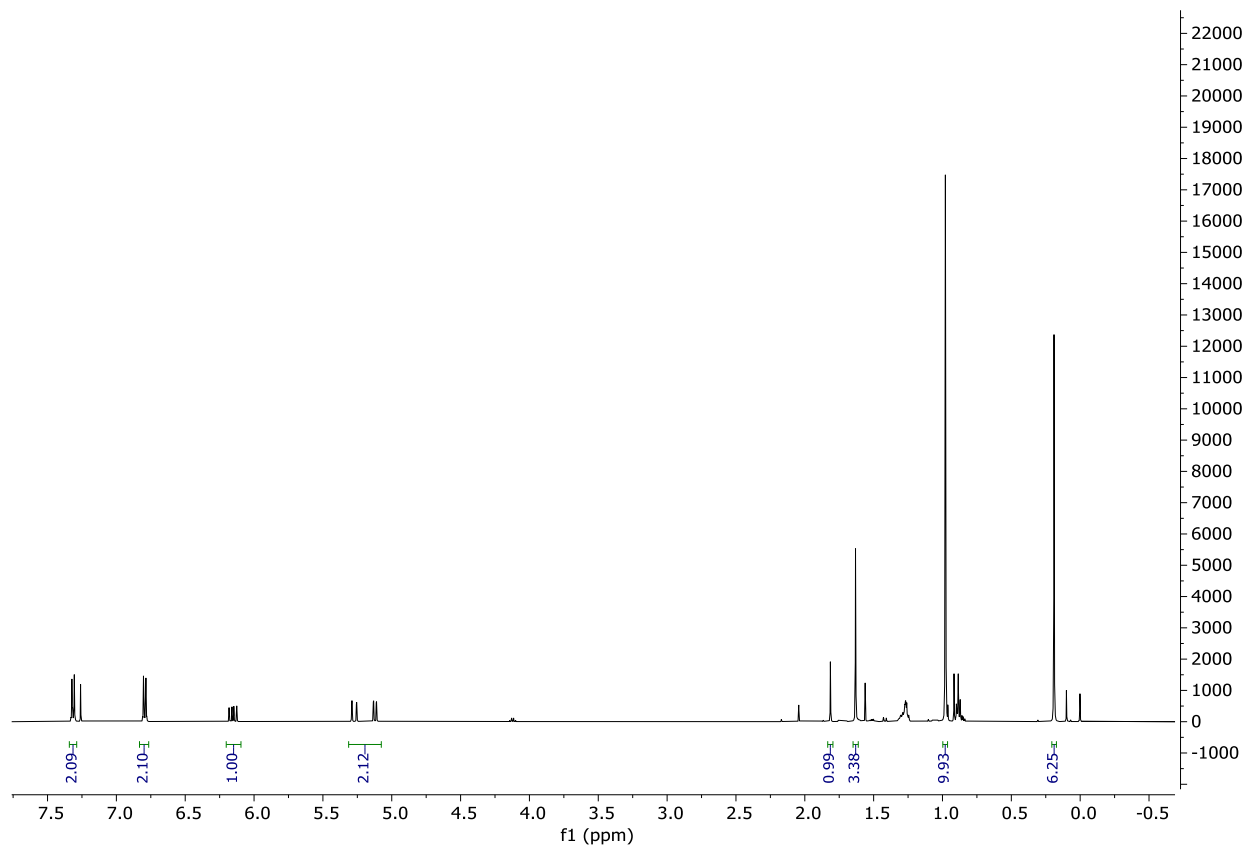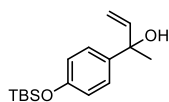
^{1}H NMR, CDCl$_3$-*d*

2-(3-methoxyphenyl)but-3-en-2-ol
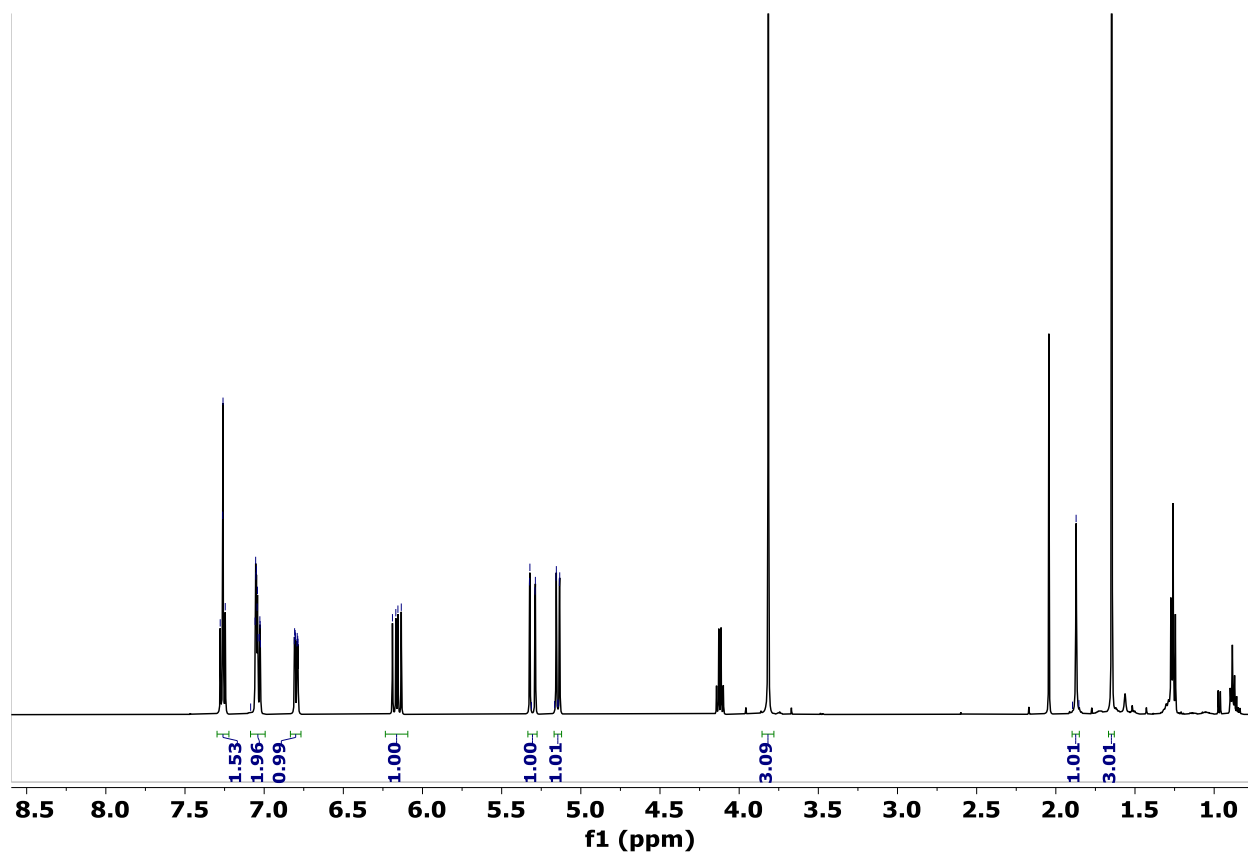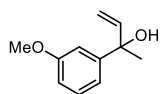
^{1}H NMR, CDCl$_3$-*d*

2-(3,5-dimethoxyphenyl)but-3-en-2-ol
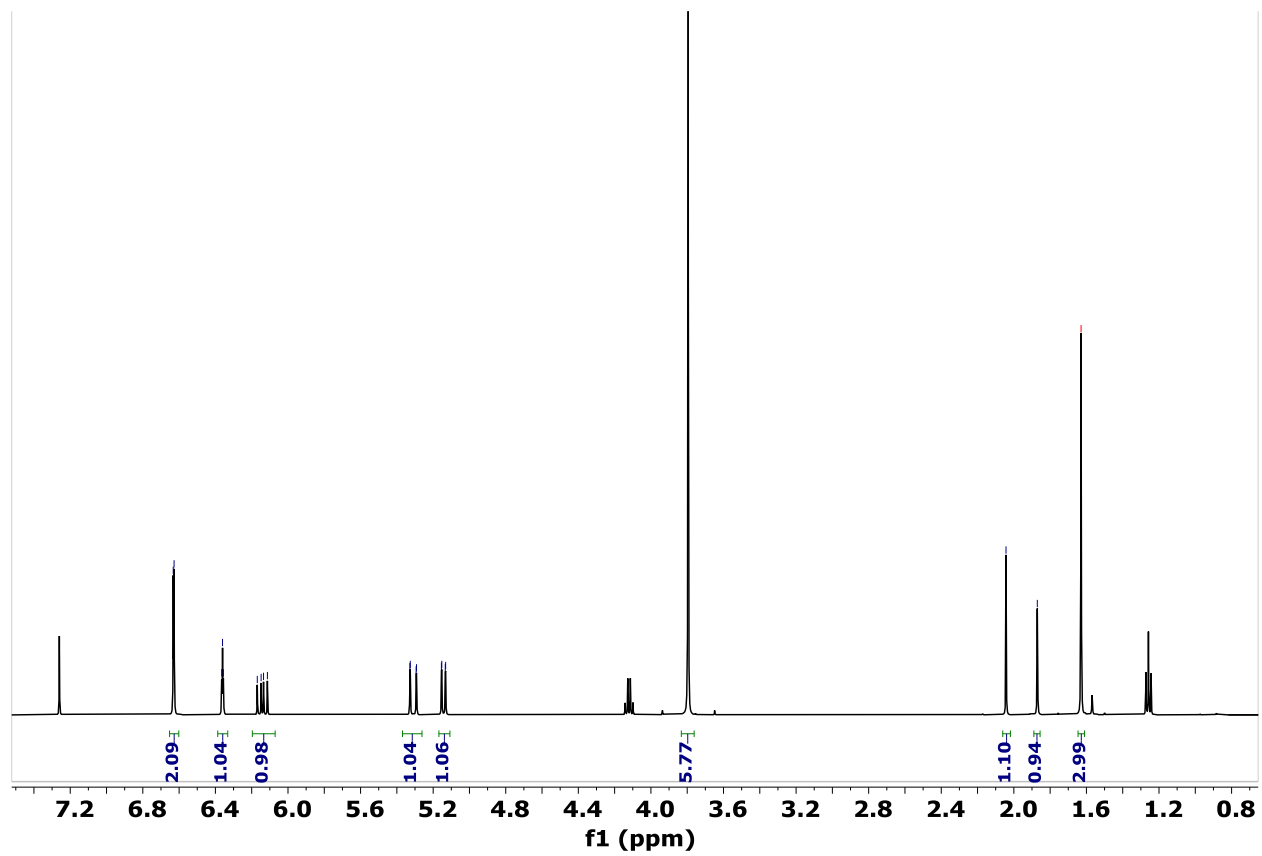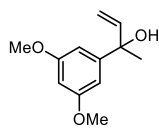
^{1}H NMR, CDCl$_3$-d

2-(4-fluorophenyl)but-3-en-2-ol
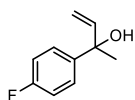
ERM-2-238.10.fid
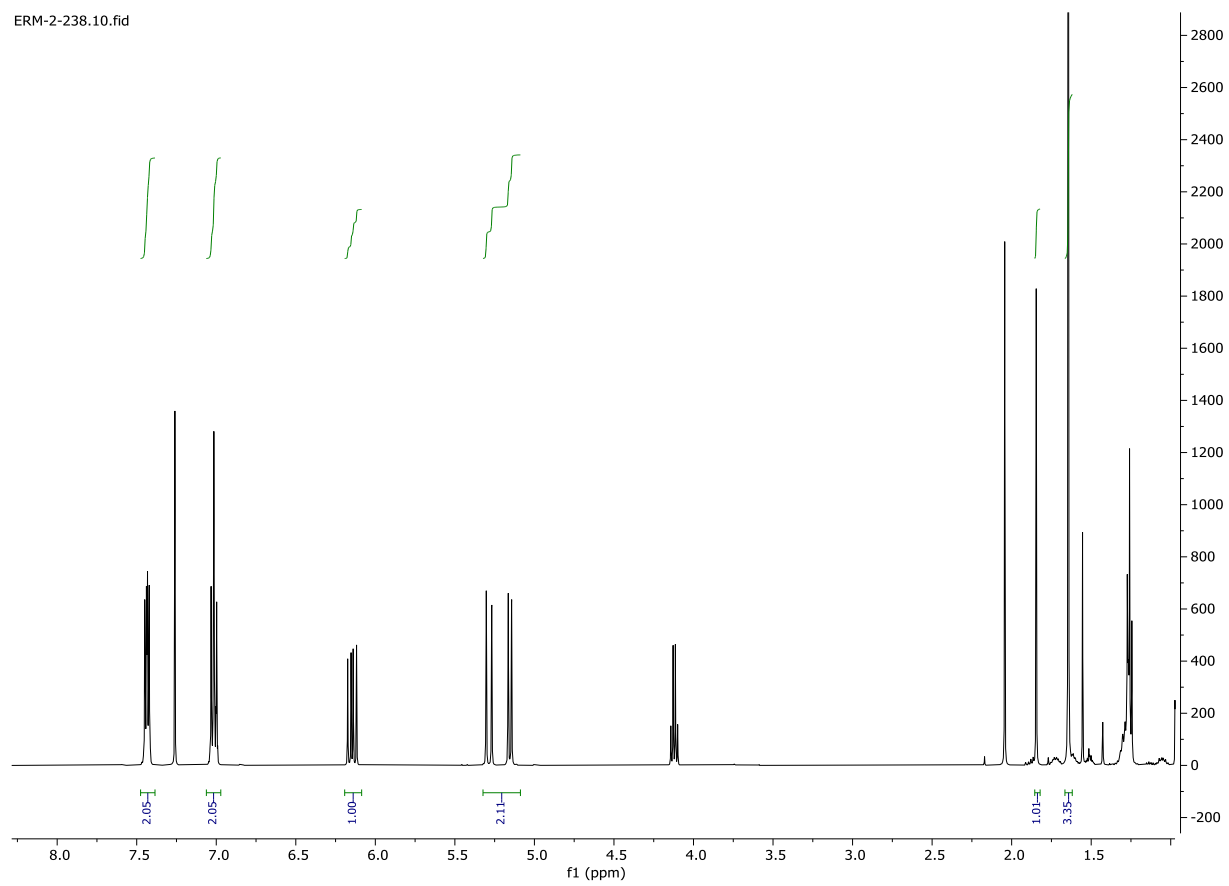
¹H NMR, CDCl₃-*d*
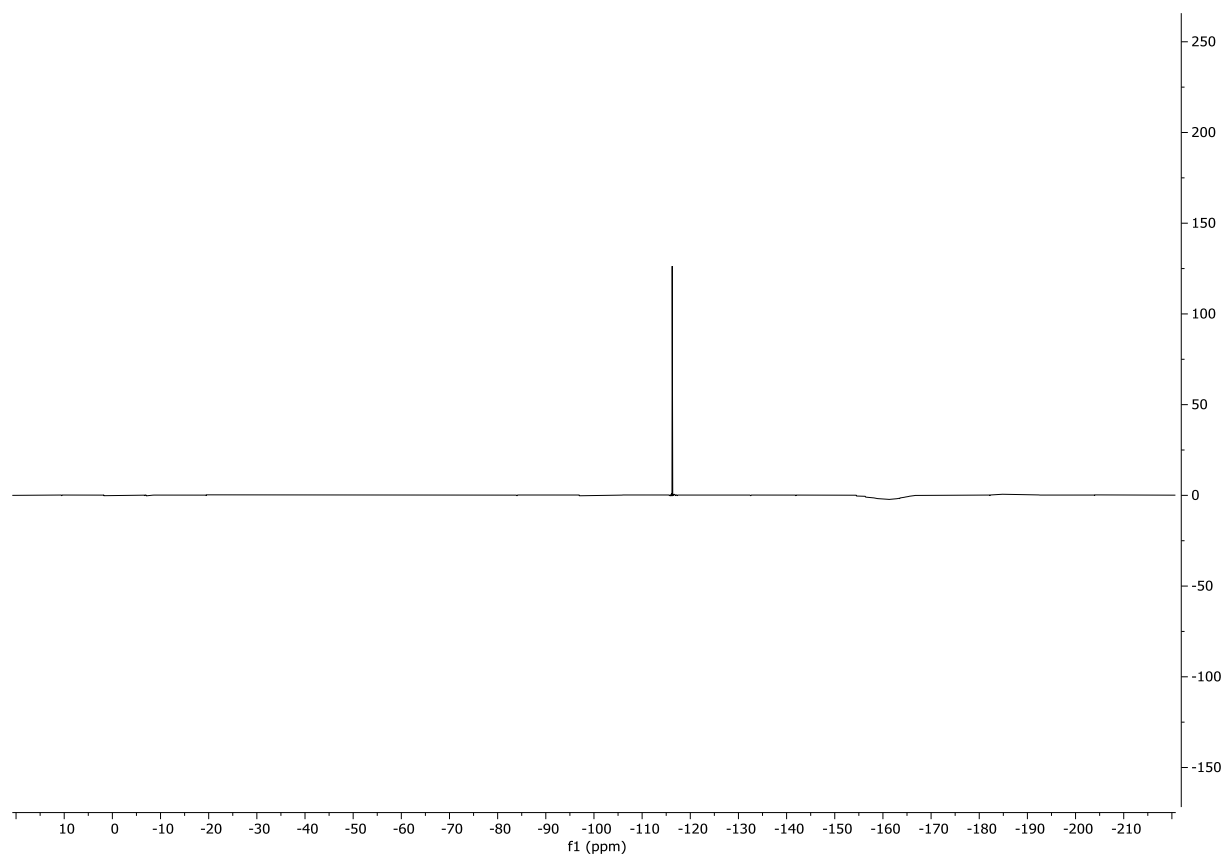
^{19}F NMR, CDCl$_3$-*d*

diethyl (1-(naphthalen-1-yl)vinyl) phosphate
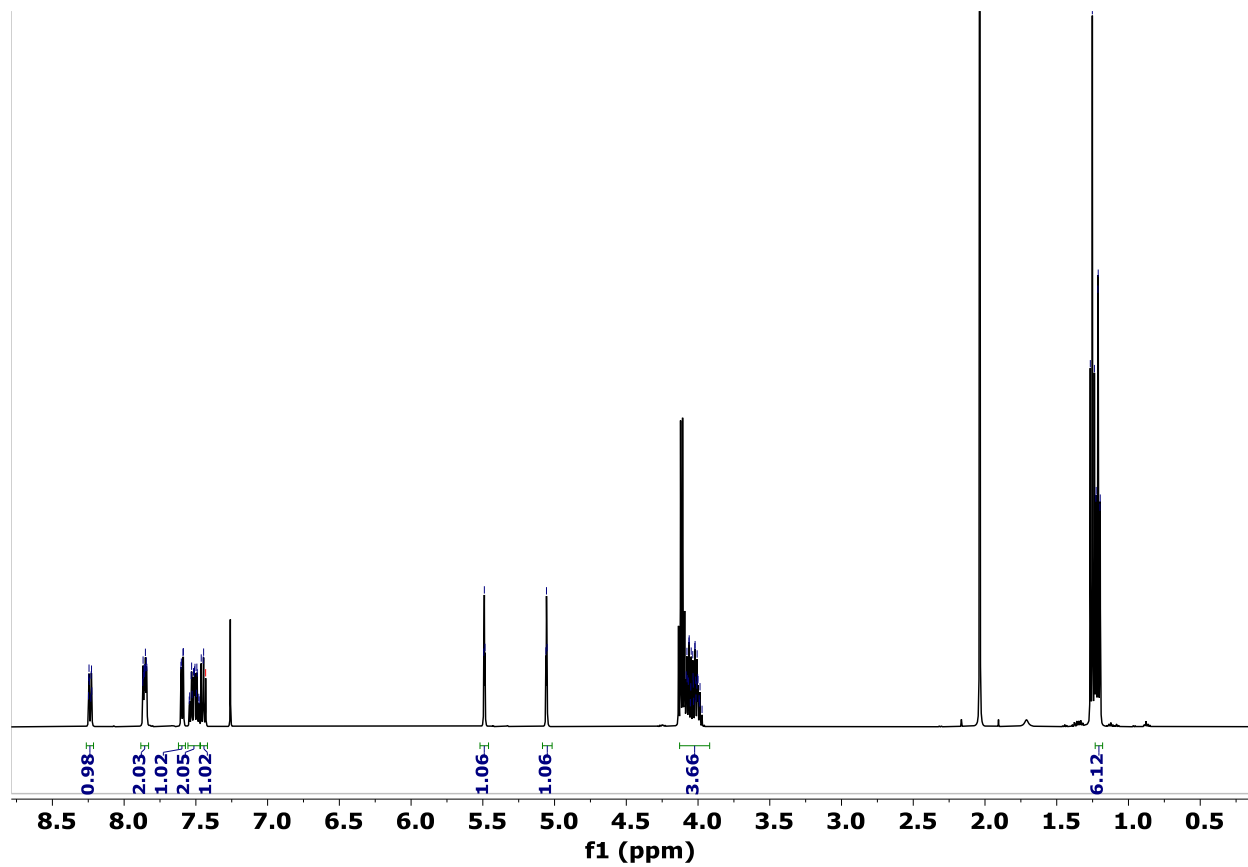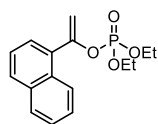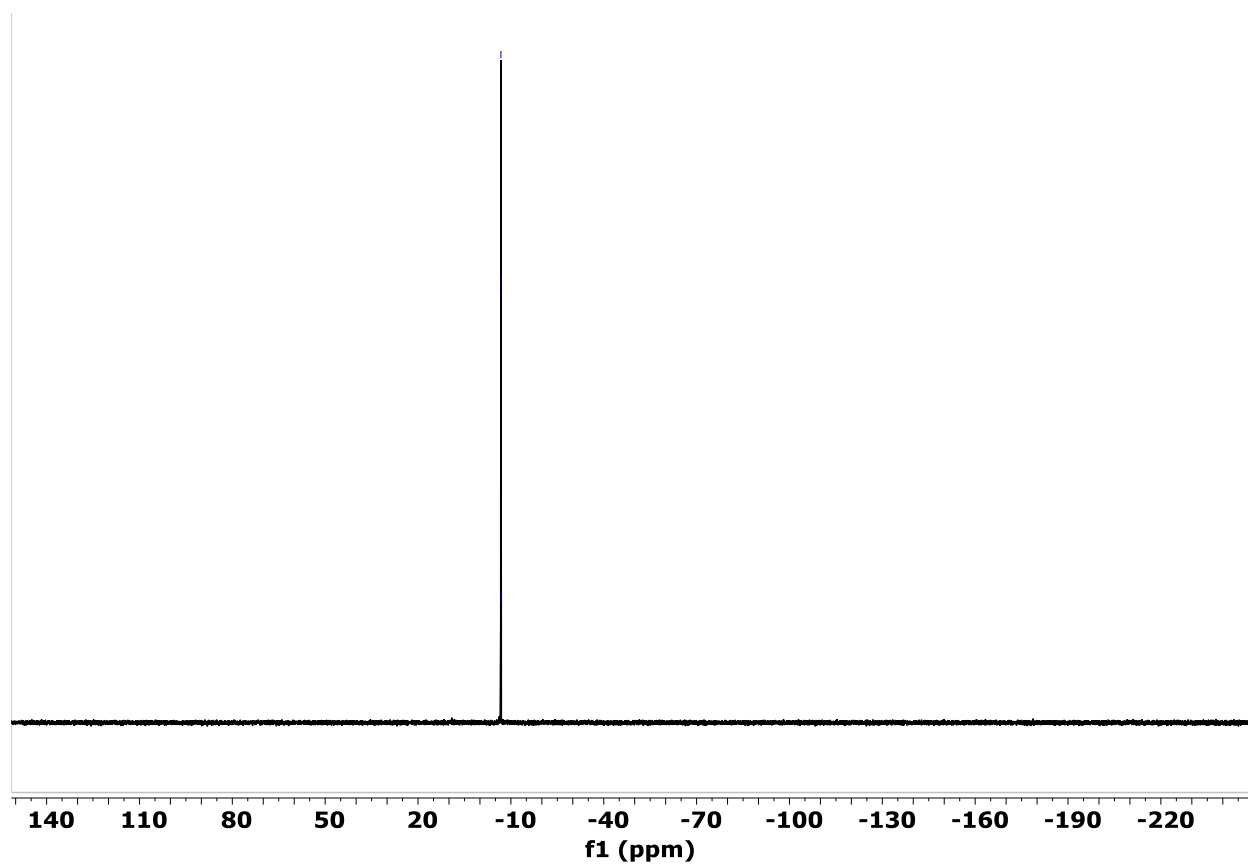
^{1}H NMR, CDCl$_3$-*d*
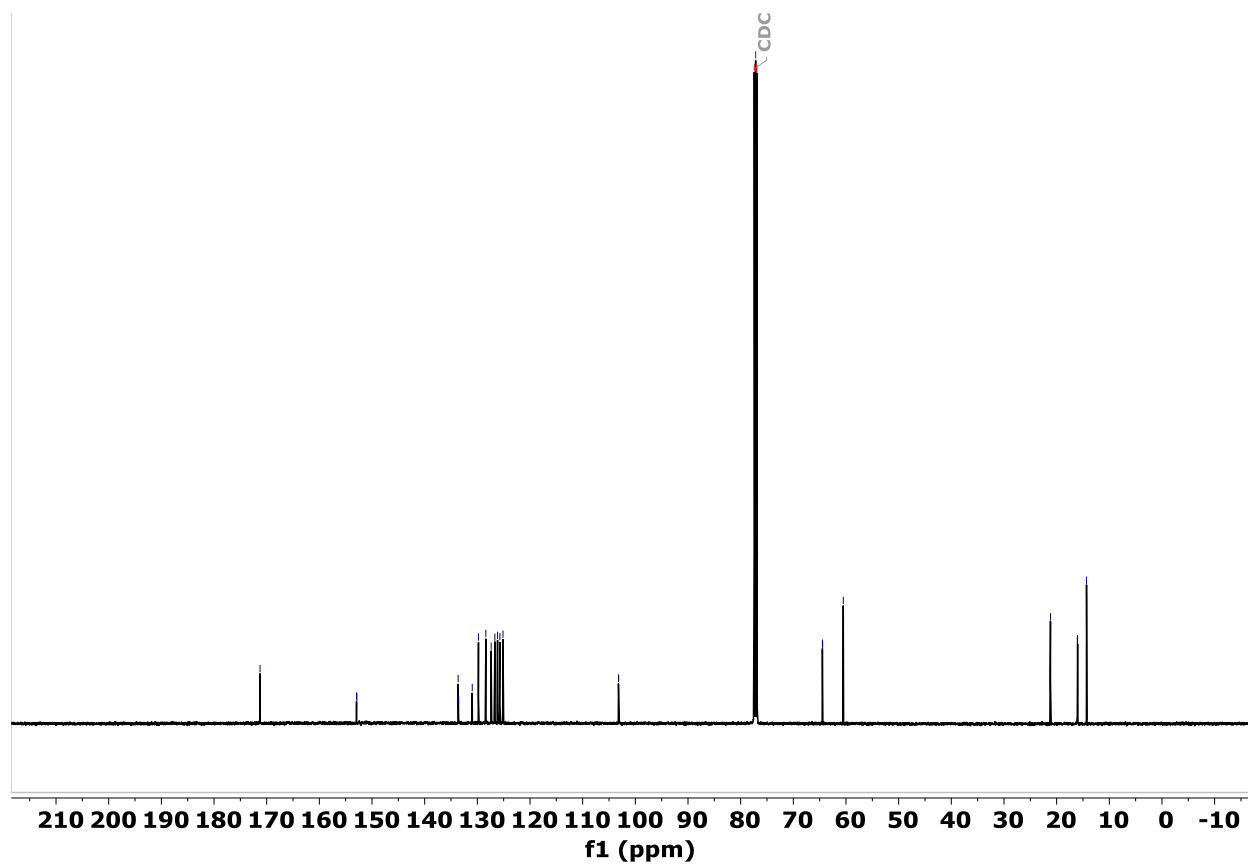
^{31}P NMR, CDCl$_3$-*d*

¹³C NMR, CDCl₃-*d*

1-(2,4-dimethylphenyl)vinyl diethyl phosphate
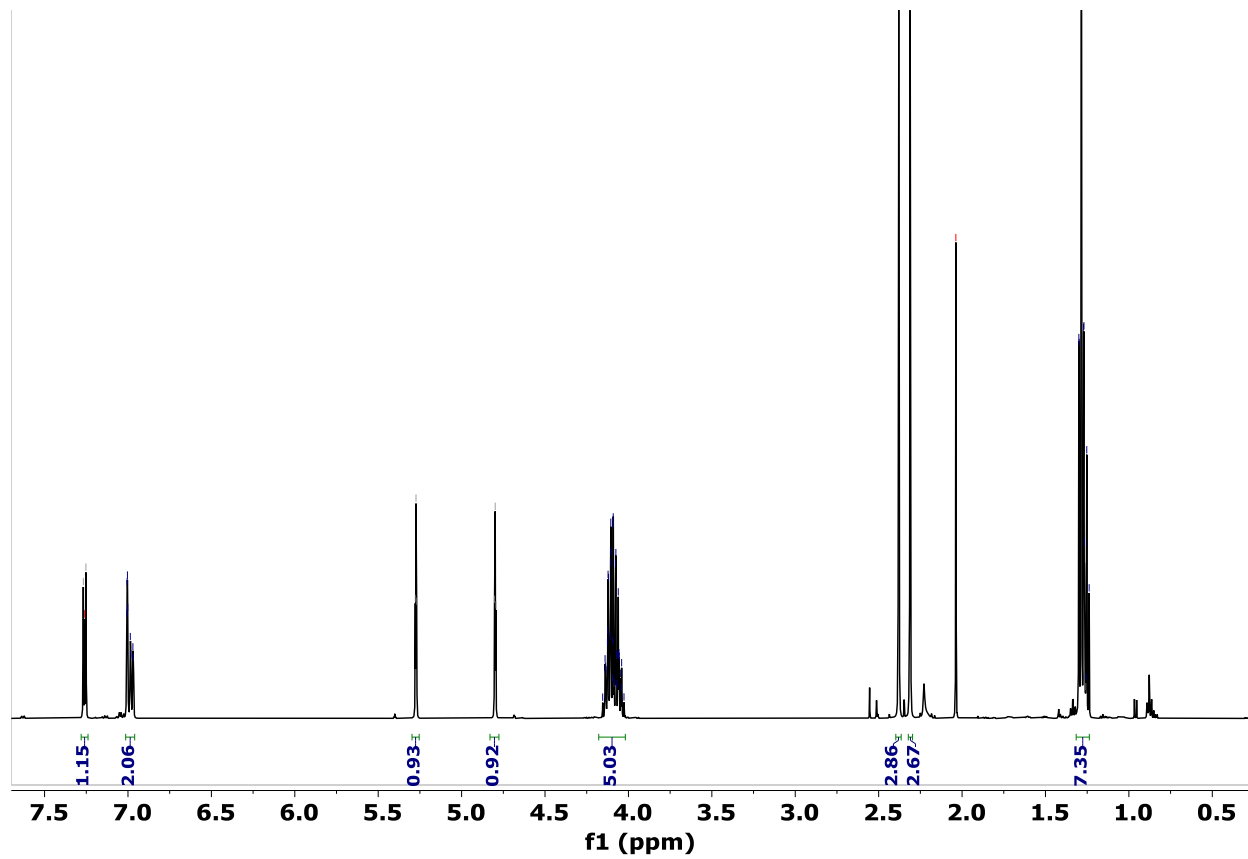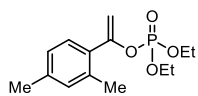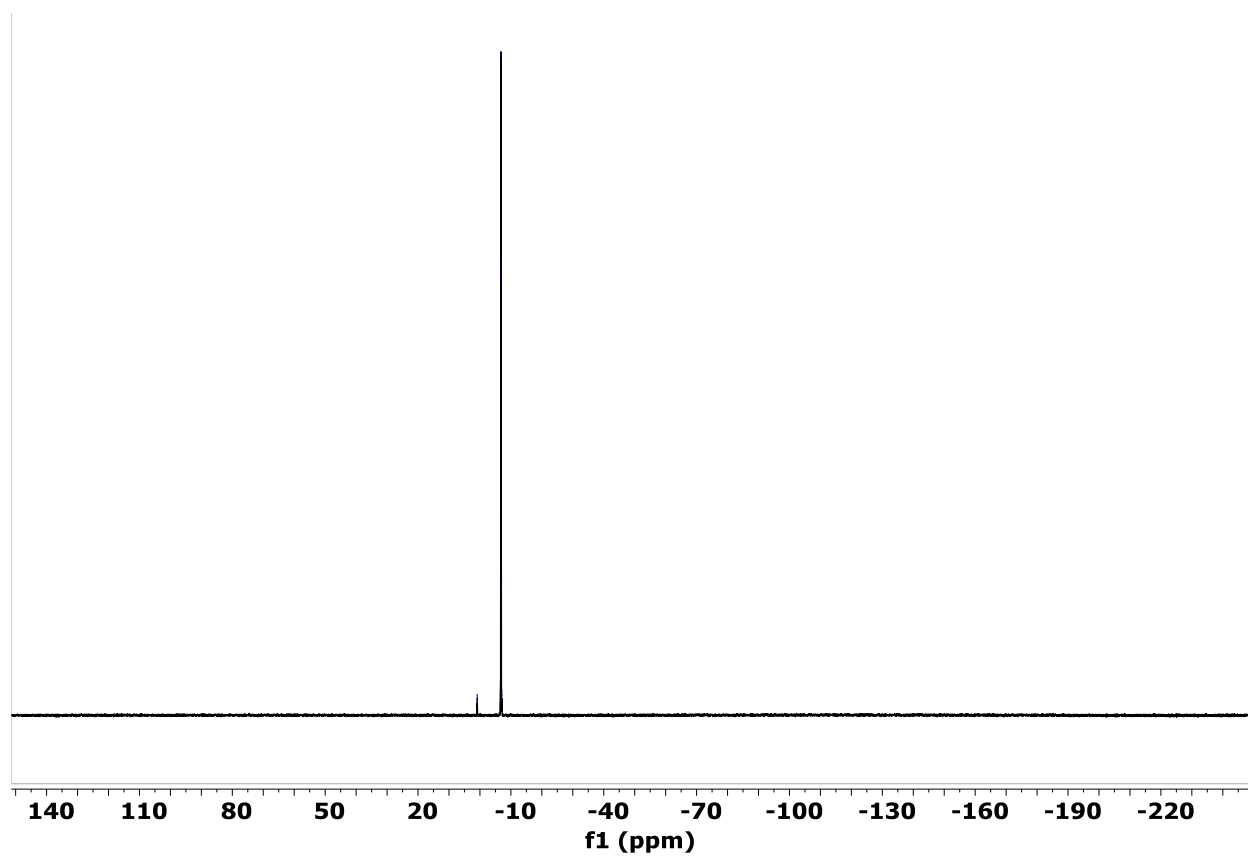
^{1}H NMR, CDCl$_3$-d

^{31}P NMR, CDCl$_3$-*d*

1-(2-((tert-butyldimethylsilyl)oxy)phenyl)vinyl diethyl phosphate
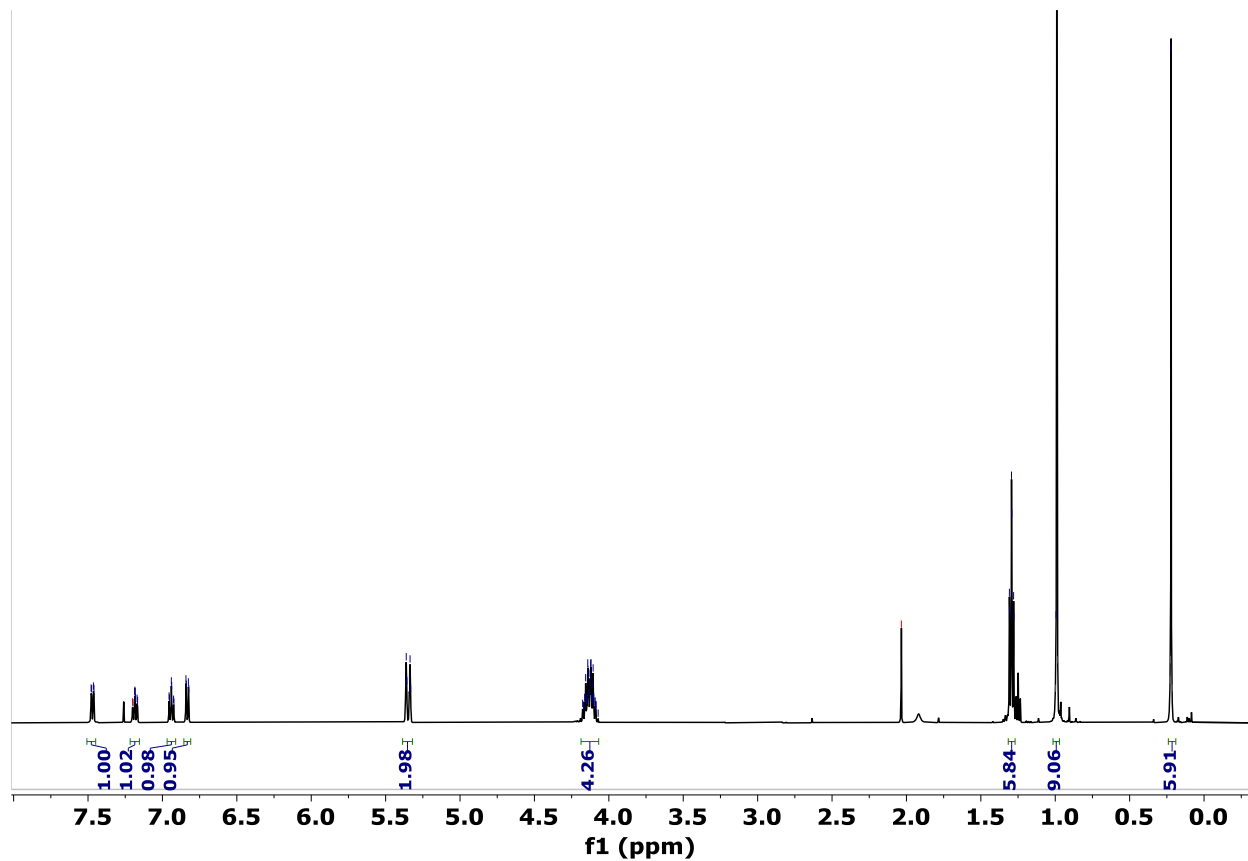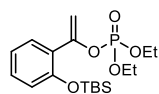
¹H NMR, CDCl₃-*d*

diethyl (1-(4-((trimethylsilyl)ethynyl)phenyl)vinyl) phosphate
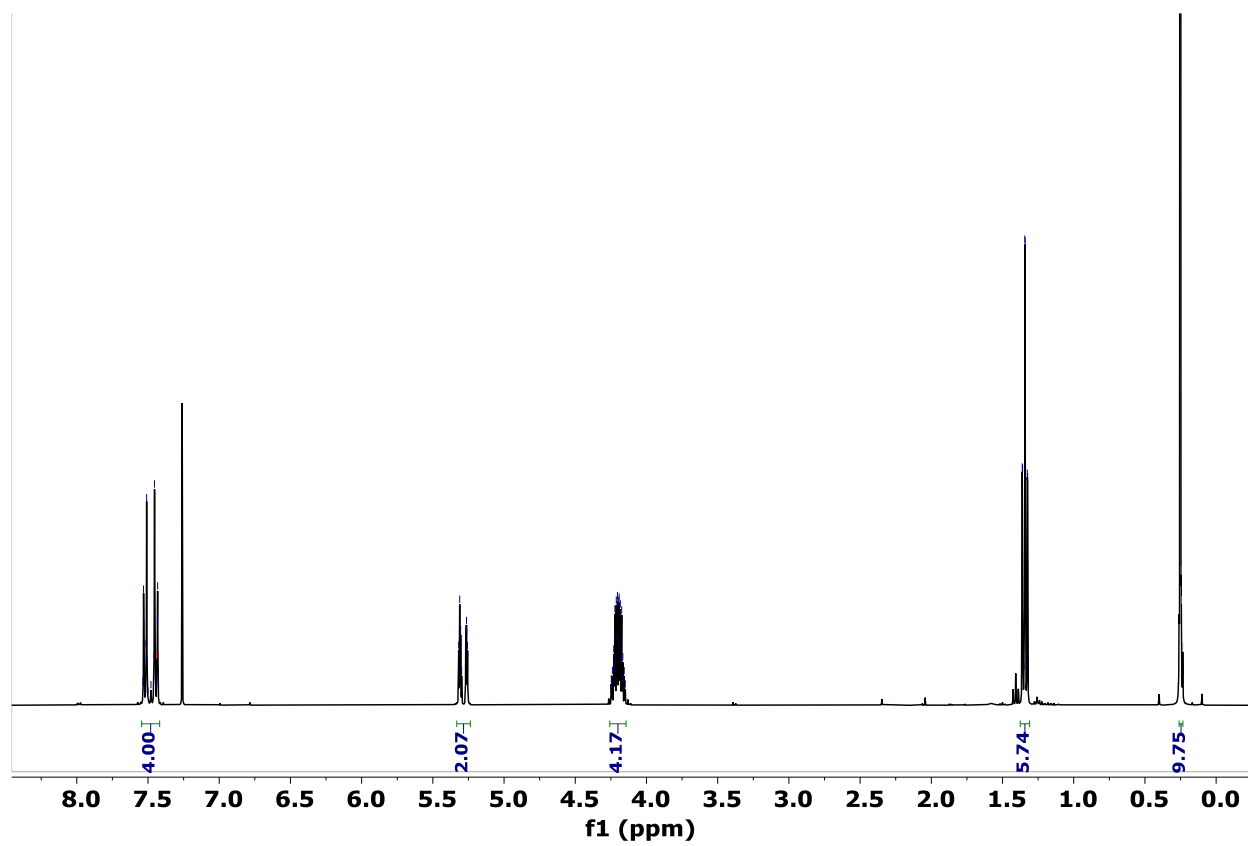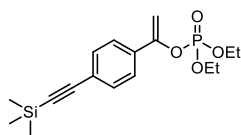
^{1}H NMR, CDCl$_3$-*d*

(4-(buta-1,3-dien-2-yl)phenoxy)(tert-butyl)dimethylsilane
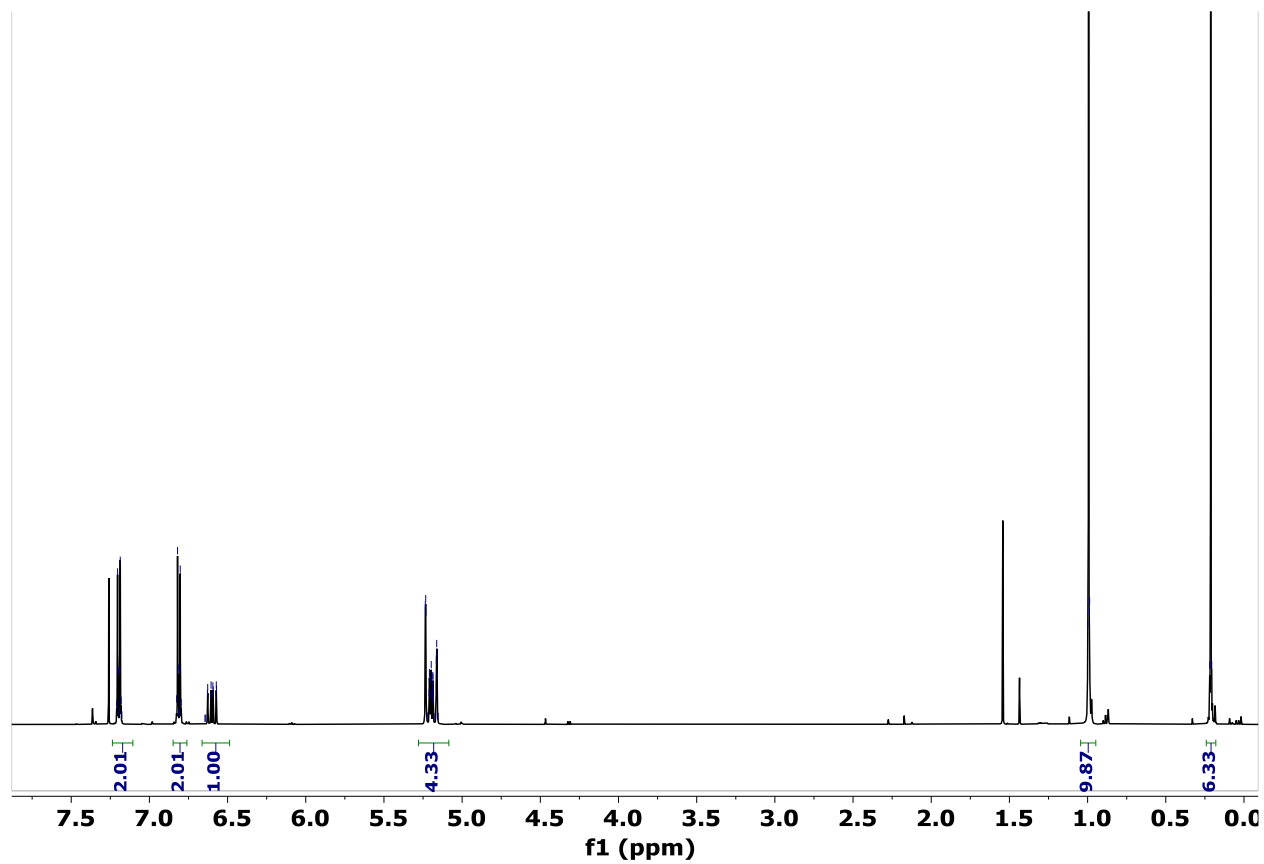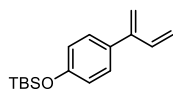
¹H NMR, CDCl₃-*d*

1-(buta-1,3-dien-2-yl)-4-fluorobenzene
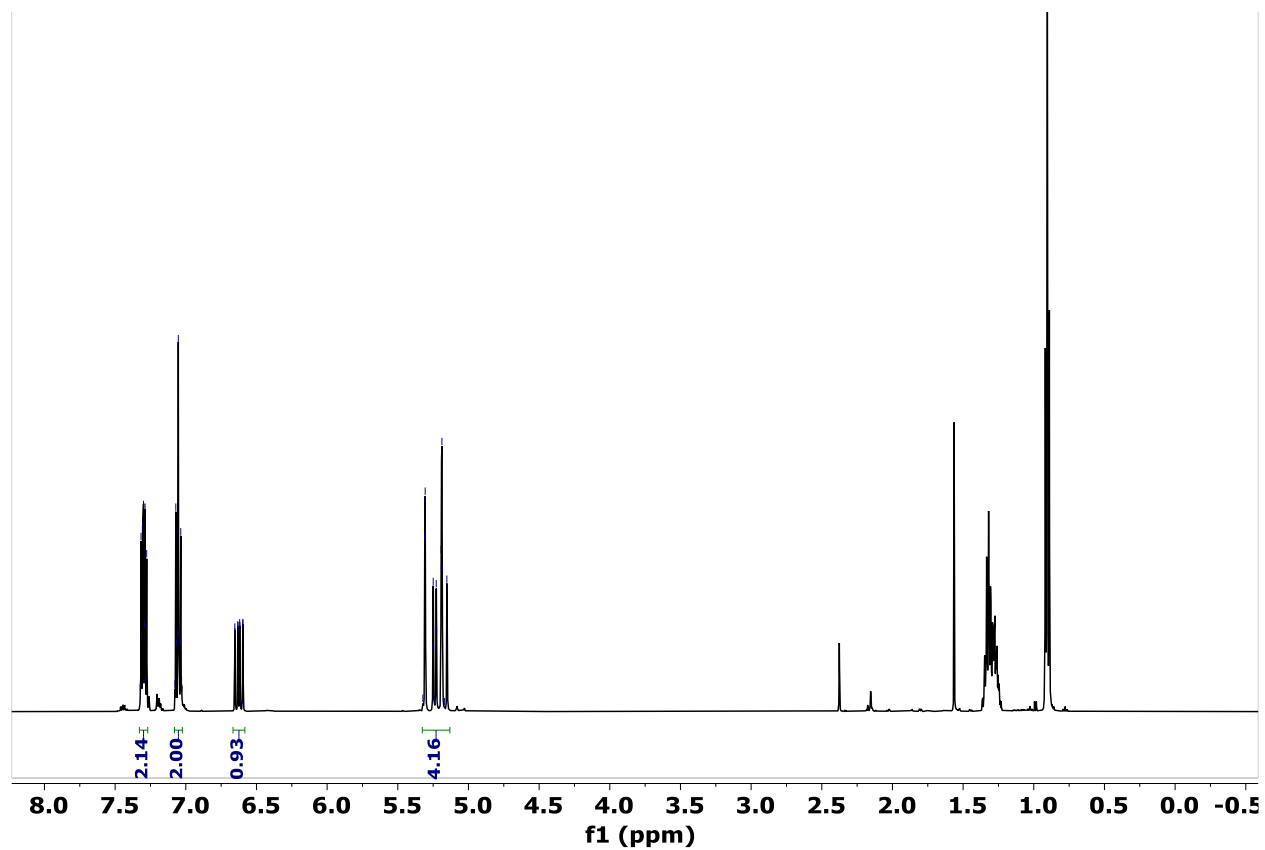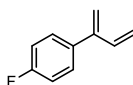
¹H NMR, CDCl₃-*d*
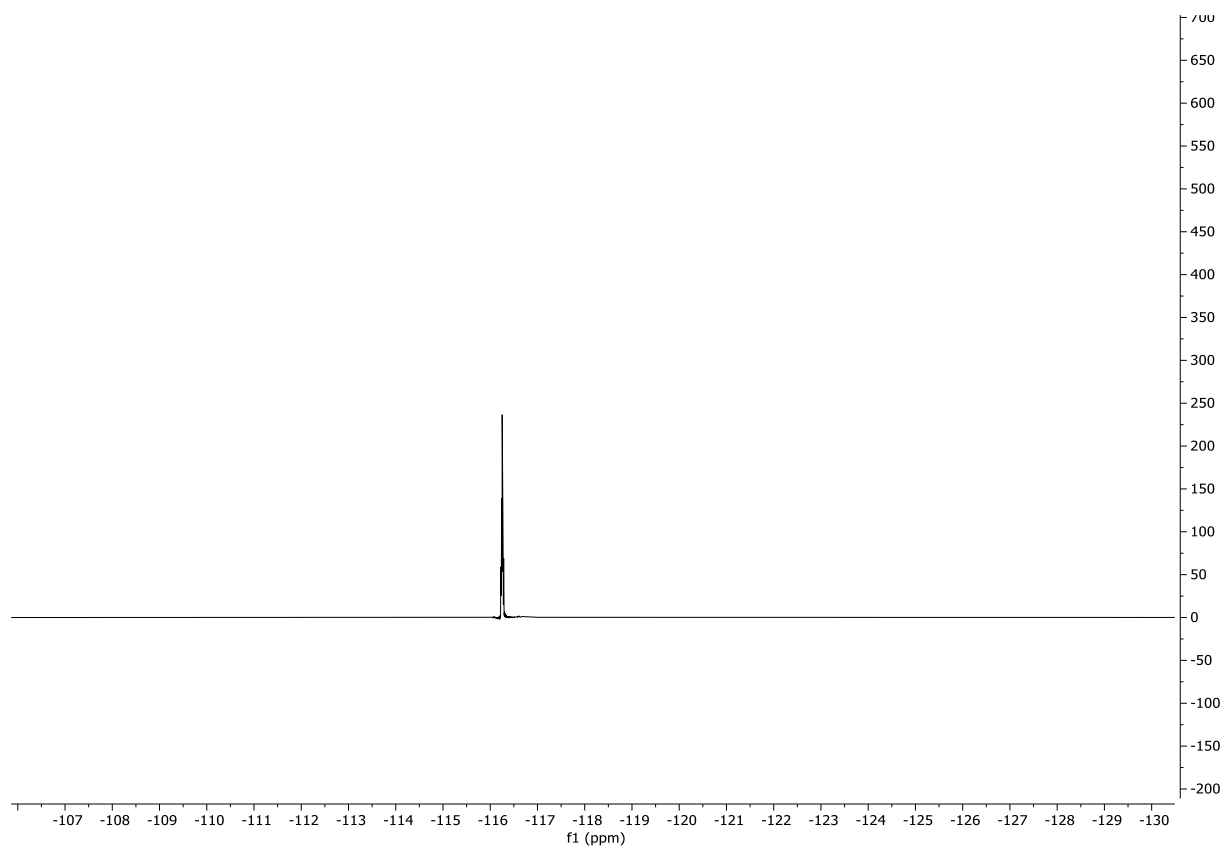
^{19}F NMR, CDCl$_3$-d

1-(buta-1,3-dien-2-yl)-3-methoxybenzene
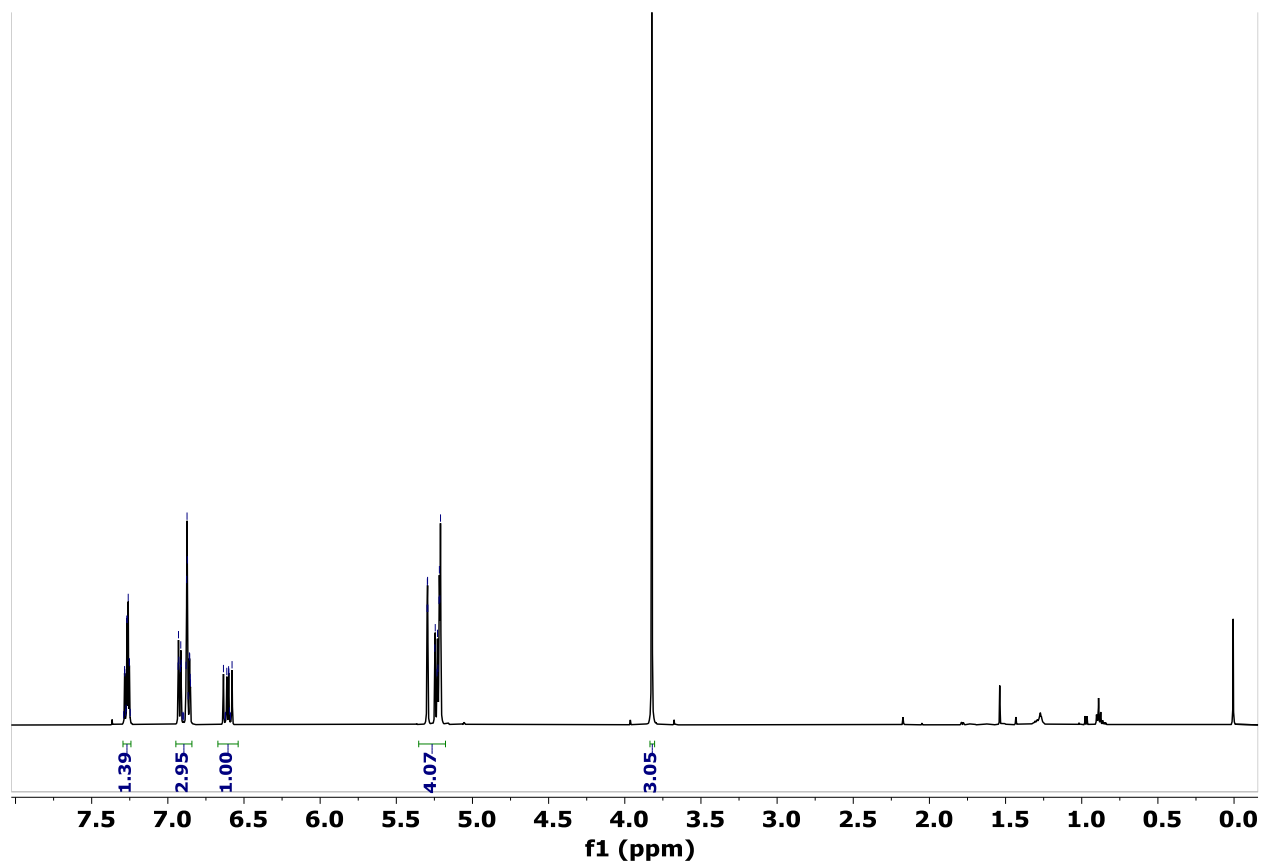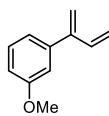
^{1}H NMR, CDCl$_3$-*d*

1-(buta-1,3-dien-2-yl)-3,5-dimethoxybenzene
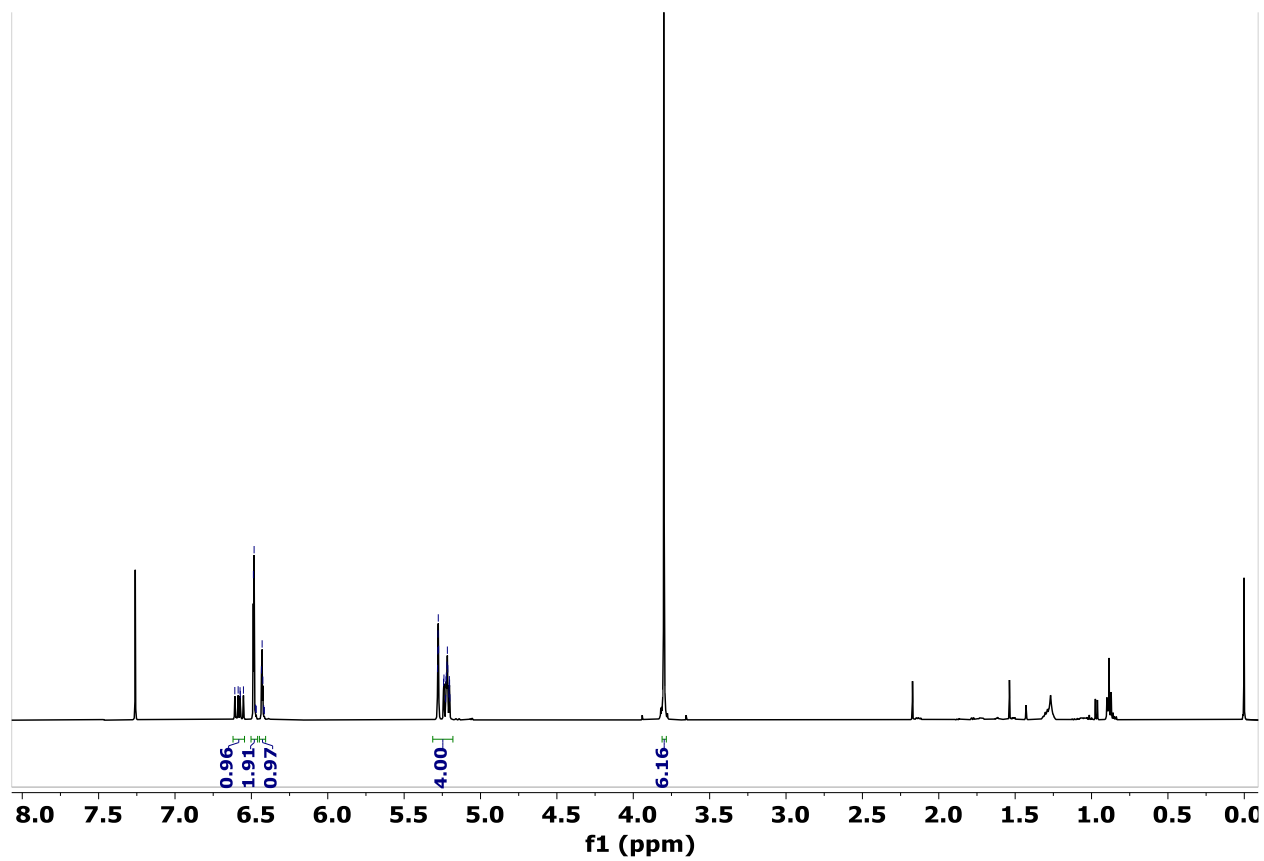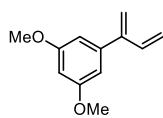
¹H NMR, CDCl₃-*d*

(2-(buta-1,3-dien-2-yl)phenoxy)(tert-butyl)dimethylsilane
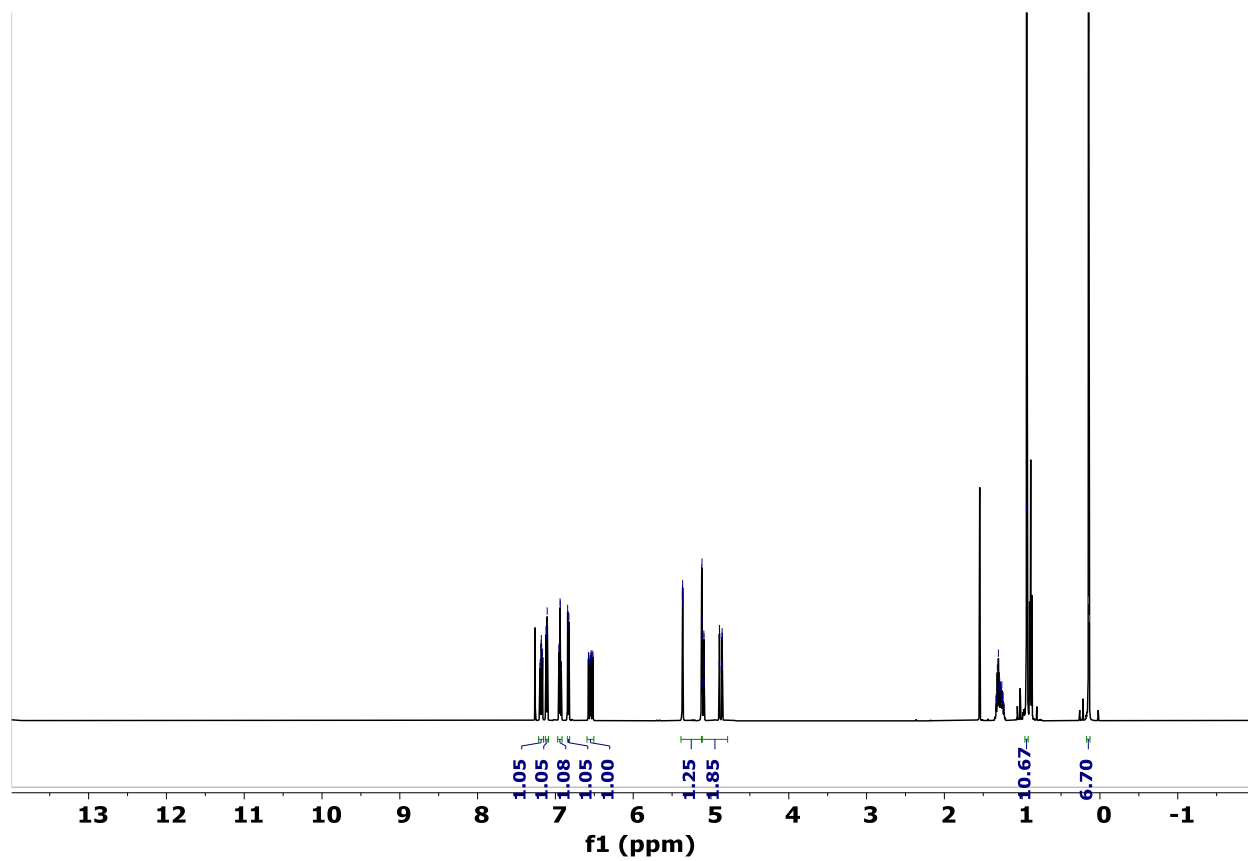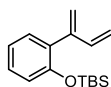
^{1}H NMR, CDCl$_3$-*d*

77.16 CD
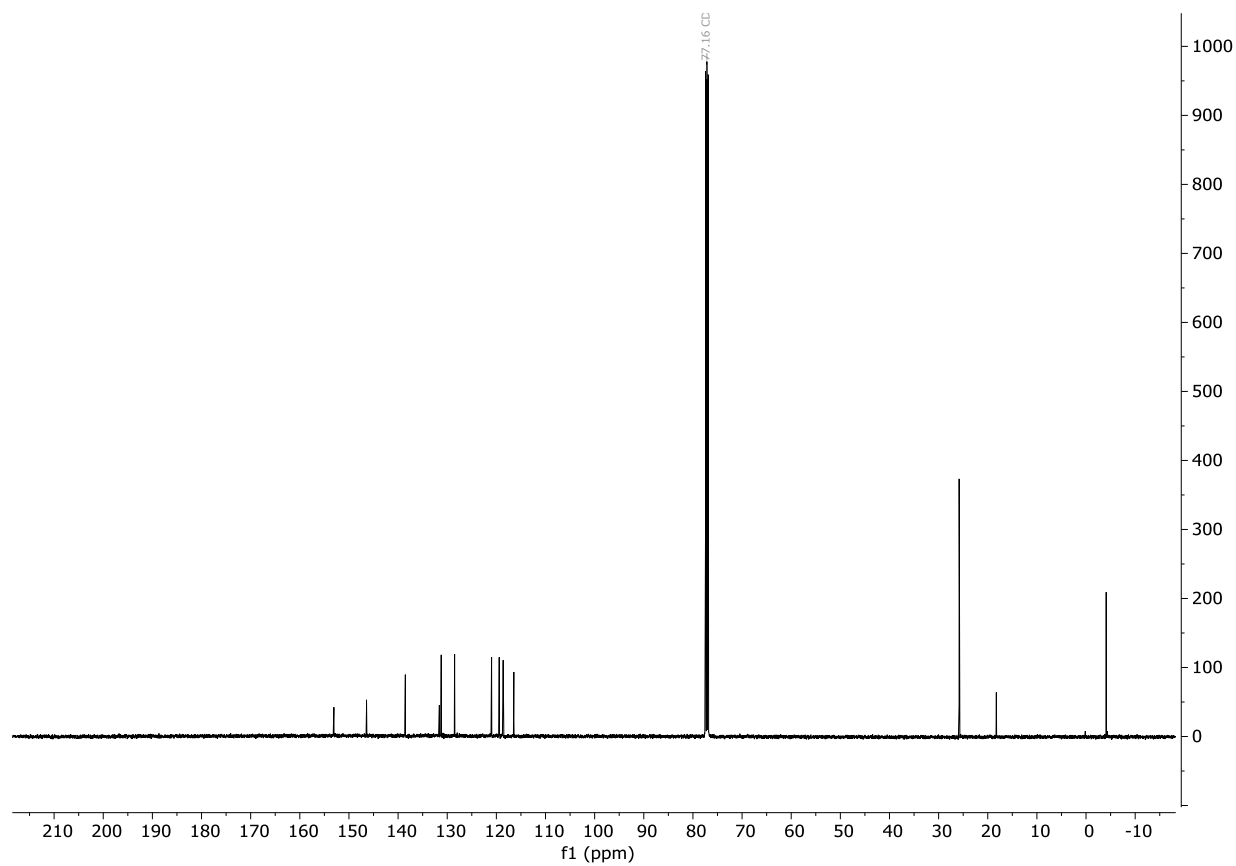
13C NMR, CDCl3-*d*

((4-(buta-1,3-dien-2-yl)phenyl)ethynyl)trimethylsilane
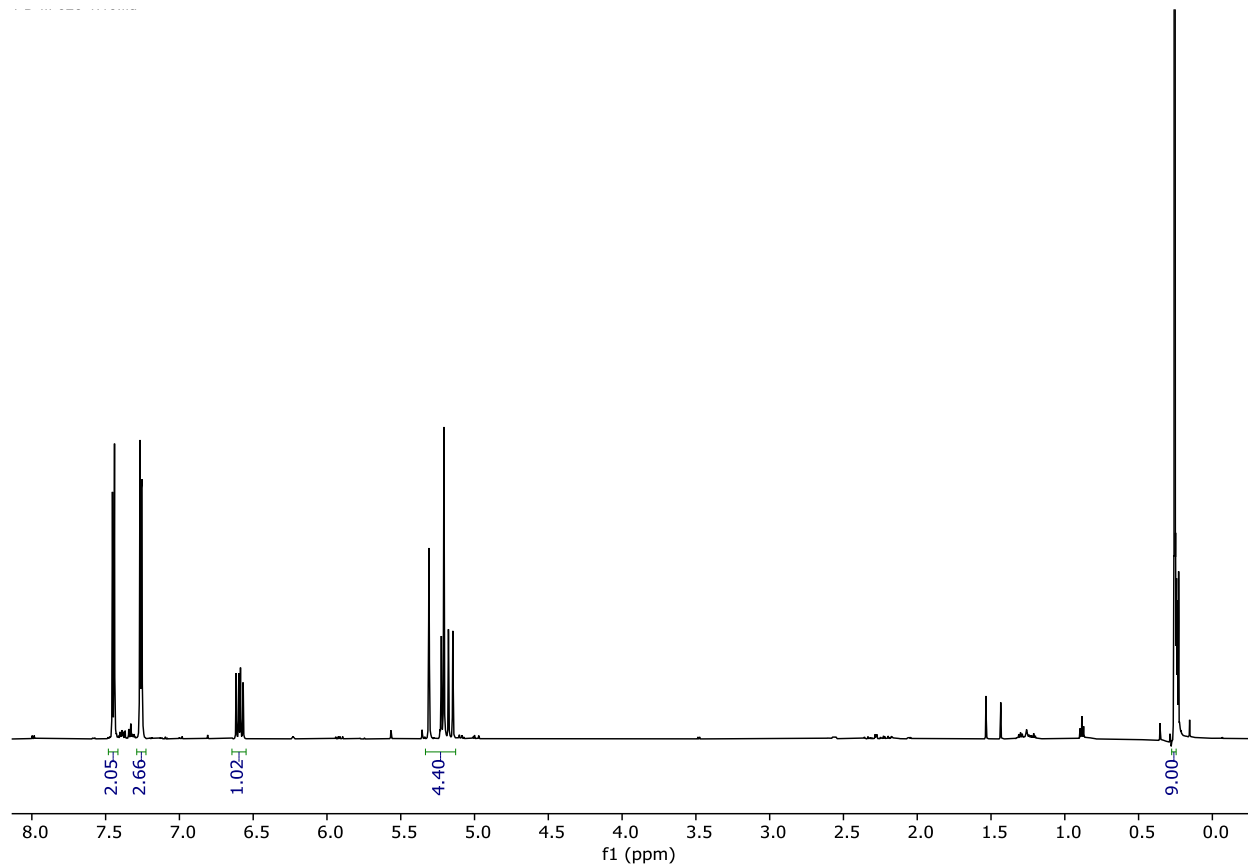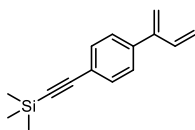
^{1}H NMR, CDCl$_3$-*d*

1-(buta-1,3-dien-2-yl)naphthalene
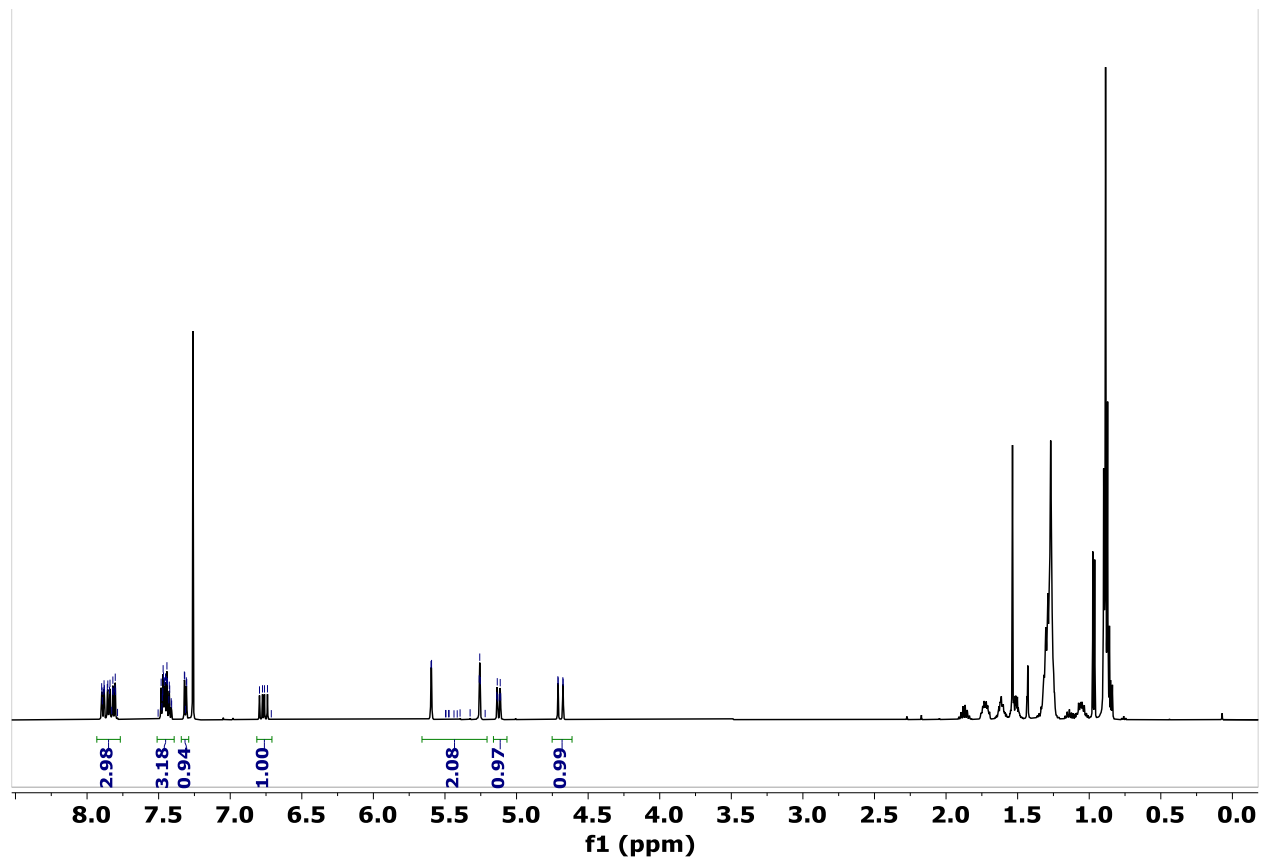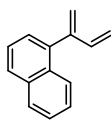
¹H NMR, CDCl₃-*d*
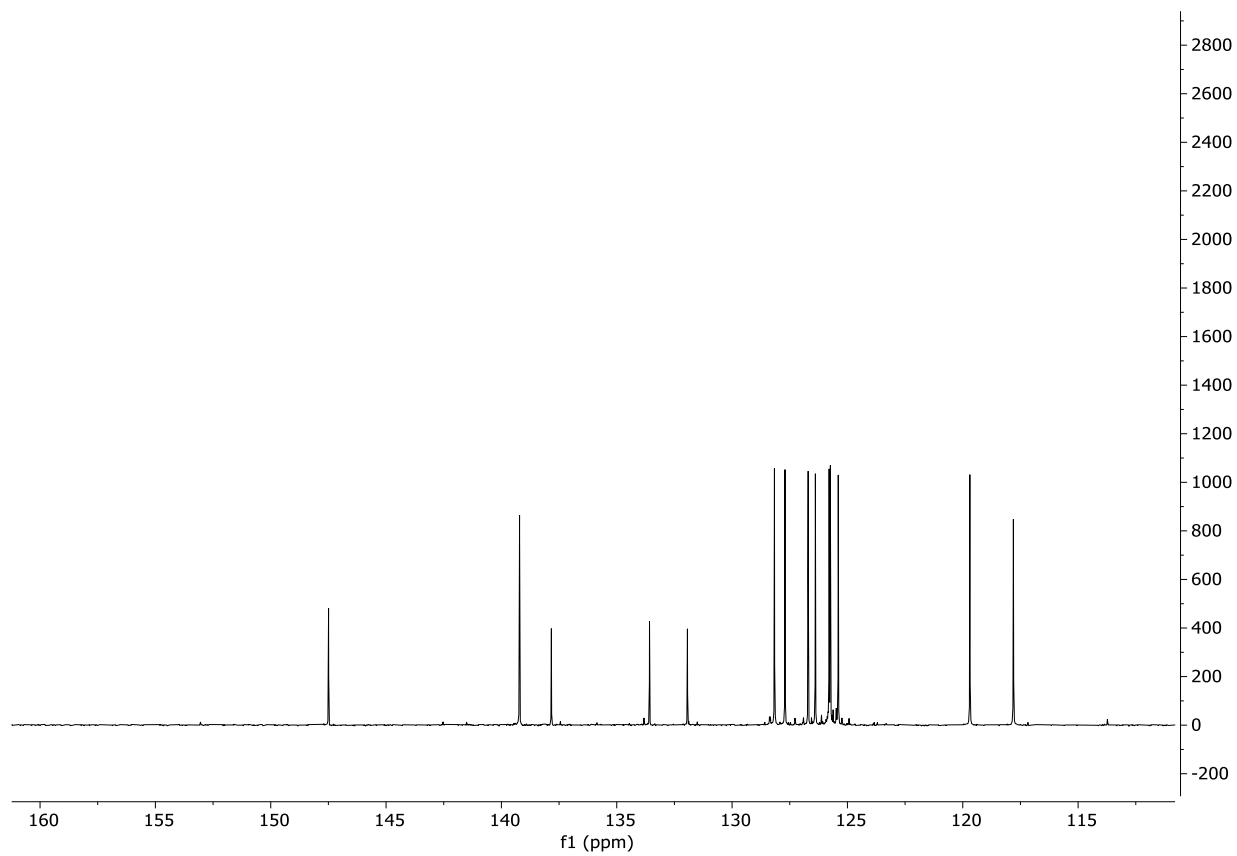
^{13}C NMR, CDCl$_3$-*d*

1-(buta-1,3-dien-2-yl)-4-methylbenzene
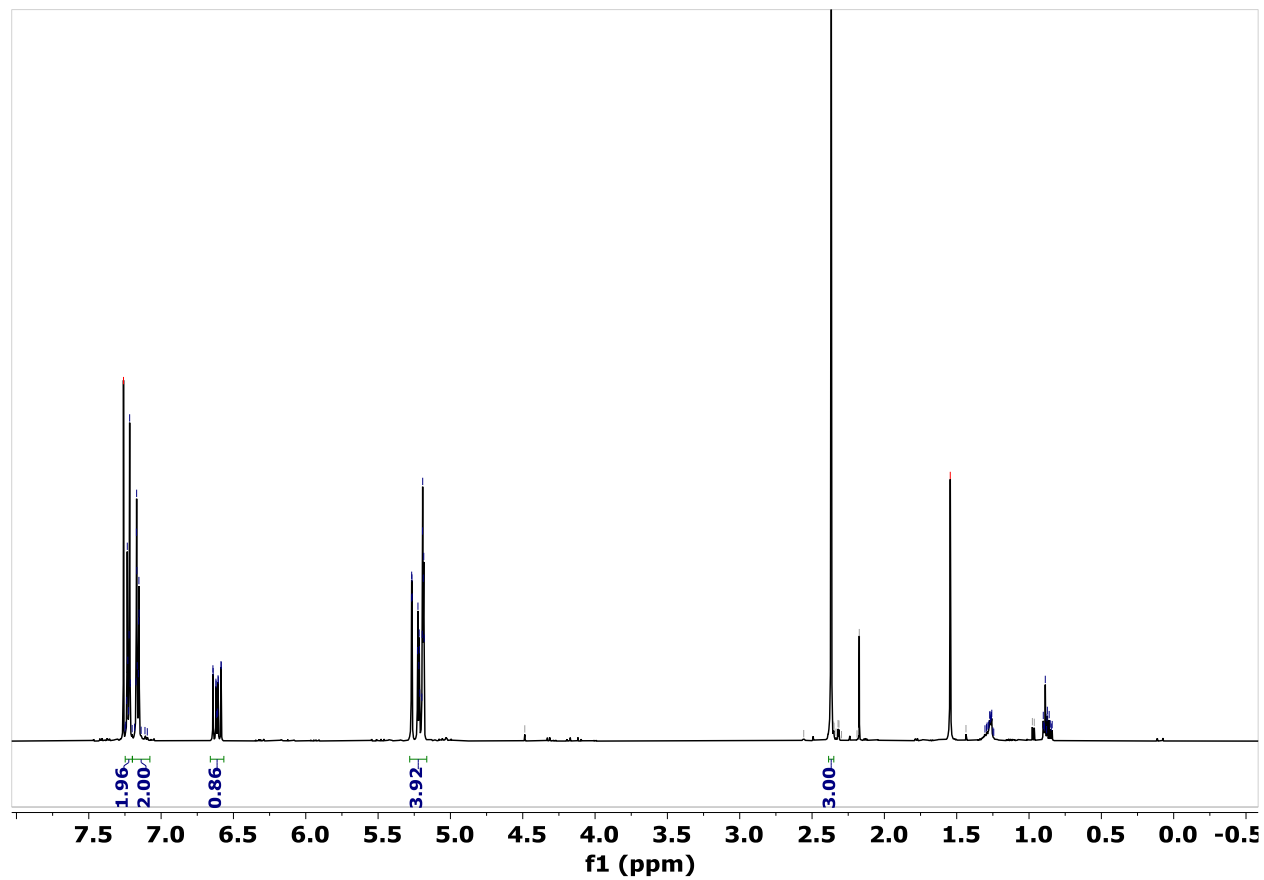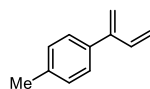
^{1}H NMR, CDCl$_3$-d
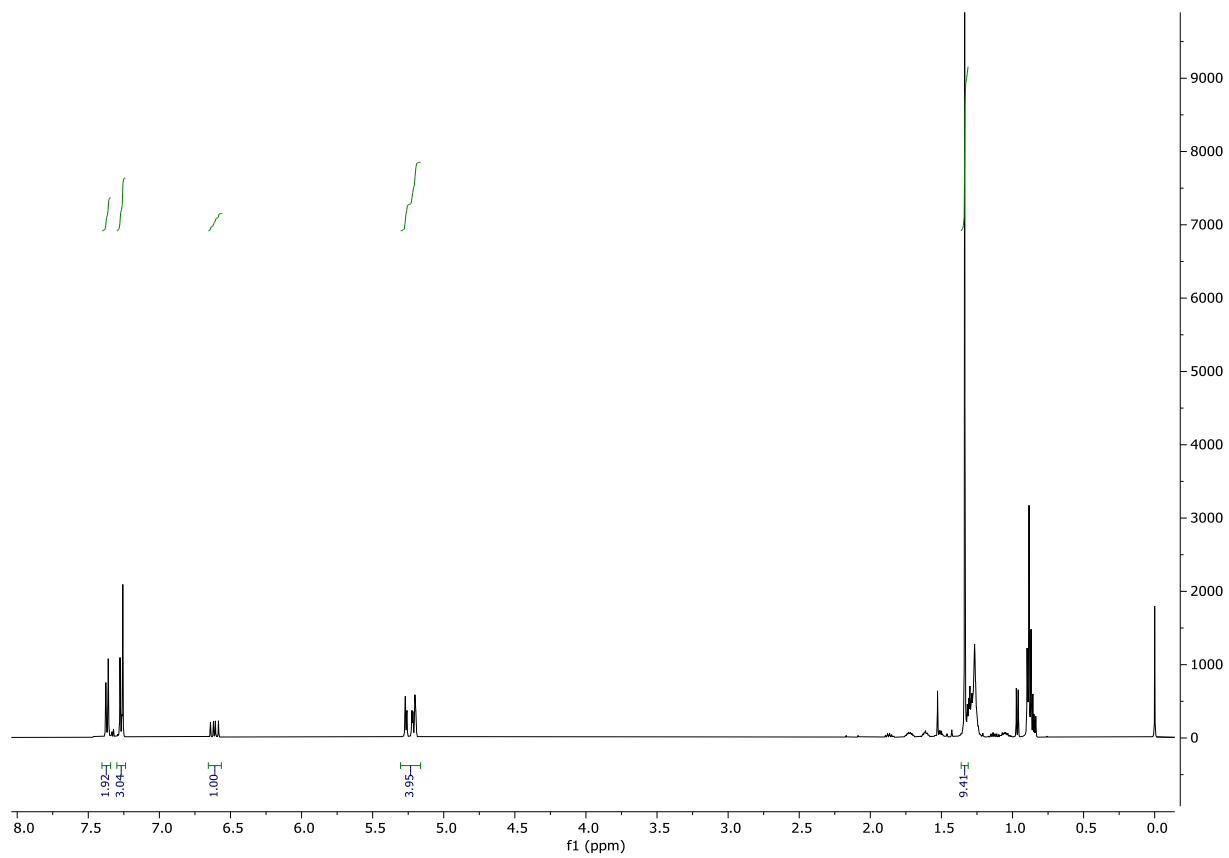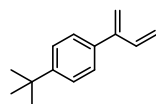
1-(buta-1,3-dien-2-yl)-4-(tert-butyl)benzene

^{1}H NMR, CDCl$_3$-d

1-(buta-1,3-dien-2-yl)-2,4-dimethylbenzene

ERM-2-142.10.fid
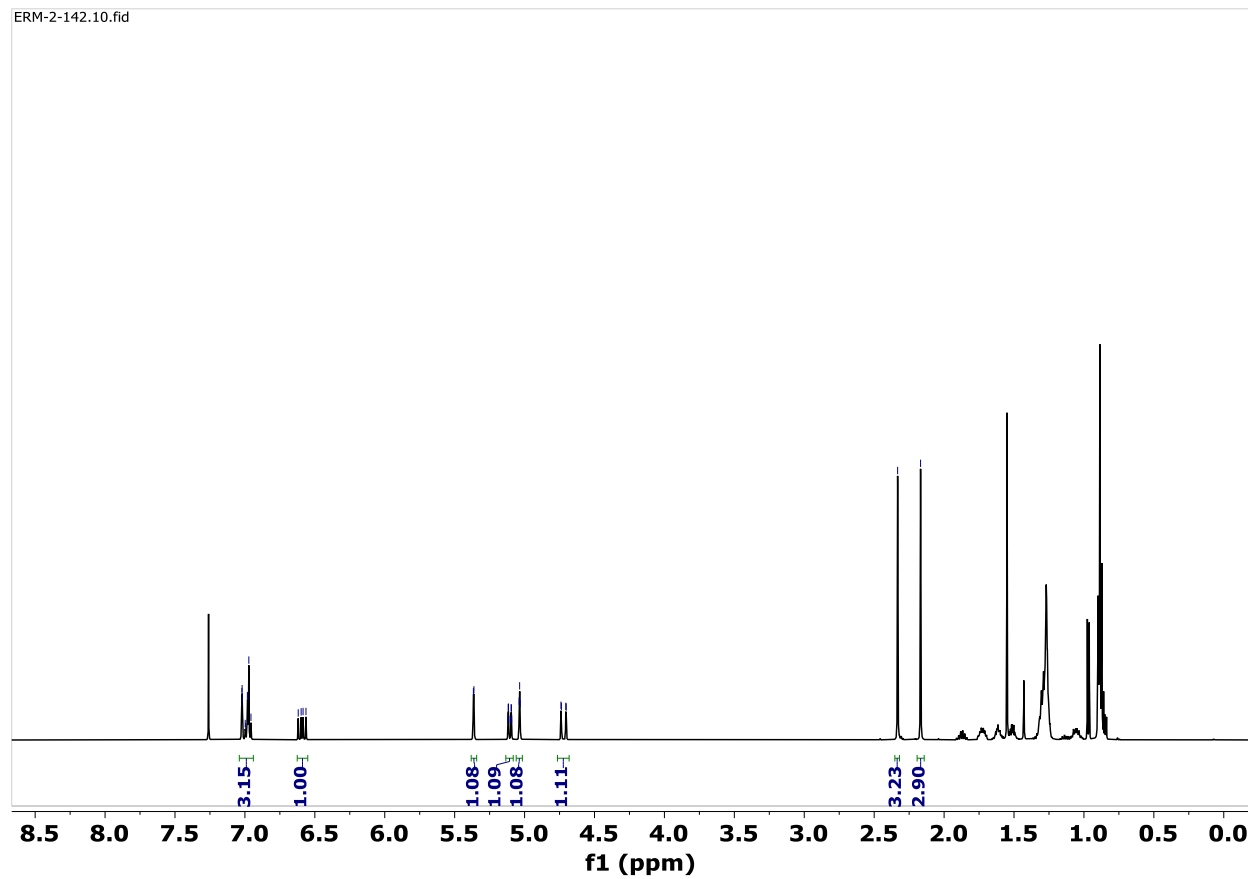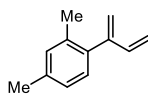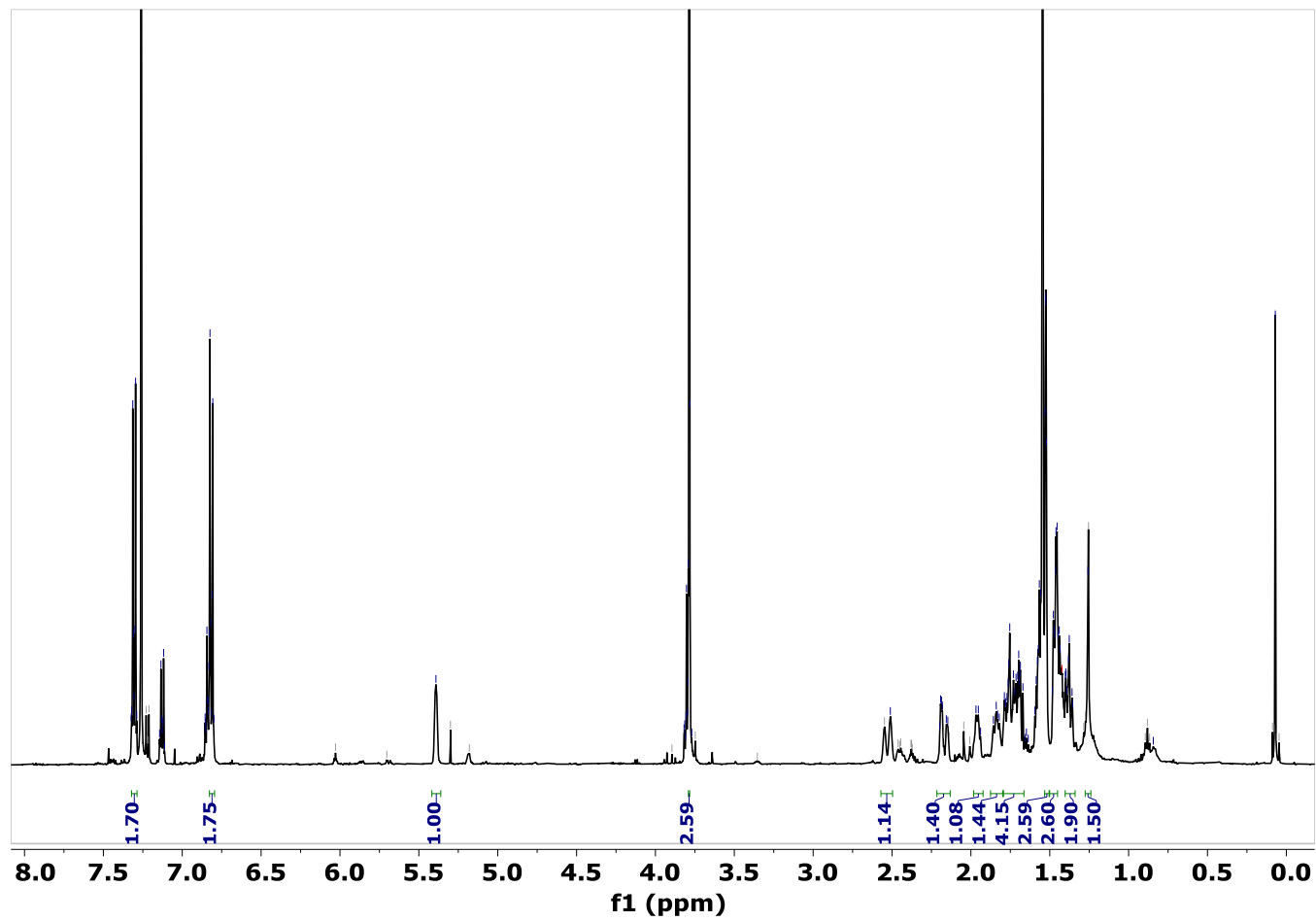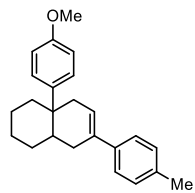
^{1}H NMR, CDCl$_3$-d
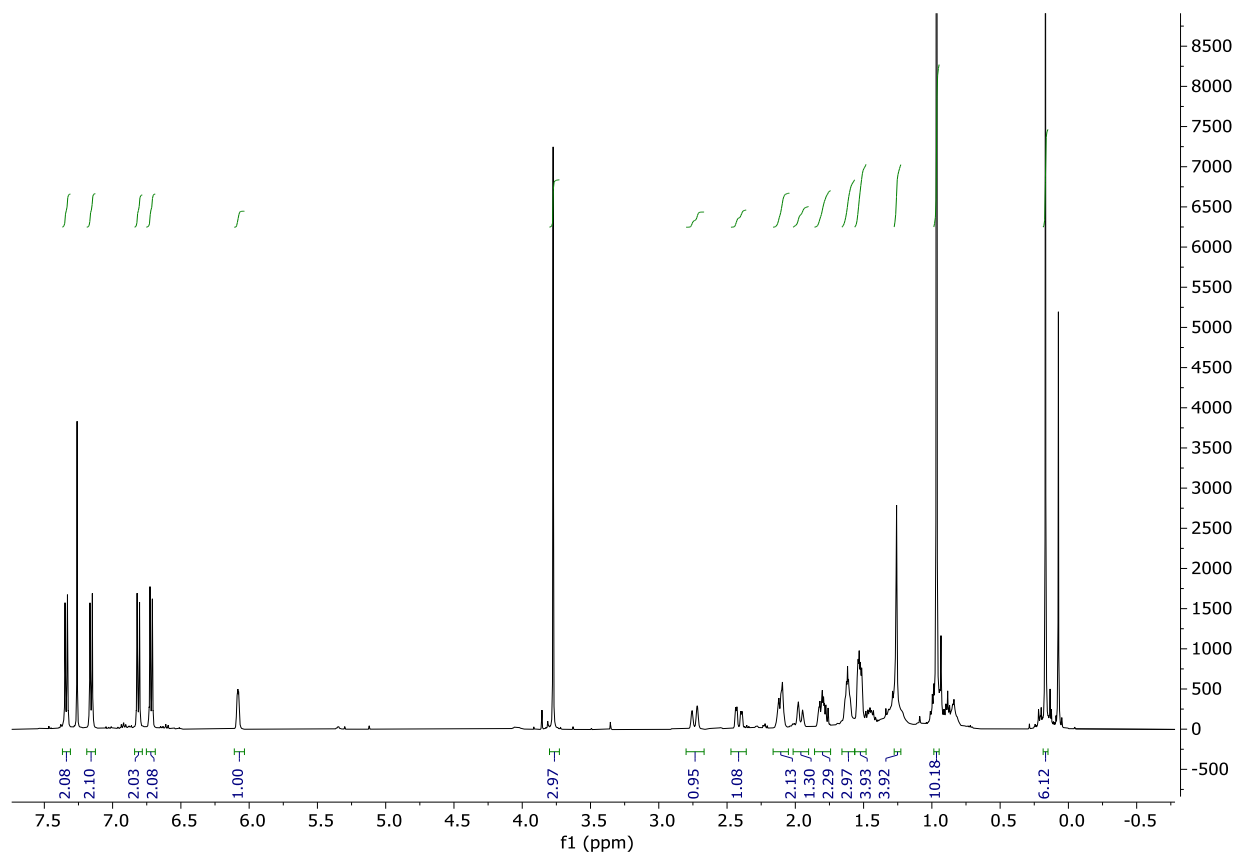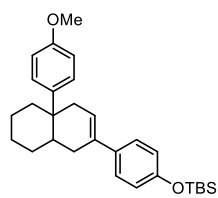
^{1}H NMR, CDCl$_3$-d
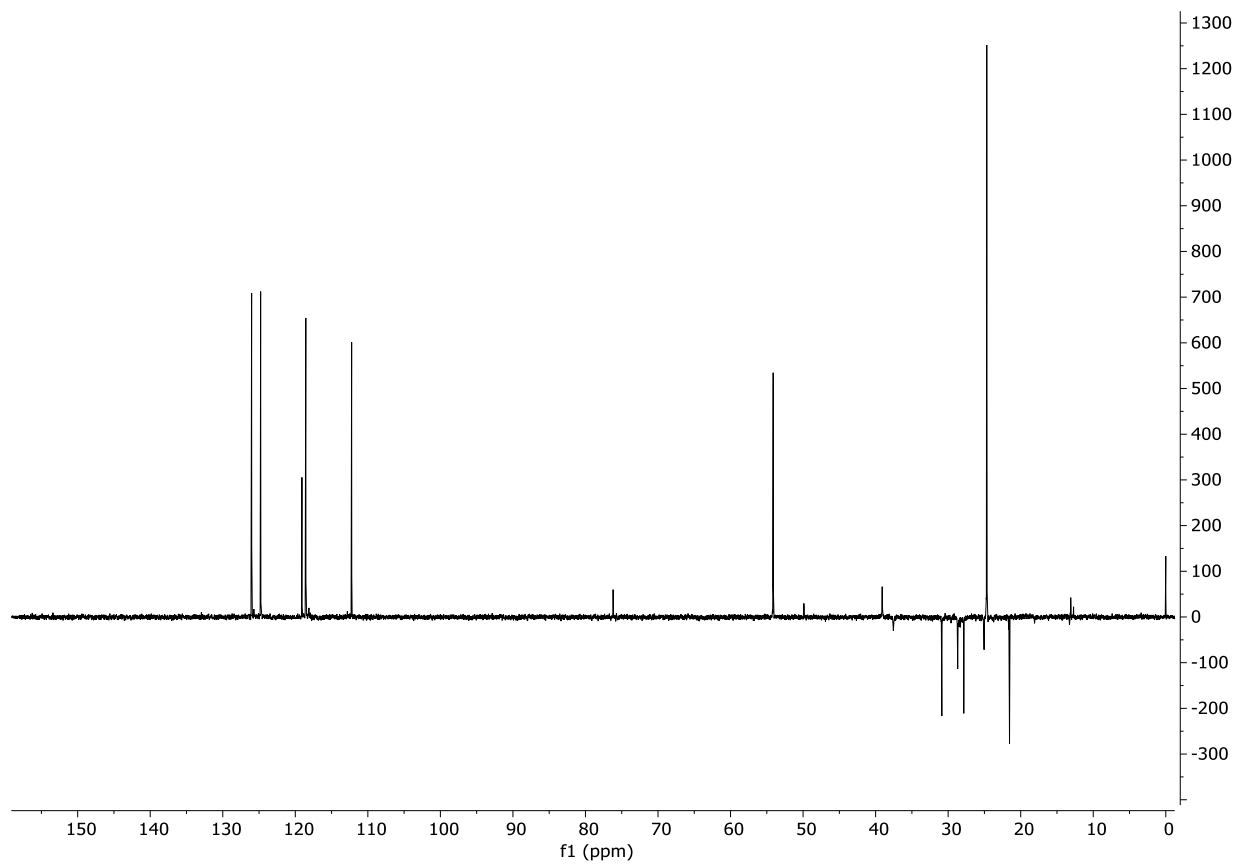
^{1}H NMR, CDCl$_3$-d

^{13}C DEPT NMR, CDCl$_3$-*d*
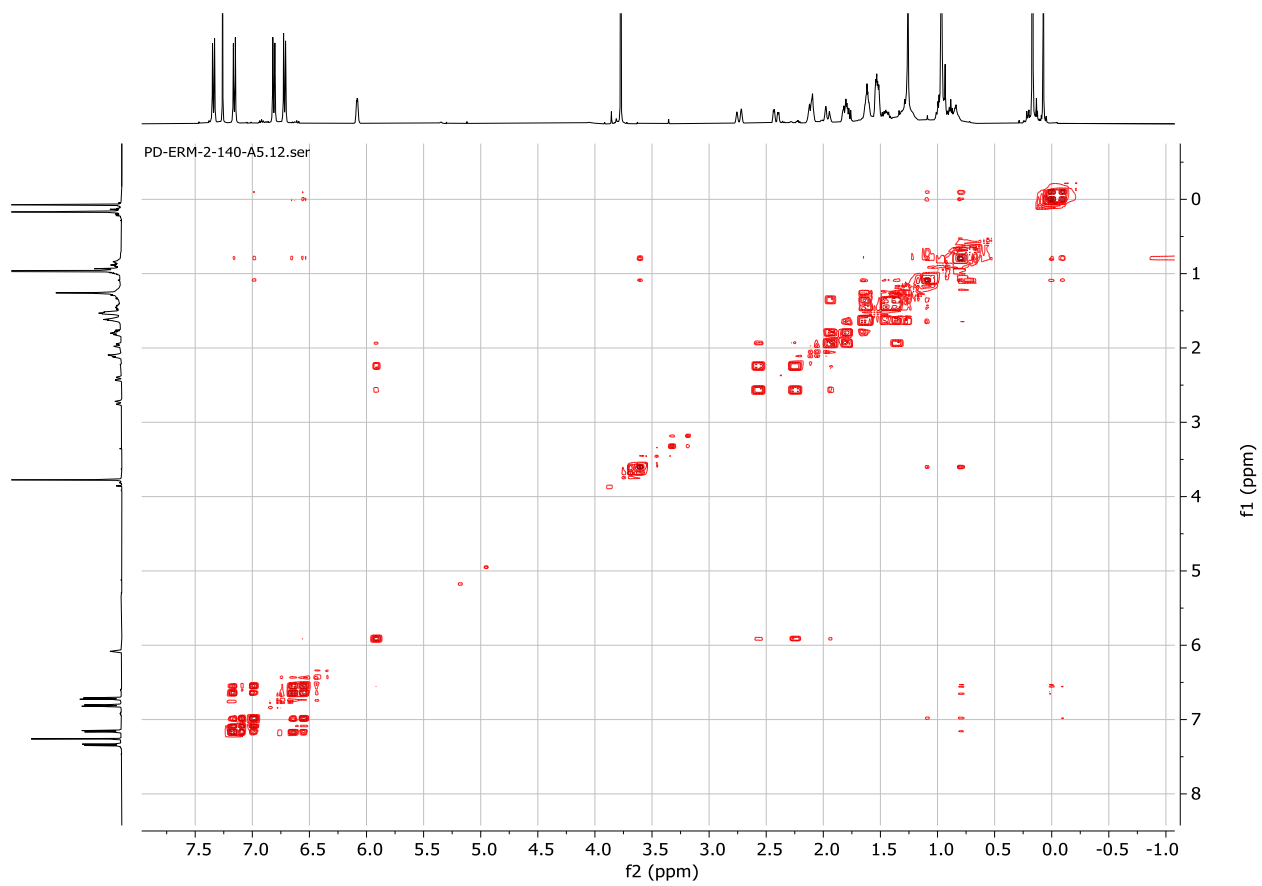
2D COSY NMR, CDCl₃-*d*
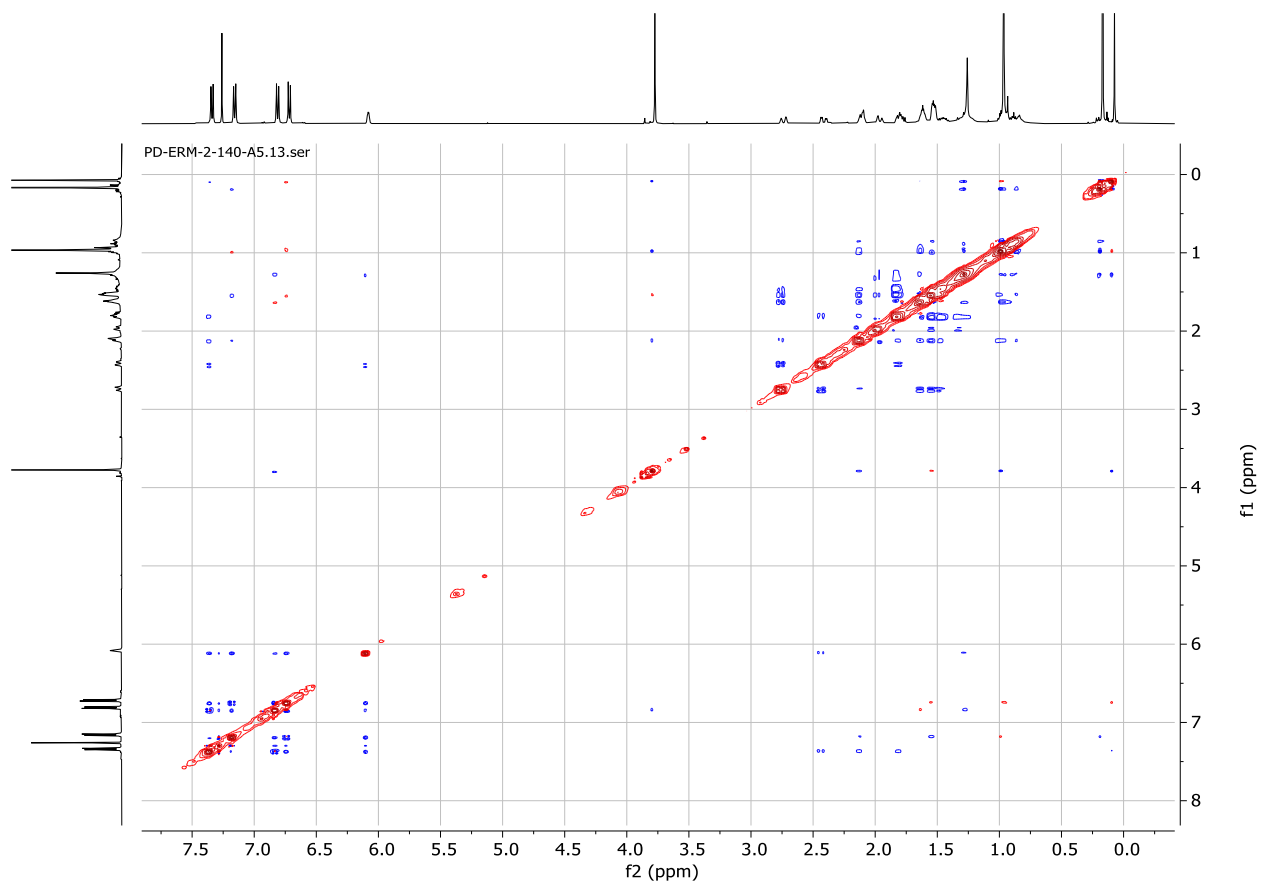
2D NOESY NMR, CDCl$_3$-d
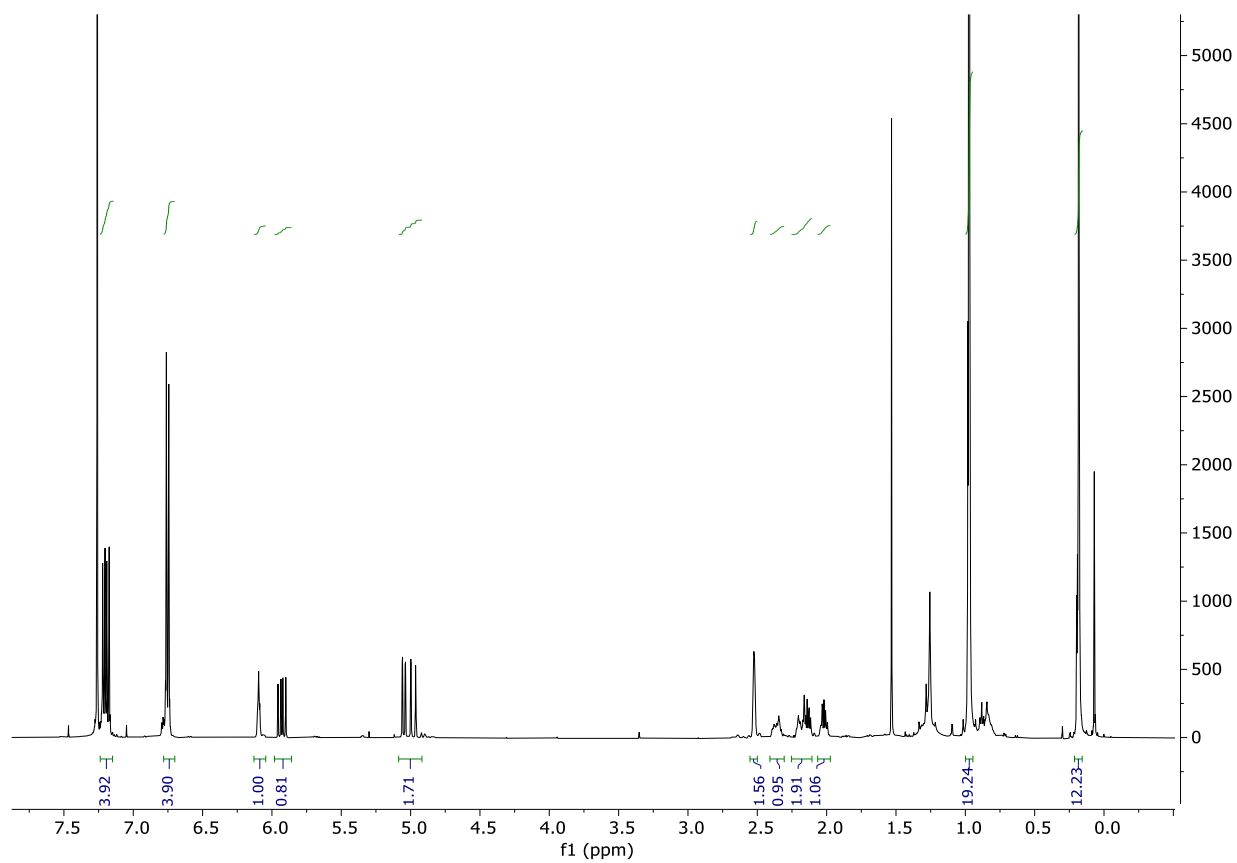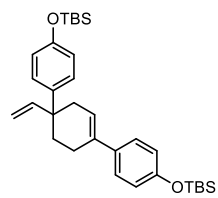
^{1}H NMR, CDCl$_3$-*d*
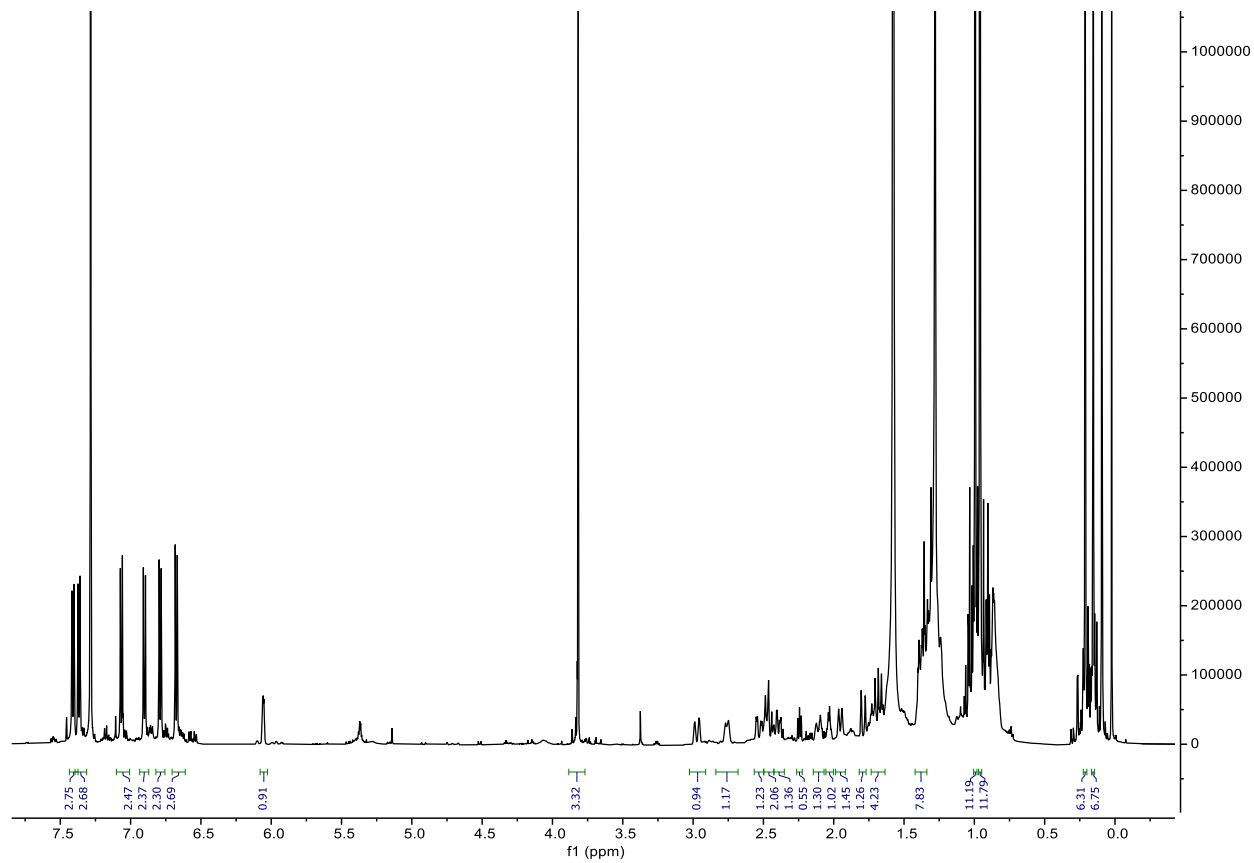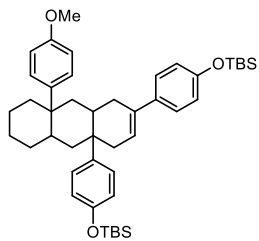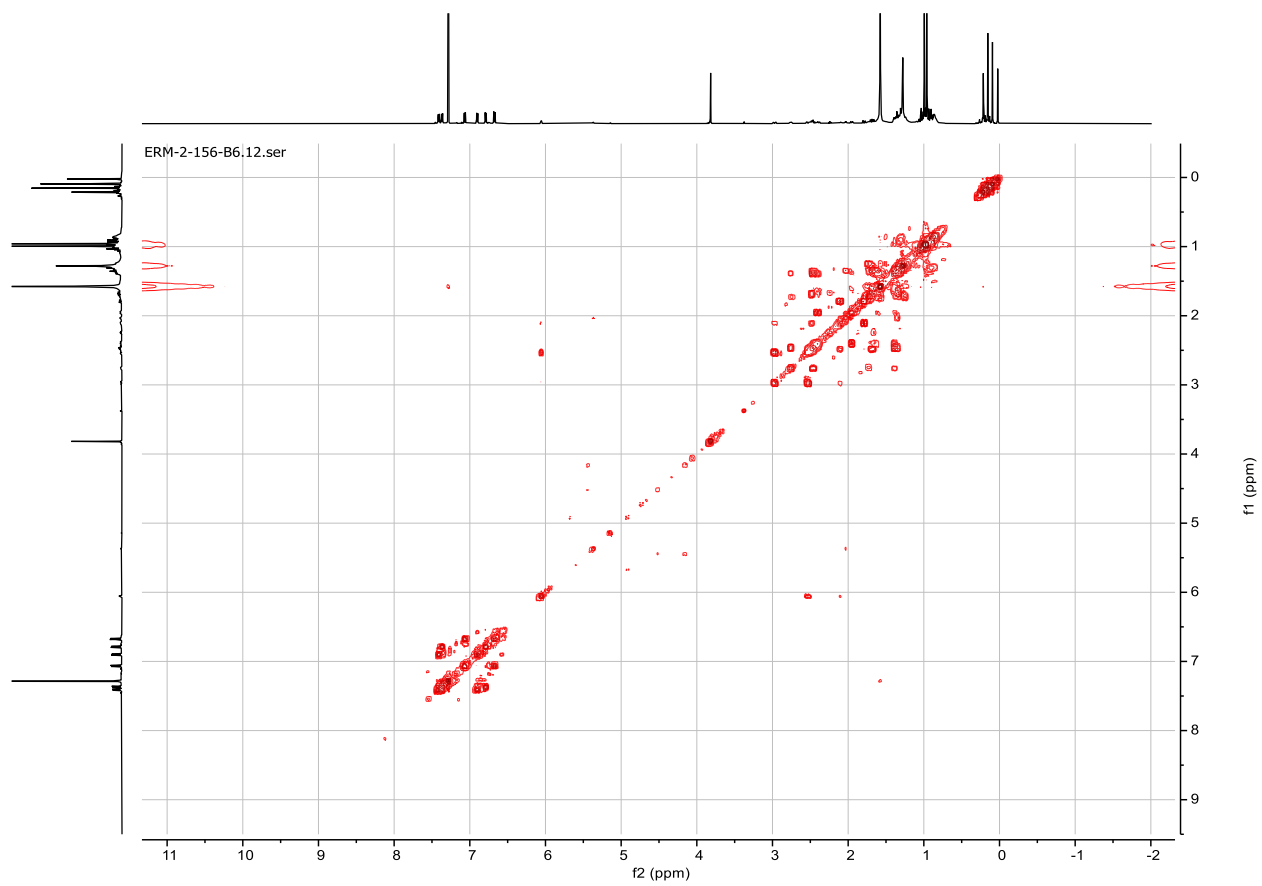
^{1}H NMR, CDCl$_3$-d

2D COSY NMR, CDCl₃-*d*
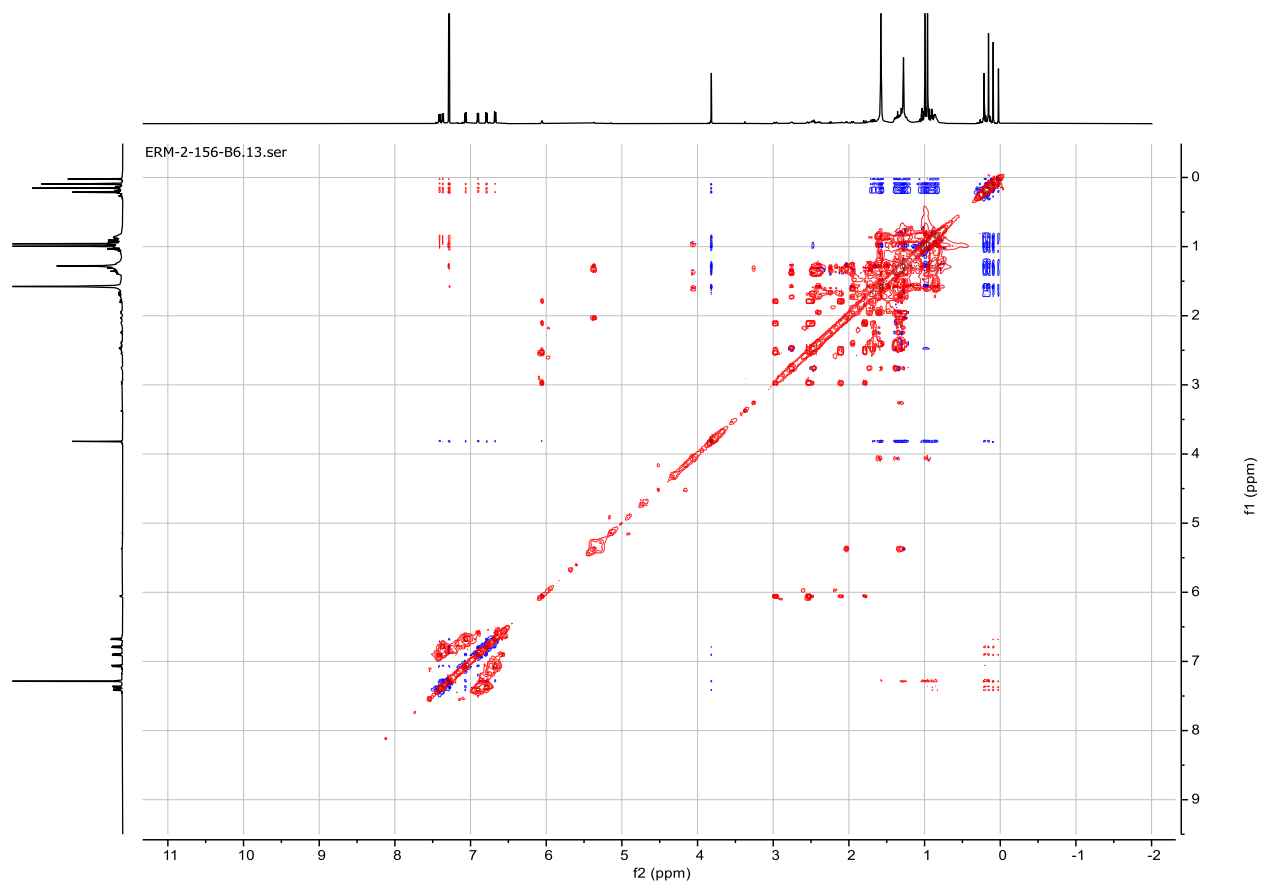
2D TOCSY NMR, CDCl$_3$-d

ERM-2-156-B6.14.ser
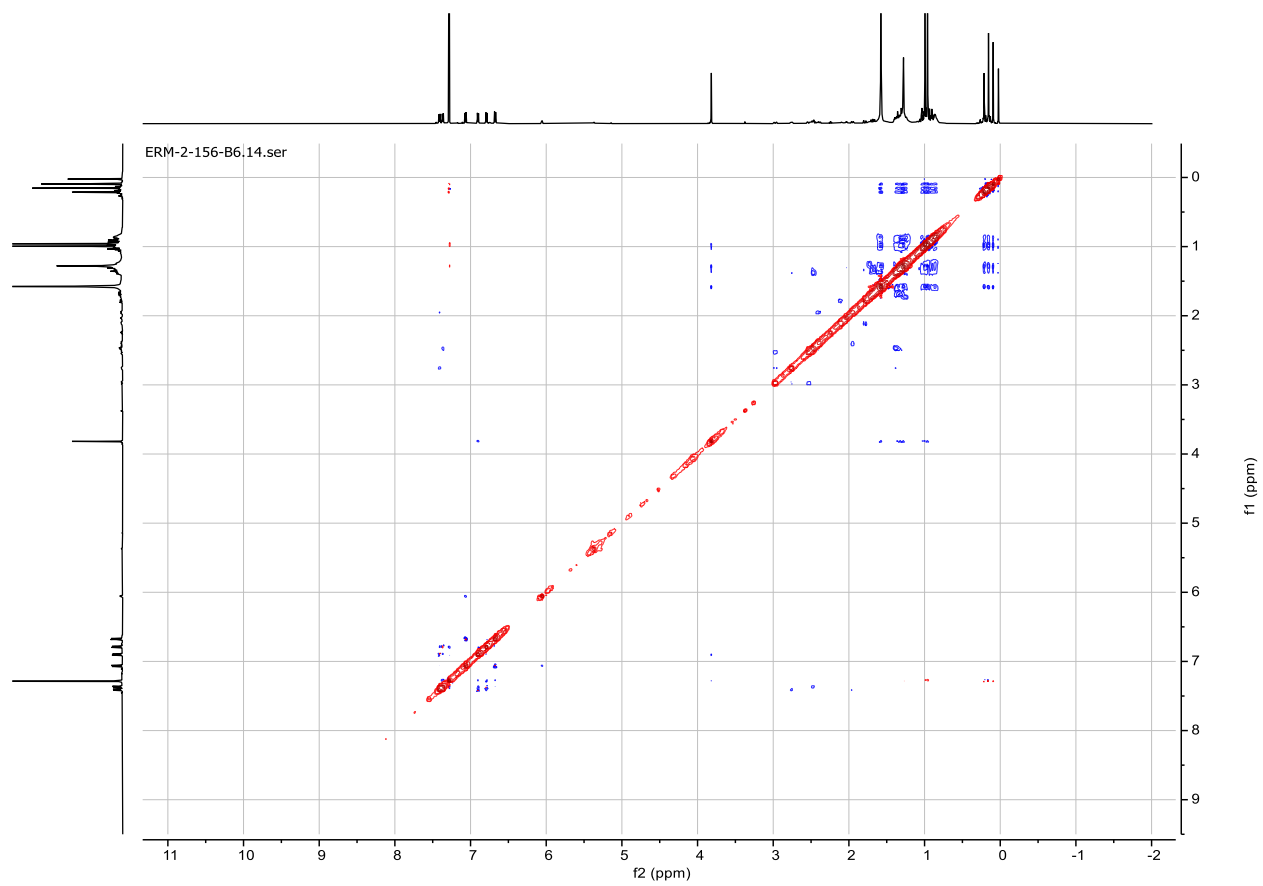
2D NOESY NMR, CDCl₃-*d*
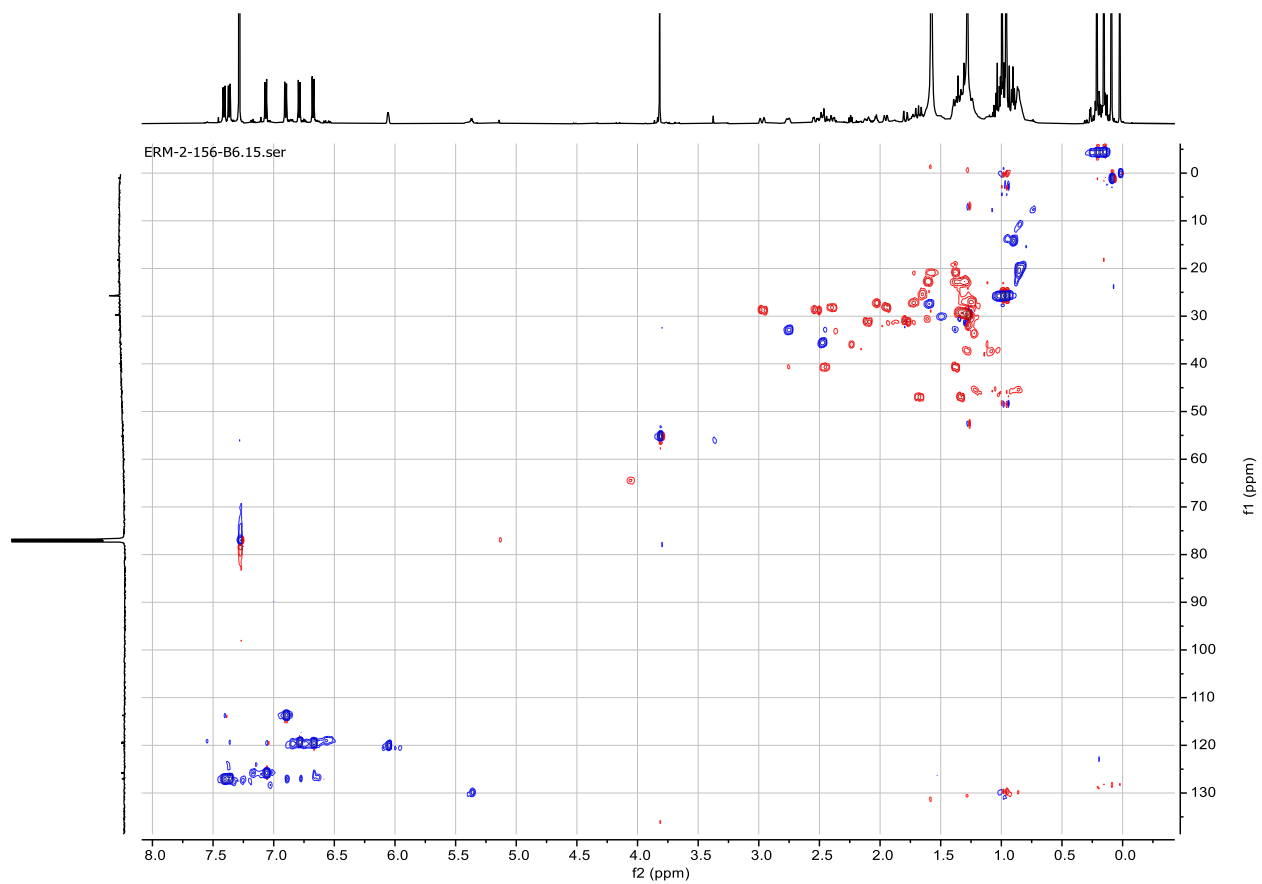
2D HSQC NMR, CDCl$_3$-d
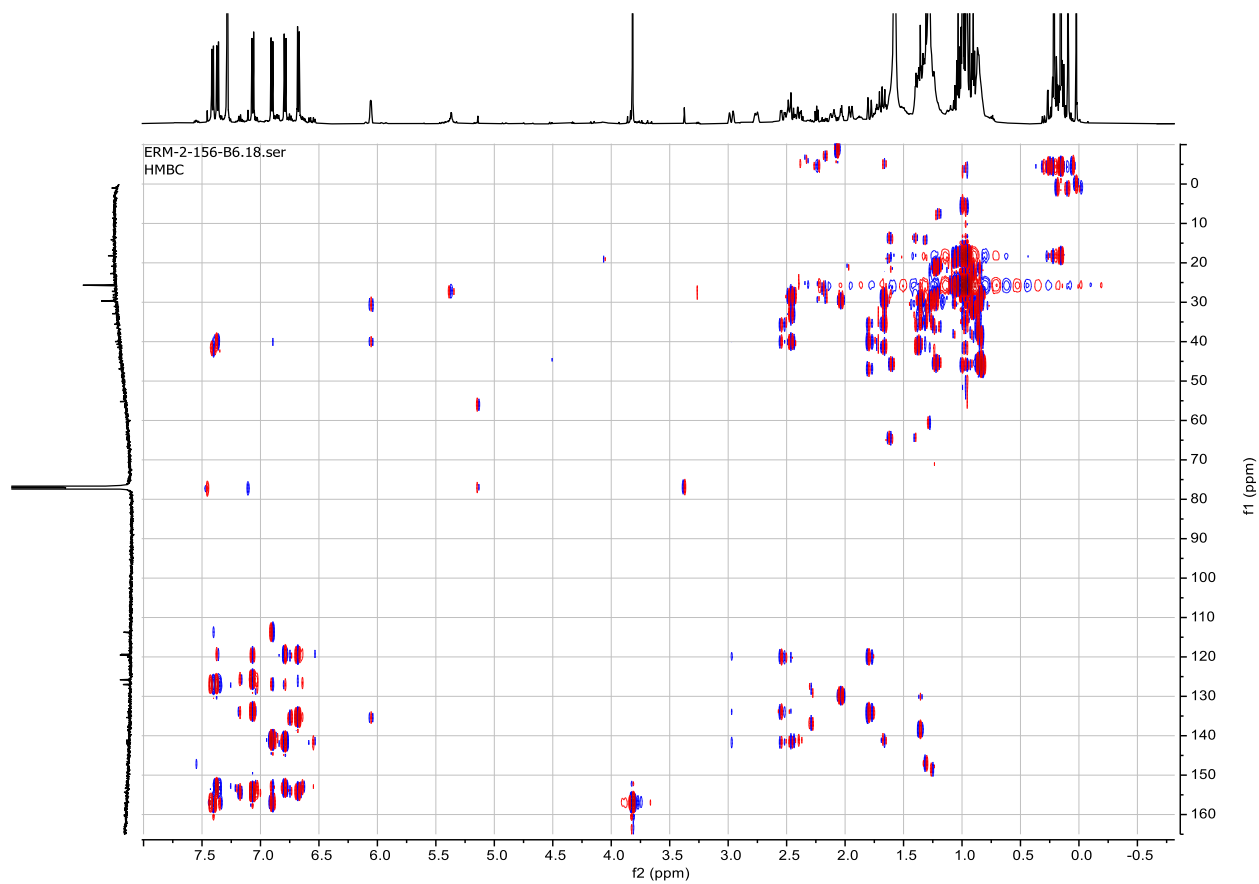
2D HMBC NMR, CDCl$_3$-*d*
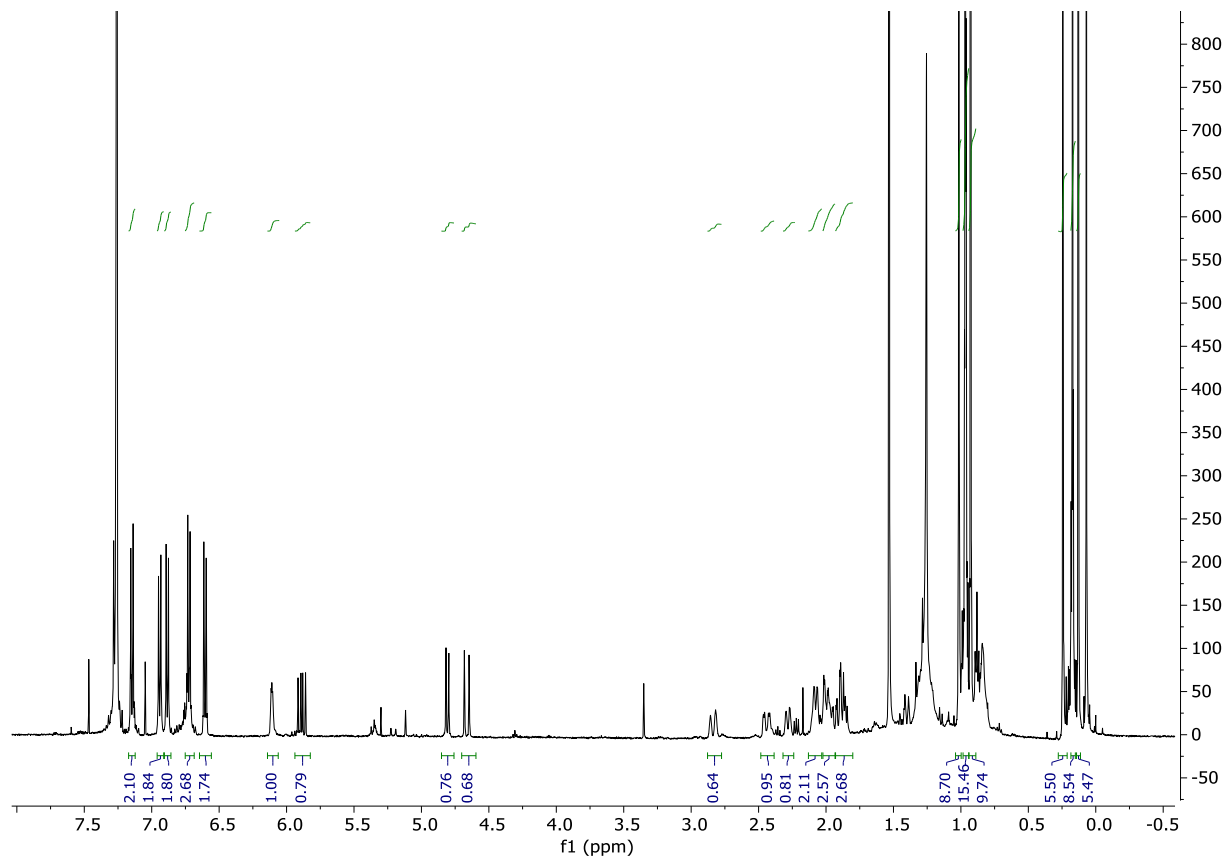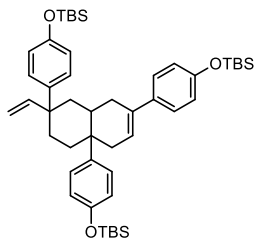
¹H NMR, CDCl₃-*d*

MALDI Spectra
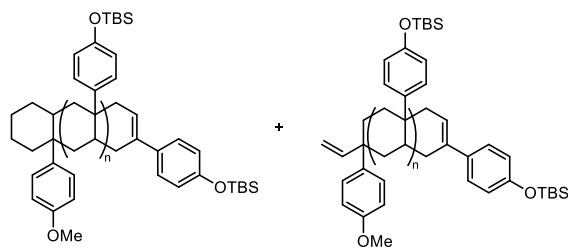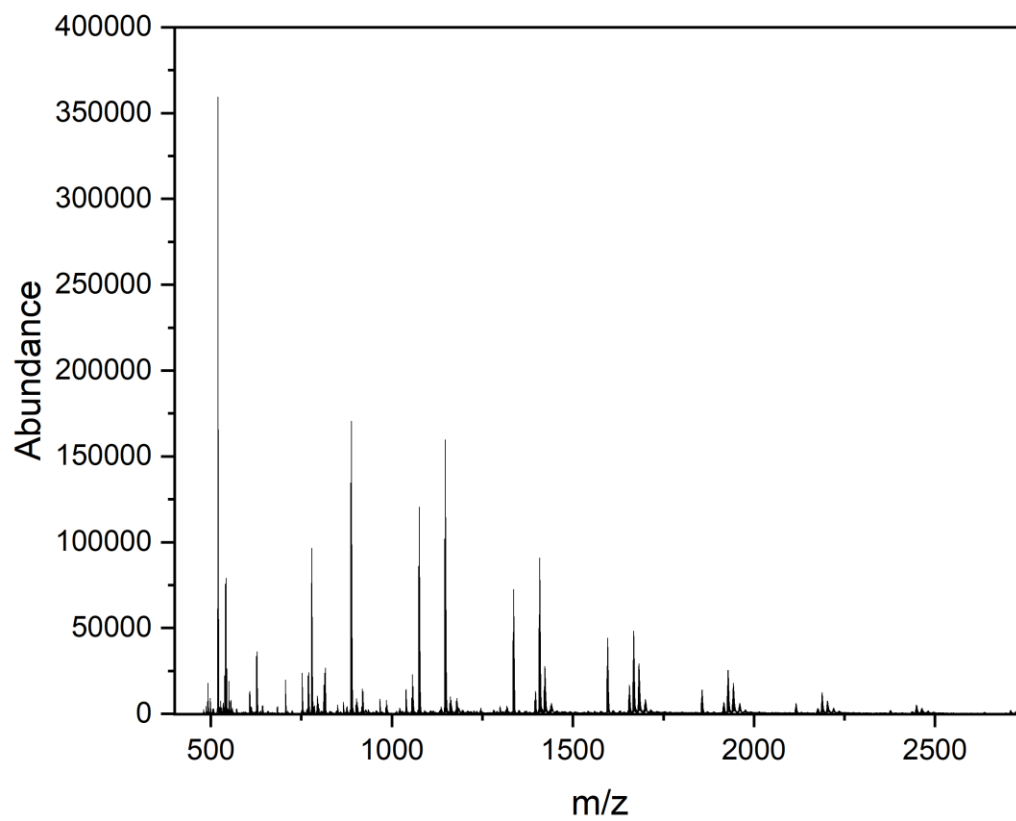
Figure 105. MALDI-TOF of LP-3b and LP-3b' (polymerization with initiator).
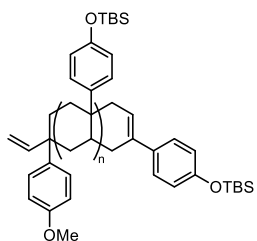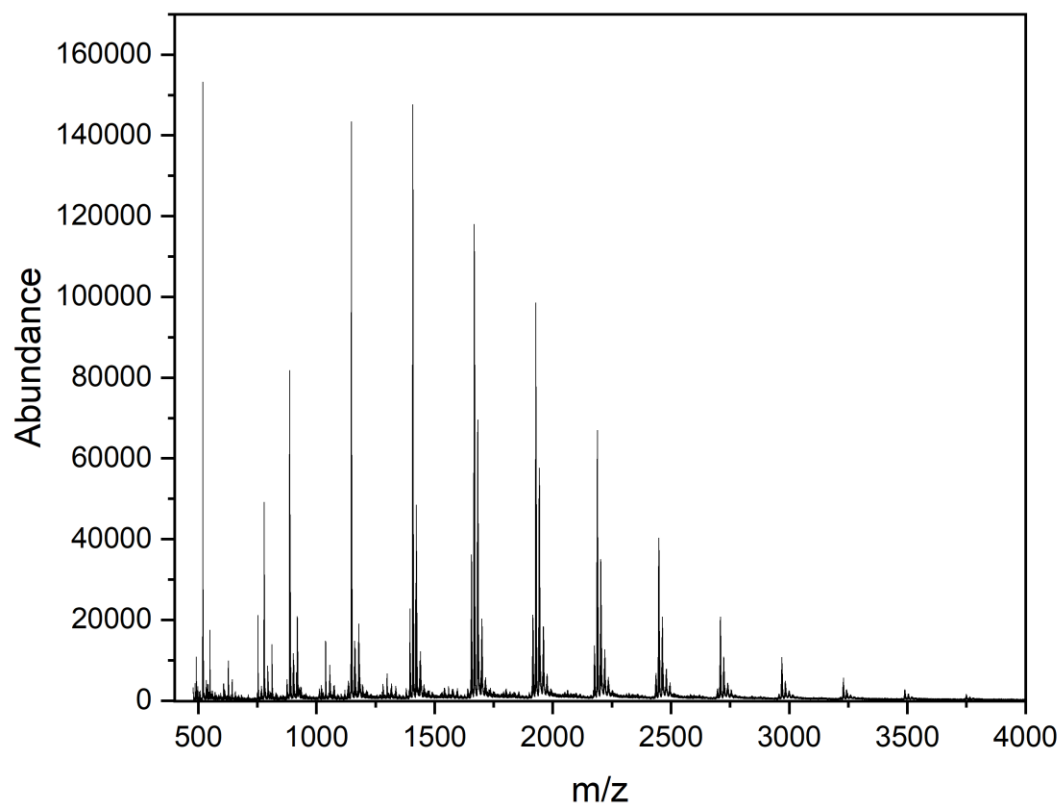
Figure 106. MALDI-TOF of LP-3b' (polymerization without initiator).
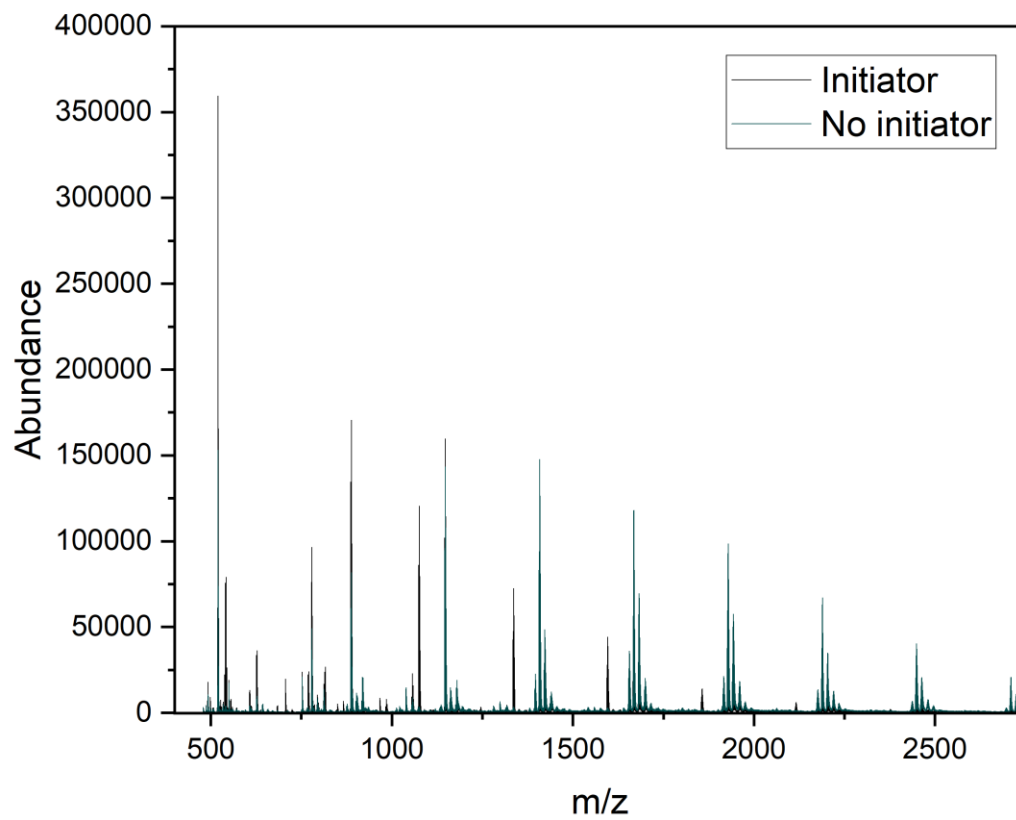
Figure 107. MALDI-TOF MS of LP-3b and LP-3b' (overlay).
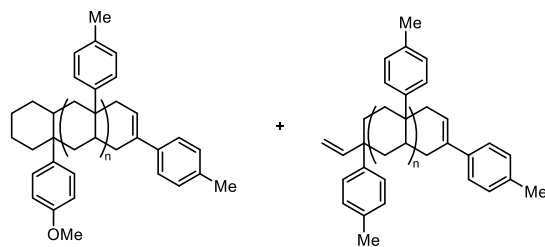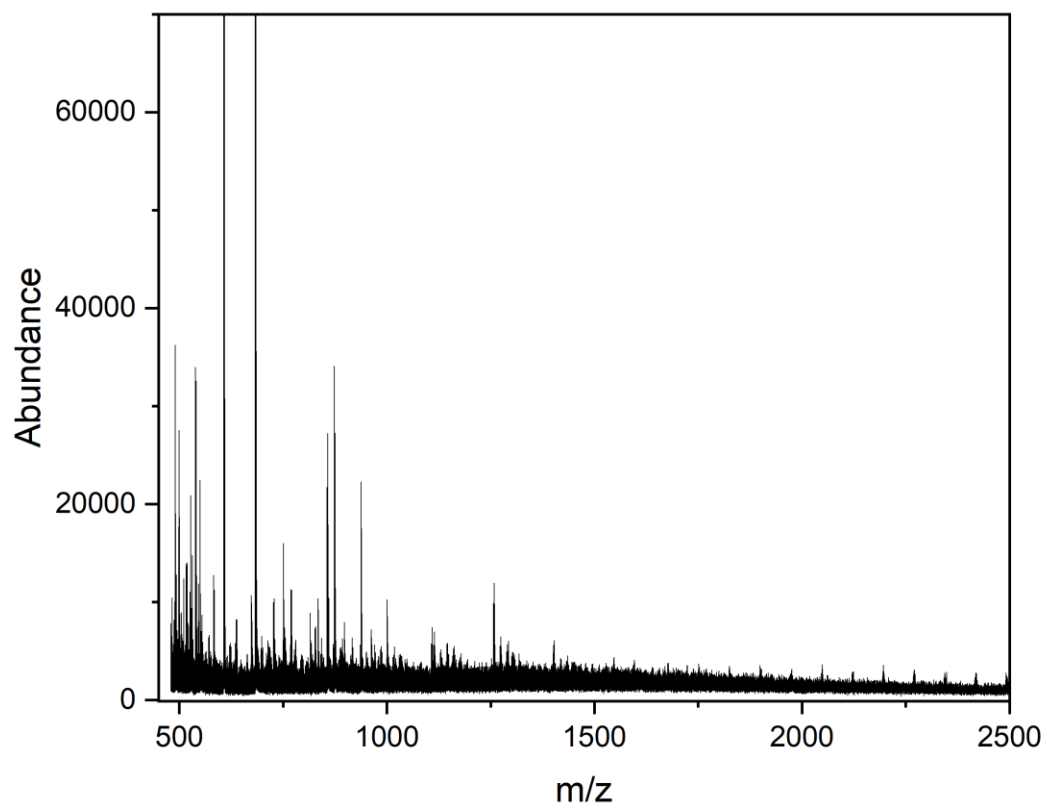
Figure 108. MALDI-TOF MS of LP-3d and LP-3d'.
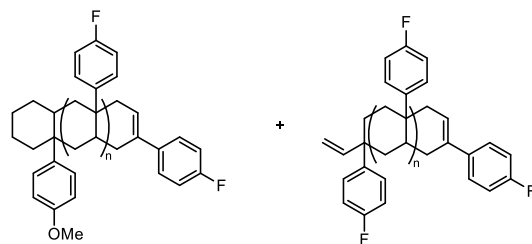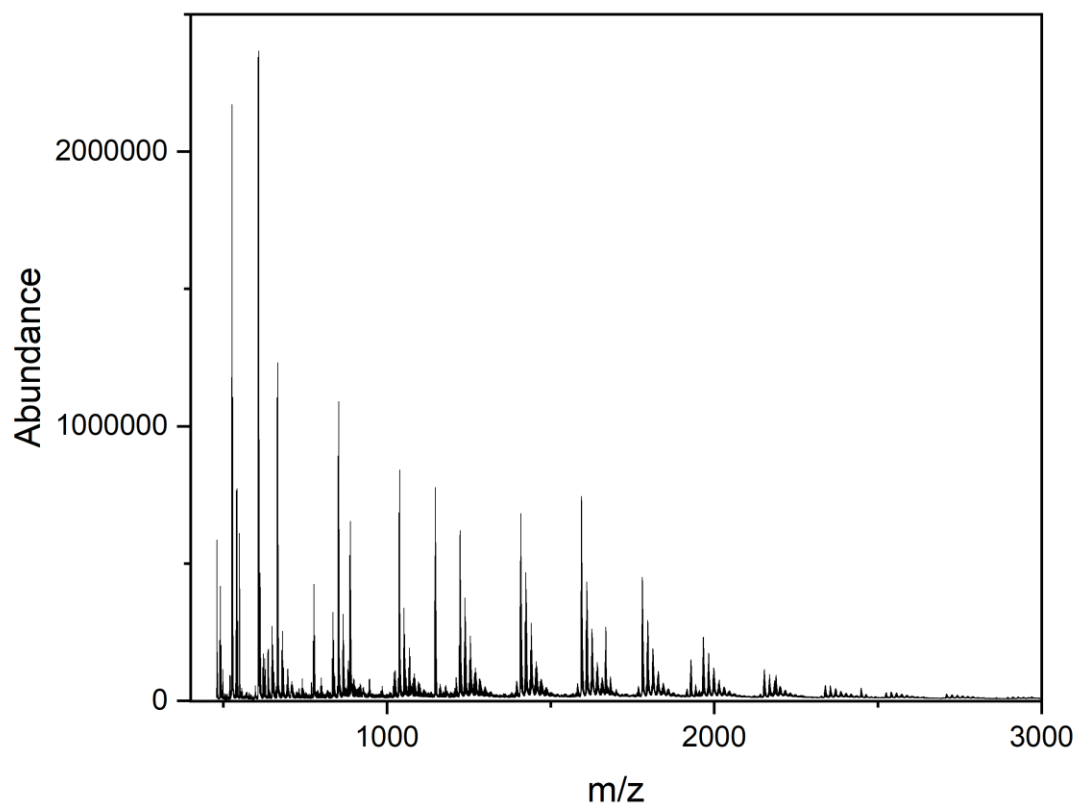
Figure 109. MALDI-TOF MS of LP-3e and PF-3e'.
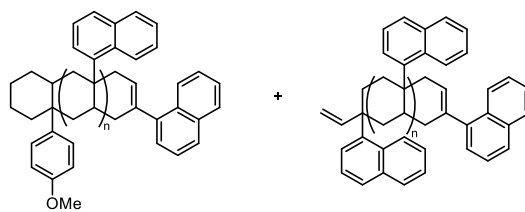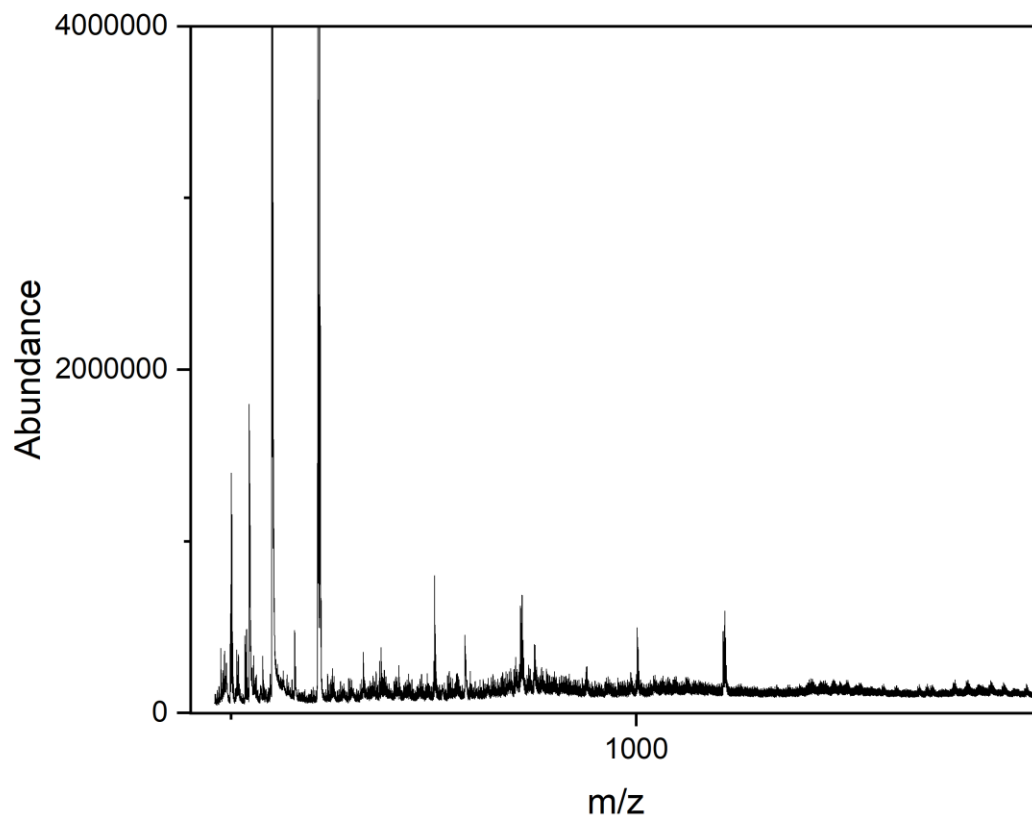
Figure 110. MALDI-TOF MS of LP-3g and LP-3g'.
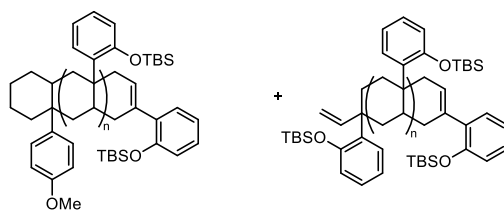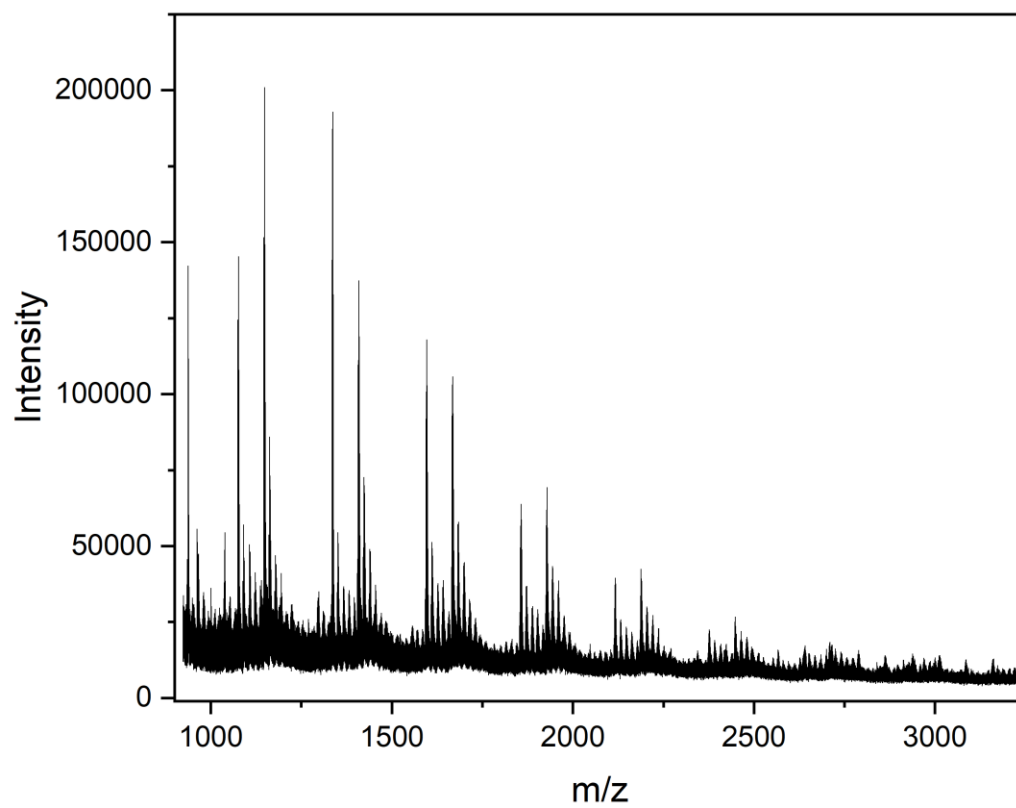
Figure 111. MALDI-TOF MS of LP-3i and 3i'.
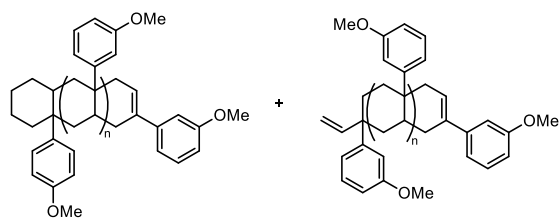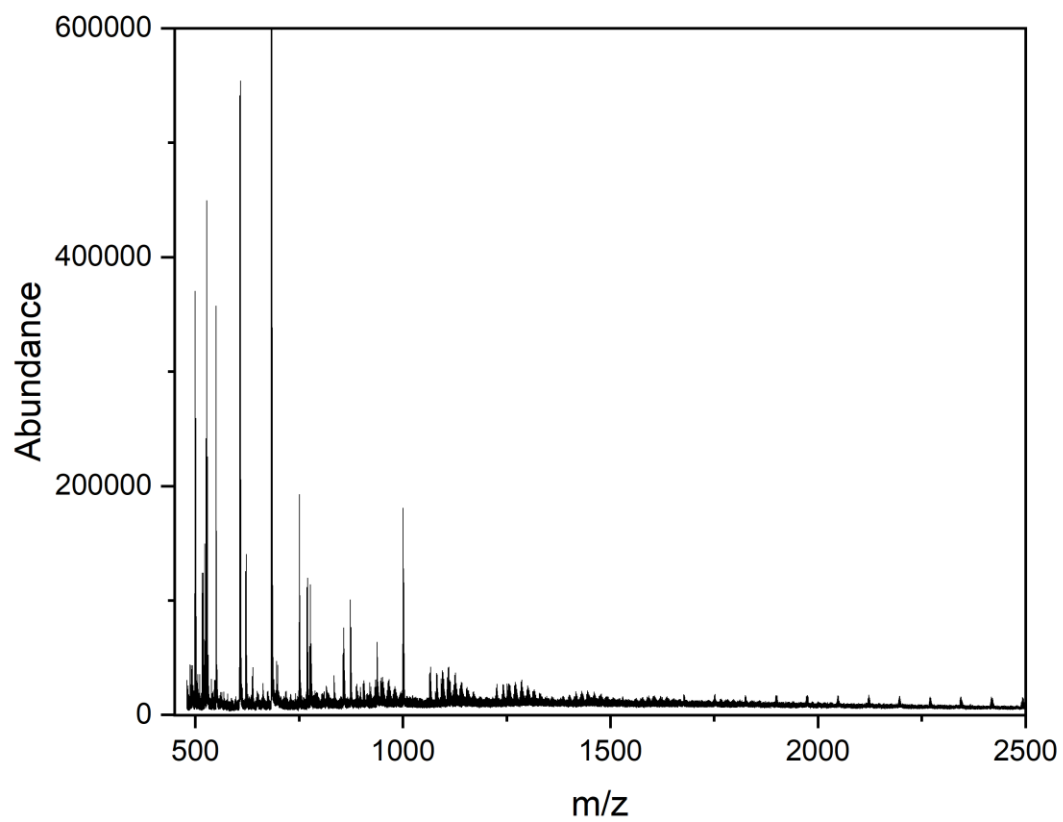
Figure 112. MALDI-TOF MS of LP-3j and LP-3j'.
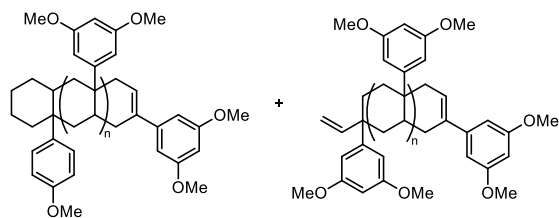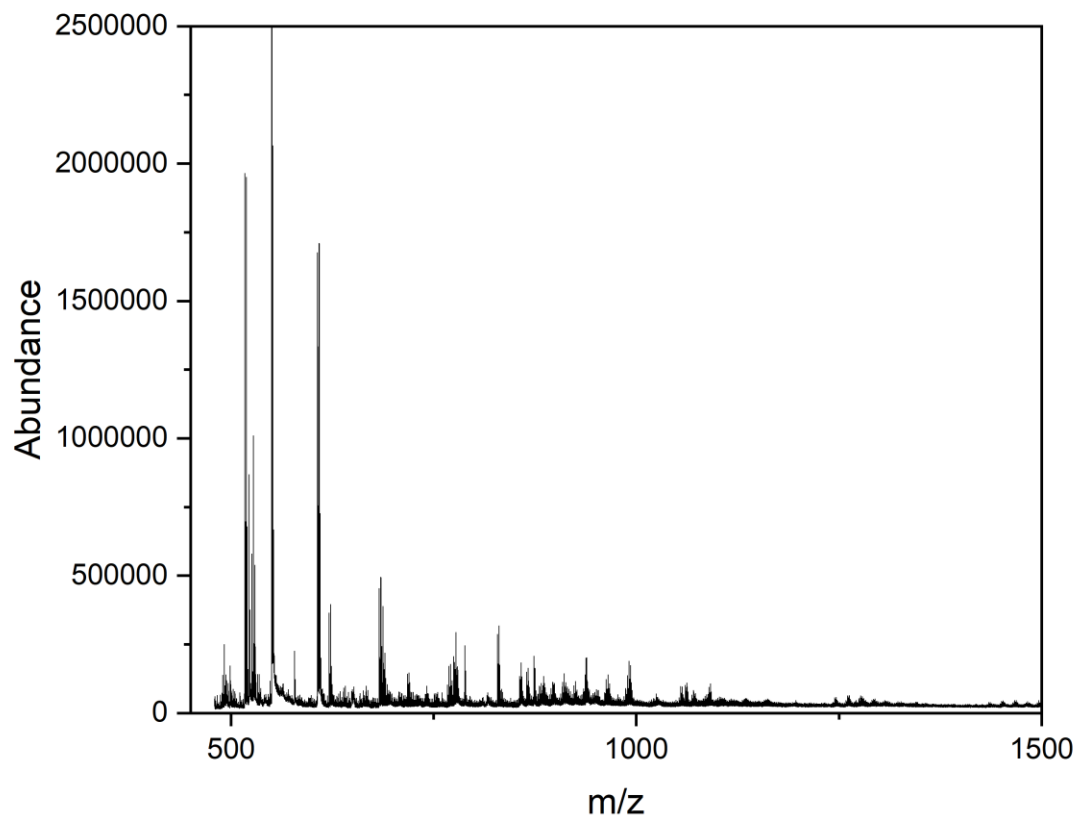
Figure 113. MALDI-TOF MS of LP-3k and LP-3k'.

Appendix B: Original research proposal: Cross-electrophile coupling for the functionalization and upcycling of poly(vinyl) chloride

October 18, 2022 at 10:30am

Abstract

Recycling of poly(vinyl chloride) (PVC) poses a significant industrial challenge due to the formation of hydrochloric acid, which damages industrial reprocessing equipment and initiates uncontrolled depolymerization reactions. Because of this, PVC is not collected even though it is a widely produced and used industrial polymer. Part of the challenge in functionalizing or reprocessing PVC arises from the low reactivity of alkyl C—Cl bonds, which present obstacles for post-polymerization modification (PPM). To develop a reaction that is suitable for PPM of PVC, I propose to develop a small-molecule transformation that will successfully functionalize linear, secondary alkyl chlorides through a cross-electrophile coupling approach. This cross-electrophile coupling will be developed and expanded to the PPM of PVC thermoplastics to install new functional groups on the polymer backbone and provide an opportunity to upcycle the material. I plan to explore the scope of this newly developed cross-electrophile coupling reaction with myriad aryl halides. Moreover, installing functional groups that can neutralize any HCl formation during reprocessing will present a viable alternative to industrial recycling. I will characterize the properties of these newly modified polymers to compare them to un-functionalized PVC and propose new applications for these functionalized materials.

Introduction and Motivation

Plastic waste and recycling presents an increasingly urgent issue in the United States, as less than 10% of plastics are recycled.[135] Indeed, plastic pollution has only increased recently due in part to the COVID-19 pandemic and the increased use of single-use plastic.[136] Plastic waste has continued to accumulate in the United States because many countries that used to import foreign recyclables—such as China—have begun to ban importation of foreign recyclables.[137] Recycling has stagnated and new solutions are crucial to maintain a sustainable, circular economy. Almost 90% of plastic waste falls within six categories of plastics, though not all these plastics can be recycled to the same extent. Most recycled polymers are thermoplastics, or unlinked polymer chains. Thermosets—crosslinked polymer chains—are not recyclable.[138] Efforts to recycle some thermoplastics—such as polyesters and high-density polyethylene—are limited by contamination and collection

errors. In other words, effective strategies to chemically recycle polymers such as polyethylene terephthalate (PET) exist, yet limitations in PET recycling arise from industrial and economic limitations.

Conversely, chemical processes to recycle polyvinyl chloride (PVC) are extremely limited. PVC is the third most-produced polymer in the world by volume.[139] While a majority of PVC is manufactured for construction purposes, it is also broadly incorporated in the manufacturing of medical equipment. The benefits of using PVC include its biocompatibility, low manufacturing cost, and robust mechanical lifetime. However, PVC begins to thermally degrade at approximately 200°C, at which point the polymer begins to dechlorinate and form hydrochloric acid.[140] Acid formation damages industrial recycling equipment, leads to depolymerization of the polymer, and can contaminate other polymers in recycling plants. The formation of HCl is a competing reaction that prevents the chemical recycling of PVC to recover monomers.[141] Due to these complications that arise from reprocessing and recycling PVC, it is neither recovered nor recycled.[142] While some plastics without chemical recycling strategies can be incinerated for energy recovery, PVC incineration results in the release of halogenated organics. Chemical strategies that aim to recycle this class of polymer should focus on mitigating the formation of HCl through single-electron pathways and maintaining or enhancing the robust mechanical properties of these materials. While chemically recycling to monomers would be entropically disfavored, PVC functionalization to form new polymers would serve as an attractive alternative to current end-of-life cycles for PVC.[143] Indeed, functionalization of polymers through activation of seemingly latent bonds has become increasingly studied and presents many new opportunities for chemical transformations.[144]

However, the C—Cl bond in PVC continues to present an obstacle for recycling and functionalization, rather than an opportunity for functionalization and upcycling to obtain new polymers with unique properties. Compared to other electrophiles, C—Cl bonds are relatively stable, which makes them less-suitable partners in typical metal-catalyzed transformations. Attempts to functionalize PVC through nucleophilic substitution at the C—Cl site have resulted in parallel formation of hydrochloric acid.[145,146] PVC has been functionalized through grafting of acrylic acid, but this method required a two-step transformation in which the PVC was first subjected to iodination before grafting via an ATRP mechanism.[147] Instead of exploring reactions that require

multiple steps—with each step leading to a decrease in % mol functionalization of the polymer—it would be prudent to develop a reaction that is able to functionalize PVC in one chemical transformation.

Alkyl halides remain under-explored as cross-coupling partners in two-electron transition-metal catalysis because they decompose via β-hydride elimination.[148,149] Researchers have avoided this elimination pathway by generating alkyl radicals that serve as partners in cross-electrophile coupling reactions.[150] This cross-electrophile coupling reaction uses starting materials that are more affordably sourced than their organometallic counterparts. Additionally, many of these cross-electrophile coupling reactions use of earth abundant catalysts—such as nickel—that make these transformations promising for industrial applications. While these cross-electrophile couplings have been expanded to include a small library of alkyl halides, their application to polymer functionalization has not yet been explored. Herein, I propose a strategy to functionalize PVC through cross-electrophile coupling of sp^3 C—Cl bonds to prevent the formation of hydrochloric acid. These transformations will also modify the polymer material properties and present a new opportunity for upcycling PVC for additional applications. By treating PVC as a feedstock for the formation of new polymers, we can open the door to additional lifecycles for an abundant polymer source.

Aim 1: Developing compatible sp$_3$ C–Cl functionalization reactions

Optimizing cross-electrophile coupling of secondary alkyl chlorides

Previous reports by Weix and coworkers demonstrate that coupling of alkyl chlorides in nickel-catalyzed cross-electrophile coupling is possible with the incorporation of specialized ligands and salt additives.[151]

Incorporation of sub-stoichiometric quantities of lithium iodide or lithium bromide promote the formation of alkyl bromides or iodides as
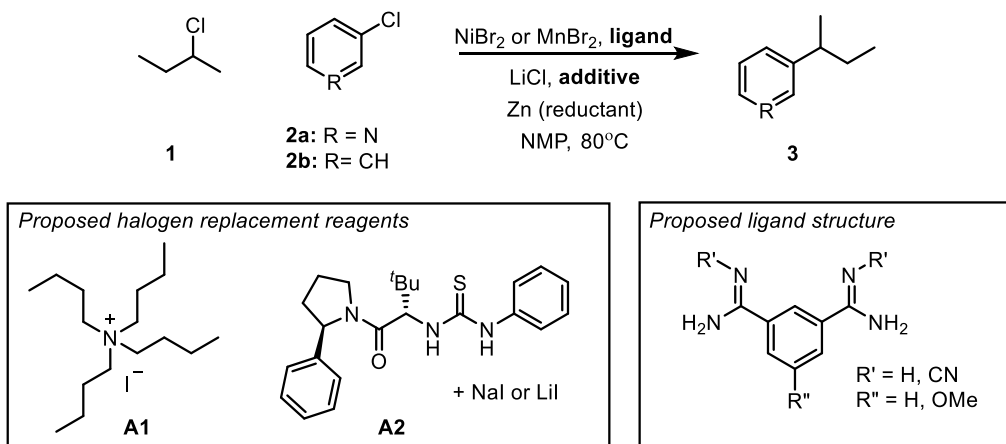
Scheme 5. Proposed cross-electrophile coupling reaction with 2-chlorobutadiene.

an intermediate prior to radical formation. While this method was applicable to the cross-coupling of primary alkyl chlorides, the yield decreased when applied to a cyclic secondary alkyl chloride. Secondary alkyl bromides have been reported as suitable cross coupling partners,[152] but linear alkyl chlorides were not explored in this method. Most likely, the slow formation of the secondary alkyl iodide or bromide (via S_N2) contributes to the low formation of product. I hypothesize that incorporating an additional catalyst to promote secondary alkyl chloride abstraction will promote alkyl iodide and radical formation. One option includes expanding the scope of salt additives to include quaternary ammonium salts (**A1**),[153] but chlorine abstraction could also be achieved through incorporation of a bis-thiourea catalyst and salt additive (**A2**) (**Scheme 5**).[154] Alternatively, substitution of the nickel to a MnBr$_2$ precatalyst could promote the formation of secondary alkyl radicals more favorably and increase the formation of cross-electrophile coupled product.[155] To develop a compatible alkyl C—Cl cross-coupling reaction, I propose first expanding the use of transition-metal catalysis to linear small molecules, such as 2-chlorobutane (**Scheme 5**). To optimize this reaction, gas chromatography mass spectrometry (GC-MS) will be employed to detect the formation of product (**3**) and unwanted side products, such as aryl dimerization. Alkyl chloride dimerization—while still somewhat undesirable—could prove a viable pathway to later functionalize PVC through crosslinking and network formation. As some secondary alkyl groups can isomerize in cross-coupling reactions with other catalytic systems,[156] nuclear magnetic resonance (NMR) spectroscopy will also be used to monitor the formation of any isomerized product. I plan to explore ligand structure, solvent, aryl halide coupling partners, and precatalyst structure as additional parameters to optimize the reaction. Developing this reaction expands the scope of viable substrates for alkyl-chloride cross-coupling transformations.

Once the reaction of 2-chlorobutane has been optimized as the alkyl chloride cross coupling partner, I plan to apply these conditions to 2,4-dichloropentane (DCP) (**Scheme 6**). DCP (**4**) can be prepared in one step[157] and is a small molecule that more closely mirrors the structure of PVC. I plan to monitor the formation of mono (**5**) and bis-substitution (**6**) of the aryl halide coupling partner as well as possible cyclization products. Moreover, since PVC varies in its tacticity,[158] I will study the effect of the stereochemical relationship between both stereoisomers of DCP on the yield of the cross-coupling reaction (**Scheme 6**). Separating these

diastereomers and studying them can also provide insight into the presence of radical rearrangements between adjacent C—Cl bonds during the mechanism. In other words, if (2*S*,4*S*)-DCP forms a racemic mixture of the mono product (**5**), I could conclude that radical rearrangements exist with neighboring alkyl chlorides. If the abundance of radicals or radical rearrangements inhibit the reaction, I propose substituting the salt additives for bromine-based halogen abstraction agents to decrease the rate of radical formation and better control the reaction. Studying this transformation will inform the design of initial parameters for applying this small-molecule reaction to the functionalization of PVC.

Experimental Challenges and Contingency Plans
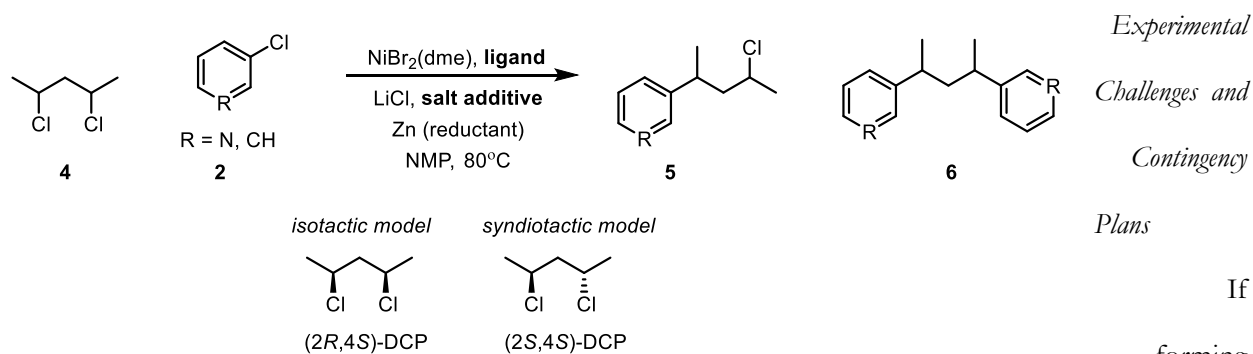
Scheme 6. Proposed cross-electrophile coupling reaction with 2,4 dichloropentane.

If forming cross-coupling products via an iodo- or bromo-alkyl intermediate is not successful, I plan to implement other synthetic strategies to achieve halogen atom abstraction and radical formation.[159,160] Incorporation of a dual catalytic system to activate the alkyl halide could improve the efficiency of the reaction; incorporation of more mild and homogenous reductants—such as amines—could also improve the yield of the desired cross-coupling product.[160] Photocatalytic strategies could also be explored as alternatives to obtain radical formation. Silyl radical precursors have enabled dual nickel/photoredox methods for the cross-electrophile coupling of primary and secondary alkyl chlorides.[161,162] Pyridiunium salts—when they form a donor-acceptor complex with Hantzsch esters—enable a single-electron transfer that also forms an alkyl radical from alkyl halide precursors.[163] The photocatalytic generation of the radical from an alkyl chloride precursor is a suitable alternative to the halogen-exchange intermediate. Photocatalytic transformations have been previously implemented in the post-polymerization functionalization and degradation of thermoplastics.[26]

Beyond photocatalysis, electrocatalytic methods also serve as an attractive alternative to promote cross-electrophile coupling of alkyl halides.[164] Several instances of cross-electrophile coupling of linear alkyl bromides[165–168] with aryl halides have been reported with a more limited exploration of activated alkyl chlorides.[169] The benefits of electrocatalysis include higher frequency and localization of reductions that lead to the generation of radicals. Therefore, I could also implement an electrochemical strategy to promote the generation of alkyl radicals from secondary alkyl chlorides. Judicious selection of an electrochemical mediator, electrode, and solvent would be parameters to explore while expanding the scope of alkyl chloride coupling partners.

Aim 2: Applying the transformation to PVC materials

Once the appropriate small molecule reaction has been optimized as outlined in Aim 1, I plan to apply this optimized reaction condition to the functionalization of PVC thermoplastics through a post-polymerization modification (PPM) reaction (**Scheme 7**). Gel permeation chromatography (GPC) will measure the polymer size and dispersity before and after the PPM reaction to ensure that the reaction does not significantly decrease polymer molecular weight through degradation pathways nor increase the molecular weight via crosslinking of PVC chains. To confirm incorporation of the aryl coupling partners, NMR and infrared spectroscopy (IR) analysis will be used to look for incorporation of sp² C—H bonds within the polymer backbone. Additionally, I will use NMR to determine the percent of C—Cl bonds that are
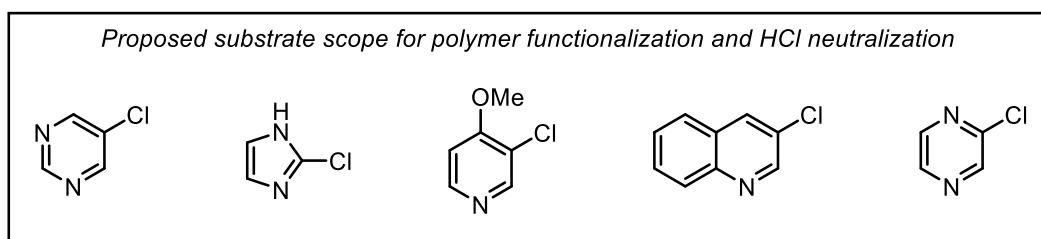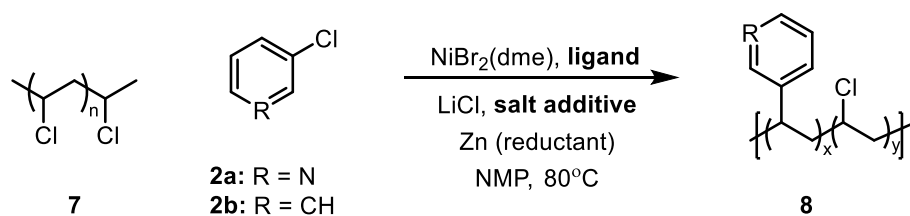
Scheme 7. Applying small-molecule cross-coupling reactions to the post-polymerization functionalization of poly(vinyl) chloride.

functionalized during the PPM reaction. Up to 30 mol % functionalization has been observed in other linear polymer modifications such as C—H activation[144,170] and grafting from PVC.[147] DOESY NMR will confirm the incorporation of the aryl coupling partners along the polymer chain. A library of aryl coupling partners will be screened to determine the scope of the PPM reaction, but 3-chloropyridine presents an especially attractive coupling partner because of the potential for pyridine to sequester any HCl generated during PVC reprocessing after functionalization. To test whether these functional groups sufficiently inhibit HCl formation and depolymerization, these materials will be reprocessed and heated, using GPC, NMR, and IR to measure the changes in polymer structure after recycling. Beyond expanding the library of aryl halide coupling partners, the reductant, catalyst, and ligand can be modified or optimized to promote PVC functionalization.

This PVC functionalization presents multiple strategies to modify and upcycle the PVC thermoplastic for additional applications. For example, I envision expanding on small molecule alkyl-alkyl reaction conditions to develop a reaction that crosslinks PVC chains to synthesize PVC thermosets.[171] Transforming PVC through crosslinking to form thermosets will develop a material with additional thermal and mechanical stability, and increase the elastic behavior of these materials.[138]

Functionalizing PVC through cross-electrophile coupling reactions will potentially mitigate the effects of harmful HCl formation. Furthermore, installing aryl moieties on the polymer chain will impart new properties on these PVC materials. To study the changes in the PPM transformation on properties such as crystallinity, melting temperature (T_m), and glass transition temperature (T_g), I plan to analyze these newly functionalized polymers through differential scanning calorimetry (DSC). Results from these experiments will inform new applications for these materials. However, I plan to design specific cross-coupling partners to modify material properties. Installing short branches of low-T_g polymers at C—Cl sites along the PVC backbone will lower the T_g of the thermoplastic.

To further characterize these modified thermoplastics and thermosets, I anticipate using dynamic mechanical analysis (DMA) to test the tensile properties of these materials compared to un-functionalized PVC polymers. I will compare the properties of the polymers through stress-strain curves. Impact testing and fracture propagation will provide additional opportunities to analyze and compare these materials to their non-

functionalized counterparts. As part of a longer goal to incorporate these polymers in industrial applications, I plan to study these polymers as components in blends with additives and other classes of polymers. In fact, modification of PVC with additional functional groups could expand the computability of these polymer chains within other polymer blends.

Experimental Challenges and Contingency Plans

Post-polymerization modification results in a broad range of % mol functionalization of the starting polymer. The most significant obstacle I anticipate for this project is functionalizing the polymer to an extent such that HCl generation is sequestered, and the resulting polymer has sufficiently unique properties for upcycling applications. Modification of solvent, ligand structure, catalyst type and equivalence, and external reductant can be investigated to increase the mol % functionalization of C—Cl bonds. While one approach could be to modify the PPM conditions to increase the mol % functionalization of PVC, I envision expanding the scope of aryl cross-coupling partners to include more basic sites and heterocycles with a higher pK_{aH} (**Scheme 7**).

The other challenge I anticipate is the functionalized PVC still forming HCl upon heating and reprocessing, leading to polymer degradation. Increasing the percent functionalization with substrates that can neutralize acid could mitigate this pathway. The focus of the transformation could be re-examined to focus on upcycling and using PVC as a feedstock for new polymer materials as an alternative approach to closed-loop recycling.

Summary and Conclusion

With the rise in plastic use, there is an increased demand for sensible recycling and end-of-life pathways for all polymers, including PVC. While many plastics have viable recycling and reprocessing pathways, PVC remains largely unexplored in industrial settings due to the lack of effective transformations. In the effort to develop new approaches to recycling PVC, I envision using PVC as a feedstock for functionalization and synthesis of new polymers. To realize this vision, I propose developing a cross-electrophile coupling reaction that successfully functionalizes secondary linear alkyl chlorides. Development of this small-molecule reaction broadens the scope of cross-electrophile coupling and will provide new mechanistic insights to this transition metal transformation. Once this transformation has been realized, I plan to apply this reaction to the

functionalization of PVC. The resulting functionalized polymers will be characterized to confirm successful modification and to test the new materials properties of the modified PVC. These functionalized material properties will provide new pathways for upcycling PVC and mitigate the harmful side reactions observed during conventional recycling methods.

References

(1)   Ciamician, G. The Photochemistry of the Future. *Science* **1912**, *36* (926), 385–394. https://doi.org/10.1126/science.36.926.385.

(2)   Rabek, J.F., Fouassier, J. P. *Radiation Curing in Polymer Science and Technology Fundamentals and Methods*; Elsevier Science Publishers LTD, 1993; Vol. 1.

(3)   Chatani, S.; Kloxin, C. J.; Bowman, C. N. The Power of Light in Polymer Science: Photochemical Processes to Manipulate Polymer Formation, Structure, and Properties. *Polym. Chem.* **2014**, *5* (7), 2187–2201. https://doi.org/10.1039/C3PY01334K.

(4)   Dewar, M. J.; Kirschner, S.; Kollmar, H. W. Orbital Isomerism as a Controlling Factor in Chemical Reactivity. *J. Am. Chem. Soc.* **1974**, *96* (16), 5240–5242.

(5)   Katz, H. Orbital Symmetry in Photochemical Transformations. *J. Chem. Educ.* **1971**, *48* (2), 84.

(6)   del Barrio, J.; Sánchez-Somolinos, C. Light to Shape the Future: From Photolithography to 4D Printing. *Adv. Opt. Mater.* **2019**, *7* (16), 1900598. https://doi.org/10.1002/adom.201900598.

(7)   Zhang, J.; Xiao, P. 3D Printing of Photopolymers. *Polym. Chem.* **2018**, *9* (13), 1530–1540. https://doi.org/10.1039/C8PY00157J.

(8)   Ma, Y.; Kottisch, V.; McLoughlin, E. A.; Rouse, Z. W.; Supej, M. J.; Baker, S. P.; Fors, B. P. Photoswitching Cationic and Radical Polymerizations: Spatiotemporal Control of Thermoset Properties. *J. Am. Chem. Soc.* **2021**, *143* (50), 21200–21205. https://doi.org/10.1021/jacs.1c09523.

(9)   Yan, Q.; Wang, S. Fusion of Aggregation-Induced Emission and Photochromics for Promising Photoresponsive Smart Materials. *Mater. Chem. Front.* **2020**, *4* (11), 3153–3175. https://doi.org/10.1039/D0QM00522C.

(10)   Mansø, M.; Petersen, A. U.; Wang, Z.; Erhart, P.; Nielsen, M. B.; Moth-Poulsen, K. Molecular Solar Thermal Energy Storage in Photoswitch Oligomers Increases Energy Densities and Storage Times. *Nat. Commun.* **2018**, *9* (1), 1945.

(11)   Jia, S.; Fong, W.-K.; Graham, B.; Boyd, B. J. Photoswitchable Molecules in Long-Wavelength Light-Responsive Drug Delivery: From Molecular Design to Applications. *Chem. Mater.* **2018**, *30* (9), 2873–2887. https://doi.org/10.1021/acs.chemmater.8b00357.

(12)   Fuhrmann, A.; Göstl, R.; Wendt, R.; Kötteritzsch, J.; Hager, M. D.; Schubert, U. S.; Brademann-Jock, K.; Thünemann, A. F.; Nöchel, U.; Behl, M.; Hecht, S. Conditional Repair by Locally Switching the Thermal Healing Capability of Dynamic Covalent Polymers with Light. *Nat. Commun.* **2016**, *7* (1), 13623. https://doi.org/10.1038/ncomms13623.

(13)   Kathan, M.; Kovaříček, P.; Jurissek, C.; Senf, A.; Dallmann, A.; Thünemann, A. F.; Hecht, S. Control of Imine Exchange Kinetics with Photoswitches to Modulate Self-Healing in Polysiloxane Networks by Light Illumination. *Angew. Chem. Int. Ed.* **2016**, *55* (44), 13882–13886. https://doi.org/10.1002/anie.201605311.

(14)   Russew, M.-M.; Hecht, S. Photoswitches: From Molecules to Materials. *Adv. Mater.* **2010**, *22* (31), 3348–3360. https://doi.org/10.1002/adma.200904102.

(15)   Jin, Y.; Yu, C.; Denman, R. J.; Zhang, W. Recent Advances in Dynamic Covalent Chemistry. *Chem. Soc. Rev.* **2013**, *42* (16), 6634–6654. https://doi.org/10.1039/C3CS60044K.

(16)   Zheng, N.; Xu, Y.; Zhao, Q.; Xie, T. Dynamic Covalent Polymer Networks: A Molecular Platform for Designing Functions beyond Chemical Recycling and Self-Healing. *Chem. Rev.* **2021**, *121* (3), 1716–1745. https://doi.org/10.1021/acs.chemrev.0c00938.

(17)   Lemieux, V.; Gauthier, S.; Branda, N. R. Selective and Sequential Photorelease Using Molecular Switches. *Angew. Chem.-Int. Ed.* **2006**, *45* (41), 6820–6824. https://doi.org/10.1002/anie.200601584.

(18)   Kathan, M.; Eisenreich, F.; Jurissek, C.; Dallmann, A.; Gurke, J.; Hecht, S. Light-Driven Molecular Trap Enables Bidirectional Manipulation of Dynamic Covalent Systems. *Nat. Chem.* **2018**, *10* (10), 1031–1036. https://doi.org/10.1038/s41557-018-0106-8.

(19)   Narayanam, J. M. R.; Stephenson, C. R. J. Visible Light Photoredox Catalysis: Applications in Organic Synthesis. *Chem. Soc. Rev.* **2011**, *40* (1), 102–113. https://doi.org/10.1039/B913880N.

(20)   Corrigan, N.; Shanmugam, S.; Xu, J.; Boyer, C. Photocatalysis in Organic and Polymer Synthesis. *Chem. Soc. Rev.* **2016**, *45* (22), 6165–6212. https://doi.org/10.1039/C6CS00185H.

(21)   Staveness, D.; Bosque, I.; Stephenson, C. R. J. Free Radical Chemistry Enabled by Visible Light-Induced Electron Transfer. *Acc. Chem. Res.* **2016**, *49* (10), 2295–2306. https://doi.org/10.1021/acs.accounts.6b00270.

(22)   Zhao, J.; Brosmer, J. L.; Tang, Q.; Yang, Z.; Houk, K. N.; Diaconescu, P. L.; Kwon, O. Intramolecular Crossed [2+2] Photocycloaddition through Visible Light-Induced Energy Transfer. *J. Am. Chem. Soc.* **2017**, *139* (29), 9807–9810. https://doi.org/10.1021/jacs.7b05277.

(23)   Fujiya, A.; Nobuta, T.; Yamaguchi, E.; Tada, N.; Miura, T.; Itoh, A. Aerobic Photooxidative Direct Asymmetric Aldol Reactions of Benzyl Alcohols Using Water as the Solvent. *RSC Adv.* **2015**, *5* (49), 39539–39543. https://doi.org/10.1039/C5RA05155J.

(24)   Zhang, Z.; Li, X.; Zhou, D.; Ding, S.; Wang, M.; Zeng, R. Controllable C–H Alkylation of Polyethers via Iron Photocatalysis. *J. Am. Chem. Soc.* **2023**, *145* (13), 7612–7620. https://doi.org/10.1021/jacs.3c01100.

(25)   Gentry, E. C.; Knowles, R. R. Synthetic Applications of Proton-Coupled Electron Transfer. *Acc. Chem. Res.* **2016**, *49* (8), 1546–1556. https://doi.org/10.1021/acs.accounts.6b00272.

(26)   Nguyen, S. T.; McLoughlin, E. A.; Cox, J. H.; Fors, B. P.; Knowles, R. R. Depolymerization of Hydroxylated Polymers via Light-Driven C–C Bond Cleavage. *J. Am. Chem. Soc.* **2021**, *143* (31), 12268–12277. https://doi.org/10.1021/jacs.1c05330.

(27)   Fors, B. P.; Hawker, C. J. Control of a Living Radical Polymerization of Methacrylates by Light. *Angew. Chem. Int. Ed.* **2012**, *51* (35), 8850–8853. https://doi.org/10.1002/anie.201203639.

(28)   Kottisch, V.; Michaudel, Q.; Fors, B. P. Cationic Polymerization of Vinyl Ethers Controlled by Visible Light. *J. Am. Chem. Soc.* **2016**, *138* (48), 15535–15538. https://doi.org/10.1021/jacs.6b10150.

(29)   Kottisch, V.; Michaudel, Q.; Fors, B. P. Photocontrolled Interconversion of Cationic and Radical Polymerizations. *J. Am. Chem. Soc.* **2017**, *139* (31), 10665–10668. https://doi.org/10.1021/jacs.7b06661.

(30)   Chen, M.; MacLeod, M. J.; Johnson, J. A. Visible-Light-Controlled Living Radical Polymerization from a Trithiocarbonate Iniferter Mediated by an Organic Photoredox Catalyst. *ACS Macro Lett.* **2015**, *4* (5), 566–569. https://doi.org/10.1021/acsmacrolett.5b00241.

(31)   Chen, D.-F.; Boyle, B. M.; McCarthy, B. G.; Lim, C.-H.; Miyake, G. M. Controlling Polymer Composition in Organocatalyzed Photoredox Radical Ring-Opening Polymerization of Vinylcyclopropanes. *J. Am. Chem. Soc.* **2019**, *141* (33), 13268–13277. https://doi.org/10.1021/jacs.9b07230.

(32)   Huang, Z.; Chen, Z.; Jiang, Y.; Li, N.; Yang, S.; Wang, G.; Pan, X. Metal-Free Hydrosilylation Polymerization by Merging Photoredox and Hydrogen Atom Transfer Catalysis. *J. Am. Chem. Soc.* **2021**, *143* (45), 19167–19177. https://doi.org/10.1021/jacs.1c09263.

(33)   Ogawa, K. A.; Goetz, A. E.; Boydston, A. J. Metal-Free Ring-Opening Metathesis Polymerization. *J. Am. Chem. Soc.* **2015**, *137* (4), 1400–1403. https://doi.org/10.1021/ja512073m.

(34)   Yang, X.; Gitter, S. R.; Roessler, A. G.; Zimmerman, P. M.; Boydston, A. J. An Ion-Pairing Approach to Stereoselective Metal-Free Ring-Opening Metathesis Polymerization. *Angew. Chem. Int. Ed.* **2021**, *60* (25), 13952–13958. https://doi.org/10.1002/anie.202016393.

(35)   Xu, J.; Boyer, C. Visible Light Photocatalytic Thiol–Ene Reaction: An Elegant Approach for Fast Polymer Postfunctionalization and Step-Growth Polymerization. *Macromolecules* **2015**, *48* (3), 520–529. https://doi.org/10.1021/ma502460t.

(36)   Stache, E. E.; Kottisch, V.; Fors, B. P. Photocontrolled Radical Polymerization from Hydridic C–H Bonds. *J. Am. Chem. Soc.* **2020**, *142* (10), 4581–4585. https://doi.org/10.1021/jacs.0c00287.

(37)   Nguyen, S. T.; Fries, L. R.; Cox, J. H.; Ma, Y.; Fors, B. P.; Knowles, R. R. Chemical Recycling of Thiol Epoxy Thermosets via Light-Driven C–C Bond Cleavage. *J. Am. Chem. Soc.* **2023**, *145* (20), 11151–11160. https://doi.org/10.1021/jacs.3c00958.

(38)   Teo, Y. C.; Lai, H. W. H.; Xia, Y. Synthesis of Ladder Polymers: Developments, Challenges, and Opportunities. *Chem. – Eur. J.* **2017**, *23* (57), 14101–14112. https://doi.org/10.1002/chem.201702219.

(39)   McCulloch, B.; Ho, V.; Hoarfrost, M.; Stanley, C.; Do, C.; Heller, W. T.; Segalman, R. A. Polymer Chain Shape of Poly(3-Alkylthiophenes) in Solution Using Small-Angle Neutron Scattering. *Macromolecules* **2013**, *46* (5), 1899–1907. https://doi.org/10.1021/ma302463d.

(40)   Cao, Z.; Leng, M.; Cao, Y.; Gu, X.; Fang, L. How Rigid Are Conjugated Non-Ladder and Ladder Polymers? *J. Polym. Sci.* **2022**, *60* (3), 298–310. https://doi.org/10.1002/pol.20210550.

(41)   Staudinger, H.; Bruson, H. A. Hochpolymere Verbindungen. 7. Mitteilung. Über Das Dicyclopentadien Und Weitere Polymere Cyclopentadiene. *Justus Liebigs Ann. Chem.* **1926**, *447* (1), 97–110. https://doi.org/10.1002/jlac.19264470110.

(42)   Bailey, W. J.; Economy, J.; Hermes, M. E. Polymers. IV. Polymeric Diels-Alder Reactions1, 2. *J. Org. Chem.* **1962**, *27* (9), 3295–3299.

(43)   Yu, L.; Chen, M.; Dalton, L. R. Ladder Polymers: Recent Developments in Syntheses, Characterization, and Potential Applications as Electronic and Optical Materials. *Chem. Mater.* **1990**, *2* (6), 649–659.

(44)   Lee, J.; Rajeeva, B. B.; Yuan, T.; Guo, Z.-H.; Lin, Y.-H.; Al-Hashimi, M.; Zheng, Y.; Fang, L. Thermodynamic Synthesis of Solution Processable Ladder Polymers. *Chem. Sci.* **2016**, *7* (2), 881–889.

(45)   Ajaz, A.; Bradley, A. Z.; Burrell, R. C.; Li, W. H. H.; Daoust, K. J.; Bovee, L. B.; DiRico, K. J.; Johnson, R. P. Concerted vs Stepwise Mechanisms in Dehydro-Diels–Alder Reactions. *J. Org. Chem.* **2011**, *76* (22), 9320–9328. https://doi.org/10.1021/jo201567d.

(46)   Vogel, T.; Blatter, K.; Schlüter, A.-D. A Soluble Polyacene Precursor. *Makromol. Chem. Rapid Commun.* **1989**, *10* (8), 427–430. https://doi.org/10.1002/marc.1989.030100808.

(47)   Chen, Z.; Amara, J. P.; Thomas, S. W.; Swager, T. M. Synthesis of a Novel Poly(Iptycene) Ladder Polymer. *Macromolecules* **2006**, *39* (9), 3202–3209. https://doi.org/10.1021/ma052451f.

(48)   Tsuda, T.; Hokazono, H. New Synthesis of Soluble Ladder Polymers by Nickel (0)-Catalyzed Cycloaddition Copolymerization of Cyclic Diynes. *Macromolecules* **1993**, *26* (20), 5528–5529.

(49)   Tsuda, T.; Maruta, K.; Kitaike, Y. Nickel(0)-Catalyzed Alternating Copolymerization of Carbon Dioxide with Diynes to Poly(2-Pyrones). *J. Am. Chem. Soc.* **1992**, *114* (4), 1498–1499. https://doi.org/10.1021/ja00030a065.

(50)   McKeown, N. B.; Budd, P. M.; Msayib, K. J.; Ghanem, B. S.; Kingston, H. J.; Tattershall, C. E.; Makhseed, S.; Reynolds, K. J.; Fritsch, D. Polymers of Intrinsic Microporosity (PIMs): Bridging the Void between Microporous and Polymeric Materials. *Chem. – Eur. J.* **2005**, *11* (9), 2610–2620. https://doi.org/10.1002/chem.200400860.

(51)   Wang, Y.; Ghanem, B. S.; Ali, Z.; Hazazi, K.; Han, Y.; Pinnau, I. Recent Progress on Polymers of Intrinsic Microporosity and Thermally Modified Analogue Materials for Membrane-Based Fluid Separations. *Small Struct.* **2021**, *2* (9), 2100049. https://doi.org/10.1002/sstr.202100049.

(52)   Thomas, S. W.; Long, T. M.; Pate, B. D.; Kline, S. R.; Thomas, E. L.; Swager, T. M. Perpendicular Organization of Macromolecules: Synthesis and Alignment Studies of a Soluble Poly(Iptycene). *J. Am. Chem. Soc.* **2005**, *127* (51), 17976–17977. https://doi.org/10.1021/ja056241u.

(53)   Benedetti, F. M.; Wu, Y.-C. M.; Lin, S.; He, Y.; Flear, E.; Storme, K. R.; Liu, C.; Zhao, Y.; Swager, T. M.; Smith, Z. P. Side-Chain Length and Dispersity in ROMP Polymers with Pore-Generating Side Chains for Gas Separations. *JACS Au* **2022**, *2* (7), 1610–1615. https://doi.org/10.1021/jacsau.2c00219.

(54)   Budd, P. M.; Ghanem, B. S.; Makhseed, S.; McKeown, N. B.; Msayib, K. J.; Tattershall, C. E. Polymers of Intrinsic Microporosity (PIMs): Robust, Solution-Processable, Organic Nanoporous Materials. *Chem. Commun.* **2004**, No. 2, 230–231. https://doi.org/10.1039/B311764B.

(55)   Carta, M.; Malpass-Evans, R.; Croad, M.; Rogan, Y.; Jansen, J. C.; Bernardo, P.; Bazzarelli, F.; McKeown, N. B. An Efficient Polymer Molecular Sieve for Membrane Gas Separations. *Science* **2013**, *339* (6117), 303–307. https://doi.org/10.1126/science.1228032.

(56)   Catellani, M.; Motti, E.; Della Ca', N. Catalytic Sequential Reactions Involving Palladacycle-Directed Aryl Coupling Steps. *Acc. Chem. Res.* **2008**, *41* (11), 1512–1522. https://doi.org/10.1021/ar800040u.

(57)   Liu, S.; Jin, Z.; Teo, Y. C.; Xia, Y. Efficient Synthesis of Rigid Ladder Polymers via Palladium Catalyzed Annulation. *J. Am. Chem. Soc.* **2014**, *136* (50), 17434–17437. https://doi.org/10.1021/ja5110415.

(58)   Lin, S.; Ischay, M. A.; Fry, C. G.; Yoon, T. P. Radical Cation Diels–Alder Cycloadditions by Visible Light Photocatalysis. *J. Am. Chem. Soc.* **2011**, *133* (48), 19350–19353. https://doi.org/10.1021/ja2093579.

(59)   Winne, J. M.; Leibler, L.; Du Prez, F. E. Dynamic Covalent Chemistry in Polymer Networks: A Mechanistic Perspective. *Polym. Chem.* **2019**, *10* (45), 6091–6108. https://doi.org/10.1039/c9py01260e.

(60)   Zhang, W.; Jin, Y. *Dynamic Covalent Chemistry : Principles, Reactions, and Applications*, First edition.; Wiley,: Hoboken, NJ, 2017.

(61)   Wojtecki, R. J.; Meador, M. A.; Rowan, S. J. Using the Dynamic Bond to Access Macroscopically Responsive Structurally Dynamic Polymers. *Nat. Mater.* **2011**, *10* (1), 14–27. https://doi.org/10.1038/Nmat2891.

(62)   Boehnke, N.; Cam, C.; Bat, E.; Segura, T.; Maynard, H. D. Imine Hydrogels with Tunable Degradability for Tissue Engineering. *Biomacromolecules* **2015**, *16* (7), 2101–2108. https://doi.org/10.1021/acs.biomac.5b00519.

(63)   Lohse, M. S.; Bein, T. Covalent Organic Frameworks: Structures, Synthesis, and Applications. *Adv. Funct. Mater.* **2018**, *28* (33). https://doi.org/10.1002/adfm.201705553.

(64)   Rottger, M.; Domenech, T.; van der Weegen, R.; Nicolay, A. B. R.; Leibler, L. High-Performance Vitrimers from Commodity Thermoplastics through Dioxaborolane Metathesis. *Science* **2017**, *356* (6333), 62–65. https://doi.org/10.1126/science.aah5281.

(65)   Gu, R. R.; Flidrova, K.; Lehn, J. M. Dynamic Covalent Metathesis in the C=C/C=N Exchange between Knoevenagel Compounds and Imines. *J. Am. Chem. Soc.* **2018**, *140* (16), 5560–5568. https://doi.org/10.1021/jacs.8b01849.

(66)   Maeda, T.; Otsuka, H.; Takahara, A. Dynamic Covalent Polymers: Reorganizable Polymers with Dynamic Covalent Bonds. *Prog. Polym. Sci.* **2009**, *34* (7), 581–604. https://doi.org/10.1016/j.progpolymsci.2009.03.001.

(67)   Rapp, T. L.; DeForest, C. A. Visible Light-Responsive Dynamic Biomaterials: Going Deeper and Triggering More. *Adv. Healthc. Mater.* **2020**. https://doi.org/10.1002/adhm.201901553.

(68)   Scott, T. F.; Schneider, A. D.; Cook, W. D.; Bowman, C. N. Photoinduced Plasticity in Cross-Linked Polymers. *Science* **2005**, *308* (5728), 1615–1617. https://doi.org/10.1126/science.1110505.

(69)   Worrell, B. T.; McBride, M. K.; Lyon, G. B.; Cox, L. M.; Wang, C.; Mavila, S.; Lim, C. H.; Coley, H. M.; Musgrave, C. B.; Ding, Y.; Bowman, C. N. Bistable and Photoswitchable States of Matter. *Nat Commun* **2018**, *9* (1), 2804. https://doi.org/10.1038/s41467-018-05300-7.

(70)   Liu, J. H.; Butt, H. J.; Wu, S. Reconfigurable Surfaces Based on Photocontrolled Dynamic Bonds. *Adv. Funct. Mater.* **2019**. https://doi.org/10.1002/adfm.201907605.

(71)   Gong, T.; Feng, J. C.; Wei, W.; Huang, W. Recent progress in diarylethene as a photoswitching unit. *Prog. Chem.* **2006**, *18* (6), 698–706.

(72)   Bandara, H. M. D.; Burdette, S. C. Photoisomerization in Different Classes of Azobenzene. *Chem. Soc. Rev.* **2012**, *41* (5), 1809–1825. https://doi.org/10.1039/c1cs15179g.

(73)   Helmy, S.; Leibfarth, F. A.; Oh, S.; Poelma, J. E.; Hawker, C. J.; de Alaniz, J. R. Photoswitching Using Visible Light: A New Class of Organic Photochromic Molecules. *J. Am. Chem. Soc.* **2014**, *136* (23), 8169–8172. https://doi.org/10.1021/ja503016b.

(74)   Klajn, R. Spiropyran-Based Dynamic Materials. *Chem. Soc. Rev.* **2014**, *43* (1), 148–184. https://doi.org/10.1039/c3cs60181a.

(75)   van Dijken, D. J.; Kovaricek, P.; Ihrig, S. P.; Hecht, S. Acylhydrazones as Widely Tunable Photoswitches. *J. Am. Chem. Soc.* **2015**, *137* (47), 14982–14991. https://doi.org/10.1021/jacs.5b09519.

(76)   Gerwien, A.; Reinhardt, T.; Mayer, P.; Dube, H. Synthesis of Double-Bond-Substituted Hemithioindigo Photoswitches. *Org. Lett.* **2018**, *20* (1), 232–235. https://doi.org/10.1021/acs.orglett.7b03574.

(77)   Kortekaas, L.; Browne, W. R. The Evolution of Spiropyran: Fundamentals and Progress of an Extraordinarily Versatile Photochrome. *Chem. Soc. Rev.* **2019**, *48* (12), 3406–3424. https://doi.org/10.1039/c9cs00203k.

(78)   Liu, D.; Sponza, A. D.; Yang, D. D.; Chiu, M. Modulating Polymer Dispersity with Light: Cationic Polymerization of Vinyl Ethers Using Photochromic Initiators. *Angew. Chem.-Int. Ed.* **2019**, *58* (45), 16210–16216. https://doi.org/10.1002/anie.201908775.

(79)   Lvov, A. G.; Yadykov, A. V.; Lyssenko, K. A.; Heinemann, F. W.; Shirinian, V. Z.; Khusniyarov, M. M. Reversible Shifting of a Chemical Equilibrium by Light: The Case of Keto-Enol Tautomerism of a Beta-Ketoester. *Org Lett* **2020**, *22* (2), 604–609. https://doi.org/10.1021/acs.orglett.9b04376.

(80)   Kathan, M.; Hecht, S. Photoswitchable Molecules as Key Ingredients to Drive Systems Away from the Global Thermodynamic Minimum. *Chem. Soc. Rev.* **2017**, *46* (18), 5536–5550. https://doi.org/10.1039/c7cs00112f.

(81)   Lemieux, V.; Gauthier, S.; Branda, N. R. Selective and Sequential Photorelease Using Molecular Switches. *Angew. Chem.-Int. Ed.* **2006**, *45* (41), 6820–6824. https://doi.org/10.1002/anie.200601584.

(82)   Gostl, R.; Hecht, S. Photoreversible Prodrugs and Protags: Switching the Release of Maleimides by Using Light under Physiological Conditions. *Chem.- Eur. J.* **2015**, *21* (11), 4422–4427. https://doi.org/10.1002/chem.201405767.

(83)   Asadirad, A. M.; Boutault, S.; Erno, Z.; Branda, N. R. Controlling a Polymer Adhesive Using Light and a Molecular Switch. *J. Am. Chem. Soc.* **2014**, *136* (8), 3024–3027. https://doi.org/10.1021/ja500496n.

(84)   Yesilyurt, V.; Webber, M. J.; Appel, E. A.; Godwin, C.; Langer, R.; Anderson, D. G. Injectable Self-Healing Glucose-Responsive Hydrogels with PH-Regulated Mechanical Properties. *Adv. Mater.* **2016**, *28* (1), 86–91. https://doi.org/10.1002/adma.201502902.

(85)   Guan, Y.; Zhang, Y. Boronic Acid-Containing Hydrogels: Synthesis and Their Applications. *Chem. Soc. Rev.* **2013**, *42* (20). https://doi.org/10.1039/c3cs60152h.

(86)   Cromwell, O. R.; Chung, J.; Guan, Z. B. Malleable and Self-Healing Covalent Polymer Networks through Tunable Dynamic Boronic Ester Bonds. *J. Am. Chem. Soc.* **2015**, *137* (20), 6492–6495. https://doi.org/10.1021/jacs.5b03551.

(87)   Hargrove, A. E.; Reyes, R. N.; Riddington, I.; Anslyn, E. V.; Sessler, J. L. Boronic Acid Porphyrin Receptor for Ginsenoside Sensing. *Org. Lett.* **2010**, *12* (21), 4804–4807. https://doi.org/10.1021/ol1019647.

(88)   Ni, N. T.; Laughlin, S.; Wang, Y. J.; Feng, Y.; Zheng, Y. J.; Wang, B. H. Probing the General Time Scale Question of Boronic Acid Binding with Sugars in Aqueous Solution at Physiological PH. *Bioorg. Med. Chem.* **2012**, *20* (9), 2957–2961. https://doi.org/10.1016/j.bmc.2012.03.014.

(89)   Chapin, B. M.; Metola, P.; Vankayala, S. L.; Woodcock, H. L.; Mooibroek, T. J.; Lynch, V. M.; Larkin, J. D.; Anslyn, E. V. Disaggregation Is a Mechanism for Emission Turn-On of Ortho-Aminomethylphenylboronic Acid-Based Saccharide Sensors. *J. Am. Chem. Soc.* **2017**, *139* (15), 5568–5578. https://doi.org/10.1021/jacs.7b01755.

(90)   Sun, X. L.; James, T. D.; Anslyn, E. V. Arresting "Loose Bolt" Internal Conversion from -B(OH)(2) Groups Is the Mechanism for Emission Turn-On in Ortho-Aminomethylphenylboronic Acid-Based Saccharide Sensors. *J. Am. Chem. Soc.* **2018**, *140* (6), 2348–2354. https://doi.org/10.1021/jacs.7b12877.

(91)   Sun, X. L.; Chapin, B. M.; Metola, P.; Collins, B.; Wang, B. H.; James, T. D.; Anslyn, E. V. The Mechanisms of Boronate Ester Formation and Fluorescent Turn-on in Ortho-Aminomethylphenylboronic Acids. *Nat. Chem.* **2019**, *11* (9), 768–778. https://doi.org/10.1038/s41557-019-0314-x.

(92)   Monajemi, H.; Cheah, M. H.; Lee, V. S.; Zain, S. M.; Abdullah, W. A. T. W. On the Kinetics and Reaction Mechanisms of Boronic Acid in Interaction with Diols for Non-Enzymatic Glucose Monitoring Applications: A Hybrid DFT Study. *Rsc Adv.* **2014**, *4* (21), 10505–10513. https://doi.org/10.1039/c3ra46964f.

(93)   Marinaro, W. A.; Prankerd, R.; Kinnari, K.; Stella, V. J. Interaction of Model Aryl- and Alkyl-Boronic Acids and 1,2-Diols in Aqueous Solution. *J. Pharm. Sci.* **2015**, *104* (4), 1399–1408. https://doi.org/10.1002/jps.24346.

(94)   Brooks, W. L. A.; Deng, C. C.; Sumerlin, B. S. Structure-Reactivity Relationships in Boronic Acid-Diol Complexation. *Acs Omega* **2018**, *3* (12), 17863–17870. https://doi.org/10.1021/acsomega.8b02999.

(95)   Martinez-Aguirre, M. A.; Flores-Alamo, M.; Medrano, F.; Yatsimirsky, A. K. Examination of Pinanediol-Boronic Acid Ester Formation in Aqueous Media: Relevance to the Relative Stability of Trigonal and Tetrahedral Boronate Esters. *Org. Biomol. Chem.* **2020**, *18* (14), 2716–2726. https://doi.org/10.1039/d0ob00201a.

(96)   Furikado, Y.; Nagahata, T.; Okamoto, T.; Sugaya, T.; Iwatsuki, S.; Inamo, M.; Takagi, H. D.; Odani, A.; Ishihara, K. Universal Reaction Mechanism of Boronic Acids with Diols in Aqueous Solution: Kinetics and the Basic Concept of a Conditional Formation Constant. *Chem.- Eur. J.* **2014**, *20* (41), 13194–13202. https://doi.org/10.1002/chem.201403719.

(97)   Kano, N.; Yoshino, J.; Kawashima, T. Photoswitching of the Lewis Acidity of a Catecholborane Bearing an Azo Group Based on the Change in Coordination Number of Boron. *Org. Lett.* **2005**, *7* (18), 3909–3911. https://doi.org/10.1021/ol051337e.

(98)   Yoshino, J.; Kano, N.; Kawashima, T. Synthesis of Organoboron Compounds Bearing an Azo Group and Substituent Effects on Their Structures and Photoisomerization. *Tetrahedron* **2008**, *64* (33), 7774–7781. https://doi.org/10.1016/j.tet.2008.05.128.

(99)   Accardo, J. V.; Kalow, J. A. Reversibly Tuning Hydrogel Stiffness through Photocontrolled Dynamic Covalent Crosslinks. *Chem. Sci.* **2018**, *9* (27), 5987–5993. https://doi.org/10.1039/c8sc02093k.

(100)   Bahrenburg, J.; Rottger, K.; Siewertsen, R.; Renth, F.; Temps, F. Sequential Photoisomerisation Dynamics of the Push-Pull Azobenzene Disperse Red 1. *Photochem. Photobiol. Sci.* **2012**, *11* (7), 1210–1219. https://doi.org/10.1039/c2pp05400k.

(101)   Bléger, D.; Schwarz, J.; Brouwer, A. M.; Hecht, S. O-Fluoroazobenzenes as Readily Synthesized Photoswitches Offering Nearly Quantitative Two-Way Isomerization with Visible Light. *J. Am. Chem. Soc.* **2012**, *134* (51), 20597–20600. https://doi.org/10.1021/ja310323y.

(102)   Samanta, S.; McCormick, T. M.; Schmidt, S. K.; Seferos, D. S.; Woolley, G. A. Robust Visible Light Photoswitching with Ortho-Thiol Substituted Azobenzenes. *Chem. Commun.* **2013**, *49* (87), 10314–10316. https://doi.org/10.1039/c3cc46045b.

(103)   Knie, C.; Utecht, M.; Zhao, F.; Kulla, H.; Kovalenko, S.; Brouwer, A. M.; Saalfrank, P.; Hecht, S.; Bléger, D. Ortho-Fluoroazobenzenes: Visible Light Switches with Very Long-Lived Z Isomers. *Chem. - Eur. J.* **2014**, *20* (50), 16492–16501. https://doi.org/10.1002/chem.201404649.

(104)   Dong, M. X.; Babalhavaeji, A.; Samanta, S.; Beharry, A. A.; Woolley, G. A. Red-Shifting Azobenzene Photoswitches for in Vivo Use. *Acc. Chem. Res.* **2015**, *48* (10), 2662–2670. https://doi.org/10.1021/acs.accounts.5b00270.

(105)   Ahmed, Z.; Siiskonen, A.; Virkki, M.; Priimagi, A. Controlling Azobenzene Photoswitching through Combined Ortho-Fluorination and -Amination. *Chem. Commun.* **2017**, *53* (93), 12520–12523. https://doi.org/10.1039/c7cc07308a.

(106)   Dong, M.; Babalhavaeji, A.; Collins, C. V.; Jarrah, K.; Sadovski, O.; Dai, Q. Y.; Woolley, G. A. Near-Infrared Photoswitching of Azobenzenes under Physiological Conditions. *J. Am. Chem. Soc.* **2017**, *139* (38), 13483–13486. https://doi.org/10.1021/jacs.7b06471.

(107)   Konrad, D. B.; Savasci, G.; Allmendinger, L.; Trauner, D.; Ochsenfeld, C.; Ali, A. M. Computational Design and Synthesis of a Deeply Red-Shifted and Bistable Azobenzene. *J. Am. Chem. Soc.* **2020**, *142* (14), 6538–6547. https://doi.org/10.1021/jacs.9b10430.

(108)   Schneider, H. J. Hydrogen Bonds with Fluorine. Studies in Solution, in Gas Phase and by Computations, Conflicting Conclusions from Crystallographic Analyses. *Chem. Sci.* **2012**, *3* (5), 1381–1394. https://doi.org/10.1039/c2sc00764a.

(109)   Taylor, R. The Hydrogen Bond between N-H or O-H and Organic Fluorine: Favourable Yes, Competitive No. *Acta Crystallogr. Sect. B-Struct. Sci. Cryst. Eng. Mater.* **2017**, *73*, 474–488. https://doi.org/10.1107/S2052520617005923.

(110)   Collins, B. E.; Metola, P.; Anslyn, E. V. On the Rate of Boronate Ester Formation in Ortho-Aminomethyl-Functionalised Phenyl Boronic Acids. *Supramol. Chem.* **2013**, *25* (2), 79–86. https://doi.org/10.1080/10610278.2012.740044.

(111)   Aguirre-Chagala, Y. E.; Santos, J. L.; Huang, Y. X.; Herrera-Alonso, M. Phenylboronic Acid-Installed Polycarbonates for the PH-Dependent Release of Diol-Containing Molecules. *Acs Macro Lett.* **2014**, *3* (12), 1249–1253. https://doi.org/10.1021/mz500594m.

(112)   Yesilyurt, V.; Ayoob, A. M.; Appel, E. A.; Borenstein, J. T.; Langer, R.; Anderson, D. G. Mixed Reversible Covalent Crosslink Kinetics Enable Precise, Hierarchical Mechanical Tuning of Hydrogel Networks. *Adv. Mater.* **2017**, *29* (19). https://doi.org/10.1002/adma.201605947.

(113)   Tang, S. C.; Ma, H.; Tu, H. C.; Wang, H. R.; Lin, P. C.; Anseth, K. S. Adaptable Fast Relaxing Boronate-Based Hydrogels for Probing Cell-Matrix Interactions. *Adv. Sci.* **2018**, *5* (9). https://doi.org/10.1002/advs.201800638.

(114)   Metanomski, W. V.; Bareiss, R. E.; Kahovec, J.; Loening, K. L.; Shi, L.; Shibaev, V. P. Nomenclature of Regular Double-Strand (Ladder and Spiro) Organic Polymers (IUPAC Recommendations 1993). *Pure Appl. Chem.* **1993**, *65* (7), 1561–1580. https://doi.org/10.1351/pac199365071561.

(115)   Diels, O.; Alder, K. Synthesen in Der Hydroaromatischen Reihe. *Justus Liebigs Ann. Chem.* **1928**, *460* (1), 98–122. https://doi.org/10.1002/jlac.19284600106.

(116)   Schlüter, A.-D. Ladder Polymers: The New Generation. *Adv. Mater.* **1991**, *3* (6), 282–291. https://doi.org/10.1002/adma.19910030603.

(117)   Corrigan, N.; Shanmugam, S.; Xu, J.; Boyer, C. Photocatalysis in Organic and Polymer Synthesis. *Chem. Soc. Rev.* **2016**, *45* (22), 6165–6212. https://doi.org/10.1039/C6CS00185H.

(118)   Xu, J.; Jung, K.; Atme, A.; Shanmugam, S.; Boyer, C. A Robust and Versatile Photoinduced Living Polymerization of Conjugated and Unconjugated Monomers and Its Oxygen Tolerance. *J. Am. Chem. Soc.* **2014**, *136* (14), 5508–5519. https://doi.org/10.1021/ja501745g.

(119)   Xu, J.; Jung, K.; Corrigan, N. A.; Boyer, C. Aqueous Photoinduced Living/Controlled Polymerization: Tailoring for Bioconjugation. *Chem. Sci.* **2014**, *5* (9), 3568–3575. https://doi.org/10.1039/C4SC01309C.

(120)   Fors, B. P.; Hawker, C. J. Control of a Living Radical Polymerization of Methacrylates by Light. *Angew. Chem. Int. Ed.* **2012**, *51* (35), 8850–8853. https://doi.org/10.1002/anie.201203639.

(121)   Tasdelen, M. A.; Uygun, M.; Yagci, Y. Photoinduced Controlled Radical Polymerization. *Macromol. Rapid Commun.* **2011**, *32* (1), 58–62. https://doi.org/10.1002/marc.201000351.

(122)   Kottisch, V.; Michaudel, Q.; Fors, B. P. Cationic Polymerization of Vinyl Ethers Controlled by Visible Light. *J. Am. Chem. Soc.* **2016**, *138* (48), 15535–15538. https://doi.org/10.1021/jacs.6b10150.

(123)   Okada, Y.; Yamaguchi, Y.; Ozaki, A.; Chiba, K. Chem Sci. 2016; 7: 6387–6393. Doi: 10.1039. *C6SC02117DEurope PMC Free Artic. Sch.*

(124)   Ischay, M. A.; Ament, M. S.; Yoon, T. P. Crossed Intermolecular [2 + 2] Cycloaddition of Styrenes by Visible Light Photocatalysis. *Chem. Sci.* **2012**, *3* (9), 2807–2811. https://doi.org/10.1039/C2SC20658G.

(125)   Fiorito, D.; Simon, M.; Thomas, C. M.; Mazet, C. Access to Highly Stereodefined 1,4-Cis-Polydienes by a [Ni/Mg] Orthogonal Tandem Catalytic Polymerization. *J. Am. Chem. Soc.* **2021**, *143* (33), 13401–13407. https://doi.org/10.1021/jacs.1c06553.

(126)   Teo, Y. C.; Lai, H. W. H.; Xia, Y. Synthesis of Ladder Polymers: Developments, Challenges, and Opportunities. *Chem. – Eur. J.* **2017**, *23* (57), 14101–14112. https://doi.org/10.1002/chem.201702219.

(127)   Lai, H. W. H.; Liu, S.; Xia, Y. Norbornyl Benzocyclobutene Ladder Polymers: Conformation and Microporosity. *J. Polym. Sci. Part Polym. Chem.* **2017**, *55* (18), 3075–3081. https://doi.org/10.1002/pola.28640.

(128)   Chaoui, N.; Trunk, M.; Dawson, R.; Schmidt, J.; Thomas, A. Trends and Challenges for Microporous Polymers. *Chem. Soc. Rev.* **2017**, *46* (11), 3302–3321. https://doi.org/10.1039/C7CS00071E.

(129)   Zhao, Y.; He, Y.; Swager, T. M. Porous Organic Polymers via Ring Opening Metathesis Polymerization. *ACS Macro Lett.* **2018**, *7* (3), 300–304. https://doi.org/10.1021/acsmacrolett.8b00041.

(130)   Cismesia, M. A.; Yoon, T. P. Characterizing Chain Processes in Visible Light Photoredox Catalysis. *Chem. Sci.* **2015**, *6* (10), 5426–5434. https://doi.org/10.1039/C5SC02185E.

(131)   Hu, G.; Xu, J.; Li, P. Sulfur Mediated Allylic C–H Alkylation of Tri- and Disubstituted Olefins. *Org. Lett.* **2014**, *16* (22), 6036–6039. https://doi.org/10.1021/ol5031348.

(132)   Fiorito, D.; Folliet, S.; Liu, Y.; Mazet, C. A General Nickel-Catalyzed Kumada Vinylation for the Preparation of 2-Substituted 1,3-Dienes. *ACS Catal.* **2018**, *8* (2), 1392–1398. https://doi.org/10.1021/acscatal.7b04030.

(133)   Maruyama, K.; Katagiri, T. Mechanism of the Grignard Reaction. *J. Phys. Org. Chem.* **1989**, *2* (3), 205–213.

(134)   Yao, C.; Liu, N.; Long, S.; Wu, C.; Cui, D. Highly Cis-1, 4-Selective Coordination Polymerization of Polar 2-(4-Methoxyphenyl)-1, 3-Butadiene and Copolymerization with Isoprene Using a β-Diketiminato Yttrium Bis (Alkyl) Complex. *Polym. Chem.* **2016**, *7* (6), 1264–1270.

(135)   Rahimi, A.; García, J. M. Chemical Recycling of Waste Plastics for New Materials Production. *Nat. Rev. Chem.* **2017**, *1* (6), 0046. https://doi.org/10.1038/s41570-017-0046.

(136)   Patrício Silva, A. L.; Prata, J. C.; Duarte, A. C.; Barcelò, D.; Rocha-Santos, T. An Urgent Call to Think Globally and Act Locally on Landfill Disposable Plastics under and after Covid-19 Pandemic: Pollution Prevention and Technological (Bio) Remediation Solutions. *Chem. Eng. J.* **2021**, *426*, 131201. https://doi.org/10.1016/j.cej.2021.131201.

(137)   Vedantam, A.; Suresh, N. C.; Ajmal, K.; Shelly, M. Impact of China's National Sword Policy on the U.S. Landfill and Plastics Recycling Industry. *Sustainability* **2022**, *14* (4). https://doi.org/10.3390/su14042456.

(138)   Scheutz, G. M.; Lessard, J. J.; Sims, M. B.; Sumerlin, B. S. Adaptable Crosslinks in Polymeric Materials: Resolving the Intersection of Thermoplastics and Thermosets. *J. Am. Chem. Soc.* **2019**, *141* (41), 16181–16196. https://doi.org/10.1021/jacs.9b07922.

(139)   Lewandowski, K.; Skórczewska, K. A Brief Review of Poly(Vinyl Chloride) (PVC) Recycling. *Polymers* **2022**, *14* (15), 3035.

(140)   McNeill, I. C.; Memetea, L.; Cole, W. J. A Study of the Products of PVC Thermal Degradation. *Polym. Degrad. Stab.* **1995**, *49* (1), 181–191. https://doi.org/10.1016/0141-3910(95)00064-S.

(141)   Coates, G. W.; Getzler, Y. D. Y. L. Chemical Recycling to Monomer for an Ideal, Circular Polymer Economy. *Nat. Rev. Mater.* **2020**, *5* (7), 501–516. https://doi.org/10.1038/s41578-020-0190-4.

(142)   Yu, J.; Sun, L.; Ma, C.; Qiao, Y.; Yao, H. Thermal Degradation of PVC: A Review. *Waste Manag.* **2016**, *48*, 300–314. https://doi.org/10.1016/j.wasman.2015.11.041.

(143)   Jehanno, C.; Alty, J. W.; Roosen, M.; De Meester, S.; Dove, A. P.; Chen, E. Y. X.; Leibfarth, F. A.; Sardon, H. Critical Advances and Future Opportunities in Upcycling Commodity Polymers. *Nature* **2022**, *603* (7903), 803–814. https://doi.org/10.1038/s41586-021-04350-0.

(144)   Williamson, J. B.; Lewis, S. E.; Johnson Iii, R. R.; Manning, I. M.; Leibfarth, F. A. C−H Functionalization of Commodity Polymers. *Angew. Chem. Int. Ed.* **2019**, *58* (26), 8654–8668. https://doi.org/10.1002/anie.201810970.

(145)   Kameda, T.; Fukuda, Y.; Grause, G.; Yoshioka, T. Chemical Modification of Rigid Poly(Vinyl Chloride) by the Substitution with Nucleophiles. *J. Appl. Polym. Sci.* **2010**, *116* (1), 36–44. https://doi.org/10.1002/app.31452.

(146)   Saleh, T.; Yousif, E.; Al-Tikrity, E.; Bufaroosha, M.; Husain, A.; Al-Mashhadani, M. H. Modification of PVC with Captopril and Complexation Reaction for Preparing Photostability and Thermal Stability of PVC. *Mater. Sci. Energy Technol.* **2022**, *5*, 311–323. https://doi.org/10.1016/j.mset.2022.07.001.

(147)   Rusen, E.; Raluca, Ș.; Busuioc, C.; Diacon, A. Hydrophilic Modification of Polyvinyl Chloride with Polyacrylic Acid Using ATRP. *RSC Adv.* **2020**, *10* (59), 35692–35700. https://doi.org/10.1039/D0RA05936F.

(148)   Curto, S. G.; de las Heras, L. A.; Esteruelas, M. A.; Oliván, M.; Oñate, E. C(Sp3)–Cl Bond Activation Promoted by a POP-Pincer Rhodium(I) Complex. *Organometallics* **2019**, *38* (15), 3074–3083. https://doi.org/10.1021/acs.organomet.9b00409.

(149)   Kwiatkowski, M. R.; Alexanian, E. J. Transition-Metal (Pd, Ni, Mn)-Catalyzed C–C Bond Constructions Involving Unactivated Alkyl Halides and Fundamental Synthetic Building Blocks. *Acc. Chem. Res.* **2019**, *52* (4), 1134–1144. https://doi.org/10.1021/acs.accounts.9b00044.

(150)   Weix, D. J. Methods and Mechanisms for Cross-Electrophile Coupling of Csp2 Halides with Alkyl Electrophiles. *Acc. Chem. Res.* **2015**, *48* (6), 1767–1775. https://doi.org/10.1021/acs.accounts.5b00057.

(151)   Kim, S.; Goldfogel, M. J.; Gilbert, M. M.; Weix, D. J. Nickel-Catalyzed Cross-Electrophile Coupling of Aryl Chlorides with Primary Alkyl Chlorides. *J. Am. Chem. Soc.* **2020**, *142* (22), 9902–9907. https://doi.org/10.1021/jacs.0c02673.

(152)   Hansen, E. C.; Li, C.; Yang, S.; Pedro, D.; Weix, D. J. Coupling of Challenging Heteroaryl Halides with Alkyl Halides via Nickel-Catalyzed Cross-Electrophile Coupling. *J. Org. Chem.* **2017**, *82* (14), 7085–7092. https://doi.org/10.1021/acs.joc.7b01334.

(153)   Zheng, Y.; Qing, F.-L.; Huang, Y.; Xu, X.-H. Tunable and Practical Synthesis of Thiosulfonates and Disulfides from Sulfonyl Chlorides in the Presence of Tetrabutylammonium Iodide. *Adv. Synth. Catal.* **2016**, *358* (21), 3477–3481. https://doi.org/10.1002/adsc.201600633.

(154)   Kennedy, C. R.; Lehnherr, D.; Rajapaksa, N. S.; Ford, D. D.; Park, Y.; Jacobsen, E. N. Mechanism-Guided Development of a Highly Active Bis-Thiourea Catalyst for Anion-Abstraction Catalysis. *J. Am. Chem. Soc.* **2016**, *138* (41), 13525–13528. https://doi.org/10.1021/jacs.6b09205.

(155)   Atack, T. C.; Cook, S. P. Manganese-Catalyzed Borylation of Unactivated Alkyl Chlorides. *J. Am. Chem. Soc.* **2016**, *138* (19), 6139–6142. https://doi.org/10.1021/jacs.6b03157.

(156)   Han, C.; Buchwald, S. L. Negishi Coupling of Secondary Alkylzinc Halides with Aryl Bromides and Chlorides. *J. Am. Chem. Soc.* **2009**, *131* (22), 7532–7533. https://doi.org/10.1021/ja902046m.

(157)   Pritchard, J. G.; Vollmer, R. L. The Meso and Racemic Forms of 2,4-Pentanediol and Certain of Their Derivatives. *J. Org. Chem.* **1963**, *28* (6), 1545–1549. https://doi.org/10.1021/jo01041a025.

(158)   Yousif, E.; Hasan, A. Photostabilization of Poly(Vinyl Chloride) – Still on the Run. *J. Taibah Univ. Sci.* **2015**, *9* (4), 421–448. https://doi.org/10.1016/j.jtusci.2014.09.007.

(159)   Juliá, F.; Constantin, T.; Leonori, D. Applications of Halogen-Atom Transfer (XAT) for the Generation of Carbon Radicals in Synthetic Photochemistry and Photocatalysis. *Chem. Rev.* **2022**, *122* (2), 2292–2352. https://doi.org/10.1021/acs.chemrev.1c00558.

(160)   Charboneau, D. J.; Barth, E. L.; Hazari, N.; Uehling, M. R.; Zultanski, S. L. A Widely Applicable Dual Catalytic System for Cross-Electrophile Coupling Enabled by Mechanistic Studies. *ACS Catal.* **2020**, *10* (21), 12642–12656. https://doi.org/10.1021/acscatal.0c03237.

(161)   Sakai, H. A.; Liu, W.; Le, C. "Chip"; MacMillan, D. W. C. Cross-Electrophile Coupling of Unactivated Alkyl Chlorides. *J. Am. Chem. Soc.* **2020**, *142* (27), 11691–11697. https://doi.org/10.1021/jacs.0c04812.

(162)   Zhang, P.; Le, C. "Chip"; MacMillan, D. W. C. Silyl Radical Activation of Alkyl Halides in Metallaphotoredox Catalysis: A Unique Pathway for Cross-Electrophile Coupling. *J. Am. Chem. Soc.* **2016**, *138* (26), 8084–8087. https://doi.org/10.1021/jacs.6b04818.

(163)   Yang, T.; Wei, Y.; Koh, M. J. Photoinduced Nickel-Catalyzed Deaminative Cross-Electrophile Coupling for C(Sp2)–C(Sp3) and C(Sp3)–C(Sp3) Bond Formation. *ACS Catal.* **2021**, *11* (11), 6519–6525. https://doi.org/10.1021/acscatal.1c01416.

(164)   Tay, N. E. S.; Lehnherr, D.; Rovis, T. Photons or Electrons? A Critical Comparison of Electrochemistry and Photoredox Catalysis for Organic Synthesis. *Chem. Rev.* **2022**, *122* (2), 2487–2649. https://doi.org/10.1021/acs.chemrev.1c00384.

(165)   Zackasee, J. L. S.; Al Zubaydi, S.; Truesdell, B. L.; Sevov, C. S. Synergistic Catalyst–Mediator Pairings for Electroreductive Cross-Electrophile Coupling Reactions. *ACS Catal.* **2022**, *12* (2), 1161–1166. https://doi.org/10.1021/acscatal.1c05144.

(166)   Jiao, K.-J.; Liu, D.; Ma, H.-X.; Qiu, H.; Fang, P.; Mei, T.-S. Nickel-Catalyzed Electrochemical Reductive Relay Cross-Coupling of Alkyl Halides to Aryl Halides. *Angew. Chem. Int. Ed.* **2020**, *59* (16), 6520–6524. https://doi.org/10.1002/anie.201912753.

(167)   Truesdell, B. L.; Hamby, T. B.; Sevov, C. S. General C(Sp2)–C(Sp3) Cross-Electrophile Coupling Reactions Enabled by Overcharge Protection of Homogeneous Electrocatalysts. *J. Am. Chem. Soc.* **2020**, *142* (12), 5884–5893. https://doi.org/10.1021/jacs.0c01475.

(168)   Perkins, R. J.; Pedro, D. J.; Hansen, E. C. Electrochemical Nickel Catalysis for Sp2-Sp3 Cross-Electrophile Coupling Reactions of Unactivated Alkyl Halides. *Org. Lett.* **2017**, *19* (14), 3755–3758. https://doi.org/10.1021/acs.orglett.7b01598.

(169)   Durandetti, M.; Nédélec, J.-Y.; Périchon, J. Nickel-Catalyzed Direct Electrochemical Cross-Coupling between Aryl Halides and Activated Alkyl Halides. *J. Org. Chem.* **1996**, *61* (5), 1748–1755. https://doi.org/10.1021/jo9518314.

(170)   Williamson, J. B.; Na, C. G.; Johnson, R. R.; Daniel, W. F. M.; Alexanian, E. J.; Leibfarth, F. A. Chemo- and Regioselective Functionalization of Isotactic Polypropylene: A Mechanistic and Structure–Property Study. *J. Am. Chem. Soc.* **2019**, *141* (32), 12815–12823. https://doi.org/10.1021/jacs.9b05799.

(171)   Breitenfeld, J.; Ruiz, J.; Wodrich, M. D.; Hu, X. Bimetallic Oxidative Addition Involving Radical Intermediates in Nickel-Catalyzed Alkyl–Alkyl Kumada Coupling Reactions. *J. Am. Chem. Soc.* **2013**, *135* (32), 12004–12012. https://doi.org/10.1021/ja4051923.

<div align="center">**Vita**</div>

Emily R. McClure

EDUCATION

Northwestern University
Evanston, IL
PhD in Chemistry (3.8/4.0)   Expected July 2023

RESEARCH EXPERIENCE

Graduate Research Assistant
Evanston, IL
Northwestern University (Prof. Julia Kalow)   August 2018-present

Photoredox ladder polymers
- Invented and pursued a new reaction to make porous polymers for gas and water purification
- Isolated and characterized small molecule side-products and polymer chains
- Developed reaction screens to optimize polymerization and small-molecule reactions
- Evaluated reaction condition efficacy using LC-MS, GC-MS, NMR and MALDI-TOF

Light-responsive hydrogels
- Designed and synthesized red-light absorbing photoswitches and measured reaction thermodynamics using proton NMR and VT-NMR
- Collaborated with computational chemists to perform calculations to elucidate the mechanism of photocontrolled dynamic chemistry
- Planned and synthesized a library of photoswitch derivatives
- Synthesized light-responsive, bio-compatible hydrogels and measured properties using rheology

Selective photochromic cross coupling
- Troubleshooted reaction optimization of a selective photocontrolled cross-coupling reaction
- Screened reaction parameters and evaluated product formation using LC-MS
- Used LC-MS to characterize degradation side products
- Proposed new reaction conditions to prevent side reactions and promote product formation

Additional experiences
- Mentored, supervised and trained junior research students by providing technical advice
- Inspected, repaired, and maintained laboratory equipment including Isolera Biotage and solvent purification system

Research Experience for Undergraduates (REU) Student
Philadelphia, PA
University of Pennsylvania LRSM (Prof. Virgil Percec) (45 hours/week)   May-August 2017
- Conceived and executed experiments to optimize a previously reported reaction and make previously uncharacterized materials
- Collaborated with senior graduate students to create and execute a summer research project

Mentored Advanced Project Student
Grinnell, IA

Grinnell College (Prof. Steven Sieck)   May-August 2016, August-December 2017

- Designed and executed experiments to optimize the yields of previously synthesized compounds and apply the optimized methodology to synthesize new compounds
- Developed a report of several years of research in a comprehensive document summarizing previous research progress and my own research progress

LEADERSHIP EXPERIENCE

Northwestern University Building on Diversity (NUBonD) Board Member
Evanston, IL
Northwestern University (3 hours/week)   June 2019-present

- Advocated for policy changes in the Chemistry department including the successful adoption of a $1,000 moving stiped for incoming graduate students
- Organized and hosted the two-day Faces of Seminar Series in Winter of 2020 and Spring 2022 with over sixty students and faculty attending two days of talks and workshops
- Facilitated orientation diversity workshops and social events through NUBonD to increase dialogue around diversity and inclusion in the department and build community
- Constructed and proposed a $5,000 budget annually that was approved to support activities and talks throughout the school year
- Provided assistance to newer board members to plan and execute events and prepare budgets
- Evaluated extent of student wellbeing and inclusion of study body by facilitating meetings with students and faculty
- Collaborated with the chemistry faculty Diversity, Equity, Inclusion committee to increase implementation of DEI programming in the chemistry department

NU Votes Ambassador and Staffer
Evanston, IL
Northwestern University Center for Civic Engagement (2 hours/week)   September 2018-present

- Organized social events and one-on-one conversations to promote voting in Northwestern graduate and undergraduate students
- Presented to research groups and classes to increase voter participation in the greater Northwestern community and maintain Northwestern's 90% eligible voter registration rate
- Canvassed at various campus locations to register students to vote and assist them in registering to vote, requesting an absentee ballot, or making a plan to vote
- Processed voter registration forms through the Center of Civic Engagement to check for errors in voter registration forms and mail voter registration forms
- Served as a resource for mail-in voting for students and colleagues

Department Organizer
Evanston, IL
Northwestern University Graduate Workers (1 hour/week)   June 2020-present

- Facilitated and attended monthly meetings to update students on the progress of the graduate student union, action items to promote graduate worker wellbeing
- Organized and hosted informational and social events every quarter to increase union presence in the chemistry department and promote union membership within the graduate worker population

- Promote union membership in the chemistry department (250 students) through one-on-one conversations and canvassing to increase chemistry membership to 30% by fall of 2022
- Served as a liaison between chemistry graduate students and the larger graduate union to communicate needs, action items and promote union events
- Collaborate with other chemistry department student groups to promote joint issues and union membership through student programming and joint meetings

Graduate Student Advisory Committee Member
Evanston, IL
Northwestern University Center for Civic Engagement (1 hour/week)   April 2021-
August 2022

- Advised and promoted programming (between 30-50 students) at the Center for Civic Engagement
- Attended "Introduction to Community-based Scholarship" workshop series which involved completing readings and discussing civically oriented scholarship with peers in graduate school

Science Policy Outreach Taskforce Board Member (SPOT)
Evanston, IL
Northwestern University (2 hours/week)   October 2018-
January 2020

- Managed social media for SPOT including the SPOT twitter account and writing monthly newsletters
- Assisted in the organization of the SPOT Symposium of 2019—a full day symposium with over 70 student attendees from multiple academic institutions
- Organized and attended monthly lunch discussions on topics relevant to science policy
- Presented at a lunch discussion regarding sustainable plastics in December of 2019

TEACHING EXPERIENCE

Instructor
Bridge II Instructor
Evanston, IL
Northwestern University (15 hours/week)   August 2020-
September 2021

- Designed a three-week curriculum to introduce sixty students to organic chemistry and prepare students to succeed academically in the organic chemistry series at Northwestern
- Lectured hour-long lesson plans to students for three weeks to reflect lecture style during full-quarter chemistry courses
- Constructed assessments (3 exams and 10 formative assessments) to evaluate student learning
- Provided feedback on daily assessments and weekly cumulative assessments
- Served as a leader to undergraduate teaching fellows and students throughout the course
- Mentored a graduate co-instructor for the 2021 Bridge II course
- Received ratings of 5.37/6 for the course, 5.1/6 for learning in the course, 5.67/6 for instructor preparedness, 5.27/6 for instructor communication, and 5.70/6 for instructor enthusiasm

Teaching Fellow/Assistant
Organic Chemistry Teaching Fellow and Assistant
Evanston, IL
Northwestern University (10 hours/week)   January 2021-
March 2022

- Lead and presented review sessions and office hours to review course material approximately 120 students per quarter
- Collaborated with instructors in the design of assessments and grading exams
- Supervised graduate student teaching assistants grading exams and provided logistical and intellectual support during the grading process
- Designed exam, quiz, and problem set questions based on lecture material and scientific literature
- Evaluated student performance by grading exams, quizzes, and lab reports
- Facilitated in class-discussions and office hours to review material for students
- Received 5.7/6 rating on ability to answer questions, preparedness for class, interest in teaching, and communication of ideas
- Supervised laboratory experiments and provide technical oversight by giving small demos to undergraduate students to ensure technique proficiency

Tutor and Facilitator
Northwestern Prison Education Program Correspondence Tutor
Evanston, IL
Northwestern University (2 hours/week)   June 2021-present

- Mentored and tutored a student at Logan Correctional Facility through correspondence to assist with studies in math, literature, chemistry, sociology, and conflict resolution
- Facilitated in-person study hours at Logan correctional facility to review and coursework

Organic Chemistry Tutor
Chicago, IL
Northwestern University (2.5 hours/week)   January 2019-present

- Supplemented student learning in class by meeting once or twice a week to review material covered in classes

Teaching Assistant Training Program—Workshop Facilitator
Evanston, IL
Northwestern University   September 2019, 2020 and 2021

- Facilitated "Feedback During Office Hours" workshop for new graduate students
- Translated personal developments from teaching experience into a live demonstration
- Constructively critiqued peers in learning how to hold office hours

Scientific Outreach Workshop Facilitator
Chicago, IL
Northwestern University   November 2018-December 2019

- Coordinated and facilitated an educational workshop on chemical transformations for middle-school aged youth for Expanding Youth Horizons (EYH) educational series at Northwestern University
- Lead a series of workshops, demonstrations, and a panel for high school students the Kovler Hawkins Career Conference at the University of Chicago in July 2019
- Communicated science and chemistry concepts to approximately 30 elementary school students as a substitute instructor for Science in the Classroom (SITC)

CERTIFICATES

Certificate in Science Communication   Received September 2022
Center for Interdisciplinary Exploration and Research in Astrophysics (Northwestern University)
Teaching Certificate Program Completion   Received June of 2022
Searle Center for Advancing Teaching and Learning (Northwestern University)

PUBLICATIONS

1. McClure, E. R.; Das, P.; Kalow, J. A. "Photoredox Ladder Polymerization." *In preparation*.
2. Das, P.; Woods, E. F.; **McClure, E. R.**; Ly, J. T.; Olding, J. N.; Presley, K. F.; Romanoff, B.; Grusenmeyer, T. A.; Weiss, E. A.; Kalow, J. A. "Controlling substrate selectivity in cross coupling with light." *Under revision.* https://doi.org/10.26434/chemrxiv-2021-8wqv0-v2
3. Wang, S.; Huang, N.; Partridge B. E.; Wang, X.; Sahoo, D.; Hoffman D. J.; Malineni, J.; Peterca, M.; Jezorek, R. L.; Zhang, N.; Daud, H.; Sung, P. D.; **McClure, E. R.**; Song S. L.; Percec, V., "An Accelerated Modular-Orthogonal Ni-Catalyzed Methodology to Symmetric and Nonsymmetric Constitutional Isomeric AB2 to AB9 Dendrons Exhibiting Unprecedented Self-Organizing Principles" *J. Am. Chem. Soc.* 2021, 143 (42), 17724-17743.
4. Accardo, J. V.; **McClure, E. R.;** Mosquera, M. A.; Kalow, J. A., "Using Visible Light to Tune Boronic Acid–Ester Equilibria." *J. Am. Chem. Soc.* 2020, 142 (47), 19969-19979.

SKILLS AND PROFICIENCIES

Chemical analysis:
- ^{1}H, ^{13}C, ^{19}F, and 2D Nuclear Magnetic Resonance Spectroscopy
- Electrospray Ionization and Electron Impact Mass Spectrometry
- Matrix-Assisted Laser Desorption Ionization Mass Spectrometry
- Cyclic Voltammetry
- Ultraviolet-Visual Spectroscopy
- Infrared Spectroscopy
- High-Performance Liquid Chromatography
- Gas Chromatography
- Gel Permeation Chromatography
- Rheology
- Thermogravimetric Analysis
- Differential Scanning Calorimetry

Software:
- Microsoft Excel, Word and PowerPoint
- ChemDraw
- MestreNova
- SciFinder
- Reaxys
- Avogadro
- Orca
- Origin
- Electronic Laboratory notebooks
- Zoom
- Microsoft Teams

Organic synthesis:
- Schlenk technique
- Glovebox chemistry
- Small- and large-scale reactions
- Polymerizations
- Column chromatography
- Reaction screens
- Distillation
- Peptide coupling
- Extraction and recrystallization

Languages:
- Proficient in Spanish reading, writing, and speaking (studied from 2001-2016)

SELECTED PRESENTATIONS AND CONFERENCES

1. **Emily R. McClure**, Pradipta Das, Julia Kalow "Photoredox Ladder Polymerization" 2022 Fall American Cehmical Society (ACS) Meeting, Chicago, IL, USA (Oral, August 2022)
2. **Emily R. McClure**, Pradipta Das, Julia Kalow "Photoredox Ladder Polymerization" Context, Community and Connections Symposium (C3), Evanston, IL (Poster, July 2022)
3. **Emily R. McClure**, Pradipta Das, Julia Kalow "Photoredox Ladder Polymerization" 3M RISE Symposium, online (Oral, June 2022)
4. **Emily R. McClure**, Pradipta Das, Julia Kalow "Photoredox Ladder Polymerization" Northwestern University 2021 Third Year Organic Seminar Series, Evanston, IL (Oral, June 2021)
5. **Emily R. McClure**, Joseph V. Accardo, Martin R. Mosquera, Julia A. Kalow, "Visible light-photoswitchable dynamic covalent cross-links for reversibly stiffened hydrogels." 2020 Fall American Chemical Society (ACS) Meeting, San Francisco, CA, University (Oral, Accepted)
6. **Emily R. McClure,** Linnea Dolph, Stephen R. Sieck: "Synthesis of α-Keto Substituted Chalcones and Alkenones." 2018 Spring American Chemical Society (ACS) Meeting, New Orleans, LA, USA (Poster, March 2018)
7. **Emily R. McClure,** Paul D. Sung, Virgil Percec: "Expanding on the Ni-Catalyzed Suzuki Coupling Reaction in the Synthesis of Constitutional Isomeric Libraries of Self-Assembling Building Blocks" Grinnell College Summer Research Department Seminar, Grinnell, IA (Oral, October 2017)
8. **Emily R. McClure,** Stephen R. Sieck: "Synthesis of α-Keto Substituted Chalcones" 2017 Fall Midstates Consortium for Undergraduate Research, St. Louis, MO, USA (Oral, November 2016)

HONORS

Weinberg College of Arts and Sciences Outstanding Graduate Teaching Award   March 2023
Nominated for Phi Lambda Upsilon Teaching Assistant Award   2020
Recipient of the Grinnell College Chemistry Department's Award for Outstanding Excellence in Organic Chemistry I and II (ACS Polymer Chemistry Award)   May 2016
Recipient of the Grinnell College Chemistry Department's Award for Fourth Year Excellence in Organic Chemistry (ACS Division of Organic Chemistry Summer Undergraduate Research Fellowship)   May 2018

(1) Kathan, M.; Kovaříček, P.; Jurissek, C.; Senf, A.; Dallmann, A.; Thünemann, A. F.; Hecht, S. Control of Imine Exchange Kinetics with Photoswitches to Modulate Self-Healing in Polysiloxane Networks by Light Illumination. *Angew. Chem. Int. Ed.* **2016**, *55* (44), 13882-13886. DOI: 10.1002/anie.201605311.